INVESTIGATION OF ENVIRONMENTAL EFFECTS ON COATINGS FOR THERMAL CONTROL OF LARGE SPACE VEHICLES

CR-123531

G.A.Zerlaut
With
J.E.Gilligan
N.A.Ashford

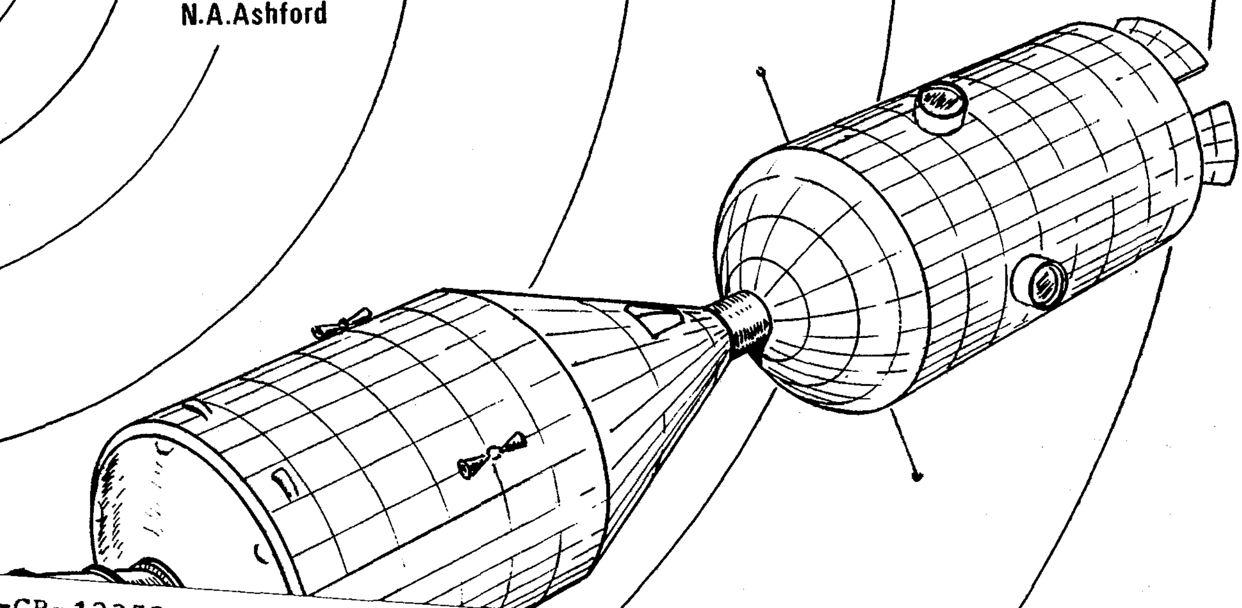

(NASA-CR-123531) INVESTIGATION OF ENVIRONMENTAL EFFECTS ON COATINGS FOR THERMAL CONTROL OF LARGE SPACE VEHICLES Final G.A. Zerlaunt, et al (IIT Research Inst.) 8 Oct. 1971 377 p CSCL 11C G3/18

N72-18576

Unclas 16974

FACILITY FORM 602

377 (ACCESSION NUMBER)	63 (THRU)
(PAGES)	(CODE)
CR-123531 (NASA CR OR TMX OR AD NUMBER)	18 (CATEGORY)

IITRI IIT RESEARCH INSTITUTE

Contract No. NAS8-5379
Report No. IITRI-U6002-97

INVESTIGATION OF ENVIRONMENTAL EFFECTS ON COATINGS FOR THERMAL CONTROL OF LARGE SPACE VEHICLES

Prepared by

G. A. Zerlaut

with

J. E. Gilligan
N. A. Ashford

of

IIT Research Institute
10 West 35th Street
Chicago, Illinois 60616

for

National Aeronautics & Space Administration
George C. Marshall Space Flight Center
Huntsville, Alabama 35812

Final Report for Period 20 May 1963 through 8 October 1971

8 October 1971

PRECEDING PAGE BLANK NOT FILMED

FOREWORD

This is Report No. IITRI-U6002-97 (Final Report) of IITRI Project U6002, Contract No. NAS8-5379, entitled "Investigation of Environmental Effects on Coatings for Thermal Control of Large Space Vehicles," performed for the George C. Marshall Space Flight Center of the National Aeronautics and Space Administration. This report covers the period from May 23, 1963 through October 8, 1971. Formal reports were issued triannually during the course of the program. They are listed in Table i. (Because of a divisional re-organization and an accompanying administrative change in 1965, the IITRI project number designating this program was changed from C6014, the original number, to project U6002, a change that was reflected in the Triannual Report issued on November 9, 1965.)

The program has been under the technical direction of G.A. Zerlaut, who was Project Leader during the course of the program. Contributors to the program, their areas of specialty, and the years that they contributed are presented in Table ii.

The work reported herein was performed under the technical direction of the Space Sciences Laboratory of the George C. Marshall Space Flight Center. Mr. Daniel W. Gates was the Project Manager and the Contracting Officer's Technical Representative (COTR).

Prior to January 1, 1970, this contract was funded under the Funding Codes presented in Table iii. The Funding Code for the period January 1, 1970 to October 8, 1971 was:
124-09-26-0000-33-0-004-000-2510.

Data taken on this research program are recorded in IITRI Logbooks numbers C13736, C14176, C14384, C14550, C14918, C15214, C15652, C16870, C17032, C18308, C18532, C18882, C18933, C19257, C19374, C19477, C19582, C19597, C20104 and C20232.

Respectfully submitted,
IIT RESEARCH INSTITUTE

G.A. Zerlaut
Manager
Polymer Chemistry Research

APPROVED:

Morton J. Klein
Director
Chemistry Research

GAZ:jss

Although the authors are indebted to many people, both in and out of Government service, at IIT Research Institute as well as in industry, we wish to especially acknowledge with sincere thanks both Conrad P. Mook (Retired), Office of Advanced Research and Technology, National Aeronautics and Space Administration, and William F. Carroll, Jet Propulsion Laboratory, California Institute of Technology, for their many helpful suggestions and their unfailing attention during the entire course of the program.

ABSTRACT

The objective of significantly advancing the state-of-the-art of "white", spacecraft-radiator coatings has been realized in a comprehensive goal-oriented, pigmented-coatings research program. The results of this study are presented in nine chapters. They are: an introductory chapter, one on general experimental aspects, two on inorganic pigments and coatings, two on silicone polymers and coatings, one on the design and construction of a combined ultraviolet-plus-proton irradiation facility (the CREF) one on the development of zinc orthotitanate pigment and coatings, and one on the effects on several low α_s/ε paints of combined ultraviolet and proton irradiation in the CREF. Major accomplishments are:

- The development of a structure/property theory that relates to the selection of the most appropriate candidate pigments for employment in space paints,
- The improvement of IITRI's Z93 zinc oxide-pigmented potassium silicate paint as an engineering material,
- The development of S-13G silicated-zinc oxide-based silicone elastomer coating as a reliable engineering material (currently being widely employed as prime thermal control on numerous satellites and spacecraft),
- The development of a rationale for selection of silicone binders that led to the discovery of Owens-Illinois 650 "Glass" resin as the most stable resin binder commercially available,
- The elucidation of ultraviolet-damage mechanisms in semi-conductor pigments,
- The development of reactive encapsulation to stabilize semiconductor pigments against ultraviolet radiation in vacuum,
- The elucidation of "plasma" annealing to stabilize reactively-encapsulated zinc orthotitanate against combined ultraviolet-plus-proton irradiation,

- The design and construction of the 12-specimen IRIF (In Situ Reflectance/Irradiation Facility),

- The design and construction of the CREF (Combined Radiation Environmental Facility) which simultaneously deposits ultraviolet at 1X to 4X solar-ultraviolet acceleration factors and 1.2 keV protons from 1.5X to 250X solar-wind acceleration factors,

- The development of a stable, reactively-encapsulated zinc orthotitanate-pigmented potassium silicate paint having a nominal solar absorptance, α_s, of 0.1 and a $\Delta\alpha_s$ of less than 0.01 in 1000 ESH of ultraviolet radiation in vacuum, and

- The development of a stable plasma-annealed, reactively-encapsulated zinc orthotitanate paint based on Owens-Illinois 650 "Glass" silicone resin that possesses a nominal α_s of 0.2 and a $\Delta\alpha_s$ of much less than 0.01 in 2000 ESH of ultraviolet irradiation in vacuum.

(In work on another program,* an Owens-Illinois 650 "Glass" resin paint pigmented with plasma-annealed, hexafluorosilicate-treated zinc orthotitanate subsequently has been shown to be stable to more than 2000 ESH of ultraviolet and simultaneous irradiation with 2 x 10^{16} H^+/cm^2-sec.)

*IIT Research Institute Project C6233, NASA-MSFC Contract No. NAS8-26791.

Table i

FORMAL TRIANNUAL REPORTS ISSUED

Triannual Report No.	Date of Issue
C6014-4	Oct. 25, 1963
C6014-8	March 5, 1964
C6014-13	July 20, 1964
C6014-18	Dec. 21, 1964
C6014-21	Feb. 23, 1965
C6014-26	July 20, 1965
U6002-31	Nov. 9, 1965
U6002-36	Feb. 21, 1966
U6002-42	July 11, 1966
U6002-47	Nov. 30, 1966
U6002-51	Feb. 28, 1967
U6002-55	Sept. 22, 1967
U6002-59	Jan. 15, 1968
U6002-63	April 15, 1968
U6002-69	Oct. 25, 1968
U6002-73	Jan. 31, 1969
U6002-77	July 11, 1969
U6002-83	Nov. 17, 1969
U6002-85	Feb. 20, 1970
U6002-90	July 1, 1970
U6002-94	Nov. 30, 1970

Table ii

CONTRIBUTORS TO IITRI PROJECT U6002

Name	Contributions	Dates
Major Contributors		
*G.A. Zerlaut	Project Leader	1963-1971
*Dr. N.A. Ashford	Solid state (EPR) studies	1968-1970
N.D. Bennett	Reflectance measurements	1965, 1966
R. Boutin	Space-simulation testing	1968-1970
*Dr. L.U. Berman	Silicone synthesis and photolysis	1964
W.E. Courtney	Space-simulation testing, IRIF and CREF design	1964-1966 1966, 1967
H. DeYoung	Laboratory paint preparation	1967, 1968
*J.E. Gilligan	General consultation, damage studies and proton irradiation studies	1964, 1965 1968-1971
*Y. Harada	Inorganic pigment and paint studies	1963, 1964
*W. Jamison	Space simulation testing	1963, 1964
G. Kimura	Space simulation testing	1966-1970
*M. Marcour	Zinc orthotitanate synthesis	1968, 1969
*Dr. G. Noble	EPR studies of silicones EPR studies of pigments	1965 1967, 1968
*F.O. Rogers	General paint technology Reactive encapsulation	1966-1971 1968-1971
S. Shelfo	Space-simulation testing	1966-1968
*Dr. G.A. Rubin	Theoretical studies and inorganic technology	1965, 1966
D.G. Vance	Silicone paint prep. and space-simulation testing	1963-1965
*E.H. Tompkins	Microporous structures	1963-1964
F. Yarke	EPR measurements of irradiated pigments	1969, 1970
Support and Special Contributions		
J. Brzuskiewicz	Reactive encapsulation studies	1970
C.A. Erdman	Silicone photolysis experiments	1965
*R.F. Firestone	Inorganic coating prep.	1964

Table ii (Cont'd)

Support and Special Contributions

Name	Contribution	Dates
*Dr. B.H. Kaye	Particle size studies	1964
W.R. Logan	Inorganic coating prep.	1965, 1966
O.H. Olson	Optical measurements	1963, 1964
H. Rechter	Inorganic coatings consultation	1963, 1964
R. Reichel	Microporous structures (prep.)	1963, 1964
W.R. Ridenour(dec.)	Space-simulator design	1965, 1966
Dr. R.G. Scholz	Mass spectra/silicone photolysis	1966
*Dr. R. Serway	Silicone photolysis (EPR)	1965

*Denotes authors and coauthors of Triannual Reports.

Table iii

PROGRAM FUNDING CODES PRIOR TO JANUARY 1, 1970

04-84-3-6001-00-000-84-2561-3
124-09-05-0014-28-4-000-2870-2512
933-50-01-0000-28-4-004-000-2801-0
908-20-02-0147-28-5-004-001-2510
124-09-05-2604-28-6-004-028-2510
124-09-05-2604-27-7-004-028-2510
124-09-18-0504-25-8-004-028-2510
124-09-18-0500-25-9-004-028-2510

TABLE OF CONTENTS

Page

PRECEDING PAGE BLANK NOT FILMED

LIST OF FIGURES

Figure No.		Page
38	SPECTRAL REFLECTANCE OF ZINC OXIDE-SILICONE PAINTS AT DIFFERENT PVC's (BASED ON $MgCO_3$-BLOCK)	127
39	EFFECT OF PARTICLE SIZE ON REFLECTANCE OF LTV-602 ZINC OXIDE PAINTS	129
40-A	REFLECTANCE OF SP500 ZINC OXIDE-PIGMENTED SR-80 RESIN AT 35% PVC	131
40-B	EFFECT OF ALUMINUM SUBSTRATE ON REFLECTANCE OF A S-13 SPECIMEN	131
41	SPECTRAL REFLECTANCE OF $CaWO_4$/O-I 650 PAINT AS A FUNCTION OF EXPOSURE TO 600 ESH OF UV IN IRIF-II	142
42	SPECTRAL REFLECTANCE OF $Ca*WO_4$/O-I 650 PAINT AS A FUNCTION OF EXPOSURE TO 600 ESH OF UV IN IRIF-II	143
43	EFFECT OF UV IRRADIATION ON A CABOT RF-1 RUTILE-PIGMENTED 650 PAINT	144
44	UV DEGRADATION OF S-13	147
45	UV DEGRADATION OF ZnO	149
46	UV DEGRADATION OF Z93	150
47	UV DEGRADATION OF SILICATE-TREATED ZnO	151
48	EFFECT OF UV IRRADIATION ON REFLECTANCE SPECTRA OF A TYPICAL PRODUCTION BATCH OF S-13G (BATCH B-581)	154
49	UV DEGRADATION OF SILICATED ZnO IN SILICONE "GLASS" RESIN (COATING A-429)	160
50	THE COMBINED RADIATION TEST FACILITY (CREF)	167
51	CLOSE-UP OF THE CREF SHOWING THE IRIF AND THE SAMPLES (REFLECTED IN THE 45° MIRROR)	168
52	COMBINED RADIATION ENVIRONMENT FACILITY	169
53	BLOCK DIAGRAM OF PRESENT CREF FACILITY	170
54	TWO-ELEMENT EXTRACTOR LENS (DISASSEMBLED) TO REDUCE FLUX FROM RF SOURCE	172
55	EINZEL LENSES; TWO VIEWS	173
56	FARADAY CUP FLUX MAPPER (OPERATED BY A MAGNETIC CHUCK)	174
57	QUADRAPOLE LENS (SWEEP/COLLIMATOR)	175

Figure No.		Page

LIST OF TABLES

INVESTIGATION OF ENVIRONMENTAL EFFECTS ON COATINGS FOR THERMAL CONTROL OF LARGE SPACE VEHICLES

1. INTRODUCTION

The temperature control of satellites and spacecraft is perhaps the most challenging technical problem that has confronted spacecraft designers and engineers. The ultimate objective of thermal design is to ensure that the spacecraft operates within the prescribed temperature range defined by the temperature limitations of the vehicle's materials and components. Therefore, the thermal design, fabrication, launch, and operation of satellites and spacecraft involves a complex balancing of various factors, each of which must be weighed in terms of overall mission requirements, performance, and reliability.

Although many materials' problems have arisen as we have progressed from the early, functionally short-lived satellites of the late 1950's to the sophisticated spacecraft planned for the 1970's, none have been as historical, as tenacious and as technically challenging as the problem of ensuring stability of optical properties of materials (and, to a lesser extent, physical properties) in the hostile radiation environment of oxygenless space. This is attested to by the fact that the multidisciplinary field of Thermophysics, although based on well-established scientific disciplines such as optics, radiation-heat transfer and radiation- and photochemistry, has exhibited most of its growth in the past ten years--growth that has gained its impetus from the need to control the thermophysical properties of surfaces and materials as an essential condition of the temperature regulation of satellites and spacecraft.

The surface temperature of an object in space depends primarily upon the absorptance of solar radiation by the surface, the re-radiation of energy from the surface, and the generation of heat in the body of the object. Secondary parameters that influence the surface temperature of a space vehicle are material properties such as the thermal conductivity and specific heat of spacecraft components.

By definition, the temperature of a spacecraft is that temperature at which the absorbed energy and the emitted, or reradiated, energy are in equilibrium. As the size of the absorbing area (because of changes in attitude) or the intensity of the incident energy changes, an exactly compensating change in temperature occurs, so that the temperature is always changing to affect a new equilibrium. Thus, the optical (reflectance) and radiometric (emittance) characteristics largely determine the limits of the surface temperature of a spacecraft.

Two fundamentally different techniques are used for regulating the temperature of satellites and spacecraft: active temperature control and passive temperature control. Active control is achieved by feedback techniques that usually employ both electrical power and moving parts. For example, bimetallic strips or thermostats control shutters and vanes, whose manipulation results in a constantly varying surface in terms of effective optical properties. Passive control, in contrast, requires neither electrical power nor moving parts. Passive control is achieved by the use of surface materials with appropriate thermophysical characteristics, namely, solar absorptance, α_s, and infrared emittance, ϵ.

Passive control techniques are more reliable than active control techniques because the latter employ both electrical and mechanical parts, which can fail. On the other hand, active control systems can readily accommodate the radiation changes caused by changes in altitude and attitude of the spacecraft, as well as for space radiation-induced changes in the optical properties of the passive surfaces. Active systems are therefore often used in conjunction with passive techniques to provide the most effective control of temperature. Regardless of which control systems are used, the thermophysical properties of the entire surface of the spacecraft must be specified, since it is the average properties of the surface that determine the temperature excursions of satellites and spacecraft.

It is therefore immediately obvious that surface coatings necessarily play a large role in the temperature control of spacecraft. It is because of this role that the technical area of thermophysics known as "spacecraft thermal-control materials technology" has developed since the launching of Explorer I (1958α) in 1958. However, it is also immediately obvious that within the framework of this materials technology the most sensitive and challenging problem of all is that of the development of space-stable, low α_s/ϵ radiator coatings, the nature of which makes them both highly important to spacecraft temperature control and highly vulnerable, optically, to space radiation damage--to both the ultraviolet environment of near space, i.e., that beneath the Van Allen radiation belts, and the ultraviolet-plus-charged particle environment that characterizes space at distances greater than the Van Allen and the induced belts. Low α_s/ϵ surfaces can be divided into those represented by diffusely-reflecting, "white", pigmented-coatings, or paints, and those represented by second-surface mirrors that obtain their low solar absorptance from the metallic reflection of the mirror (usually aluminum or silver) and their emittance from the selectively-transmitting substrate (usually quartz, FEP Teflon, etc.).

Because of the very significant engineering advantages of sprayable coatings, the former type, the "white", low-α_s/ϵ coatings, were chosen for study on the research program for which this final report is presented. Historically, the research effort has been divided into four major phases: (1) Inorganic pigment technology; (2) silicone-photolysis and silicone-paint investigations, (3) the design and characterization of two ultraviolet- (the IRIF's) and a combined-radiation (the CREF) environmental facilities and (4) general coatings investigations. However, for the convenience of reporting on and discussing these aspects, the research results are presented as eight (8) independent chapters: One is on the general experimental aspects of the program (Chapter 2), two are on inorganic technology (Chapter 3 on pigments and Chapter 4 on coatings), two are on silicone technology (Chapter 5 on silicone polymer photolysis and Chapter 6 on silicone coatings), one chapter is on the development of a combined-radiation environmental testing capability (Chapter 7), another chapter is devoted solely to the development of zinc orthotitanate pigment and zinc orthotitanate-pigmented coatings (Chapter 8), and the last chapter, exclusive of a brief summary, is on the effects of combined ultraviolet-plus-proton irradiation of several thermal-control coatings (Chapter 9).

The relative emphasis on each major task has varied during the course of the program according to the urgency of the various problems elucidated by our investigations. However, the major emphasis during the past four years has involved the investigation of new, potentially-stable white pigments, particularly zinc orthotitanate and zinc orthotitanate-pigmented silicate and silicone coatings, and on the design, construction and utilization of a combined-radiation environment facility (CREF) that is capable of simultaneously irradiating evacuated specimens with simulated solar-wind protons and extraterrestrial ultraviolet radiation.

Finally, it is appropriate to briefly examine the philosophy that has guided this program from its inception. The approach employed throughout was predicated almost solely on the application of sound materials sciences practices within the framework of a highly goal-oriented research and development program. Basic mechanisms studies were instituted whenever needed, however not with the frequency nor the intensity that we, as scientists and research technologists would have preferred, yet with a sufficiency of frequency and intensity that we, as practical chemists and engineers,deemed necessary within the framework and limitations imposed by the reality of the program requirements.

The silicone photolysis studies were not completed due to more pressing problems in terms of time and funds as well as to the emergence of Owens-Illinois 650 resin as a strong candidate for a stable binder. The value of the silicone photolysis results presented in Chapter 5 relate more to their relevancy as a point of departure for the future research required than as a solution, to the combined radiation-environment problem of stabilizing binders for long-term, deep-space. On the other hand, the much more complete mechanism study reported in Chapter 8 for zinc orthotitanate served as a guide to the stabilization of this material utilizing surface treatment techniques and, as such, has provided far more than a point of departure for the stabilization studies that are currently underway on a subsequent research program (the results of which have provided strong confirmation of our choice of zinc orthotitanate as a pigment and of the approach selected for its stabilization).

Consistant with the decision to perform goal-oriented developmental research has been the operating ground rule that any candidate chemical structure, whether pigment or binder, in order to be studied must be capable of being developed as a practical, and therefore manufacturable, engineering material. Because of this ground rule and because of the fact that during the entire time of this program coatings have been required for (field) application to spacecraft of all sizes (with emphasis on large systems), we have selected systems the stabilization of which depends on <u>impurity effects as a secondary</u> rather than a primary <u>variable</u>. Thus, the assurance of maintaining coatings' stability when applied to large space vehicles tends to be a much more straightforeward extension of laboratory-scale preparations for such systems compared, for example, to systems the stabilization of which depends on maintaining an exceedingly high degree of purity as a first order variable. Indeed, the fact that field-engineered, commercially-feasible coatings have been continuously available as best-option selections based on the expanding state-of-the-art is, we believe, testimony to the philosophy that has guided this study.

2. EXPERIMENTAL

2.1 Test and Evaluation Philosophy

Tests of proposed candidate thermal control materials should be made under conditions resembling as nearly as possible those existent in the real space environment. Since these conditions vary with distance from the earth--and sometimes even temporarily--simulation facilities must be able to operate over a range of conditions. Yet, whatever the real space conditions are, the equipment can rarely reproduce them. Therefore, and most importantly, we must make certain that the net effect of the real space conditions is being achieved. This implies that we must be certain that the effects induced in a test material by our simulation facilities must be qualitatively--and, as nearly as possible, quantitatively--the same as those induced by the space environment for the same exposure.

In space simulation testing of thermal control materials, the damaging environments are the ultraviolet component of the solar electromagnetic spectrum and charged particles (Van Allen Belt and the solar wind). The hard vacuum of space in itself does not constitute a damaging environment but indirectly has much to do with the effects caused by ultraviolet and charged particle radiation. The net effect of the vacuum of space is such that, if a molecule or atom leaves an exterior spacecraft surface, the probability of its returning is infinitesmally small. Hence, all surface reactions involving the loss of atoms or molecules are in effect irreversible.

The solar spectrum has always been very difficult to simulate. Although it is possible to achieve good spectral matches in certain spectral regions, the cost of doing so virtually prohibits routine use of exact simulators. Also, most of these simulators "age"; that is, certain spectral lines exhibit disproportionate decreases in certain spectral emission lines relative to others. In short, even the best solar simulators are not very close in spectral match in the ultraviolet region; their spectral outputs change with time.

Fortunately, most materials not only have relatively steep absorption spectra at their fundamental absorptions, but also exhibit broad and nearly constant absorption at wavelengths below their fundamental absorption edges. Consequently, the most important simulation parameter is total energy absorbed. This varies considerably between different kinds of ultraviolet sources but not so much with time in any single source. For any given material the amount of ultraviolet absorbed fundamentally will be some definite (but usually unknown)fraction of that which is incident. For this reason the measure of ultraviolet exposure--the equivalent sun-hour (ESH)--has a meaning which depends upon the total ultraviolet content of the source relative to that of the sun. It is a convenient and constant, but by no means accurate, measure of actual ultraviolet absorption. The equivalent sun-hours of ultraviolet exposure were determined by the technique employed in an earlier program (Ref. 1), a technique that simply relied on the computation of total energy deposited employing an Eppley Model S Pyrheliometer.

The philosophy employed throughout this program has been that, regardless of whether an ultraviolet, proton, or combined-radiation screening test, the shortest exposure was performed that always permitted the extablishment of the degree of instability exhibited by the most stable specimen in any one test. In other words, if 500 ESH of ultraviolet was sufficient to degrade all specimens in any given screening test, that test was terminated. On the other hand, the tests were always continued to 2000 ESH even if only one specimen of twelve was sufficiently stable to warrent such a test.* This philosophy has become even more important as the need for and ability to test in the expensive, simulated (combined) ultraviolet-plus-proton radiation environment

*This rule did not extend to Z93, S-13G or second surface OSR's used as controls.

has become established. The only cases where this philosophy has not prevailed are where either low-ESH quality-control tests of "specification" surfaces, or high-ESH simulation tests of experimental surfaces "for record," were required.

2.2 Vacuum Considerations

The use of oil diffusion-pumped facilities has all but ceased in space environment-effects studies. It has been found that the oil back-streaming encountered with even highly baffled systems is sufficient to contaminate specimens being irradiated by either ultraviolet, charged particles or both. Oil diffusion-pumped systems have not been used on this program.

Indeed, it has been found necessary and is now common practice to regularly clean the ion-pumped facilities that are now almost universally employed in space-irradiation facilities. At IITRI, the vacuum pumps are themselves regularly dismantled and cleaned. Because the bake-out techniques carbonize many of the low molecular weight organic molecules collected by getter-ion pumps, the residue builds up in the pump and usually it eventually causes arcing and deterioration of pump performance. Non-carbonized molecules that are removed from ion pumps and chamber structures and walls by bake out are often collected on the colder portions of chamber structures and walls.

Oil-based mechanical "roughing" pumps are rarely employed in space irradiation facilities because of the impracticability of eliminating oil contamination of the vacuum chamber. The use of turbomolecular pumps (if used properly) and/or 'sorption pumps to evacuate facilities to pressures required to "start" ion pumps has helped solve the major vacuum pumping problems inherent in space-radiation-effects studies.

The non-in situ Quad-Ion ion pumped facility described in paragraph 2.3.1 was rough-pumped with a well-trapped, oil-based mechanical pump. The IRIF (para. 2.3.2) and CREF (para. 2.3.3 and Chapter 6) were pumped with 400 liter/sec. ion pumps that

A BETTER QUALITY OF THESE

PAGES IS REPRODUCED AT THE END OF

THIS PUBLICATION

were rough-pumped with the Geleral Electric "Gulper," a fast 'sorption pumping system that itself is rough pumped with a cryo-trapped carbon-vane mechanical pump.

The vacuum levels that have been employed during the course of this program have ranged from 5 x 10^{-6} torr (for the Quad-Ion System) to 10^{-9} torr for the CREF (when utilized for ultraviolet irradiation only). We have shown in other studies that vacuums greater than 10^{-5} torr are not required from the standpoint of the partial pressure of oxygen necessary to interfere with observable damage kinetics (Ref. 2). As a consequence, the vacuums of 10^{-7} torr that have been routinely achieved - with the IRIF and CREF are deemed entirely sufficient for these studies.

2.3 Space Simulation Facilities

2.3.1 The Quad-Ion Ultraviolet Facility

The Quad-Ion ultraviolet-irradiation facility that was employed until 1966 is shown in Figure 1. It was the facility used to perform all non-in situ tests described in this report. The Quad-Ion facility is a multiple-chamber, ultraviolet-irradiation system that was pumped with 20 liter/sec. Ultec ion-pumps, each equipped with a 180 liter/sec. titanium-sublimation pump. This system employs four chambers and four ion-pumps with a common rough-pumping system. The four chambers, which are provided with liquid-cooled samples tables, are mounted such that the lamp-to-sample distance is variable, thus providing different solar intensities during a given space-simulation test.

This system is not currently being used.

2.3.2 The IRIF-I and IRIF-II Facilities

The IRIF, an acronym for "In-Situ Reflectance/Irradiation Facility," is a multiple-sample ultraviolet-simulation facility possessing in situ hemispherical spectral-reflectance-measurement capabilities. Two IRIF's are available; I and II. Both facilities exhibit exceptional precision (repeatability) in the measurement of spectral reflectance in the 220- to 2700nm wavelength range.

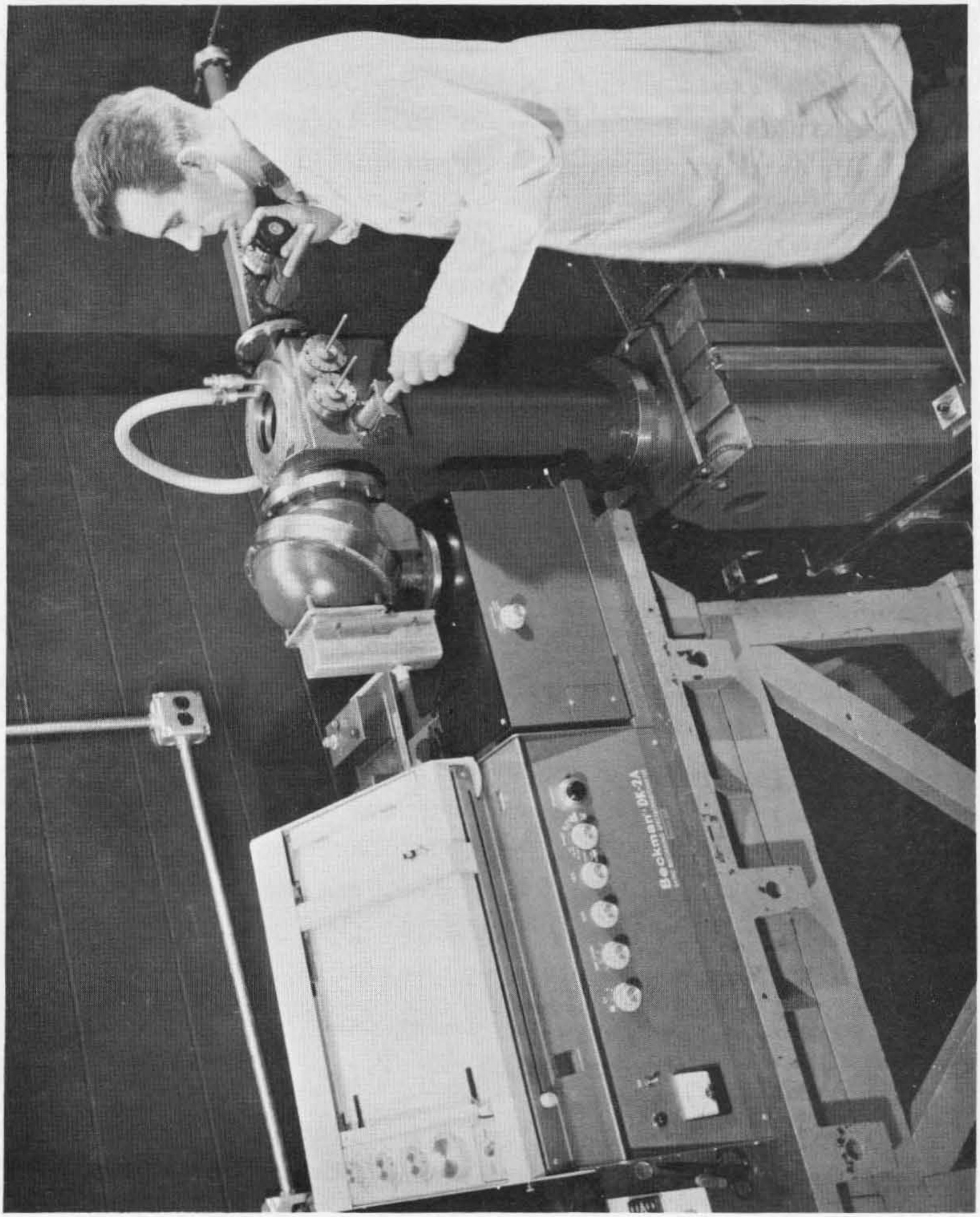

Figure 1 THE IRIF MATED TO THE BECKMAN DK-2A SPECTROREFLECTOMETER

IRIF-II is currently mated to a solar wind simulator, and together with this facility, is known as the CREF (Combined Radiation Environment Facility), which is described in detail in Chapter 6.

Each IRIF incorporates an integrating sphere with center-mounted sample. IRIF-I employs a Beckman DK-2A and IRIF-II (the CREF), a Beckman DK-1 spectrophotometer. The major features of the IRIF's include:

1. Operation of the integrating sphere in vacuum at $\sim 10^{-7}$ torr.

2. A sample exchange mechanism that maintains, during irradiation, each of the 12 samples in contact with a temperature-controlled sample table and that permits the transfer of any one of them to the integrating sphere for measurement and the subsequent return to the sample table for continued irradiation.

The IRIF's are pumped with 400 liter/sec. ion pumps and are rough-pumped with a General Electric "Gulper" cryosorption pump. The IRIF has been described in detail by Zerlaut and Courtney (Ref. 3). It is shown in Figure 2; the A-H6 mercury argon ultraviolet source that is employed with IRIF-I is not shown. (A schematic of IRIF-II which is essentially identical to IRIF-I, is shown as part of the CREF facility in Figure 52, Chapter 7).

2.3.3 The CREF

The CREF is described in detail in Chapter 7 of this report and will not be discussed here. A 5-kw Hanovia mercury-xenon source is employed with the CREF.

2.4 Ultraviolet Sources

2.4.1 The A-H6 Mercury-Argon Source

Because of a number of factors, chief among them being economical operation, the General Electric 1000 watt A-H6 lamp is widely employed as an ultraviolet source. Another factor that prompts its use is the high ratio of ultraviolet to total (radiant) energy. Accelerated ultraviolet testing at several equivalent solar factors, based on total ultraviolet only, is possible.

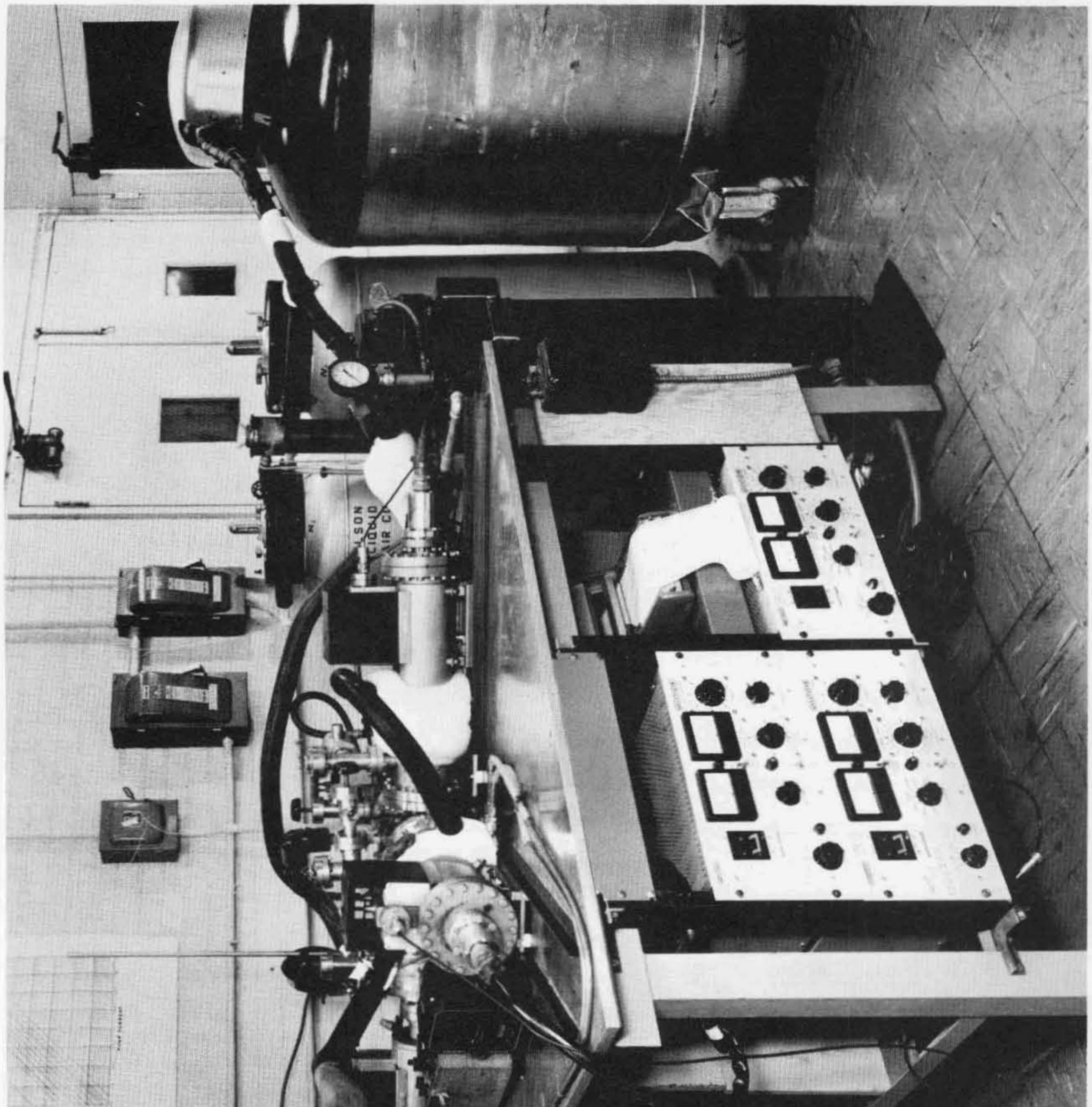

Figure 2 QUAD-ION SOLAR SIMULATION FACILITY

Accelerations of 10 equivalent solar factors are easily achieved with an A-H6 lamp (compared to a maximum of about 4 to 6 for a 5kw mercury-xenon source and about 1.5 for 5kw xenon sources).

The principal problems associated with the use of high-pressure mercury-argon sources are twofold: (1) They possess a low-order continuum with strong superimposed mercury emission lines, and (2) they exhibit short lifetimes and considerable instability of spectral distribution as a function of age and the number of starts. For that reason, we change A-H6 lamps every 72 hr during tests of longer duration at IIT Research Institute.

Lamp intensity (in equivalent solar factors) is determined by first comparing the lamp to be employed to the characteristics of an "average" lamp. The "average" lamp characteristics have been determined over a period of time by plotting the output in watts of a number of lamps as a function of lamp-to-detector distance. A linear plot (Figure 3) was drawn as an "average" to be used for calibrating A-H6 lamps. The detector employed is a Model S wide-angle temperature-compensated thermopile obtained from the Eppley Laboratories; it possesses a constant of 6.98 $mv \cdot cal^{-1} \cdot cm^{-2} \cdot min^{-1}$. The operating characteristics of any given lamp are determined by measuring its output at 25 cm. These data are then plotted on Figure 3 and a line is drawn through this point parallel to the average data curve (tedius calibration is thus avoided on a routine basis). Reference is then made to Figure 4, which is a plot of the equivalent solar (ultraviolet) factor as a function of total radiation received (by the thermopile). Figure 4 was prepared by assuming that 30% of A-H6 radiation is in the 200- to 400-nm range and that "one" solar factor is 13 mv/cm^2. These two plots are thus sufficient to establish the lamp-to-sample distance of a given lamp required to achieve a given solar factor.

2.4.2 Xenon and Mercury-Xenon Sources

Xenon and mercury-xenon burners (100- to 10,000 watt short-arc lamps) are being employed more and more frequently as

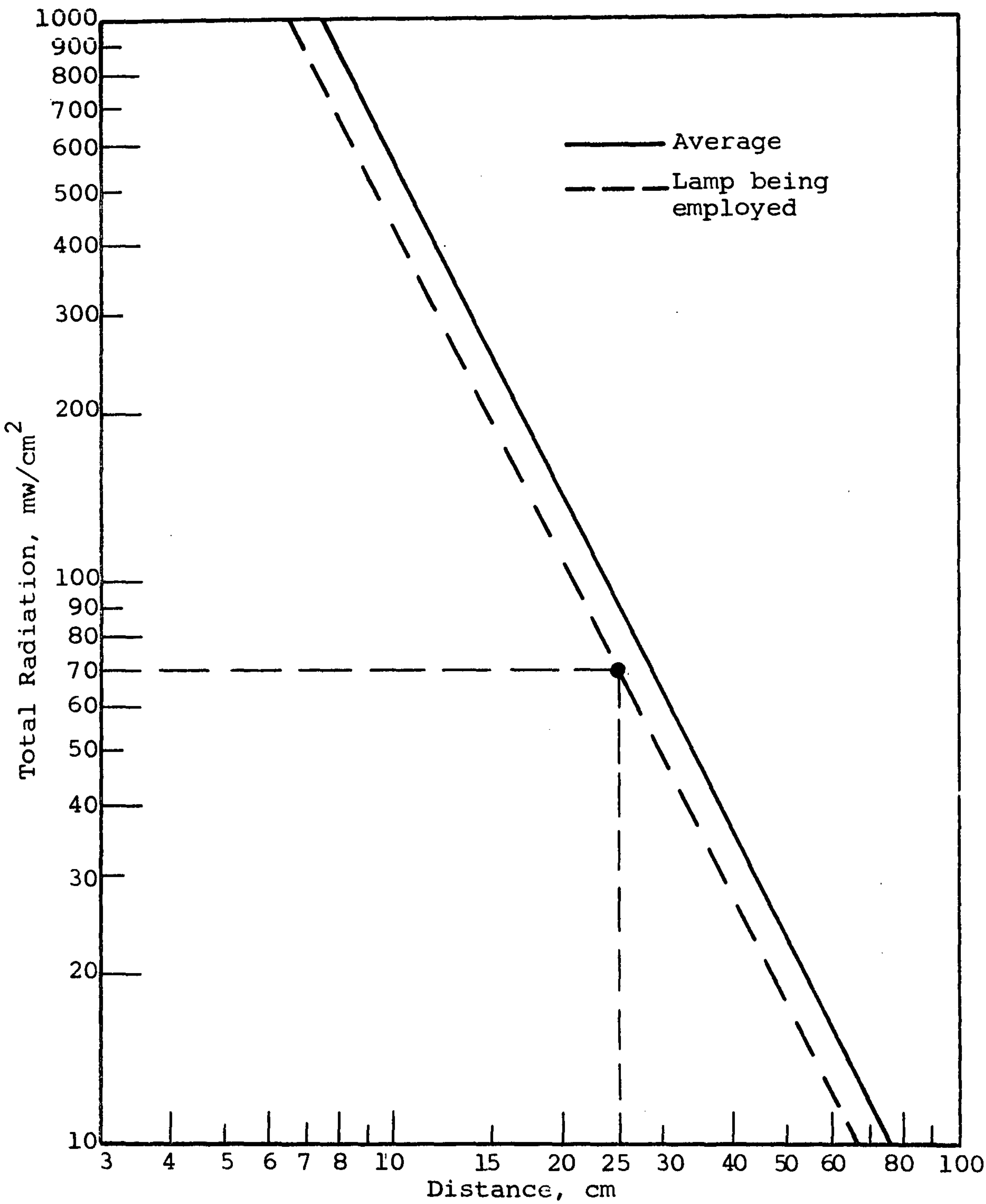

Figure 3 RADIATION DISPLAY (EPPLEY THERMOPILE) FOR AN AVERAGE A-H6 LAMP

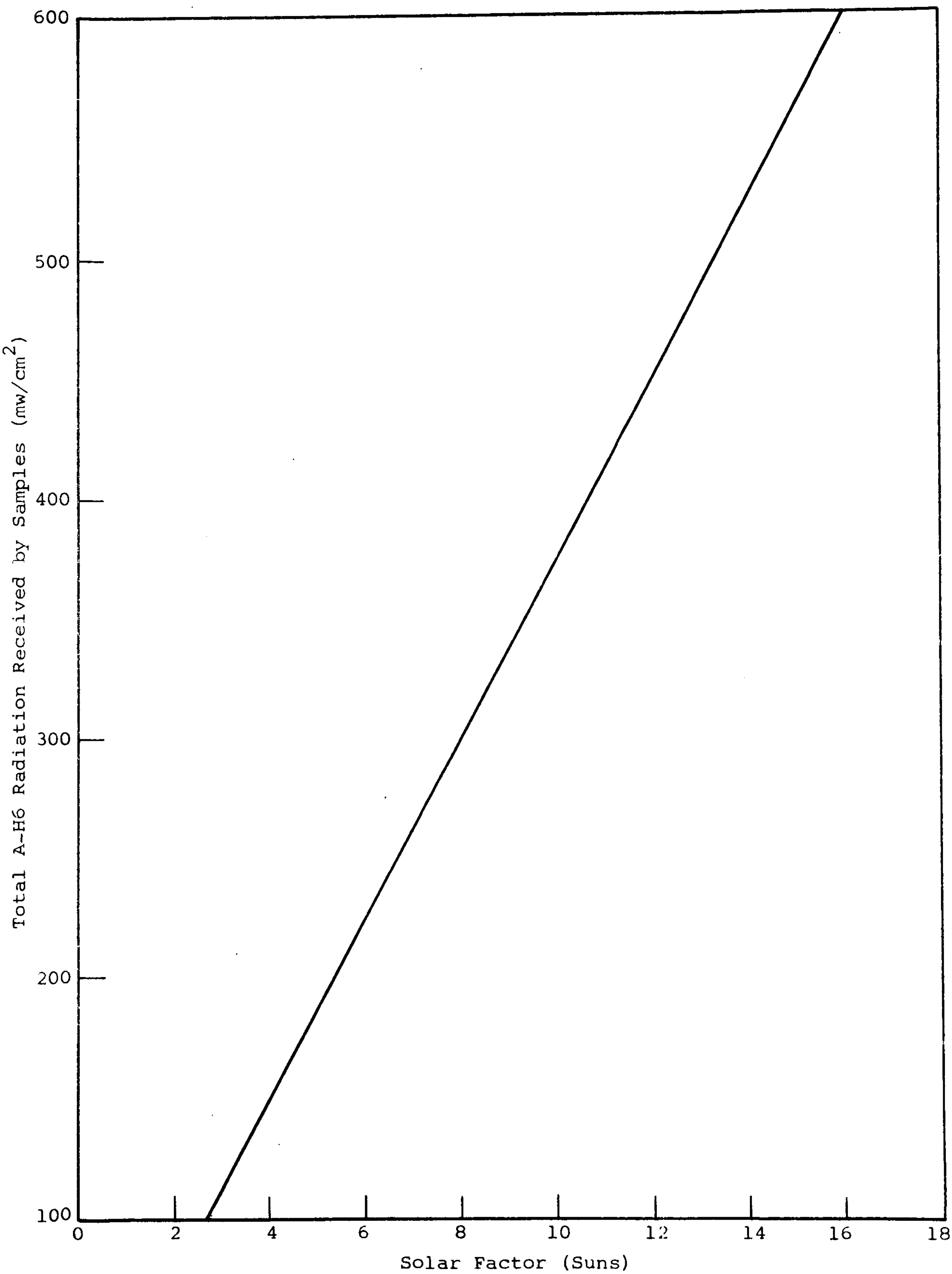

Figure 4 SOLAR FACTOR AT SAMPLE SURFACE AS A FUNCTION OF TOTAL ENERGY RECEIVED

ultraviolet sources; both 5000-watt Hanovia xenon and mercury-xenon burners are employed at IIT Research Institute. Their principal disadvantages are initial cost and only modest lifetimes; they cannot be operated with confidence in the horizontal position.

We prefer the mercury-xenon to the xenon source for two reasons: (1) Hg-Xe sources possess a greater amount of ultraviolet in the 200- to 230-nm wavelength region, permitting accelerated testing, and (2) xenon sources possess intense emission bands in the near infrared (850- to 1000-nm) that require filtering. The combination of filtering and low ultraviolet intensity at short wavelengths make accelerated testing with xenon lamps difficult, if not impossible, for single arrays. The lamp output of the two typical sources are compared for 1000-watt burners in Table 1 below (Ref. 4).

Table 1

COMPARISON OF SPECTRAL OUT-PUT OF SHORT ARCS

Spectral Range (nm)	Total Watts Radiated Hg-Xe	Total Watts Radiated Xe
200 - 210	0.19	0.04
210 - 220	0.72	0.07
220 - 230	1.09	0.10
230 - 240	2.15	0.14
240 - 250	2.86	0.18

2.5 Computation of Solar Absorptance

Solar absorptance is computed from the hemispherical spectral reflectance data by integration with the standard Johnson solar energy spectrum. The computation of solar reflectance is performed simply by the addition of the reflectances (x 0.02) of 50 equal-energy wavelengths. The reflectances are listed by employing a photo-positive overlay over the raw-data reflectance*

*Providing the 100% line does not necessitate compensation.

chart-paper: Two overlays (one for the 325- to 700-nm and one for the 700- to 2700-nm wavelength regions) are employed for the Beckman DK-2A and one overaly is used in reducing the DK-1 data.

The data are sometimes divided into two solar-absorptance components, $\alpha 1$ and α_2; these two components are chosen such that each encompasses one-half of the integrated energy in the Johnson spectrum. Thus, α_1 represents all energy below about 700-nm and α_2 represents all energy of greater wavelength, such that the following identity can be made:

$$\alpha_1 + \alpha_2 = \alpha_s$$

Computation and reporting of solar absorptance data in this manner permits quick and easy reference to that portion of the spectrum that undergoes the greatest amount of damage.

2.6 Pigment-Powder Specimen Preparation

The "water-mull" technique of pigment powder preparation, which was developed by Y. Harada at IITRI, and which has been described in various Triannual Reports and widely used in the thermal-control coatings field, was employed in all pigment studies except the screening tests described in section 3.1. The water mull, also called the "wet-powder" spray method consists of preparing a dilute water suspension of the pigment by gently mulling the pigment in distilled water (if necessary). The water suspension is then sprayed, preferrably with an air brush, onto a substrate, usually aluminum pre-heated to ~200°F. This technique permits the successful build-up of thick, reflective coatings of most pigment materials; nominal thicknesses of 5 mils are achieved. Indeed, we have found the technique to work for IRIF specimens that are inverted by the mechanical sample transfer in order to measure reflectance in the evacuated Edwards-type integrating spheres that are modular attachments to the IRIF's.

3. SUMMARY OF PIGMENT TECHNOLOGY

3.1 Pigment Screening Studies

3.1.1 Introduction

All pigment screening studies performed before 1965 were performed prior to the advent of in situ reflectance measurements. The facility described in paragraph 2.3.1 was employed in such experiments. Even though the space ultraviolet simulation employed during the period 1963 through 1965 would not be acceptable technology today, the work is germane to the extent that: (1) pigments and materials shown to degrade by post-exposure measurements performed in air have been shown to never have degraded less when the measurements were subsequently performed in situ in vacuum, and (2) generally only the semiconductor pigments have been found to be very sensitive to oxygen bleaching and the data on the many dielectric pigments examined are largely useful, though generally disappointing.

Reflectance spectra of the degraded "screened" pigments are not presented, since, with only a very few exceptions, chief among which were the zinc titanates, all pigments degraded severely--as evidenced by the data presented in tabular form.

3.1.2 Reflectance of Various White Crystalline Materials

The reflectances of a large number of white materials were determined (versus magnesium oxide) utilizing a Cary 14 spectroreflectometer (Ref. 5, 6). More than 40 potential pigments were examined as pressed compacts (50-60 psi), making a total of about 100 that were examined at IITRI in the period 1963-1964. (Over 50 potential candidate pigments were screened previously in the Stable White Coatings program for the Jet Propulsion Laboratory (Ref. 1).)

The white pigment candidates listed in Table 2 are typical of those examined in the early part of the program (Ref. 5-7). The candidate materials were calcined to determine the effect of heat treatment on their reflectance.

Table 2

EFFECT OF HEAT TREATMENT ON REFLECTANCES OF VARIOUS MATERIALS

Material Trade Name (Chemical Name)	Heat Treatment	% Reflectance* at 0.325μ	0.700μ	2.0μ
Lithafrax	None	90.5	91.5	92.5
(Lithium Aluminum Silicate)	800°C/6 hr	89.0	91.5	96.0
White Barytes	None	76.5	91.5	90.0
(Barrium Sulfate)	800°C/6 hr	78.0	90.0	95.0
Kona-F-4	None	75.0	86.0	89.5
(Potassium Aluminum Silicate)	800°C/6 hr	74.5	91.0	96.0
Nepheline Syenite	None	83.0	87.0	87.0
(Sodium Potassium Aluminum Silicate)	800°C/6 hr	79.0	88.0	94.0
Talc	None	71.0	84.5	75.0
(Magnesium Silicate Hydrate)	800°C/6 hr	45.5	72.0	90.5
Petalite	None	76.5	83.5	80.0
(Lithium Aluminum Silicate)	800°C/6 hr	81.0	87.0	90.0
Potassium Metaphosphate	None	85.5	94.5	80.5
	500°C/16 hr	81.0	93.5	91.0
Spinel	None	91.5	91.0	62.0
Magnesium Aluminate	500°C/16 hr	93.5	93.0	71.0
Edgar 4SP	None	31.0	86.0	67.5
Aluminum Silicate	800°C/16 hr	32.0	91.0	88.0
Superpax	None	64.0	88.0	82.5
Zirconium Silicate	800°C/16 hr	63.0	90.0	89.0

* Based on magnesium oxide.

All materials listed in Table 5 showed enhanced reflectance in the infrared to varying degrees as a result of heat treatment. In the visible and ultraviolet portions of the spectrum, improved reflectance was relatively minor and was not realized for all materials. Petalite, Kona F-4 and Edgar ASP revealed the most significant increases. The approach to enstatite through partial loss of water of talc (900°C is the water-loss temperature) colored the material significantly. These experiments indicate a method by which optical properties of a pigment can be altered.

Earlier work (Ref. 1) with zinc oxide powders has also shown that improved resistance to ultraviolet-vacuum can be obtained by calcination. Although no similar beneficial effect from heat treatment was observed for alumina, zirconia, and zircon (Ref. 5), the possible volatilization of contaminants and elimination of defects suggested that heat treatment should be a standard procedure for pigments.

3.1.3 Ultraviolet Stability of Pigment Candidates

3.1.3.1 China Clays

The effect of ultraviolet irradiation on a number of aluminum and magnesium silicates is presented in Table 3 (Ref. 7). A decrease in solar absorptance for the Molochite china clay was realized both from acid leaching and calcination. The higher solar reflectance resulted from an increase in the infrared portion of the spectrum, as indicated by the α_2 values. Increased stability also occurred as a result of the treatments; the most significant was that from acid leaching.

The mullite from fused grain (Mullnorite from the Norton Company) and the Enstatite (American Lava) both showed severe damage, especially the Mullnorite, which received only 200 ESH of ultraviolet irradiation (Ref. 8).

The Foresterite (American Lava) showed exceptional stability to 2000 ESH of ultraviolet irradiation. Unfortunately it

Table 3

EFFECT OF ULTRAVIOLET IRRADIATION IN VACUUM ON NON-IN SITU OPTICAL PROPERTIES OF CHINA CLAYS, ETC. (COMPACTS)

Pigment	Remarks	Solar Factor	Exposure (ESH)	Solar Absorptance α_1	α_2	α_s	$\Delta\alpha_s$
Molochite No. 6[1] ($3Al_2O_3 \cdot 2SiO_2$)	--	0	0 0	0.101	0.099	0.200	---
		9.5	700	0.182	0.108	0.290	0.090
Molochite No. 6	Leached in hot HCl	0	0	0.099	0.085	0.184	---
		9.5	700	0.134	0.088	0.222	0.038
Molochite No. 6	800°C/16 hr	0	0	0.105	0.062	0.167	---
		9.5	700	0.146	0.066	0.212	0.045
Mullnorite[2] ($3Al_2O_3 \cdot 2SiO_2$)	Fused Grain	0	0	0.144	0.140	0.284	---
		10	200	0.203	0.147	0.350	0.066
Enstatite[3] ($MgSiO_3$)	--	0	0	0.100	0.093	0.193	---
		10	2000	0.222	0.106	0.328	0.135
Forsterite[3] ($2MgO \cdot SiO_2$)	--	0	0	0.170	0.057	0.227	---
		10	2000	0.179	0.063	0.242	0.015

[1] Paper Malcers Importing Company

[2] Norton Company

[3] American Lava

possesses a poor solar reflectance and we were unable to obtain improvements by beneficiation (Ref. 9).

3.1.3.2 Zirconium Compounds

The stability of a number of zirconias and zircons are presented in Table 4 (Ref. 7, 8). Of the zirconium oxides examined as compacted powders, only the 99% pure Fluorescent Grade produced by TAM was reasonably stable. TAM's very pure HP grade (99.9%) was badly degraded, although it was examined in a very severe test (i.e., 2370 ESH).

The double zirconium silicates were surprisingly stable except for the barium zirconium silicate (Ref. 9). These data led us to examine the double zircons in much greater detail. The results of further studies are presented in paragraphs 3.2.7.4, a literature survey and 4.5.2, which deals with potassium silicate-based paints.

3.1.3.3 Aluminum Oxide Pigments

The results of irradiation of a number of aluminas from three manufacturers (Norton, Gulton, and Alcoa) are presented in Table 5 (Ref. 8, 9). These data were surprising in that it indicated that heat treatment at calcining temperatures had a strongly deleterious effect on Al_2O_3. Because we believe that degradation is due to surface states and that lowering the surface area (and hence the surface energy) of a pigment improves resistance to degradation, the behavior of the Al_2O_3 is believed to be due largely to a change in stoichiometry, which obviously greatly effects the kinetics of the oxygen reactions at the surface and in the bulk.

3.1.3.4 Other Pigment Candidates

The data for several pigment compacts (50-60 psi) are presented in Table 6. Typical of the stability of most of the remaining materials examined are the results of irradiation of dysprosium oxide and barrium sulfate (Ref. 7), and of the oxides

Table 4

EFFECT OF ULTRAVIOLET IRRADIATION IN VACUUM ON NON-IN SITU OPTICAL PROPERTIES OF ZIRCONIA AND DOUBLE ZIRCON COMPACTS

Pigment	Manufacturer	Remarks	Solar Factor	Exposure (ESH)	Solar Absorptance			
					α_1	α_2	α_s	$\Delta\alpha_s$
Zirconium Spinel	TAM	1000°C/16 hr	0	0	0.050	0.057	0.107	---
			8.5	230	0.084	0.056	0.140	0.033
HP ZrO_2 (99.9%)	TAM	Calcination at 2000°F	0	0	0.051	0.031	0.082	---
			10	2370	0.248	0.079	0.327	0.245
ZrO_2 (99%)	TAM	Fluorescent Grade	0	0	0.071	0.042	0.113	---
			10	1760	0.104	0.045	0.149	0.036
ZrO_2 (98%)	Norton	Zirnorite (7.5μ)	0	0	0.176	0.183	0.359	---
			10	200	0.196	0.189	0.385	0.026
$ZnZrSiO_5$	TAM	--	0	0	0.078	0.045	0.123	---
			10	2000	0.132	0.049	0.181	0.058
$CuZrSiO_5$	TAM	--	0	0	0.083	0.032	0.115	---
			10	2000	0.120	0.039	0.159	0.044
$MgZrSiO_5$	TAM	--	0	0	0.072	0.030	0.102	---
			10	2000	0.123	0.070	0.160	0.058
$BaZrSiO_5$	TAM	--	0	0	0.122	0.039	0.161	---
			10	2000	0.215	0.058	0.273	0.112

Table 5

EFFECT OF ULTRAVIOLET IRRADIATION IN VACUUM ON NON-IN SITU OPTICAL PROPERTIES OF ALUMINA COMPACTS

Pigment	Manufacturer	Remarks	Solar Factor	Exposure (ESH)	Solar Absorptance α_1	α_2	α_s	$\Delta\alpha_s$
Alundum 38	Norton	95%; 3μ	0	0	0.038	0.041	0.071	---
			10	200	0.189	0.060	0.249	0.178
C33	Alcoa	99%	0	0	0.019	0.080	0.099	---
			10	200	0.340	0.156	0.496	0.397
38900	Norton	99.6%; 7.5μ (1650°F)	0	0	0.088	0.066	0.154	---
			10	300	0.133	0.064	0.197	0.043
Alucer MC	Gulton	As received	0	0	0.038	0.025	0.063	---
			10	500	0.122	0.031	0.153	0.090
Alucer MC	Gulton	1000°C/1 hr	0	0	0.019	0.017	0.036	---
			10	500	0.113	0.032	0.145	0.109
Alucer MC	Gulton	1620°C/1 hr	0	0	0.024	0.008	0.032	---
			10	500	0.128	0.021	0.149	0.117

Table 6

EFFECT OF ULTRAVIOLET IRRADIATION IN VACUUM ON
THE NON-IN SITU OPTICAL PROPERTIES OF MISCELLANEOUS PIGMENT COMPACTS

Pigment	Manufacturer	Remarks	Solar Factor	Exposure (ESH)	Solar Absorptance α_1	α_2	α_s	$\Delta\alpha_s$
$ZnTiO_3$	TAM	Metatitanate	0	0	0.077	0.034	0.111	---
			10	1000	0.126	0.065	0.191	1080
Zn_2TiO_4	New Jersey Zinc	Orthotitanate	0	0	0.092	0.055	0.147	--
			10	1000	0.116	0.076	0.192	0.045
Dysprosium Oxide	--	--	0	0	0.062	0.145	0.206	---
			8.5	230	0.108	0.141	0.249	0.043
$BaSO_4$	--	White Barytes (800°C/16 hr)	0	0	0.067	0.063	0.130	---
			8.5	230	0.141	0.066	0.208	0.078
CaO (99.9%)	Whittaker, Clark & Daniels	--	0	0	0.024	0.075	0.099	---
			10	2370	0.272	0.136	0.408	0.309
CaO (99.9%)	Whittaker, Clark & Daniels	2000°F/1 hr	0	0	0.019	0.073	0.092	---
			10	2370	0.227	0.096	0.323	0.231
SnO_2	M&T Company	--	0	0	0.097	0.043	0.140	---
			10	300	0.203	0.152	0.353	0.213
SnO_2	M&T Company	1000°F/1 hr	0	0	0.102	0.052	0.154	---
			10	300	0.246	0.213	0.459	0.305
MoO_3	IITRI	99%	0	0	0.199	0.191	0.390	---
			10	300	0.437	0.442	0.879	0.489
Ta_2O_5	TAM	HP	0	0	0.051	0.018	0.069	---
			10	300	0.130	0.033	0.164	0.095

of tin, calcium, molybdenum and tantalum (Ref. 8). As with aluminum oxide, heat treatment had a deleterious effect on the stability of the tin oxide (contrary to our previous and more recent experience in heat treating, e.g., calcining, pigments, in general).

The most exciting data obtained in the pigment screening tests was the generally better stability of the zinc titanates (Ref. 9). It was on the basis of these data that greater emphasis was placed on zinc titanate-potassium silicate paints prepared from the experimental materials obtained from the New Jersey Zinc Company. These additional data are presented in the next chapter (Chapter 4), the results of which subsequently led to the concentration on zinc orthotitanate as a new stable-white-pigment candidate (see Chapter 8).

3.1.4 Summary of Pigment Screening

As pointed out in the introduction to this section, the irradiation results on pigments (and coatings) whose post-exposure reflectance measurements were performed in air (rather than in situ in vacuum) are considered valid for those "dielectric" pigments that do not exhibit significant oxygen-bleaching reactions in air. This concept was proven in studies on another program, also performed for NASA's George C. Marshall Space Flight Center (Ref. 2).

The zinc titanates, however, were later found to exhibit fast oxygen bleaching. Nevertheless, the basically good stability exhibited by Zn_2TiO_4 in these studies gave impetus to the studies that have now resulted in the development of new, low-solar absorptance, stable white coatings.

3.2 Potentially-Stable, New* White Pigments

3.2.1 Basic Considerations

Theoretical considerations led us to believe that certain binary and ternary systems containing complex and/or polynegative

*In addition to zinc orthotitanate.

anions should be candidates for highly-reflective, space-stable, white pigments. Not only do such materials offer the strong possibility of possessing high refractive indices, but the very structure that assures high refractivity, namely high (electron) density, was also believed to be important to stability. That is, these less symmetrical structures should have stabilities that are related to the reduction of vacancy formation and ionic mobility.

Although these factors may not be as important to semiconductors that exhibit "gaseous-sorption" bleaching, such as the ultraviolet-induced, "bleachable" damage exhibited by rutile titanium dioxide, and certain zinc orthotitanates, reduced ionic mobility in semiconducting systems might at least preclude additional, complicating reactions at the surface. Significant gaseous-sorption bleaching of optical degradation is believed to be limited to materials having semiconductor character, and such instability should be amenable therefore to reactive encapsulation techniques that have been found useful with zinc oxide, titanium dioxide, and zinc orthotitanate (see Chapter 8). We have not attempted at this time to ascertain the semiconducting properties of the pigments described in section 3.2.2.

On the basis of ionic refractivities after Fajans and Joos (Ref. 10), the double titanates, tungstates and stannates can be expected to possess high refractive indices. In general, high refractive indices can be obtained by utilizing the following concepts:

1. a cation of high atomic weight and low charge
2. an anion of high charge and high atomic weight, or
3. complex ions.

Also, "if a compound of element A has a high refractive index, then a compound of B, in the same group but of a greater atomic weight, may be expected to have a higher one" (Ref. 11)

It was decided to investigate the optical and physical properties, first through a thorough literature search, and then on selected materials in the laboratory, of the following groups of compounds: titanates, tungstates, stannates and double zirconium silicates.

3.2.2 Literature Search

3.2.2.1 Titanates

A thorough literature search on the properties and methods of preparation of the zinc titanates was reported in a Triannual Report (Ref. 12) and is the subject of Chapter 5; they therefore will not be discussed here.

3.2.2.1.1 Lithium Titanates

Six lithium titanates are discussed in the literature:

$LiTiO_2$ (or $Li_2O \cdot Ti_2O_3$)

Li_2TiO_3 (or $Li_2O \cdot TiO_2$)

$Li_2Ti_2O_5$ (or $Li_2O \cdot 2TiO_2$)

$Li_2Ti_3O_7$ (or $Li_2O \cdot 3TiO_2$)

$Li_4Ti_5O_{12}$ (or $2Li_2O \cdot 5TiO_2$)

$Li_4Ti_7O_{16}$ (or $2Li_2O \cdot 7TiO_2$)

Lundberg and Anderson (Ref. 13) mention the existence of a series of compounds with the general formula of $Li_xTi_{4-x/4}O_8$. They explain that this series of compounds has a ramsdellite structure with "tunnels" that can accommodate a varying number of lithium atoms. No other reference could be found in the literature which substantiates Lundberg and Anderson's thesis. $LiTiO_2$ is described by Reuter and Weber (Ref. 14) and by Lecerf (Ref. 15). The latter author gives the color of $LiTiO_2$ as black.

Li_2TiO_3 is repeatedly mentioned in the liaterature, notably by Kutolin and Seegeva in Russia (Ref. 16) and Lecerf in France (Ref. 15), who implies, although he does not definitively state it, that Li_2TiO_3 crystals are white. Jonker (Refl 17), Yamaguchi (Ref. 18) and Barblau (Ref. 19) have all synthesized Li_2TiO_3, although each author used different methods and reacted the products of synthesis at widely varying temperatures ranging from 650 to 1250°C in environments such as vacuum, CO_2 or atmospheric conditions. The structure $Li_2Ti_3O_5$ is only mentioned by Barblau and his coworkers (Ref. 20), where $Li_2Ti_3O_7$ is discussed by two separate investigators - the previously cited Lundberg and Anderson (Ref. 13) and Jonker (Ref. 17). There is some doubt as to the very existance of $Li_4Ti_7O_{16}$, which was reported by Bertant and Durif (Ref. 21), since Jonker claims that the x-ray pattern of $Li_4Ti_5O_{12}$ agrees with the pattern previously attributed to $Li_4Ti_7O_{16}$.

3.2.2.1.2 Lanthanum Titanates

Five different titanates are reported in the literature:

La_2TiO_5 (or $La_2O_3TiO_2$)

$La_2Ti_2O_7$ (or $La_2O_32TiO_2$)

$La_2Ti_3O_9$ (or $La_2O_33TiO_2$)

$La_4Ti_9O_{24}$ (or $2La_2O_39TiO_2$)

$LaTiO_3$

$La_2Ti_2O_7$ is of special interest to us because of its outstanding transmission properties, which were reported by Merker and Herrington (Ref. 22). Transmission data were not available for the other titanates, but at least one of them must be ruled out as totally unsuitable: It is $LaTiO_3$, which is reported to be black by Kestigian and Ward (Ref. 23). $LaTiO_3$ and compounds in the solid solution series between $La_{0.69}TiO_3$ and $LaTiO_3$ are reported to have a cubic perovskite structure by Kestigian and Ward, but this is contested by Johnston and Sestrich (Ref. 24), who claim that the crystals are orthorombic. They relate this orthorombic structure to the previously reported cubic perovskite structure by doubling the cubic unit cell in the c direction and using face diagonals for a and b.

The various authors agree on the structure of $La_2Ti_2O_7$: It has a distorted pyrochlore structure. This is reported by Merker and Herrington who synthesized this compound by flame fusion and by Collongues and his coworkers (Ref. 25), who prepared it by coprecipitation of $LaCl_3$ and $TiCl_3$. The colors of $LaTiO_3$ and $La_2Ti_2O_7$ are complete opposites in spite of the rather small difference in oxygen content. This should not deter the selection of $La_2Ti_2O_7$ as a potential space stable pigment, however. $La_2Ti_2O_7$ and $LaTiO_3$ are made from different initial components - namely Ti_2O_3 for the former and TiO_2 for the latter. Furthermore, no author reports significant problems in synthesizing either compound. In fact, MacChesney and Aauer (Ref. 26) do not show the presence of $LaTiO_3$ in their phase diagram of the La_2O_3-TiO_2 system.

The other three titanates are described by MacChesney and Sauer. They personally discovered the existence of La_2TiO_5 and $La_4Ti_9O_{24}$, and received a personal communication from Jonker who identified $La_2Ti_3O_9$. The existence of this latter compound was later confirmed by Kestigian and Ward (Ref. 27) and Repp (Ref. 28). The optical properties of these compounds are unfortunately not discussed in these papers; the emphasis was placed on methods of preparation and the measurement of dielectric properties.

3.2.2.1.3 Gadolinium Titanates

Two forms of gadolinium titanates are reported in the literature:

Gd_2TiO_5 (or $Gd_2O_3TiO_2$)

$Gd_2Ti_2O_7$ (or $Gd_2O_32TiO_2$)

We will discuss our findings since they have a definite academic interest. However, it should be noted that the cost of gadolinium oxide, which is quoted by American Potash and Chemical Corporation to be $300/lb, would probably prove to be a deterrent to the use of $Gd_2Ti_2O_7$ as a pigment. This is especially true if one considers that the equivalent lanthanum titanate can be made from La_2O_3, which costs \$7/lb. $Gd_2Ti_2O_7$ has excellent transmission properties which are very similar to those of $La_2Ti_2O_7$. Both are reported by Merker and Herrington (Ref. 22). They believe that the weak absorption at 0.9 micron in the gadolinium titanate-transmission curve is due to contamination by ytterbium. Roth (Ref. 29) indicates that $Gd_2Ti_2O_7$ has a pyrochlore structure with cubic symmetry. Both Queyroux (Ref. 30) and Collongues and his coworkers (Ref. 25) describe Gd_2TiO_5 as being monoclinic derived from the fluorite type and the cell dimensions reported by these two authors are in good agreement. Queyroux (Ref. 30, 31) makes an interesting observation concerning gadolinium oxide: It has a cubic cell structure at ordinary temperatures which becomes monoclinic when heated to 1000°C according to Perez y Jorba (Ref. 32), where Queyroux notes that this transformation occurs at 1250°C. They both agree that the reaction is reversible and Perez y Jorba states that the cubic structure can be restored by grinding the monoclinic oxide, followed by prolonged heating at 900°C.

3.2.2.1.4 Tin Titanates

A thorough search in Chemical Abstracts did not provide any information on crystal types, cell dimensions or transmission properties of tin titanates. A British patent (Ref. 33) was granted to Siemens and Halske for the production of titanate mixtures of tin, but no mention is made of the synthesis of pure tin titanate. The existence of preparation procedures is implied in the abstracts of two Russian publications (Ref. 34, 35) on the dielectric properties of tin titanate. Khodakov and Kromakov studied the small dielectric losses of solid solutions of $SnTiO_3$ and $BaTiO_3$, whereas Kaczmarek discussed variations in dielectric constants of solid solutions of $BaTiO_3$ and $SnTiO_3$ in a pulsed electric field. A phase diagram of the SnO_2-TiO_2 was developed by Padurow (Ref. 36).

3.2.2.2 Tungstates

A publication by Cockayne and Ridley (Ref. 37) indicated that not only calcium tungstate, but barium and strontium tungstates as well, have outstanding transmission properties. This opens the possibility of preparing solid solutions of two or three of these tungstates that hopefully will have transmission properties and stability superior to that of the individual components. Calcium, barium and strontium ions have different sizes and it is believed that a judicious apportionment of these cations could relieve some of the stresses now present in the calcium tungstate lattice.

3.2.2.2.1 Calcium Tungstate

The most commonly prepared form of calcium tungstate is $CaWO_4$, Nassau and Broyer (Ref. 38) report the existence of Ca_6WO_9. Chang et al (Ref. 39) reports the existence of Ca_3WO_6 as a stable compound; they report melting points of 1580°C and 2250°C for $CaWO_4$ and Ca_3WO_6, respectively. The phase diagram is shown in Figure 5 (Ref. 39).

Cell dimensions of $CaWO_4$ are reported in two different publications and are in good agreement. A very careful study of interatomic distances in $CaWO_4$ was carried out by Kay, Frazer and Almodovar (Ref. 40). They report that the slightly distorted WO_4 tetrahedron contains a W-O distance of 1.788 Å and O_1-W-O_2 angles of 113°27' and 107°56'. Nassau and Broyer (Ref. 38) state that the distorted $(WO_4)^{2-}$ ions are held apart by Ca^{2+} ions which are surrounded by eight oxygens at the corners of a distorted cube. The structure, a sheelite structure, is described as "very compact." The melting point of the $CaWO_4$ has been reported to be 1535°C, 1566°C or 1576 ± 5°C by three different investigators.

Lange's Handbook of Chemistry lists the refractive index of $CaWO_4$ as 1.9200.

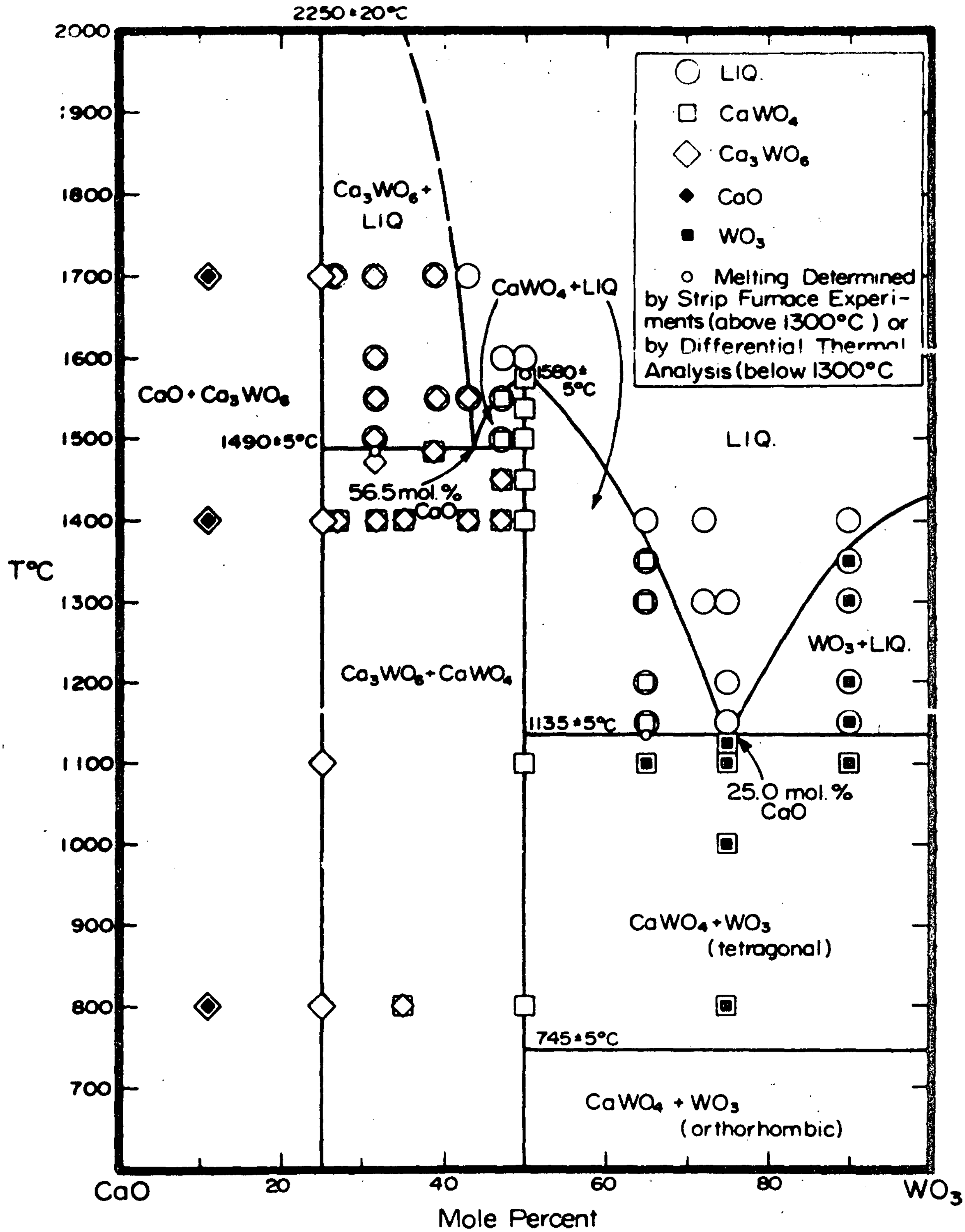

Figure 5 PHASE RELATIONS IN THE SYSTEM $CaO-WO_3$ (REF. 39)

Fairly good agreement exists between the transmission spectra given by Nassau and Broyer and the data of Cockayne and Ridley (Ref. 37). The former report that their data does not entirely agree with data presented by Gillette (Ref. 41) and they attribute the structure in the 500- to 3000-nm region shown by Gillette to the presence of either impurities or excess WO_3.

Various investigators report preparing $CaWO_4$ by precipitation from Na_2WO_4 and $CaCl_2$ solution. Reduction of W^{6+} to W^{5+} by heating $CaWO_4$ in hydrogen at 1000°C produces a black compound that can be reoxydized to white $CaWO_4$ by heating in oxygen.

3.2.2.2.2 Barium Tungstates

No less than six different barium tungstates have been reported in the literature; $BaO \cdot WO_3$ and $3BaO \cdot WO_3$ have been repeatedly discussed and used whereas $BaO \cdot 2WO_3$, $BaO \cdot 3WO_3$, $BaO \cdot 4WO_3$ and $5BaO \cdot 12WO_3$ are described only by Shivahare (Ref. 42). He formed these compounds by titrating a solution of Na_2WO_4 with $BaCl_2$ in the presence of nitric acid. He observed that upon aging the following reaction took place:

$$5BaO \cdot 12WO_3 \xrightarrow{H_2O} 4(BaO \cdot 3WO_3) + Ba(OH)_2, \quad (1)$$

whereas the normal $(BaO \cdot WO_3)$ and the $(BaO \cdot 2WO_3)$ tungstates were quite stable.

Normal barium tungstate appears to be a promising candidate as a pigment for space vehicles; it exhibits good optical properties, which are described by Cockayne and Ridley (Ref. 37), and has a rather high heat of formation, which is discussed by Rezukhina and his coworkers (Ref. 43).

The preparation of $BaO \cdot WO_3$ can be performed by the method employed by Shivahare (Ref. 42). This precipitation technique was also utilized by Kislyakov and his coworkers (Ref. 44). An entirely different approach to synthesis was used by Zmud and Ostapchenko (Ref. 45), who heated mixtures of WO_3 and $BaCO_3$ to 1600°C. A third technique used in the synthesis of $BaWO_4$ is described by Van Uitert and Soden (Ref. 46). $BaWO_4$ crystals were grown by crystallization from a Na_2WO_4 melt.

This technique was used to grow single crystals and it gave a yield superior to the method previously employed to grow single crystals in a NaCl melt.

3.2.2.2.3 Strontium Tungstates

A considerable number of strontium tungstates are reported in the literature.

$SrO \cdot WO_3$	$SrO \cdot 2WO_3$
$3SrO \cdot WO_3$	$SrO \cdot 3WO_3$
$3SrO \cdot 8WO_3$	$SrO \cdot 4WO_3$
$5SrO \cdot 12WO_3 \cdot 28H_2O$	$3SrO \cdot 7WO_3 \cdot 16H_2O$
	$4SrO \cdot 10WO_3 26H_2O$

Two general methods of preparation have been employed. The first one consists of precipitating various strontium tungstates by adding strontium chlorides to the corresponding sodium tungstates. This method yielded five different strontium tungstates and is discussed by Shivahare (Ref. 47). The other method used to prepare the strontium tungstates consists of reacting $SrCO_3$ and WO_3 at temperatures ranging from 800 to 1200°C. This is discussed by Fesenko (Ref. 48) and Belyaev (Ref. 49) and their coworkers.

3.2.2.3 Stannates

A quite complete discussion of the properties of the meta and orthostannates by Dupuis (Ref. 50) indicated that the zinc, magnesium and calcium stannates offered the possibility of being white and potentially useful as space-stable radiator coatings. We must rule out iron, copper, nickel, cobalt and manganese metastannates, since they are not white.

3.2.2.3.1 Calcium Stannates

Two forms of calcium stannate are reported in the literature: The metastannate ($CaSnO_3$) and the orthostannate (Ca_2SnO_4). The crystalline structure of the metastannate is the object of much controversy. Colin (Ref. 51) and Nagay-Szabo (Ref. 52) indicate that $CaSnO_3$ has a cubic cell but disagree on the size of the unit cell, with Nagay-Szabo doubling the edge dimension. Megaw (Ref. 53) believes the structure of $CaSnO_3$ is monoclinic whereas Tanaka (Ref. 54), Smith and Welch (Ref. 55), Couganour (Ref. 56) and Rooksby (Ref. 57) all believe that $CaSnO_3$ has an orthorombic structure although they give it extremely different cell dimensions.

The structure of calcium orthostannate is reported to be orthorombic byTroemel (Ref. 58).

3.2.2.3.2 Barium Stannates

Barium metastannate has a cubic structure which is described by four different authors. Nagay-Szabo (Ref. 52), Megaw (Ref. 53), and Smith and Welch (Ref. 55) show very good agreement on the cell dimensions (a=4.12Å) whereas Wagner and Binder (Ref. 59) attribute a larger dimension to $CaSnO_3$ (a=4.28Å). Barium orthostannate has been synthesized and described by Weiss and Faivre (Ref. 60). It has a tetragonal structure.

3.2.2.3.3 Zinc Stannates

We could find only one reference on zinc metastannate: Dupis (Ref. 50) claims that, upon heating, the metastannate is stable up to 500°C and is completely transformed to the orthostannate when the temperatures reaches 900°C.

Zinc orthostannate (Zn_2SnO_4) has a spinel structure. Very good agreement is found between Colin (Ref. 51) and Natta and Passerini (Ref. 61) on cell dimension.

3.2.2.4 Double Zirconates

These were of interest primarily because of the screening studies performed very early in the program on the double-zirconium silicates. Results of a preliminary survey of the literature are given in the following paragraphs.

3.2.2.4.1 $CaO-ZrO_2-SiO_2$

The $CaO-ZrO_2-SiO_2$ system has been well characterized (Ref. 62) and the phase relations are shown in Figure 6. For each pair of constituent oxides, a 1:1 compound exists. Only in the $CaO-SiO_2$ system compounds of other molal ratio are formed. A ternary compound was identified as $Ca_3ZrSi_2O_9$. This compound and Ca_2ZrSiO_{12} were reported previously (Ref. 63) but the latter was thought to be in error (Ref. 62).

A ternary composition, unless of a confirmed compound, will yield a mixture of phases whose make-up will be determined by the method of preparation and the starting materials. The phase composition of a quenched melt can be predicted from the phase diagram.

A method has been described as to selectively dissolve constituents of the $CaO-ZrO_2-SiO_2$ system for purposes of phase composition analysis (Ref. 64). Various organic and mineral acid reagents are used to successively dissolve free CaO, Ca_2SiO_4, $CaSiO_3$, other calcium compounds, SiO_2, and ZrO_2, leaving $ZrSiO_4$ as a residue.

The refractive indices of these compositions would increase with higher ZrO_2 content. The ternary compound is low in ZrO_2 and therefore may not have good pigment qualities.

3.2.2.4.2 $MgO-ZrO_2-SiO_2$

The $MgO-ZrO_2SiO_2$ system has recently been investigated in some detail (Ref. 65) and no ternarys are reported. The phase diagram is shown in Figure 7. Compounds of MgO and ZrO_2 with SiO_2 are well known, while MgO forms solid solutions with ZrO_2

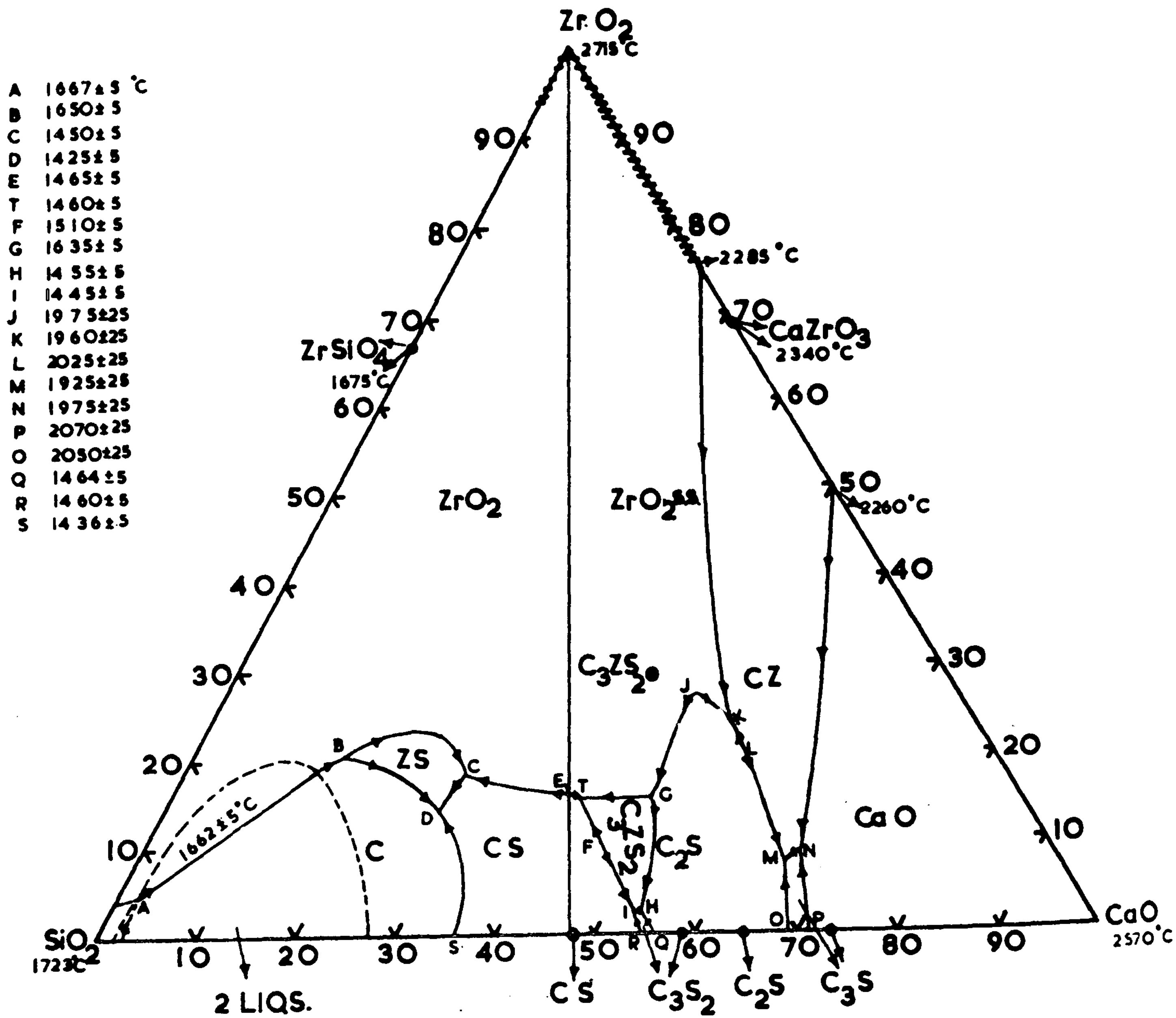

Figure 6 THE CaO-ZrO_2-SiO_2 SYSTEM (REF. 62)

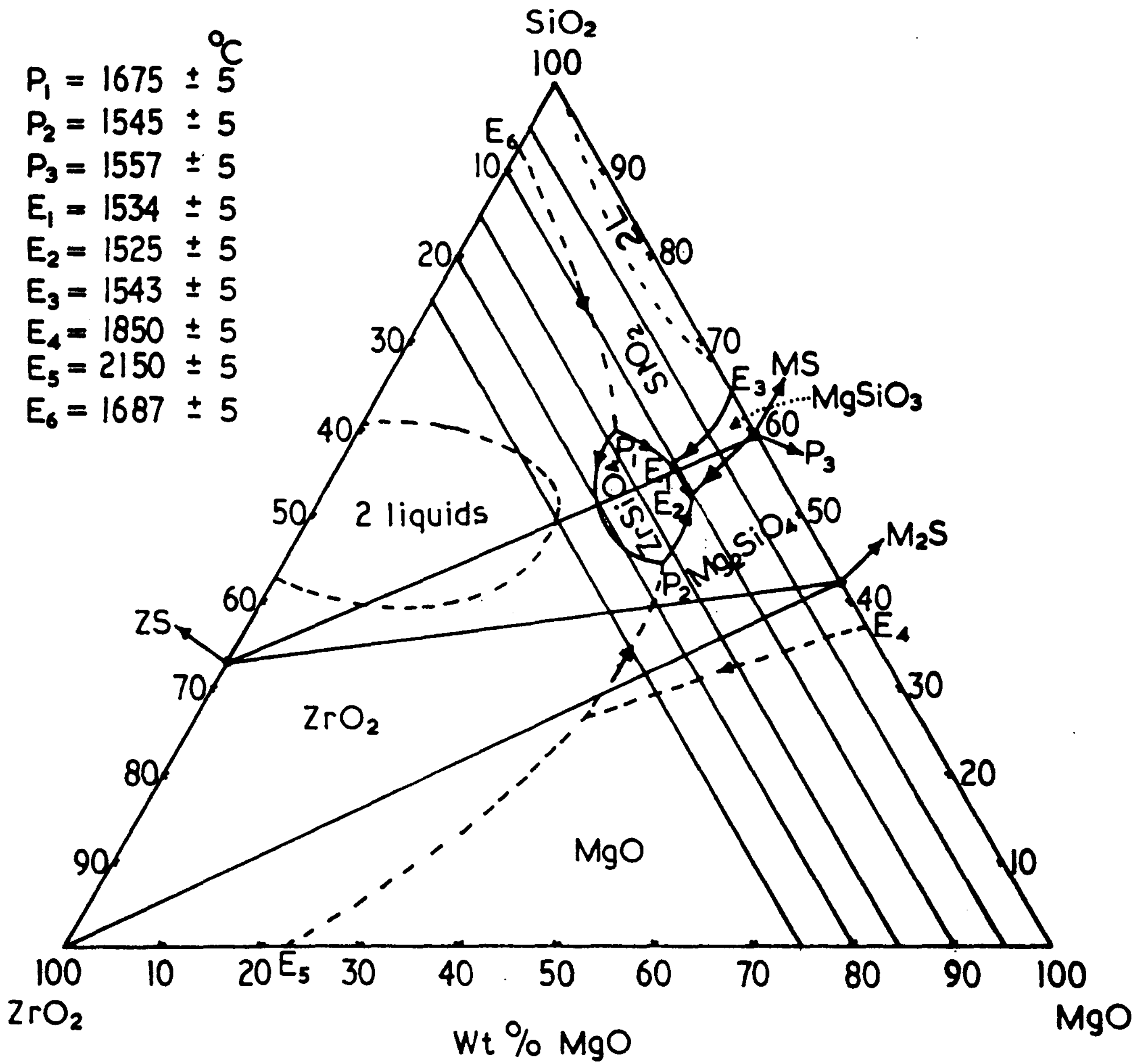

Figure 7 THE $MgO-ZrO_2-SiO_2$ SYSTEM (REF. 65)

stabilizing a cubic crystal structure, but no compounds have been reported in the $MgO-ZrO_2$ system. Ternary compositions would produce a phase mixture and increasing zirconia content would tend to increase the refractive index.

3.2.2.4.3 <u>$BaO-ZrO_2-SiO_2$</u>

Two ternary compounds have been reported for the $BaO-ZrO_2-SiO_2$ system, namely $Ba_2Zr_2Si_3O_{12}$ and $BaZrSi_3O_9$ (Ref. 66). Binary phase relationships in the $BaO-ZrO_2$ system are unavailable. However, high purity, ultra-fine size strontium zirconate ($SrZrO_3$) powder has been synthesized by simultaneous hydrolytic decomposition of Sr and Zr alkoxides (Ref. 67). There is reason to believe that $BaZrO_3$ could be synthesized likewise.

3.2.2.4.4 <u>$ZnO-ZrO_2-SiO_2$</u>

The ternary system $ZnO-ZrO_2-SiO_2$ has not apparently been investigated and only the ZnO and ZrO_2 binary systems with SiO_2 are established. Commercially available $ZnO-SnO_2$ compositions are mixtures of the components, rather than a binary compound and commercially available $ZnO-ZrO_2-SiO_2$ is a phase mixture, whose x-ray diffraction pattern is essentially that of $ZrSiO_4$ and ZnO (Ref. 68).

3.2.2.4.5 <u>Summary</u>

Because of the information obtained in this survey of the literature, coupled with the lack of good results achieved in the earlier pigment screening and paint (Chapter 4) studies, no synthesis experiments were performed.

3.2.3 <u>Experimental Investigations</u>

Various tungstates were obtained from Sylvania Electric Products, Inc. and several new pigments described in the preceding paragraphs were prepared by high-temperature solid-solution reactions. The reflectances and ultraviolet stability of wet-powder sprayed specimens of these pigments were determined (Ref. 69).

3.2.3.1 Reflectances of Several Pigments

3.2.3.1.1 Tungstates

The reflectances of five (5) tungstates purchased from Sylvania Electric Products, Inc. were determined using the wet-powder spray technique described earlier. The data which is presented in Figures 8 through 12, was obtained with the Edwards-sphere mounted Beckman DK-2A spectroreflectometer, and is in substantial agreement with the data shown by Cockayne and Ridley (Ref. 37) for the tungstates of calcium, barium, and strontium. We performed reflectance measurements further into the ultraviolet region than Cockayne and Ridley and it is interesting to notice that calcium tungstate has a definite absorption band at approximately 280-nm wavelength. Strontium tungstate has the highest reflection in the 325 to 255-nm region and barium tungstate appears to be the least promising of the three compounds.

Zinc tungstate has a definite absorption edge at 375-nm wavelength. As shown by Figure 12, $ZnWO_4$ exhibits a gradual loss of reflectance between 460 and 380 nm. Zirconium tungstate exhibits a lower reflectance in the infrared region than the other tungstates that were tested; it also has a gradual loss of reflectance from 470 to 320-nm wavelength.

3.2.3.1.2 Stannates

We prepared a number of stannates; the reaction conditions are presented in Table 7. The most promising calcium stannate prepared was $CaSnO_3$ (Batch A-773) reacted for 19.5 hr at 1000°C (Figure 13). When higher reaction temperatures were used, the reflectances of the resulting compounds progressively decreased, probably because of the decomposition of stannic oxide.

Zinc orthostannate, Zn_2SnO_4, reacted for 19.5 hr at 1000°C (batch A-770) is more reflective than all the other zinc stannates that were prepared (see Figure 14). Zinc stannates prepared at higher temperatures are less reflective and it is believed that this also is due to the decomposition of stannic oxide.

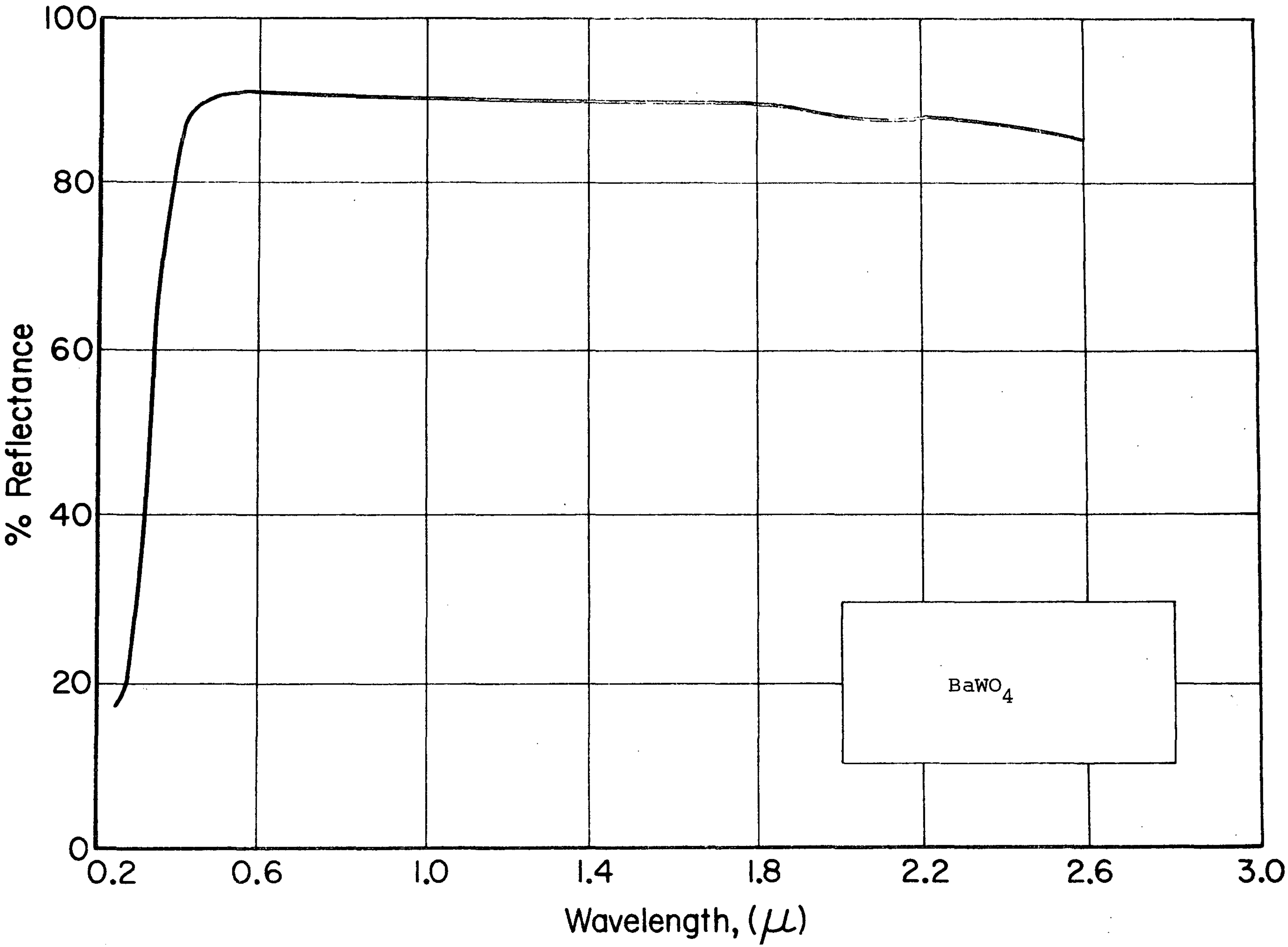

Figure 8 ABSOLUTE HEMISPHERICAL REFLECTANCE OF WET-POWDER SPRAYED BARIUM TUNGSTATE

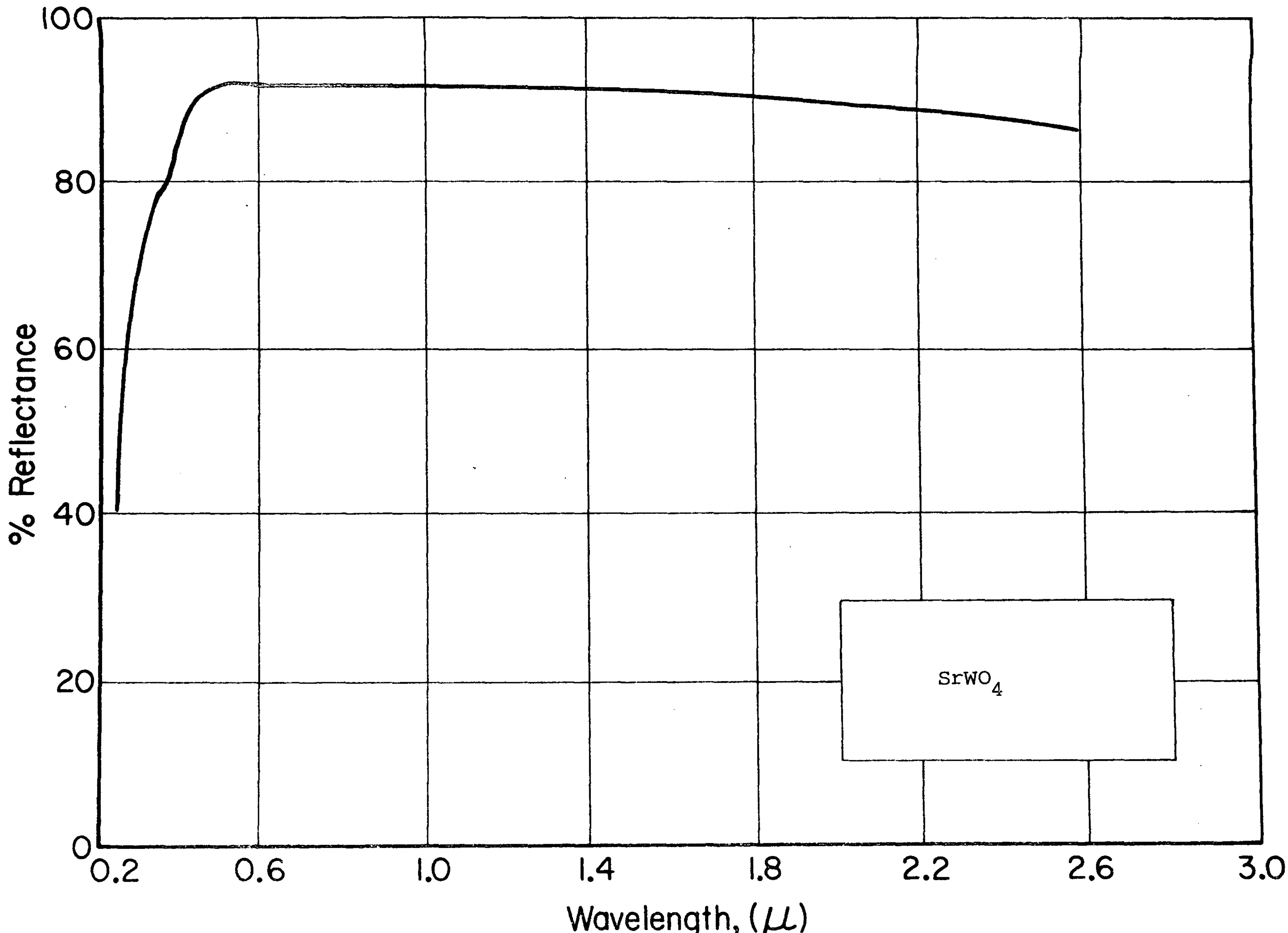

Figure 9 ABSOLUTE HEMISPHERICAL REFLECTANCE OF WET-POWDER SPRAYED STRONTIUM TUNGSTATE

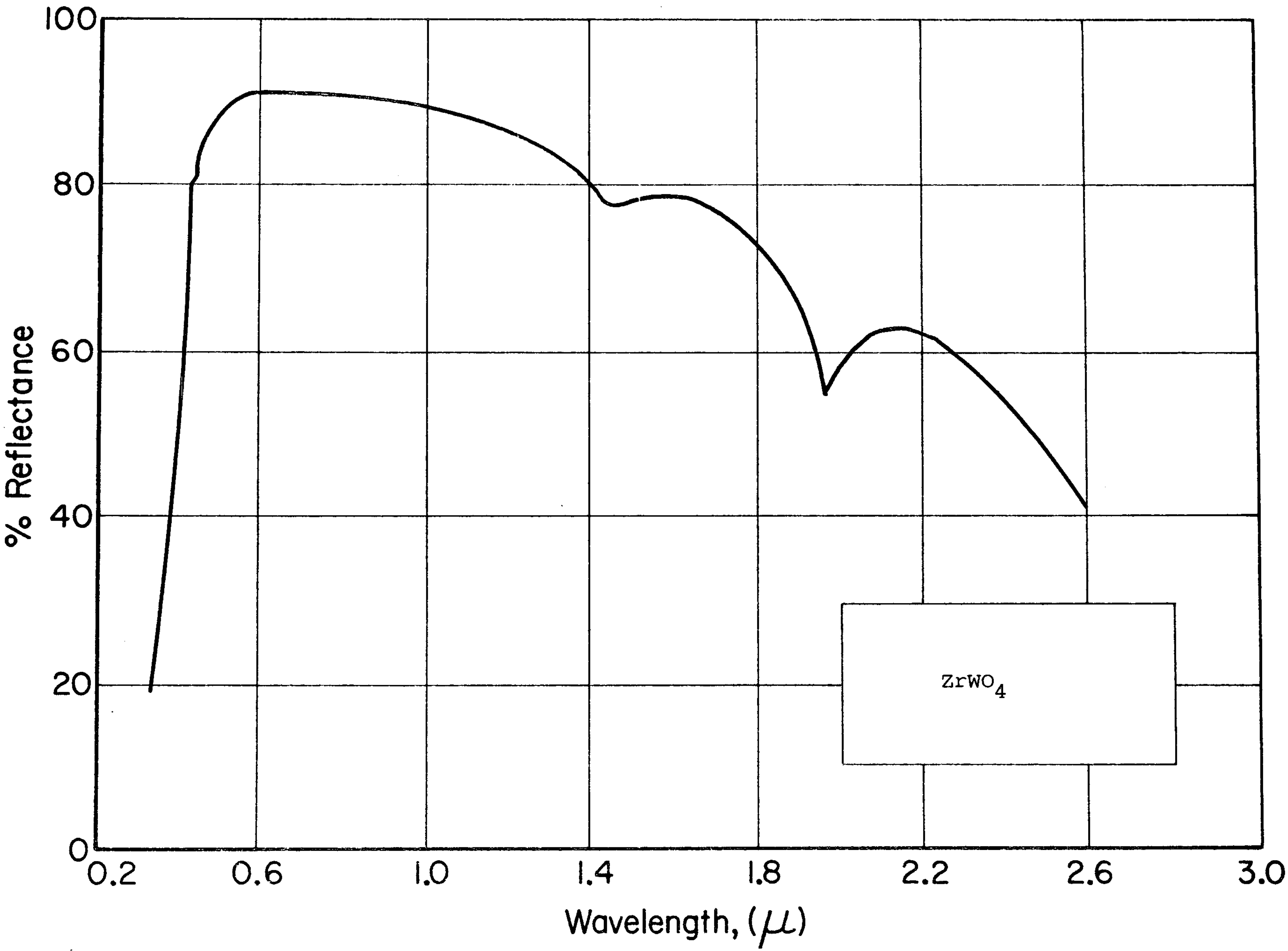

Figure 10 ABSOLUTE HEMISPHERICAL REFLECTANCE OF WET-POWDER SPRAYED ZIRCONIUM TUNGSTATE

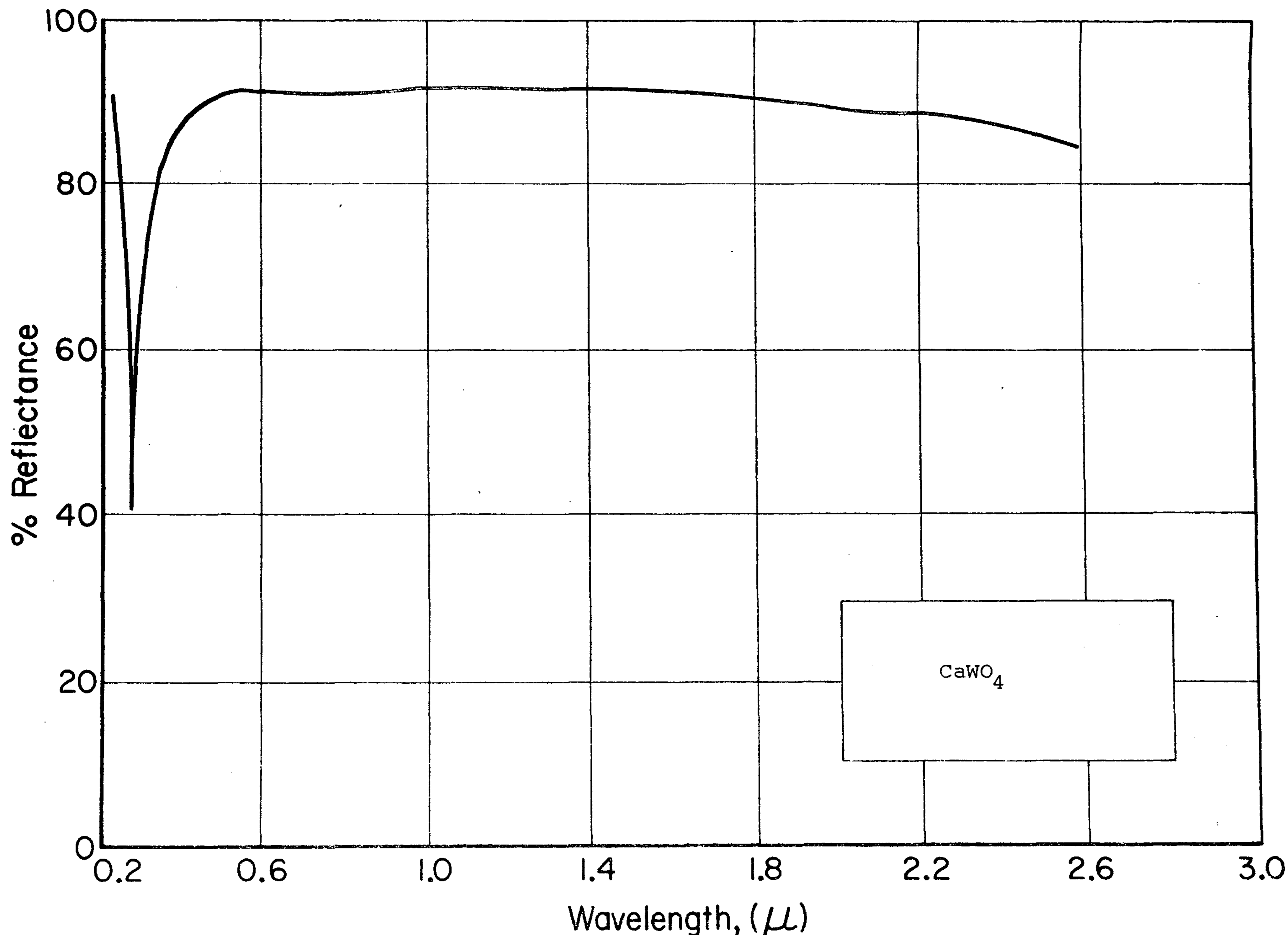

Figure 11 ABSOLUTE HEMISPHERICAL REFLECTANCE OF WET-POWDER SPRAYED CALCIUM TUNGSTATE

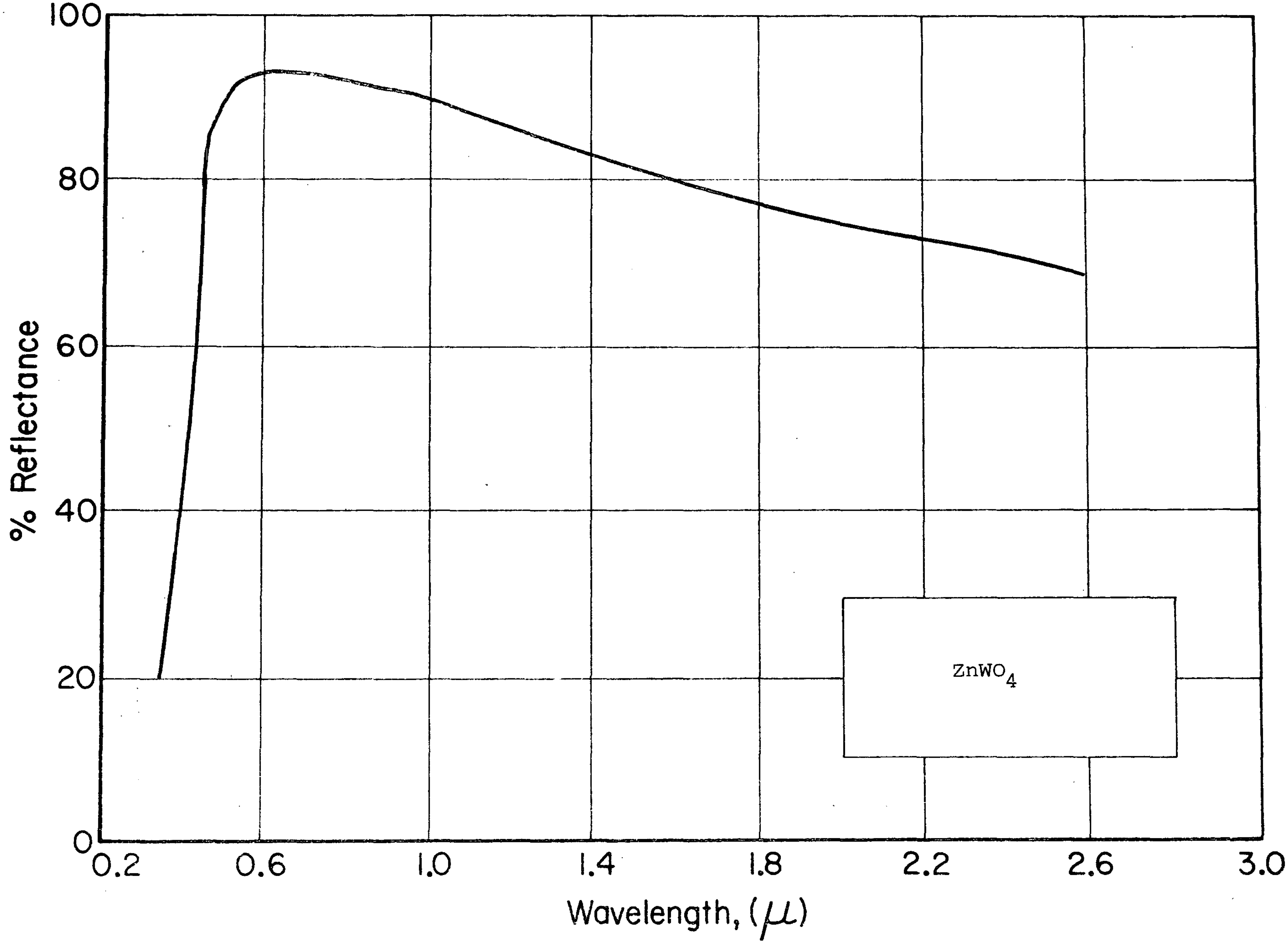

Figure 12 ABSOLUTE HEMISPHERICAL REFLECTANCE OF WET-POWDER SPRAYED ZINC TUNGSTATE

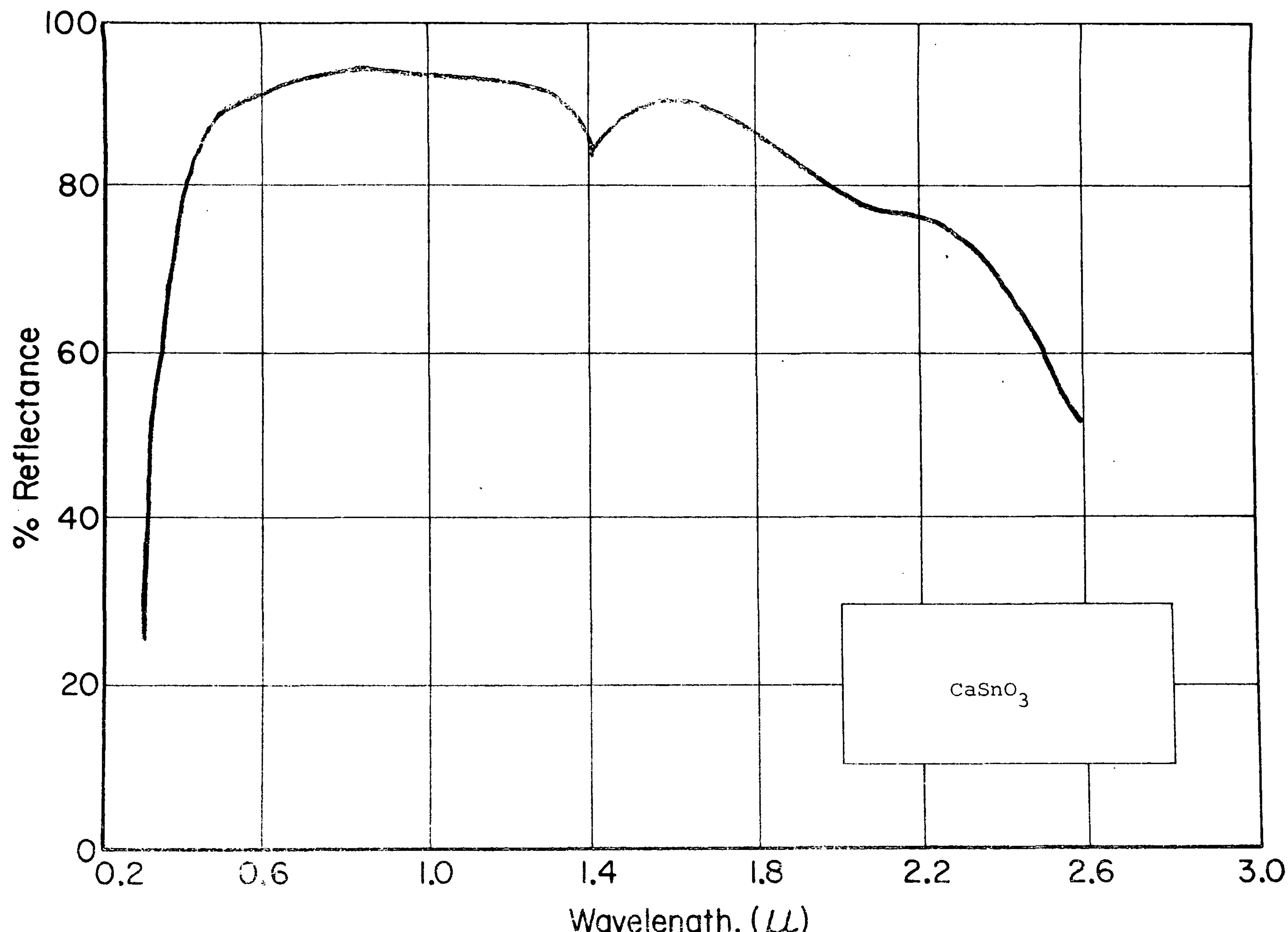

Figure 13 ABSOLUTE HEMISPHERICAL REFLECTANCE OF A WET-POWDER SPECIMEN OF CALCIUM METASTANNATE (Batch A-770; 1000°C)

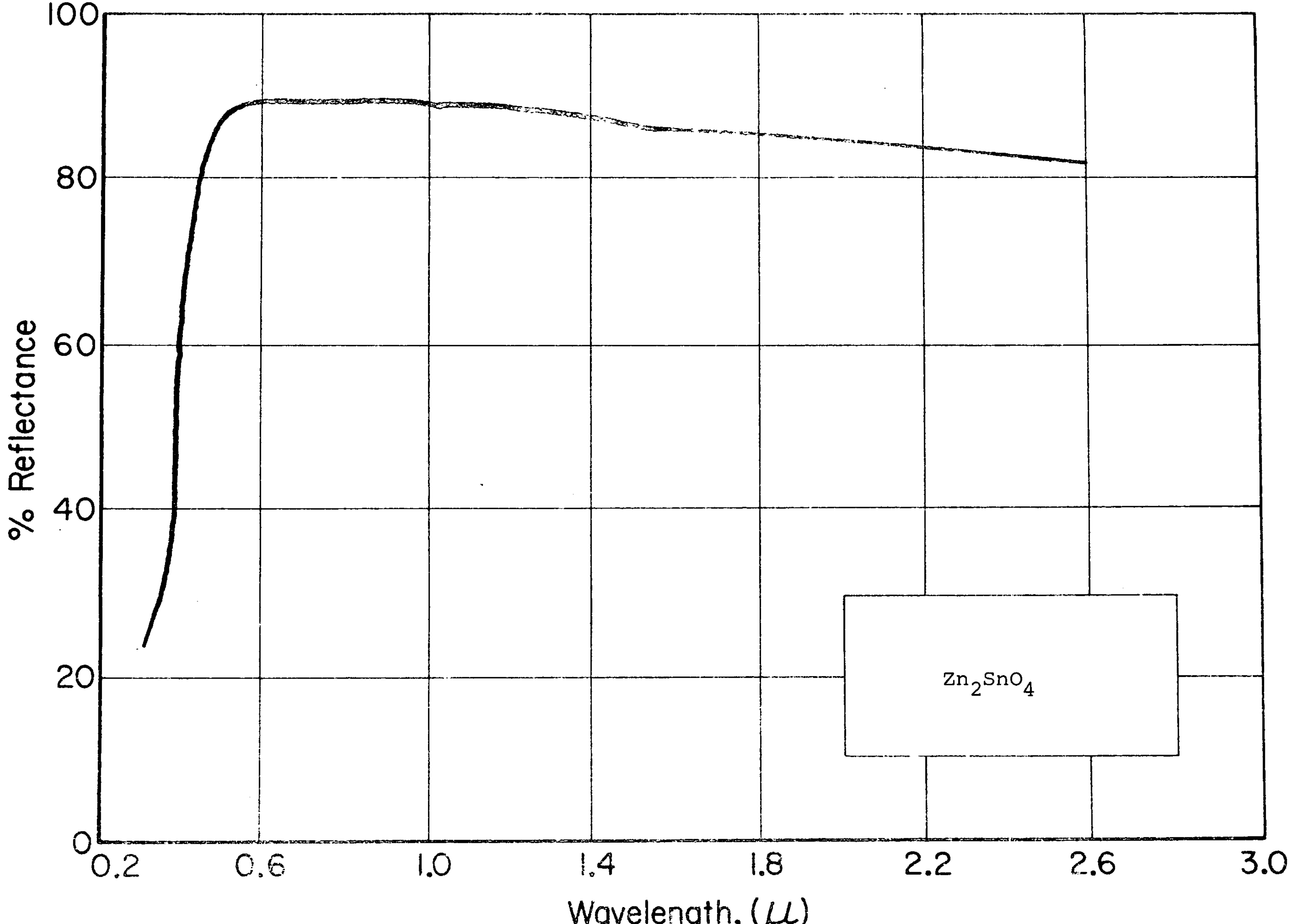

Figure 14 ABSOLUTE HEMISPHERICAL REFLECTANCE OF A WET-POWDER SPECIMEN OF ZINC ORTHOSTANNATE (Batch A-773; 1300°C)

Table 7

EXPERIMENTAL PIGMENT SYNTHESES

Pigment Compound	Temperature Degree Centigrade	Time, Hours	Batch No.
$CaSnO_3$	500	5.75	A-747
$CaSnO_3$	500+ 1200	5.75 2.5	A-751
$CaSnO_3$	800	20	A-767
$CaSnO_3$	1000	19.5	A-773
$CaSnO_3$	1300+ 1400	12 2	A-777
Zn_2SnO_4	800	20	A-764
Zn_2SnO_4	1000	19.5	A-770
Zn_2SnO_4	1200	17	A-782
Zn_2SnO_4	1300+ 1400	12 2	A-775
$SrSnO_3$	1100	3	A-745
Sr_2SnO_3	1200	17	A-781

Examination of Figure 14 shows that, while the product prepared at 1300°C (Figure 12) is less reflective in the visible portion of the spectrum, it exhibits greater reflectance in the 1500-nm wavelength region. This is attributed primarily to the greater particle size of the high-temperature product.

It should be emphasized that prior to reaction, ZnO and SnO_2 were dry mixed and that no attempt was made to extract unreacted elementary oxides from the final product. There can be little question that slurrying and extraction of unreacted oxides would improve the initial reflectance of zinc orthostannate.

3.2.3.2 Stability of Several Pigments

3.2.3.2.1 Tungstates

The effects of 1000 ESH of ultraviolet irradiation on three calcium tungstate powders are presented in Table 8. Different

Table 8

EFFECT OF 1000 ESH UV IRRADIATION ON CALCIUM TUNGSTATE PIGMENTS

No.	Remarks	(ESH) Exposure	Solar Absorptance α_1	α_2	α_s	$\Delta\alpha_s$
Lot 54	Sylvania Crystal Grade	0	.167	.131	.298	
		1000	.196	.136	.332	.034
MM 54	# 54 heated 15.5 hr at 1000°C	0	.111	.081	.192	
		1000	.161	.087	.248	.056
MM 61	Lot # 61 heated 15.5 hr at 500°C	0	.164	.123	.287	
		1000	.189	.130	.319	.032

lots of calcium tungstate have been observed to vary in stability, as exemplified by the differences between the heat treated lots 54 and 61.

Because of these discrepancies, a series of calcium tungstate-powder specimens were prepared, the objective of which was their stabilization by selected heat treatments. The data, including the heat treatments, are presented in Table 9. Although the various heat treatments employed were not effective in stabilizing Lot No. 600-16 (Sylvania Electric Products, Inc.), the results of subsequent irradiation of a heat-treated specimen of Lot No. 8802-78 was encouraging. The spectral-damage curves for the Lot No. 600-16 control are shown in Figure 15; the spectra for the 800°C-treated Lot No. 8802-78 are presented in Figure 16.

A series of mixed tungstates of calcium, strontium and barium were prepared according to the schedule contained in Table 10. These materials were irradiated for 360 ESH of Hg-Xe (ultraviolet) radiation in IRIF-II. The results are also presented in Table 10. (An exposure of 360 ESH was sufficient for differentiating between the specimens being tested.)

Again, the tungstates were very disappointing. Only $BaWO_4$ exhibited reasonable stability. We believe that most of the difficulties are due to intrinsic impurities in the percursor tungstates. Also, the system is apparently very susceptible to surface contamination and grinding.

Because of the erratic behavior of the calcium tungstates when irradiated as powders (behavior that we also observed for the $CaWO_4$-pigmented paints described in Chapter 4), coupled with the disappointing behavior of the other/mixed tungstates, and the increasing emphasis that was placed on the zinc orthotitanate system, we suspended further studies on the tungstates until more concentrated efforts could be placed on the synthetic and solid-state chemistry aspects of the problem.

Table 9

SPECTRAL DAMAGE SUSTAINED BY $CaWO_4$ POWDERS (WET SPRAYED)

Lot No.	Heat Treatment Temp., °C	Heat Treatment Time, Hr	Exposure[1] (ESH)	ΔR_λ (λ, nm) 325	400	700	2400
600-16	No Heat Treatment		1000	15.0	9.0	0.5	0.0
600-16	500	16	1000	14.4	8.8	0.3	0.0
600-16	750	17	1000	15.0	8.3	0.2	0.0
600-16	1000	15	1000	18.0	11.0	0.0	0.0
600-16	1250	2	1000	16.0	9.0	1.0	0.5
600-16	1250	16	1000	17.0	9.0	-0.4	-0.3
1802-78	800	4	2500	4.0	2.0	2.0	0.0

[1] The 1000-ESH exposures were performed in IRIF-I; the 2500-ESH exposure was performed in IRIF-II.

Table 10

SPECTRAL DAMAGE SUSTAINED BY PIGMENT POWDERS (WET SPRAYED) IRRADIATED FOR 355 ESH IN IRIF-II

Description	ΔR_λ (λ, nm) 336	407	818	2362
$SrWO_4$ (Sylvania Elec. Prd.)	14.2	8.0	1.0	0.8
$BaWO_4$ (Sylvania Elec. Prd.)	2.0	4.0	1.0	2.0
$ZnWO_4$ (Sylvania Elec. Prd.)	0.0	2.3	10.0	9.0
$ZrWO_4$ (Sylvania Elec. Prd.)	6.5	20.6	30.2	-2.2
$CaWO_4 \cdot 2\ BaWO_4$ (12 hr/1300°C)	23.0	18.7	1.5	0.6
$2\ CaWO_4 \cdot BaWO_4$ (12 hr/1300°C)	8.6	6.0	0.7	0.0
$CaWO_4 \cdot 2\ SrWO_4$ (12 hr/1300°C)	13.1	7.1	1.0	0.0
$2\ CaWO_4 \cdot SrWO_4$ (12 hr/1300°C)	13.8	9.8	3.4	0.3
$SrWO_4 \cdot 2\ BaWO_4$ (12 hr/1300°C)	19.4	12.3	2.0	1.2
$2\ SrWO_4 \cdot BaWO_4$ (12 hr/1300°C)	18.8	12.8	1.2	1.2
$CaWO_4 \cdot BaWO_4 \cdot SrWO_4$ (12 hr/1300°C)	15.0	8.0	1.0	0.0

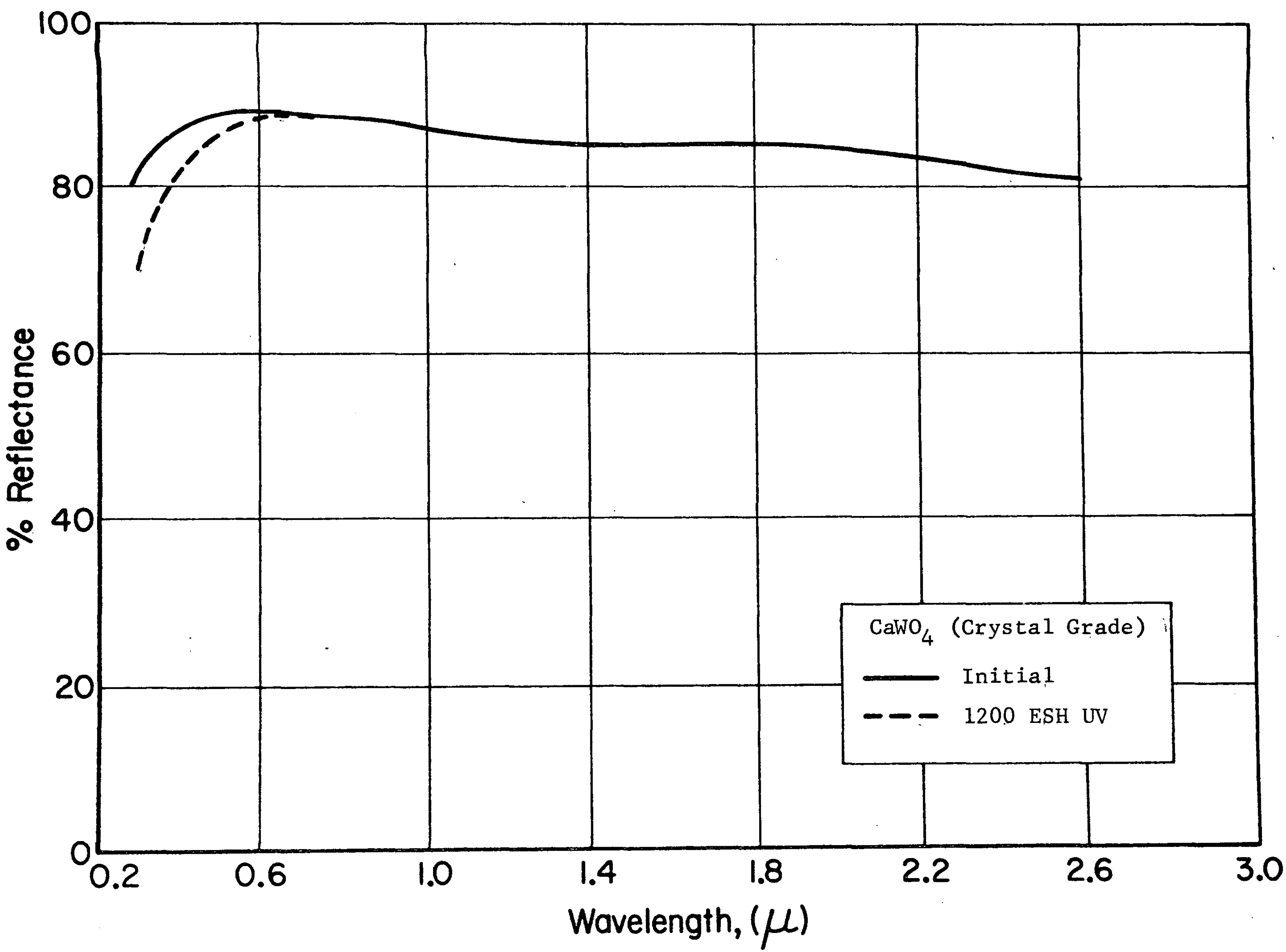

Figure 15 EFFECT OF UV IRRADIATION IN VACUUM ON CALCIUM TUNGSTATE (LOT 600-16)

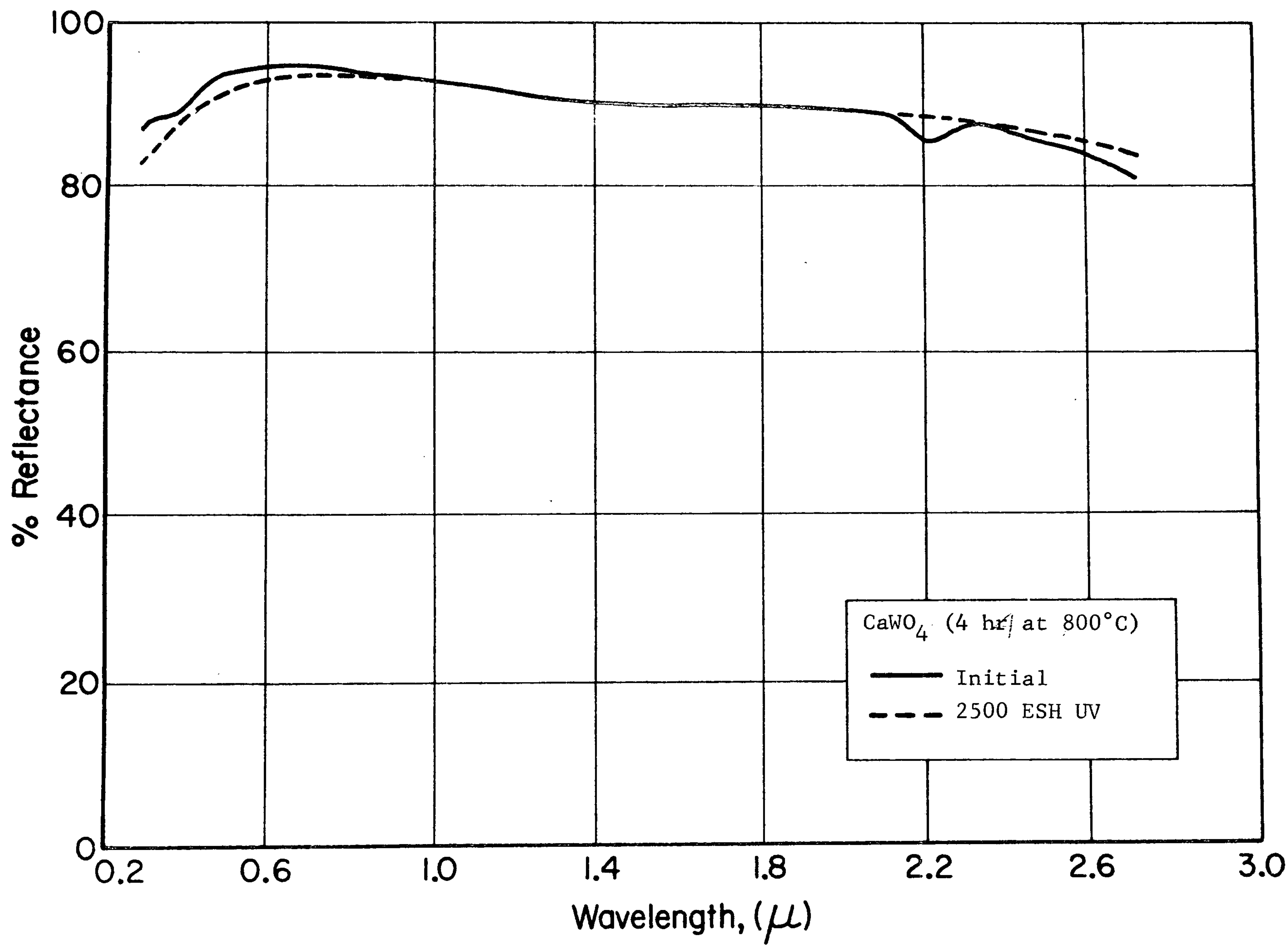

Figure 16 EFFECT OF UV IRRADIATION IN VACUUM ON CALCIUM TUNGSTATE HEAT TREATED FOR 4 HR. AT 800°C (LOT 8802-78)

3.2.3.2.2 Stannates

Both calcium and zinc stannate were prepared by solid-solution reaction. Exactly 325.6 g (4 moles) of SP500 ZnO and 301.4 g (2 moles) of SnO_2 (reagent grade) were each slurried for 5 min in distilled water (600 and 1200 g respectively). They were then mixed and slurried for 15 min. The slurry was vacuum filtered and dried at 110°C for 16 hr. One hundred grams of the dried powder mixture (ZnO + SnO_2) was placed in an alumina crucible and fired for 16 hr at 950°C (1740°F). The results of irradiation for 1000 ESH are presented in Table 11.

Table 11

SPECTRAL DAMAGE SUSTAINED BY WET-SPRAYED STANNATE POWDERS IRRADIATED FOR 1000 ESH

	ΔR_λ (λ, nm)			
Pigment	325	400	700	2400
$CaO \cdot SnO_2$	7.1	10.0	0.8	-1.5
$2ZnO \cdot SnO_2$	0.0	2.0	0.0	4.6

The zinc orthostannate specimen was remarkably stable in all wavelength regions except the long wavelength region beyond 1200 nm. The spectra are plotted in Figure 17.

The damage exhibited by the Zn_2SnO_4 was confined to the 1500- to 2600-nm wavelength region - damage that is very similar to that exhibited by ZnO, but much less intense. This damage bleached out completely on admission of oxygen to the irradiation chamber. The damage is therefore believed to be due to residual (unreacted) ZnO.

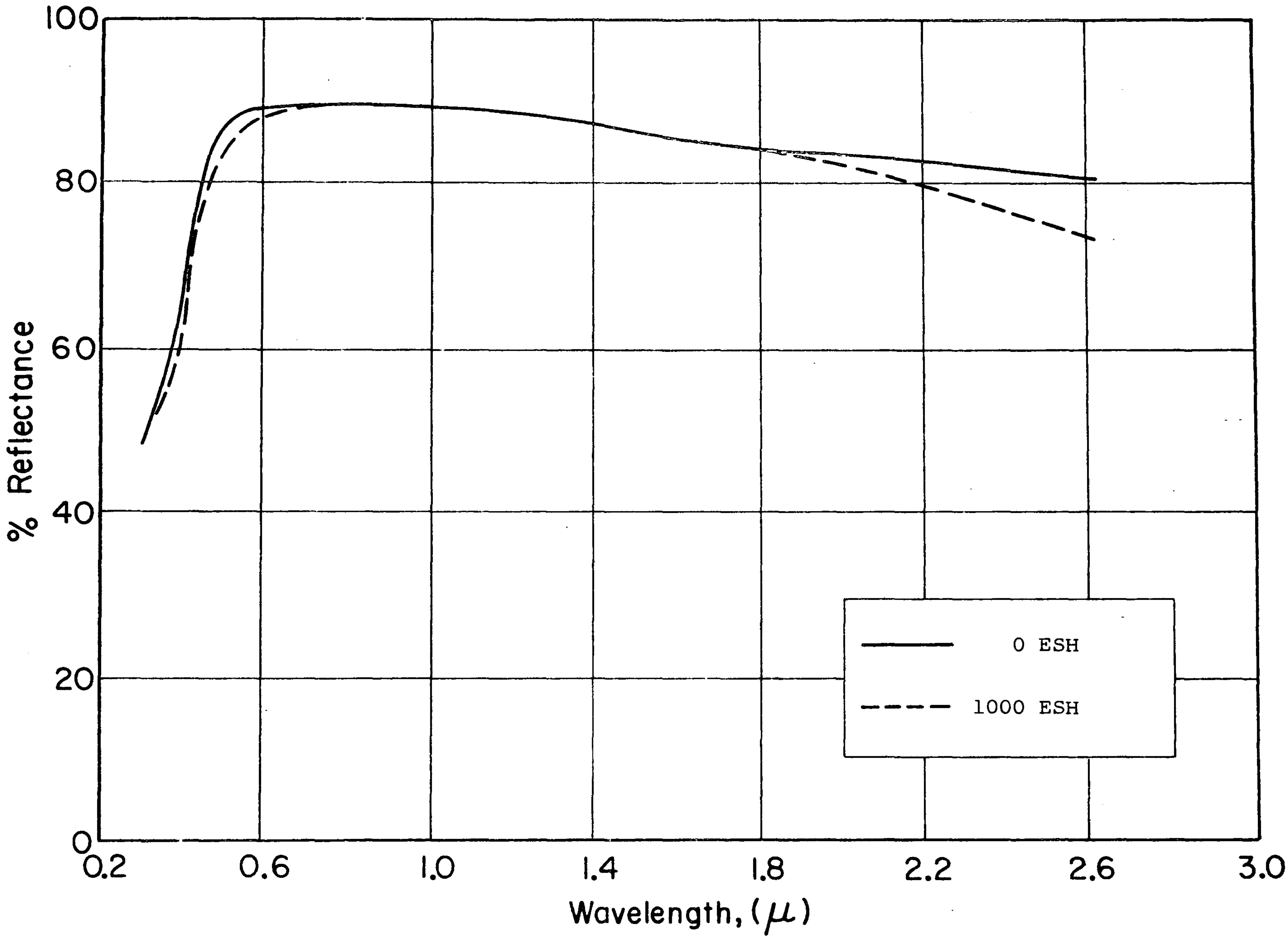

Figure 17 DAMAGE SPECTRA OF ZINC ORTHOSTANNATE IRRADIATED FOR 1000 ESH

4. SUMMARY OF INORGANIC COATINGS TECHNOLOGY

4.1 Porcelain Enamels

White, fused vitreous porcelain enamels were considered for early U.S. spacecraft but were not employed for three principal reasons: (1) they required high firing temperatures, (2) they were heavy at thicknesses that provide adequate reflectance, and (3) they possess generally poor infrared reflectance due to the low concentration of opacifier employed in such enamels. Although these disadvantages are accurate from an historical standpoint, we have long believed that improved infrared reflectance could be be achieved and that low-temperature-vitrifying glasses could be developed, the realization of which would eliminate all three objections.

Experiments at IIT Research Institute in 1965 (Ref. 8) indicated that porcelain enamels could be developed that would be very stable and we have since strongly advocated that greater attention be devoted to such systems. The results of early studies are presented in Table 12, along with the results of a subsequent long-term irradiation exposure performed in the IRIF-I in situ facility. The damage spectra of the rutile-opacified enamel irradiated in the IRIF-I is presented in Figure 18. Examination of this spectra shows that the high initial solar absorptance is due to poor infrared reflectance, but that the coating is quite stable. The rate curve is presented in Figure 19, which is adapted from References 2 and 70. The flight curve is also for a rutile enamel and is adapted from Neel (Ref. 71).

The stability of porcelain enamels, including the surprising stability of the antimony oxide-opacified system, is believed to relate to the prevention of oxygen reactions at the pigment (opacifier) particle-glass matrix interface. The matrix density and intimacy of the glass/oxide interface simply do not permit the oxygen to escape--and, of course, the oxygen that is desorbed in vitrification is not replaced on cooling for the same reasons.

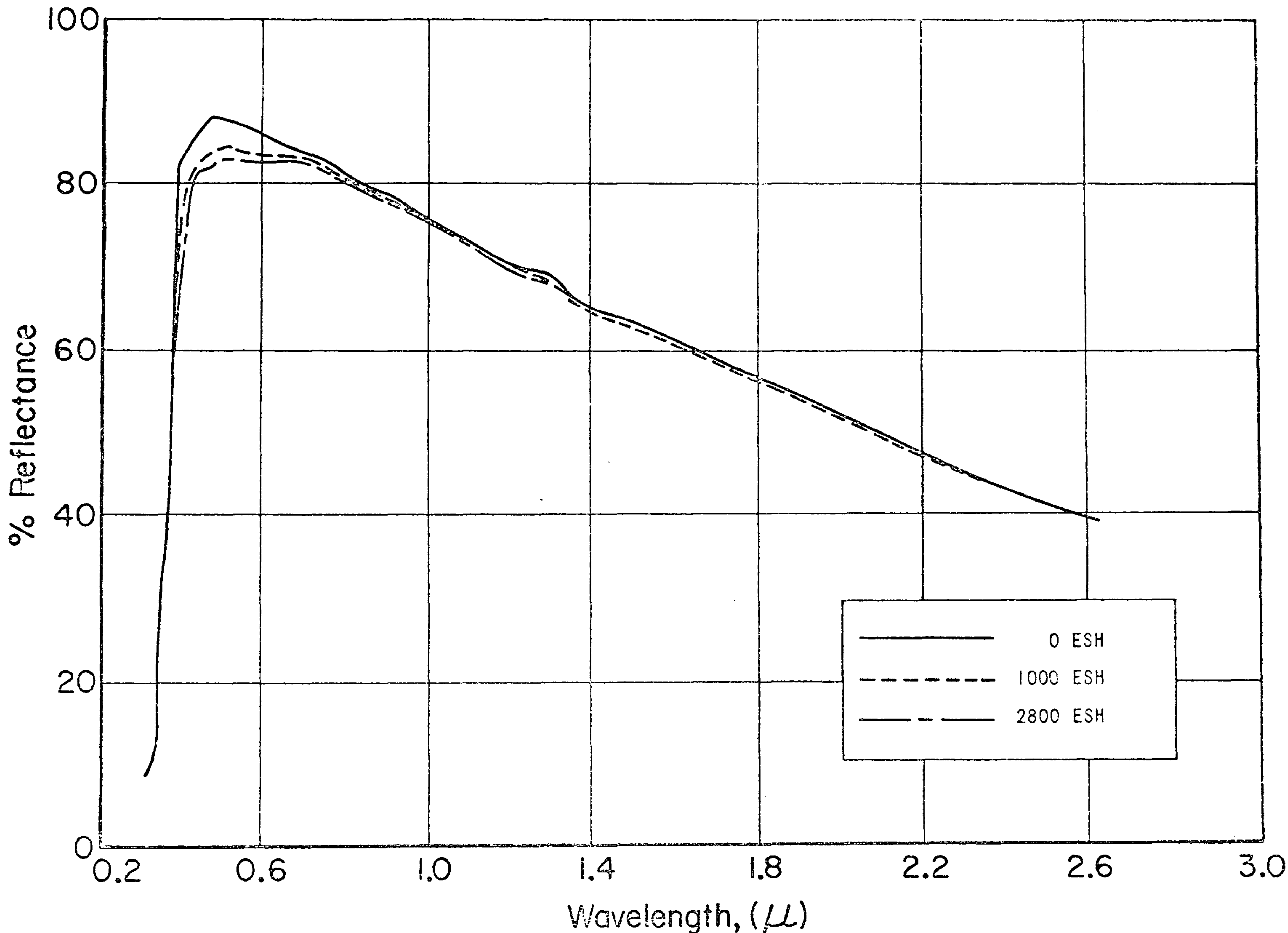

Figure 18 UV DEGRADATION OF RUTILE PORCELAIN ENAMEL

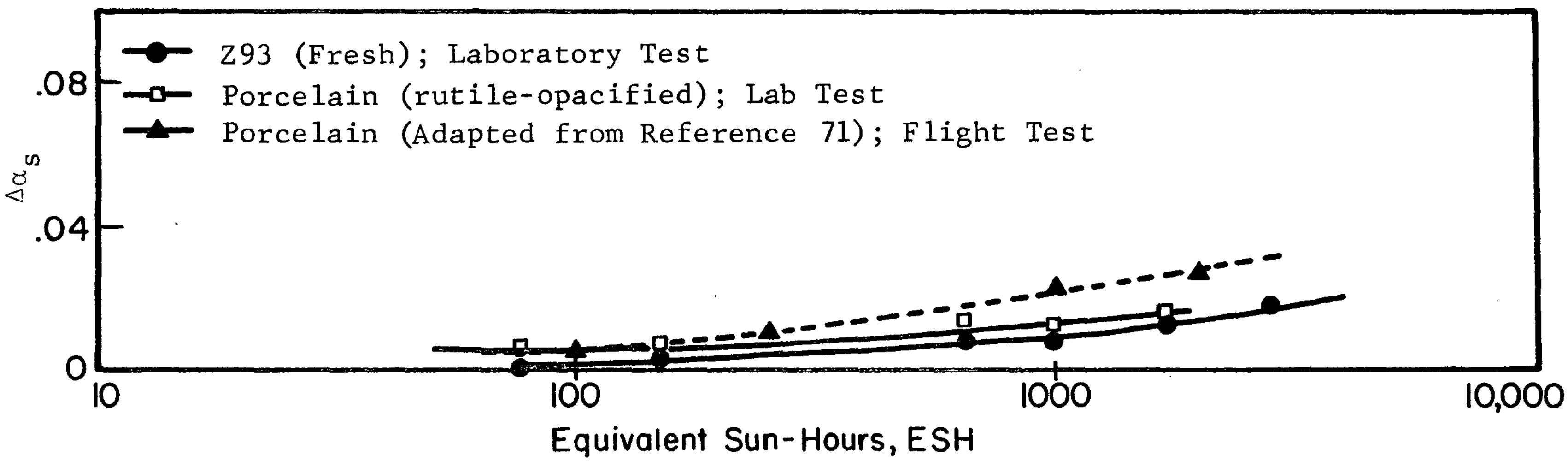

Figure 19 DEGRADATION RATES OF PORCELAIN AND Z93 EVALUATED IN THE IRIF-I (ADAPTED FROM REFERENCE 70)

Table 12

RESULTS OF ULTRAVIOLET IRRADIATION OF BOROSILICATE GLASS ENAMELS* (SOLAR FACTOR = 10X)

Opacifier	In Situ Meas.	Exposure (ESH)	Solar Absorptance α_s	$\Delta\alpha_s$
r-TiO_2	No	2350	0.242	0.016
r-TiO_2	No	2150	0.252	0.008
ZrO_2	No	2150	0.409	-0.014
Sb_2O_3	No	2150	0.355	0.030
r-TiO_2	Yes	2800	0.306	0.021

*Obtained from Chicago Vitreous Company.

Therefore, as will be discussed in more detail in Chapter 5, electrons are not free to accumulate either in low-energy surface traps, in anion vacancies, or in the conduction band (as in the case of ZnO). The opacifier is thus virtually stabilized by the glass matrix.

Although neither high-temperature ultraviolet nor charged particle (low-energy protons and electrons) irradiations of porcelain enamels have been reported, their potential for use on critical areas, where either high temperatures are reached or where their cleanability and non-outgassing characteristics are needed, has been demonstrated. Providing that current studies* result in improved infrared reflectance and in reasonably low-temperature vitrifying characteristics, porcelain enamels may very well receive greater attention in the future.

4.2 Z93 Thermal-Control Paint

Although IIT Research Institute's Z93 thermal-control coating was developed for the Jet Propulsion Laboratory in an earlier program (Ref. 1, 72), we have continued to evaluate Z93's

*NASA Contract NAS8-27439, Hughes Aircraft Co.

characteristics in order to learn how to better handle and apply this material. Z93 is a zinc oxide-pigmented potassium silicate paint formulated in a pigment-to-binder weight ratio (PBR) of 4.3 and a solids content of 57%. The original specification called for calcination of New Jersey Zinc Company's SP500 ZnO at 700°C for 16 hr; the binder is Sylvania Electric Products Corporation's PS7 potassium silicate (35% sdn.).

4.2.1 Experiments with Various ZnO Pigments

A limiting solar absorptance for zinc oxide-potassium silicate paints of about 0.13 is observed due mainly to ZnO's strong ultraviolet absorptance. Increasing the reflectance both in the near-ultraviolet region and also in the infrared portion of the spectrum is necessary for attaining lower solar absorptance.

An investigation of the optical characteristics of various zinc oxide powders as functions of particle size and manufacturer was conducted. The reflectances of a number of commercial zinc oxide powders were measured.

Sample preparation consisted of pouring the powder into a copper ring placed on a vellum-covered steel plate. A steel disc of 1-1/2 in. diameter (equal to the inside diameter of the ring) is fitted into the ring covering the pigment. A pressure of 5,000 psi applied on the steel disc results in a specimen with one exposed face for reflectance determination. No binders or lubricants were used, thus averting the possible effects of foreign materials.

Information concerning the physical properties of the various powders as well as solar absorptance values are presented in Table 13. Absorptance values are reported as α_1 and α_2 for the reasons that were given in section 2.5.

Spectral reflectance curves are graphically illustrated in Figures 20, 21 and 22. Among the "AZO" series shown in Figure 20, lowest solar absorptance is exhibited by AZO-66. Although the

Table 13

PROPERTIES OF ZINC OXIDE POWDERS

Manufacturers Designation	Manufacturer	Purity %	Mean Particle Size, μ	Remarks	Solar Absorptance α_1	α_2	α
AZO-88	American Zinc Sales	99.20	0.90		0.145	0.075	0.219
AZO-77	American Zinc Sales	99/80	0.14		0.093	0.070	0.163
AZO-66	American Zinc Sales	99.80	0.20		0.086	0.050	0.136
AZO-33	American Zinc Sales	99.20	ca. o.40	Acicular	0.106	0.073	0.179
SP500	New Jersey Zinc	>99.90	0.25-0.35	Spectrographic grade	0.092	0.037	0.128
SP500	New Jersey Zinc	>99.90		Calcined: 700°C/16 hr	0.091	0.037	0.128
SP500	New Jersey Zinc	>99.90		Calcined: 700°C/112 hr	0.096	0.037	0.133
SP500	New Jersey Zinc	>99.90		Calcined: 1000°C/1 hr	0.116	0.043	0.159
SP500*	New Jersey Zinc	>99.90	2.1 (initial)	Calcined: 700°C/40 hr	0.116	0.041	0.157
USP 12	New Jersey Zinc	99.80	0.30		0.089	0.046	0.136
XX 254	New Jersey Zinc	99.60	1.5		0.114	0.056	0.170
E-P 730	Eagle-Picher	99.50	5.4		0.164	0.085	0.249

*Large particle size, 2.1μ, SP500 supplied by the manufacturer.

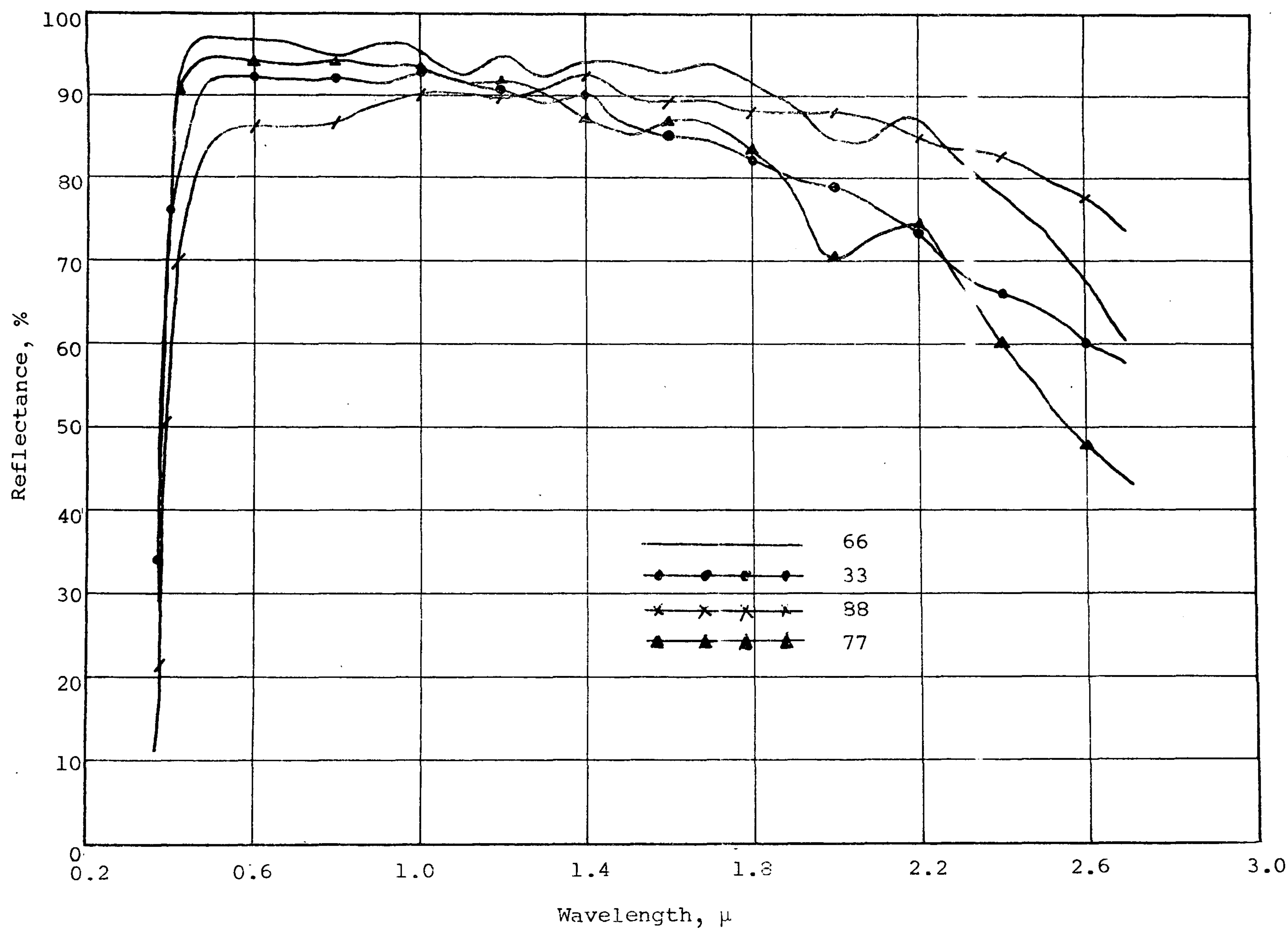

Figure 20 SPECTRAL REFLECTANCE CURVES FOR AZO ZINC OXIDE POWDERS

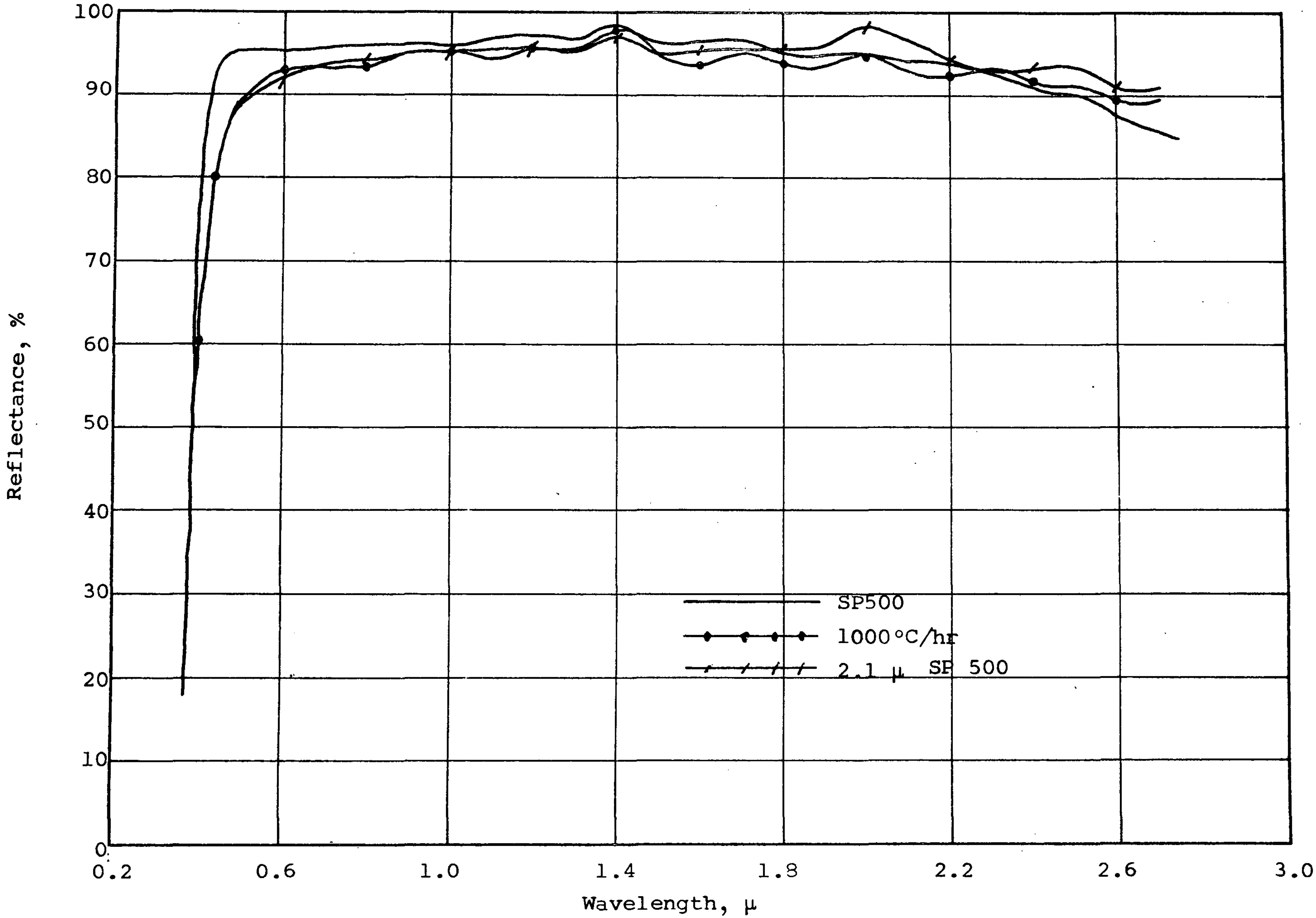

Figure 21 SPECTRAL REFLECTANCE CURVES FOR SP500 ZINC OXIDE POWDERS

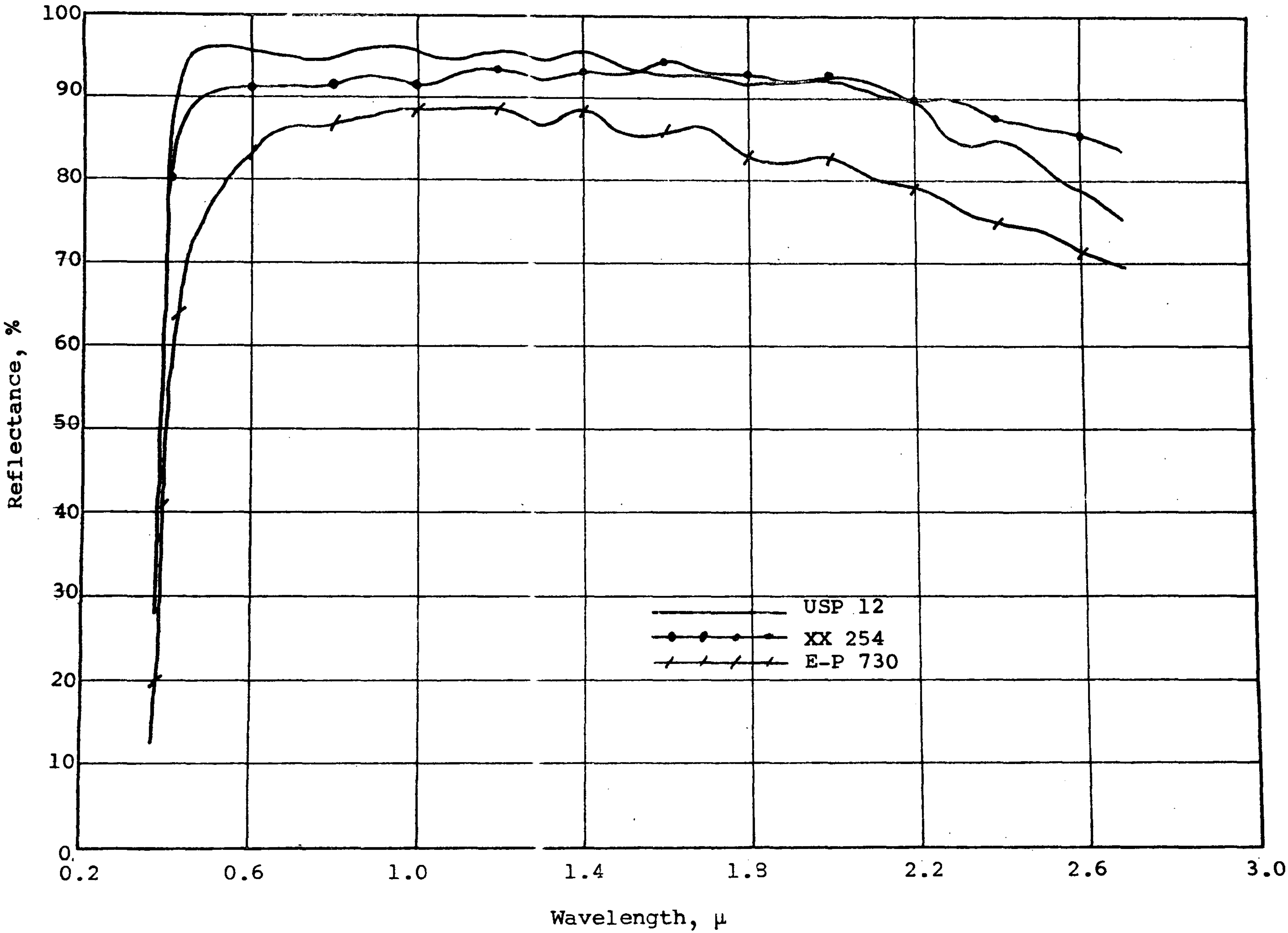

Figure 22 SPECTRAL REFLECTANCE CURVES FOR MISCELLANEOUS ZINC OXIDE POWDERS

reflectance of AZO-77 approaches that of AZO-66 in the visible portion of the spectrum, a rapid reflectance drop-off in its infrared reflectance contributes to a higher solar absorptance. The larger particle-sized AZO-88 displayed a higher infrared reflectance, but its poor reflectance in the visible caused a relatively high solar absorptance.

Spectrographic grade SP500 ZnO possessed the lowest solar absorptance among the commercial zinc oxides. AZO-66 is more reflective in the visible region, i.e., 0.38-0.70μ, than SP500 whereas AZO-77 possesses about the same reflectance as SP500 in this region. This high purity material manifests its superior reflectance in the infrared wavelength region. As tabulated in Table 13, the α_2 of SP500 is 0.037 and is considerably less than that of AZO-66 (0.050) or AZO-77 (0.070). Calcination of SP500 at 700°C did not significantly affect the solar absorptance. However, a higher temperature, 1000°C, causes a distinct reflectance loss in the visible. Use of a calcined, larger particle size SP500 (2.1μ) results in lower visible reflectance and a slight increase at wavelengths greater than 2.0μ. Curves for these powders appear in Figures 20 and 21. Not illustrated are the 700°C calcined SP500 materials which display curves practically identical to the uncalcined powder.

Figure 22 illustrates the spectral reflectance of USP 12 which also has a relatively low solar absorptance and of two materials of larger particle size, XX254 and E-P 730. The Eagle-Picher material was visually yellow and had the highest solar absorptance of the zinc oxides studied.

These studies indicate that reflectance at the longer wavelength is improved with the use of larger particles, which is consistent with light-scattering theories. However, since half of the solar flux is concentrated in the portion of the spectrum below 0.7μ, and therefore it is this region in which the reflectance must be optimized, SP500 ZnO was deemed still to be the best choice of ZnO for the Z93 formulation in terms of initial optical properties.

4.2.2 Calcination of SP500 ZnO

4.2.2.1 Calcination at New Jersey Zinc Company

A series of potassium silicate-bonded zinc oxides were prepared from as-received, calcined New Jersey Zinc SP500 zinc oxide (Ref. 73). The average particle size for three lots varied as follows (provided by New Jersey Zinc Company):

Sample	5221	5222	5223
Particle Size (microns)	0.52	0.47	0.56

Table 14 shows the ultraviolet degradation of three Z93 paints, also designated 5221, 5222 and 5223, prepared from the "precalcined" SP500. This precalcined material is heat treated at a temperature between 600 and 700°C for one hour, presumably in air.

Table 14

COMPARISON OF Z93 PAINTS PREPARED FROM
SP500 ZINC OXIDE PIGMENTS CALCINED BY NJZ (Solar Factor: 7X)

Sample No.	Exposure ESH	Solar Absorptance α_1	α_2	α_s	$\Delta\alpha_s$
5221	0	0.076	0.052	0.128	
	1650	0.101	0.051	0.152	0.024
5222	0	0.081	0.060	0.141	
	1650	0.106	0.059	0.165	0.024
5223	0	0.091	0.064	0.155	
	1650	0.112	0.063	0.175	0.020

The change in solar absorptance is relatively high compared to values that are usually obtained on paints containing "standard" SP500 zinc oxide calcined at IITRI. Typical of the results is the $\Delta\alpha_s$ of -0.016 reported for specimen 7173 of Z93 reported in Table 4 of section 3.2.4.

4.2.2.2 Calcination at IITRI

Although the original specification for Z93 calls for calcination of the SP500 ZnO pigment for 16 hr at 700°C, our experience with currently furnished material is that 700°C is too high a temperature and slight yellowing results. We have recently found that 635°C is the optimum calcination temperature for currently-furnished SP500 ZnO; a higher temperature is too yellow and a temperature of 610°C, although slightly superior in optical properties, results in a tendency to produce checking of the cured paint.

4.2.3 Stability of Z93-Type Paints Prepared from Various Zinc Oxides

Potassium silicate-bonded coatings with four different zinc oxide pigments, which had been prepared more than one year previously (and stored under normal laboratory conditions) were irradiated for 2150 ESH of ultraviolet irradiation. The data, presented in Table 15, show that the degradation resistance of these coatings is not impaired by storage. Of the four coatings, the standard Z93 was affected least by ultraviolet irradiation in vacuum. The negative $\Delta\alpha$ for the paint (Z93) is attributed to the reflectance increase in the α_2-region as a result of loss of water by the silicate vehicle.

4.2.4 Grinding Z93 Paint

Because of the propensity for yellowing on grinding exhibited by zinc oxide pigments, especially SP500, care must be exercised in the preparation of paints pigmented with zinc oxide. The yellowing has been attributed to a zinc interstitial that results from lattice distortion during grinding and has been studied by Gilligan (Ref. 74). (Work with S-13, the precursor paint to S-13G, has also shown that the space environment stability of overground ZnO is impaired seriously; see Chapter 6).

Table 15

ULTRAVIOLET DEGRADATION* OF POTASSIUM SILICATE PAINTS PREPARED FROM SEVERAL ZINC OXIDE PIGMENTS
(PS7 Potassium Silicate at a PBR of 4.3; Solar Factor: 10X)

Pigment	Manufacturer	Purity	Average Size	Exposure (ESH)	Solar Absorptance α_1	Solar Absorptance α_2	Solar Absorptance α_s	$\Delta\alpha_s$
55LO	American Zinc	99.2	0.4μ	0	0.097	0.049	0.146	
				2150	0.098	0.045	0.143	-0.003
XX254	New Jersey Zinc	99.6	1.5μ	0	0.106	0.070	0.176	
				2150	0.111	0.064	0.180	+0.004
EP730	Eagle Pitcher	99.5	5.4μ	0	0.150	0.090	0.246	
				2150	0.101	0.091	0.252	+0.012
SP500	New Jersey Zinc	99.9	0.3μ	0	0.083	0.069	0.152	
				2150	0.088	0.048	0.136	-0.016

*Pre-in situ measurements

**Z93 formula

We have therefore historically ground Z93 (and S-13G) to a much coarser grind than is standard practice in the paint and enamel industry and the standard Hegman Gage is of no value in registering and monitoring fineness of grind. Our current practice is to employ a PB-20 Peanut Butter gage (Gardner Laboratories) for determining the correct dispersion of Z93 (and S-13G)

The original specification calls for a paint grind of 6 hr in a laboratory pebble mill. This is much too long and current practice is to grind as little as possible but usually between 35 and 45 min. A typical laboratory batch of Z93, ground for 40 min in a small pebble mill, has a PB-20 fineness of grind of about 6. Recently a series of Z93 grinds was prepared in order to correlate fineness of grind with solar absorptance. The results are represented by Figure 23. The fineness curve is easily explained from grinding theory. The solar absorptance curve may be explained as follows: At grind times of less than 40 min (PB fineness >6-1/2), the lack of dispersion has an adverse effect on light scattering efficiency and the total reflectance (solar) is less than optimum; at grind times treater than 60 min (PB fineness <5), yellowing due to lattice distortion overcompensates for the increasing light scattering efficiency and the solar absorptance increases. A composite of many years of experience in observing the stability of over- and underground Z93 is presented in the "dashed" curve of Figure 23. The poorer stability at low grind times is attributed to unprotected islands of silicate binder. On the other hand, the poorer stability of overground Z93 is attributed primarily to the greatly increased solar energy absorption resulting from lattice distortion, i.e., the creation of the now recognized B-band in ZnO (Ref. 74).

It must be noted that the data represented by Figure 23 should be plotted for every combination of mill-type, ball-to-charge ratio and mill speed employed in the manufacture of Z93. Examination of the curves in Figure 23, which is quite typical

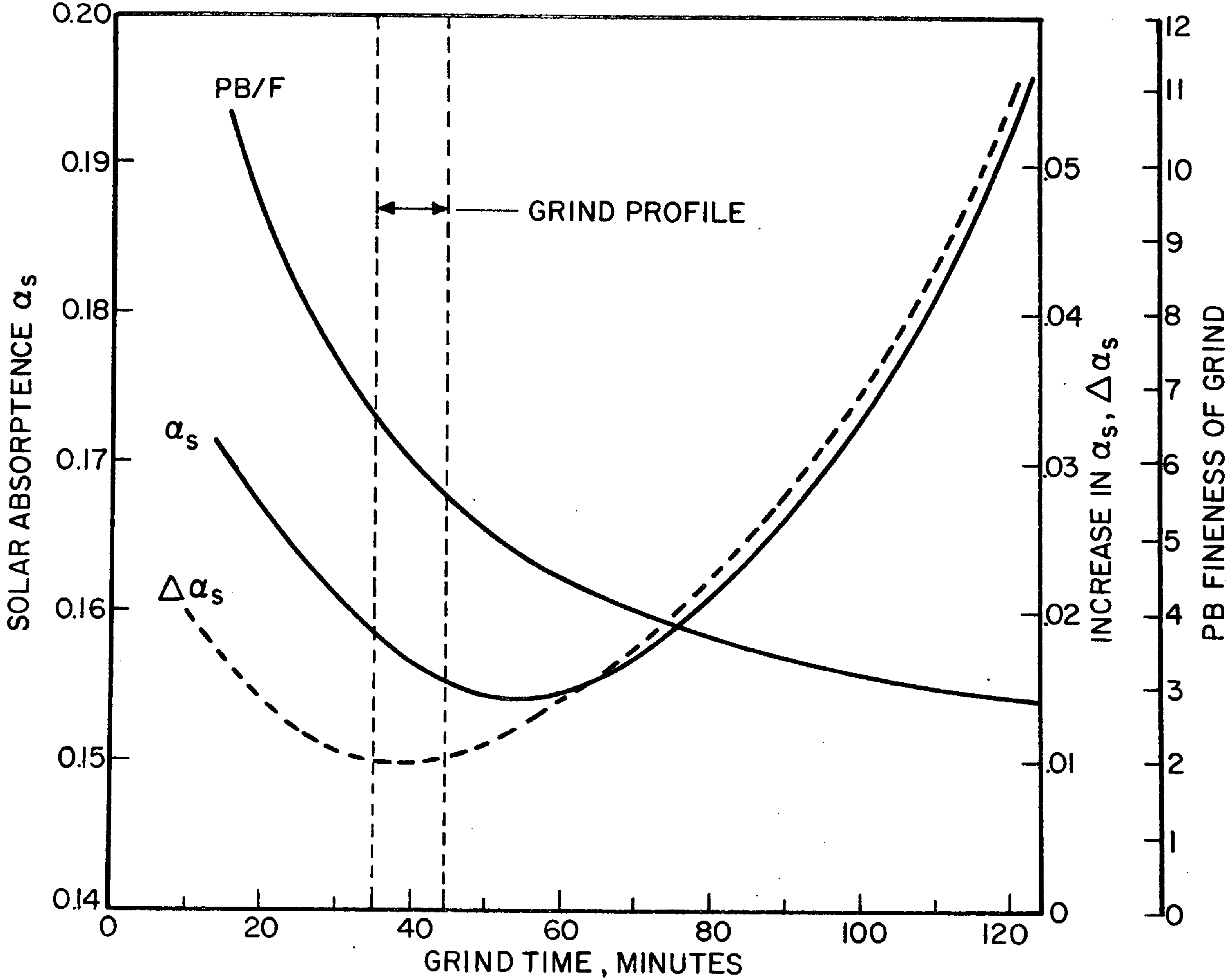

Figure 23 GRIND PROFILE FOR Z93

for 1-qt laboratory pebble mills operated at a standard 50% charge and 70% of critical speed, show that about 40- to 70 min. grind time is required for optimum reflectance but that 30- to 60-min. is optimum for space ultraviolet stability. We therefore currently grind Z93 to a fineness of not less than 5-1/2, which is usually between 35 and 45 min. for the mills employed.

4.2.5 Surface Preparation for Z93

Two simple procedures have been found necessary for preparation of metal surfaces for Z93, procedures which, if not performed, will likely result in early adhesion failure of the cured paint, but which, if properly performed, will ensure an exceptional bond. The first is to clean the metal surfaces to the extent that they are break-free to water. This is accomplished in various ways; a typical sequence for aluminum is:

Vapor degrease
5% NaOH
De-smut with 15% HNO_3
— Standard De-Ox procedures employed in the Aerospace Industry will usually suffice.
Rinse with water
Rinse (scrub if necessary) with ethanol
If not break free to water, scrub with 5% Alconox or an abrasive cleanser such as COMET, etc. Rinse thoroughly.

The second important procedure consists of immediately rub-priming with Z93 (employing a lint-free swab) to effect a "washed," thin coating. Although rub-priming is not necessary for most aluminum surfaces, it is absolutely necessary for magnesium, stainless steel, brass and beryllium--and we recommend it also for all aluminum alloys as well. Indeed, we have successfully coated 1-mil 304 stainless steel sheets (6-ft diameter) with 4 mils of Z93, with the result that flexing of the stainless steel sheet did not adversely affect the Z93 coating. This was made possible only by rub-priming the surface first.

We have been successful in applying Z93 to plastic and plastic fiberglass surfaces providing the surfaces can be primed with Randolph Products' Non-Chromated Epoxy Primer W-2248-A (at a thickness of 1 mil).

4.2.6 Summary

Z93 has proven to be the most ultraviolet-stable, diffusely-reflecting, thermal-control coating currently being employed on U.S. spacecraft. Typical of the data on Z93 for near-earth orbit are the data of Pearson (Ref. 75) and Millard (Ref. 76), which are included in Figure 19, page 60. Furthermore, because of its exceptional stability to ultraviolet radiation in space, Z93 has been employed as a standard against which the experimental paints discussed in Chapters 6 and 8 were compared.

Although at various times Z93 has been reported to have failed in adhesion, examination has shown that in nearly 100% of the cases, improper surface preparation was responsible for the failure. Indeed, even in the cases reported concerning discoloration of Z93-painted surfaces, improper surface preparation has usually been responsible (external contamination has been found responsible for the remaining cases of discoloration reported).

The studies reported in the previous paragraphs have confirmed that the original Z93 formula (Ref. 1, 72), i.e., the specific ingredients (SP500 ZnO and PS7 potassium silicate) and the formula weights employed, is optimum. However, these studies have shown that the proper calcining temperature for currently furnished SP500 ZnO is 635°C (rather than 700°C), and that a much shorter grind time is required in pebble mill manufacture of the paint (about 40 min. rather than 6 hr). Also, rub-priming for Z93 with Z93 has been found desirable for aluminum surfaces and mandatory for all other metal surfaces. Finally, we have found Randolph Products' W-2248-A epoxy primer to be satisfactory for priming plastic and plastic-fiberglass surfaces for application of Z93.

4.3 Reflective Topcoats for Z93

Attempts were made to improve the reflectance of a zinc oxide-silicate system by application of an ultraviolet-reflecting topcoat. Because of its good ultraviolet reflectance and reasonably good stability, a thin zirconia-silicate coating with a pigment-to-binder ratio (PBR) of 4.30 was selected. It was brush-painted on a portion of several 1 x 3-in. zinc oxide-silicate (Z93) samples. For a 0.4 mil ZrO_2-silicate paint (~0.07g), the reflectance improvement is given in Figure 24 (Ref. 5). The solar absorptance changes due to topcoating are concentrated in the ultraviolet, i.e., the α_1 region of the spectrum.

A space-simulation experiment was conducted to determine the stability of Z93 overcoated with 0.4 mil of silicate-bonded zirconia. Figure 25 illustrates the complete experimental sample measuring 1 x 3 in. and the 1 x 1/2-in. test specimens (Nos. 1 to 4) which were cut from the parent. Samples 1 and 3 were heated at 400°C for 2 hr; Samples 2 and 4 received no treatment. Data for this experiment, conducted at an accelerated solar factor of 11.0 suns in the Quad-Ion Facility (see section 2.3.1), are tabulated in Table 16.

Table 16

EFFECT OF ULTRAVIOLET IRRADIATION IN VACUUM ON Z93 TOPCOATED WITH A ZIRCONIA-SILICATE PAINT

Sample	Exposure ESH	Solar Absorptance α_1	α_2	α_s	$\Delta\alpha_s$
1	0	0.088	0.085	0.172	
	2560	0.130	0.081	0.211	0.039
2	0	0.068	0.081	0.149	
	2560	0.163	0.087	0.251	0.102
3	0	0.101	0.076	0.176	
	2560	0.107	0.070	0.178	0.002
4	0	0.102	0.080	0.182	
	2560	0.122	0.073	0.194	0.012
5-19-6*	0	0.080	0.120	0.200	
	2560	0.141	0.110	0.251	0.051

*Silicate-bonded zirconia coating only.

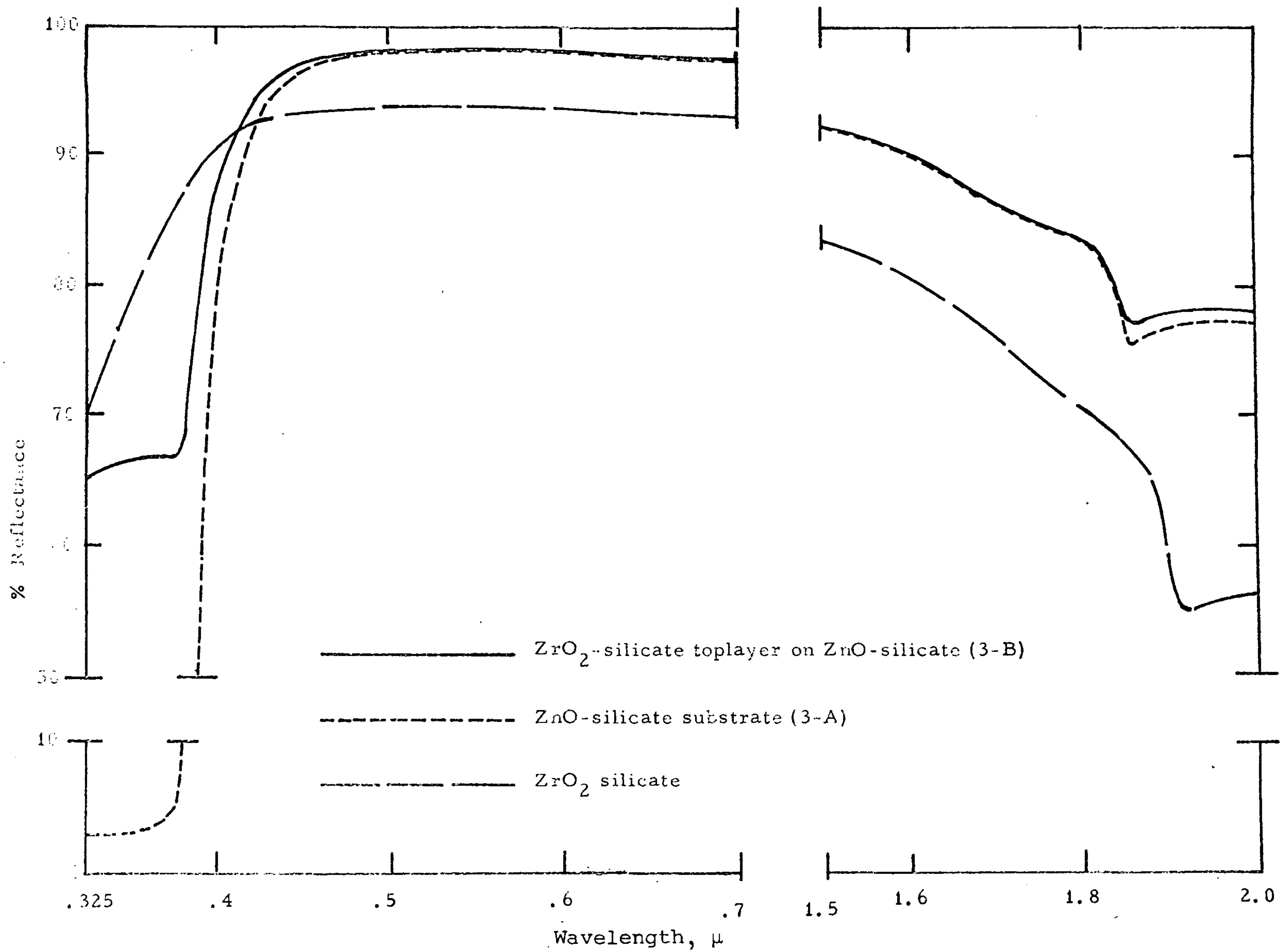

Figure 24 EFFECT OF THIN ZIRCONIA-SILICATE TOPLAYER ON SPECTRAL REFLECTANCE OF ZINC OXIDE-SILICATE SUBSTRATE

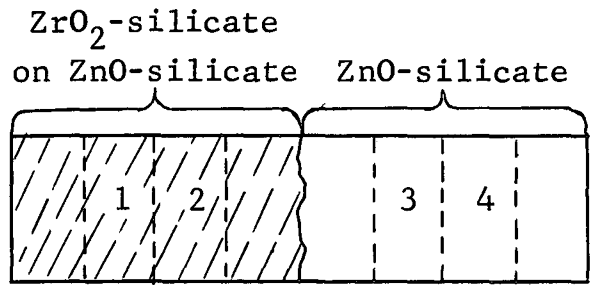

Figure 25 EXPERIMENTAL SAMPLE AND CUT SPECIMENS

As can be seen from Table 16, a comparison of original values, i.e., before irradiation, of samples 2 and 4 reveals the improvement in reflectance of the topcoated specimens. Upon heat treatment, the reflectance of zirconia (No. 1) decreased, but that of zinc oxide (No. 3) did not. Comparison of α_2 values of Z93 and the dual system with those of 5-19-6 shows the superior infrared reflectance of the dual systems.

Irradiation resulted in significant degradation of the topcoated samples. The heat-treated sample, however, was considerably more stable than the air-dried sample. A curious result was the inferior stability of the composite (Sample 2) in comparison to that of the pure zirconia coating.

4.4 Effect of Heat Treatment on Silicate Coatings

4.4.1 Effect on Reflectance

Although a number of experiments were performed to determine the effect on reflectance (and on optical stability) of heat treatment (Ref. 6), typical of the results are those obtained with potassium silicate paints pigmented with SP500 zinc oxide (Z93) and zirconium oxide (zirconia, Fluorescent Grade).

Coatings of these two materials were examined (Cary Spectrophotometer) before and after a 500°C treatment. Spectral curves appear in Figure 26. The zirconia film was applied on a Pyrex substrate, and the Z93 was applied on abraded aluminum. Both samples showed significant improvement in the infrared region;

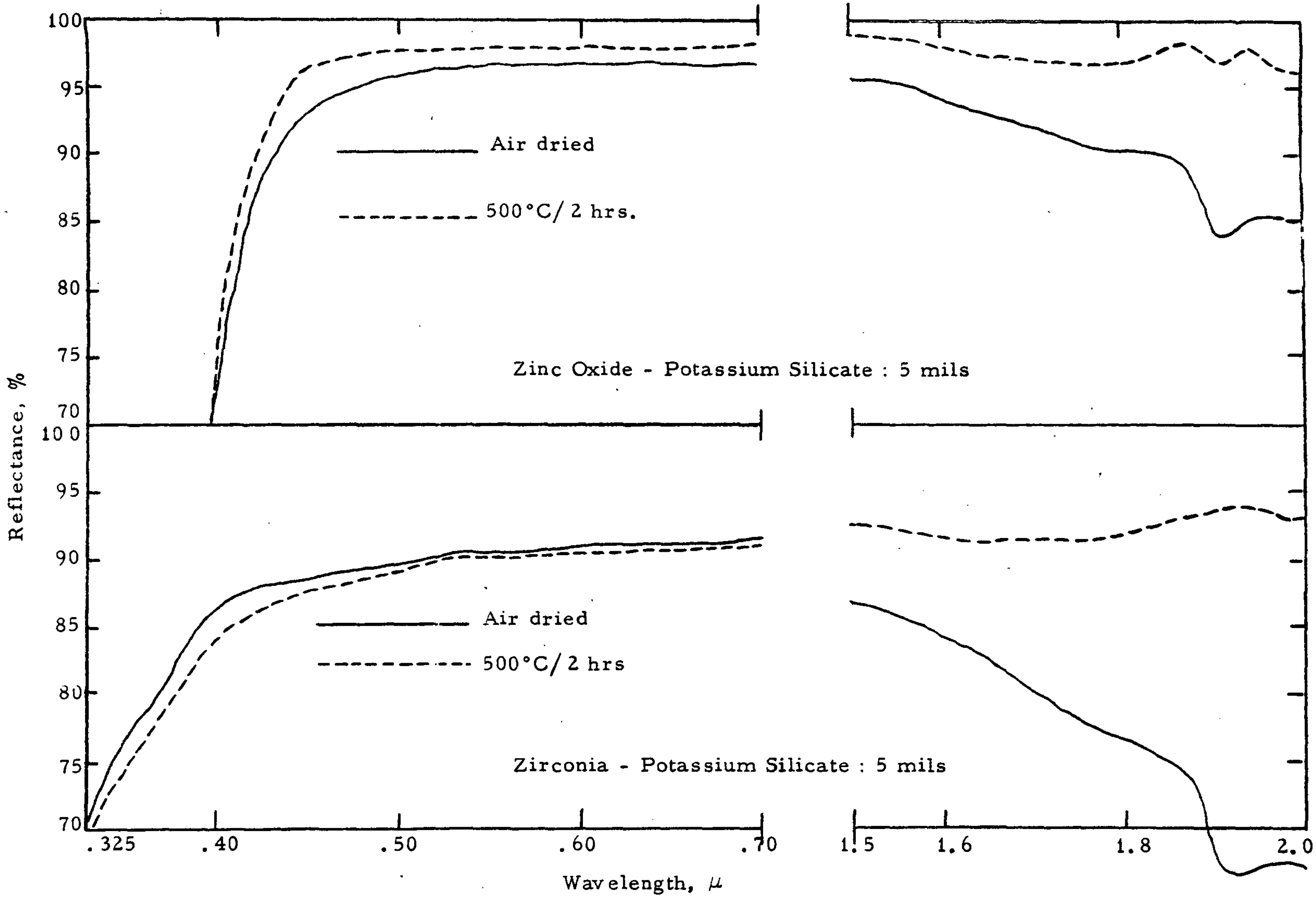

Figure 26 EFFECT OF HEAT TREATMENT ON REFLECTANCE OF ZnO AND ZrO_2 COATINGS

apparently the heat treatment results in volatilization of water and thus eliminates the water-absorption band that exists at about 1900 nm wavelength.

The observed improved reflectance in the infrared for silicate bonded coatings with heat treatment is not an irreversible phenomenon. Optical examination of heat-treated samples after periods of time showed that infrared reflectance drops slightly with time, indicating a reintroduction of the water band at about 1900 nm. However, this is a relatively slow process and time lapses of 30 days has only a small effect on solar absorptance.

4.4.2 Effect on Stability

A series of space-simulation experiments was conducted to examine the effects of heat treatment on the stability of silicate-bonded coatings. Samples of air dried and heat-treated silicate-bonded diatomaceous earth and zirconia (TAM C.P.) paints were subjected to ultraviolet irradiation in vacuum for 2000 ESH in one and 1020 ESH in another test. The results are given in Table 17.

The beneficial effect of the 500°C treatment on stability is obvious for both compositions and is stronger for the zirconia sample. A 150°C treatment did not appear to change the degradation characteristics for diatomaceous earth. In all cases a bleaching effect in the infrared portion of the spectrum resulted from irradiation for 2000 ESH.

A lowering of initial α_s was realized at lower heat treatments in the series irradiated for 1020 ESH; an increase resulted at the higher temperatures. The heat-treated paints exhibited a curious effect at the lower temperatures; mild heating produced a more degradable coating. Improvement in ultraviolet-vacuum resistance became apparent at 400 and 500°C. Also included in this experiment was a pigment sample of TAM's C.P. zirconia.

Table 17

EFFECT OF HEAT TREATMENT ON ULTRAVIOLET STABILITY OF SEVERAL SILICATE PAINTS*

Pigment	Heat Treatment	Exposure ESH	Solar Absorptance α_1	α_2	α_s	$\Delta\alpha$
Diatomaceous earth	None; air dried	0	0.075	0.097	0.172	
		2000	0.131	0.098	0.229	0.057
Diatomaceous earth	150°C/66 hr	0	0.075	0.094	0.170	
		2000	0.133	0.095	0.228	0.058
Diatomaceous earth	500°C/2 hr	0	0.072	0.090	0.163	
		2000	0.108	0.093	0.200	0.037
Zirconia	None; air dried	0	0.066	0.106	0.172	
		2000	0.141	0.106	0.247	0.075
Zirconia	500°C/2 hr	0	0.081	0.102	0.183	
		2000	0.110	0.100	0.210	0.027
Zirconia	Air dried	0	0.066	0.109	0.175	
		1016	0.162	0.103	0.265	0.090
Zirconia	Air dried	0	0.067	0.108	0.175	
	200°C/2 hr	0	0.068	0.103	0.171	
		1020	0.177	0.114	0.291	0.120
Zirconia	Air dried	0	0.067	0.107	0.174	
	300°C/2 hr	0	0.064	0.102	0.286	
		1020	0.174	0.112	0.286	0.120
Zirconia	Air dried	0 0	0.066	0.110	0.176	
	400°C/2 hr	0	0.075	0.108	0.183	
		1020	0.168	0.113	0.280	0.097
Zirconia	Air dried	0	0.068	0.110	0.177	
	500°C/2 hr	0	0.075	0.106	0.182	
		1020	0.140	0.109	0.249	0.067
Zirconia Pigment		0	0.041	0.056	0.097	
		1020	0.181	0.072	0.253	0.156

*Binder for all paints was PS7 potassium silicate. Diatomaceous earth paints had a pigment-to-binder ratio of 2.15 and the zirconia paints 4.30.

Much stronger degradation occurred for this pigment than for the silicate-bonded paints, indicating a protective effect for the vehicle.

4.5 Stability of PS7 Paints Prepared from Various Pigments

A large number of potassium silicate paints were prepared from various white pigments and were irradiated in the Quad-Ion facility described in section 2.3.1. As pointed out earlier, these non-in situ data are valid because, except for zinc orthotitanate, the pigments are dielectrics, which do not exhibit significant O_2-bleachable spectral damage. Additionally, the zinc orthotitanate-coatings data largely are relevant since potassium silicate paints do not exhibit significant O_2-bleachable spectral damage, even when pigmented with sensitive semiconductor pigments (e.g., zinc oxide and rutile titanium dioxide).

4.5.1 Early Zinc Titanates-Pigmented Silicate Coatings

Ultraviolet damage data for several zinc titanate paints are presented in Table 18. The earlier pigment studies led to the preparation of a series of silicate paints (Ref. 7, 9, 77), based on New Jersey Zinc Company's A-54-2 zinc titanate, later determined by x-ray analysis to be the orthotitanate. Although these data were certainly not conclusive, the results of the short exposure of the high-PBR paint (5.38), with a $\Delta\alpha_s$ of 0.005, and the heat-treated paint prepared from unheat-treated pigment, with a $\Delta\alpha_s$ of 0.029 in 2000 ESH of ultraviolet irradiation, led to further consideration, which subsequently resulted in research to successfully stabilize Zn_2TiO_4 (see Chapter 5). It should be noted also that the poor stability of the paint prepared from New Jersey Zinc pigment 602-26-1M, which did not contain excess zinc oxide, was considerably less stable than paints prepared from A-54-2, which contained excess ZnO.

4.5.2 Silicate Paints Prepared from Double Zircons

A series of silicate paints pigmented with double zirconium silicates, obtained from TAM, were prepared and irradiated in a

Table 18

EFFECT OF ULTRAVIOLET STABILITY ON
ZINC TITANATE-PIGMENTED POTASSIUM SILICATE PAINTS

Pigment No.	Heat Treatment		PBR	Exposure	Solar Absorptance			
	Pigment	Paint		ESH	α_1	α_2	α_s	$\Delta\alpha_s$
A-54-2*	700°C/16 hr	None	4.3	0	0.059	0.063	0.122	
				700	0.076	0.065	0.141	0.019
A-54-2	700°C/16 hr	500°C/2 hr	4.3	0	0.056	0.062	0.118	
				700	0.082	0.069	0.150	0.032
602-26-1M*	700°C/4 hr	500°C/2 hr	4.3	0	0.067	0.061	0.128	
				170	0.092	0.067	0.159	0.031
A-54-2	700°C/16 hr	None	5.38	0	0.039	0.027	0.066	
				330	0.044	0.027	0.071	0.005
A-54-2	None	500°C/1 hr	4.3	0	0.053	0.040	0.093	
				2000	0.081	0.041	0.122	0.029

*A-54-2 possessed excess ZnO; 602-26-1M did not possess excess ZnO.

series of Quad-Ion space simulation tests (Ref. 9, 73). The data are summarized in Table 19.

Examination of the compilation presented in Table 19 demonstrates that the solar absorptance, α_s, of unirradiated paints, as well as the change of solar absorptance due to irradiation, varies considerably with the heat treatment applied. These data indicate that annealing of the paint may cause a more significant improvement of the paint than calcination of the pigment alone. Heat treatment of the paint probably results in a better pigment-vehicle bond and thus in the formation of a more effective absorption-desorption barrier with respect to the surface of the pigment particles. Calcination of the pigment powder on the other hand essentially reduces the surface free energy of the pigment and may give rise to an improved ultraviolet stability of powder compacts due to a lower concentration of surface defects. A lower surface free energy of the pigment powder however, may also result in a decreased chemical activity and consequently in a poorer pigment-vehicle bond in the paint with the resultant possibility of photoinduced desorption of gases from the pigment particles.

The following conclusions were made:

1. Heat treatment of the double zirconium silicate powders increased $\Delta\alpha_s$. This might have been due to "fresh" surfaces that were created in "breaking" the powder after the heat treatment. The largest increase in $\Delta\alpha_s$ occurred with $CaZrSiO_5$ which had the lowest MP and thus would "sinter" at lower temperatures than the other two zirconium silicates.

2. The paints tended to be less stable than the pigments alone except for $CaZrSiO_5$.

3. In general, pigments heat-treated prior to paint preparation, except for $MgZrSiO_5$, exhibited inferior stability to paint heat-treated after application.

Table 19

EFFECT OF TREATMENT ON ULTRAVIOLET-STABILITY OF DOUBLE ZIRCONIUM SILICATES

Material	Treatment*	Binder	α_s Non-Irradiated	$\Delta\alpha_s$ (ESH)
$ZnZrSiO_5$	A	None	0.123	0.058 (2000)
	B	None	0.156	0.084 (2000)
	C	PS7	0.154	0.097 (1000)
	D	PS7	0.176	0.104 (2650)
	E	PS7	0.212	0.032 (2000)
	F	PS7	0.186	0.076 (2000)
$CaZrSiO_5$	A	None	0.115	0.044 (2000)
	B	None	0.136	0.080 (2000)
	C	PS7	0.165	0.012 (1000)
	D	PS7	0.138	0.126 (2650)
	E	PS7	0.178	0.021 (2000)
	F	PS7	0.136	0.099 (2000)
$MgZrSiO_5$	A	None	0.102	0.058 (2000)
	B	None	0.167	0.060 (2000)
	C	PS7	0.138	0.067 (1000)
	D	PS7	0.171	0.064 (2650)
	E	PS7	0.145	0.032 (2000)
	F	PS7	0.176	0.065 (2000)

*Treatment:
- A - As received, powder compact.
- B - Heat treated 800°C/12 hr powder compact.
- C - As received pigment, paint.
- D - Pigment heat treated 800°C/12 hr, paint.
- E - Pigment as received, paint heat treated 500°C/1 hr.
- F - Pigment heat treated 800°C/12 hr, paint heat treated 500°C/1 hr.

4. Except for $CaZrSiO_5$, heat-treatment of the paint increases stability. Heat treatment of the paints (using non-heat-treated pigment) has the most favorable effect on $\Delta\alpha_s$.

4.5.3 Silicate Paints Prepared from Other Pigments

A number of other pigments were employed in potassium silicate paints, variously heat treated, and irradiated in the Quad-Ion facility (Ref. 7, 9 77). Data from several space simulation tests are presented in Table 20. Of the various pigments employed in these coatings, the zirconium silicates (Zircon) and tantalum oxide paints were the most stable, albeit none of these coatings were of interest from the standpoint of resistance to ultraviolet-induced damage. Generally, like for the double zirconium silicates discussed in the previous section, these data show that heat treatment of the silicate paint has a beneficial effect on stability. This was particularly true for the yittria-, lanthana- and tantala-pigmented coatings.

The lithium fluoride data are included in Table 20 for another reason. The results of irradiation of pure lithium fluoride powder and the paint is a good example of the escalation of damage of the binder--even the reasonably stable PS7 potassium silicate, by a highly-ultraviolet-transparent dielectric pigment. The deep, multiple scattering in the system may have so effectively increased the path length of ultraviolet in the film that the silicate receives, in essence, a much greater dose of ultraviolet in any small volume ΔV within the film, with the result that the total extinction is greatly increased as a manifestation of the damage.

4.6 Stability of Calcium Tungstate-Pigmented Silicate Paint

Although both single and mixed tungstates, and zinc stannate, were studied as pigments, only calcium tungstate was examined as a paint (both PS7 potassium silicate and Owens-Illinois "650" silicone resin paints). However, only one specimen of calcium tungstate-pigmented potassium silicate was irradiated. It was prepared at a PBR of 4.3.

Table 20

EFFECT OF ULTRAVIOLET IRRADIATION ON SEVERAL SILICATE PAINTS

Pigment	Heat Treatment: Pigment	Heat Treatment: Paint	PBR	Exposure ESH	Solar Absorptance: α_1	α_2	α_s	$\Delta\alpha_s$
$ZrSiO_4$	800°C/16 hr		4.3	0	0.075	0.092	0.168	
				700	0.149	0.091	0.240	0.072
$ZrSiO_4$	800°C/16 hr	500°C/2 hr	4.3	0	0.076	0.079	0.155	
				700	0.140	0.085	0.225	0.070
Magnesium Aluminate Spinel	500°C/16 hr		2.5	0	0.038	0.099	0.137	
				700	0.178	0.104	0.282	0.145
Zirconium Spinel	1000°C/16 hr		4.3	0	0.058	0.047	0.104	
				2100	0.143	0.050	0.193	0.089
Zirconium Spinel	1000°C/16 hr	500°C/2 hr	4.3	0	0.043	0.034	0.076	
				2100	0.115	0.042	0.157	0.081
Y_2O_3			4.3	0	0.034	0.050	0.084	
				330	0.126	0.050	0.177	0.093
Y_2O_3		500°C/2 hr	4.3	0	0.028	0.044	0.072	
				330	0.084	0.048	0.132	0.060
La_2O_3			4.3	0	0.021	0.051	0.072	
				330	0.157	0.052	0.210	0.138
La_2O_3		500°C/2 hr	4.3	0	0.035	0.056	0.091	
				330	0.090	0.053	0.142	0.051
Ta_2O_5	800°C/2 hr		4.3	0	0.085	0.089	0.174	
				330	0.149	0.092	0.241	0.067
Ta_2O_5	800°C/2 hr	500°C/2 hr	4.3	0	0.070	0.060	0.131	
				330	0.082	0.055	0.137	0.006
Ta_2O_5		500°C/2 hr	4.3	0	0.108	0.087	0.195	
				2000	0.141	0.095	0.236	0.041
LiF		No binder used		0	0.017	0.024	0.041	
				330	0.050	0.027	0.078	0.037
LiF			4.3	0	0.039	0.061	0.099	
				330	0.144	0.062	0.206	0.107

The effect of 1200 ESH of ultraviolet irradiation in IRIF-II on a 5-mil specimen of this paint is shown in Figure 27. The spectral data shows that calcium tungstate-potassium silicate paints are certainly worthy of further study, since the paint was not severely degraded in the ultraviolet and visible spectral regions (the $\Delta\alpha_s$ was 0.03).

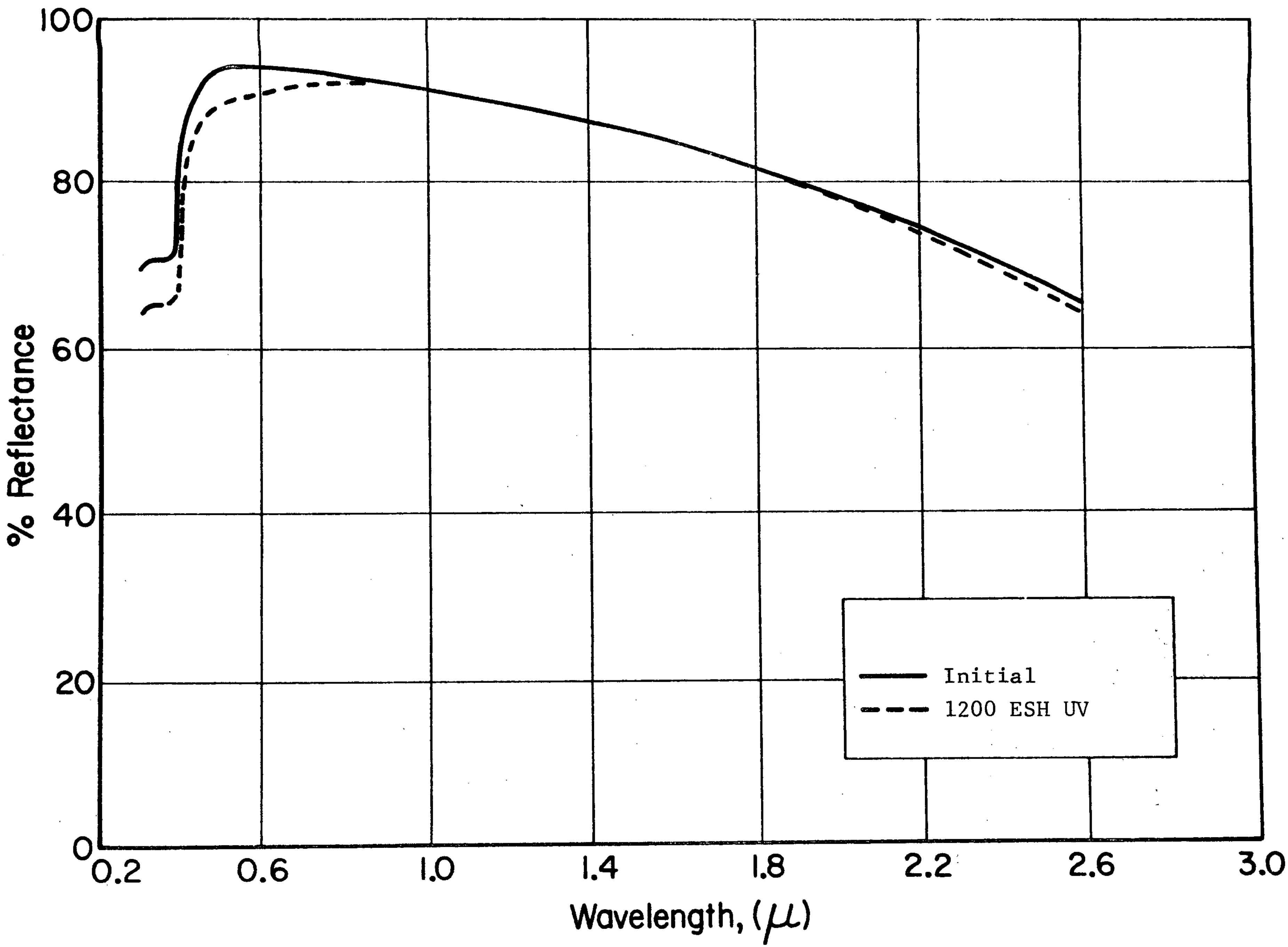

Figure 27 EFFECT OF UV IRRADIATION IN VACUUM ON A CALCIUM TUNGSTATE-PIGMENTED SILICATE (PS7) PAINT

5. SILICONE BINDER PHOTOLYSIS

5.1 Introduction

Silicone paint-binders were selected for use on early U.S. spacecraft due primarily to their high-energy -Si-O-Si- backbone compared to other polymeric binders then commercially available. These early coatings were based on heat-cured polyphenylmethylsiloxane resins. In studies performed in 1959-1961, one of the authors, G.A. Zerlaut (Ref. 78), found that the 100% methyl silicone resins were quite superior in optical properties and space ultraviolet stability to the then used phenyl/methyl systems. Subsequent study has not only confirmed these early results but also has shown that siloxane polymers, depending on the silicon ligand selected,are potentially the most stable candidates for use in the combined ultraviolet-plus-charged particle environment of deep space.

It was on the basis of the early experience with methyl silicone resins, the conclusions of which were subsequently reinforced by studies at IIT Research Institute for the Jet Propulsion Laboratory (Ref. 2, 72), that more basic synthesis and photolysis studies were undertaken on this program. These studies (Ref. 6, 7, 8, 12, 77, 79), which will be reviewed here, were undertaken for the dual purpose of improving upon both the physical characteristics and the ultraviolet radiation stability of methyl silicone resins, with the goal being their use as binders for white, spacecraft radiator coatings.

The synthesis studies reported were terminated when we discovered in 1964 that Owens-Illinois, Inc., of Toledo, Ohio, manufactured a 100% polymethylsiloxane resin, designated "650" Glass Resin, in pilot-production quantities. (Although both General Electric's Silicone Department and Dow Corning Corporation manufactured linear polydimethylsiloxane elastomers, neither commercially furnished a polymethylsiloxane resin. To the best of knowledge, no other 100% methyl resin is commercially available even today.)

However, even though the studies reported were not carried to completion due to the changed priorities created by the availability of the Owens-Illinois "650" resin, we are including the work here because of both its germaneness to the stability concepts of space-coatings materials in general, as well as because the work provides a likely departure for future research to extend the use of polysiloxanes to greater lifetimes and more hazardous radiation environments.

5.2 Radiation-Induced Changes in Polymers

Organic materials undergo chemical changes when subjected to radiation processes. These processes can be photolytic, gamma- or x-ray, or electron and other charged-particle radiation. The resulting chemical and physical changes that occur as a consequence of radiation depend on the conditions of the environment surrounding the system in question, i.e., the presence or absence of oxygen, pressure, temperature, etc. In polymeric systems, the degradative changes generally will be accompanied by cross-linking (chain scission and recombination), chain scission alone, and certain oxidative changes. These result from the reaction of free radicals formed in the polymer by the radiation processes.

Although the mechanisms can be both ionic and free radical, the latter processes are believed to predominate in polymers since free radicals are observed in solid polymers by electron paramagnetic resonance spectroscopy (EPR) in concentrations comparable to the resulting cross-link density (Ref. 80). For example, free radicals, trapped in the polymer, have been shown to cause color formation (Ref. 81-83). Miller (Ref. 84) demonstrated with EPR spectroscopy that irradiated polyvinyl chloride that has been exposed to air loses radicals at a much greater rate than when retained in vacuum. This loss of free radicals has been correlated with a loss of color formation which has been attributed to the formation of a peroxy radical by several investigators (Ref. 85, 86). Yegorova and coworkers (Ref. 87) have shown that the free-radical formation is temperature dependent, and St. Pierre and Dewhurst (Ref. 88) have demonstrated the total inhibition of carbon-carbon cross-links by the introduction of sufficient oxygen. The latter workers (Ref. 89) also demonstrated that oxygen terminates the radiation-induced free radicals by the formation of a carboxylic acid and two types of peroxides during the radiolysis of the dimer hexamethyldisiloxane. The loss of color (Ref. 90) in the presence of oxygen and the formation of oxidized end groups (Ref. 91) have also been demonstrated in the radiation of polyamides.

In the absence of oxygen, the generated free radicals are not destroyed. Indeed, in polymers below their glass transition temperatures, trapped free radicals are known to have very long lifetimes in the absence of both oxygen and light. In such cases, the resultant reactions are mainly disproportionation, which gives rise to chain scissions and migration, which in turn result in the formation of cross-links (Ref. 92, 93). In addition, if the free radicals are long-lived, color formation will be observed, as noted previously.

Lawton and coworkers (Ref. 94) have stated that the trapping of free radicals in polymer systems occurs (1) within the crystallites of the polymers, (2) in the amorphous phase below the glass transition temperature, and (3) in the heavily cross-linked polymers where radical recombination is less possible due to shielding of or attachment to the network. More recently, Ormerod (Ref. 95) has shown that hydrogen has a marked effect on radical decay rates in irradiated polyethylene, since free radicals can travel intra- and inter-molecularly.

5.3 Radiation-Induced Changes in Polysiloxanes

In 1960 Miller (Ref. 96) examined the electron irradiation of a linear polydimethylsiloxane oil in the absence of oxygen and found that both $\equiv Si \vdots CH_3$ and $\equiv SiCH_2 \vdots H$ scissions occurred with the evolution of H_2, CH_4 and C_2H_6 as the gaseous products, cross-linking was also observed on the basis of solubility characteristics. He also observed some anomalies in the overall radiation chemical effects in the transition from the fluid to the solid state. Subsequently, Miller (Ref. 97) observed a decrease in cross-linking in the presence of oxygen as a function of its partial pressure; he concluded that the residual cross-links were not peroxide bonds. He also found that hydrogen transfer agents (e.g., mercaptans) retarded cross-linking and that scission of the siloxane backbone was negligible in comparison to the propensity for cross-linking.

Subsequently, Ormerod and Charlesby (Ref. 98) examined the effect of electron radiation on a linear, unblocked dimethylsiloxane in the absence of oxygen. They also found a temperature-linked anomaly in the cross-linking reaction and concluded that the radiation chemistry differed between the solid and liquid states. They suggested that an ionic cross-linking mechanism might be possible at low temperatures, although a free-radical mechanism appears to predominate at room temperature where radicals are difficult to detect because of rapid reactions. As further confirmation of the two temperature-dependent mechanisms, they reported that stable free radicals could be produced in a vinyl-containing polysiloxane at room temperature, but not at low temperatures.

In a somewhat later paper, Charlesby and Garratt (Ref. 99) added small amounts of anthracene to the dimethylsiloxane polymer and found no protection against cross-linking. Sulfur gave more protection against cross-linking than could be explained in terms of radical combination--which is needed to explain the results with anthracene. Benzophenone afforded cross-linking protection, but from the lack of dose intensity dependence with anthracene combined with the results obtained with the other additives, they concluded, it was necessary to modify some present views on cross-linking. They proposed a different mechanism with each of the additives.

Miller (Ref. 97), by using electron radiation, had previously reported that benzene and tetralin both suppressed cross-linking in polydimethylsiloxane oils, with the suppression a function of added aromatic. In a later paper, Miller (Ref. 100) reported work on trimethylsilyl endblocked polydimethylsiloxane and on diphenylmethylsilyl endblocked polyphenylmethylsiloxane. He concluded that the radiation stability depends not only on total aromatic content but also on the types and positions of the aromatic substituents. Thus, conjugated aromatic substituents (e.g., biphenylyl and naphthyl) confer a greater stability than a single phenyl group. In addition, the aromatic group is most effective when it is attached to the same Si atom as the radiation-sensitive methyl group; he stated that the stabilizing effect of an aromatic group could not be effectively transmitted to a methyl group on a different Si atom. However, Koike and Danno (Ref. 101), by using gamma radiation, reported that in polydimethyldiphenylsiloxane the protective effect of the phenyl group may extend over 5 or 6 neighboring units of dimethylsiloxane.

Koike (Ref. 102) independently agreed with the work of Ormerod and Charlesby (Ref. 98) by concluding that below $-100°C$ the cross-linking of polydimethylsiloxane was due to non-radical processes. In contrast, however, Koike stated that cross-linking in polydimethyldiphenylsiloxane was temperature dependent and due to radical processes. They attempted to relate cross-linking to molecular motion of the group attached to the Si atom. Like the polymer studied by Ormerod and Charlesby, their polymer was not end-blocked.

It should be emphasized that, in the literature surveyed, radiation protection was synonymous with protection from cross-linking reactions. The optical properties of the polysiloxanes have been relatively ignored. Thus, we find that although aromatic groups confer radiation protection, only rare mention is made of their color-forming propensities, especially when irradiated with ultraviolet light.

In summary, color formation in polymers results from two general processes: (1) permanent color due to the formation of conjugated unsaturation, or of other chromophoric chemical groups, and/or (2) transient coloration due to the trapping of free radicals (i.e., electrons with unpaired spin) within the polymer network at temperatures below their glass transition points. Trapped radicals usually give rise to absorption bands whose presence are optically observable when the band intensity is sufficient to cause absorption at optical wavelengths; this absorption then becomes important in terms of increases in the solar absorptance of coatings prepared from them. Although degradation of polymers is manifested in both physical deterioration and optical changes, we generally estimate that greater than 10^{18} defects/cm^3 are required to cause physical changes in a polymeric material, while, on the other hand, only little more than 10^{14} defects/cm^3 are required to be visually observable. It is not surprising therefore that we have confined most of our investigations of materials for thermal control of spacecraft to the problem of coloration.

Since an important notion is that <u>the properties and behavior of the color centers produced are unrelated to the agency that created them</u>, the literature pertaining to electron- and gamma-irradiation of polymers has given us many qualitative ideas about what to look for and what to expect when we expose our polysiloxane polymers to ultraviolet and ultraviolet-plus-proton radiation.

5.4 Photolysis Studies

Ultraviolet photolysis experiments were conducted on five silicone polymers: three model polymers (a linear, unblocked polydimethylsiloxane, a nonlinear poly<u>dimethyl</u>siloxane resin and an oxidatively cross-linked poly<u>dimethyl</u>siloxane), General Electric Company's RTV-602 poly<u>dimethyl</u>siloxane elastomer, and Owens-Illinois "650" Glass Resin, a poly<u>monomethyl</u>siloxane.

5.4.1 Experimental

5.4.1.1 Synthesis of Model Polysiloxane

5.4.1.1.1 Linear, Unblocked Polydimethylsiloxane

A linear, low-molecular-weight model polymer was prepared by standard techniques but with the scrupulous avoidance of any aromatic contamination. It was prepared by first synthesizing octamethylcyclotetrasiloxane (Ref. 103), from which the polymer was later prepared.

A 2-liter 3-neck flask was assembled with a thermometer, stirrer, condenser, and an adding funnel protected with a drying tube. By using a syringe, the plastic bag technique was employed for transferring 400 ml of dichlorodimethylsilane (Union Carbide Corporation) in an atmosphere of prepurified nitrogen to the adding funnel. The silane was added as rapidly as dropwise addition would permit to 1200 ml of water, which had been previously charged into the flask. With the intermittent application of an ice bath, the temperature was maintained at 15 to 20°C throughout the vigorously stirred addition. The nonaqueous phase was extracted with 300 ml of diethyl ether, washed with water until neutral, and dried over sodium sulfate. After filtration, the solvent was removed on a rotating evaporator (Rinco), and the residue (~250 ml) was distilled rapidly through a 6 x 3/4-in insulated Vigreaux column. The fraction boiling at 164 to 171°C/745.5 mm was collected and weighed (123 g).

This fraction was then carefully redistilled by using the previously described apparatus. The fraction boiling at 170.0 to 173.0°C/738.7 mm was collected in two equal parts. Each of the two parts had an index of refraction, $N_D^{27.6} = 1.3932$. This value is in essential agreement with that reported by Hunter (Ref. 104) and the boiling point reported (Ref. 103) is the same. A total of 81 g of the cyclic tetramer was obtained, from which the linear polydimethylsiloxane was prepared by catalytic rearrangement.

Into a 250 ml g.s. Pyrex bottle was charged 52 ml of the cyclic tetramer (octamethylcyclotetrasiloxane), 25 ml diethyl ether, and 9.6 ml of conc. sulfuric acid. The stopper was secured by wire and the bottle allowed to shake in an Eberbach shaking machine for 24 hr at ambient room temperature. After this time, the thick mass was diluted with 50 ml of diethyl ether, 25 ml of water was added and the bottle was shaken for 1 hr. The solvent was separated and washed with three 10-ml portions of water. The still-acid solvent layer was diluted a little further with ether and dried over solid, anhydrous potassium carbonate.

The filtrate was placed on a rotating evaporator to remove the solvent, and the residue was distilled through a long Claisen adaptor by using a Woods' metal heating bath. At still-pot temperatures up to 360°C, a few milliliters of liquid distilled at temperatures up to 117°C. The residue was allowed to cool in an atmosphere of prepurified nitrogen. The molecular weight of the residue averaged 3,030 by Mechrolab vapor pressure osmometer determination.

Analysis (Ref. 105): Found: H, 7.77, 8.09; C, 31.90, 31.84; Si, 34.59, 34.89. Calcd. for $(CH_3)_2SiO$: H, 8.16; C, 32.38; Si, 37.86.

The absorption spectrum of this polymer in isooctane was better than 98% transparent from 400- to less than 190-nm wavelength, as shown in Figure 28. The CH_3:Si ratio was close to the theoretical value of 2. At the pressures required for photolysis and at room temperature, about 10 to 15% of the polymer distilled over a 16-hr period.

5.4.1.1.2 <u>Oxidatively Cross-Linked Polydimethylsiloxane</u>

A flask equipped with a two-way addition tube fitted with a gas-inlet tube and a reflux condenser was employed to cross-link a cyclic polysiloxane by the method of Hyde and Delong (Ref. 106). The flask was charged with the cyclic polysiloxanes

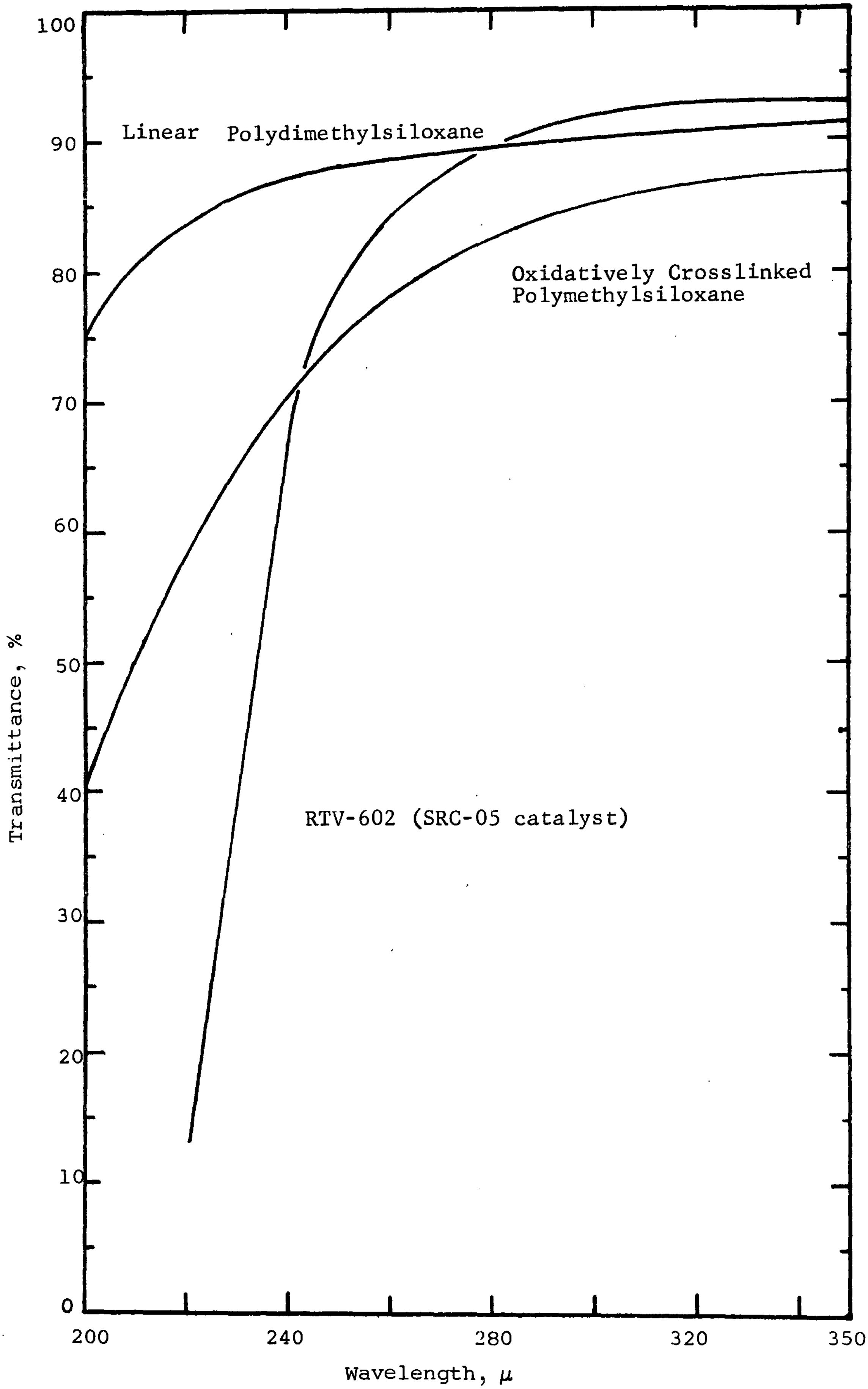

Figure 28 TRANSMITTANCE OF SILICONE POLYMERS

(pentamer and higher) obtained from the hydrolysis of dimethyldichlorosilane. This material was heated by means of a Woods metal bath to 220 to 230°C (pot temperature) for 16 hr while a slow current of air was continuously bubbled through the polymer. The resulting cross-linked material was of jello-like consistency and was water-white with an excellent ultraviolet transmission, 65% at 220 mμ and 40% at 200 mμ.

Analysis (Ref. 105): Found: C, 32.34; H, 8.06; Si, 33.51. Calcd. for $(CH_3)_2SiO$: C, 32.38; H, 8.16; Si, 37.88.

The transmission spectra of the oxidatively cross-linked polymer is also shown in Figure 28 and is compared with the linear polymer from which it was prepared and the linear RTV-602 obtained from the General Electric Company.

5.4.1.1.3 <u>Nonlinear, Polydimethylsiloxane Resin</u>

Six-tenths moles (77.4 g) of dimethyldichlorosilane (99.4%) and 0.4 moles (60 g) of methyltrichlorosilane (95%) were mixed in 300 g of anhydrous ethyl ether. The resultant mixture was added dropwise with agitation, over a period of 40 min, to 1000 g of ice. The ether layer was separated and washed once with distilled water. It was then washed once with a 5% solution of sodium bicarbonate, followed by three washings with distilled water. The ether solution was then dried overnight with Drierite and evaporated at reduced pressure leaving a semi-viscous, colorless oil. The Me/Si was calculated to be 1.6.

The above stock was then distilled at an average temperature of 100°C and 4×10^{-3} torr. The upper molecular weight fraction was collected and employed in photolysis studies. The molecular weight was found to be 2050 by vapor osmometry.

5.4.1.2 <u>Photolysis</u>

5.4.1.2.1 <u>Facility</u>

The photolysis investigation was conducted in the facility shown in Figure 29. The glass vacuum manifold was pumped by a

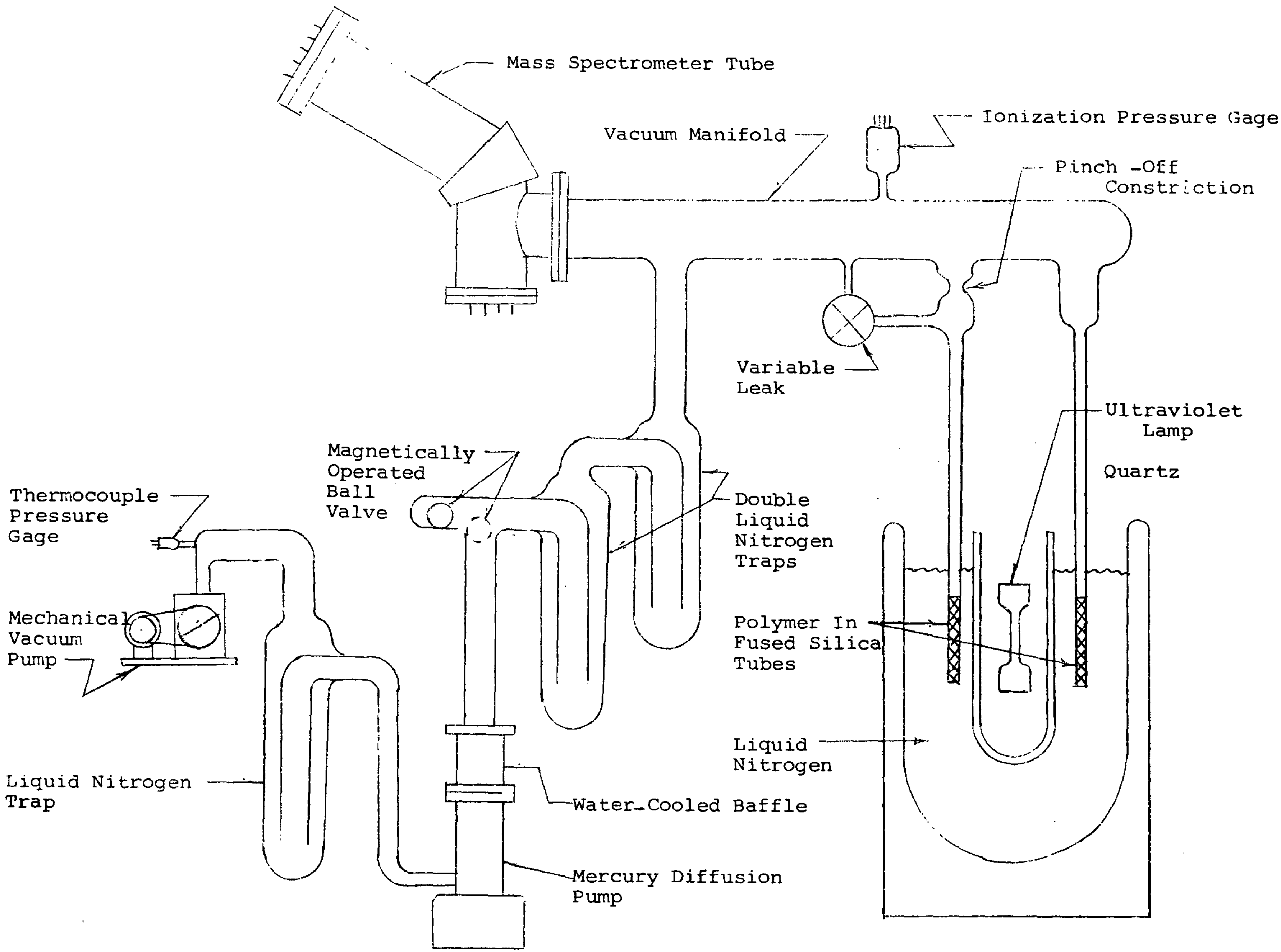

Figure 29 GLASS VACUUM SYSTEM FOR POLYMER IRRADIATION STUDIES

mercury diffusion pump through two liquid nitrogen traps, producing a net pumping speed of approximately 1 liter/sec for noncondensible species. Pressures in the range of low to mid 10^{-7} torr were ordinarily produced in the empty system after a mild bake-out at 150°C. Pressures in the 10^{-3} to 10^{-7} torr range were measured with a hot-filament ionization gage. The residual gases in the manifold were analyzed with a 60-degree-sector field Nier-type mass spectrometer (Vacuum Electronics Corp., model GA-4). This instrument has an ultimate sensitivity for nitrogen of 10^{-13} torr and a working sensitivity in these experiments below 10^{-10} torr. The mass range is 2 to 300 AMU.

The polymer specimens were contained in 4-mm OD fused-silica tubes and were irradiated with an A-H6 lamp through a quartz envelope of approximately 1-mm thickness at a distance of 4 cm measured from the lamp centerline to the polymer centerline, with about 3 cm of the intervening distance filled with liquid nitrogen.

5.4.1.2.2 Procedures

The polymer was irradiated by attaching the fused silica polymer tube onto the glass manifold with graded seals. A vacuum below 10^{-6} torr was obtained, and liquid nitrogen was slowly admitted to the Dewar surrounding the sample tube. The liquid nitrogen was replenished automatically by a controller, which maintained the liquid level at approximately ± 2 cm from a preset level. Tests were conducted with a continuous gaseous nitrogen purge of the lamp cavity to preclude condensation of water from the atmosphere on the inside of the quartz tube.

The polymer was irradiated for a predetermined time. The unshunted polymer tube was then removed, still under a typical vacuum and at liquid nitrogen temperature, for electron spin resonance measurements. The shunted polymer tube was warmed to room temperature, and the evolved gases were analyzed with the mass spectrometer. After irradiation, the left polymer tube was sealed from the vacuum manifold at the constriction, and the evolving gases were bled into the manifold with the variable leak at a rate sufficiently slow that accurate mass spectrometric analyses could be made.

Mass spectrometer analyses of the residual gases were made on the empty system before the polymer tubes were attached, on the system with the polymer tubes attached and at room temperature, after cooling to liquid nitrogen temperatures, during irradiation, after irradiation while the polymer was still cold, while the evolved gas from the room temperature sample was being bled into the system, and again with the empty system after the polymer tubes were removed.

5.4.2 EPR Analyses

5.4.2.1 Linear, Unblocked Polydimethylsiloxane (Me/Si=2)

Although two irradiation experiments were performed employing the facility described in Figure 29, no EPR spectra could be generated in either test (at exposures of 2 and 5 hr A-H6 irradiation). No color developed in either sample, although slight gellation occurred in the 2 hr exposure. The extreme transparency probably accounts for the lack of gross effects, the conclusion of which is that insufficient energy was absorbed.

5.4.2.2 Nonlinear Polydimethylsiloxane (Me/Si=1.6)

The EPR absorption spectrum observed in the ultraviolet-irradiated, silicone polymer of Me/Si=1.6 is essentially the same as those observed by other investigators (Ref. 98, 107). Trace recordings of the spectrum are shown in Figures 30 and 31, where Figure 31 is the same as Figure 30 multiplied in amplitude by a factor of five. This spectrum is essentially the same as that observed in this laboratory on the irradiated, solid, cross-linked polydimethylsiloxane (Section 5.4.2.4). Note in Figure 31 the weakest lines labeled a_i. Although the lines a_2 and a_4 are observed in these traces, if they are postulated to exist so as to form a quartet spectrum, this group of lines may be identified with $\cdot CH_3$ radicals which are unstable at 77°K. This probably

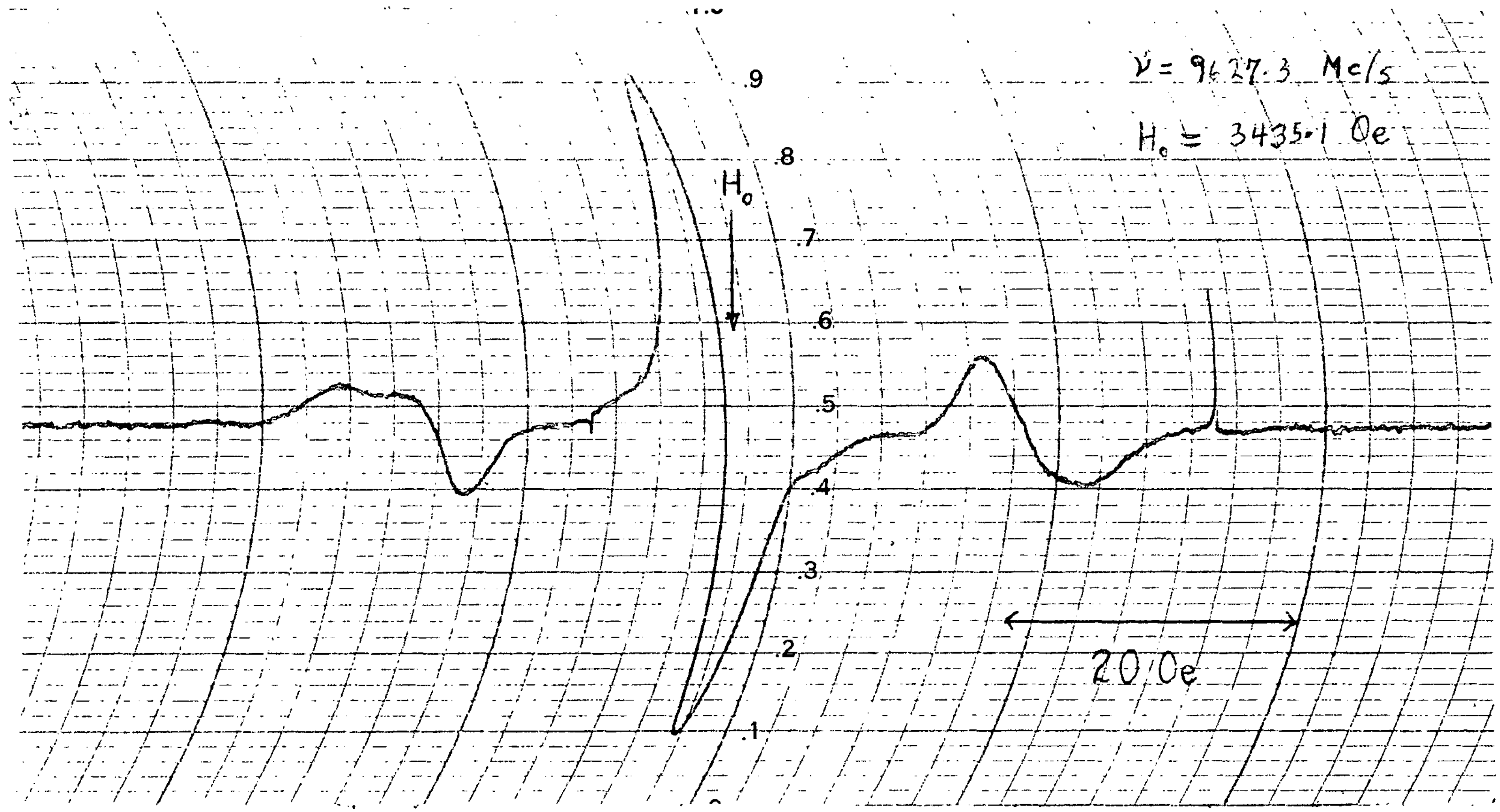

Figure 30 ELECTRON-SPIN-RESONANCE-ABSORPTION SPECTRUM OF LP-5 POLYDIMETHYLSILOXANE IRRADIATED WITH UV AT 77°K

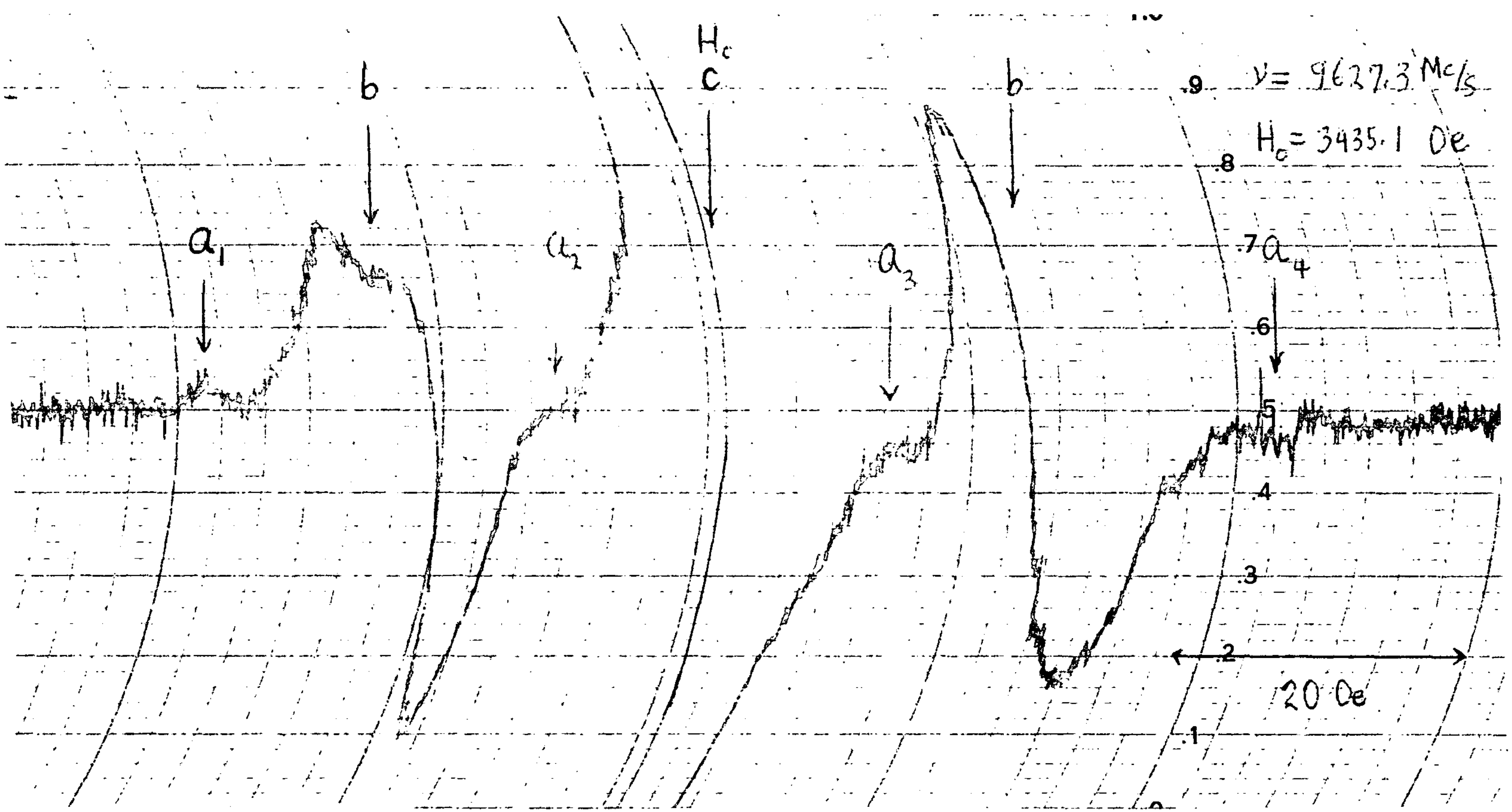

Figure 31 ELECTRON-SPIN-RESONANCE-ABSORPTION SPECTRUM OF LP-5 POLYDIMETHYLSILOXANE IRRADIATED WITH UV AT 77°K (Same as Figure 30 with Gain Times 5)

explaines their low intensity since these spectra were taken several hours from the time of irradiation.

The unpaired electron of the methyl radical interacts with three hydrogen nuclei, each having a nuclear spin quantum number of 1/2. Four magnetic dipole transitions are expected for this system corresponding to the nuclear magnetic quantum numbers $m = 3/2, 1/2, -1/2, -3/2$. The $m \pm 3/2$ transitions are the outer lines labeled a_1 and a_4 in Figure 31. The $m \pm 1/2$ would be the lines labeled a_2 and a_3 and are predicted to be three times more intense than the $m = \pm 3/2$ transitions since there are more ways of adding up the individual magnetic quantum number of the three hydrogen nuclei to give $m = \pm 1/2$. Energy eigen values for this system in the strong field limit are given by

$$E(M,m) = g\beta HM + AMm \qquad (2)$$

where β is the Bohr magneton, H is the external magnetic field, g is the gyromagnetic ratio, A is the hyperfine splitting constant, and where we have neglected the nuclear Zeeman interaction (Ref. 108). Transitions labeled a_1 and a_4 correspond to the $m = 3/2 \rightarrow 3/2$, $M = 1/2 \rightarrow 1/2$ and $m = -3/2 \rightarrow -3/2$, $M = -1/2 \rightarrow -1/2$ transitions where M is the electron magnetic quantum number having two possible values $\pm 1/2$. The condition of resonance of these transitions are obtained from Equation (2) using the selection rules $\Delta M = \pm 1$, $\Delta m = 0$ giving

$$E(1/2,\ 3/2) - E(-1/2,\ 3.2) = g\beta H_1 + \frac{3}{2} A \qquad (3)$$

$$E(1/2,\ -3/2) - E(-1/2,\ -3/2) = g\beta H_4 - \frac{3}{2} A \qquad (4)$$

where H, and H_4 are the resonance field position of a_1 and a_4. Since these transitions occur at constant microwave frequency ν, we set Equations (3) and (4) equal to $h\nu$, divided by $g\beta$ and solve for A and g. The result is

$$\frac{A}{g\beta} = H_4 - H_1 \qquad (5)$$

$$g = \frac{2h\nu}{H_1 + H_4} \tag{6}$$

From the experimental data we have H_1 = 3400.2 oe, H_4 = 3466.1 oe at ν = 9627.8 Mc/s. Substituting these values in Equations (5) and (6) gives $A/g\beta$ = (22.1 ± 0.5) oersteds and g = 2.0037 ± 0.0010. These results are in good agreement with the values $A/g\beta$ = (21.9 ± 0.2) oersteds, g = 2.0026 (1) and $A/g\beta$ = 22.9 oersteds, g = 2.00242 (8) for CH_3 radicals trapped in Zeolite and CH_4 matrices, respectively (Ref. 108). The errors in the parameters for the present case are large since the spectral lines are weak and not completely resolved.

Although Tsvetkov et al (Ref. 107) have given tentative assignments to the remaining spectra labeled b and c in Figures 30 and 31, it is not clear that these identifications are correct. For example, the lines which they call group b appear to be a superposition of at least two spectra whereas this point was previously overlooked (Ref. 98). It is not obvious that lines labeled b belong to a triplet spectrum as suggested by Tsvetkov. It may be possible to preferentially bleach out some of the lines at various temperatures to determine if these assignments are valid. The g-value measured for the central component labeled c in Figure 31 is given by g = 2.0026 ± 0.0005.

5.4.2.3 Uncured RTV-602 (Me/Si=2)

Figure 32 is a trace of the EPR spectrum of ultraviolet irradiated RTV-602 polydimethylsiloxane taken at 77°K immediately following the irradiation. It is noted that this spectrum is significantly different from that obtained with the irradiated specimen of Me/Si=6 (see Figures 30 and 31) with the appearance of at least two other lines labeled H_{x_1} and H_{x_2} on the recorder tracing. This suggests the presence of three or more paramagnetic species, one associated with the components $H_y{}^1$, $H_y{}^2$ and H_o (where $H_y2 - H_y1$ = 35 gauss) the second associated with H_{x_1} and H_{x_2} and the third associated with H_{z_1} , H_o and H_{z_2}

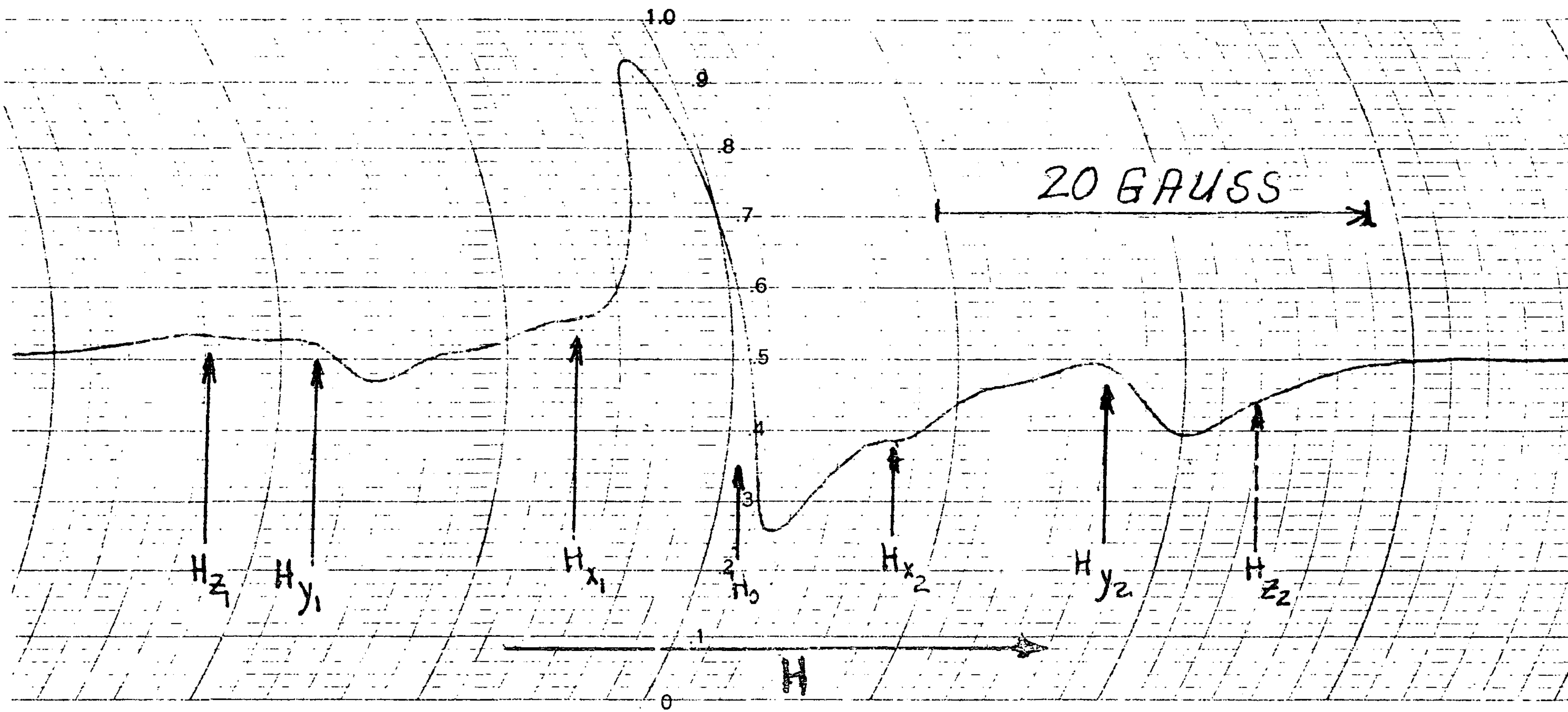

Figure 32 ESR SPECTRUM OF ULTRAVIOLET IRRADIATED RTV-602 (LP-4)

(unresolved). Also, the central line is highly asymmetric. The line width measured between points of inflection is approximately 4.5 gauss. The large asymmetry in the central line (labeled H_o) is probably due to the superposition of two or more lines which are shifted by some small amount. If the radicals associated with the y and z species give triplet spectra when their central components would be shifted from one another to give the asymmetric line observed at H_o. Since the central component is stronger than the sum of the outer components of y and z there is most likely at least one singlet at this field position.

5.4.2.4 <u>Oxidatively Cross-linked Polydimethylsiloxane</u>

Figure 33 presents the electron paramagnetic resonance spectrum of the irradiated, solid, oxidatively-cross-linked polymer. The results show the presence of one central strong line and groups of weaker lines. The center line has a g value of 2.0026 which is very close to the free spin value of 2.0023. The subsidiary lines could be hyperfine lines associated with the main line, but this is unlikely in view of the fact that the weaker lines appear to be broader than the main line. Rather it seems that the weaker lines are due to a separate paramagnetic species associated with a center having a nuclear spin I of 1/2. There are some structures associated with these weaker lines, suggesting that a further set of weaker lines exists. The data are consistent with this third center being associated with two nuclei, each of spin 1/2, although the resolution of the spectrum is not high enough to allow this to be stated unequivocally.

5.4.2.5 <u>Owens-Illinois 650 Polymonomethylsiloxane</u>

A fairly weak EPR spectrum was observed in one sample; <u>no EPR spectra could be induced by ultraviolet in a second specimen.</u> Three lines similar to the RTV-602 spectra (Figure 32) were observed. The central line is again highly asymmetric and the high field satellite line is unresolved. The spectra is

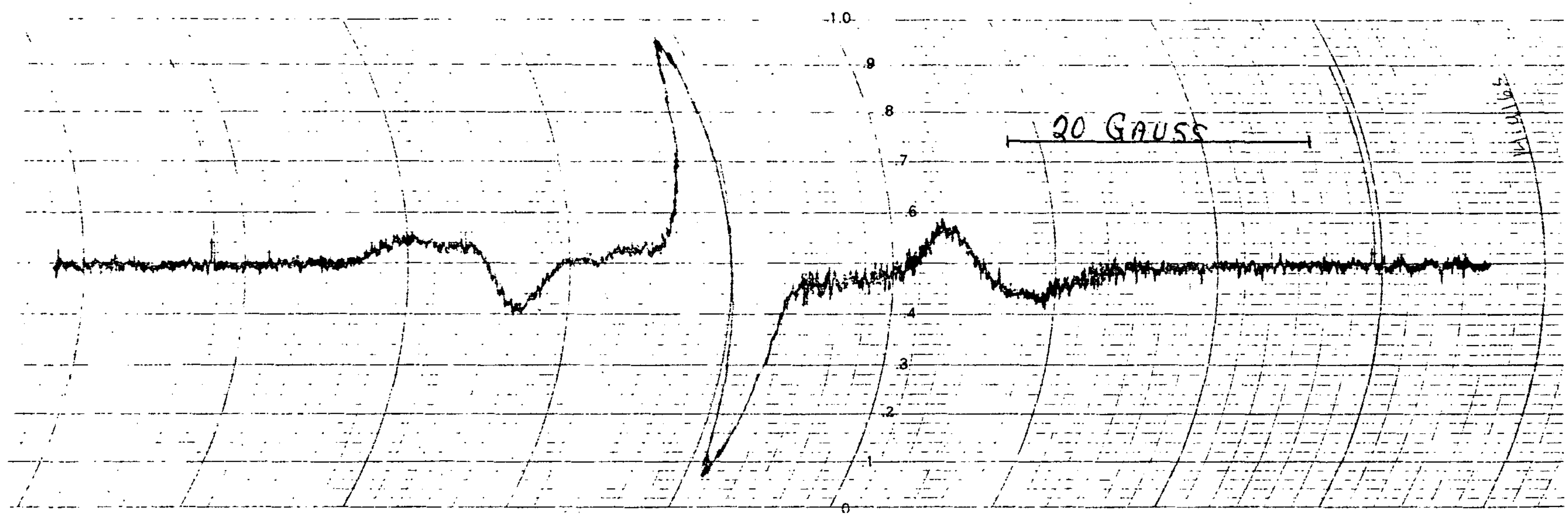

Figure 33 ELECTRON-SPIN-RESONANCE-SPECTRUM OF IRRADIATED, SOLID, CROSS-LINKED POLYDIMETHYLSILOXANE

presented in Figure 34. This spectrum is seen to be different from previous spectra because of the absence of the low field satellite line.

5.4.3 Mass Spectrometry

5.4.3.1 Linear, Unblocked Polydimethylsiloxane (Me/Si=2)

Although mass spectra data were taken, and reduced to tabular form, the data were too inconclusive to warrent presentation. Hydrogen, methane and carbon dioxide were evolved when the irradiated, liquid polymer was warmed from 77°C to room temperature.

5.4.3.2 Nonlinear Polydimethylsiloxane (Me/Si=1.6)

Mass spectra of the irradiated nonlinear polydimethylsiloxane with Me/Si of 1.6 were obtained but not resolved.

5.4.3.3 RTV-602 Polydimethylsiloxane (Me/Si=2.0)

The mass spectra data for the uncured RTV-602 are tabulated in Table 21. An increase in hydrogen was observed after completion of ultraviolet irradiation when the gas from the warmed polymer was bled into the mass spectrometer. The hydrogen content decreased from a relative peak height of 140 prior to irradiation to approximately 50 during irradiation; the peak height increased when the A-H6 lamp was turned off, however. The methane content (14, 15 and 16 m/e) decreased during radiation with no subsequent change after irradiation. The water content (18 m/e) decreased during the irradiation.

5.4.3.4 Oxidatively-Cross-linked Polymethylsiloxane (Me/Si 2)

The mass spectra from the irradiation of the oxidatively cross-linked polymer are given in Table 22. Only modest amounts of methane evolution was observed; however, a significant increase in m/e 12 (C^+) was observed. The hydrogen content of the system increased somewhat when the polymer tubes were attached, although no increase in intensity resulted from the irradiation.

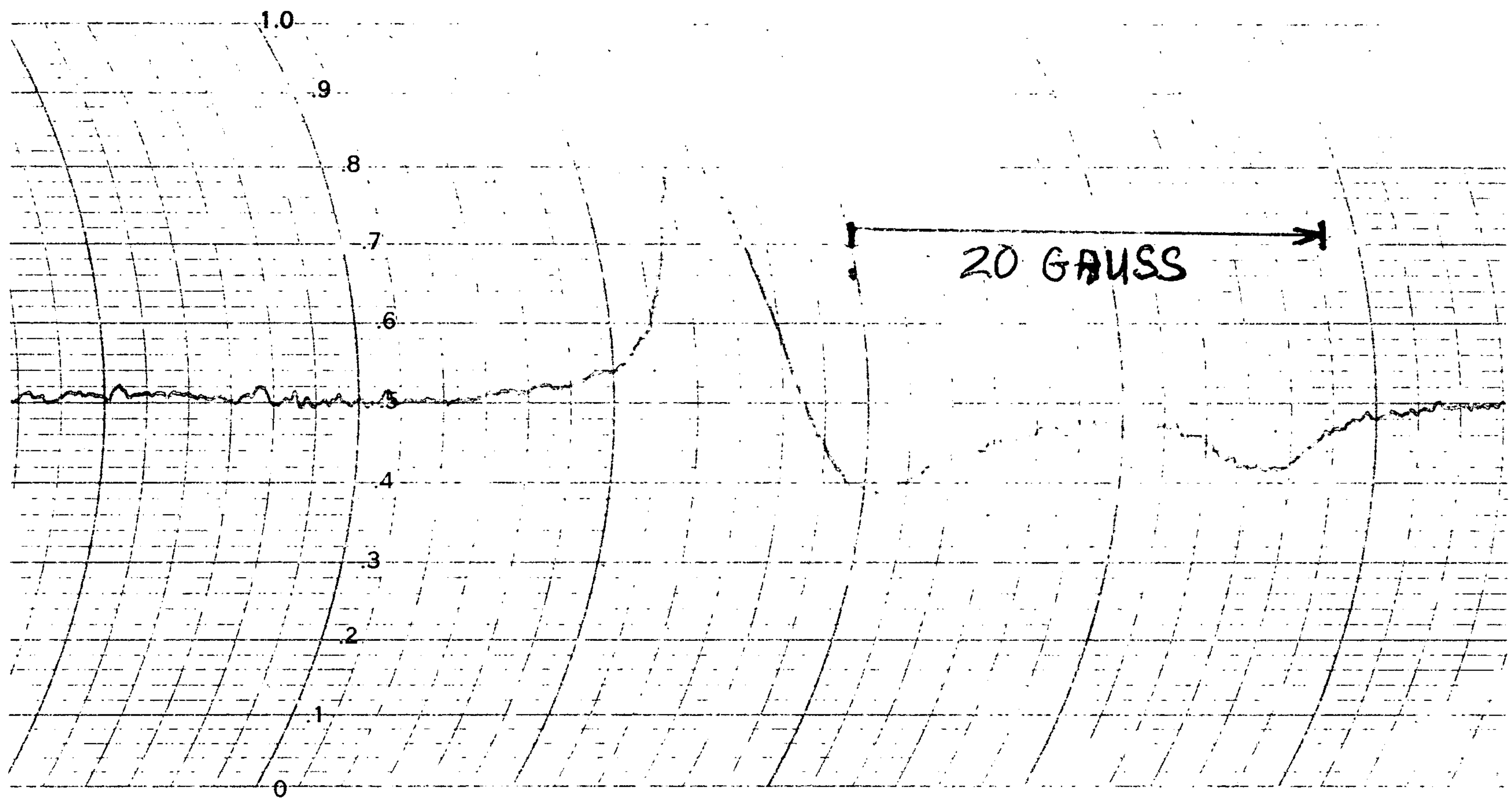

Figure 34 ESR SPECTRUM OF ULTRAVIOLET IRRADIATED OWENS-ILLINOIS TYPE 650 SILICONE

Table 21

MASS SPECTRA OF IRRADIATED UNCATALYZED RTV-602

m/e	Probable Gas Species	Warm Polymer Background	Polymer under LN_2	Polymer under UV + LN_2	Polymer under LN_2 only	Warm Polymer Gas Bleed
2	H^+	140	49	50	114	366
12	C^+	6	4.6	4.6	1.4	1.7
13	CH^+	0.6	0.5	0.3	0.3	Trace
14	CH_2^+, N^+	6	8.9	8.9	8.5	9.4
15	CH_3^+	5	3.3	2.4	3.8	3.1
16	CH_4^+, O^+	10.6	6.8	5.5	0.5	4.7
17	OH^+, CH_5^+	22	8.6	5.6	3.1	3.1
18	H_2O^+	109	26.4	16.1	10	11.3
25	C_2H^+	Trace	Trace	Trace		
26	$C_2H_2^+$	1.1	0.9	0.7	0.4	0.6
27	$C_2H_3^+$	1.9	1.1	1.1	0.7	1.2
28	$C_2H_4^+, CO^+, N_2^+$	100	100	100	100	100
29	$C_2H_5^+$	2.2	1.4	1.1	1.3	2.2
30	$C_2H_6^+$	0.6	Trace	0.3	0.2	Trace
32	O_2^+	1.8	1.7	1.6	0.5	Trace
39	$C_3H_3^+$	0.2	0.2	Trace	Trace	Trace
40	C_2O^+, A^+	0.2	0.2	0.5	0.9	0.9
44	CO_2^+	4.3	4.3	4.8	1.7	1.3

Table 22

MASS SPECTRA OF IRRADIATED OXIDATIVELY CROSSLINKED POLYDIMETHYLSILOXANE

m/e	Probable Gas Species	Warm Polymer Background 2.4×10^{-6}	Polymer under LN_2 7.5×10^{-7}	Polymer under LN_2 & UV 8×10^{-7}	Warm Polymer Gas Bleed 8.5×10^{-7}
2	H^+	1300	3400	1770	1350
12	C^+	37	43	164	176
13	CH^+	10	22	15	32
14	CH_2^+, N^+	21	51	34	36
15	CH_3^+	44	104	30	37
16	CH_4^+, O^+	56	116	100	158
17	OH^+, CH_5^+	28	12	27	5
18	H_2O^+	67	20	40	7
25	C_2H^+	2	4	2	7
26	$C_2H_2^+$	8	14	8	3
27	$C_2H_3^+$	11	16	8	3
28	$C_2H_4^+, CO^+, N_2^+$	100	100	100	100
29	$C_2H_5^+$	6	5	4	2
30	$C_2H_6^+$	2	2	1	1
32	O_2^+	0.3	0.4	Neg.	Neg.
36	C_3^+	1.3	1.3	Neg.	Neg.
39	$C_3H_3^+$	3.9	3.9	2	Neg.
40	C_2O^+, A^+	0.9	1.4	Neg.	Neg.
44	CO_2^+	14	4.1	16	4

It appears, however, that the irradiation again liberated carbon dioxide (CO_2^+, 44 m/e; C^+, 12 m/e).

5.4.3.5 Owens-Illinois 650 Polymonomethylsiloxane (Me/Si=1)

The mass spectra of the irradiated Owens-Illinois Type 650 resin are tabulated in Table 23. Although the hydrogen peak decreased on irradiation, considerable hydrogen was trapped in the frozen polymer. Little increase in m/e 12 through 16 was observed; however, the peak corresponding to m/e 17 (OH^+, CH_5^+) increased after an initial decrease during irradiation; the peak increased still further when the polymer was warmed. The peak for m/e 18 behaved similarly to that corresponding to m/e 17. Peaks corresponding to m/e 29 ($C_2H_5^+$) and m/e 31 exhibited significant increases when the frozen polymer was warmed.

5.4.3.6 RTV-602 Polydimethylsiloxane Cured with SRC-05 Catalyst (Amine Functional)

The mass spectra results of solid RTV-602 (catalyzed at 0.4% with SRC-05) are presented in Table 24. The hydrogen peak not only increased when the LN_2-cooled polymer was irradiated but increased still further when the polymer was warmed and the gases bled to the spectrometer. Methane peaks (12, 13, 15, 16 and 17 m/e) increased on irradiation and peaks at 14, 15 and 17 increased still further when the gases trapped in the polymer were bled to the spectrometer. Water (18 m/e) appears to have been trapped in the irradiated, frozen polymer. An interesting observation is the increase in the m/e 29 peak, which could have been $C_2H_5^+$, when the irradiated polymer is warmed. Similarly, the m/e 39 peak ($C_3H_3^+$) increased when the polymer was warmed.

5.5 Summary of Photolysis Studies

The pertinent data from the photolysis experiments are tabulated in Table 25. Although these studies were incomplete, the data were strongly predictive of the direction that silicone binder technology for near-earth spacecraft has gone--namely to the "cleanest" polymethylsiloxanes possible.

Table 23

MASS SPECTRA OF IRRADIATED OWENS-ILLINOIS TYPE 650 RESIN (HEAT CURED)

m/e	Probable Gas Species	Warm Polymer Background	Polymer under LN_2 only	Polymer under LN_2 + UV	Warm Polymer Gas Bleed
2	H^+	2110	760	248	554
12	C^+	10.8	5	13.5	13.4
13	CH^+	6*	1	3.4	3.5
14	CH_2^+, N^+	23	12	11.1	10.2
15	CH_3^+	53	15	20	26.8
16	CH_2^+, O^+	44.5	16	27	23.2
17	OH^+, CH_5^+	32.8	20	25.7	32
18	H_2O^+	97.5	72	77	98
25	C_2H^+	12	Trace	0.3	0.4
26	$C_2H_2^+$	72	4	2.7	1.8
27	$C_2H_3^+$	16.9	8	4.9	2.9
28	$C_2H_4^+, CO^+, N_2^+$	100	100	100	100
29	$C_2H_5^+$	16.4	5	3.4	14.7
30	$C_2H_6^+$	4.8	2	2.7	2.9
31		4.2	1	0.3	15.3
32		3	3	2.7	8.9
36	C_3^+	Trace	1	0.9	Trace
39	$C_3H_3^+$	3.6	2	1	0.1
40	C_3O^+, A^+		1	0.6	0.3
41		20	3	2	0.4
42		3	1	0.4	0.3
43		Trace	4	0.4	1.4
44	CO_2^+	7.2	14	24	13

*m/e = 13.5 value trace

Table 24

SUMMARY DATA OF TEST SP-3 (RTV-602/0.4% SRC05)

m/e	Probable Gas Species	Warm Polymer Background	Polymer under LN_2 only	Polymer under LN_2 + UV	Warm Polymer Gas Bleed
2	H^+	370	140	382	470
12	C^+	5.8	5	10	0.3
13	CH^+	1.8	2.5	4.2	4.7
14	CH_2^+, N^+	9.7	7.5	12.5	14.9
15	CH_3^+	23.6	25	35	59.3
16	CH_4^+, O^+	18	28	35	14.4
17	OH^+, CH_5^+	43	14	10	25
18	H_2O^+	182	46	27.6	84
25	C_2H^+	0.4	Trace	0.8	3
26	$C_2H_2^+$	3.3	3	5	11
27	$C_2H_3^+$	10.8	8	11.6	10
28	$C_2H_4^+, CO^+, N_2^+$	100	100	100	100
29	$C_2H_5^+$	5.1	3.5	4.2	54
30	$C_2H_6^+$	12.2	5.0	4.2	5.8
31		0.8	Trace	Trace	1
32		0.4	1	2.1	1.2
36	C_3^+	Trace	Trace	Trace	1
39	$C_3H_3^+$	1.7	1	0.8	3.9
40	C_2O^+, A^+	1.1	2.5	1.7	1.9
41		2.5	2.5	2.5	1.9
42		3.2	4	2.5	3.1
43		6.2	3	2.5	36
44	CO_2^+	16.7	17.5	10.8	8.1

Table 25

SUMMARY OF METHYL SILICONE PHOTOLYSIS EXPERIMENTS

Material	Solid or Liquid	Pertinent EPR Characteristics	Pertinent Mass Spectra Characteristics
Linear PDMS (Me/Si = 2)	L	Negative	H^+, CH_3^+, CO_2^+ (weak)
Nonlinear PDMS (Me/Si = 1.6)	L	Quartet (Q); Triplet (T)	Not resolved
RTV-602 PDMS (Me/Si = 2)	L	Q; T; Singlet (S)	sH^+
O_2-Crosslinked PDMS (Me/Si 2)	S	Q; S	sC^+, CO_2^+
Owens-Illinois PMMS (Me/Si = 1)	S	Q; T; S	sH^+, mCH_5^+, $mC_2H_5^+$
RTV602 PDMS (cured SRC-05)	S	Positive but not analyzed	sH^+, C^+, sCH_2^+, sCH_3^+, sCH_4^+, $C_2H_5^+$

Although Tsvetkov (Ref. 107) assigned the triplet $\cdot CH_2Si\equiv$ to an EPR peak that we have also observed in all the spectra examined, there is some doubt as to the correctness of this conclusion. However, in all cases where we observed the Tsvetkov-assigned triplet state, we also observed large quantities of H^+ being emitted in the mass spectra determinations, a result wholly consistent with the assignment of the triplet state to the structure.

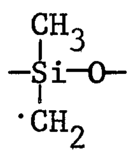

Ormerod and Charlesby (Ref. 98) also detect spectra similar to those observed in these studies and suggest that the singlet and quartet species are:

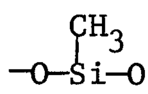

Singlet

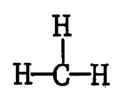

Quartet

In the present case the data are slightly different from those reported by Ormerod and Charlesby. Specifically, the separation in the doublets is 34 gauss compared to 40 gauss. However, these values may fall within our experimental errors.

Since polymer I was the precursor for polymer IV, and in a sense, III was the precursor for VI (they were from the same lot), the greater effects of ultraviolet on the solid polymers (IV, V and VI) are of interest. It could be speculated that contamination of the POMS (I) occurred during oxidative cross-linking--and, certainly, the ethanol/butanol solvent used for casting the Owens-Illinois 650 resin could have contributed to its behavior. The amine cure of RTV-602, although not fully understood, presents sufficient problems relative to its presence after cure has taken place, that research has been prompted on the problem.*

*Hughes Aircraft Corporation, Contract AF33615-69-C-1287.

Aromatic, as well as ultraviolet-active aliphatic, contamination may act as energy traps and store energy for relatively long periods of time. Through such insidious mechanisms as energy transfer and photosensitization, in which the energy donor is not damaged, infinitesimally small amounts of aromatic contaminants can give rise to inordinately large deleterious effects.

6. SILICONE COATINGS TECHNOLOGY

6.1 Introduction

The ultraviolet/vacuum-radiation stability of the silicone polymers had been demonstrated to be superior to all other commercial, soluble polymers by the time this investigation commenced (Ref. 1, 72, 78). Except to verify the ultraviolet stability, or instability, of other polymeric pigment binders from time-to-time, we confined all non-inorganic paint studies to the silicone-based systems. This section therefore treats the investigations of silicone paints from the period preceding the employment of the IRIF space simulation facilities, with their capability for determining in-situ the post exposure reflectance of irradiated specimens as an absolute hemispherical reflectance measurement, to the present time.

No data are given in this section, as elsewhere in this report, on pre-in situ reflectance data unless it either represents paints that (1) do not exhibit oxygen-bleachable spectral damage, or (2) the data are useful for purposes other than describing the stability in the infrared (~2500-nm for zinc oxide and ~950-nm for unstabilized zinc orthotitanate paints).

6.2 Microporous Coatings

6.2.1 Introduction

In theory, a coating composed of appropriately sized voids, uniformly dispersed in a matrix, should scatter light not unlike a pigmented film. That is, each void (or microbubble) behaves as a scattering center in which the scattering power depends upon refractive index ratios of less than unity (compared with ratios greater than unity for classical pigmented systems): It matters not whether the optical disparity is a crystalline oxide pigment ($n \sim 2$ to 2.7) surrounded by a lower refractive index polymer binder ($n \sim 1.4$ to 1.6) or whether it is a void with an index of unity surrounded by a binder of higher refractive index. Therefore, the micropores in a foamed coating are in theory the ultimately stable, wholly transparent, non absorbing pigment. A white paint appears white because the numerous scattering events that take place within the white coating effectively scatter the incident radiation back out of the coating without selective absorption. Therefore, it is obvious why foamed plastics are white and good reflectors of visable light.

A highly reflective microbubble coating must contain voids whose average diameter is roughly 0.5μ. Such voids must be uniformly dispersed throughout the material and in sufficient concentration to give rise to a high scattering density. To remain effective as such a scatterer, its voids must remain consistant in number and dimensions. Hence, the foam structure must not only be photochemically stable but also mechanically stable.

To obtain a coating whose mechanical characteristics are as stated, it is necessary to select a matrix, blow voids into it, rigidize it so that the voids are firmly constrained, and construct it thick enough to attenuate at least 95% of solar radiation.

From the inception of these studies (Ref. 5, 6, 7, 109) it was realized that matrix stability would become very important. Not only should the polymeric matrix material itself be very stable, i.e., remain very transparent, but contamination had to be avoided if the resultant foams were to be stable to ultraviolet irradiation in vacuum. We chose to concentrate on methyl silicones, especially the elastomeric RTV-602, after preliminary experimentation (Ref. 1, 109).

6.2.2 Experimental Methods

6.2.2.1 Mechanical Methods

Vigorous agitation of an emulsion, a suspension, or a solution of the resin produces a froth which is then gelled and fused or cured. Originally developed for producing latex foam, this method has been adapted to foaming polyvinyl acetal, polyvinyl chloride plastisols, and urea-formaldehyde resins. This method cannot be used to produce a bubble structure in silicone resins due to their slow cure characteristics.

6.2.2.2 Physical Methods

Physical methods use materials as bubble-forming agents that change their physical state during the foaming operation, e.g., compressed gases, volatile liquids, or soluble solids (e.g. starch). Our best results were obtained with a solution of a silicone resin (plus catalyst) in methylene chloride or Freon 11 (trichloromonofluoromethane) which was sprayed with an airbrush on a heated plate. By this means bubble formation in the resin layer occurred through the sudden evaporation of the organic solvent and the trapping of air bubbles in the rapidly curing resin. Reflectance was poor due to the lack of numerical density of the microbubbles and to the thin coatings that were produced.

6.2.2.3 Chemical Methods

In chemical bubble formation, the expanding gas is generated in situ, i.e., within the matrix of the polymer. The cell-forming gas can be produced as a by-product of a chain extension or cross-linking of the polymer, e.g., the formation of polyurethane foams with carbon dioxide liberated from the reaction between carboxyl-bearing alkyd resins and an isocyanate.

Chemical blowing agents, frequently called foaming agents in the plastics industry, are inorganic or organic materials that decompose under the influence of heat to yield at least one gaseous decomposition product. The most characteristic property of chemical foaming agents is the temperature at which the gas is liberated. In fact, the decomposition temperature determines the usefulness of a foaming agent in a given plastic material and also governs the conditions under which the foamable compound is to be processed. Since we relied only on certain silicone resins with specific curing properties, the selection of a suitable blowing agent was especially critical. The range of potential blowing agents extends from baking powder to explosives. Indeed, in the past 40 years at least a thousand different products have been proposed as chemical foaming agents. The compounds which we selected for our investigations are listed together with their trade name and decomposition temperature in air in Table 26.

6.2.3 Results

Typical of the results of many formulations was that of an RTV-602 coating foamed with 10% by weight Porofor N. The effects of only 170 ESH of ultraviolet irradiation are shown for a 1/4" thickness shown in Figure 35. The damage in all foamed specimens tested was severe and catastrophic. Although Porofor N residue could account for some of the damage seen, the deep and random scatter of the ultraviolet into the film accounts for a large portion of the damage. Indeed, coloration was observed deep in the foamed coating.

Unfortunately, the very character of microbubble systems that makes them attractive as solar-reflecting coatings may also tend to preclude their use in the ultraviolet environment of space. This can be seen by considering the nature of scattering by totally non-absorbing particles.

First, consider the ray behavior and the path length of ultraviolet in a coating pigmented with an ultraviolet-absorbing pigment (e.g., rutile, zinc oxide, and zinc orthotitanate). This is shown schematically in Figure 36. Such a pigment effectively absorbs all the ultraviolet (below its absorption edge) in the first two or three interactions, thus providing protection to the matrix. Unlike the ultraviolet-absorbing pigment shown in Figure 36, the ultraviolet-transparent microbubbles depicted in Figure 37 deep-scatter the ultraviolet rays by the very mechanism (multiple refraction) that accounts for the reflectance of white paints as well as foams. Thus, when the ultraviolet-absorbing pigment (Figure 36) is replaced by ultraviolet-transparent microbubbles or pigment particles, the

Table 26

CHEMICAL BLOWING AGENTS

Chemical Name	Structure	Trade Name	Decomp. Range in Plastics, °C	Gas Yield, cc/g (STP)	Remarks
Azodicarbonamide	$H_2N{-}CO{-}N{=}N{-}CO{-}NH_2$	Celogen AZ	160 - 200	225	Residue colorless and odorless. Original color is yellow.
Azobisisobutyronitrile	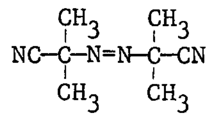	Porofor N	105 - 120	115	Residue colorless, toxic. No residue at 600°F.
Dinitrosopentamethylene tetramine	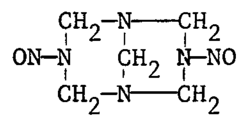	Unicel N	130 - 190		Residue colorless. Amine odor (hexamethylene tetramine). 60% silica filler.
Diazoaminobenzene	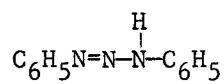	Porofor DB Unicel	100 - 130	130	Has phenyl groups and brown color. Residue staining and toxic.
4,4'-Oxybis(benzenesulfonyl hydrazide)	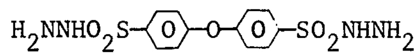	Celogen OT	120 - 130	225	Residue colorless and odorless. OT refers to oil treated.
N,N'-Dimethyl-N,N'-dinitroso-terephthalamide	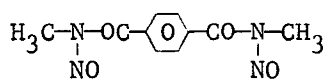	Nitrosan	90 - 105	310	Residue colorless. Residue is dimethyl terephthalate.
Benzenesulfonylhydrazide	$C_6H_5SO_2{-}NHNH_2$	Porofor BSH	95 - 100		Colorless and odorless residue.
Ammonium nitrite	NH_4NO_2		70		
Ammonium carbonate	$(NH_4)_2CO_3$		58		

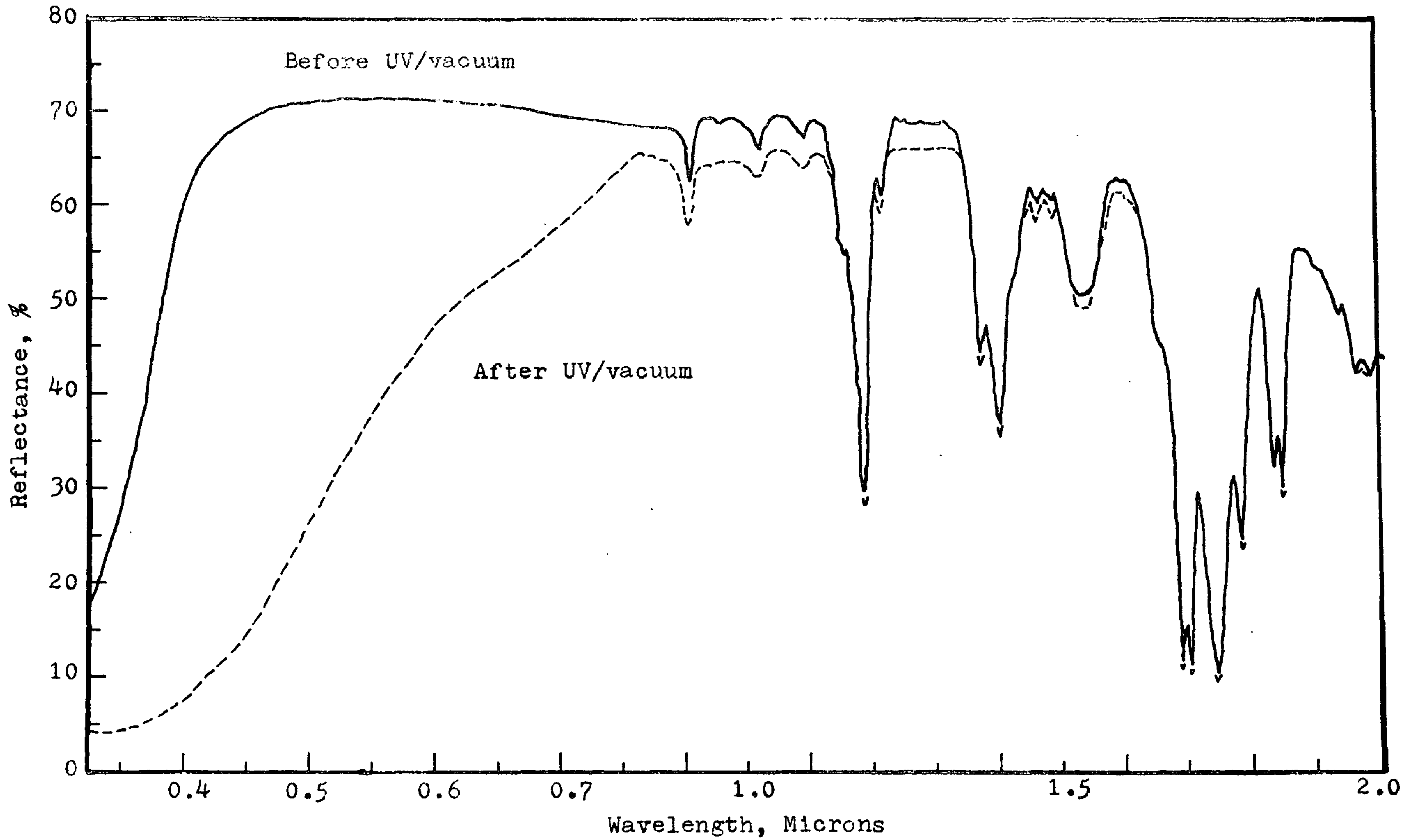

Figure 35 REFLECTANCE OF FOAMED LTV-602 FILM CONTAINING 10% POROFOR N BEFORE AND AFTER ULTRAVIOLET EXPOSURE

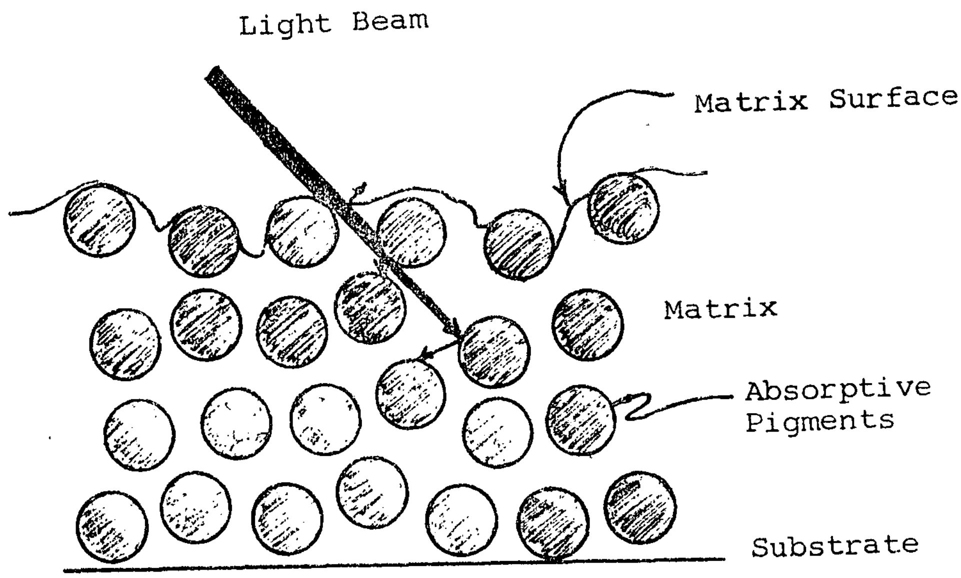

Figure 36 RAY BEHAVIOR IN IDEALIZED PAINT FILM CONTAINING TOTALLY ABSORBING PIGMENTS

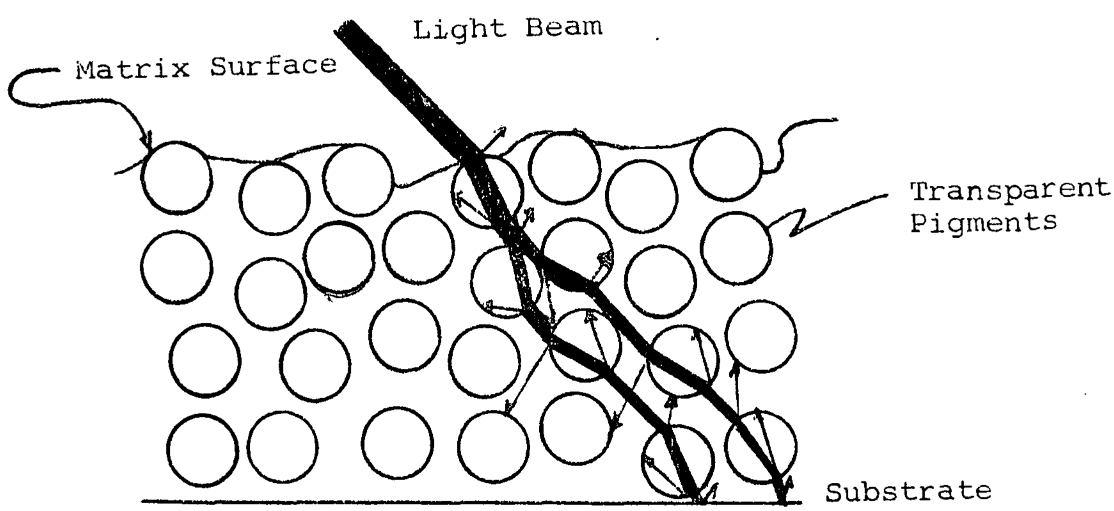

Figure 37 RAY BEHAVIOR IN IDEALIZED PAINT FILM CONTAINING TOTALLY TRANSPARENT PIGMENTS

ultraviolet path length in the matrix will be many orders of magnitude greater, and the probability of a photon being absorbed to cause a color center is greatly enhanced. The penetration and random scattering of the ultraviolet photons within the film will greatly increase the probability of damage, which in this instance, is manifested as increased spectral absorption and evidenced visually by coloration.

From the foregoing discussion and from experimental evidence, the following can be listed as the attributes that are absolutely essential to stable microbubble coatings:

1. The matrix must be completely transparent to solar radiation - at all wavelengths.
2. It must have an index of refraction different from unity.
3. It must have a void structure whose dimensional characteristics are stable and are important in terms of interaction with optical wavelengths.

The key point is that <u>all</u> the components of the matrix <u>must</u> be transparent; otherwise the absorbing component will eventually color and/or cause other components to degrade. Obviously, if there is no absorption, there will be no damage. Consequently, it is imperative that only pure, <u>highly stable</u> polymers be used as matrices for microporous coatings intended for utilization in the space environment. Commercial foams, while very reflective, are not sufficiently stable and in fact have been observed to char after only a few hours of ultraviolet radiation in vacuum.

Even though the concept of a closed-cell foamed (and, therefore, insulative) polymer that would also possess solar absorptances of less than 0.1 is very attractive for many space missions, the utilization of this concept must await the development of foamable polymers that are still more stable than the systems available today.

6.3 General Paint Technology

6.3.1 Introduction

Although the following paragraphs, which treat the subjects of pigment volume, spray-up method and particle size, utilize untreated zinc oxide-pigmented RTV-602 paints, they are included here rather than in the section on S-13G (section 6.6) due to the universality of application of the results.

6.3.2 Effect of Pigment Volume Concentration (PVC)

SP500 zinc oxide-pigmented methyl silicone (General Electric Company's RTV-602 elastomer) specimens were prepared with pigment volume concentrations (PVC) of 15, 20, 25, 30, 35 and 40%. The thickness of each film was 6.7 $\pm$ 0.1 mils; this was achieved by painting nearly 100 specimens and measuring the reflectance on those with thicknesses between 6.6 and 6.8 mils. The spectral reflectances of these films (applied to 6061 aluminum) were then determined in the wavelength range of 0.325 to 2.0μ.

The reflectance curves of five of the six films are presented in Figure 38. These data show the effect of increased particle-packing on the reflectance in the various regions of the spectrum. As the particles (mean diameter 0.3μ) are packed more closely together, they tend to behave as a particle with a diameter larger than that of any single particle but smaller than the diameter of the aggregate. Thus, the packing of the particles as increased pigment concentrations appears to have a greater effect on the near-infrared reflectance.

Simply stated, the PVC of all space paints should be maintained at just under the critical PVC (CPVC). The CPVC is that concentration of pigment at which there is just sufficient binder to cement the particles in a continuous, nonfragile film.

6.3.3 Effect of Particle Size

Solar absorptance values were determined on a series of paints which were prepared from specific mixtures of SP500 and

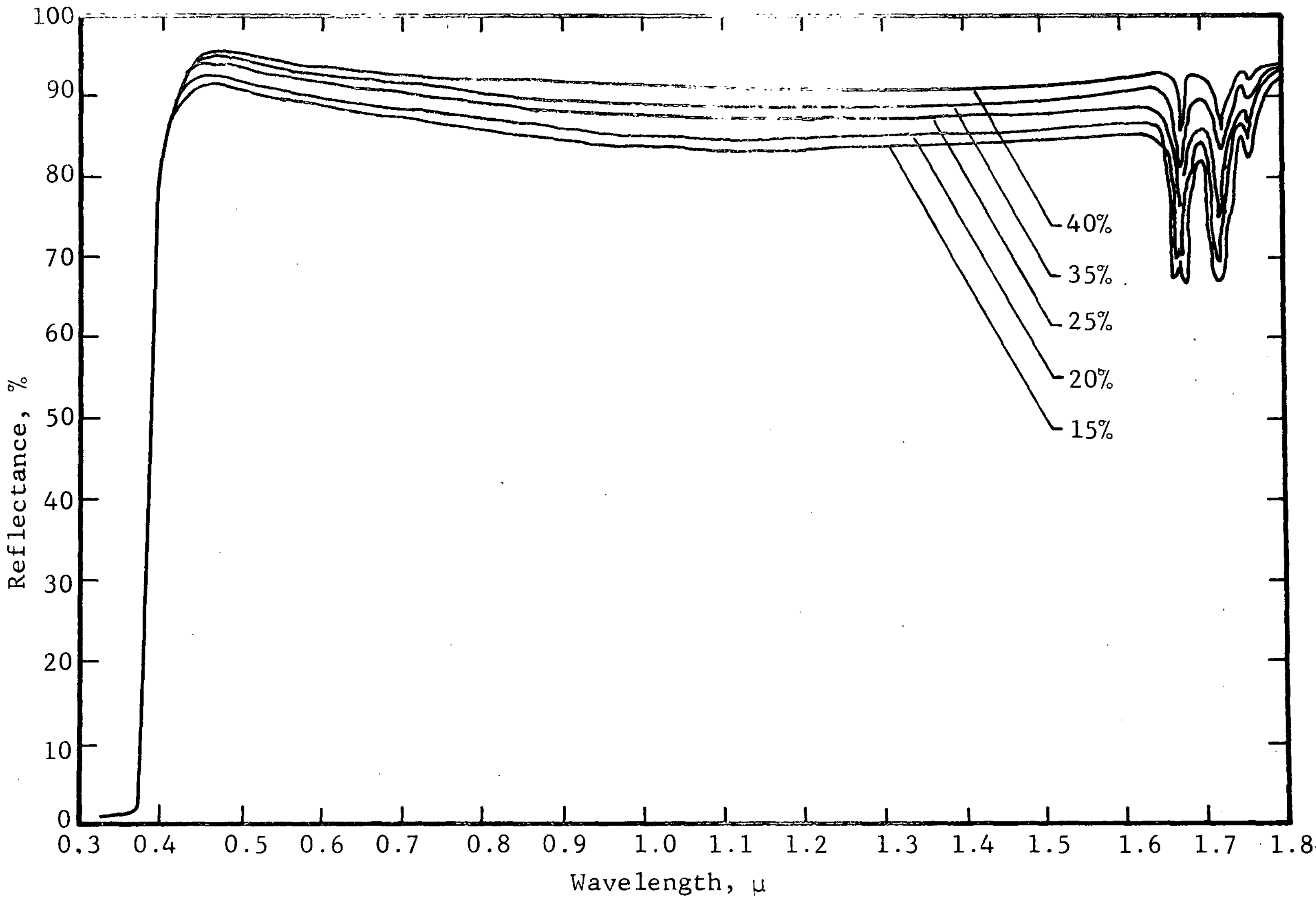

Figure 38 SPECTRAL REFLECTANCE OF ZINC OXIDE-SILICONE PAINTS AT DIFFERENT PVC'S (Based on $MgCO_3$-Block)

XX 254 zinc oxide pigments at a PVC of 32%. The mean particle size for SP500 is reported by the manufacturer to be 0.3μ diameter and that for the XX254 is 1.5μ diameter. The pertinent data are given in Table 27. The paints were prepared at 100, 80, 50, 20 and 0% SP500 pigment. Except for the 0% SP500 (100% XX254), the films were cast with a Garner knife at 10-mil wet-film thickness. The dry-film thickness of the five specimens are given in Table 27, and their reflectances are shown in Figure 39.

Table 27

SOLAR ABSORPTANCE AS A FUNCTION OF PIGMENT PARTICLE SIZE (32% PVC)

Paint No.	Percent SP500	Percent XX254	Thickness, mill	Solar Absorptance α_1	α_2	α_s
1	100	0	5.3	0.10	0.11	0.21
2	80	20	6.5	0.11	0.11	0.22
3	50	50	6.8	0.12	0.11	0.23
4	20	80	6.8	0.13	0.11	0.24
5	0	100	13.0	0.13	0.11	0.24

Examination of the data shows the effect of mixing two zinc oxides of different particle-size distributions. (Although paint 5 is considerably thicker than the other paints, the effect of the mixing is most apparent in α_1.) The effect of the larger pigment tends to be much more noticeable in the visible portion of the spectrum (which is manifested in α_1). Examination of the curves in Figure 39 shows that paint 5, prepared entirely from the larger XX254 pigment, possesses a more sharply defined near-infrared spectra compared to the other specimens and in this respect is analogous to the spectra observed for the microbubble coatings.

Although the general application of light scattering is discussed in more detail in Chapter 8, it should be pointed out

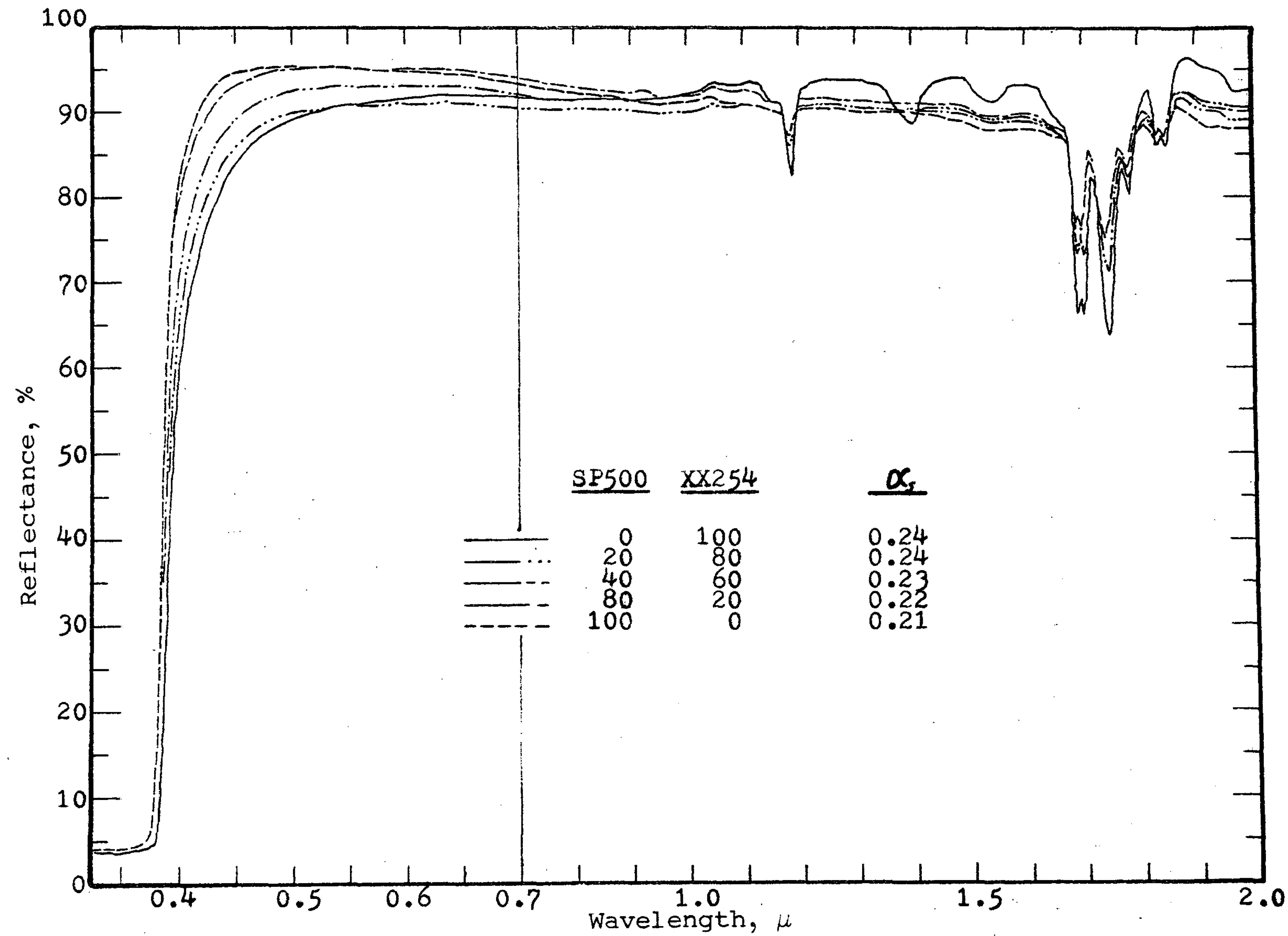

Figure 39 EFFECT OF PARTICLE SIZE ON REFLECTANCE OF LTV-602 ZINC OXIDE PAINTS

here that the results of the particle size experiment are in concert with our present views on the maximization of solar reflectance. As we point out in Chapter 8, the extensions to the Mie theory for single particle scattering are useful only in dilute suspension and the theory breaks down in the multiple-scattering systems represented by our highly-pigmented space paints. The data presented here show that if only 20% of the SP500 pigment is replaced with a larger size, it seriously detracts from the visable portion of the spectrum where the solar output is greatest.

We conclude therefore that the solar reflectance is optimized by using a particle size that is just under that which Mie theory predicts for optimization at the solar maximum and increasing the PVC to the greatest extent permissable.

6.3.4 Effect of Multiple Layers

The reflectances of two SP500 zinc oxide/silicone paint specimens prepared at equal thickness (32% PVC) are presented in Figure 40. One specimen was prepared in one application of about 8-mil film thickness. The other specimen was prepared in four applications of about 2-mils each. The one-coat specimen was carefully shaved (scapel) to 6.7 mils, and the multiple-coat film was shaved to 6.8 mils. This experiment was conducted in order to determine the degree of spectral reflectance which the multiple-coat paint films would exhibit compared to that of a single, equally thick coating. As indicated in Figure 40, the reflectance of the multiple-coat film is 1 to 2% higher than the single-coat film in the bulk of the solar spectrum. This is attributed to refractive index changes at the interfaces of the separately cured layers and represents a solar absorptance improvement of 0.02%.

6.3.5 Effect of Substrate Reflectance

The contribution to spectral reflectance of an unpolished, clean aluminum substrate is shown in Figure 40. The bottom

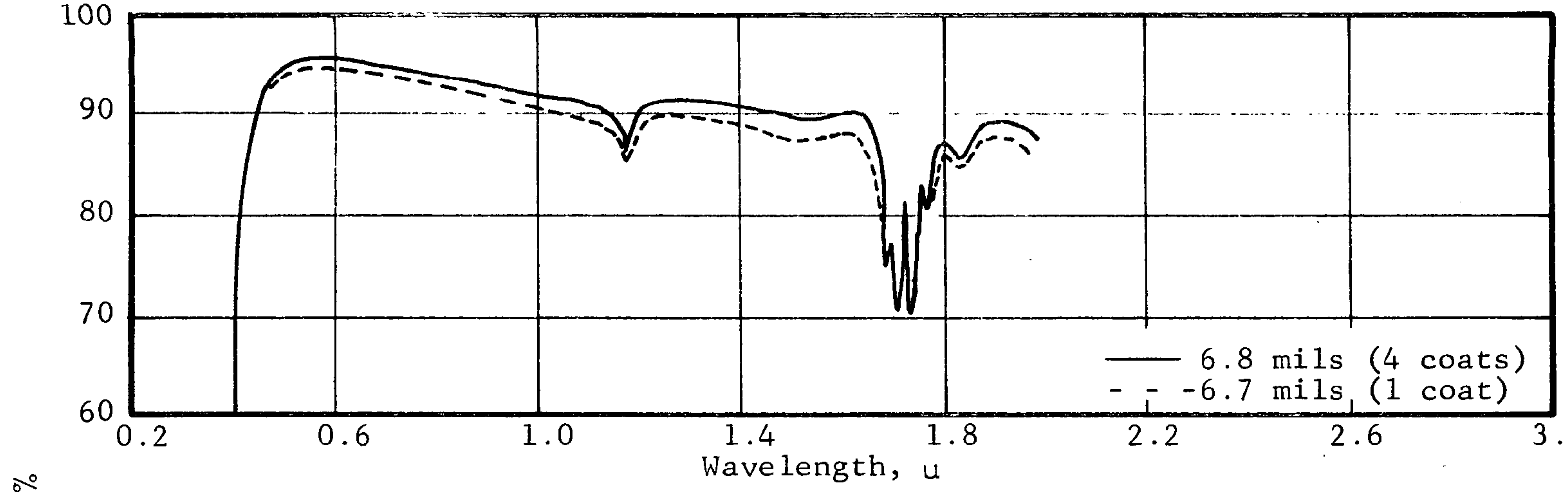

Figure 40-A REFLECTANCE OF SP 500 ZINC OXIDE-PIGMENTED SR-80 RESIN AT 35% PVC

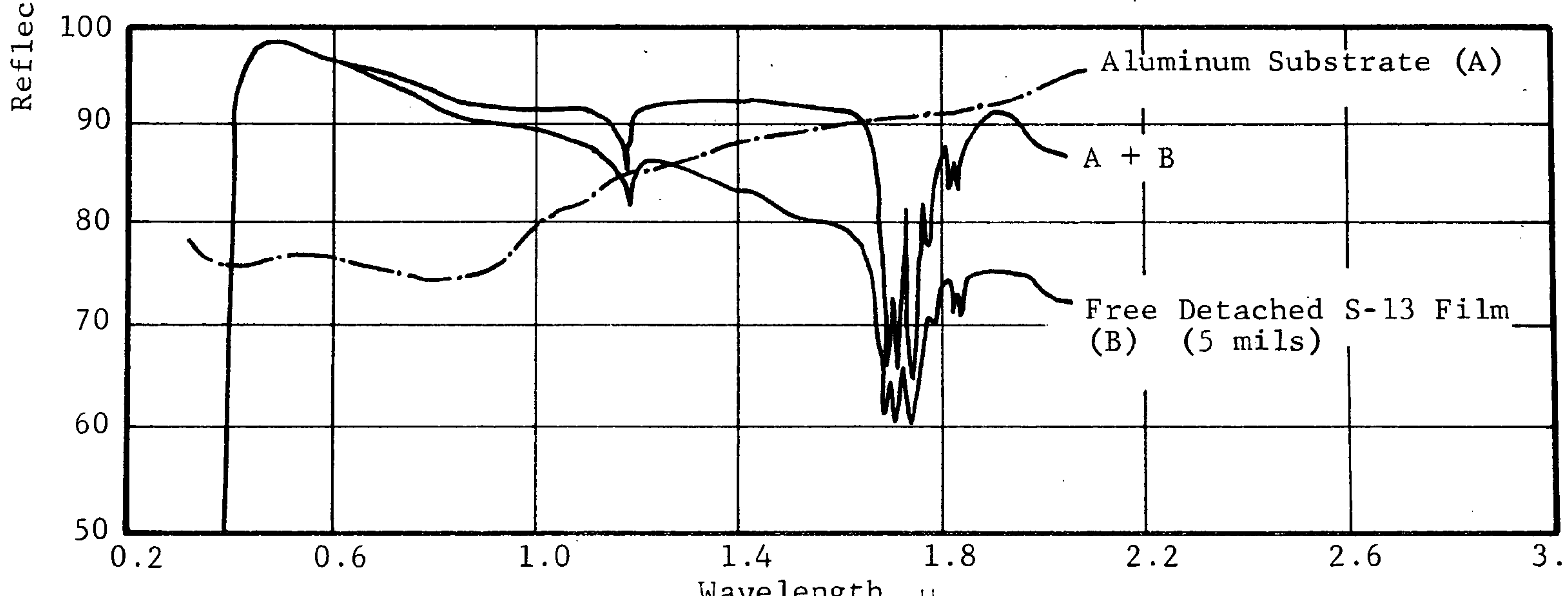

Figure 40-B EFFECT OF ALUMINUM SUBSTRATE ON REFLECTANCE OF A S-13 SPECIMEN

cure is the reflectance of an unbacked, free detached film of S-13 (30% PVC SP500 in RTV-602 silicone): The detached S-13 coating was backed with optical-black paper. The dashed curve is the spectral reflectance of the aluminum substrate. These curves illustrate the importance of the substrate reflectance, even for 5-mil-thick coatings.

6.4 The Silicone Binders Employed

6.4.1 General Electric RTV-602

General Electric's proprietary RTV-602 is a linear hydroxy-terminated polydimethylsiloxane elastomer that is used primarily in the electrical and mechanical encapsulating/potting industry. The RTV-602 contains a reactive, low-molecular weight silanol that is not necessary for cure*; the use of the silanol is unclear since its removal (Ref. 110) gives superior film and optical properties and is indeed unnecessary for cure, as indicated by the General Electric Company (Ref. 110, 111).

Although General Electric supplies a proprietary catalyst for RTV-602, designated as SRC-05, this polymer may be cured by a number of curing agents. We have successfully employed the following in addition to SRC-05, a mixture of diethylenetriamine and tetramethylguanadine (the best physical properties were obtained with the "starred" candidates):

*Tetramethylguanadine (TMG)
Diethanolamine
Ethylene diamine
Diethylamine
Tin octoate
*Shell H-Z

Akawie (Ref. 111) in more recent studies has employed the following in an attempt to cure RTV-602 without leaving catalyst in the system as a contaminant.

*Personal communication with General Electric Silicone Products Department.

NH_3 (gas)
Triethylamine
Tetramethylammonium hydroxide
Tetrabutyl phosphonium hydroxide

Current studies at IIT Research Institute (Ref. 110) employing "spinning dish" molecular distillation has effectively reduced the outgassing behavior of S-13G paints (see paragraph 6.6) prepared from RTV-602 (VCM* $>$ 0.04% weight), in addition to improving both film toughness and ultraviolet stability.

Adhesion of RTV-602 requires the use of General Electric Company's proprietary primer SS4044, although General Electric's SS4155 and Dow Corning's 4098 primers may also be employed (without real advantages, however).

Because RTV-602 is a 100% solids material, solubility characteristics had to be established for paint manufacture and spray application. A wide variety of solvents and solvent combinations were employed involving flow-out tests on glass plates. The results of these tests are presented in Table 28; these experiments involved flow-out tests on glass plates.

While RTV-602 is quite soluble in a variety of solvents, a smooth pour, free from "crawling," "ridging," discontinuous breaks, and "rainbow" bands was observed using the following single solvents only; isopropanol, isopropyl acetate and isopropyl ether. The diluent petroleum ether (which is not a solvent) also resulted in a smooth film.

The isopropyl ether gave the best solution and film but resulted in extremely rapid evaporation and was, therefore, too fast to handle. Based upon these tests, both a paint formulation solvent and a spray thinner were selected for use with RTV-602 paints (S-13G):

*VCM = Vacuum condensible material.

Table 28

SOLUBILITY OF RTV-602 IN VARIOUS SOLVENTS

Group	Solvent	Solution	Film
Hydrocarbons	Light petroleum ether	Insoluble	(Even, smooth)
	Benzine	Borderline, colloidal suspension or gel	Shrinkage or creep-up of the pour, rainbow fringes
	Benzene	Soluble	Shrinkage or creep-up of the pour, rainbow fringes
	Toluene[a]	Soluble	Shrinkage or creep-up of the pour, rainbow fringes
	Xylene	Soluble	Shrinkage or creep-up of the pour, rainbow fringes
	Turpentine	Soluble	Shrinkage or creep-up of the pour, rainbow fringes
Alcohols	Methanol	Insoluble	
	Ethanol, 190p	Insoluble	
	Ethanol, 200p	Insoluble	
	Isopropanol[a]	Soluble	Discontinuous pour, even, smooth
	Butanol	Soluble	Shrinkage or creep-up of the pour, rainbow fringes, discontinuous pour
	Methyl isobutyl carbinol	Excellent	Rainbow fringes, discontinuous pour
	Diisobutyl carbinol	Excellent	Rainbow fringes, discontinuous pour
Ketones[b]	Acetone	Insoluble	Discontinuous pour
	Methyl ethyl ketone	Soluble	Rainbow fringes
	Methyl isobutyl ketone	Soluble	Rainbow fringes
	Diethyl ketone	Soluble	Rainbow fringes
	Diisobutyl ketone	Soluble	Rainbow fringes
	Diacetone	Borderline, colloidal suspension or gel	Rainbow fringes
	Isophorone	Insoluble	
	Cyclohexane	Insoluble	
Acetates	Ethyl acetate	Soluble	Rainbow fringes
	Isopropyl acetate[a]	Excellent	Even, smooth
	n-Butyl acetate	Soluble	Rainbow fringes
	Amyl acetate	Soluble	Rainbow fringes
	Methyl amyl acetate	Soluble	Rainbow fringes
	Methyl cellosolve acetate	Insoluble	Discontinuous pour
	Cellosolve	Borderline, colloidal suspension or gel	Discontinuous pour
	Butyl acetate	Insoluble	Discontinuous pour
Miscellaneous	Methyl cellosolve	Insoluble	Discontinuous pour
	Cellosolve	Borderline, colloidal suspension or gel	Discontinuous pour
	Butyl cellosolve	Borderline, colloidal suspension or gel	Discontinuous pour
	Dioxane	Borderline, colloidal suspension or gel	Discontinuous pour
	2-Nitropropane	Insoluble	
	Isopropylether	Excellent	Very smooth

[a]Best of group.

[b]None of the ketones is a good solvent.

T25 Solvent	
Toluene	40 pbw
Isopropanol	50 pbw
n-Butanol	10 pbw
	100

X99 Spray Thinner	
Toluene	40 pbw
Xylene	20 pbw
Isopropanol	20 pbw
n-Butanol	15 pbw
n-Butyl acetate	10 pbw
	100

In order to pass Rule 66 (California Air Pollution Control Board), the following formulation solvent must be employed for use in and shipment to California:

X66 Solvent	
VM&P Naptha	38 pbw
Isopropanol	20 pbw
Methylisobutyl Carbitol	15 pbw
Isopropyl Acetate	5 pbw
Cellosolve	5 pbw
Ethyl Benzene	12 pbw
	100

It should be noted that we have observed no poor shelf or ultra-violet stability with specimens prepared from the X66 solvent. We prefer the X99 solvent because of only slightly superior flow-out characteristics compared to the X66 system.

6.4.2 Owens-Illinois 650 "Glass" Resin

The "650" glass resin is a condensation product (polymonomethylsiloxane) of the hydrolysis of methyltriethoxysilane and has sufficient stereoregularity to warrent denoting it as a "broken-ladder polymer." This polymer is cured by thermally-induced cross-linking at the residual hydroxies. Its principal disadvantage has been its propensity for embrittlement on aging (termed "coasting") as a pigmented film, a characteristic that is of little consequence to the electrical industry for whom it was developed. However, it's exceptionally stable optical properties have made it the most promising pigment-binder currently available in commercial quantities. Type 650 resin is supplied as a B-staged flake that is soluble in ethanol and butanol and combinations thereof. However, it does not produce a smooth, easily applied film from either solvent alone. We have found that the solvent system given below is excellent for both formulation and spray thinning:

n-Butanol	35 pbw
Isopropanol	30 pbw
Toluene	15 pbw
Methylisobutylketone	20 pbw
	100

As indicated earlier, thick (~7 mils), pigmented films of Owens-Illinois 650 do not age well. Typical of the early results of Owens-Illinois 650 "Glass" resin coatings is the behavior exhibited by the films discussed in Table 29.

The quality control of the 650 resin has been greatly improved and pigmented coatings of the currently-supplied, B-staged polymer exhibit much improved properties compared to Table 29. Pigment volume is a critical factor and must not exceed 35% PVC. The cure schedule currently employed is:

24 hr Air dry
16 hr 200°F
16 hr 350°F

Although current Owens-Illinois 650-resin paints are much superior to the earlier coatings in terms of physical properties, 5-mil pigmented films still cannot be bent with a conical mandrel without failure at small radii.

Because of the brittleness of ~5-mil films, which still exhibit "coasting" with low-temperature thermal aging, we have initiated plasticizer studies for the Owens-Illinois 650 "Glass" resin in a current program for NASA-Marshall Space Flight Center. These studies, which have been summarized in a recent Triannual Report (Ref. 110), have been largely successful in that improved physical properties were realized without detriment to the optical and ultraviolet stability characteristics of coatings prepared from them. Thermally cured 5-mil films of modified resin can be bent without failure around a conical mandrel.

Table 29

PROPERTIES OF OWENS-ILLINOIS TYPE 650 GLASS RESIN PAINTS PIGMENTED WITH SP500 ZINC OXIDE

Lot	PVC, %	Curing and Heating Schedule	Finish	Remarks
1004	30	1 hr @ RT + RT to 195°F in 1 hr + 24 hr @ 195°F + 195 to 300°F in ½ hr + ½ hr @ 300°F	Semi-gloss	Smooth, very hard surface after room temperature cure. After the 300°F cure, 60% of the specimens exhibited small cracks. After standing at room temperature for 16 hrs, the remaining 40% of the specimens developed small cracks.
1004	35	16 hrs @ RT + RT to 300°F in 2 hr with IR lamps	Matte	Coating was hard after 16 hrs of room temperature cure. Heating with the IR lamps had no effect.
276	35	N/A	N/A	Paints (liquid) gelled in one week at room temperature.
1025	35	N/A	N/A	Paints (liquid) gelled in one week at room temperature.
1025	25	16 hrs @ RT	Gloss	Very hard coating which cracked after the 16 hrs at room temperature.
1034	25	16 hrs @ RT	Gloss	Cracked after several hours at room temperature.
1034	30	1 hr @ RT + 1 hr at 140°F + 1 hr at 150°F	Matte	No change was observed as paints were cured (heated). No cracks observed. Cracked when immersed in liquid nitrogen.
1040	25	1 hr @ RT + 1 hr at 140°F + 1 hr @ 150°F	Gloss	Cracked when cooled to room temperature after heating to 400°F
1040	30	1 hr @ RT + 1 hr @ 140°F + 1 hr @ 150°F	Semi-gloss	Cracked when cooled to room temperature after heating to 400°F.

6.5 Stability of Silicone Paints

6.5.1 Pre-IRIF Results

The space-ultraviolet stability of a number of silicone paints is presented in Table 30. These paints, which are selected as representative of those studied (in terms of the results of space simulation), were all pigmented at between 30 and 32% PVC (Ref. 8, 9, 12, 79). Although the three semiconductor pigments r-TiO_2, ZnO and Zn_2TiO_4 all exhibit oxygen-bleachable infrared damage, the data presented is worthy of reporting because of the stabilities displayed in the α_1-spectral region (the near-ultraviolet and visible regions).

The RF-1 "Flame Process," a chloride-process, rutile produced by Cabot Corporation, is the most stable rutile titania examined. Because of the difficulty of preparing low-α_s silicone paints from rutile, i.e., paints with α_s's below 0.17, and because of the $\Delta\alpha$ of 0.05 (compared to 0.01 for both ZnO and Zn_2TiO_4), we chose not to investigate r-TiO_2 paints on the basis of either a materials science or solid-state chemistry approach.

The excellent stability of the R-9 resin, prepared in identical fashion to the non-linear polydimethylsiloxane resin whose synthesis is described in paragraph 5.4.1.1.3, but at a Me/Si of 1.43, was largely responsible for our early acceptance of Owens-Illinois 650 resin. The R-9 resin was the basis of IITRI's S-33 paint developed for the Jet Propulsion Laboratory (Ref. 1, 72). ($\Delta\alpha_s$ = -0.008 for the ZnO-pigmented paint.)

Similarly, the excellent stability exhibited by the zinc orthotitanate-pigmented Owens-Illinois 650 resin, coupled with the results of concurrent Zn_2TiO_4 pigment-powder and potassium silicate-paint studies (see Chapters 3 and 4), prompted the subsequent attention devoted to the zinc orthotitanate system. Unfortunately both ZnO and Zn_2TiO_4 proved to exhibit oxygen-bleachable damage and extensive investigations were therefore necessitated to stabilize these pigments. The zinc oxide/silicone

Table 30

EFFECT OF ULTRAVIOLET IRRADIATION ON SEVERAL SILICONE PAINTS

			Solar Absorptance			
Pigment	Binder	Exposure (ESH)[1]	α_1	α_2	α_s	$\Delta\alpha_s$
r-TiO_2 (RF-1)[2]	RTV-602	0	0.089	0.086	0.175	
		2150	0.117	0.107	0.224	0.049
ZnO (SP500)[3]	R-9 PMDS[4]	0	0.092	0.094	0.186	
		2000	0.096	0.089	0.185	-0.001
ZnO (SP500)	OI-650	0	0.086	0.058	0.144	
		2000	0.086	0.050	0.136	-0.008
α-Al_2O_3 (Alucer MC)[5]	OI-650	0	0.029	0.057	0.068	
		2000	0.080	0.067	0.147	0.061
α-Al_2O_3 (Alucer MC)	RTV-602	0	0.038	0.062	0.100	
		2000	0.200	0.074	0.274	0.174
Zn_2TiO_4 (A-54-2)[3]	OI-650	0	0.088	0.072	0.160	
		2000	0.100	0.075	0.175	0.015
Zn_2TiO_4 (A-54-2)	RTV-602	0	0.071	0.053	0.124	
		2000	0.090	0.059	0.149	0.025

[1] Fluence deposited at between 3 and 5 solar intensities, depending on test.
[2] Cabot Corporation
[3] New Jersey Zinc Company
[4] IITRI resin employed in S-33 paint (Ref. 1, 72)
[5] Gulton Industries

paint studies (S-13 and S-13G) are presented in section 6.6 of this Chapter and the zinc titanate system is the subject of Chapter 8.

The two α-Al_2O_3 and two Zn_2TiO_4 paints, all irradiated for 2000 ESH of ultraviolet in vacuum, are presented in Table 30 to show the importance of the matching, or mismatching, of the ultraviolet spectra of pigment and binder. The results of irradiation of these four coatings largely confirmed the selection of the semiconductor pigments ZnO and Zn_2TiO_4 for study rather than dielectrics such as Al_2O_3, SiO_2, MgO, etc., with their absorption edges below 210 nm wavelength. Where the absorption edge of the pigment is at a greater wavelength than the binder, as with the zinc orthotitanate-pigmented OI-650 resin ($\Delta\alpha_s$ = 0.015), the paint's instability is largely due to the pigment ($\Delta\alpha_1$ = 0.012). However, when the binder's edge is at a much greater wavelength (see Figure 28, Chapter 5) than the pigment, as with the α-alumina-pigmented RTV-602 ($\Delta\alpha_s$ = 0.174), the damage is largely in the binder where the mechanism is, quite simply, the fundamental instability of the binder multiplied by some factor associated with the manifoldly-increased pathlength in the film. Thus, as shown in section 6.2.3 (Figures 36 and 37) of this chapter, the multiple scattering associated with a highly ultraviolet-transparent pigment can easily destroy any but the most stable polymeric binder*--and none have been reported to be more stable than either Owens-Illinois 650 "Glass" resin or IITRI's R-9 nonlinear polydimethylsiloxane (Me/Si = 1.43). We have, on the basis of these as well as other considerations delineated in Chapter 8 (8.1), confined our efforts in this program to the stabilization of ultraviolet-absorbing pigments that behave as a screening agent to <u>help</u> protect the binders in which they are dispersed.

*While FEP Teflon is as stable, it cannot be formulated into highly reflective pigmented coatings.

6.5.2 IRIF Test Results on OI-650 Paints

Although the results of irradiation of silicated zinc oxide- and zinc orthotitanate-pigmented Owens-Illinois 650 resin paints are presented in section 6.7 of this Chapter and in Chapter 8, respectively, the behavior of several other pigmented Type 650 resin paints is worthy of note. The results of ultraviolet irradiation of three such paints are shown in Table 31 and Figures 41, 42 and 43.

The stability of the calcium tungstate-pigmented 650-resin paint prepared from Crystal Grade powders was exceptional, although a $\Delta\alpha_1$ of 0.006 was noted (visable region), which was offset by a concommitant decrease (bleaching) in the infrared region, i.e., the $\Delta\alpha_2$ region. The high initial solar absorptance of about 0.21 for the Type 650 silicone paints dissuaded us from giving greater attention to calcium tungstate paints, especially in light of the somewhat erratic behavior observed for irradiated $CaWO_4$ powders and silicate paints (Chapters 3 and 4).

Table 31

EFFECT OF ULTRAVIOLET IRRADIATION IN THE IRIF ON THE SOLAR ABSORPTANCE OF SEVERAL OI-650 RESIN COATINGS

Figure	Description	Exposure (ESH)	Solar Absorptance α_1	α_2	α_s	$\Delta\alpha_s$
41	$CaWO_4$ (Crystal Grade)	0	0.116	0.089	0.205	-----
		600	0.122	0.083	0.205	0.000
42	$Ca*WO_4$ (Phosphor Grade)	0	0.128	0.103	0.231	-----
		600	0.139	0.108	0.247	0.016
43	Cabot's RF-1 $r-TiO_2$	0	0.128	0.116	0.244	-----
		550	0.168	0.153	0.321	0.077
		1200	0.170	0.156	0.326	0.082
		Air	0.141	0.118	0.259	0.015

The difference between measurement in air and in vacuum of the reflectance of irradiated semiconductor-pigments, and coatings prepared from them, can be realized by comparing the data for the Cabot $r-TiO_2$ paint presented in Table 31 (Figure 43) with the

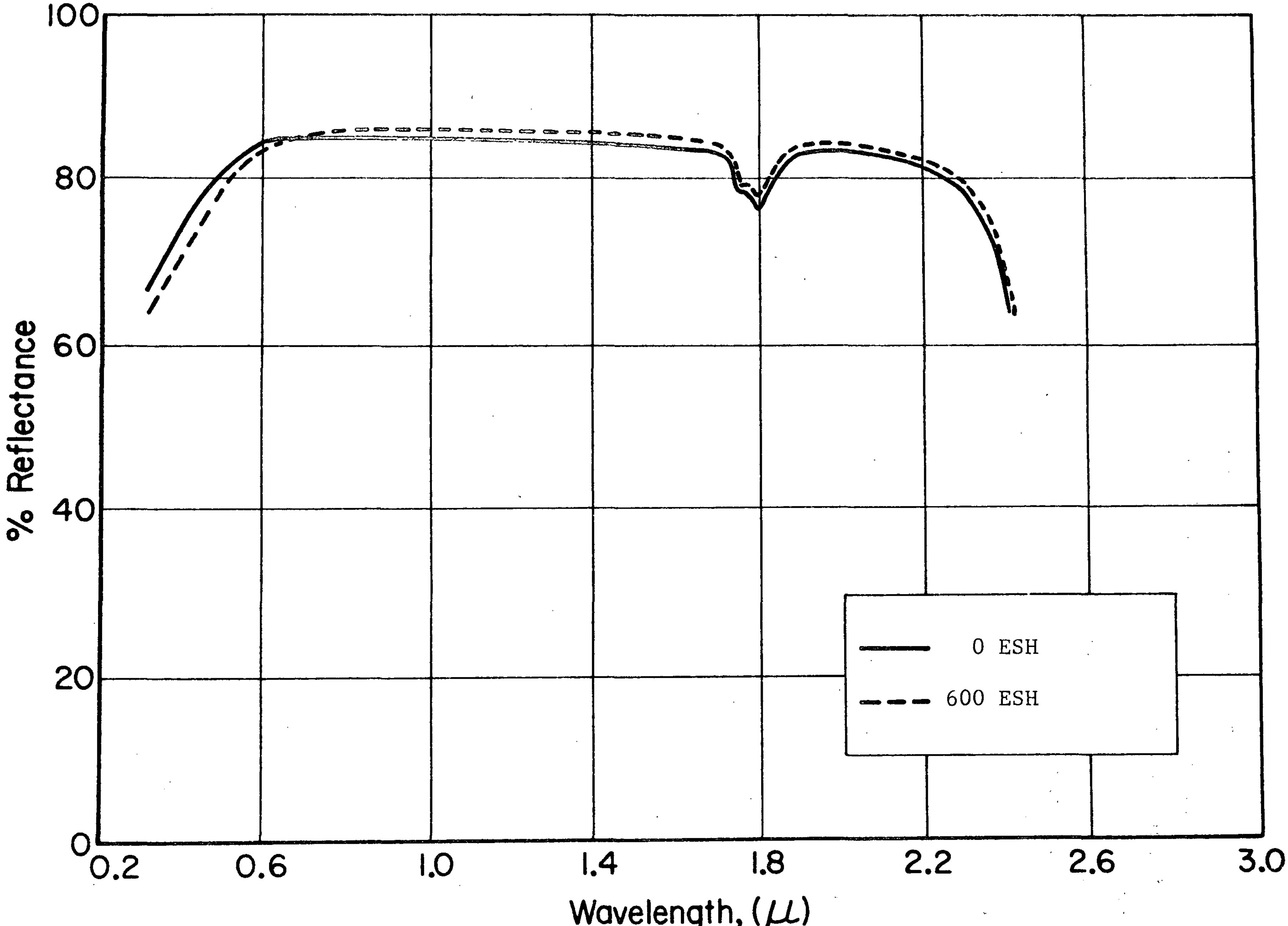

Figure 41 SPECTRAL REFLECTANCE OF $CaWO_4$/O-I 650 PAINT AS A FUNCTION OF EXPOSURE TO 600 ESH OF UV IN IRIF-II

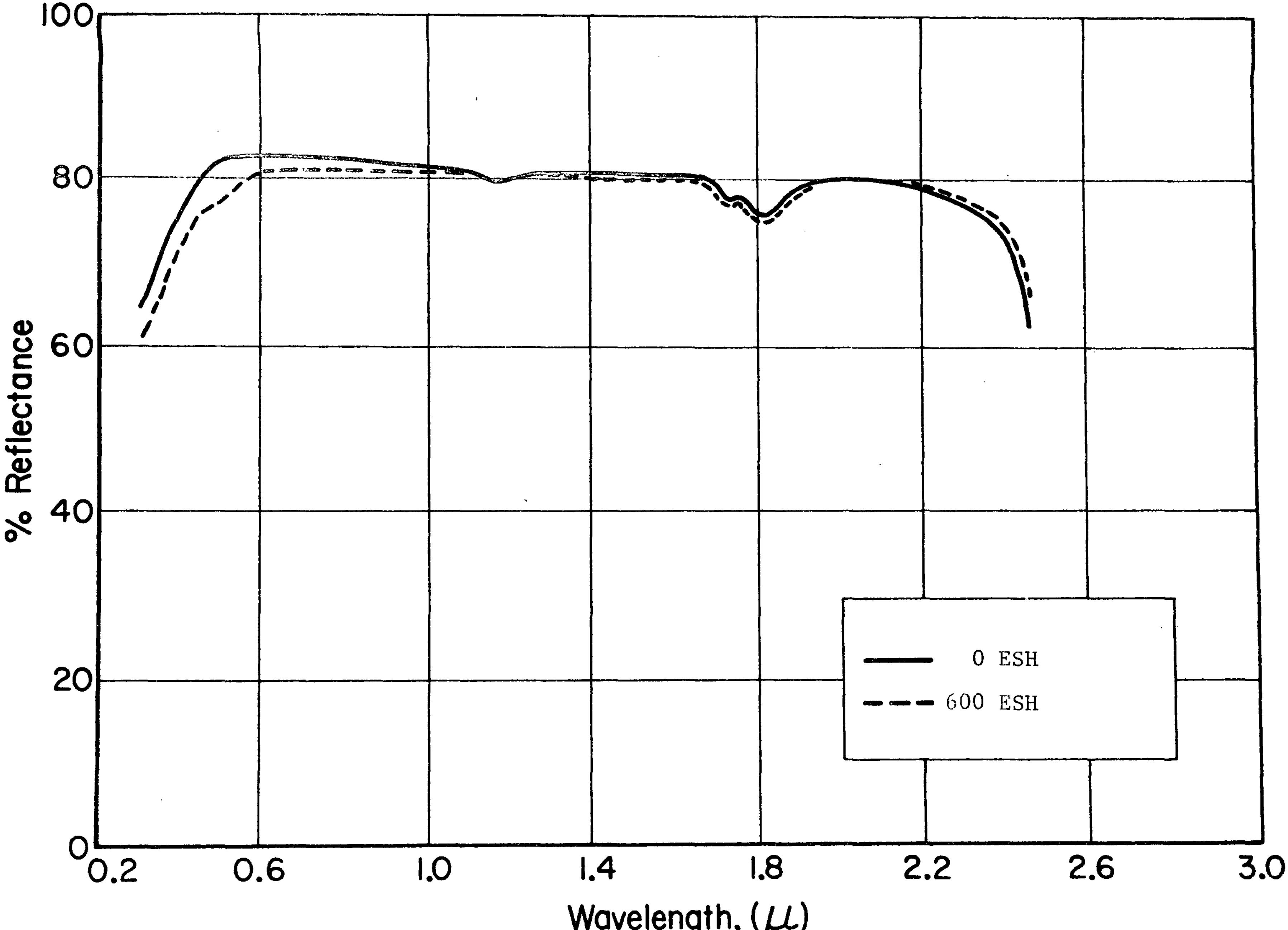

Figure 42 SPECTRAL REFLECTANCE OF Ca* WO_4/O-I 650 PAINT AS A FUNCTION OF EXPOSURE TO 600 ESH OF UV IN IRIF-II

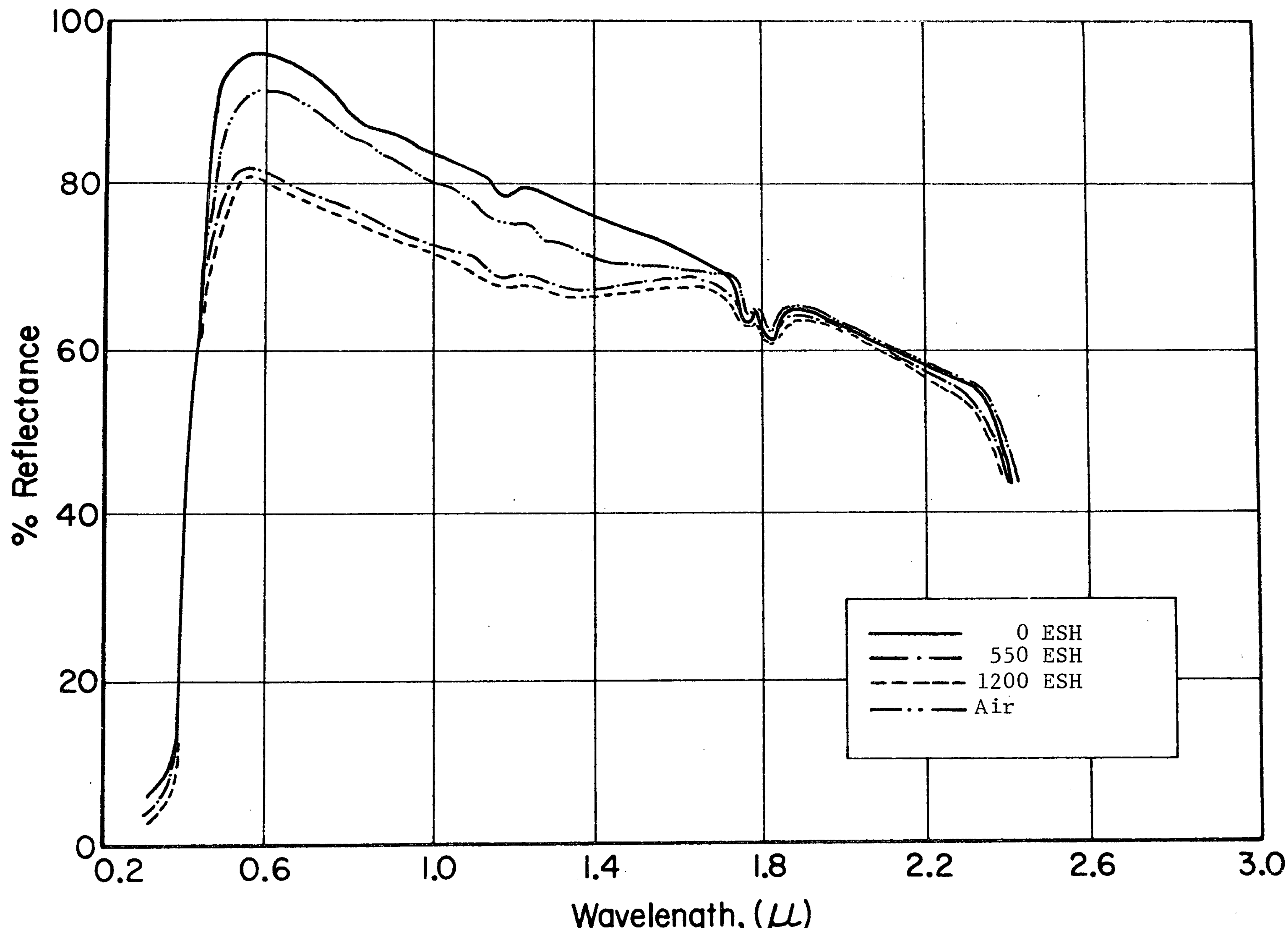

Figure 43 EFFECT OF UV IRRADIATION ON A CABOT RF-I RUTILE-PIGMENTED 650 PAINT

data presented in Table 30 of the previous section (6.5.1). While the binder was RTV-602 in the earlier and Type 650 resin in the later case, neither degrade in the infrared (α_2-region). The extent of oxygen-bleachable damage is graphically shown in Figure 43 and, from Table 31, represented a $\Delta\alpha_s$ of 0.067. Similar to the zinc orthotitanate-pigmented Owens-Illinois 650 resin paints described in Section 8.4.4.4 of Chapter 8, it is believed that rutile titanium dioxide degradation in the 400- to 1500-nm wavelength region (in rutile) is enhanced by the degradation of the binder, however slight it may be for the Owens-Illinois 650 resin. The reader is referred specifically to section 8.7.2 of Chapter 8 for a possible explanation. Damage in this broad wavelength region is believed to be due to a shallow electron trap that is associated with the ultraviolet-induced reduction $Ti^{+4} \longrightarrow Ti^{+3}$ (Ref. 112); Perny and Lorang (Ref. 113) have examined the many radiation-induced absorption bands of both rutile and anatase titanium dioxide and relate an absorption band at 860 nm to the Ti^{+3} species: It is interesting to note from Figure 43 that it is the spectral region centered at about 975-nm that bleached completely on admission of air to the IRIF.

6.6 The Development of S-13G

6.6.1 Introduction

Although the development of S-13G is the subject of previous reports (Ref. 9, 114, 115) and a communication to the 3rd Thermophysics Conference (Ref. 116), it will be summarized here. The conceptual development of S-13G as well as most of the subsequent innovations were carried out under this research program (NASA Contract NAS8-5379). However, the pilot-production scale-up and field engineering of S-13G were performed under contract to the Jet Propulsion Laboratory (Ref. 115), Subcontract 951737 under NASA Contract NAS7-100. Production scale-up was performed for the Astronautics Laboratory of the George C. Marshall Space Flight Center under NASA Contract NAS8-23268. The S-13G coating is currently manufactured by IIT Research Institute to George C.

Marshall Space Flight Center Specifications 10M01835 and 10M01836, under a non-exclusive arrangement with the National Aeronautics and Space Administration.

6.6.2 Zinc Oxide and the In-Situ Problem

Zinc oxide (ZnO) was, until 1965, thought to be the most stable white pigment available in terms of the stability of its optical properties to ultraviolet irradiation in vacuum (Ref. 1, 117, 118). However, in 1965 serious challanges to ZnO's purported behavior were reported as discrepancies between laboratory-simulation data and flight-experiment data obtained from the materials' experiments flown on OSO-II (Ref. 119) and the Pegasus (Ref. 120) spacecraft.

These data indicated that ZnO-based silicone coatings were considerably less stable than predicted by the extensive space-simulation testing to which they had been subjected. This instability has since been attributed to the formation of an easily-bleached (by oxygen) infrared adsorption band that is not observed by the postexposure reflectance measurements that were at that time performed in air. This absorption band was first observed in the laboratory by MacMillan et al (Ref. 121) during in-situ measurements of the bidirectional reflectance of in vacuo, ultraviolet-irradiated ZnO. Confirmation was reported by Miller (Ref. 122) and subsequently by Zerlaut et al (Ref. 9).

The effect of ultraviolet irradiation on IITRI's S-13 thermal control coating*, the polydimethylsiloxane (General Electric RTV-602) paint pigmented with untreated ZnO that had degraded severely in flight tests (Ref. 119, 120) is shown in Figure 44.

The S-13 paint exhibits a reflectance decrease of about 35% at 2000 nm (2μ) after approximately 800 equivalent sun hours (ESH) of ultraviolet irradiation in vacuum, Figure 44. However, an essentially instantaneous increase in infrared reflectance

*S-13 was described in Reference 1 as being stable.

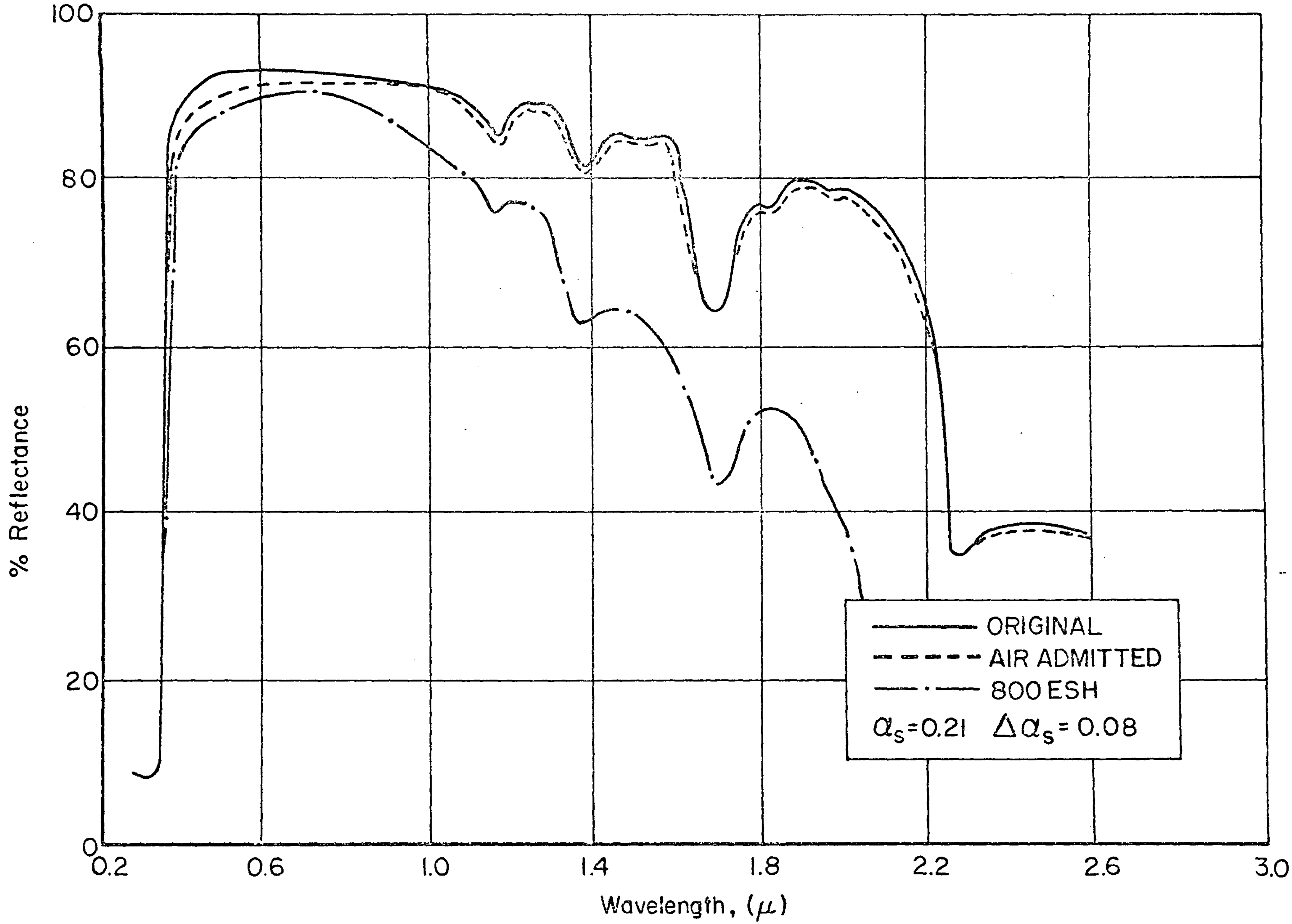

Figure 44 UV DEGRADATION OF S-13

occurs when either air or oxygen are admitted to the irradiated specimen; the recovery is very nearly total after only two minutes of exposure to air. The effect of 1000 ESH of ultraviolet radiation on a "water-sprayed" specimen of SP500 ZnO is shown in Figure 45. These data show that the bulk of the solar absorptance increase exhibited by ZnO as a powder, and as a paint in the S-13 coating, is due to the oxygen-bleachable damage sustained in the infrared.

The rapidity with which the ultraviolet-induced infrared absorption band develops in ZnO and the abruptness with which oxygen annihilates the absorption strongly indicated that the infrared phenomenon is not related to bulk diffusion phenomena but is associated with the photodesorption of adsorbed oxygen. Of particular significance was the fact that IITRI's Z93 thermal control coating, an SP500 ZnO-pigmented potassium silicate paint, did not undergo the bleachable infrared damage exhibited by S-13 and pure ZnO. Figure 46 is a typical example of the spectra of irradiated and unirradiated Z93, which is seen to be quite stable to ultraviolet radiation in vacuum.

The absence of damage to ZnO-pigmented alkali silicate coatings suggested that the reaction of ZnO with the potassium silicate may have precluded the bleachable infrared degradation exhibited by ZnO powder and ZnO-pigmented silicone paints. The polydimethylsiloxanes do not "wet" the pigment particles and consequently we conjectured that they do not offer an effective barrier to photodesorption reactions on the surface of ZnO. We, therefore, performed a series of experiments in which ZnO was first reacted with potassium silicate and then extracted and dried as a new, treated ZnO pigment. We showed that a ZnO powder treated (reactively encapsulated) in this way does not exhibit infrared degradation. The reflectance spectra of an irradiated silicate-treated ZnO specimen are presented in Figure 47.

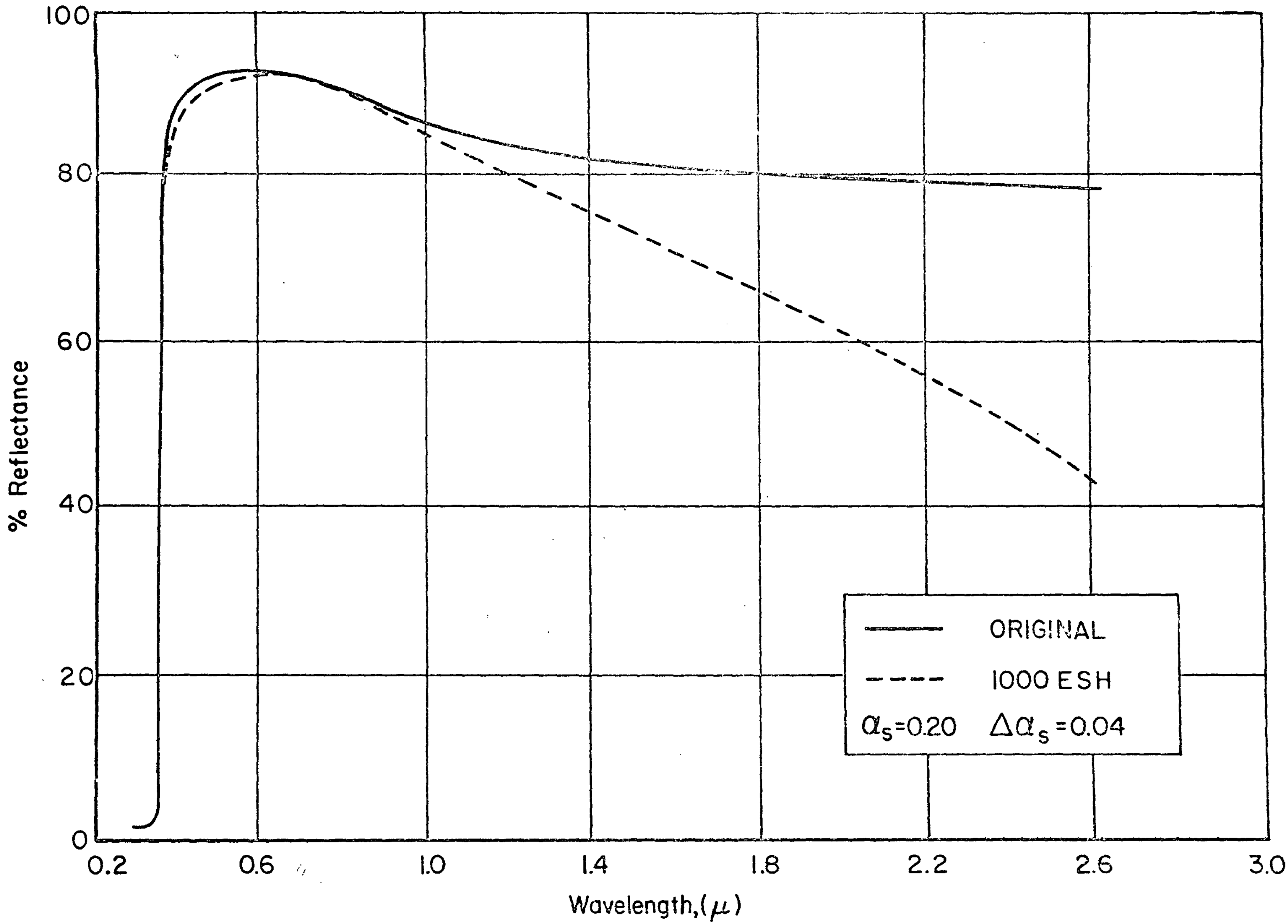

Figure 45 UV DEGRADATION OF ZnO

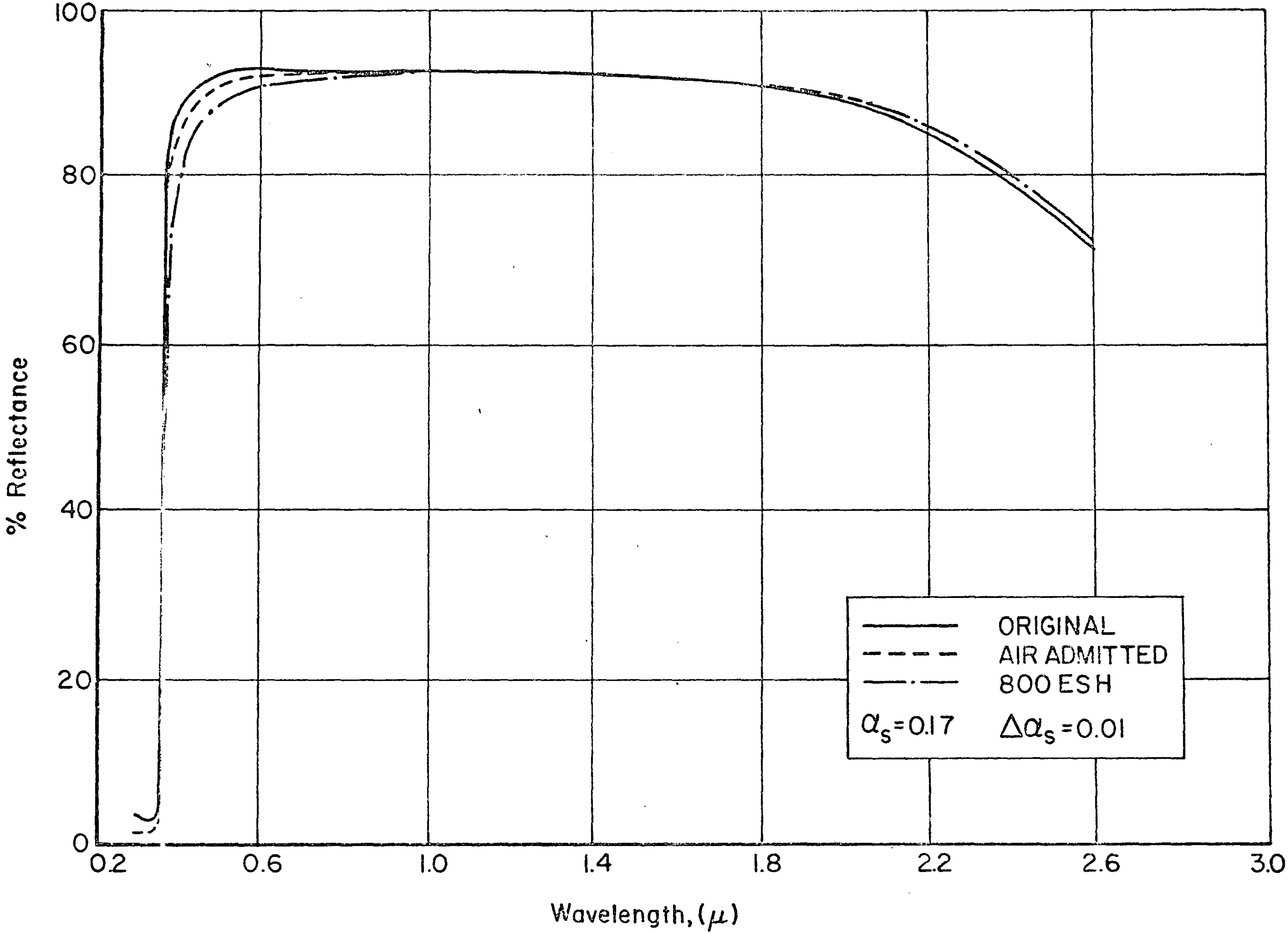

Figure 46 UV DEGRADATION OF Z93

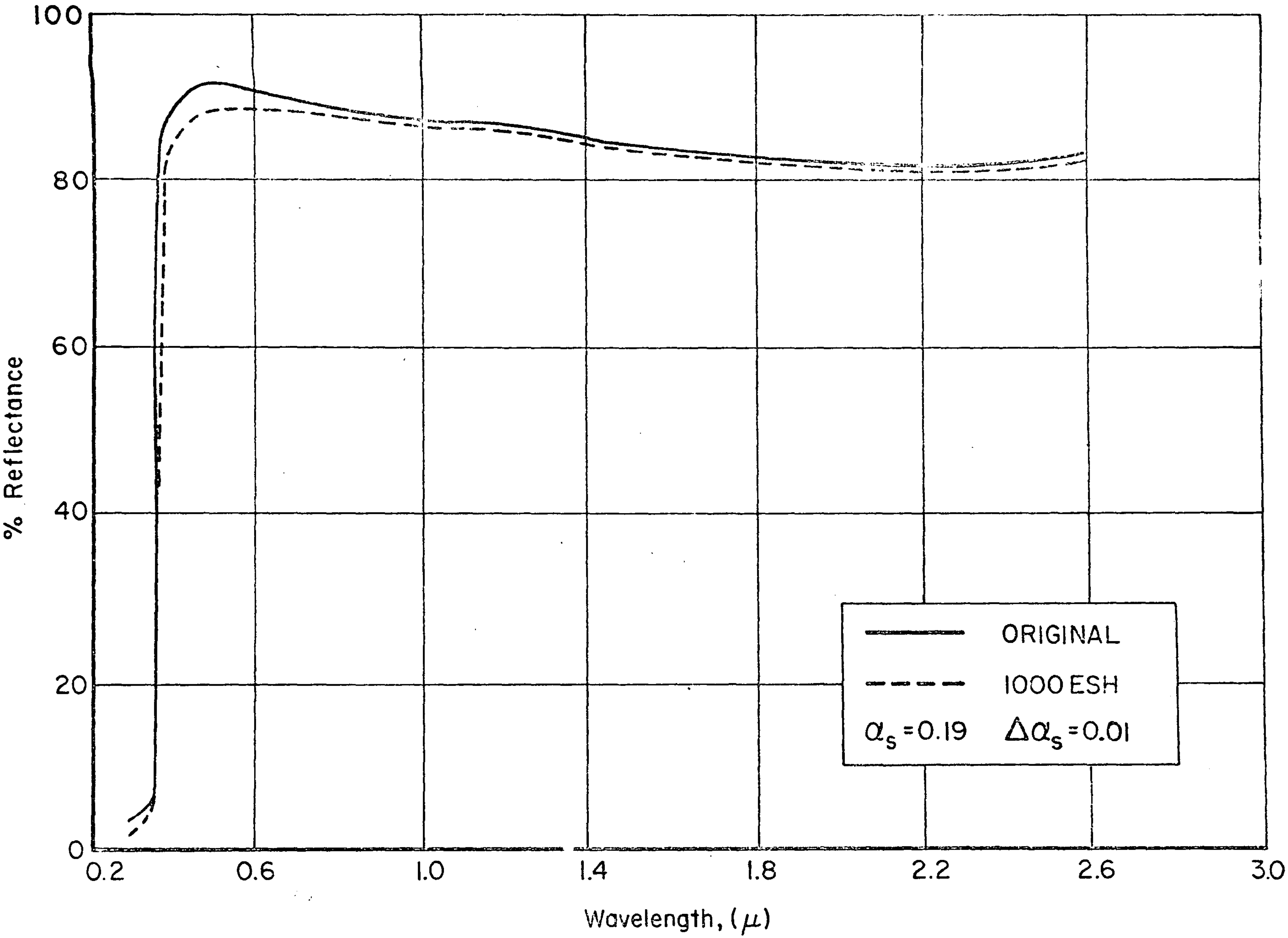

Figure 47 UV DEGRADATION OF SILICATE-TREATED ZnO

Although a complete description of the proposed mechanism for damage in ZnO and its prevention by reactive encapsulation with potassium silicate is presented in section 8.4.2 of Chapter 8, the basic aspects of the mechanism, which is beginning to be understood, should be presented here. We believe that the infrared optical behavior of ZnO can be explained on the basis of a free-carrier absorption mechanism. Gilligan (Ref. 74), in studies conducted for the Jet Propulsion Laboratory, concluded that the absorbed photon creates an electron-hole pair with the hole migrating to the surface to discharge adsorbed oxygen species. The valence-band holes are attracted to the surface, where they discharge adsorbed oxygen (and other absorbate gases). The surface thus becomes electron rich with the result being that the electrons accumulate in the infrared-active conduction band where, if their concentration is high enough, we observe them as the so-called free-carrier absorption.

Obviously silicating with potassium silicate interferes with the kinetics of electron accumulation in the conduction band. We postulate in Chapter 8 that the polynegativity of the silicate anion attracts the "positive" holes preferentially with the result that the electrons are no longer as free to accumulate in the conduction band. While this concept is not without viable counter-arguments, the <u>usefulness</u> of this thesis was proven when other polynegative "reactive" anions were employed to also effect a stabilization of zinc orthotitanate (Chapter 8).

6.6.3 S-13G

The S-13G paint was formulated to replace the S-13 coating which had been specified for a large number of spacecraft. The elastomeric S-13G paint was desired for those applications where the use of Z93 was precluded or presented difficulties. For example, the silicone coating is more easily applied, can be manufactured and shipped (as opposed to Z93) and is, unlike Z93, easily cleaned.

We quickly realized during the course of the early studies that the development of stabilized ZnO-pigmented RTV-602 silicone paints is largely a process problem. Factors that had to be considered in engineering S-13G were (Ref. 115, 116):

1. Initial ZnO-silicate reaction parameters such as materials' balance, reaction temperature, reaction time, and mixing during reaction
2. Pigment filtration and silicate extraction (washing) procedures
3. Pigment-drying and -grinding procedures
4. Silicone paint-manufacturing procedures
5. Optimization of paint formula relative to pigment volume concentration (PVC), solvents employed, catalyst concentration, etc.

The two major problems that arose during the course of the research, both of which were completely solved, were (1) decreased stability of S-13G compared to S-13 in the 385- to 450-nm wavelength region, and (2) intermittently poor shelf life of production batches that varied from 3 to 200 days. Current production batches of S-13G possess nominal solar absorptance values of 0.19 for 8-mil films and engineering values for $\Delta\alpha_s$ of 0.02 in 1000 ESH of ultraviolet irradiation in vacuum. The reflectance spectra of a typical, irradiated production batch of S-13G is presented in Figure 48.

6.6.4 Engineering Considerations

S-13G is currently furnished at 66% solids, a pigment volume of 32% PVC, and a viscosity of 27 seconds (No. 4 Ford Cup). The solvents and thinners employed with S-13G are those best suited to the RTV-602 binder and are delineated in section 6.4. The shelf-life of S-13G is warranted by IIT Research Institute for 30 days from date of manufacture (DOM), which is the date the paint is removed from initial refrigeration. The paint currently exhibits a shelf life of greater than one year. Indeed, we now have production-batch retains that are still re-dispersable after two years.

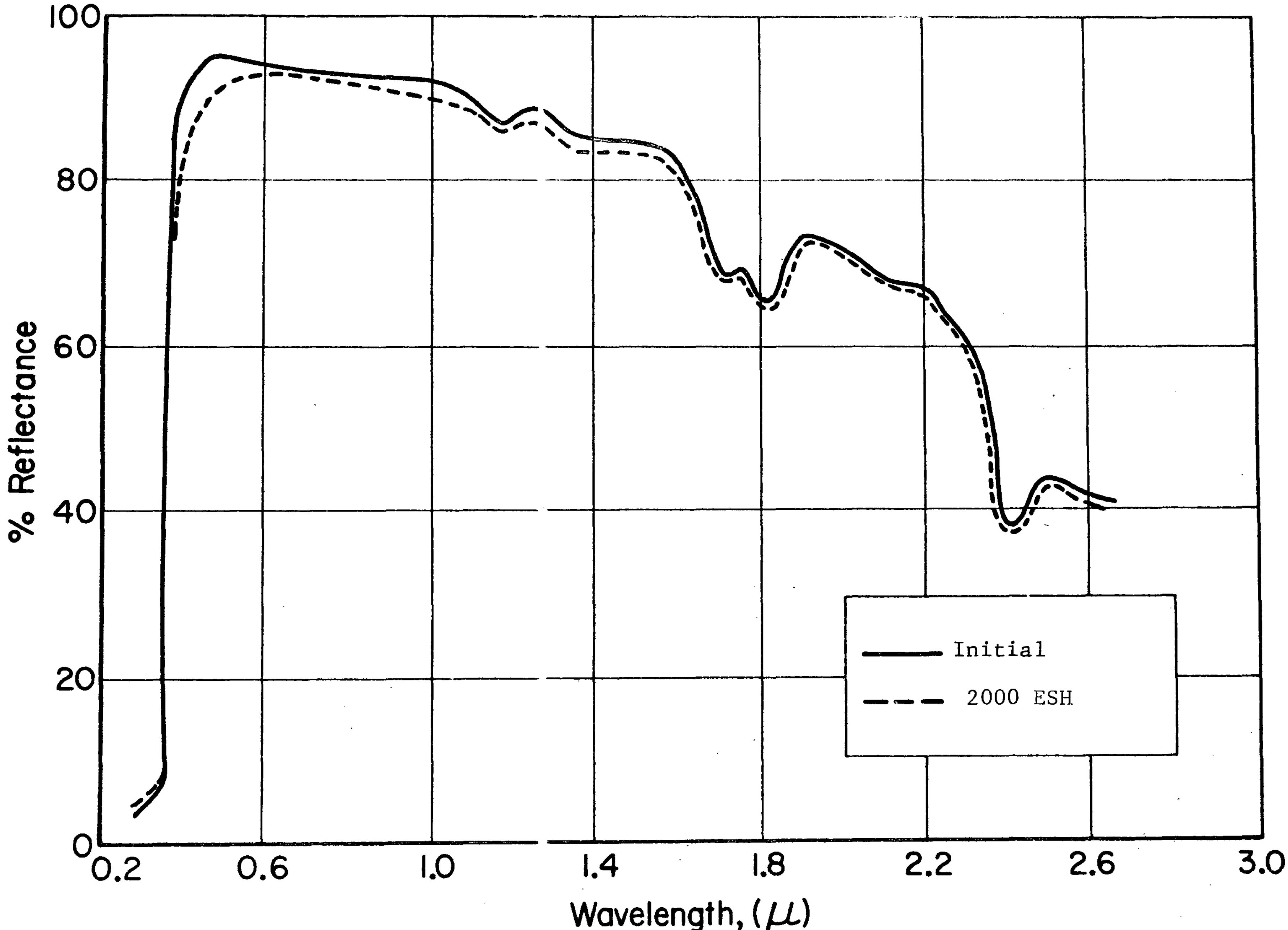

Figure 48 EFFECT OF UV IRRADIATION ON REFLECTANCE SPECTRA OF A TYPICAL PRODUCTION BATCH OF S-13G (BATCH B-581)

Although General Electric's SS4044 proprietary primer is recommended for S-13G, both GE's SS4155 and Dow Corning's OC4098 may be used without added advantage. It is mandatory however that the primer be kept less than 1 mil in thickness, and less than 0.4 mils thickness if the S-13G is to be subjected to a programmed "slow" cryovac exposure to LN_2-temperatures, or the S-13G/primer system may completely loose adhesion to the base metal.

6.7 The Development of A-429 Thermal-Control Paint

6.7.1 Introduction

Once we learned how to prevent the infrared degradation of zinc oxide by the now well-known treatment with potassium silicate (aimed at incorporation into the RTV-602 silicone elastomer), an obvious course of action was the preparation of silicate-treated zinc oxide paints based on the highly ultraviolet-stable Owens-Illinois 650 resin. Unfortunately, the very chemical functionality of the Type 650 resin, the residual hydroxies that allow it to be thermally cured at low temperatures without the use of catalysts, causes nearly instantaneous gellation when mixed with silicate-treated zinc oxide. The highly alkaline surface of the treated pigment acts as an alkaline catalyst to promote rapid polymerization of the B-staged resin.

The previous work (Ref. 9, 114, 115, 116) dealing with the development of S-13G as an engineering material indicated that some advantage could be gained from an acid phosphate-treatment of the silicate-treated zinc oxide. This was especially true for the case where the silicate-treated zinc oxide was calcined prior to incorporation into the S-13G paint; no loss in the protective effectiveness of the silicate treatment in the infrared region was observed in the phosphate-treated material.

We therefore reasoned that sodium acid phosphate might successfully be employed to neutralize the alkaline surface of the silicate-treated zinc oxide, thereby making it a useful pigment for the Owens-Illinois resin, without affecting the infrared stability of the pigment that is achieved by silicating. Experiments were accordingly performed to determine the effect of different methods of phosphate treatment of the silicated zinc oxide pigment.

6.7.2 Experimental

The starting point in all of these experiments was a filter cake from the silicate treatment of the zinc oxide as regularly produced in the manufacture of pigment for S-13G paint. In order to obtain better process control, all variations in treatment were made upon one sample of filter cake only, from a production batch of S-13G pigment.

<u>Silicate-Treatment Procedure (Cake 1)</u>

> Twelve (12) lb of New Jersey Zinc's SP500 zinc oxide (bulking at 0.257 gal), 21 lb of Sylvania Electric's PS7 potassium silicate solution (bulking at 1.91 gal), and 3.25 lb of distilled water (0.39 gal) were reacted together in a double boiler in the following manner: The water and the potassium silicate were heated to 165°F. The zinc oxide was then added under high-speed agitation and the temperature was maintained for 20 min with high-speed agitation. The heat was then removed, a cold water-jacket replaced the hot; 13.25 lb of distilled water (1.625 gal) was immediately added. The slurry was then mixed for 15 min and filtered through a Buchner funnel. The filter cake was wrapped in unplasticized Mylar and allowed to "sweat" for 18 hr. The filter cake so produced is labeled "cake 1". It analyzed at 62% solids with a K_2O content of 3.8% and a SiO_2 content of 15% (the balance was ZnO). The entire filter cake (cake 1) would normally be re-filtered, and finally dried at 212°F for 18 hr. (The pigment so produced usually shows an analysis of 7 to 9% SiO_2 and 1 to 3% K_2O.)

Even though the K_2O content of the final pigment (cake 3) has been as low as 0.7%, the S-13G pigment has always been too alkaline to permit dispersion in Owens-Illinois 650 resin. The cake-1 silicate-treated zinc oxide described above was employed as the starting material in all of the acid phosphate treatments, including controls, that are discussed in the following paragraphs.

Acid Phosphate-Treatment Procedures

Pigment A-413-1 (control): Ninety (90)g of Cake 1 was slurried with 50 g of distilled water for 15 min and filtered. The resultant cake 2 was re-dispersed in 50 g of water, slurried 15 min, filtered and dried for 18 hr at 212°F. The product was designated Cake 3.

Pigment A-413-2 (control): Ninety (90)g of Cake 1 was treated identically to A-413-1 except that it received an additional re-dispersion in water. The final product was designated as Cake 4.

Pigment A-413-3 (phosphate-treated): Ninety (90)g of cake 1 was slurried for 15 min with 50 g of a 1% solution of NaH_2PO_4. The resultant cake 2 was redispersed in 50g of 1% NaH_2PO_4, slurried 15 min, filtered and dried for 18 hr at 212°F. The product was designated Cake 3.

Pigment A-413-4 (phosphate-treated): Ninety (90)g of Cake 1 was treated with 1% NaH_2PO_4 identically to A-413-3 except that it received an additional redispersion in 50g distilled water. The final, dried product was designated Cake 4.

Pigment A-413-5 (phosphate treated): Ninety (90)g of Cake 1 was slurried for 15 min with 50 g of a 3% solution of NaH_2PO_4. The resultant cake 2 was redispersed in 50 g of 3% NaH_2PO_4, slurried 15 min, filtered and dried for 18 hr at 212°F. The product was designated Cake 3.

Pigment A-413-6 (phosphate-treated): Ninety (90)g of Cake 1 was treated with 3% NaH_2PO_4 identically to A-413-5 except that it received an additional redispersion in 50 g of distilled water. The dried product was designated Cake 4.

Owens-Illinois 650-Resin Paints

Owens-Illinois 650-resin-based paints were prepared from each of the pigments described above by grinding 15 parts of the 28% O-I 650-resin solution (see section 6.5.2) with 10 parts of pigment by weight (the PVC was approximately 32% in all six cases).

6.7.3 Results

Shelf-life studies of the six paints were performed. The results are presented in Table 32. Although additional studies are obviously necessary, the data show that washing with sodium acid phosphate has an advantageous effect on the shelf life of the A-429 O-I 650 paint. In the absence of more definitive studies, we concluded that the "fourth" water redispersion of the 1% acid phosphate-treated pigment (A-413-4) removed the neutralizing influence of the acid phosphate and A-413-4 gelled due to alkaline polymerization of the polyfunctional 650 "silicone" resin. On the other hand, we hypothesize that the A-413-5 paint gelled by acid polymerization due to the 3% acid phosphate employed in the neutralization--a factor which the additional water dispersion employed in making pigment A-413-6 militated against. It should be noted, however, that the acid phosphate was not "fixed" on pigments A-413-4 and A-413-6 by drying prior to the last redispersion in water.

The two paints that possessed a three-day shelf life were prepared on IRIF coupons and irradiated in the IRIF. The results are presented in Table 33. The reflectance spectra of the most stable of the two paints is presented in Figure 49. Examination of these data show that the specimen prepared from the 3% acid phosphate wash was the superior of the two. Indeed, this paint, designated A-429, gave the greatest stability to ultraviolet irradiation in vacuum achieved with a zinc oxide-polymethylsiloxane paint prior to 1971.

Table 32

SHELF-LIFE OF O-I 650/SILICATE ZnO PAINTS (A-429 SERIES)

Pigment No.	Description	Cake No.	Gellation Time hr
A-413-1	Control	3	1
A-413-2	Control	4	2.5
A-413-3	1% Phosphate	3	≈72
A-413-4	1% Phosphate*	4	1.5
A-413-5	3% Phosphate	3	4
A-413-6	3% Phosphate*	4	≈72

*The last redispersion made in distilled water only.

Table 33

EFFECT OF ULTRAVIOLET IRRADIATION IN THE IRIF ON TWO SILICATE-TREATED ZINC OXIDE O-I 650 RESIN PAINTS

Description	Exposure (ESH)	Solar Absorptance α_1	α_2	α_s	$\Delta\alpha_s$
Paint No. A-429 (I) (3% Acid-Phosphate Washed Silicated ZnO in O-I 650 Resin)	0	0.127	0.098	0.225	
	550	0.131	0.098	0.229	0.004
	1200	0.129	0.097	0.226	0.001
Paint No. A-429 (II) (1% Acid Phosphate washed Silicated ZnO in O-I 650 Resin)	0	0.158	0.170	0.328	
	550	0.168	0.170	0.338	0.010
	1200	0.169	0.171	0.340	0.012

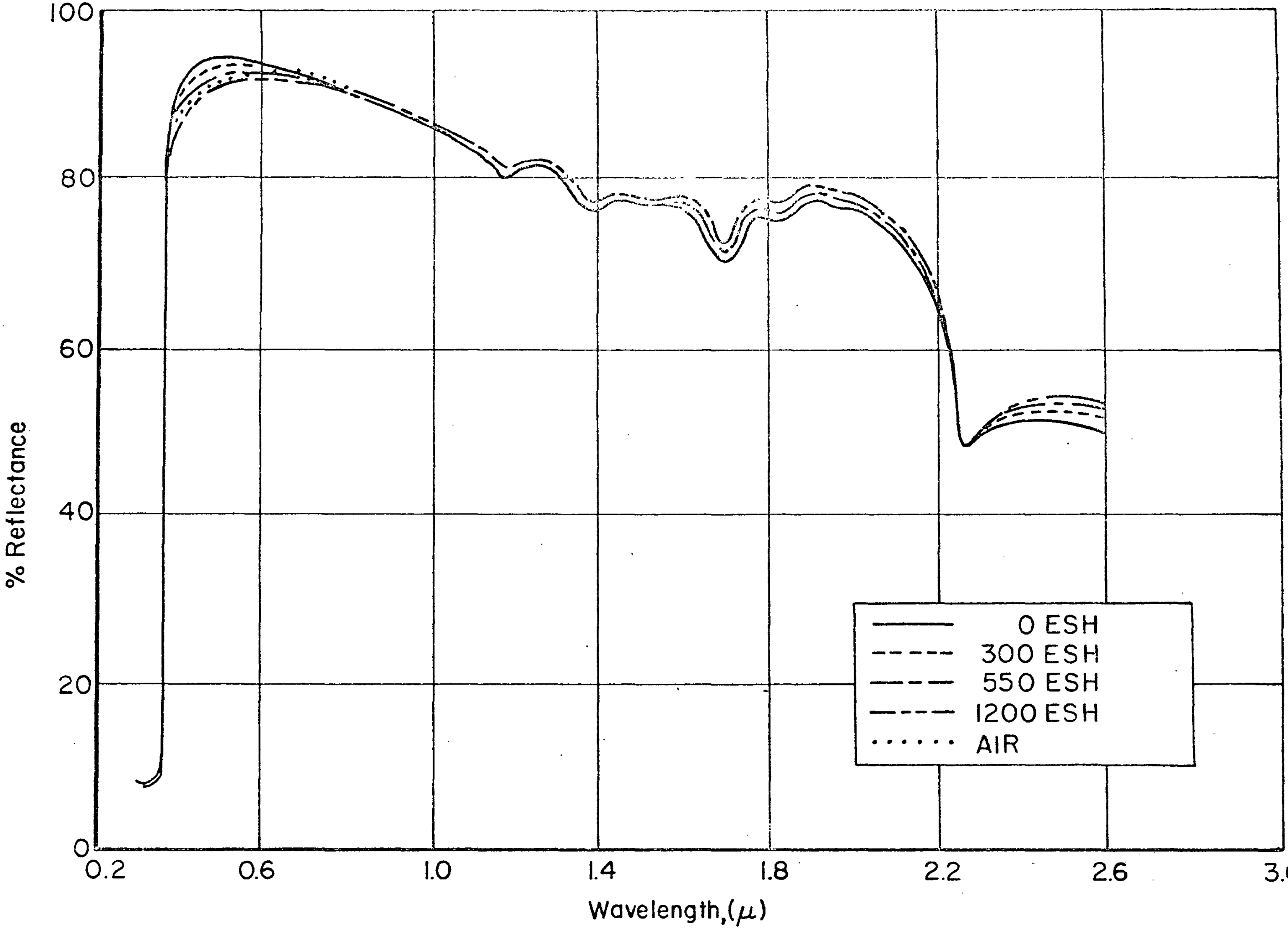

Figure 49 UV DEGRADATION OF SILICATED ZnO IN SILICONE "GLASS" RESIN (COATING A-429)

7. COMBINED-ENVIRONMENT SIMULATION

7.1 Introduction

For approximately ten years researchers in the field of spacecraft temperature control materials have been attempting to develop low solar absorptance coatings which are unaffected by the hostile elements of the space environment. During this period we have learned much about the manner in which we should test candidate materials. Nevertheless, it was not until six (6) years ago that the need for in-situ testing (Ref. 9, 121) was clearly demonstrated. Accordingly, IITRI designed the IRIF, the In-Situ Reflectance Irradiation Facility (Ref. 3). As more sophisticated missions were considered and as spacecraft missions to the moon and planets became more common, the requirements of these missions for stable spacecraft thermal control materials became more demanding. The solar wind environment had to be added to the testing scheme, because the environment of deep space includes not only solar electromagnetic radiation but also solar-wind protons (and low-energy electrons) and auroral electrons.

There are two points which from experience we know are highly important in the evolution of a simulation laboratory and the policy under which it operates. First, we firmly believe that responsible testing requires a materials science approach to the research and development of thermal control materials, a basic knowledge of the effects of ionizing radiations on materials, and an understanding of the operating principles and characteristics of the systems employed. Second, we recognize a strong need for credible simulation criteria. The greatest need we have at present in this sense is to assess the effects of nonsimulation--i.e., the differences in effects on materials when spectral compositions, flux rates and/or spectral flux rates are not close to space values.

IITRI's Combined Radiation Environment Facility, the CREF, evolved after consideration of the above and many other points. A definite need exists for determining the effects of the deep space environment, where the solar wind and solar ultraviolet radiation are concurrent. Since these two types of radiation are fundamentally different--one massive and the other electromagnetic, we expect, therefore, that the mechanisms of their interactions will be fundamentally different.

7.2 Charged Particle Interactions - General Remarks

Charged particles lose their kinetic energy primarily in interactions with the deeper-lying electronic levels of an atom. As a fast-moving particle approaches an atom lying in its path, part of its kinetic energy is transferred through the coulombic field interaction to the electrons of the atom, with the result that some of the electrons are either expelled (the atom is ionized) or are raised from their ground states to highly excited states; some of the atoms may be ejected also. Some of the ejected ions and electrons, in turn, possess sufficient energy to displace, ionize and excite other atoms. The probability of energy transfer is greatest for multiply-charged, slow-moving particles. The passage of charged particles through matter therefore involves a series of interactions, the nature of which depends upon the charge and initial energy of the particle. As it slows down, its potential for causing displacements and thus secondary interactions decrease; the probability for direct ionization also decreases with decreasing velocity--until finally only minor excitations will occur. The interactions most important in terms of optical stability are displacement of atoms, ionization, and excitation. By no means do all of the displaced atoms or excited electrons remain permanently away from their previous or similar equilibrium positions; most in fact, do return. One should note therefore that the excitation process is followed by a recovery (luminescence) process in which x-rays and ultraviolet radiation are emitted. It is thus highly probable that charged particle interactions will induce damage characteristic of high energy electromagnetic radiation as well as that due to atomic displacements and chemical reactions (for example, with protons).

Each incident proton will generate a multitude of hard ultra-violet photons. If long wavelength radiation is not also present, the damage will generally not be bleached.

Seitz, amongst others, developed equations showing that the rate of energy loss is directly proportional to: material density, charge on the moving particle, and the atomic number of the stationary atom; and that it is inversely proportional to: the energy of the moving particle, and in the case of displacements, to the mass of the stationary atom, and the displacement energy. The rate of displacement can be calculated also--from knowledge of the rate of charged particle incidence and the displacement energy. This gives a rough idea of the maximum instantaneous rate of formation of interstitials and vacancies, i.e., potential color centers (Ref. 123).

For energetic reactions, in which the <u>particle velocity greatly exceeds</u> the orbital electron velocities in the encountered atom, we can use the overall energy loss rate of a particle from the expression:

$$\frac{-dE}{dx} = \frac{4\pi z^2 e^4}{M_e V_p^2} N_o Z \log(\varepsilon/B) + \frac{2\pi z^2 e^4}{\varepsilon} Z_i \log(\varepsilon/B_i), \qquad (7)$$

where

$\frac{dE}{dx}$ = the energy loss per unit distance per incident particle

z = number of charges on the charged particle

e = electronic charge

M_e = electronic mass

V_p = velocity of charged particle

N_o = density of stationary atoms

Z = atomic number of stationary atoms

B = a parameter characteristic of the electronic energy structure of the stationary atoms (of the order of the ionization potentials)

Z_i = number of electrons per atom in the outer shell, and

B_i = an energy parameter characteristic of that shell (similar to B).

The energy loss spent in displacement of atoms per incident charged particle can be calculated from

$$\frac{-dE}{dx} = \frac{2\pi z^2 Z^2 e^4 N_o}{M V_p^2} \log\left(\frac{E}{E_D} \cdot \frac{4\mu^2}{mM}\right) \tag{8}$$

where

m = mass of the charged particle, and

M = atomic mass of stationary atom.

The displacement energy, E_D, is the minimum energy which must be transferred to an atom to eject it from its lattice site.

Regarding the fates of displaced ions and electrons, it is a fortunate fact that the actual (net) induced vacancy and interstitial concentrations of irradiated materials are orders of magnitude less than those calculated from theory; this is because the displaced atoms/ions eventually return to fill the vacancies they generated. The estimation of induced vacancy and interstitial concentrations therefore bears little relation to the actual permanent concentrations of these defects.

In summary then, charged particle damage is certain to produce effects which ultraviolet produces, as well as some which result from massive interactions, and in combined radiation environments radiative bleaching is undoubtedly going to create "synergism" and invalidate any reciprocity which might have existed in single environment testing.

7.3 Space Simulation Criteria

7.3.1 Real Versus Simulated Space Environments

Ideal simulation implies exact duplication of the real space environment, not simply the effects of the real space environment.

Since the nature and composition of the real space environment differ from one place to another, the effects likewise differ. For example, the environment at 500 miles above the earth's surface differs very much from that 20,000 miles above it. However, beyond the radiation environment trapped in the earth's magnetic field, the space environment becomes geometrically uniform and depends only upon distance from the sun and temporal variations in solar radiations. To reproduce these environments in a laboratory we must have a reasonably good characterization of the solar electromagnetic spectrum as well as of the solar particulate radiations; the former is well known, the latter reasonably well known (Ref. 124, 125). There are, however, several other important questions involved in designing and operating simulation equipment and in the evaluation of the data.

First, and foremost, it is essential that in an operating system the response of materials be as nearly as possible the same as their response would be in the actual space environment. This condition is met when the exact conditions of the space environment are duplicated, i.e., when the electromagnetic spectrum, the charged particle energy spectrum, the rates at which both of these are incident on a surface, and when electrical neutrality and vacuum-thermal conditions are achieved--all <u>simultaneously</u>!

7.3.2 <u>The Electric Neutrality Problem</u>

The incidence of energetic protons upon a dielectric material will create a charge build-up in the material; in the case of protons the charge of the proton (or any positive ion, in general) in the dielectric material accummulates. This accumulation is further compounded by a secondary electron release in the case of energetic ions. In most materials the rate at which these secondary electrons are emitted can be and often is higher than is the rate of incidence of the charged particles producing them. The net charge buildup therefore can easily proceed at a rate higher than that due to the proton beam alone. Whether or not these conditions exist in space is a question of major significance. In our opinion, it is not possible for a very large voltage to build up on a spacecraft coating because the solar wind is electrically neutral (Ref. 126). The build up of a positive charge would in fact attract more strongly the electrons and tend to repel protons. It also would tend to attract the secondary electrons back to the surface so that the net charge buildup could not possibly get much beyond the material's work function (for the escape of electrons). This is of the order of possibly 5 to 10 electron volts. In the CREF the secondary electrons which escape from the samples are replaced by a thermal ion source. Although there may be some buildup of positive charge on the coatings of a spacecraft, it is probably not significant enough to affect spectral reflectance. In our opinion, however, this question is not completely resolved. Yet, because it is likely that charge build-up is not a significant problem on a space vehicle, it, therefore, should not be permitted in simulation facilities.

7.4 Design and Construction of the CREF

The Combined Radiation Environment Facility (CREF) described in a triannual report (Ref. 127) is a fully operational system combining ultraviolet, proton and electron radiation sources with an in-situ measurement capability (Ref. 3). Photographs of the facility are presented in Figures 50 and 51. Its components are shown schematically in Figure 52 and a block diagram of it is shown in Figure 53. Except for the ultraviolet irradiation facility (i.e., the burner and power supply), the entire integral simulation laboratory is shown in Figure 50. The Beckman DK-1 ultraviolet/visible spectrophotometer is shown to the rear (behind the CREF in the photograph); the control facilities, including the high-voltage divider, are shown in the left of the photograph. The IRIF (Ref. 3) and the interface with the accelerator are shown in Figure 51. The vacuum integrating sphere is shown on the left of this photograph. The 12 samples,

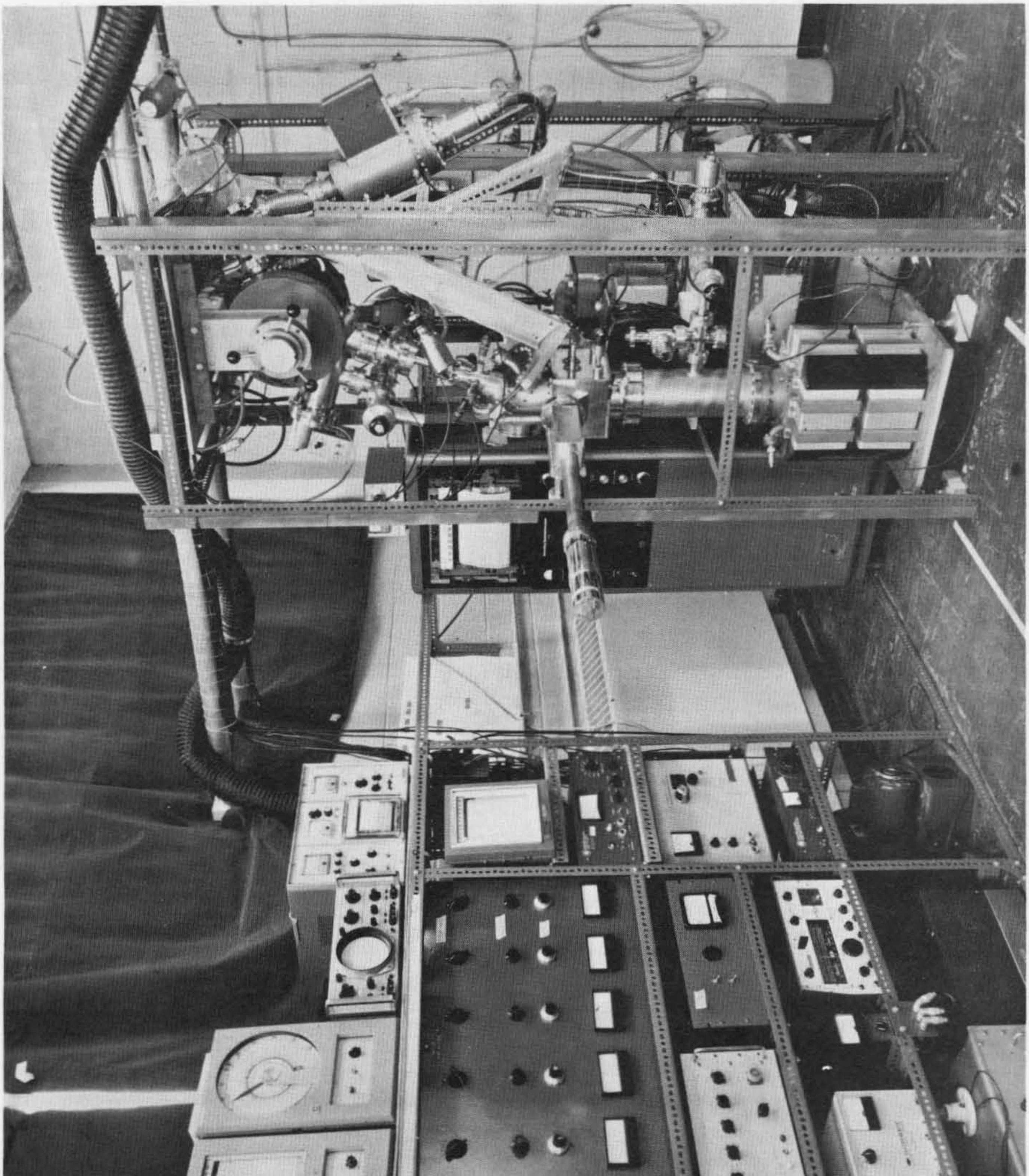

Figure 50 THE COMBINED RADIATION ENVIRONMENT TEST FACILITY (CREF)

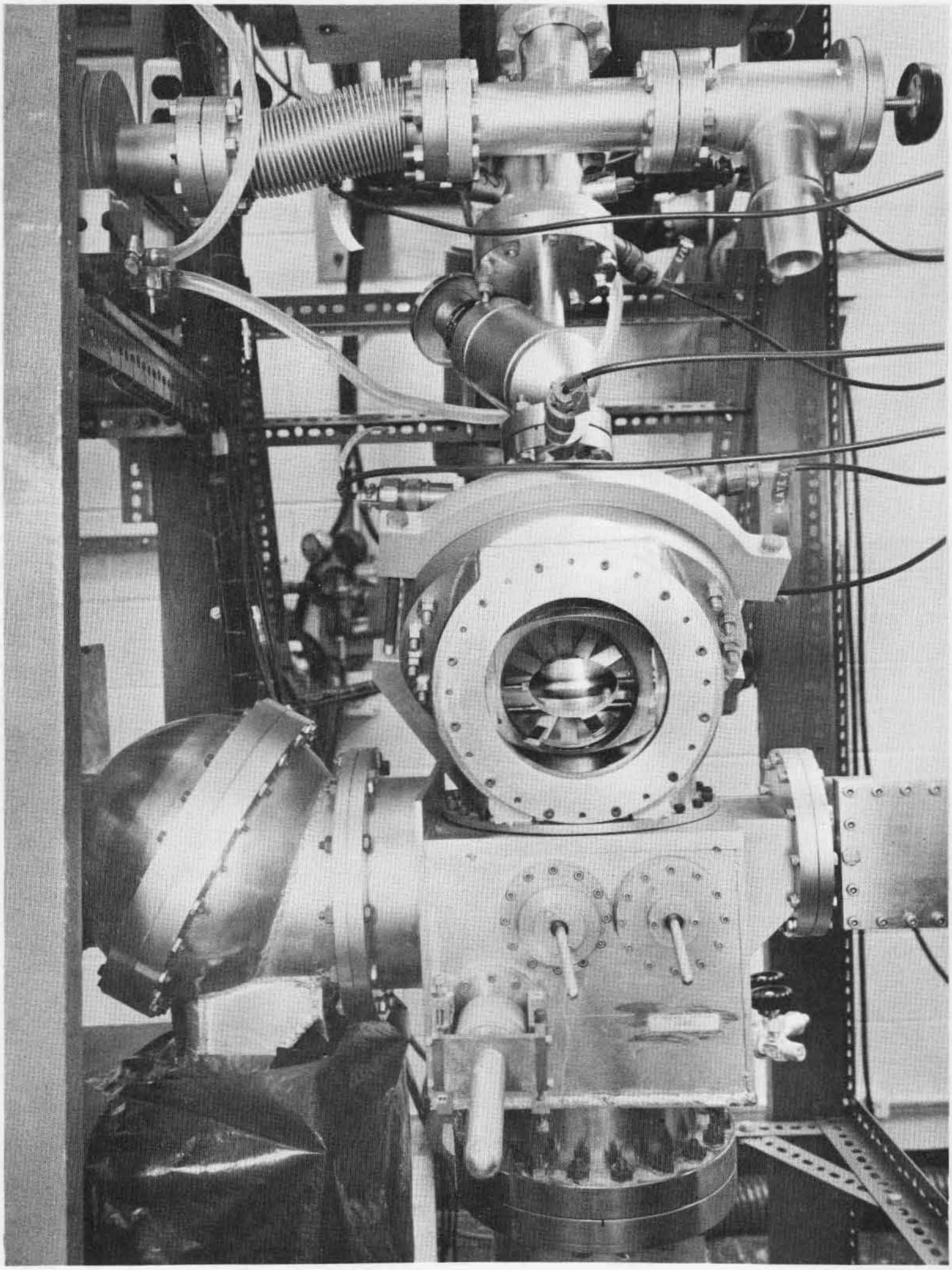

Figure 51 CLOSE-UP OF THE CREF SHOWING THE IRIF AND THE SAMPLES (REFLECTED IN THE 45° MIRROR)

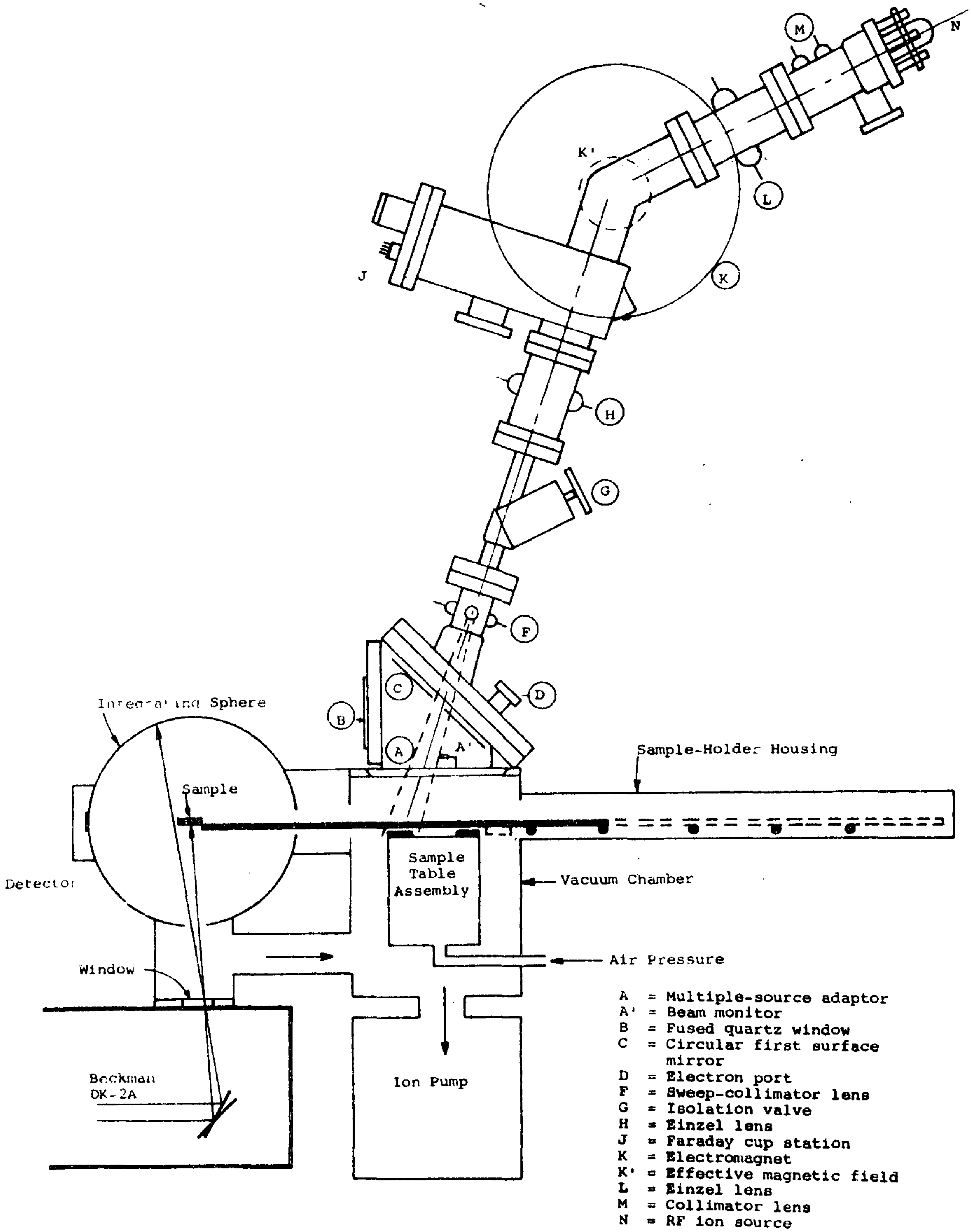

Figure 52 COMBINED RADIATION ENVIRONMENT FACILITY

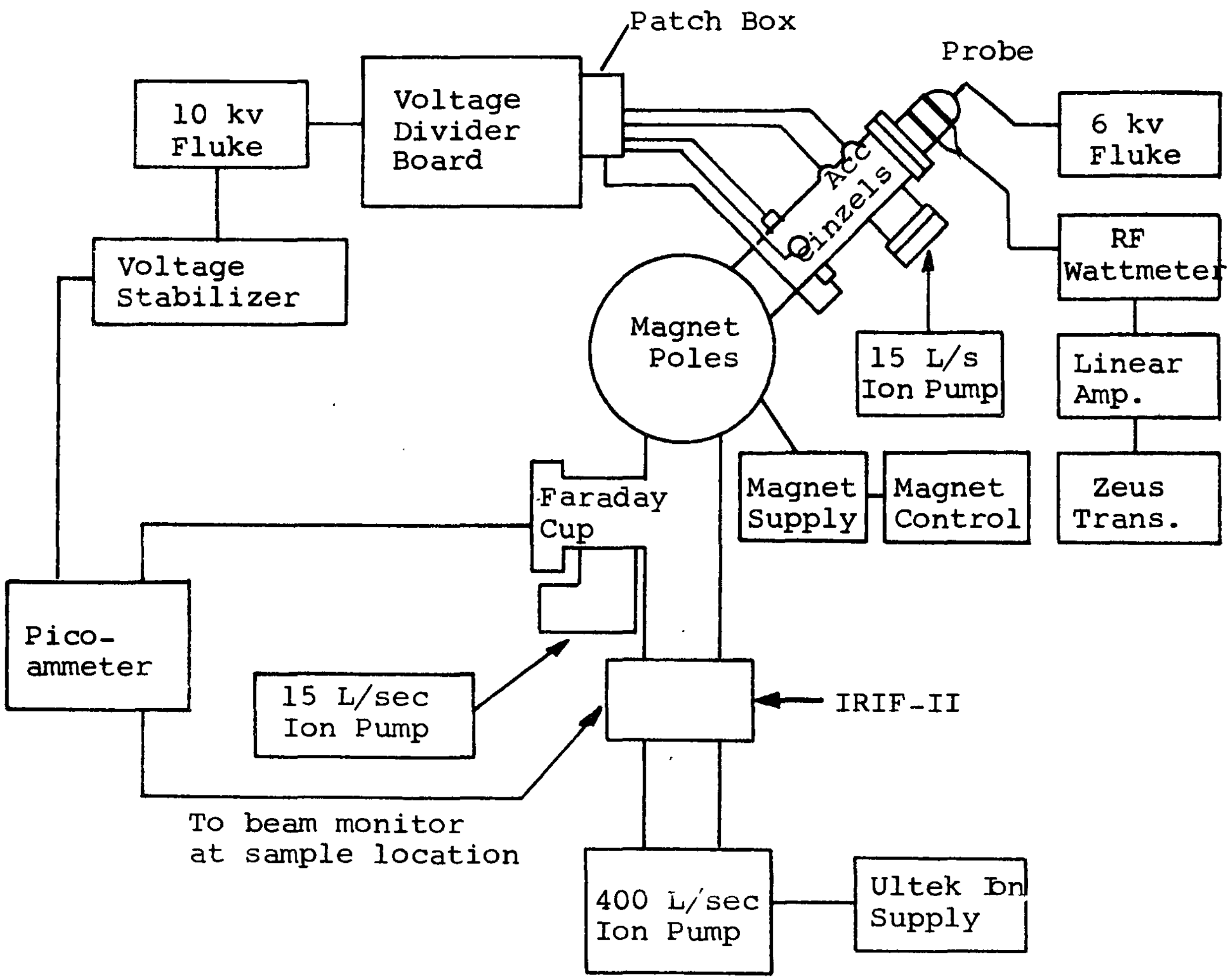

Figure 53 BLOCK DIAGRAM OF PRESENT CREF FACILITY

mounted radially in the IRIF, are shown reflected in the 45° first surface mirror (located in the multiple-source adaptor housing) employed to direct ultraviolet down onto the samples; the proton-beam port in the mirror is clearly shown.

The protons are generated in the RF (plasma) source at a potential of 1220 volts. The flow of hydrogen into the RF source (glow discharge) tube is controlled with a pressure regulator and a palladium leak. The proton beam is extracted through a small hole in the RF source into the extractor region; two collimator lenses with small diameter holes reduce the beam current from the proton source, originally of the order of 175 microamps, to about 40 microamperes. The extractor lenses, which are shown in Figure 54, also shape the beam, which then moves to the first einzel lens, which, in turn, focuses the beam into the magnet. The einzel lenses are shown in Figure 55. The highly regulated magnetic field selectively bends the ion components of the beam and thus physically separates the H^+, H_2^+ and other species. The field strength is adjusted to obtain a 45° deflection of the H^+ beam, which focuses it into another einzel lens, which, in turn, focuses the beam (through a valve) into a quadrapole lens. A Faraday Cup is located immediately downstream of the analyzer magnet and this is used to characterize the beam after it emerges from the magnet. The Faraday Cup assembly is shown in Figure 56. The angular (geometric) separation, energy and uniformity of the beam can be determined with this cup. After final focusing in the second einzel lens, the beam passes through a valve into the quadrapole sweep/collimator lens, shown in Figure 57, and then into the multiple-source adaptor housing (which connects the proton accelerator to the basic IRIF and possesses ports for simultaneous irradiation with protons, ultraviolet light, and low-energy electrons).

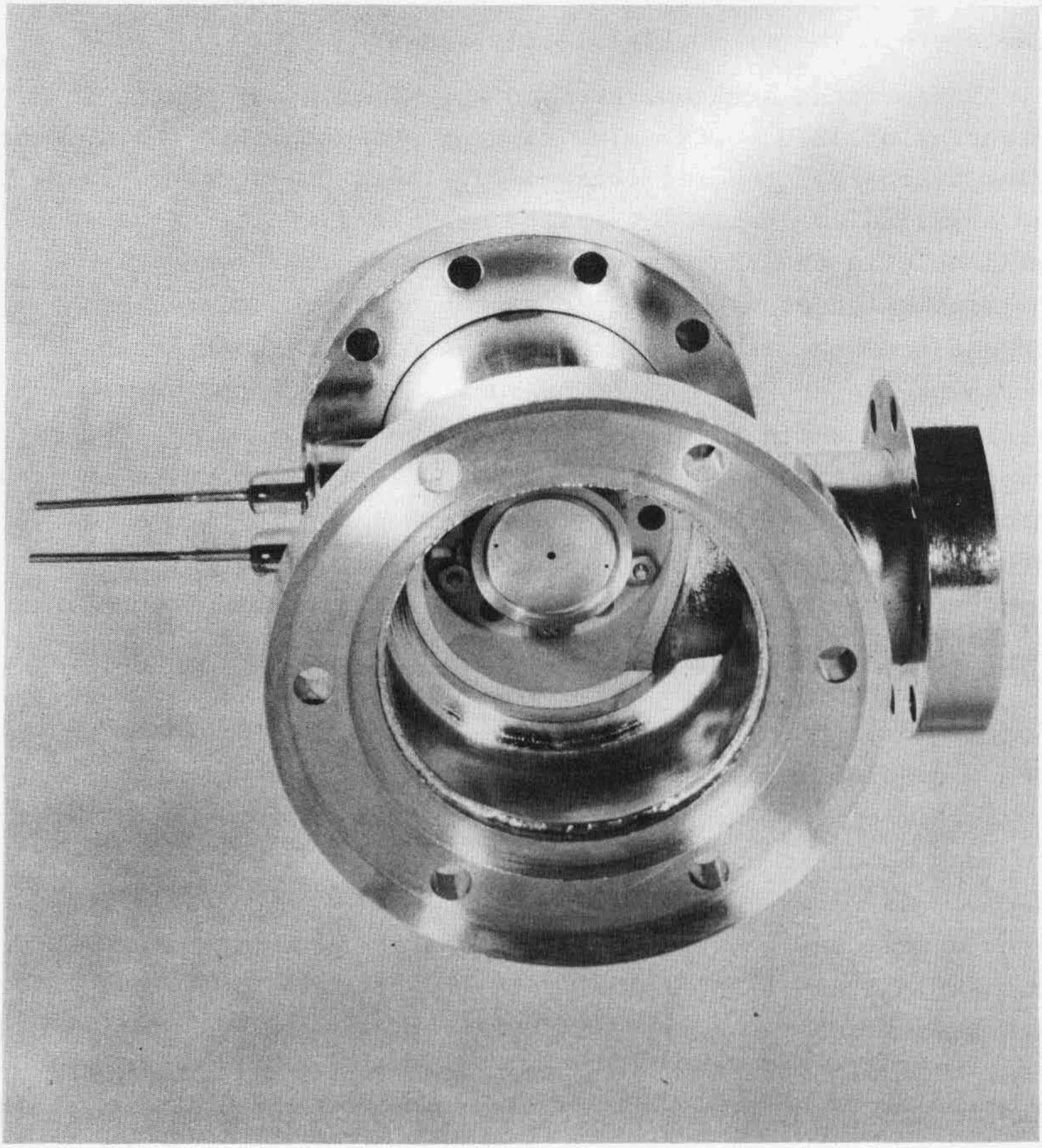

Figure 54 TWO-ELEMENT EXTRACTOR LENS (DISASSEMBLED) TO REDUCE FLUX FROM RF SOURCE

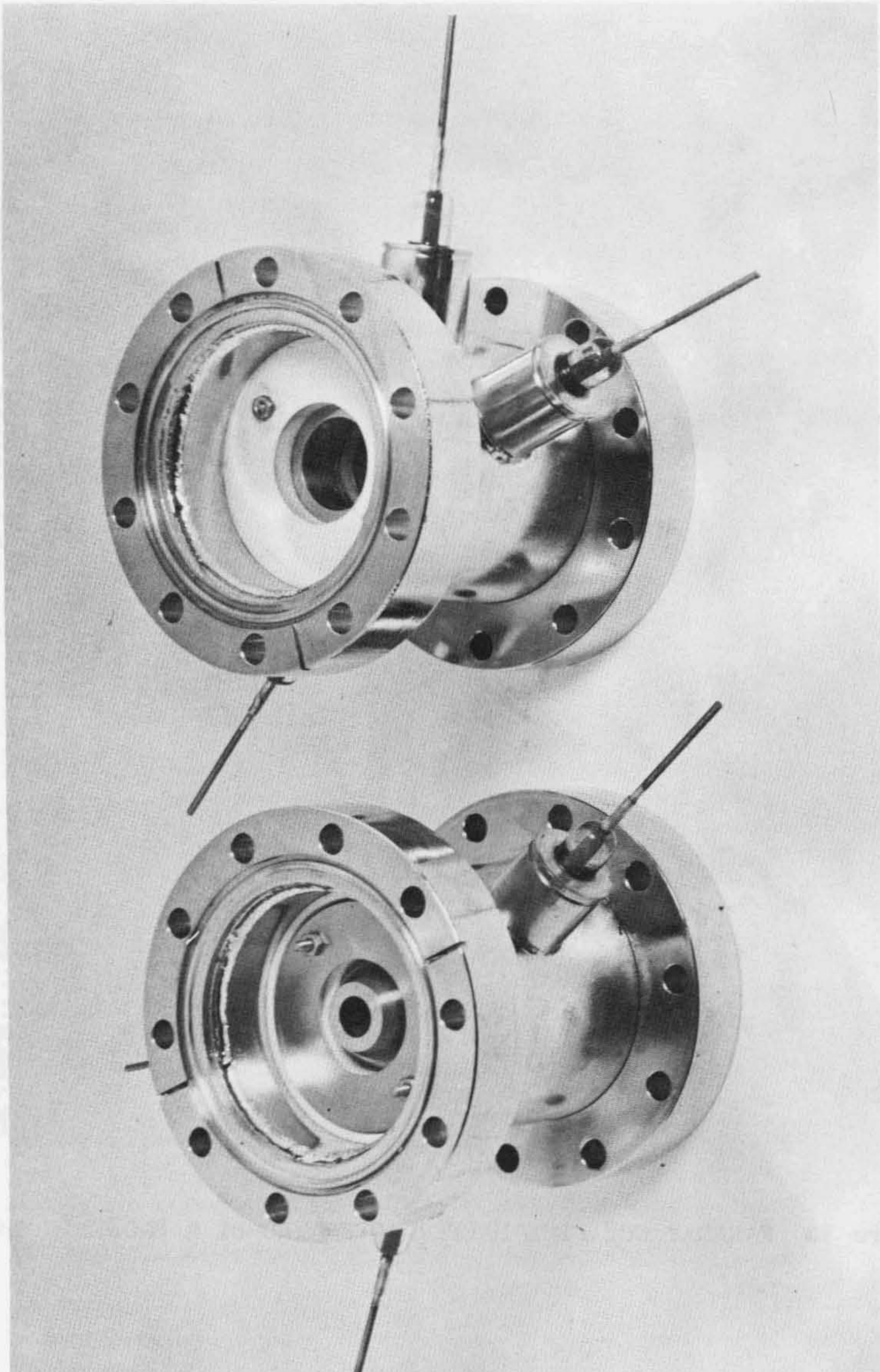

Figure 55 EINZEL LENSES: TWO VIEWS

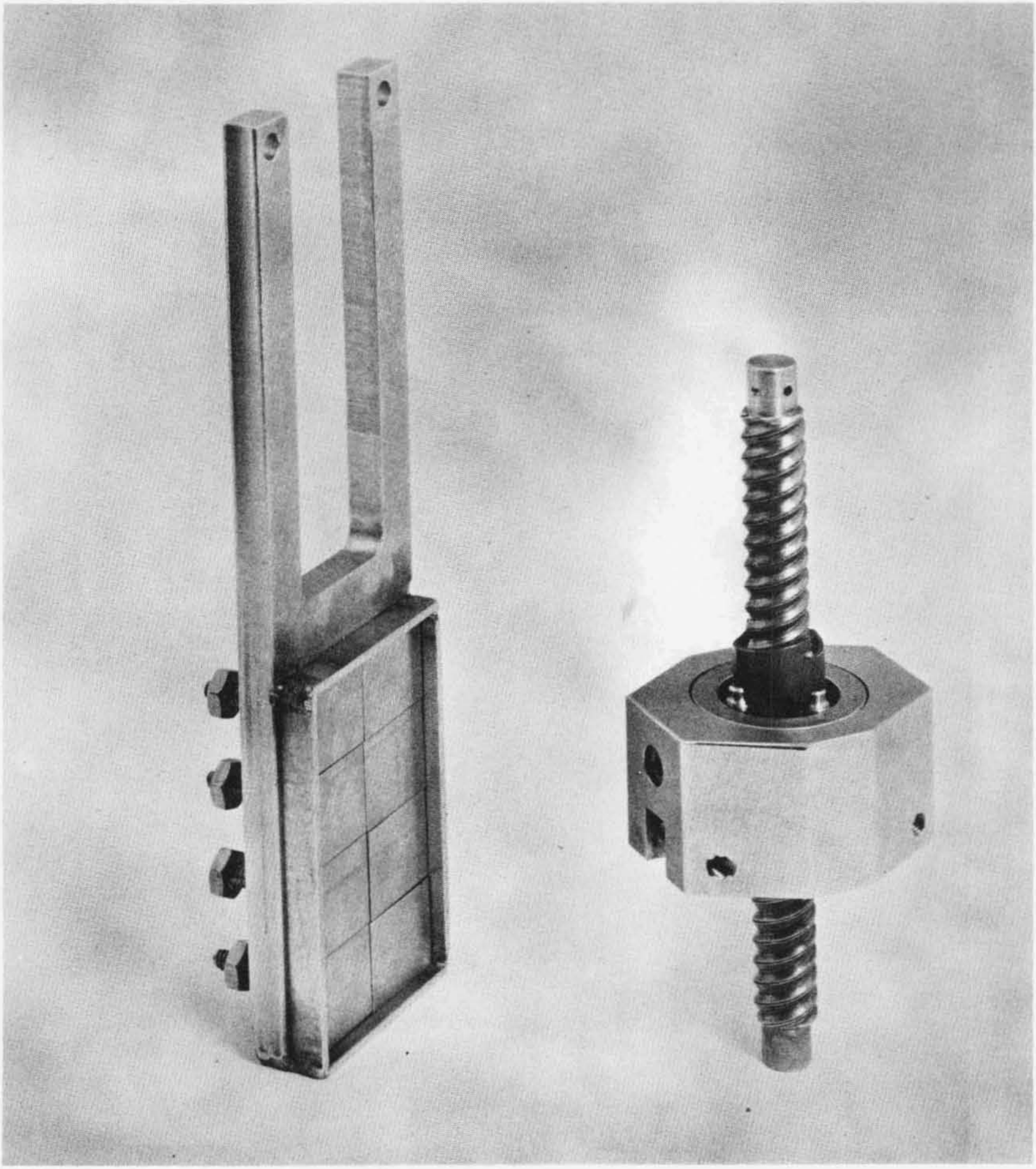

Figure 56 FARADAY CUP FLUX MAPPER (OPERATED BY A MAGNETIC CHUCK)

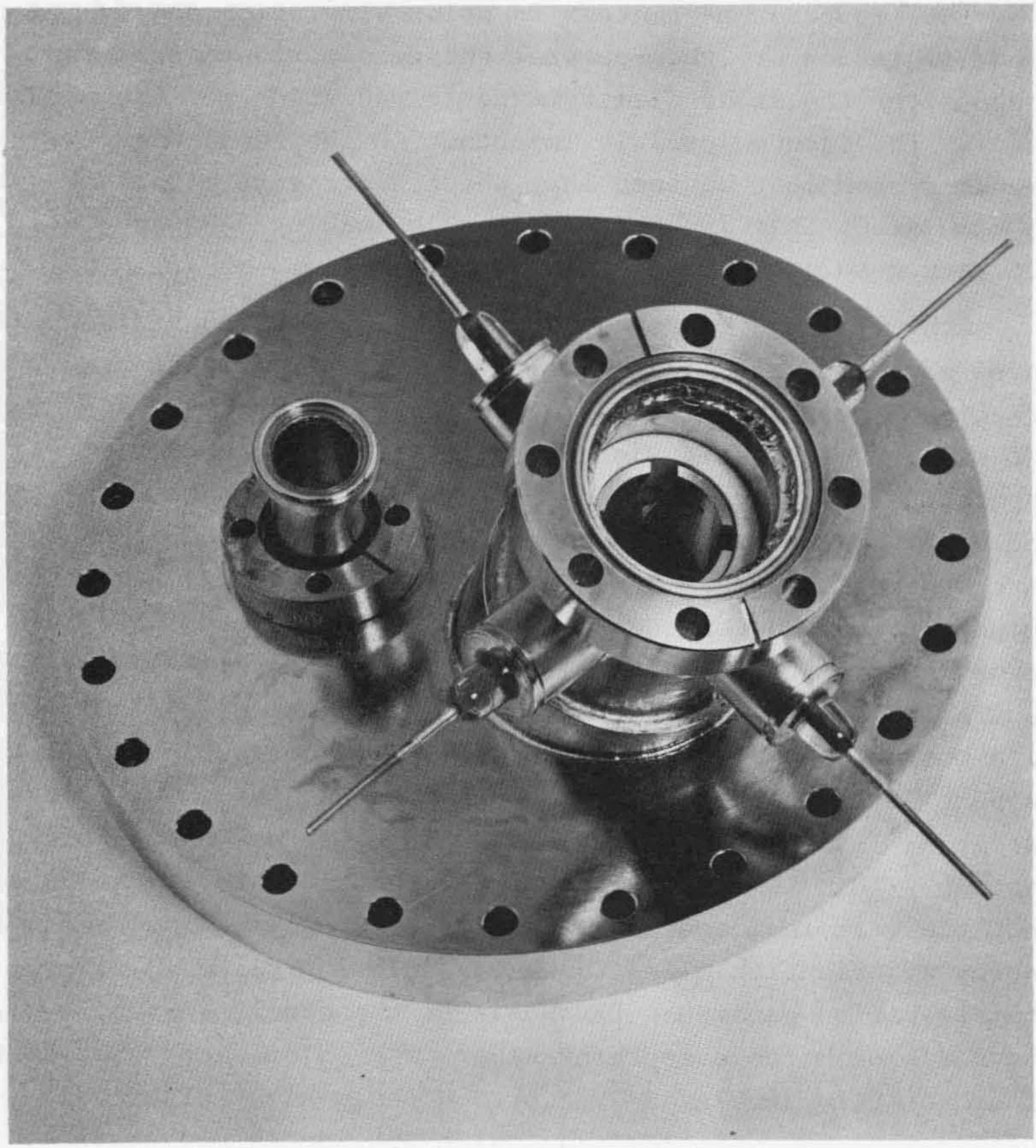

Figure 57 QUADRAPOLE LENS (SWEEP/COLLIMATOR)

7.5 Simulation Parameters

The important parameters in solar simulation and in solar wind simulation are the spectral energy distribution of the protons, of the solar electromagnetic radiation and the vacuum level. The vacuum level is important in the sense that the vacuum system must be such that the net pressure effect of space is simulated, that is, that a molecule leaving a surface will not return to it.

Achieving the correct energy distribution and average energy level of the protons in the solar wind is a difficult task. In practice, the methods for doing this are generally divided into two categories--one is electrostatic, the other magnetic. Separation is a parameter that determines the amount of H_2^+, H_3^+ and other species that may be incident upon the samples. The term separation generally refers to the geometrical relationships between the components of an analyzed beam. Since the magnetic separation is energy-selective, there will be an energy separation as well. Thus, for a given magnetic field the protons with the highest energy (in a Maxwellian distribution) will not be bent as much as the lower-energy protons, while the lowest-energy H_2^+ ions will be bent most, and there may be a geometrical overlap. This is illustrated in Figure 58, where it can be seen that the beam incident on the x-axis after separation have an energy distribution along the beam-isolation plate. In space the separation parameter for H^+ is of the order of 0.96, i.e., the ratio of H^+ to everything else. The solar wind, therefore, is effectively simulated by a pure H^+ beam along with the accompanying thermal electrons which provide an essentially neutral beam. In practice there also has to be an uniformity of the incident beam. Consequently, uniformity becomes a practical requirement. The rates at which the particles strike the surface along with the rates of the solar electromagnetic radiation should be very nearly that of space. The ratio of the two fluxes (particulate and electromagnetic) should be very nearly unity;

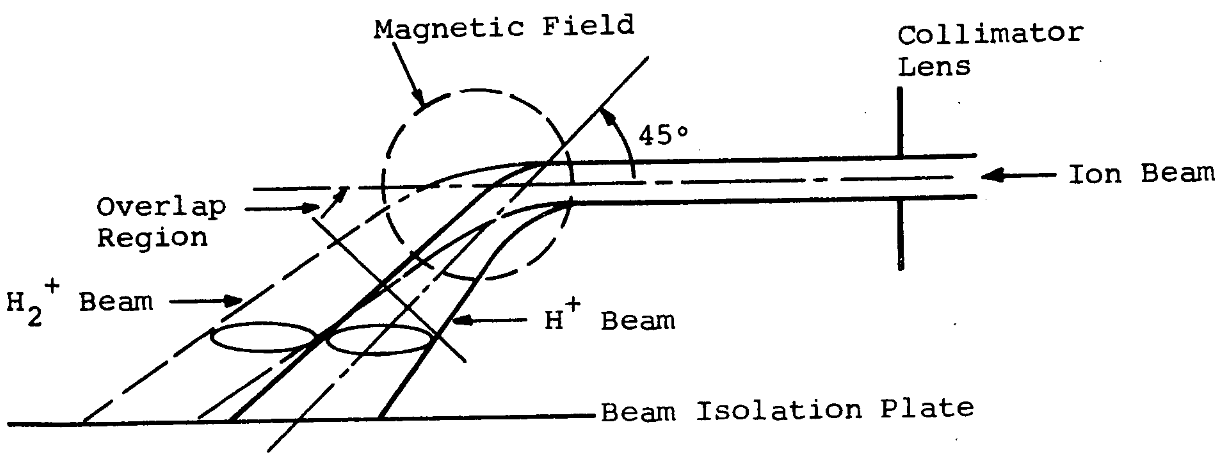

Figure 58 MAGNETIC ANALYSIS AND PHYSICAL ISOLATION OF PROTON BEAM

that is, the ratios of the intensities of these two fluxes should be very nearly that of the space environment.

The solar wind consists of 2.5 x 10^8 protons/cm^2-sec with ion energies centered approximately at 1.8 keV; they may rise during solar flares to approximately 5 keV, where the energy distribution of these protons is of the order of 0.01 of the maximum energies, or 0.01 of the average energy (in other words about a 1% spread of energy). In practice the flux rate corresponds to a current level of 4.0 x 10^{-11}amp/cm^2. The methods that are used to determine the degree to which a simulation device is achieving its purpose are difficult to decide upon. The detector/monitor for a solar wind simulator must be a Faraday Cup which has the capability of scanning the entire beam to measure its intensity in a horizontal plane. It must also be able to measure the intensity of the beam on a unit area basis and it must be able to scan the beam energy distribution. Consequently, devices for measuring both the flux incident per unit area and the energy of the beam itself must be provided at the sample location. The total environment of the samples must be such that they will respond to the incident beam solar electromagnetic and particulate radiations in very much, if not identically, the same way they would respond in space. Consequently one must also provide a charge buildup detector, because in reality the buildup of charge induced by proton reactions will occur and provisions for effectively neutralizing the charge must be provided.

7.6 Performance

7.6.1 Objectives

The calibration and characterization measurements performed on the CREF have been quite successful. The system has been operational since June 1969. In general, the CREF operates quite well within the tolerance levels that were anticipated. Major operational problems have not occurred. Our experience with the CREF indicates that the basic design of the system as a whole is fundamentally sound. Individually, the components and ancillary equipment operate well within satisfactory limits. Typical of some of the minor problems that we have encountered to date was the necessity for maintaining the system electromagnetically shielded (i.e., not allowing RF to get out of the building). A not unusual number of electrical problems such as ground connections and ground loops, interaction between instruments and power grounds, faulty connectors and connections, etc., occurred at first and were all corrected. Care in selection of components was necessary in order to avoid problems such as poor construction, insufficient ratings, or general defects. Operational problems have been relatively minor except for the usual problems attendant to high vacuum engineering.

The objectives of early experiments were mainly to determine the effects of each of the major parameters on the performance characteristics of the system as a whole. In general, we have wished to vary the proton flux at the sample locations from roughly one solar wind, or 4×10^8 protons/cm^2-sec, up to approximately 25 solar winds, or 10^{10} protons/cm^2-sec. We have also wanted the beam purity, that is the proton (H^+) species, to be greater than 95%, and approximately $\pm$ 5% energy spread about the effective energy. Geometric uniformity at the sample location is a little more difficult to achieve in most cases; for example, the microscopic flux at the sample location should be within 20% of the total beam flux averaged over the whole sample location.

These objectives have largely been met and the effects that each of the major components have on these individual performance objectives have been determined.

7.6.2 Characteristics of Operation

Rather than indicate the effects each component (for example, each Einzel lens) may have on the succeeding elements and eventually on the conditions at the sample position, we will present some of the more important variables which fix these conditions or have the most important effect on them.

The probe voltage, which is a positive voltage applied directly to the RF-source tube, determines directly the beam energy. This voltage is critical; the voltage drop between the power supply and the probe must be accounted for or made extremely minimal. The actual energy of the protons eminating from the system is slightly less by some small amount (roughly 25-30 eV) than the actual set energy as determined by the probe voltage. The probe voltage also affects the flux and the ionic composition of the emergent particle flux. All of these, of course, affect the strength of the magnetic field required to separate (analyze) the protons, and this in turn affects the focal properties of the beam, the space charge, and the energy distribution of the beam.

We have found in measuring, or monitoring, the proton flux that it is very important to account for the secondary electron emission. The net effect of the secondary electrons is to increase the apparent beam flux so that the actual beam flux is slightly less (sometimes much less) than the apparent flux. At approximately 1.2 kilovolts (kv) the correction is of the order of 20%. At 2 kv the correction is of the order of about 100% (for aluminum targets). In other words, an indicated flux of 2×10^8 2-keV protons would in fact be 1×10^8 protons/cm^2-sec under these conditions.

To measure beam purity, the separated (individual) beams are scanned across the Faraday Cup using the magnetic separator (or analyzer) and the resulting scan of Faraday Cup current (beam intensity) versus magnetic field strength (such as Figure 59 shows) can be used to determine the magnetic separation between the two beams and the amount of field strength required to produce these two beams at their individual locations on the Faraday Cup. Since the Faraday Cup is divided into eight elements each of known size and geometrical relationship to one another, the beam can be tracked across each of the cups and the amount of field strength required to move it from one element to another can then be determined. The purity then can be determined by the fact that, sufficiently far from the magnet, the divergence of the two beams, H^+ and H_2^+, is great enough to cause them (these respective beams) to hit different elements of the Faraday Cup. This divergence ordinarily is greater than the diameter of the downstream aperture into which one beam or the other is effectively focused. In effect the H^+ beam (first peak) is focused directly into the downstream aperture and only that part of it is focused which is at the top of the peak. Beam purity is thus achieved by magnetic separation followed by geometric isolation. The beam energy spread is determined by a scan, such as presented in Figure 59, in which the bias potential on the Faraday Cup is increased up to the order of the beam energy. When the current drops effectively to zero, the shape of the curve in this region is related to the energy spread (indicated by the dotted line). The peak of the distribution is at the effective energy of the proton beam. The width of the curve indicates its energy spread and this is taken to be the energy difference between the half power points as indicated by the $\pm E_{1/2}$ points on the curve. For an energy of 1.2 kv this energy spread has generally been of

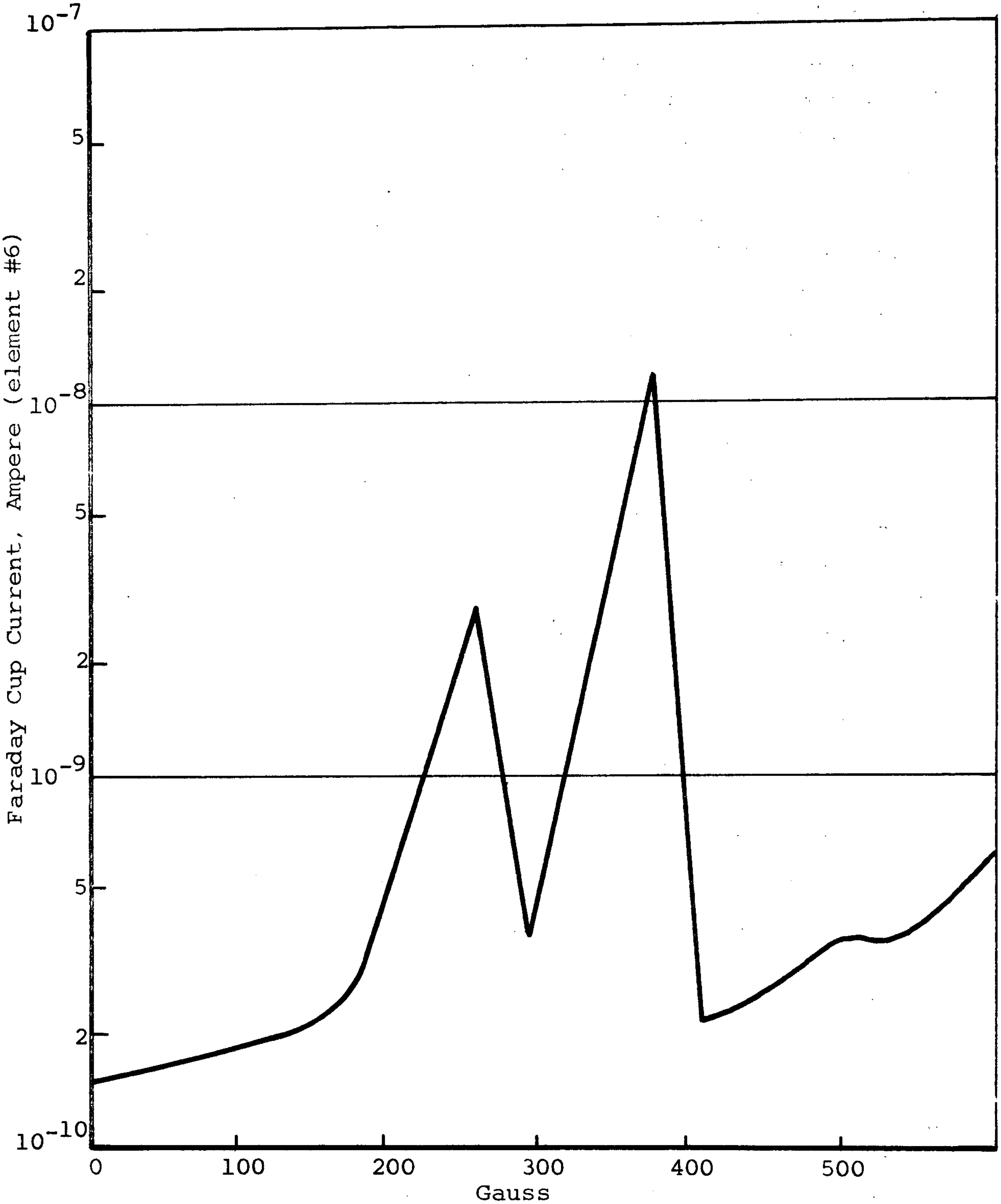

Figure 59 ION CURRENT VS MAGNETIC FIELD STRENGTH, GAUSS (B-SCAN)

the order of about 50 volts; the total spread has been slightly less than about 1/10 of a kv or less than about ± 5%.

Beam uniformity has been measured at the sample location using a 23-element Faraday Cup detector that is shown in Figure 60. In this method the entire Faraday Cup is placed above the sample location and all 23 locations, or elements, of the Faraday Cup are scanned. In general, the quadrapole lens has a fairly strong effect on the beam uniformity. The beam can be spread out across all of the samples by simply increasing the voltage across any two of the lenses. A voltage of approximately -800v applied on two of the four quadrapoles gives a beam uniformity of about 80%. Each element of the detector is one cm^2 in cross-section and the geometric relationship between each detector is known; hence the relative flux uniformity throughout the sample area can be determined quite well. Intensities at the center of the sample location were determined to be of the order of 1.1×10^{-10} ampere/cm^2 which is roughly 4 solar winds. Correcting for secondary-electron emission, this flux would be slightly less than 4 solar winds.

The total flux or the flux at the sample location can be decreased to a flux of the order of 1 solar wind by one of several means. An aperture located just above the second einzel lens can be installed with a much smaller diameter; another possibility is increasing the voltage potential on the first collimator lens.

Figure 61 shows the relationship between the potential applied to this lens and the resulting maximum flux at the sample location; on the right side of the figure are the intensities in solar winds. Figure 62 shows the flux distribution over the sample area at the sample location. This plot is at full scale and shows the beam energy distribution, the samples and the Faraday Cup elements superimposed upon each other. Figure 63 is a plot of the total flux at the sample location versus the voltage required to suppress it.

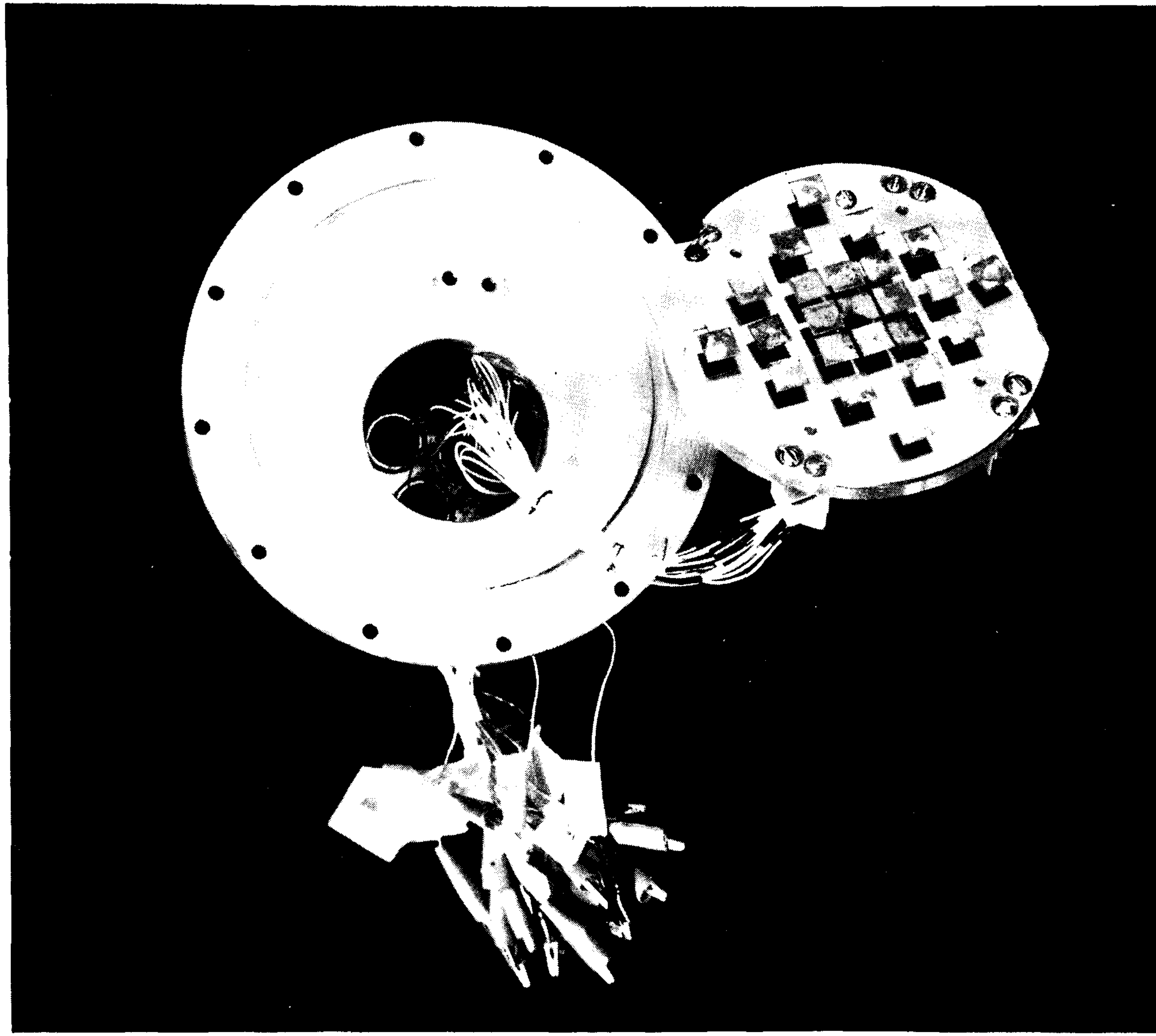

Figure 60 23-ELEMENT FARADAY CUP FOR BEAM MAPPING AT SAMPLE LOCATION

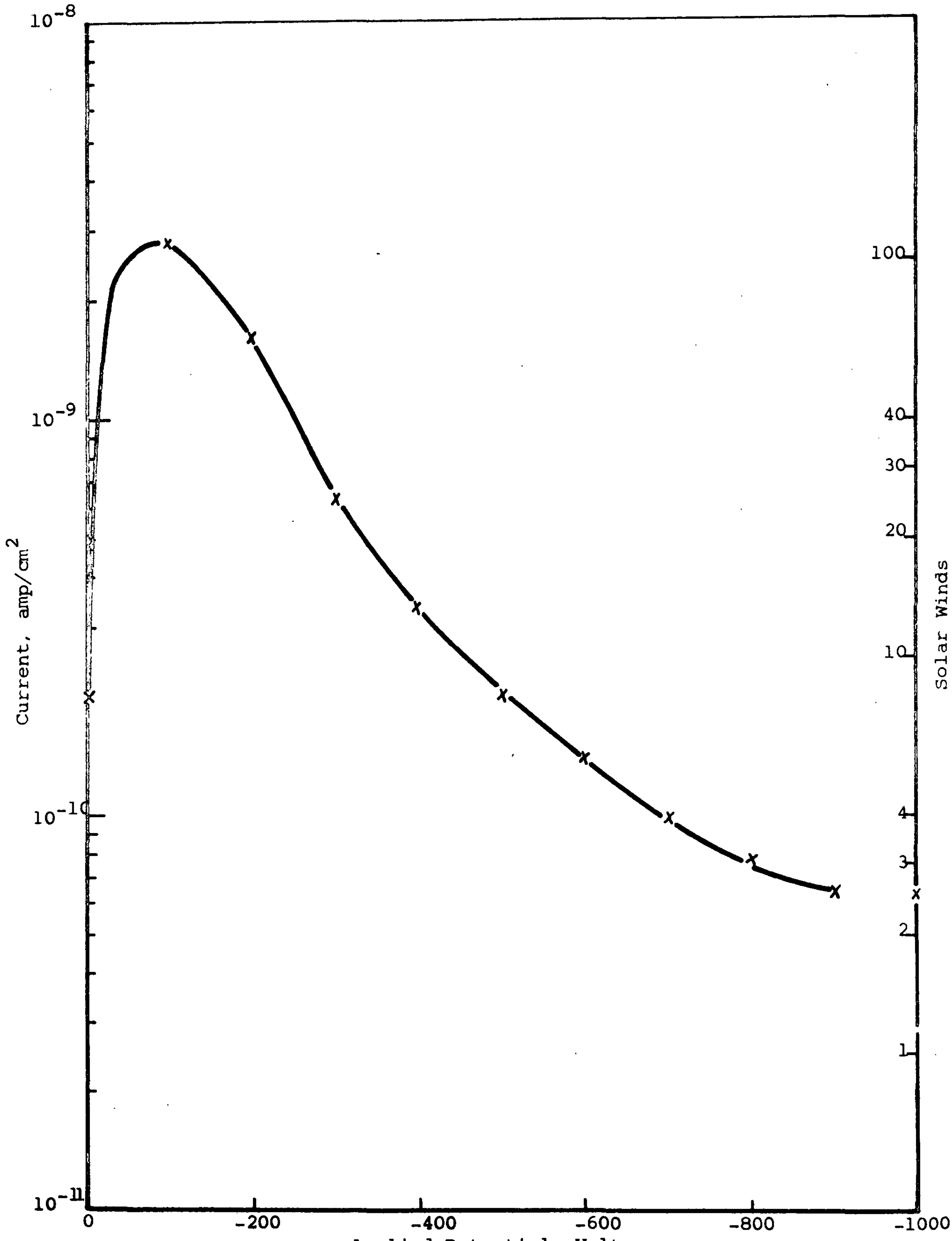

Figure 61 FLUX INTENSITY AT SAMPLE LOCATION VS COLLIMATOR LENS POTENTIAL

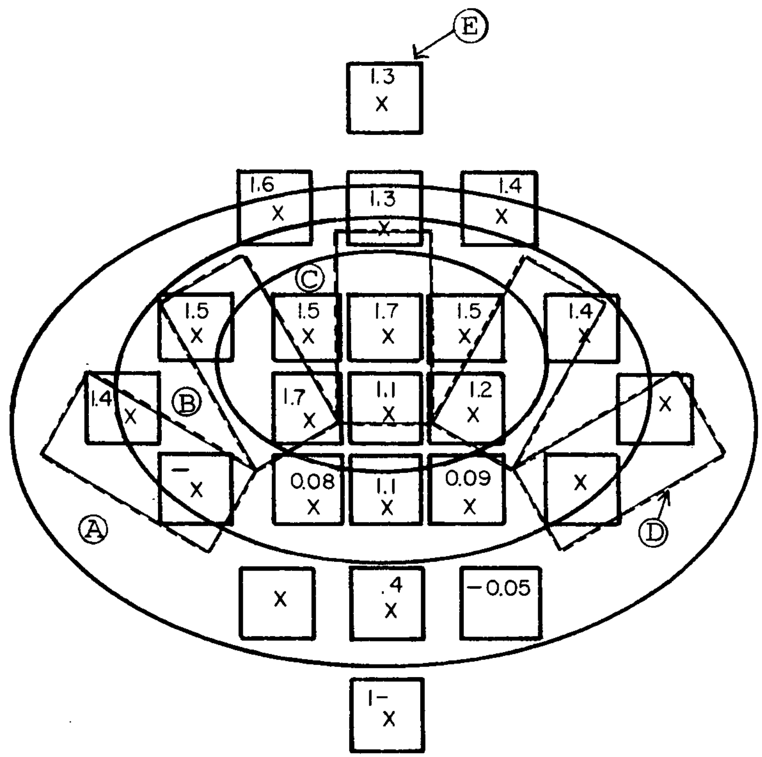

Ⓐ 2 ± 0.1 SW Intensities
Ⓑ 4 ± 0.3 SW Intensities
Ⓒ 5 ± 0.5 SW Intensities
Ⓓ IRIF Samples
Ⓔ Faraday Cup (23 elements)

Note: Intensity units are in Solar Winds. One Solar Wind $\approx 2.5 \times 10^8 p/cm^2$-sec.

Figure 62 FLUX INTENSITY MAP AT SAMPLE LOCATION (SCALE 1:1)

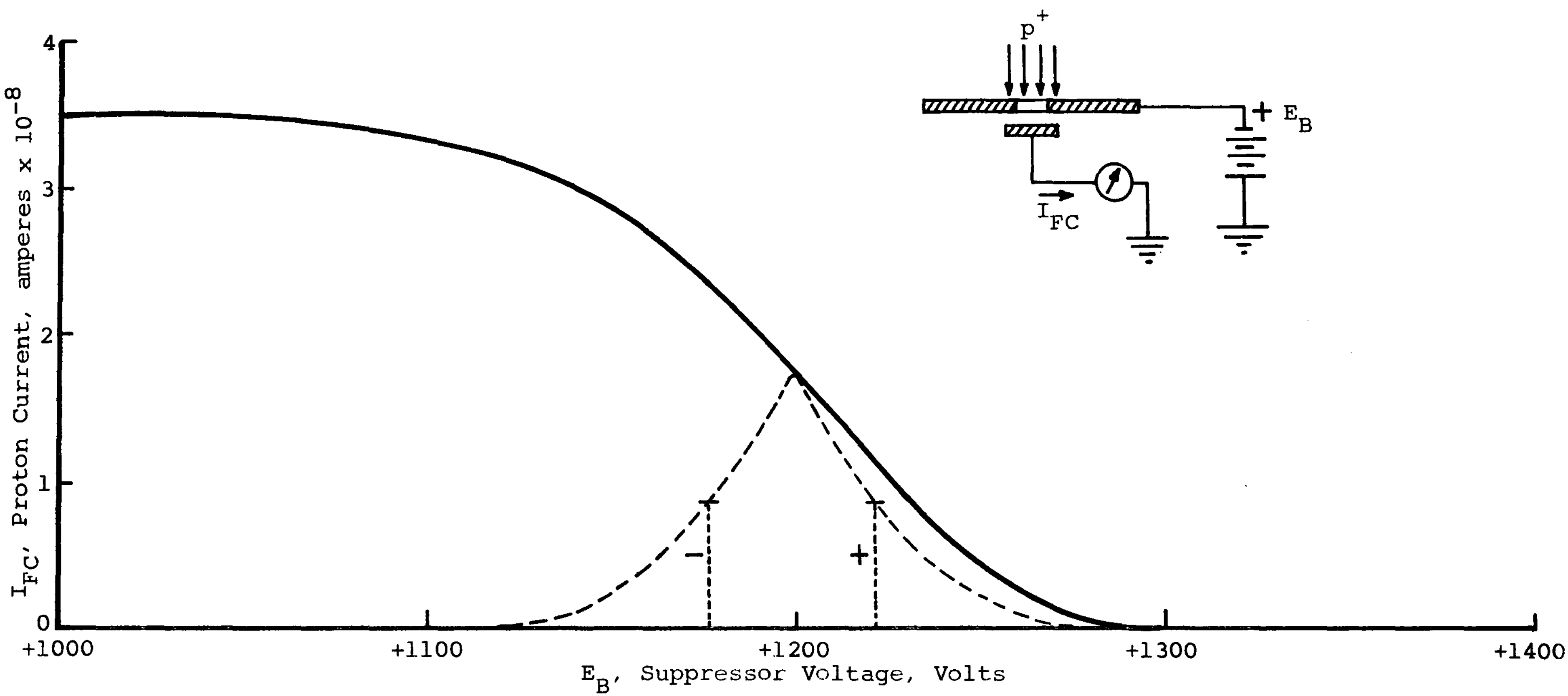

Figure 63 PROTON CURRENT VS SUPPRESSOR VOLTAGE

7.6.3 Operating Conditions

We have found a number of operational procedures which seem to stabilize and regulate the beam intensity. The hydrogen supply system was found to be quite critical. We use a very high-purity (research grade) hydrogen gas. We pass this through a regulator and control the inlet pressure to a palladium leak at 16 psig. The differential pressure across the palladium leak is therefore kept very constant. The intensity of the flux is maintained constant for the reason that there are no pressure surges or transients in the ion source. The heater current to the palladium leak is another critical factor. This must be highly regulated and for this purpose we use a titanium sublimation pump power supply.

The general philosophy in the development of procedures was to proceed from the ion source down to the sample location, characterizing the effect at the sample location of each of the lenses in the system. The total ion current extracted from the source is shown in Figure 64 as a function of applied (probe) potential. The relationship is essentially linear. The primary investigation, however, was to determine the focusing properties of each of the lenses and the effects that each lens would have on the succeeding lens, and also, for example, the ability of the einzel lens to focus the beam into the analyzer magnet. The conditions best suited for this latter situation were found to be with the middle element of the einzel lens at approximately +800 volts, or roughly 2/3 of the probe potential, and the two outer lenses grounded. Further down the system the einzel immediately following the analyzer lens has a very small aperature which geometrically selects the H^+ beam. This lens has in all cases been grounded because the aperture on the exit side of the einzel lens was inadvertently made too small to allow the einzel lens to function effectively as a focusing element. Fortunately, however, the four quadrapole lenses have a very strong focusing effect.

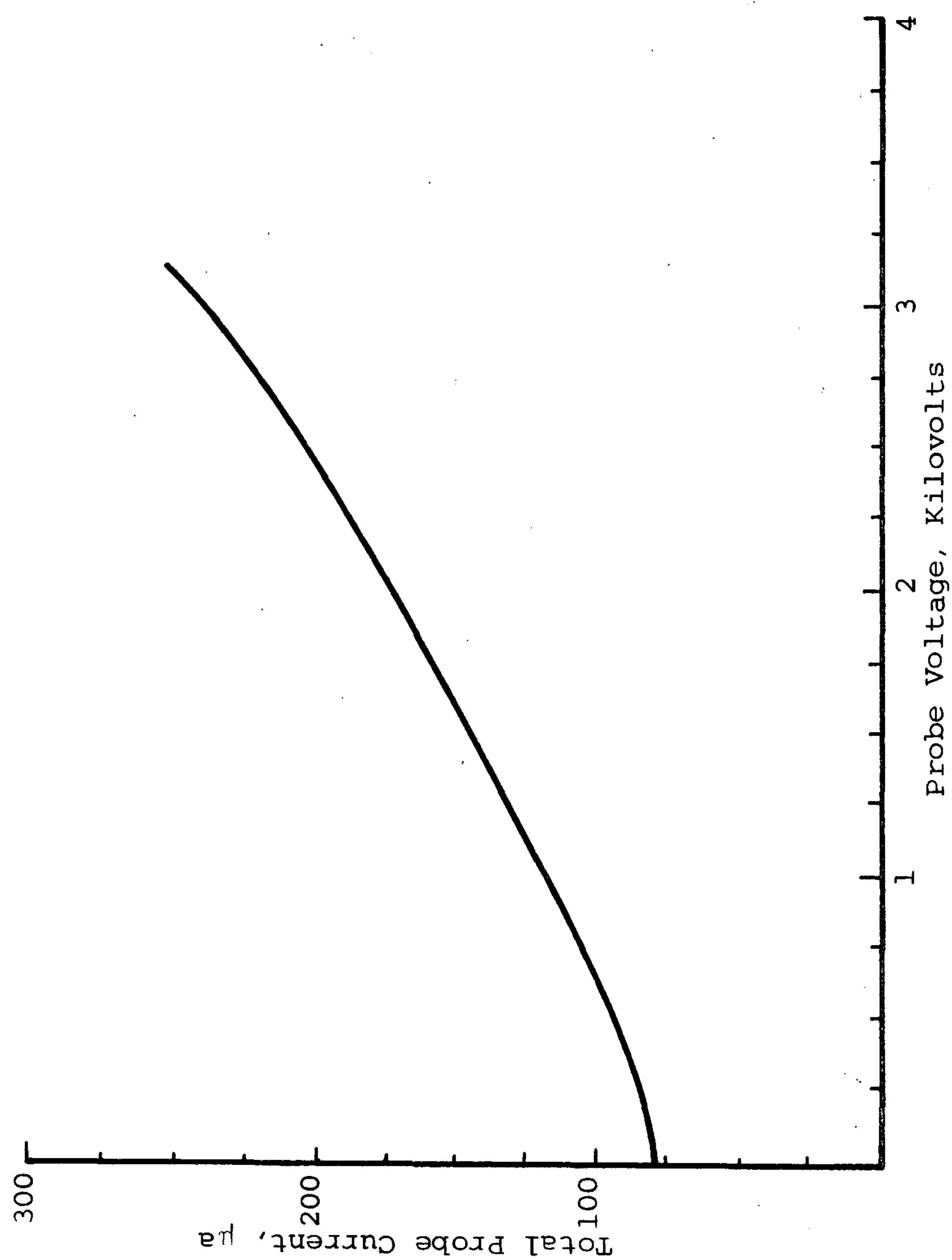

Figure 64 PLASMA CURRENT VS APPLIED POTENTIAL

The current operating conditions are: the first collimator lens is set at -1200 volts, the second collimator lens at -1300 volts, the three elements of the first einzel lens at 0, +800, and 0 volts respectively, all elements of the second einzel at 0 (ground, two of the four quadrapole elements at -830 volts and two at 0) and with zero bias on the samples.

7.6.4 Performance Summary

The performance of the CREF may best be appreciated from the information presented in Table 34. The validity of our design approach was confirmed in a more recent and independent study by King and Zuccaro (Ref. 128). Their design concept of an ideal solar-wind simulator coincided with IITRI's actual design--in all important aspects.

Table 34

CREF PERFORMANCE DATA

	Objectives	Actual
Flux, p^+/cm^2-sec	$2 \times 10^8 - 4 \times 10^9$	$2 \times 10^8 - 1.5 \times 10^{10}$
Purity, p^+/I_c	>0.95	>0.98
Energy, eV	$E_p \pm 5\%$	$E_p \pm 2\%$
Energy Spread ($\Delta E/E_p$)	± 0.05	± 0.04 - 0.06
Flux Uniformity	± 20%	Variable

The flux-analyzed protons at the sample location can be varied from slightly less than one "wind" to approximately sixty (60) winds. For discussion purposes one "wind" is a flux of 2.5×10^8 p^+/cm^2-sec. The purity of the beam, as determined by measuring the ratio of p^+ current to total ion current, exceeds 0.98. The proton energy (we have standardized on 1.2 KeV) is highly stable, and reproducible to within better than 2%. The fractional energy spread, which is a function of random losses in the ionization process and of focussing and defocussing losses in the optics, is of the order of $\pm$ 0.05, that is, the total energy spread is about 120 eV. The geometrical uniformity of the beam at the sample location depends very strongly on the quadrature field settings. At four winds the uniformity is better than the 20% initially desired; at 10 winds, it is about 20-25%, measured as the difference in fluxes at the edge and at the center of the beam, compared to that at the center of the beam. At higher intensities the uniformity decreases rapidly. The overall performance of the CREF, as Table 34 indicates, has exceeded design expections, in every important way.

8. ZINC ORTHOTITANATE

8.1 Selection of Zn_2TiO_4 for Study

8.1.1 Optical Properties

The solar reflectance of a white pigmented coating depends upon the coating's ability to scatter light of a very broad wavelength distribution.

Light-scattering theory has its origins in Maxwell's equations and modern theory is based largely on the mathematical developments of Mie, who performed a complete analysis of the interaction of an electromagnetic wave with a spherical particle. The complex Mie functions, which treat the entire range of particle size-to-wavelengths ratios for both real and complex refractive indices, have been discussed by many workers and, except for the work of Jaenicke (Ref. 129), will not be reviewed here.

Jaenicke summarized his analysis of Mie theory by the relation:

$$d(\lambda) = \frac{0.90\ (m^2 + 2)}{n\ \pi\ (m^2 - 1)}\ \lambda \tag{9}$$

where d is the particle diameter at which maximum scattering occurs for wavelength λ, n is the refractive index of the medium surrounding the particle, and m is the ratio of the refractive index of the material in the particle to that of the medium.

Applying Jaenicke's relation to rutile titanium dioxide dispersed in a vehicle of refractive index 1.48, we find that maximum scattering at wavelength λ occurs at a particle diameter of 0.41λ. In order to optimally reflect radiation such as that of extraterrestrial solar energy, this equation <u>suggests</u> that it is desirable to utilize a particle size distribution whose distribution curve possesses a shape identical to the solar distribution curve, but with the wavelength axis concentrated by the factor 0.41. Applying the same relation to zinc oxide, we find that $d = 0.85\lambda$. We have found this simple relation to be a useful guide in choosing the particle size distribution for dilute suspensions. However, the equation is not strictly applicable to concentrated pigment dispersions such as white paints, due primarily to multiple scattering phenomena associated with close-packed systems. In highly pigmented systems, a somewhat smaller particle size distribution is desirable because the agglomerated particles scatter light of longer wavelength than their primary particle size dictates from single-particle light scattering theory (on which Jaenicke based his analysis).

From these considerations, it can be shown that in a system designed for maximum reflection over the very broad wavelength region represented by the solar spectrum, it is necessary to <u>maximize</u> the <u>pigment volume concentration</u> (PVC) with pigment whose size does not exceed that defined by the Jaenicke expression for the solar maximum (500 nm), and to employ <u>thick coatings</u> in order to compensate for the decreased infrared scattering power of such a system (compared to its scattering efficiency in the region of the solar maxima).

Implicit in the concept of maximization of solar reflectance by pigmented coatings is the stringent requirement for complete <u>transparency</u>, or lack of absorption, of the vehicle, whether polymeric or inorganic in nature. That is, the very process of light scattering by multiple refraction <u>greatly</u> increases the path length in the film of light interacting with the surface. Thus, absorption centers, or color, in the film, regardless of whether inherent or radiation induced, tend to frustrate the randomness of internal reflection and refraction, and the statistical probability of photon absorption is greatly enhanced.

As the number of closely packed layers increases, the number of scattering events, or changes in the direction of incident photons, also increases. Increasing amounts of light in the deeper layers are lost by absorption and are converted to thermal and molecular energy modes. An increasing number of scattering events leads to an increasingly effective absorption path length for each penetrating photon. If the absorption path is long enough, the absorption mechanism of energy loss predominates in the deepest layers of the suspension even when the absorption efficiency is low, as is the case with most common pigments and binders in the major portion of the solar spectrum.

These considerations relate most importantly to the concept of ultraviolet stability in the following manner. In ultraviolet absorbing, semiconductor pigments such as rutile TiO_2 and ZnO, the high extinction for ultraviolet at wavelengths below their edge (which is 385 nm in ZnO), serves to <u>effectively screen</u> the ultraviolet from the binder. The binder is thus essentially totally protected below the outermost 10μ of film in the case of ZnO-pigmented coatings. The total extinction of visable light contributed by damage in a 10-μ thick pigmented film is not great even for only a moderately stable binder.

On the other hand, in low-refractive index, dielectric pigments such as Al_2O_3, MgO, SiO_2, etc., which by our definition are transparent in most of the solar ultraviolet (down to approximately 200 nm), and which therefore are effective scatterers of ultraviolet, the total ultraviolet pathlength in the film is manifoldly increased and the probability of creating serious, observable spectral damage in the binder is increased by orders of magnitude. That is, both the increased damage per infinitesimally small unit volume (ΔV) due to increased path length of ultraviolet light in that volume, coupled with the greater depth that damage, i.e., color, is caused to occur, serve to enhance the total extinction contributed by the binder, and even reasonably stable binders are observed to degrade.

Since approximately 8% of extraterrestrial solar energy lies below the absorption edge of zinc oxide, and since it is impossible to achieve perfect reflectance over the remainder of the solar spectrum, one can readily see why it is very difficult to obtain coatings based on it with solar absorptances of less than 0.15.

Also, since none of the three binders currently employed in the thermal-control coatings field (Sylvania's PS7 potassium silicate, GE's RTV-602 silicone elastomer, and Owens-Illinois 650 silicone resin) absorb in the 300- to 400-nm wavelength region, where 80% of the solar ultraviolet energy lies; accounting for about 6% of the total solar energy, employment of a stable semiconductor pigment with an edge at about 300 nm would serve two purposes. It would still effectively screen the most harmful ultraviolet from the deep layers of the paint system and at the same time would offer an excellent chance of diminishing the solar absorptance by the solar absorptance factor 0.06 (=0.8 x 0.08), <u>providing its refractive index is at least as high as ZnO</u> (n=2.00) and that equally thick and equally concentrated (pigment-wise) paints are employed.

8.1.2 <u>Ultraviolet-Damage Considerations</u>

Our preference for semiconductor over dielectric pigments also involves their intrinsic characteristics relative to the location of damage sites, or color centers, in their respective particles. The ultraviolet transparency of dielectric pigments such as Al_2O_3 or MgO means that the damage is a bulk phenomena, with its optical manifestations relating, among other things, to bulk diffusion properties in the crystal. That is, the damage, which is manifested in color centers, occurs in the interior of the particles where, as shown by the voluminous literature, bulk doping is required.

Semiconductor pigments such as ZnO and Zn_2TiO_4 possess high extinction for the damaging ultraviolet and the damage is therefore confined predominantly to the surface, where we have found it can be treated more effectively (as will be shown for Zn_2TiO_4 in the following paragraphs).

8.1.3 Summary of Criteria for Selection of Zn_2TiO_4

Of the many pigments examined during the course of our investigations in the past several years, only zinc orthotitanate appears to possess a maximum of the criteria that we had established. These criteria are presented in tabular form in Table 35.

Because we at IITRI believe that sufficient doping to stabilize dielectric pigments such as MgO and Al_2O_3, against ultraviolet damage would in all probability be accomplished at too great a sacrifice to basic optical properties, we have continued to devote most of our pigment studies during the past three years to the stabilization of the semiconductor pigment zinc orthotitanate.

8.2 Preparation of Zinc Orthotitanate

8.2.1 Literature

Zinc orthotitanate is a spinel that is formed from 2 moles of ZnO and 1 mole of TiO_2. A complete discussion of the literature pertaining to zinc titanates will not be attempted here. However, the most pertinent literature results will be given.

In 1960, Dulin and Rase (Ref. 130) of the State University of New York's College of Ceramics published a study of "Phase Equilibria in the System ZnO-TiO_2." They confirmed the existence and structure of the orthotitanate but also reported the definite existence of metatitanate as a compound ($ZnTiO_3$) having the hexagonal structure of ilmenite and stable up to a temperature of 925°C (their phase diagram is reproduced in Figure 65). The orthotitanate melts congruently at 1549°C while the metatitanate decomposes to form the orthotitanate and rutile at above 945°C. Their's was the first thorough study of zinc titanates in nearly 30 years and, along with Bartram and Slepetys (Ref. 131) in 1961, to some extent cleared up the discrepancies in previous studies. Bartram and Slepetys listed the orthotitanate as most easily prepared from sulfate type anatase and zinc oxide; a reaction time of 3 hr at 800° to 1000°C is required. The metatitanate,

Table 35

CRITERIA FOR SELECTION OF
PIGMENT AND PROPERTIES OF ZINC ORTHOTITANATE

Criteria	Zn_2TiO_4
1. High refractive index; $n \geq 2.0$	n = 2.4
2. Edge between 290 and 300 nm	Edge at 325 nm
3. No absorption from edge to 2700 nm	No absorption from 325 to 2700 nm
4. Synthesizable in laboratory, pilot and production	Yes (not produced in quantity yet, i.e., > 5 lbs.)
5. Acceptable impurities and unreacted materials	Yes (unreacted precursors subject of much study)
6. Stability to ultraviolet	Basically stable in bulk--stabilized by surface treatment
7. Stability to charged particle radiation	Appears to be stable when surface treated properly

they found, required chloride process rutile and an optimum temperature of 850°C. The solid solution phenomenon claimed by earlier writers appeared to be explained by the claim of Bartram and Slepetys to a third zinc titanate ($Zn_2Ti_3O_8$), the sesquititanate. This is a defect spinel structure made from anatase and zinc oxide in ratios of 2 moles ZnO and 3 moles TiO_2 reacted at a temperature of 700°C for at least 100 hr.

In 1962, Loshkarev in three papers found only orthotitanate as a compound using only rutile and zinc oxide and temperatures up to 1400°C (Ref. 132-134). The reaction between rutile and zinc oxide did not begin below 740°C. The existence of unreacted zinc oxide in the final product, regardless of composition, temperature or time, was observed by Loshkarev and has been confirmed by these studies. They report "very intense shrinkage" (from 15 to 18%) in forming the orthotitanate at temperatures

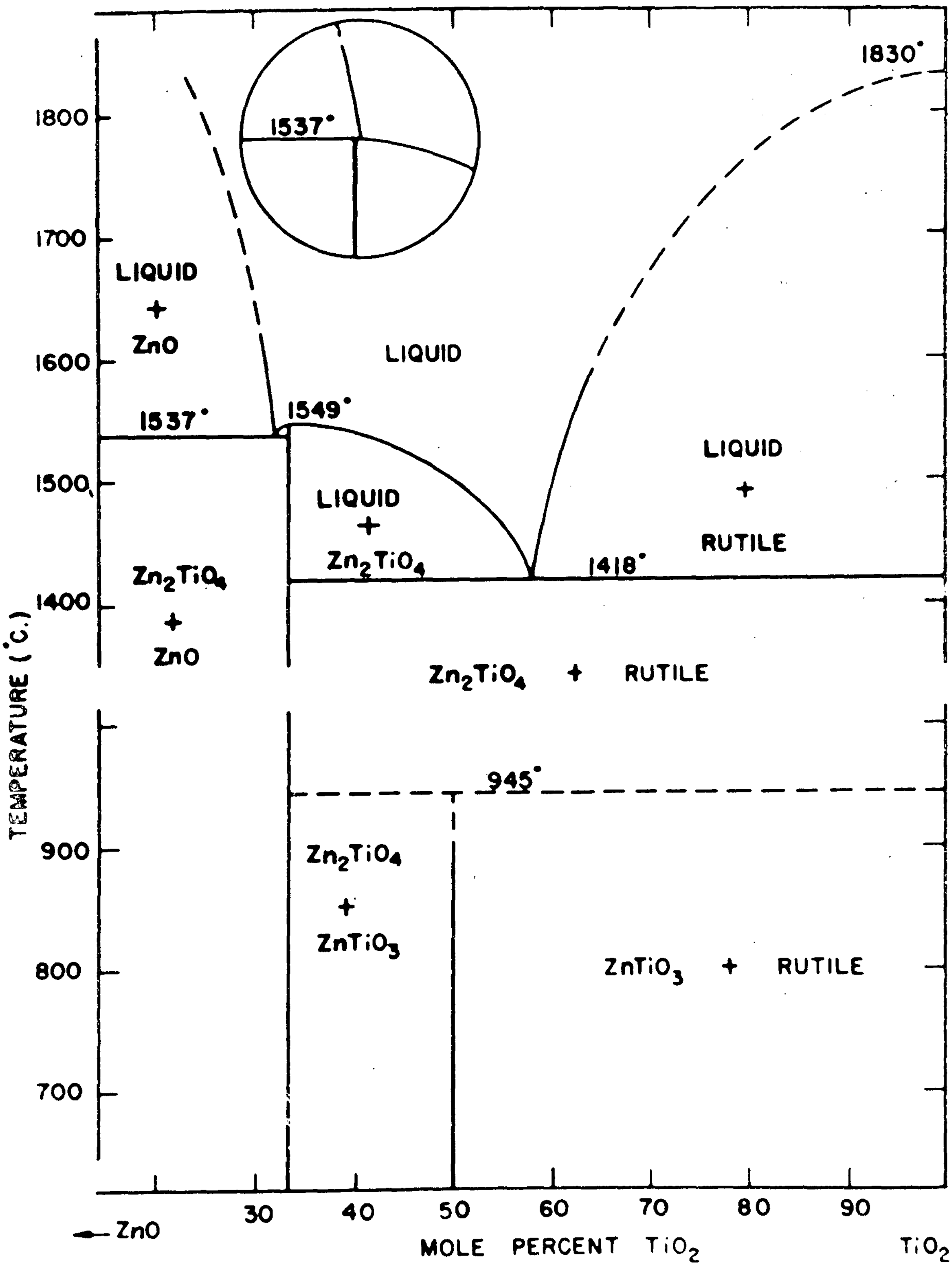

Figure 65 $ZnO-TiO_2$ SYSTEM (REF. 130)

above 1000°C. They therefore recommended slow heating when reaching this range. (We follow this advice in our studies; the high shrinkage is quite apparent.) The Russian papers do not concede the existence of the metatitanate, $ZnO \cdot TiO_2$, nor the sesquititanate listed by Bartram and Slepetys.

A more recent publication on the subject is a paper by Kubo et al in which they acknowledge the existence of the three titanates and report success in making the metatitanate of exceptional purity (Ref. 135).

Summarizing the literature, all workers agree on the composition, crystal structure and characteristics of the orthotitanate. A few agreed upon the existence and structure of the metatitanate, and only one claimed the existence and structure of the defect spinel, $Zn_2Ti_3O_8$, which we call the sesquititanate. It was considered best therefore to first attempt to form an orthotitanate using the method of Bartram and Slepetys.

8.2.2 Synthesis

The synthetic schedule for the three zinc orthotitanates that were prepared is given in Table 36. The metatitanate was the yellowest of the three stoichiometries prepared and possessed an absorption edge similar, but considerably more gentle, in slope than the rutile from which it was prepared. Like the orthotitanates discussed later, the metatitanate possesses unreacted ZnO, which can be extracted easily with acetic acid. The spectra of metatitanate ($ZnTiO_3$) and sesquititanate ($Zn_2Ti_3O_8$) are presented in Figure 66.

The sesquititanate is whiter than the metatitanate and its absorption edge at ~365 nm is intermediate between that of the metatitanate (~400 nm) and the orthotitanate (~325 nm).

The orthotitanate is a very white pigment, brighter to the eye and more reflective than either of the pigments from which it is prepared. The reflectance spectra of zinc orthotitanate are presented in Figure 67. The "step" in the reflectance spectra

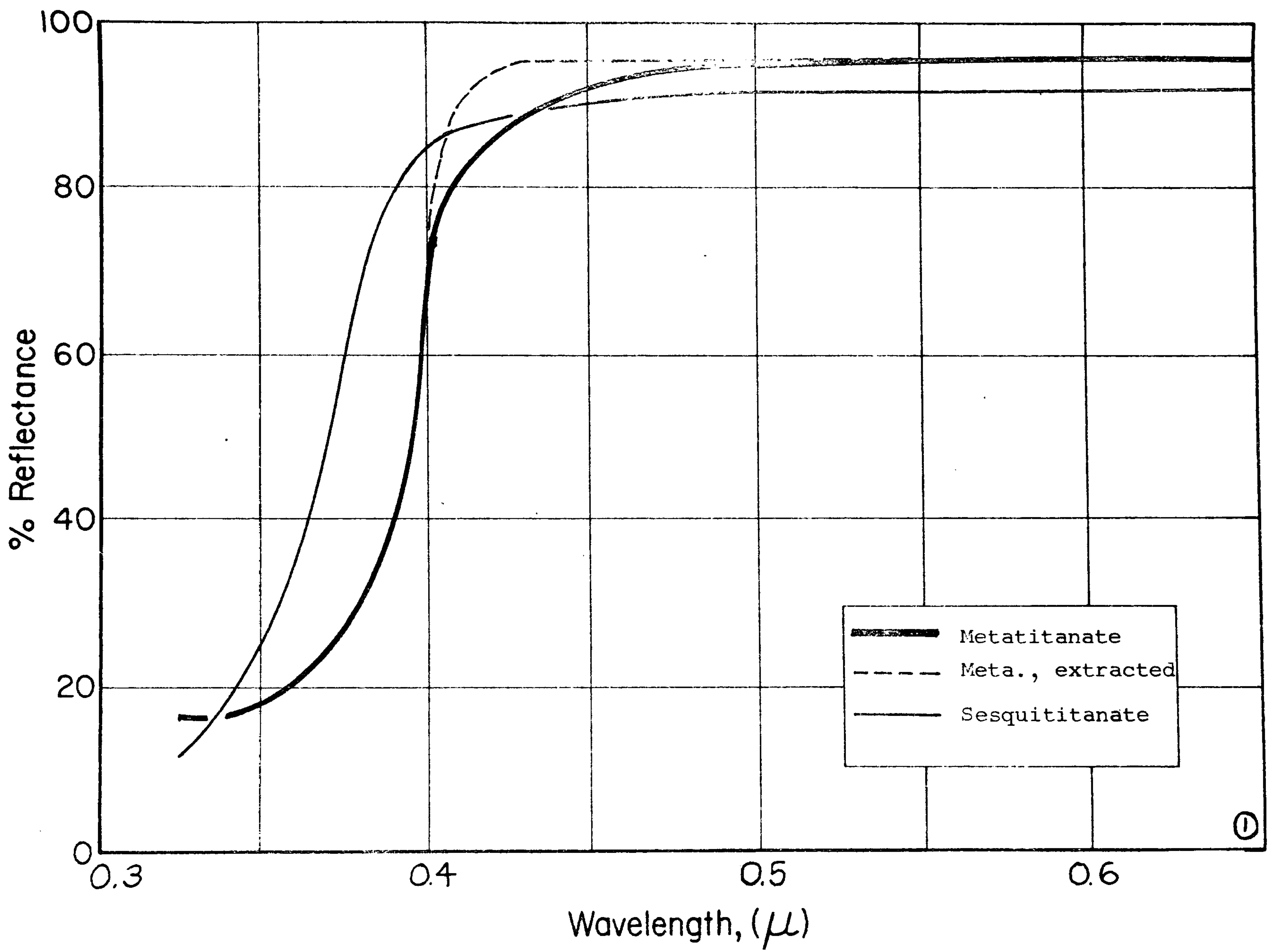

Figure 66 SPECTRA OF META- AND SESQUITITANATES

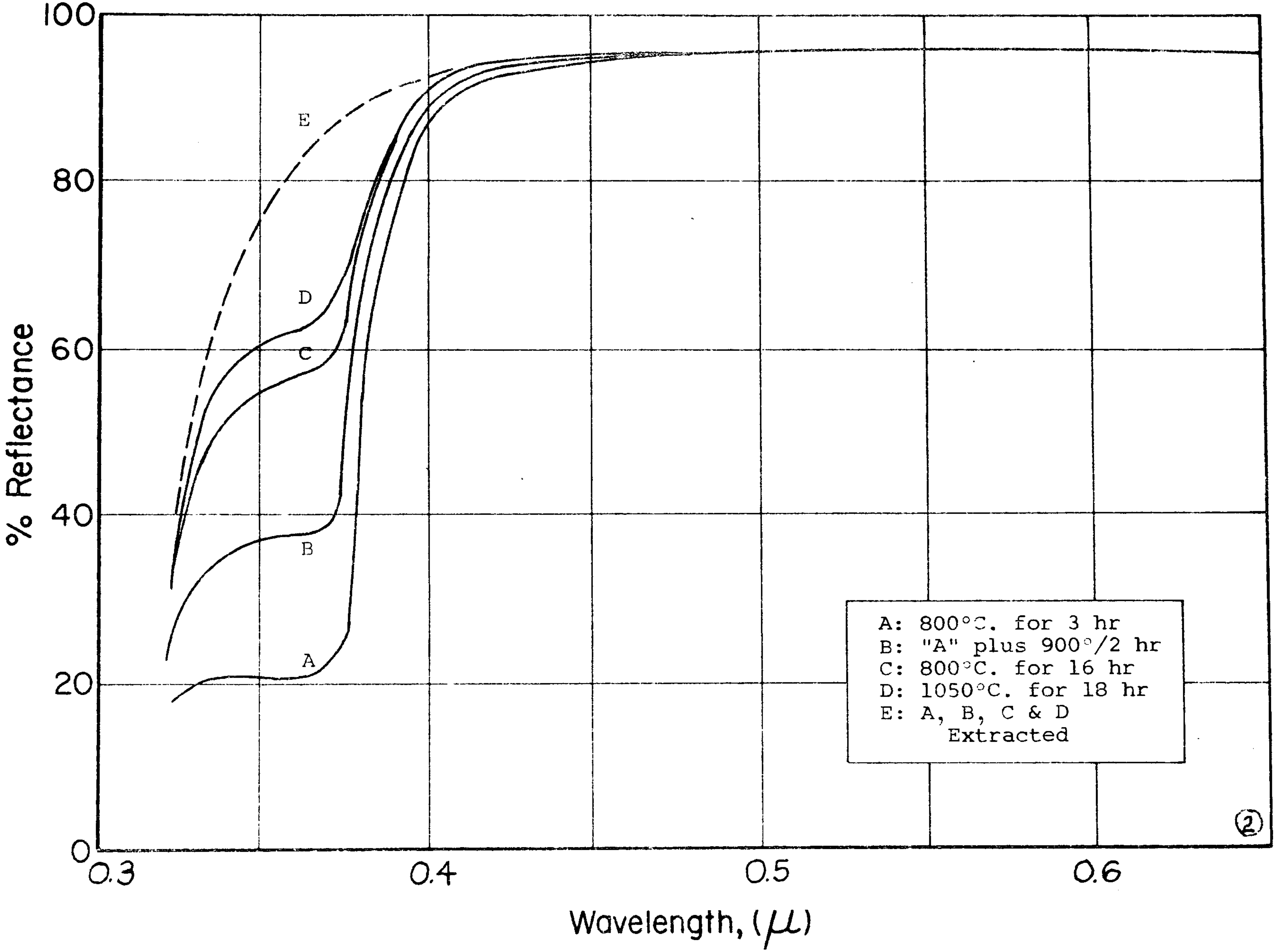

Figure 67 SPECTRA OF ZINC ORTHOTITANATE

Table 36

SYNTHESIS SCHEDULE OF
SEVERAL DIFFERENT ZINC TITANATES OF STOICHIOMETRY

Batch No.	Ratios of Reactants ZnO	TiO_2	Temp. °C	Time, hr	Structure
B-129	1 mol	1 mol (rutile)	850	17	meta
B-130	1 mol	1 mol (anatase)	700	64	sesqui
B-131	2 mol	1 mol (anatase)	700	64	sesqui
B-132	2 mol	1 mol (anatase)	1050	17	ortho
B-133	3 mol	2 mol (anatase)	1050	17	ortho

of all four heats is interpreted as being due to unreacted ZnO in all cases, extraction with acetic acid results in a powder that exhibits the spectra of curve E in Figure 67. Zinc oxide's presence has been confirmed by x-ray diffraction.

8.2.3 Irradiation

The effect of 970 ESH of ultraviolet irradiation on zinc orthotitanate prepared at 925°C is presented in Figure 68. (These data were obtained utilizing the IRIF-I simulation facility described in Chapter 2.) The absorption band at about 950-nm wavelength is characteristic of zinc orthotitanate and since has been attributed to an electron trap associated with the Ti^{+3} species (Ref. 136, 137). This conclusion is the result of electron paramagnetic resonance spectroscopy studies that are the subject of a later section (section 8.5).

Studies have shown that 0.5% excess zinc oxide is essential in minimizing the production of Ti^{+3} (Ref. 137). This absorption band is fast-bleachable with oxygen and has been studied by Gilligan and Zerlaut (Ref. 2).

The importance of reaction temperature on the stability of zinc orthotitanate is seen from the effects of 1000 ESH of ultraviolet irradiation on pigment prepared at 1050°C (see Figure 69). The high temperature product exhibited a $\Delta\alpha_s$ of less than 0.01

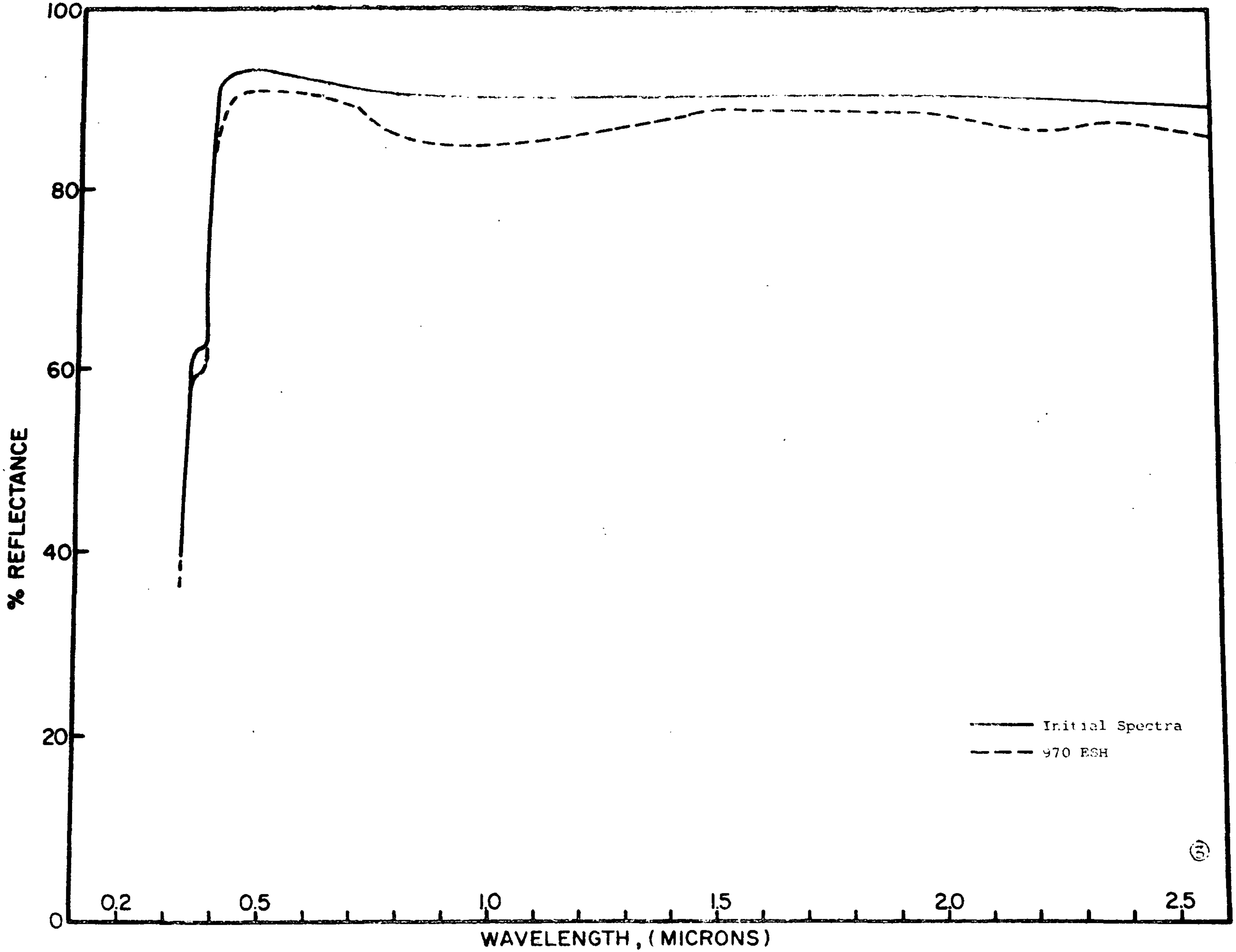

Figure 68 EFFECT OF ULTRAVIOLET ON B-229 CONTROL Zn_2TiO_4

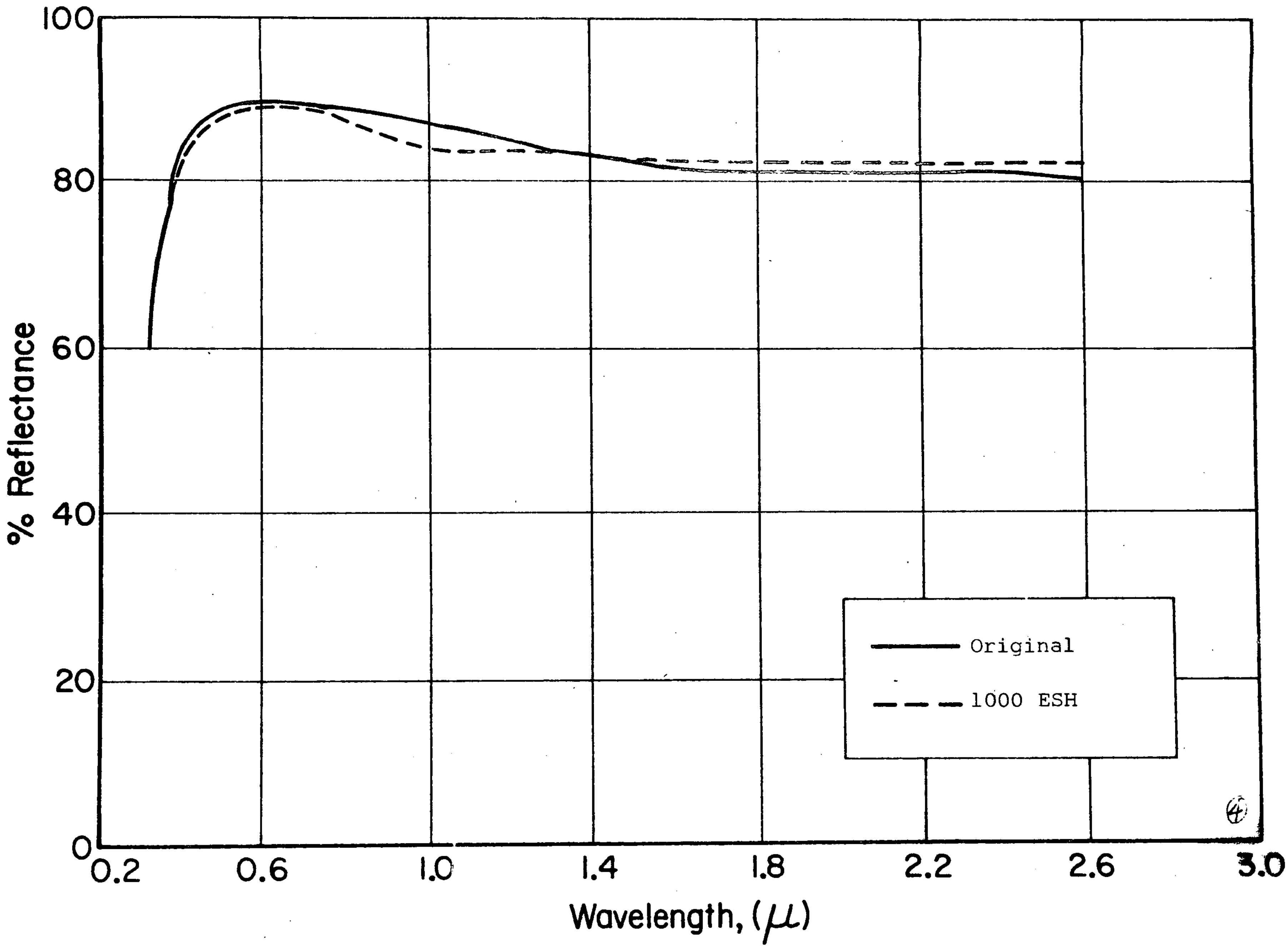

Figure 69 EFFECT OF ULTRAVIOLET ON A-132 Zn_2TiO_4 (1050°C)

but was of such hardness and agglomeration that the material could not be ground into paint. The 1050°C product has a Mho hardness of ~6.

Because we were unsuccessful in preparing stable zinc orthotitanate at lower reaction temperatures, i.e., at temperatures that produce soft, small particle-sized material, the employment of surface treatments was initiated. Both very high-temperature plasma annealing and reactive encapsulation were subsequently employed.

8.3 Plasma Annealing

8.3.1 Rationale

The employment of a high-temperature plasma facility to anneal the surface of zinc orthotitanate was considered because it was thought, quite correctly it turns out, that it might be possible to stabilize this pigment as an aerosol without either aggregation or grain growth. That is, we hoped that sufficiently high temperatures and sufficiently short residence times (in the plasma) could be achieved such that the defects residing on the surface could be annealed out without an accompanying increase in the effective particle size.

8.3.2 Experimental

The plasma heat treatments were performed by Mr. E.P. Farley of Stanford Research Institute utilizing SRI's rf-excited, induction plasma facility. These experiments were performed under separate contract to NASA-Marshall Space Flight Center (Ref. 138). The facility, which is shown schematically in Figure 70 is described by Bartlett in Reference 138. The procedure employed consisted of passing an Argon/Oxygen aerosol of the pigment being treated through the plasma reactor with variable mean effective retention times and boundary layer temperature gradients, ΔT.

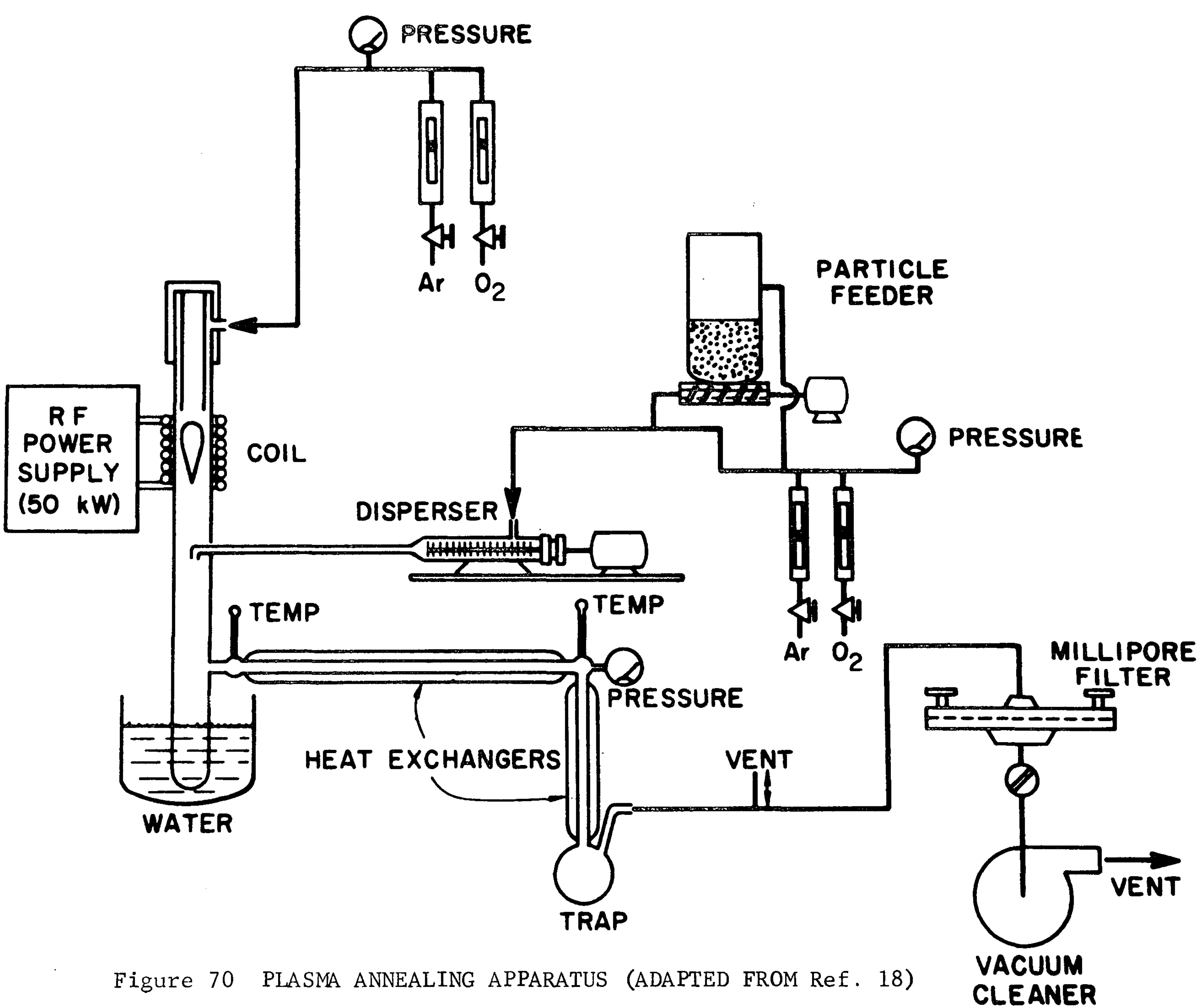

Figure 70 PLASMA ANNEALING APPARATUS (ADAPTED FROM Ref. 18)

8.3.3 Early Results

Although the objective of the early experiments was to establish the general range within which the reactor parameters should be varied, some rather basic information was quickly accumulated. Namely, it was found that the higher the temperature, the greater the damage sustained in the 1000- to 2600-nm wavelength region on ultraviolet irradiation. Also, it was observed that plasma annealing removed the 363-nm "shelf" absorption characteristic of Zn_2TiO_4, providing the retention time was not too large and the temperature ΔT, not too high (Ref. 139). Figure 71 is an example of the results of irradiation of one of the early plasma-treated pigments.

The infrared damage was immediately ascribed to conduction-electron absorption associated with increasing amounts of ZnO condensed on the surface as a result of the reaction

$$Zn_2TiO_4 \xrightarrow{\Delta} ZnO + ZnTiO_3 \tag{10}$$

The decrease in the 363-nm shelf was attributed to decreased unreacted ZnO from the original stoichiometry, an absorption that reappeared when very severe infrared damage occurred.

The effect of plasma heat treatment at two temperature gradients, ΔT, (1900 and 2900°C) of zinc orthotitanates prepared under different conditions was then determined. The treatment history of these pigments is given in Table 37.

The specimens were irradiated for 1000 ESH of ultraviolet irradiation. The results are presented in Table 38 and Figures 72 through 77. Examination of the data show that plasma heat treatment at the lower temperature tends to de-stabilize the zinc orthotitanate by creating free-carrier-like damage in the infrared (similar to that exhibited by ZnO). High-temperature heat treatment, as exemplified by the calculated plasma temperature gradient ΔT (Ref. 139), also produces a very strong increase in ultraviolet absorption at 363-nm wavelength. This absorption is

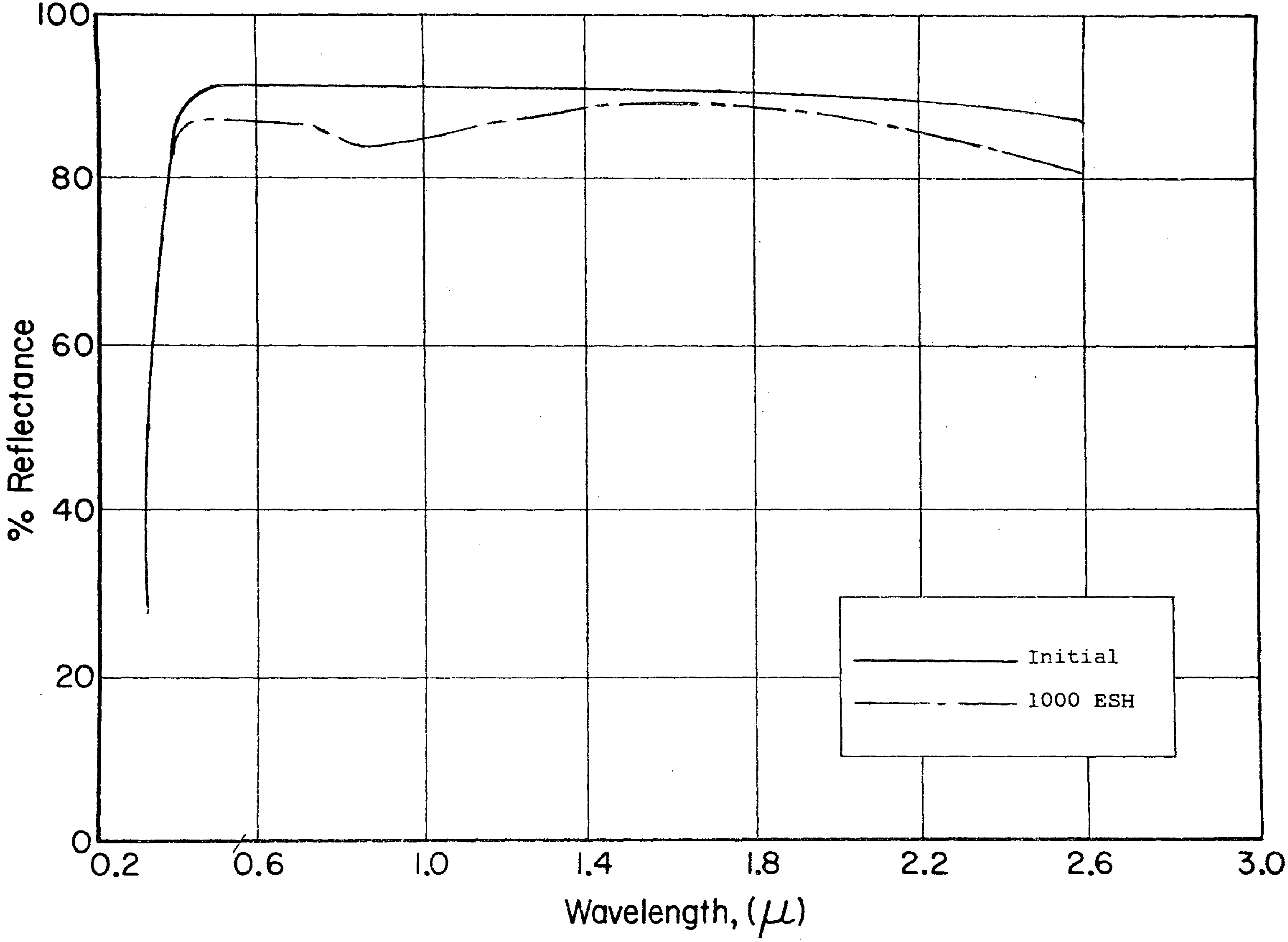

Figure 71 EFFECT OF 1000 ESH UV ON SPECIMEN B-072 OF Zn_2TiO_4 (ΔT = 1270°C)

Table 37

HISTORY OF PLASMA ANNEALED ZINC ORTHOTITANATES

Batch No.	Pigment No.[1]	Initial Reaction 925°C	Initial Reaction 1050°C	Plasma Heat Treatment, ΔT[2] 1900°C	Plasma Heat Treatment, ΔT[2] 2900°C
B-183	3*	18 hr	---	Yes	---
B-184	6*	---	18 hr	Yes	---
B-185	4**	18 hr	5 hr	---	Yes
B-186	6**	---	18 hr	---	Yes
B-187	3**	18 hr	---	---	Yes
B-188	4*	18 hr	5 hr	Yes	---

1 From Table 2; * = low ΔT; ** = high ΔT.

2 ΔT = plasma temperature gradient.

Table 38

DESCRIPTIVE NATURE OF PLASMA HEAT-TREATED ZINC ORTHOTITANATE ULTRAVIOLET DAMAGE SPECTRA

Batch No.	Pigment No.	Shoulder at 363nm ($R_{450}-R_{363}$)	Damage, $\%\Delta R_\lambda$ 363nm	Damage, $\%\Delta R_\lambda$ 700nm	Damage, $\%\Delta R_\lambda$ 2600nm	Peak Damage λ_{nm}	Peak Damage ΔR_λ, %
B-183	3*	Weak; 11%	6.5	2.5	0	900	4.0
B-184	6*	Weak; 10%	7.0	2.0	0	900	5.0
B-185	4**	Very strong; 54%	0	1.6	10.5	960	3.0
B-186	6**	Very strong; 57%	-4.0	1.6	20.0	1000	4.0
B-187	3**	Very strong; 64%	0	2.0	22.0	960	3.4
B-188	4*	Weak; 9%	6.5	1.8	0	900	2.5

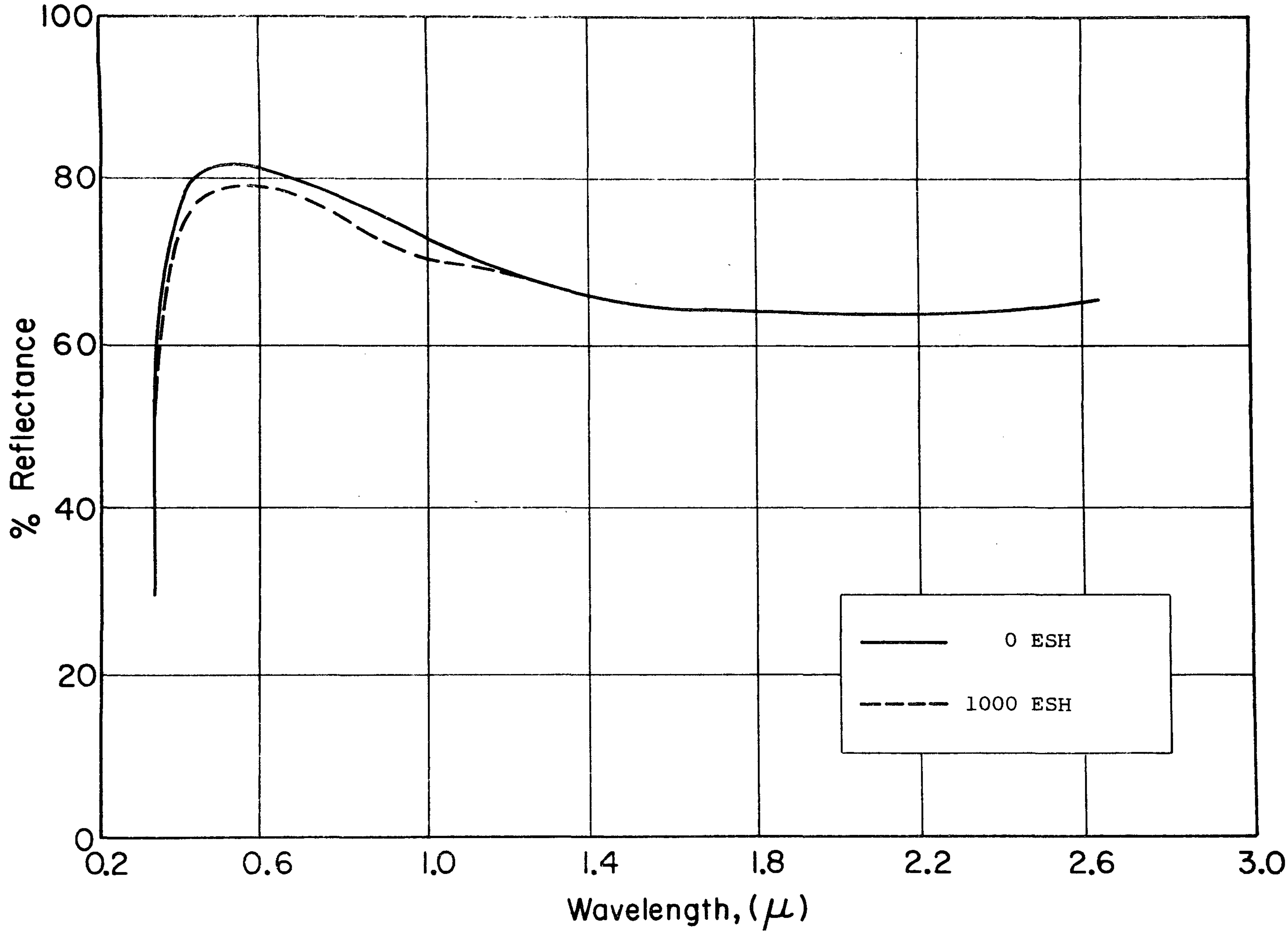

Figure 72 EFFECT OF 1000 ESH UV RADIATION ON BATCH 183 Zn_2TiO_4

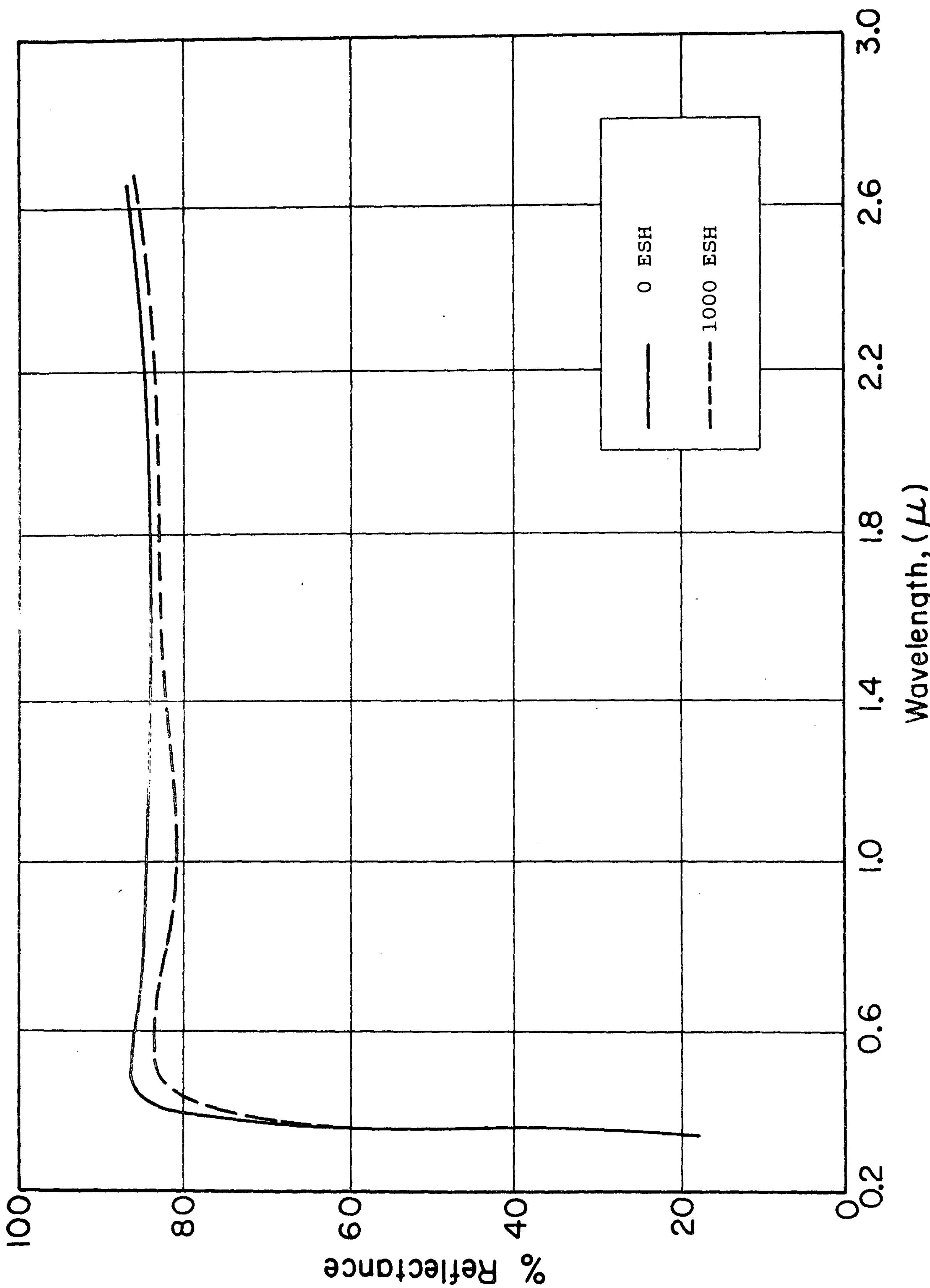

Figure 73 EFFECT OF 1000 ESH UV RADIATION ON BATCH 184 Zn_2TiO_4

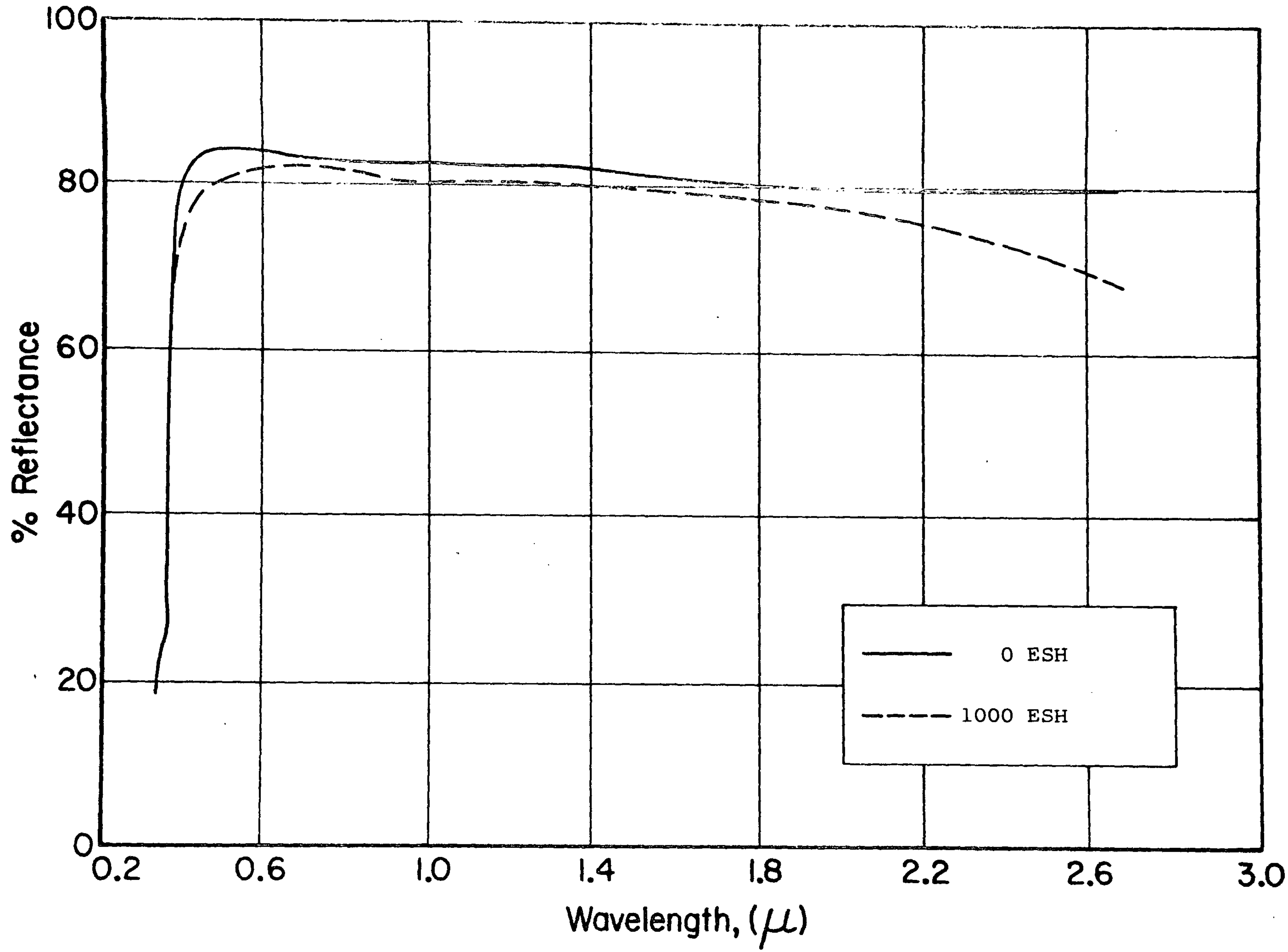

Figure 74 EFFECT OF 1000 ESH UV RADIATION ON BATCH 185 Zn_2TiO_4

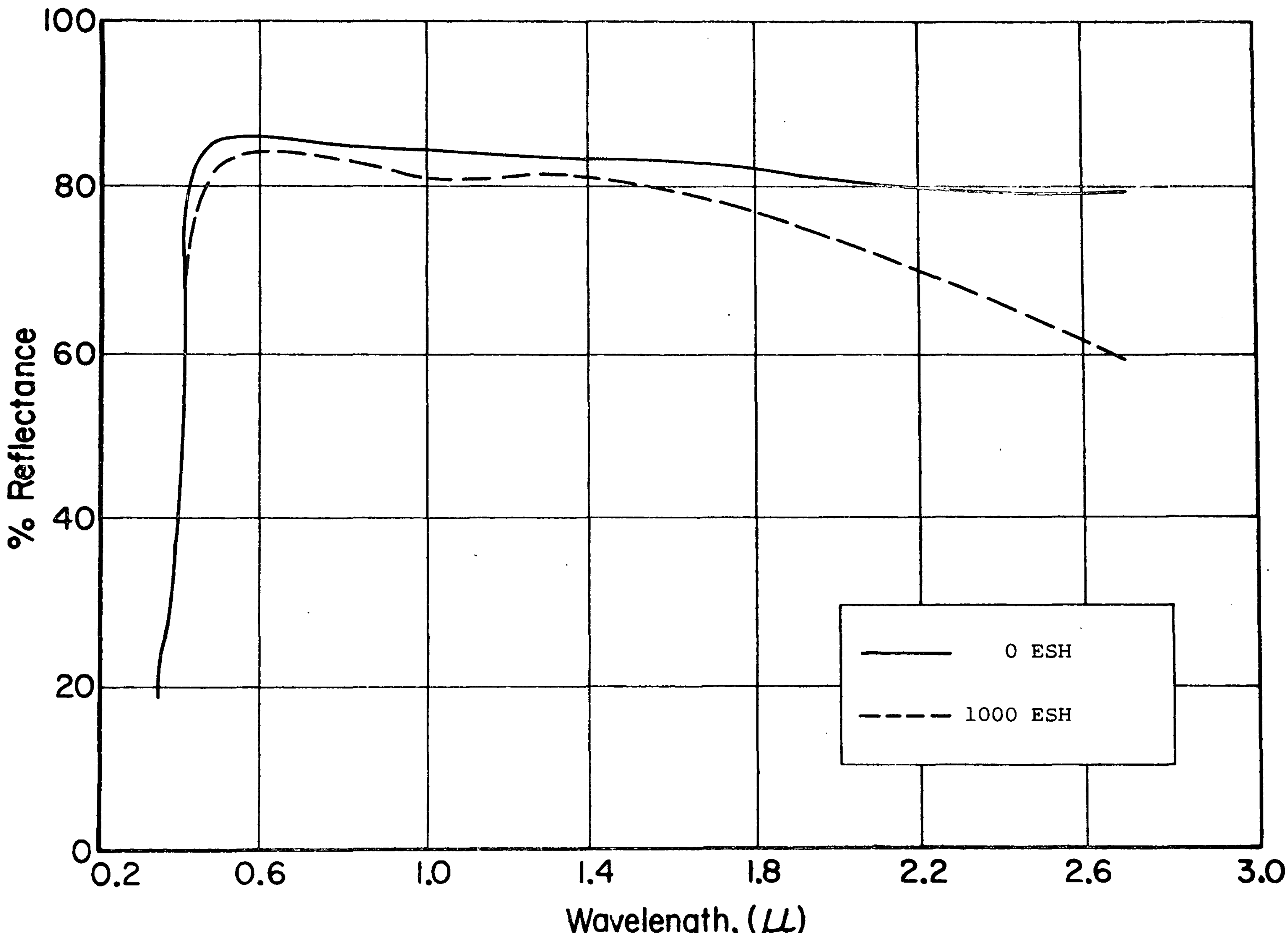

Figure 75 EFFECT OF 1000 ESH UV RADIATION ON BATCH 186 Zn_2TiO_4

5④

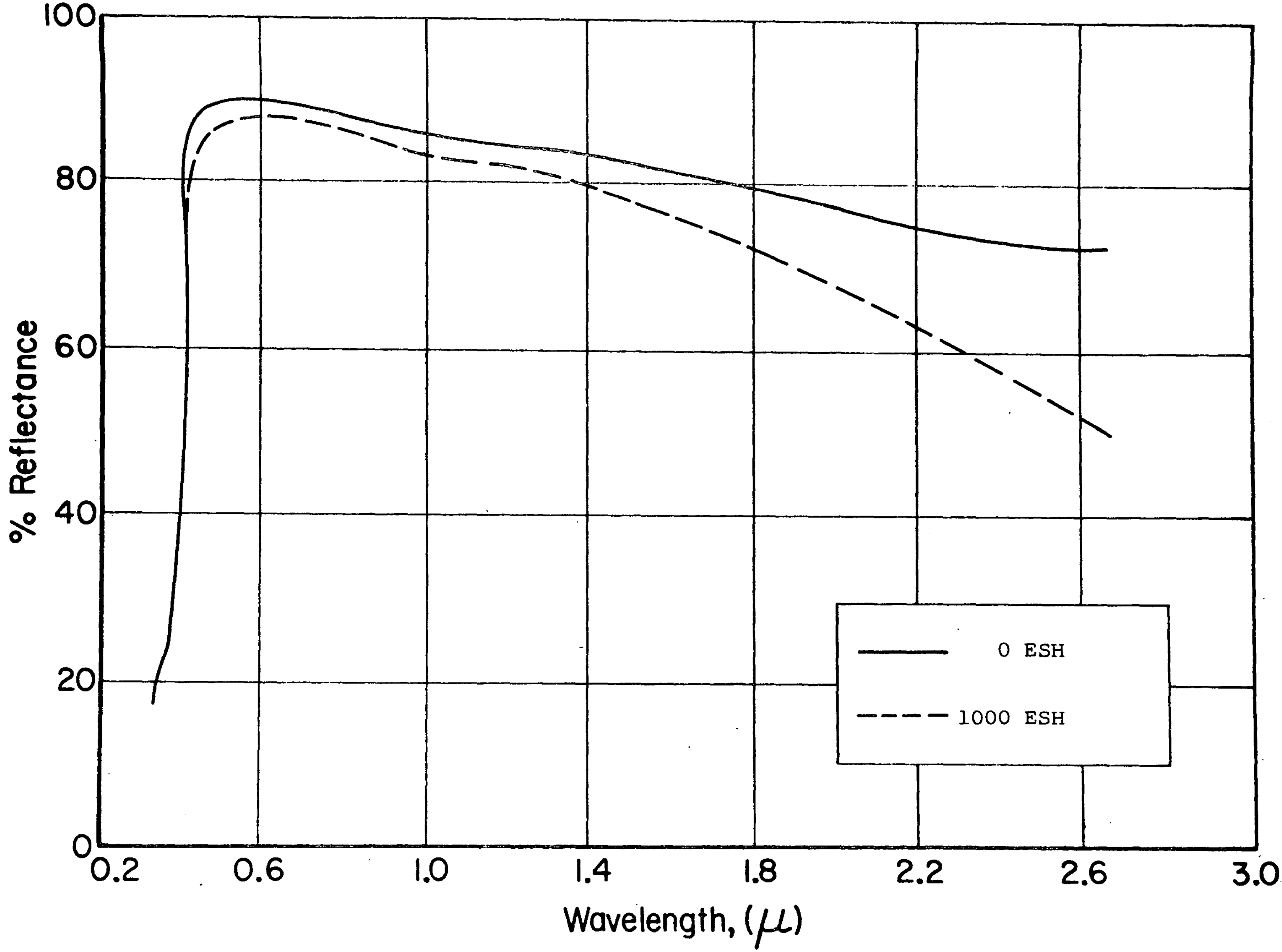

Figure 76 EFFECT OF .000 ESH VU RADIATION ON BATCH 187 Zn_2TiO_4

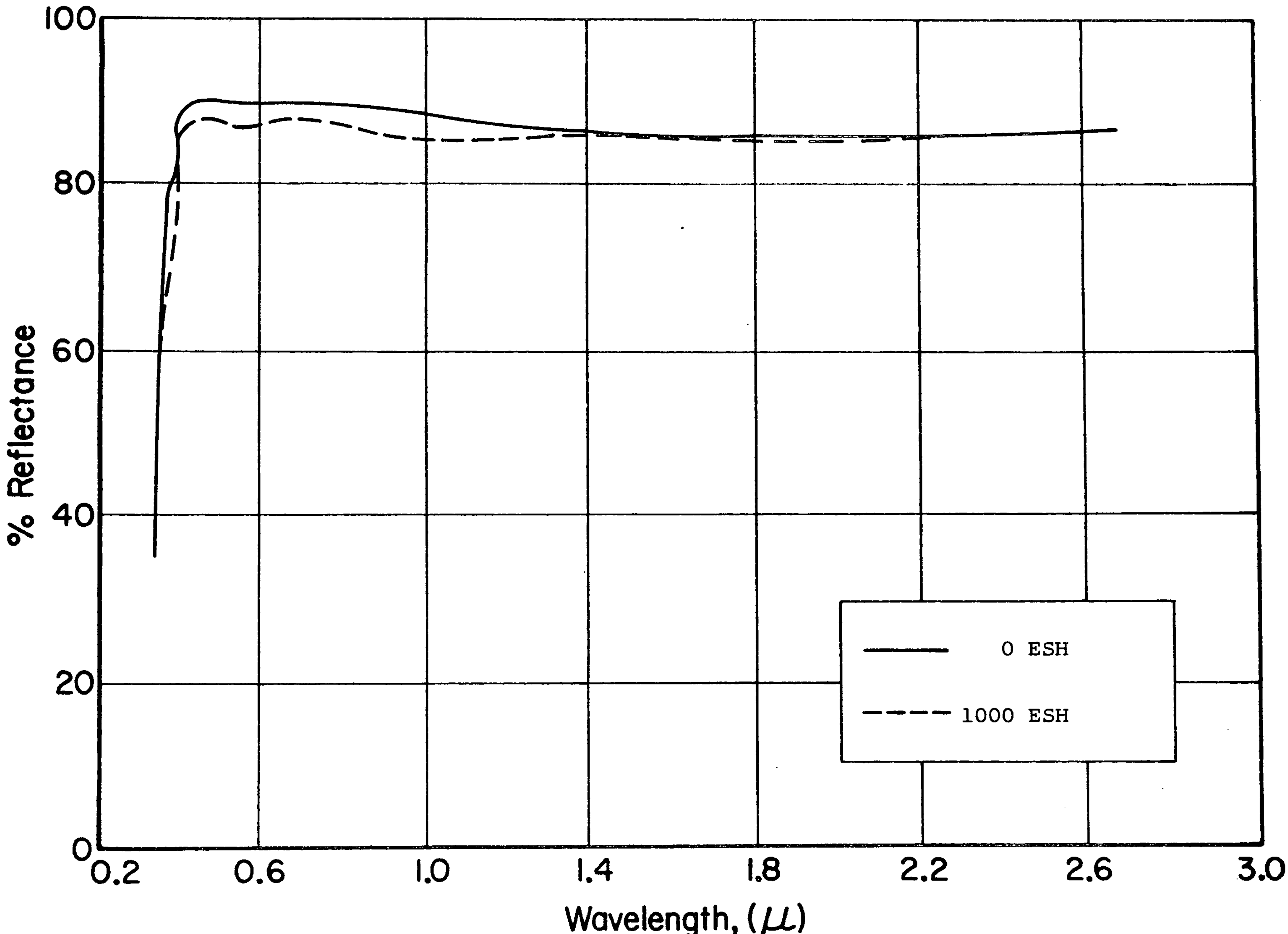

Figure 77 EFFECT OF 1000 ESH UV RADIATION ON BATCH 188 Zn_2TiO_4

believed to be due both to the creation of TiO_2 and ZnO at 2900°C ΔT. Unlike the strong absorption at 363 nm in the precursor materials, which is to a large extent extractable with acetic acid in each case, and is therefore due to unreacted ZnO, ZnO-type infrared damage occurred when the absorption was increased, or created completely, by plasma annealing.

The infrared damage in the 1500- to 2600-nm wavelength region (Figures 72-77) is therefore attributed to ZnO that was first created by the reaction

$$Zn_2TiO_4 \xrightarrow{\Delta} TiO_2 + 2ZnO, \qquad (11)$$

in which case the volatile ZnO condenses on the Zn_2TiO_4 surfaces where it is unprotected and subject to photodesorption of oxygen.

Not only does the 925°C product (3**) exhibit the strongest absorption as a result of high-temperature plasma annealing, but it also exhibits the greatest damage in the infrared. The fact that no damage is observed at 363 nm is attributed to the screening effect of the ZnO. Conversely, low-temperature annealing resulted in damage at 363-nm wavelength to all three specimens, which is consistent with the fact that the reflectance at 363 nm was nearly maximized at the ΔT of 1900°C. (It should be noted that the 1050°C product (6**) exhibited ZnO-type luminescence bleaching at 363 nm as a result of ultraviolet irradiation.)

Low-temperature plasma annealing was most effective in stabilizing the 925°C/1050°C product (#4,Table 34). Although the damage at 363-nm increased slightly, that in the 700- to 850-nm region was all but eliminated (see Table 38).

Finally, it should be noted that plasma heat treatment resulted in an increase in the peak wavelength and in the width of the 800- to 1000-nm absorption attributed to Ti^{+3} (Ref. 131). The greatest increase in peak damage that occurred in this region was exhibited by all three pigments plasma annealed at the higher temperature gradient; with the longest wavelength being associated with specimen 6** (which exhibited luminescence bleaching at 363 mn). It should be noted that the assignment of peak wavelengths is difficult due to the well-known spectral imprecision in powder-reflectance measurements (see Table 38).

8.3.4 Summary of Parameters Study

The results of plasma heat treatment at several mean boundary-layer temperature gradients, ΔT, and a reactor retention time of 1.1 sec, are presented in Table 39. These parameters are discussed fully in a recent SRI report by Farley (Ref. 139).

Table 39

EFFECT OF ULTRAVIOLET IRRADIATION ON PLASMA TREATED B-229 Zn_2TiO_4 AT A RETENTION TIME OF 1.1 SECOND

Figure No.	Plasma Temp. ΔT (°C)	Exposure (ESH)	Reflectance Decrease* ΔR_λ (λ = nm), %					Solar Absorptance	
			362	425	700	950	2400	α_s	$\Delta\alpha_s$
78	2000	1010	0.4	2.4	2.0	2.6	8.2	0.160	0.028
79	1400	1010	1.0	1.8	3.5	5.8	-1.2	0.130	0.029
80	2450	1010	-2.6	0	2.5	6.0	3.5	0.143	0.026
81	1670	2500	-4.0	0	0	0	10.0	0.145	0.010

*(-) values denote reflectance increases, i.e., bleaching.

These data and the corresponding spectra, which are presented in Figures 78 through 81, showed that a ΔT of 1670°C produced the most stable pigment in terms of $\Delta\alpha_s$. The resultant stability was deemed insufficient however, and it was decided that plasma heat treatments should be performed on reactively encapsulated Zn_2TiO_4. These studies are presented in paragraph 8.4.4.1.2.

8.4 Reactive Encapsulation of Zn_2TiO_4

8.4.1 Early Rationale for Reactive Encapsulation

The efficacy of reactive encapsulation as a method of stabilization of pigments against the degrading influence of space ultraviolet radiation was first established with Z93 as a result of comparison with S-13, a comparison that led to the

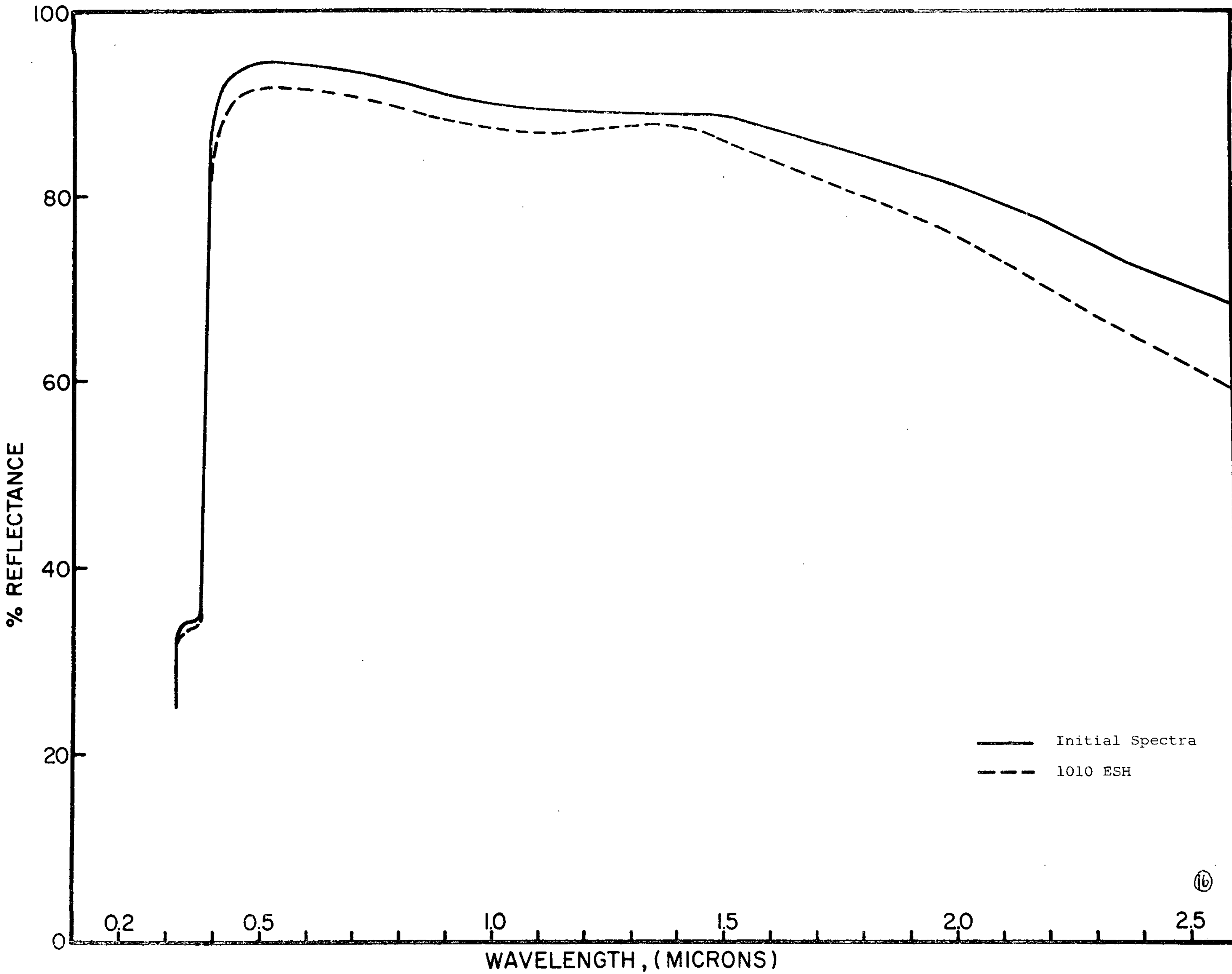

Figure 78 EFFECT OF UV ON 2000°C AT Zn_2TiO_4

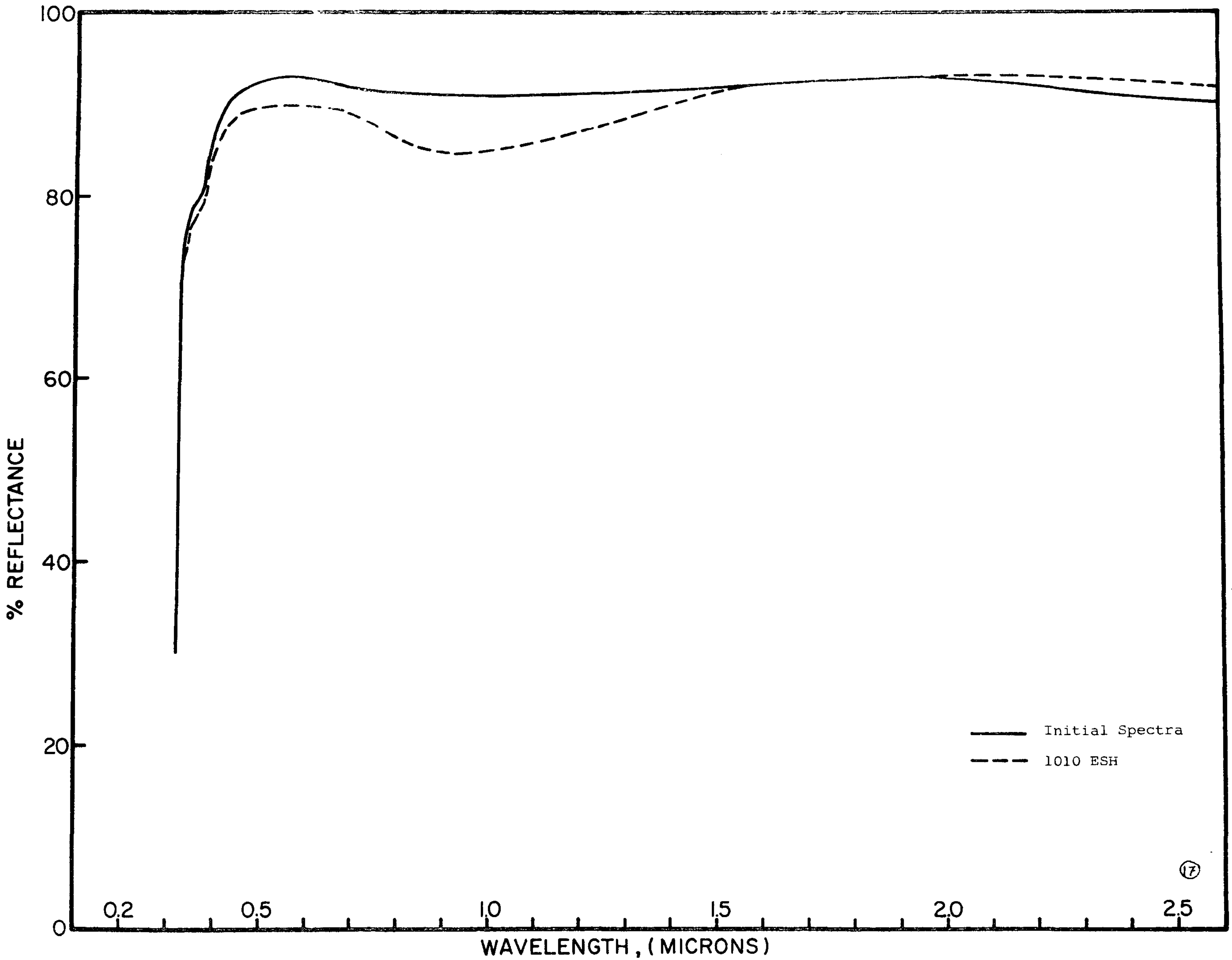

Figure 79 EFFECT OF UV ON 1400°C ΔT Zn_2TiO_4

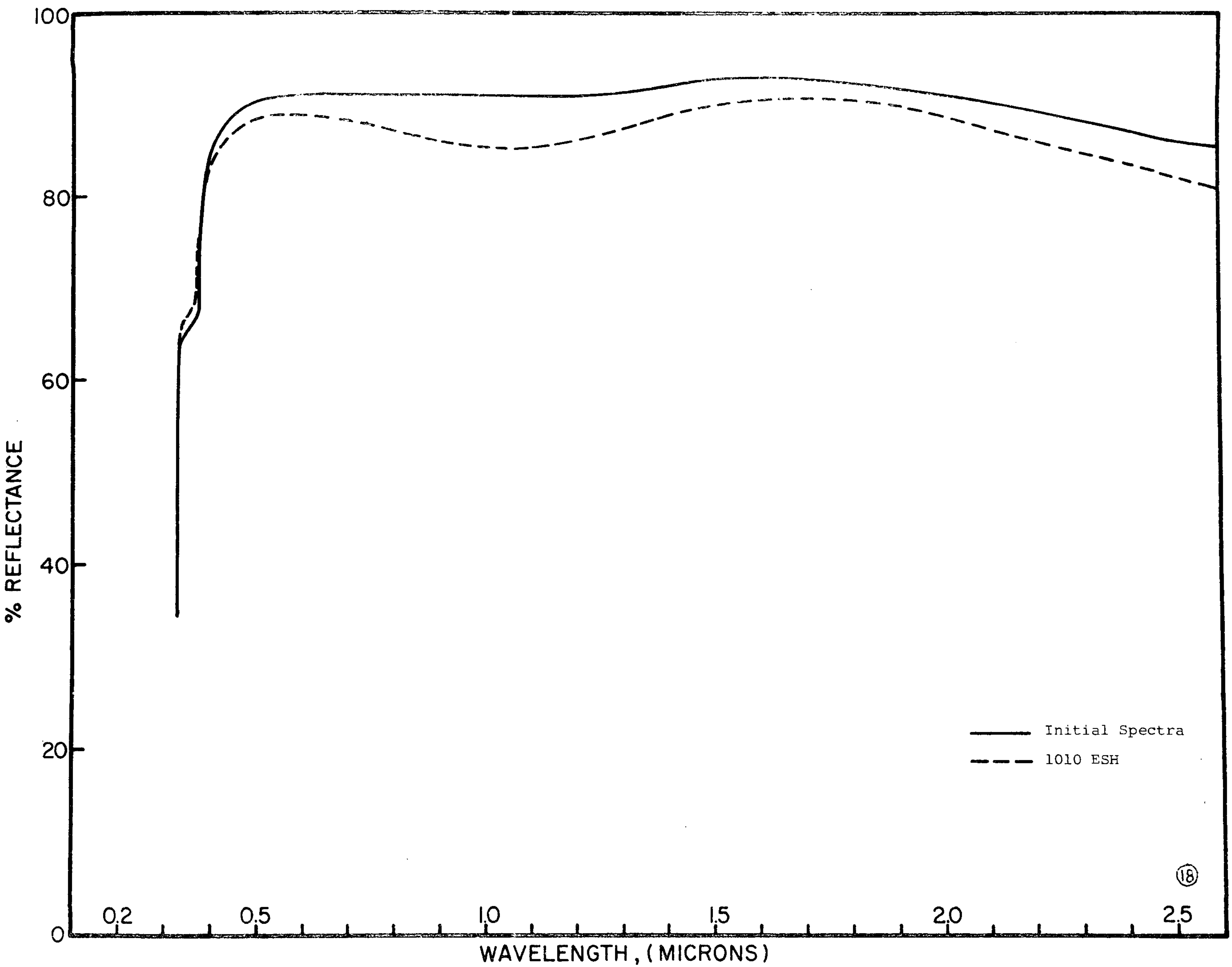

Figure 80 EFFECT OF UV ON 2450°C AT Zn_2TiO_4

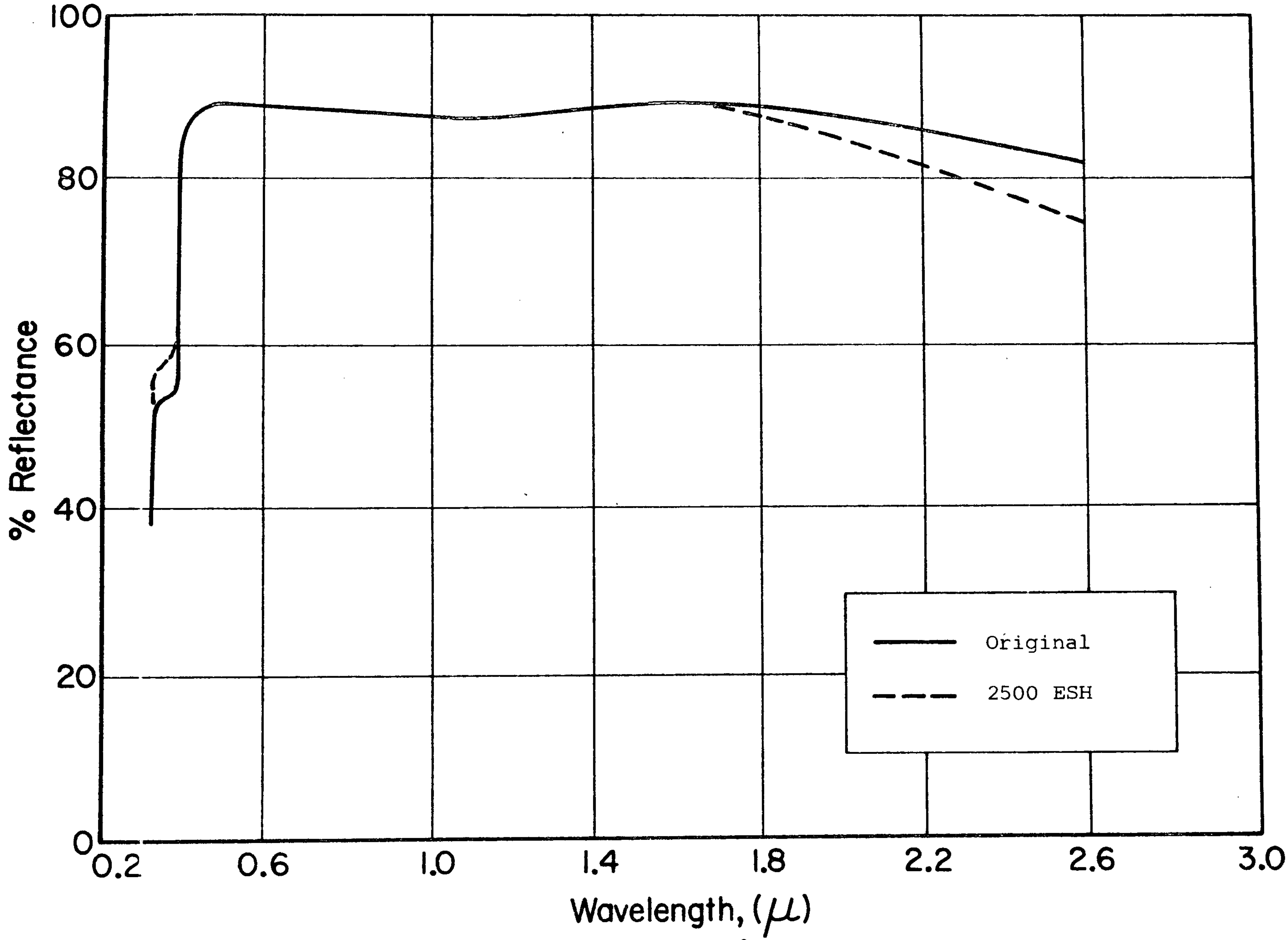

Figure 81 EFFECT OF UV ON 1670°C AT Zn_2TiO_4

development of S-13G (see Chapter 6). However, it was not until S-13, an elastomeric silicone paint based on untreated ZnO, was discovered to be unstable that the protective mechanisms associated with Z93's exceptional stability were deduced. These early experiments showed that zinc oxide was the unstable component in S-13 and that, therefore, the potassium silicate employed in the stable Z93 provided a stabilizing influence on the otherwise unstable zinc oxide (Ref. 9).

The idea of utilizing potassium silicate as a treatment to stabilize ZnO prior to its incorporation into the elastomeric silicone binder was thus developed (Ref. 119) and the concept of reactive encapsulation was subsequently postulated. The now widely employed S-13G thermal-control paint utilizes this thesis in its formulation, in which the zinc oxide is first reacted in slurry with potassium silicate, is extracted and is then dried prior to being milled into the silicone elastomer binder.

8.4.2 Theoretical Considerations

We have speculated previously on the possible mechanisms that may explain why silicate treatment is a practical method of preventing degradation of ZnO and ZnO-pigmented coatings (Ref. 119 and Chapter 6). We postulated that the effectiveness of silicate treatment of ZnO can be explained by the barrier mechanism concept in which the silicate coating on the pigment surface forms a barrier to charge and/or excitation transfer. Although subsequent experience has not disproven this concept, we are now of the opinion that the protection could also be afforded by other mechanisms, chief among which is the hole (p^+) withdrawing effect of the polynegative anions employed in reactive encapsulation.

Ultraviolet radiation produces electron-hole pairs with the electron entering the conduction band, leaving a hole (p^+) in the valence band. The holes combine with the chemisorbed oxygen (and other chemisorbed gases), now thought to be present on ZnO as O^-, releasing the oxygen at the surface,

$$O^-_{ads} + p^+ \longrightarrow O \qquad (12)$$

Some lattice oxygen can be expected to be discharged by the holes, although this is believed to be unimportant in ZnO. The non-recombined electrons in the conduction band either accumulate there, or fall into traps. Oxygen vacancies, i.e., from the discharge of lattice oxygen, will attract electrons because of their double positive charge.

On the basis of our studies of ultraviolet-irradiated zinc oxide involving optical spectroscopy and gas-adsorbate bleaching experiments (Ref. 2, 70), we have concluded that the predominant behavior in ZnO, that which manifests itself in the well-known broad infrared absorption that commences at approximately 1000 nm, is attributed to conduction band electrons. Shallow traps have been considered by others as being responsible for the observed infrared damage in ZnO. Nevertheless, we do not believe that a shallow trap with a transition energy of only about 0.03 eV, as necessitated by the infrared band observed, would permit the electron population required to be spectroscopically observable (i.e., $\sim 10^{14}$/cc). This is not to say though that shallow traps, lying 0.03 eV below the conduction band, are not present.

We previously postulated that when the surface is treated with potassium silicate, the O^- is displaced by the more highly charged, and thus more tightly bound, silicate anion. Although in a physical sense this may be true, we now believe that the surface chemistry of protection is much more complicated and that it is only possible to say with any certainty that reactive encapsulation interferes with the oxygen chemistry at the pigment/binder interface in favor of stabilization. We do believe, however, that the most probable explanation involves the interaction of the "encapsulating" anion with the highly prevalent hydroxyl (and other, namely, carboxyl) ions that are chemisorbed on all metal oxide surfaces. Whether this interaction involves hydrogen bonding with the hydroxyls, or the displacement of the hydroxyls, remains to be determined. Likewise, the concept that the high hole affinity of the polynegative anion precludes hole/O^-_{ads} combination (as shown by Eq. 12) or that the O^-_{ads} is displaced by the polynegative anion that acts as a physical barrier to hole/O^-_{ads} combination, also remains to be determined. As stated earlier, we presently favor the hole affinity concept as applied to the polynegative anion reacted on the oxide surfaces.

Regardless of whether the barrier mechanism or the hole affinity concept is, in reality, operative, it is obvious that oxygen is not photodesorbed when the electron-hole pair is produced in the pigment surface (where photon absorption takes place), and the kinetics of conduction electron formation are radically altered. Hence, as the electrons go into the conduction band, any holes left at the pigment/anion interface are captured preferentially by the polynegative anion, which is not desorbed. In the case of ZnO, the polynegative anion is silicate. We then postulate that a charge is built up in the polynegative anion, attracting electrons from the conduction band, and reducing their concentration to the point that they are not spectroscopically observable, or thermodynamically important from the standpoint of spacecraft heat transfer.

8.4.3 Pigment Treatment Scheme

The complete history of all reactive-encapsulation studies performed are presented schematically in Figures 82 and 83. The exact experimental procedures employed in the preparation of each batch are presented in the Appendix. The open circles and squares in Figures 82 and 83 represent surface-treated (reactively encapsulated) powders that were irradiated in the IRIF and/or employed as pigment material for silicate and silicone paints. The first row of "filled" circles represents PS7 potassium silicate-based inorganic paints and the second row of filled circles (the last row) represents silicone paints prepared from Owens-Illinois 650 Glass Resin.

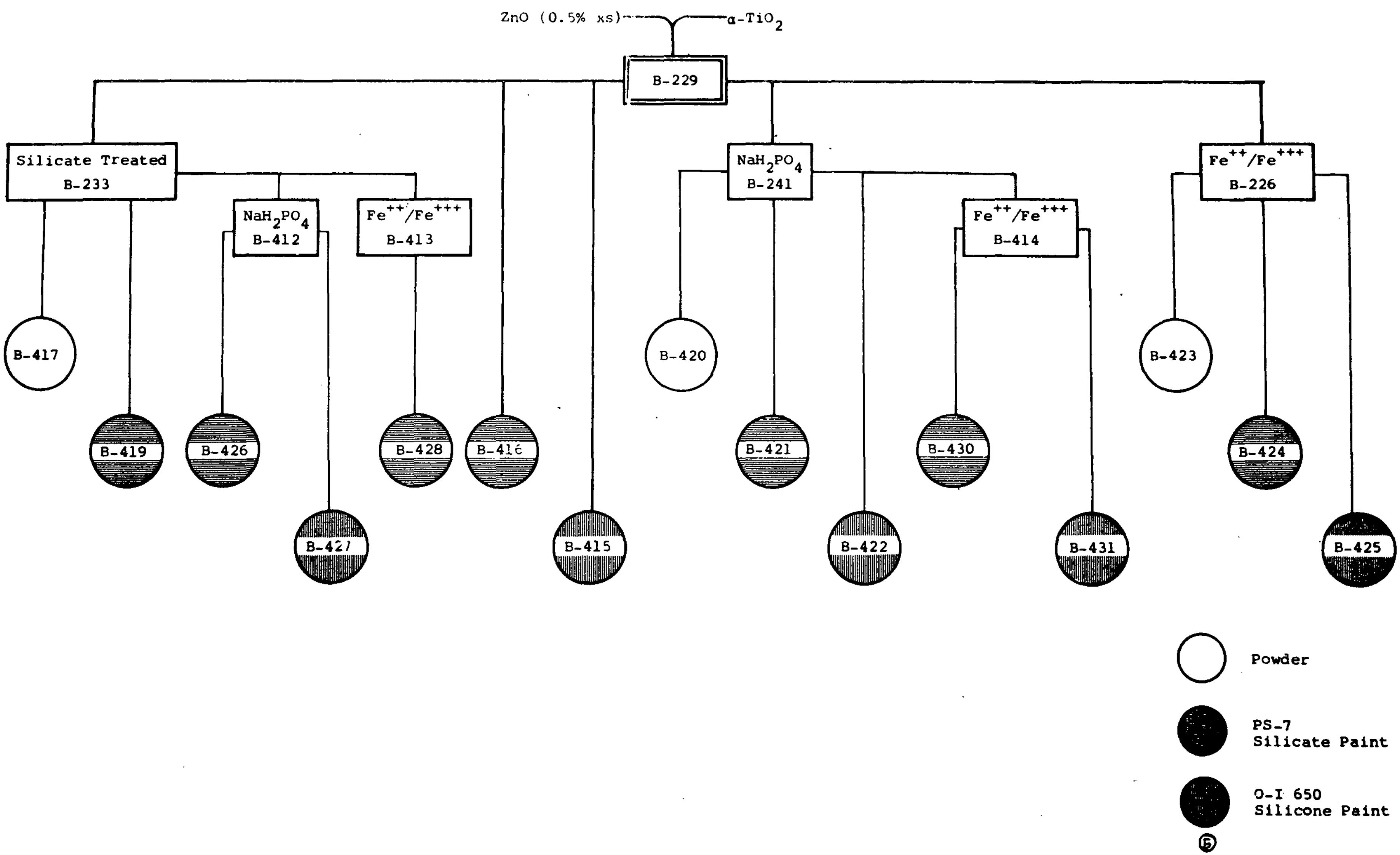

Figure 82 SCHEME FOR REACTIVE ENCAPSULATION-I

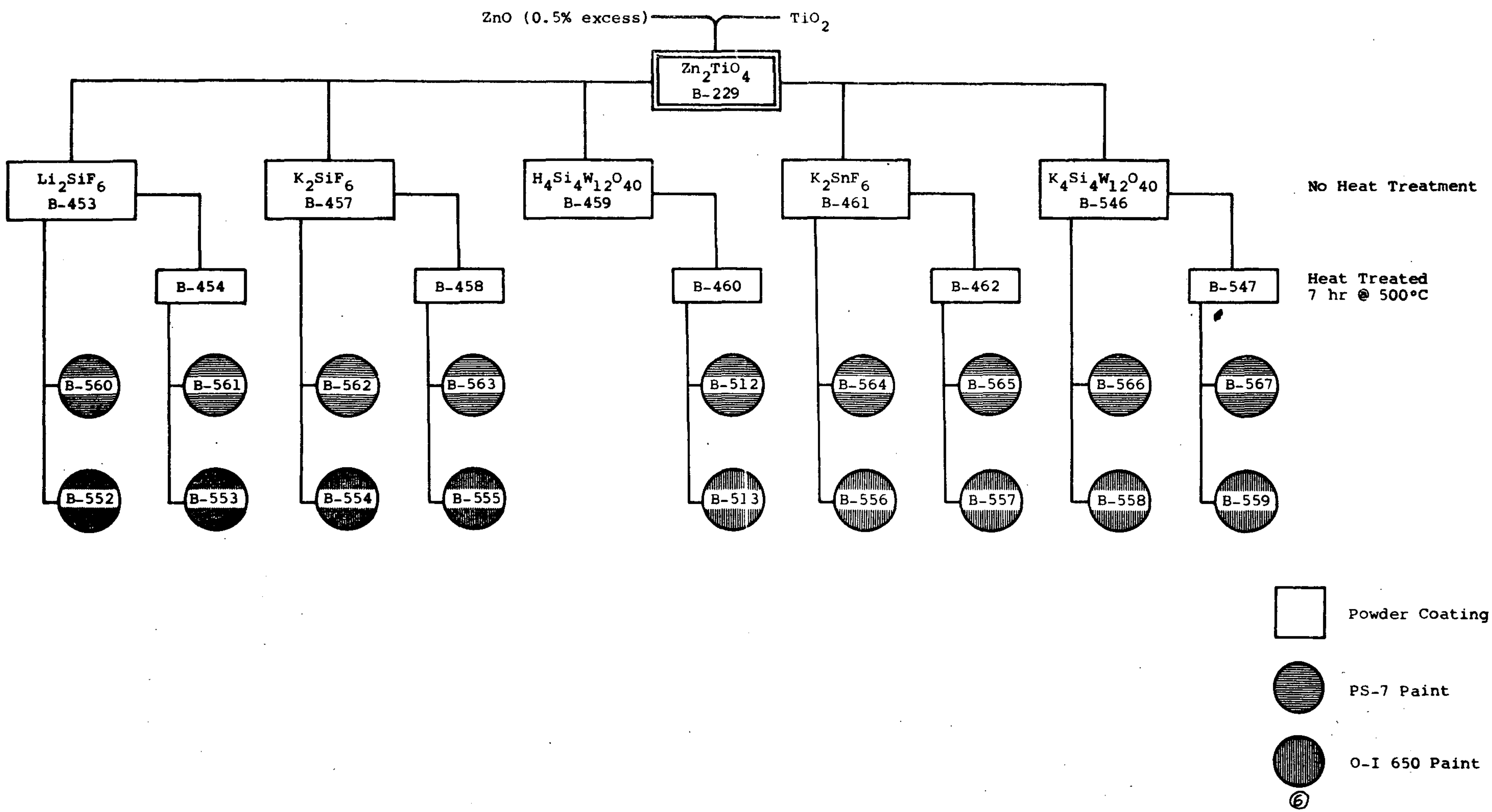

Figure 83 SCHEME FOR REACTIVE ENCAPSULATION-II

The rationale for selecting these reactive encapsulants is based on the thesis that: (1) Photodesorption of oxygen by the migrating "hole" produced by the interacting (ultraviolet) photon provide for a permissive state in which the resultant electron is free to enter the conduction band, if ZnO is present or to reduce Ti^{+4} to Ti^{+3} in any case, and (2) highly polynegative anions should have a high "hole" affinity the use of which was expected to favorably interfere with the kinetics of the $Ti^{+4} \longrightarrow Ti^{+3}$ reduction. The use of the Fe^{++}/Fe^{+++} couple was suggested because of the application to ZnO reported by Sancier (Ref. 140), who discussed its efficacy in terms of the high electron cross-section of the Fe^{+++} and the "hole" cross-section of the Fe^{++}. These treatments are discussed in greater detail in paragraph 8.7.2.

8.4.4 Results of Ultraviolet Irradiation

8.4.4.1 Reactively Encapsulated Pigments

The effect of ultraviolet irradiation in vacuum on a series of zinc orthotitanate pigments that were reactively encapsulated with soluble alkali salts of the polyvalent anions of interest are shown in Table 40. This table presents the spectral reflectance changes for five (5) pertinent wavelengths; the corresponding spectral data are presented in Figures 68 and 84 through 92.

Of those specimens prepared according to the schedule presented in Figures 82 and 83, only those treatments that are most effective, or are otherwise instructive, are discussed in this report.

The silicating of zinc orthotitanate clearly stabilizes the surface against formation of the broad damage spectra in the region 1000- to 2600-nm wavelength (Figure 84). However, as with the silicated zinc oxide employed in IITRI's S-13G, the stability of the powder (as opposed to a silicate, or silicone, paint) is decreased in the 400-nm wavelength region by silicating. No explanation is available for this phenomenon except to note

Table 40

EFFECT OF IRRADIATION ON
THE SPECTRAL REFLECTANCE OF CHEMICALLY TREATED Zn_2TiO_4 POWDERS

Figure No.	Batch No.	Chemical	Hr. @ Temp., °C	Exposure (ESH)	ΔR_λ (λ = nm), % 362	400	700	950	2400
68	B-229	None	(Control)	970	2.0	4.0	4.0	4.5	2.8
84	B-417	PS7	---	970	4.5	8.0	1.5	1.0	1.5
85	B-420	NaH_2PO_4	---	970	7.0	7.5	6.0	5.0	1.5
86	B-423	Fe-CN	---	970	2.6	7.0	5.4	6.2	3.3
87	B-453	Li_2SiF_6	---	1010	8.0	7.2	3.0	2.5	1.0
88	B-454	Li_2SiF_6	7 @ 500	1010	1.0	2.8	1.0	1.7	1.7
89	B-457	K_2SiF_6	---	1010	5.0	5.3	3.1	3.0	1.8
90	B-458	K_2SiF_6	7 @ 500	1010	2.7	3.0	1.6	2.2	0.3
--	B-461	K_2SnF_6	---	1010	8.0	6.5	1.0	1.5	1.5
91	B-462	K_2SnF_6	7 @ 500	1010	9.0	6.0	1.3	2.5	1.7
--	B-546	$K_4Si_4W_{12}O_{40}$	---	1010	0.8	4.2	5.0	4.8	1.5
92	B-547	$K_4Si_4W_{12}O_{40}$	7 @ 500	1010	0.5	3.3	2.1	2.1	1.3

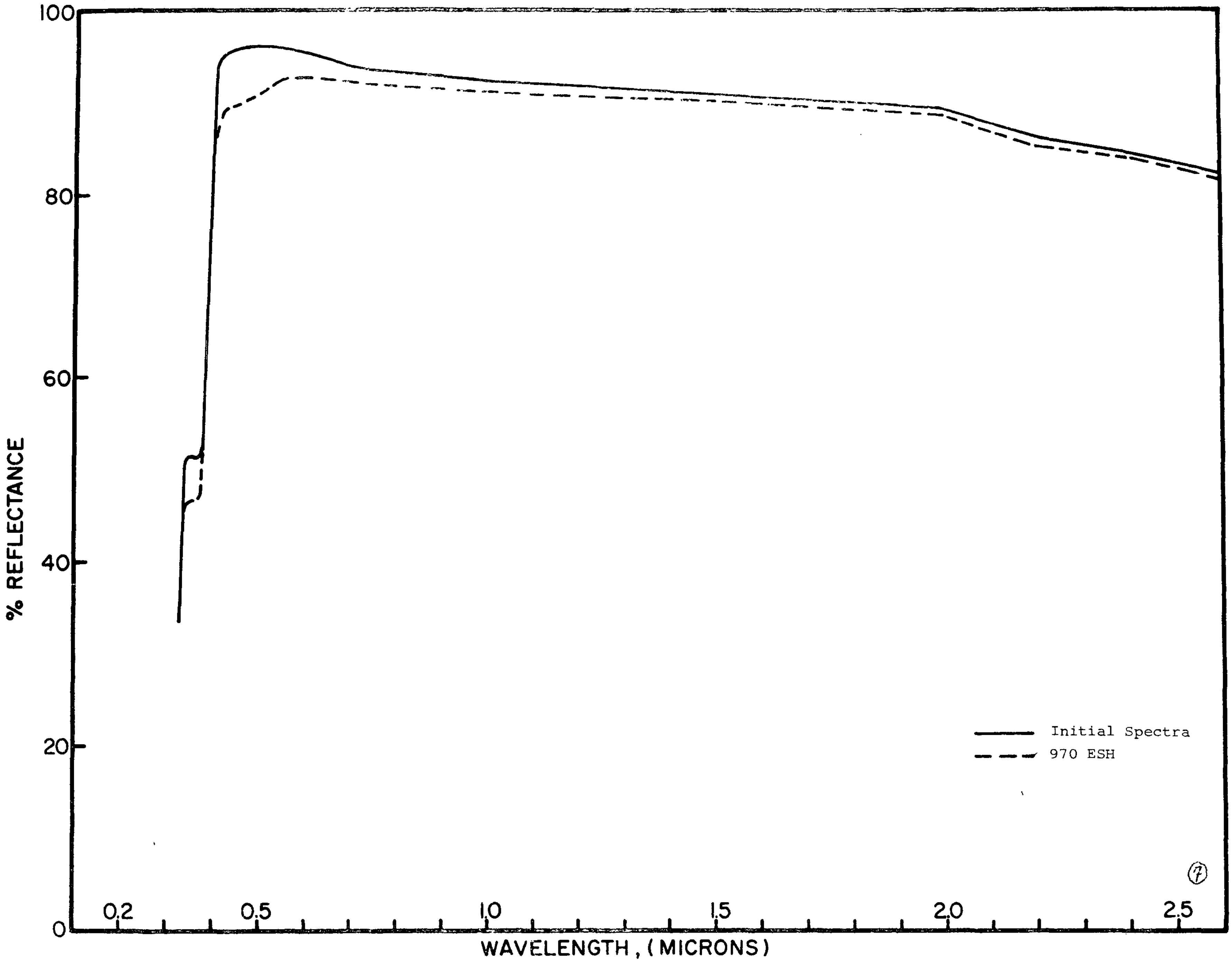

Figure 84 EFFECT OF UV ON B-417 Zn_2TiO_4

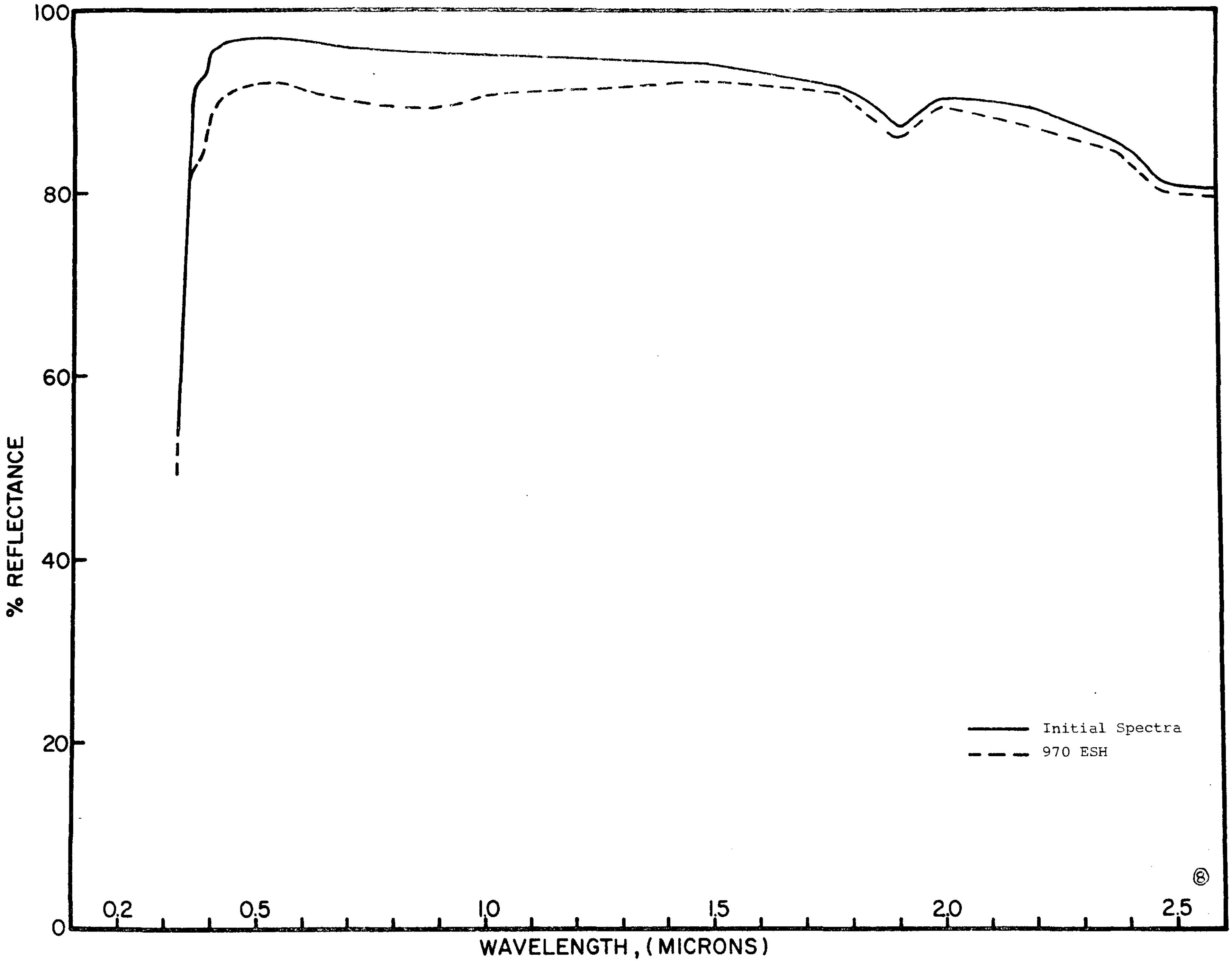

Figure 85 EFFECT OF UV ON B-420 Zn_2TiO_4

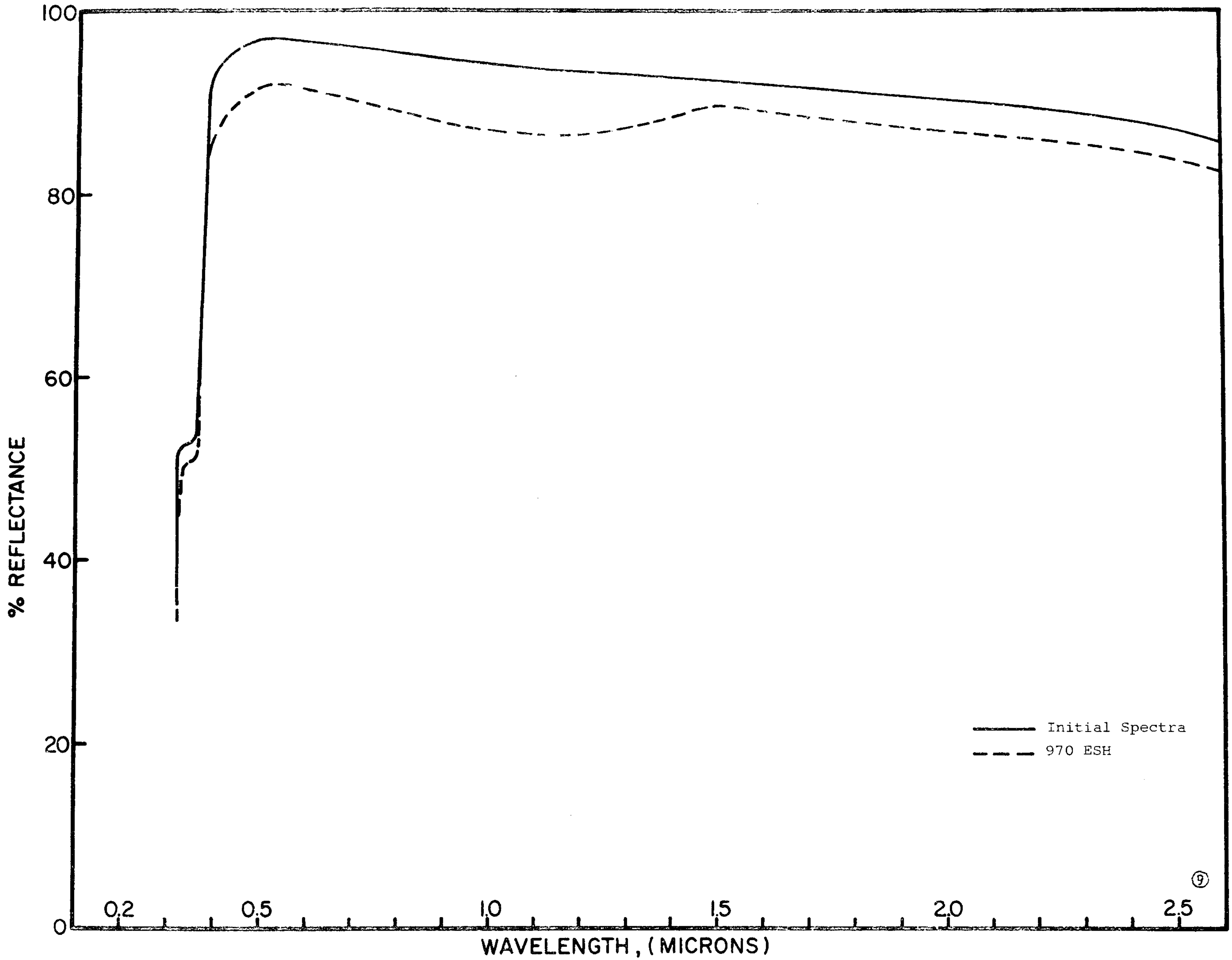

Figure 86 EFFECT OF UV ON B-423 Zn_2TiO_4

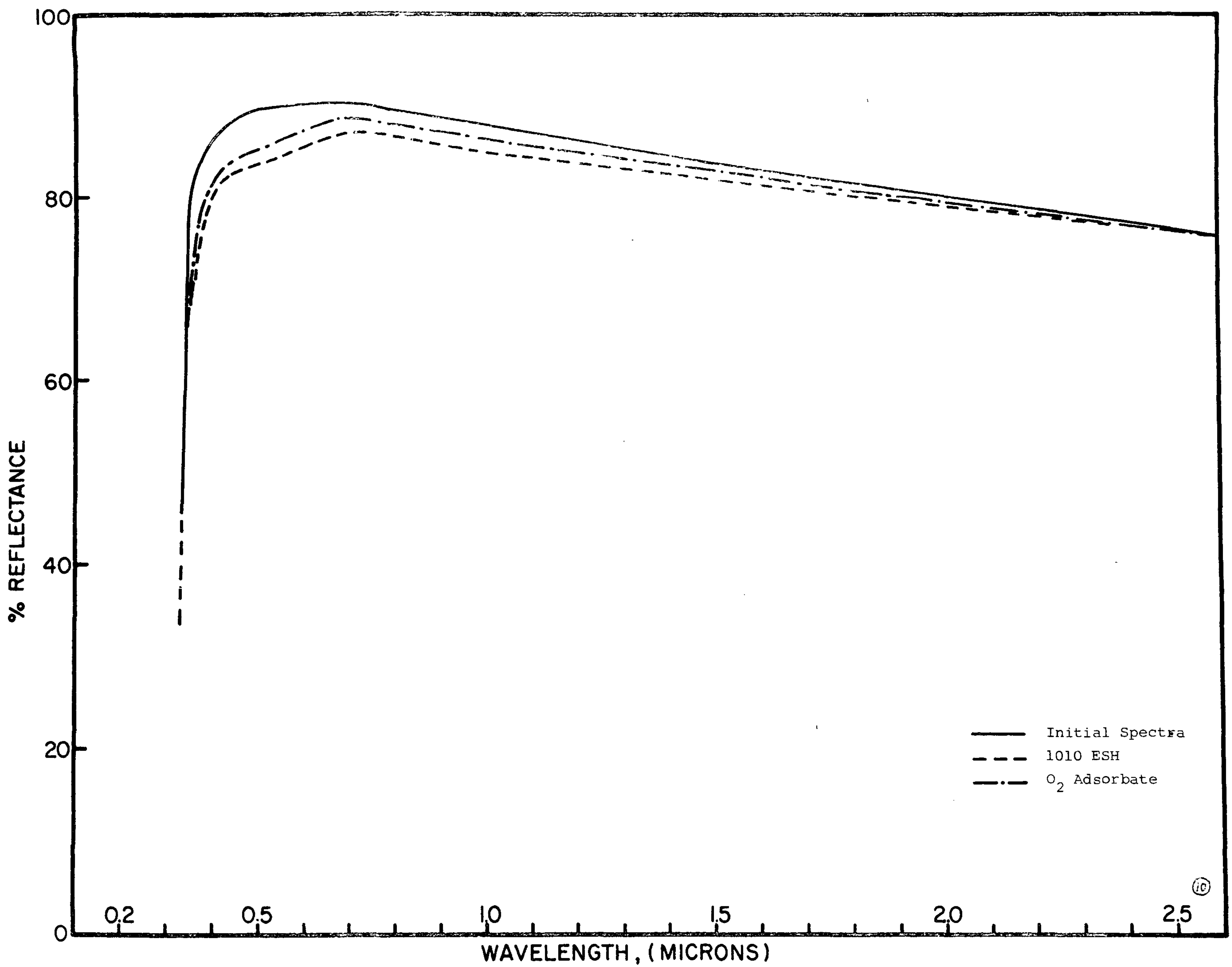

Figure 87 EFFECT OF UV ON B-453 Zn_2TiO_4

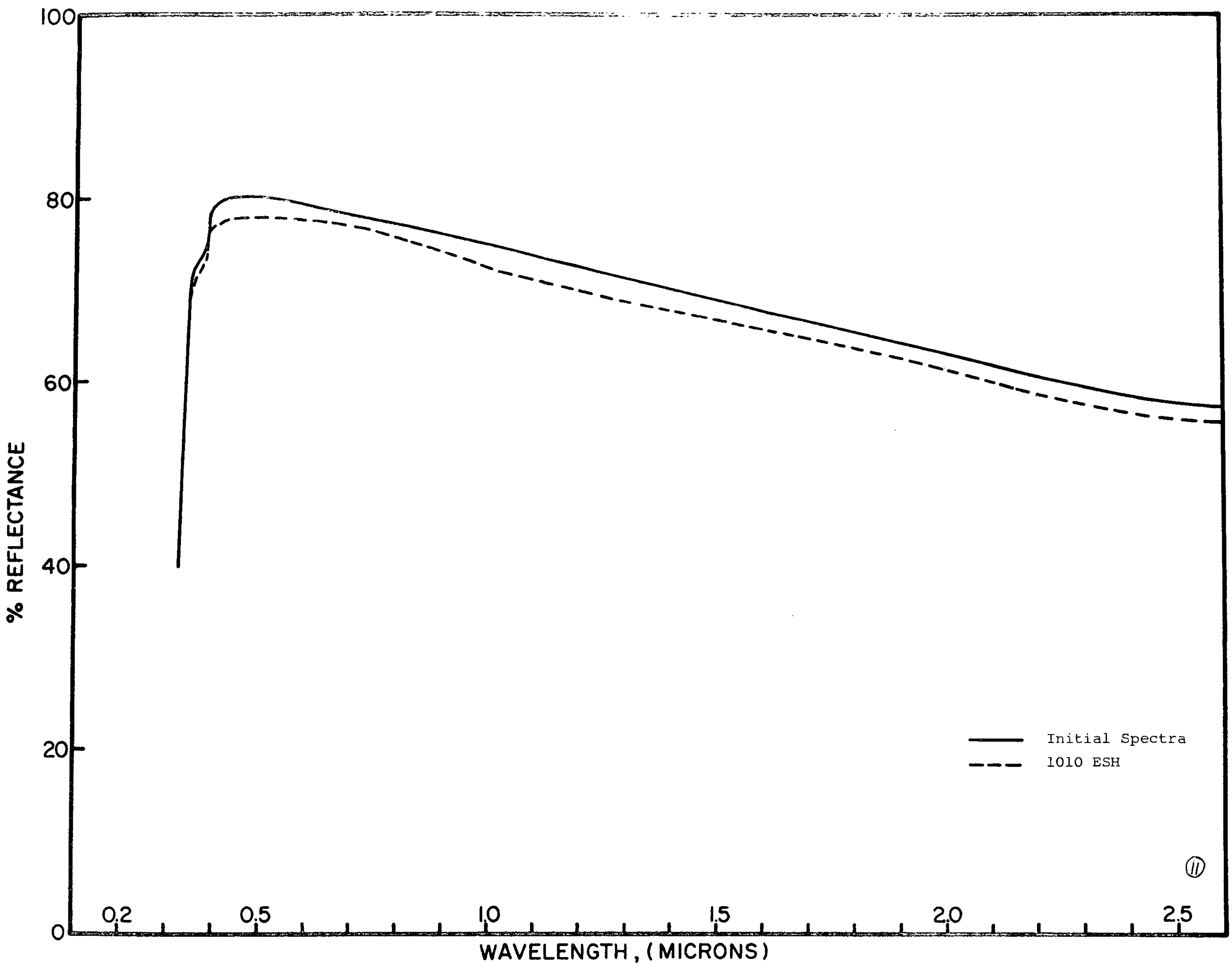

Figure 88 EFFECT OF UV ON B-454 Zn_2TiO_4

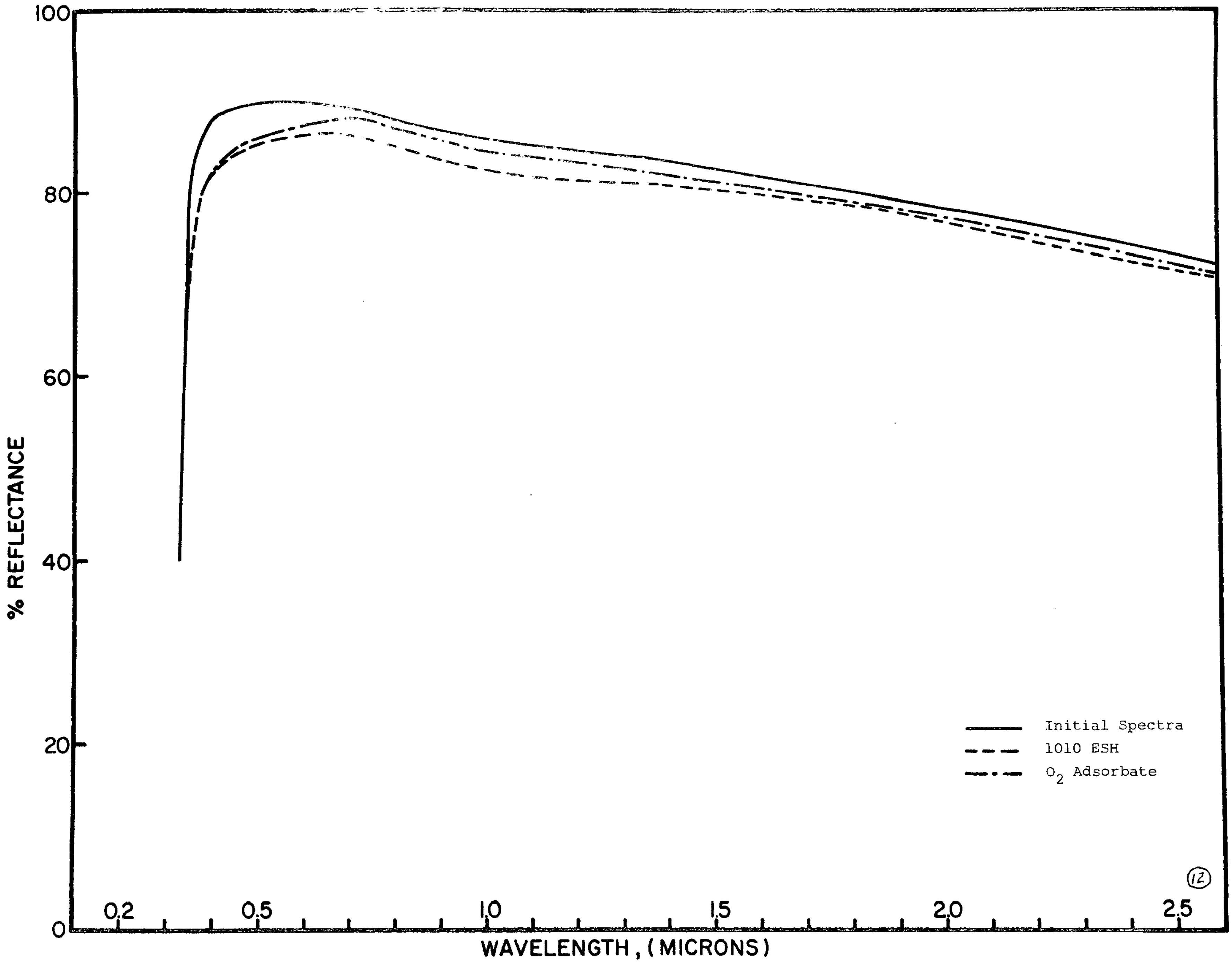

Figure 89 EFFECT OF UV ON B-457 Zn_2TiO_4

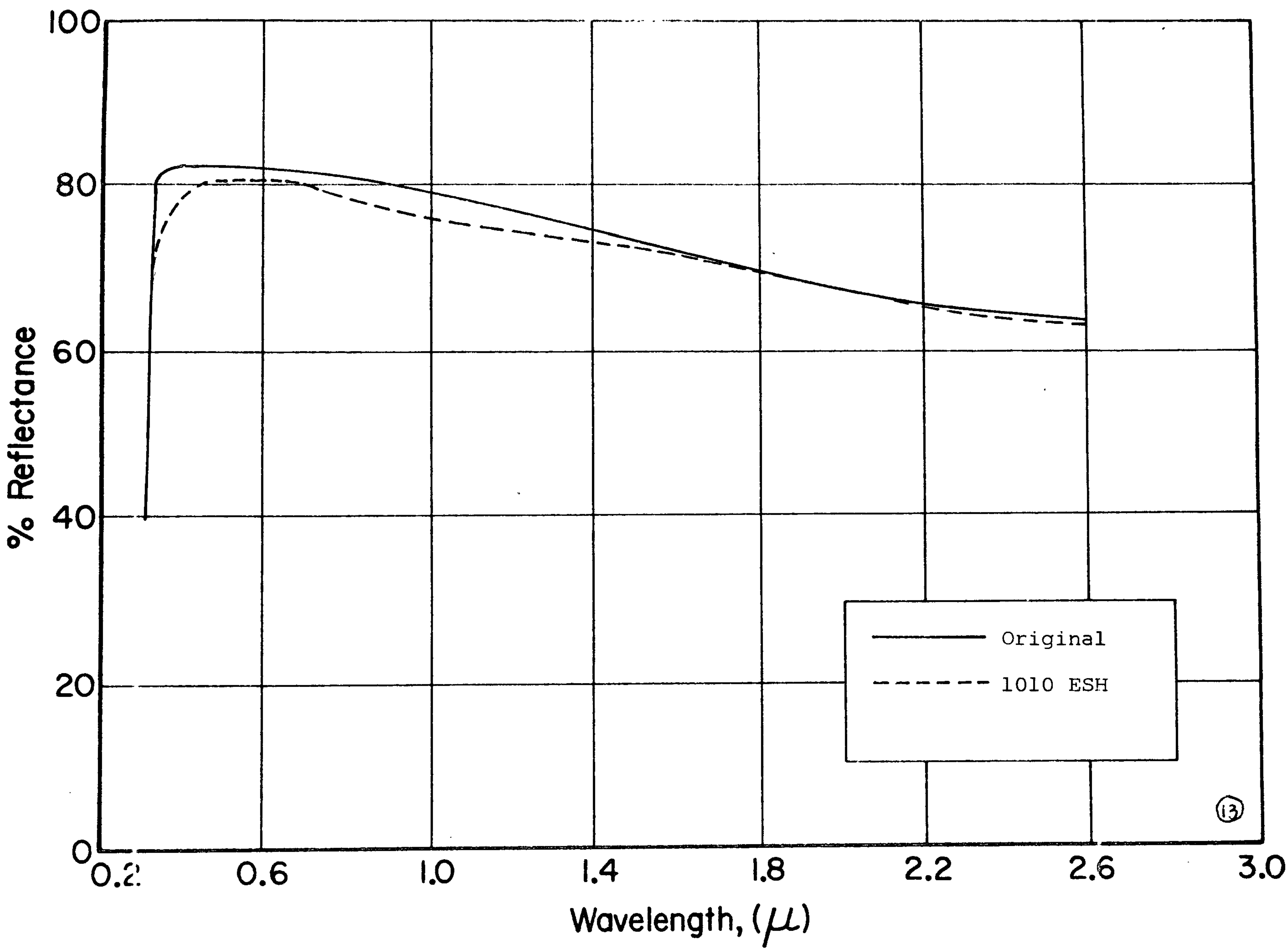

Figure 90 EFFECT OF UV ON B-458 Zn_2TiO_4

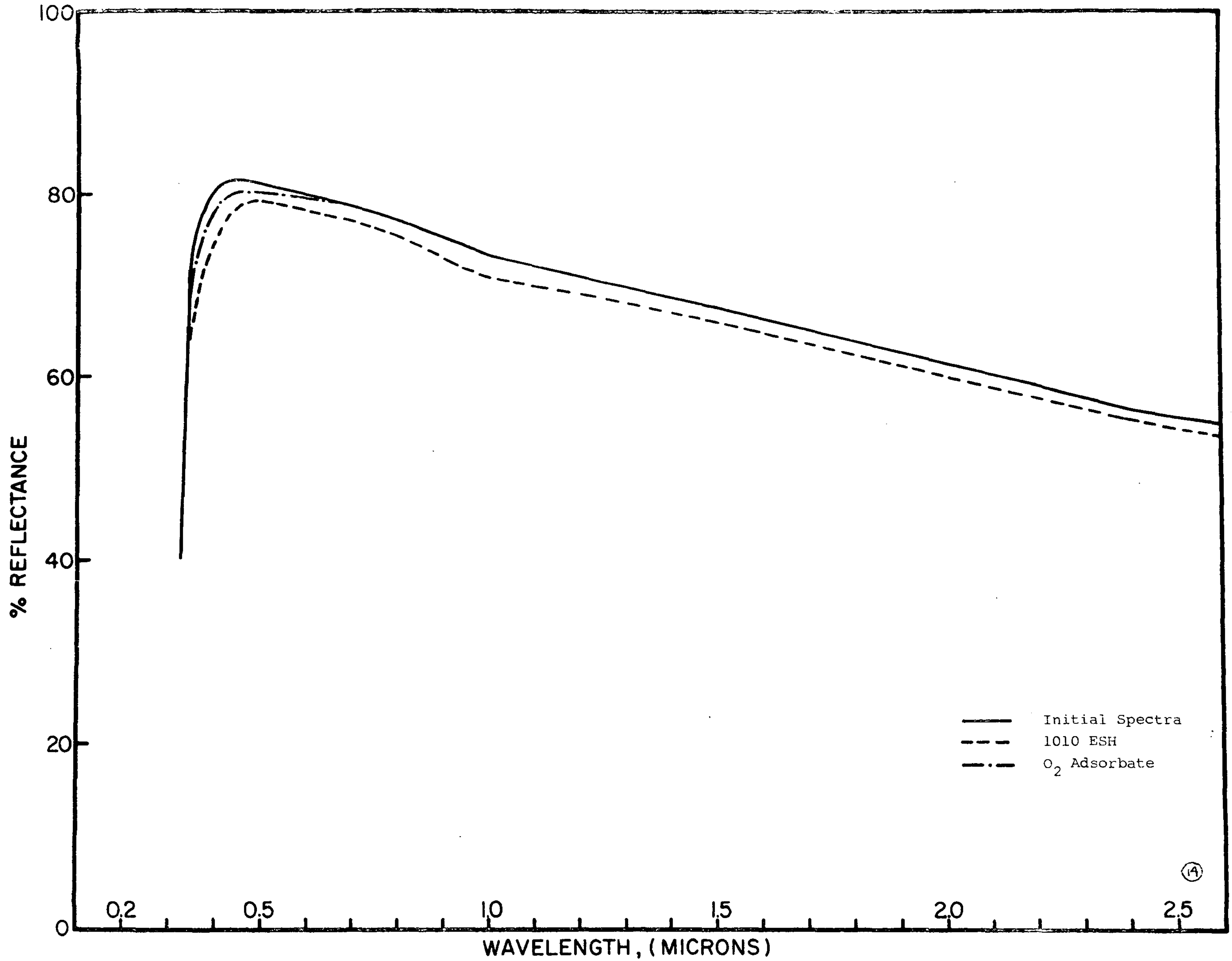

Figure 91 EFFECT OF UV ON B-462 Zn_2TiO_4

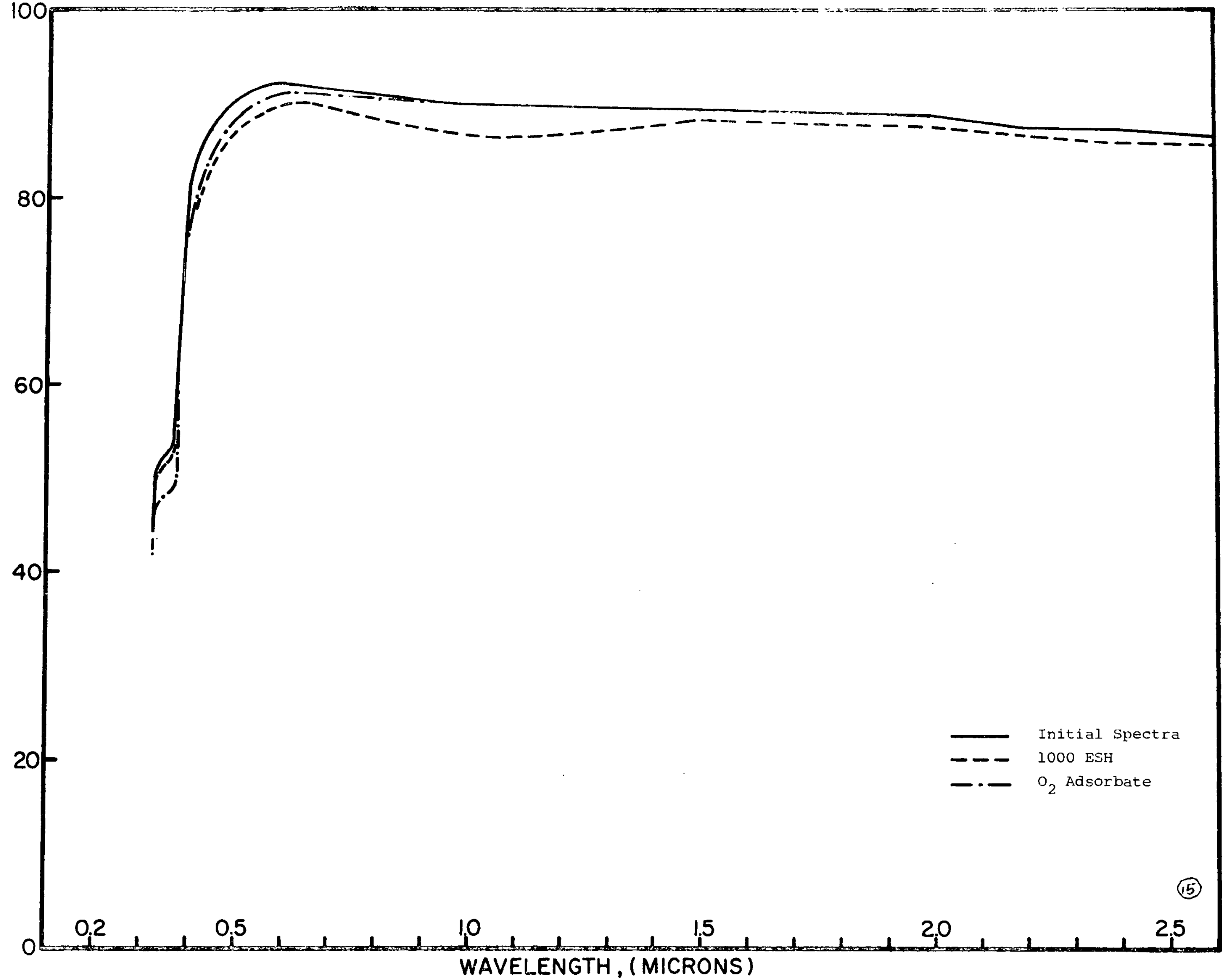

Figure 92 EFFECT OF UV ON B-547 Zn_2TiO_4

that, in the case of zinc oxide, the stability of the pigment in this region of the spectrum is greater than that of the potassium silicate.

The phosphate treatment (Figure 85) improved the reflectance in the ultraviolet by essentially removing the shoulder at ~362-nm that has been attributed to unreacted zinc oxide (Ref. 136, 137). The damage exhibited by the phosphated powder is greater than that sustained by an earlier specimen and cannot be explained except that it is conceivable that, in the present case, not all unreacted NaH_2PO_4 was removed from the surface by washing after phosphating.

Treatment with ferro/ferricyanide (Figure 86) also has a deleterious effect on the spectral stability of zinc orthotitanate powders irradiated by ultraviolet.

Of the reactive encapsulants Li_2SiF_6, K_2SiF_6, K_2SnF_6 and $K_4Si_4W_{12}O_{40}$, all three fluorinated materials substantially reduced the infrared damage in the 700- to 2400-nm wavelength region that is characteristic of untreated zinc orthotitanate (without subsequent heat treatment of the reacted powder). Of these, the fluorostannate treatment was the most effective in preventing infrared damage in the non-heat treated powder; however, the fluorostannate treatment had a highly deleterious effect on the stability of zinc orthotitanate in the 350- to 600-nm wavelength region and, in this respect, was more deleterious than the potassium silicotungstate treatment (see Figure 91).

Heat treatment of all four chemically-treated zinc orthotitanate powders resulted in pigment having greater stability than the untreated control (B-229) in the infrared region 700- to 2400-nm wavelength. The lithium and potassium silicofluoride-(hexafluorosilicate) treated pigment that was heat treated for 7 hr at 500°C exhibited improved stability in the near-ultraviolet and visible wavelength regions, as well.

Although the heat-treated product prepared from the potassium silicotungstate-treated powder (B-547) was nearly as stable as the the silicofluoride-treated products, this chemical treatment was not effective in removing the 362-nm shoulder absorption that is present in the Zn_2TiO_4 control--an absorption band that contributes significantly to the solar absorptance of coatings prepared from zinc orthotitanate. Treatment with the three fluorinated salts resulted in considerably decreased, if not completely eliminated, absorption at 362-nm wavelength (B-458, Figure 90); this change is presumably due to the extraction of unreacted zinc oxide during the reflux operation.

The poorer reflectance of the heat-treated powders (Figures 88, 90, 91) is attributed primarily to the lesser thicknesses of the treated oxide when "wet sprayed." The heat treated, encapsulated powder, perhaps by virtue of the decreased surface free energy, is more difficult to build-up by the "wet spray" method than the nonheat-treated, encapsulated powders.

8.4.4.2 Plasma-Heat Treated Pigments

The data for a series of plasma-annealed zinc orthotitanate powders that were previously silicated are presented in Table 41 and Figures 93 through 95. The data for the B-229 control pigment is included from Table 39 as a reference.

The subtleties in the spectra of plasma-annealed zinc orthotitanate have been discussed previously (Ref. 2 and para. 8.3.3.1). The infrared damage sustained by the specimen annealed at ΔT of 1670°C is attributed to conduction electrons as a result of free zinc oxide that is presumably condensed on the surface of the aerosol powder in the plasma.

Examination of the data and Figures 78 through 81 clearly shows that a ΔT of 1670°C is essentially optimum for Zn_2TiO_4. This temperature is clearly shown to be superior for the silicated/ phosphated zinc orthotitanate (Batch B-412) annealed at 1670°C (Figures 93 through 95). The data for the 1670°C product represents

Table 41

EFFECT OF ULTRAVIOLET IRRADIATION ON PLASMA-TREATED Zn_2TiO_4 (CONTROL AND SILICATED)

IITRI Pigment	Figure No.	Plasma Temp. ΔT (°C)	Exposure (ESH)	Reflectance Decrease, ΔR_λ (λ = nm), %					Solar Absorptance	
				325	425	700	950	2400	α_s	$\Delta\alpha_s$
B-229	81	1670	2500	-4.0	0	0	0	10.0	0.145	0.010
B-412*	93	1450	2500	1.4	3.3	0.3	0	0	0.140	0.003
B-412*	94	1890	2500	-2.7	0	0	0	2.5	0.150	0.008
B-412*	95	1670	2500	0	0	0	0	0.6	0.135	0

*Silicate and phosphated B-229

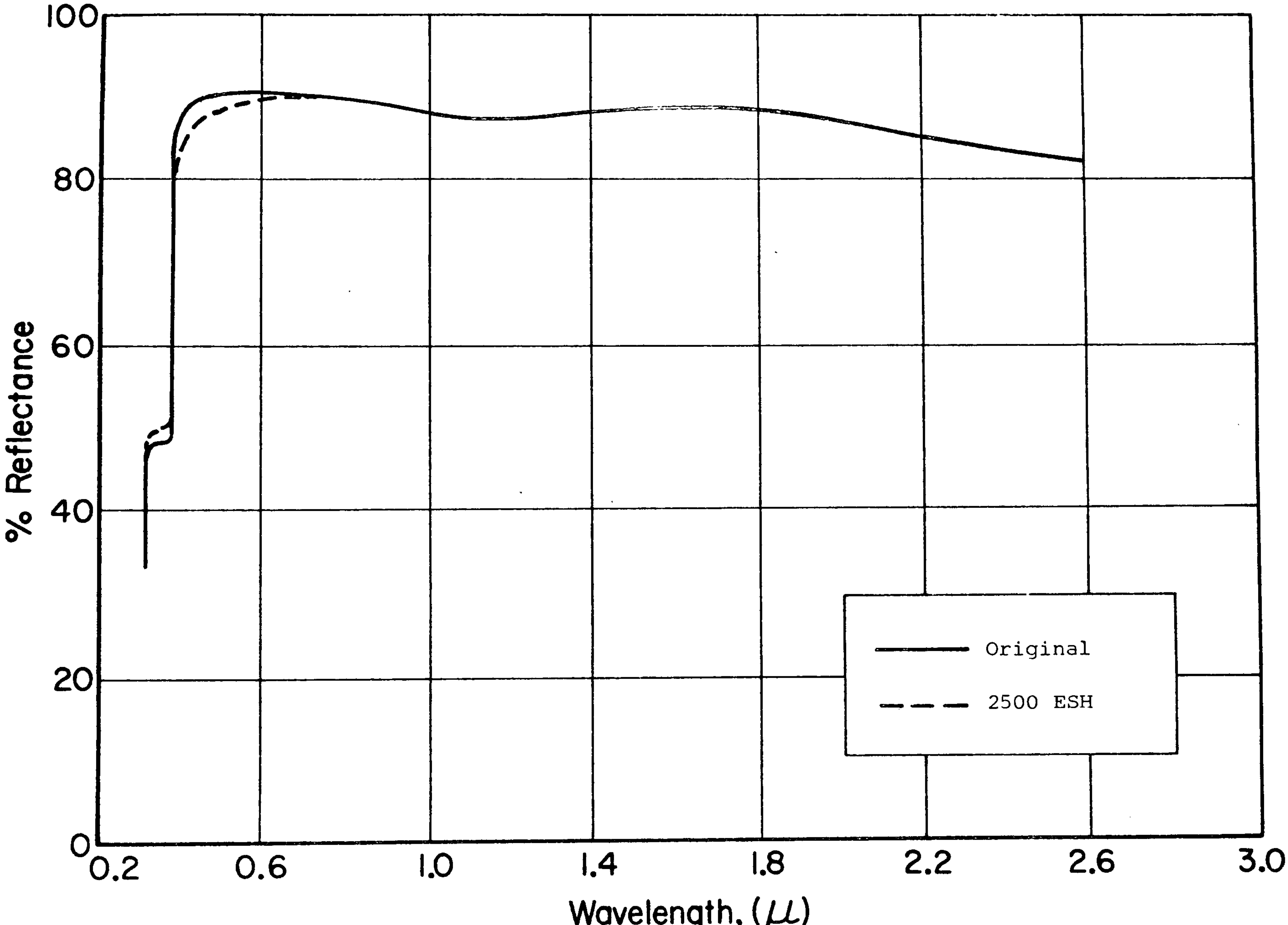

Figure 93 EFFECT OF UV ON 1450°C ΔT SILICATED Zn_2TiO_4

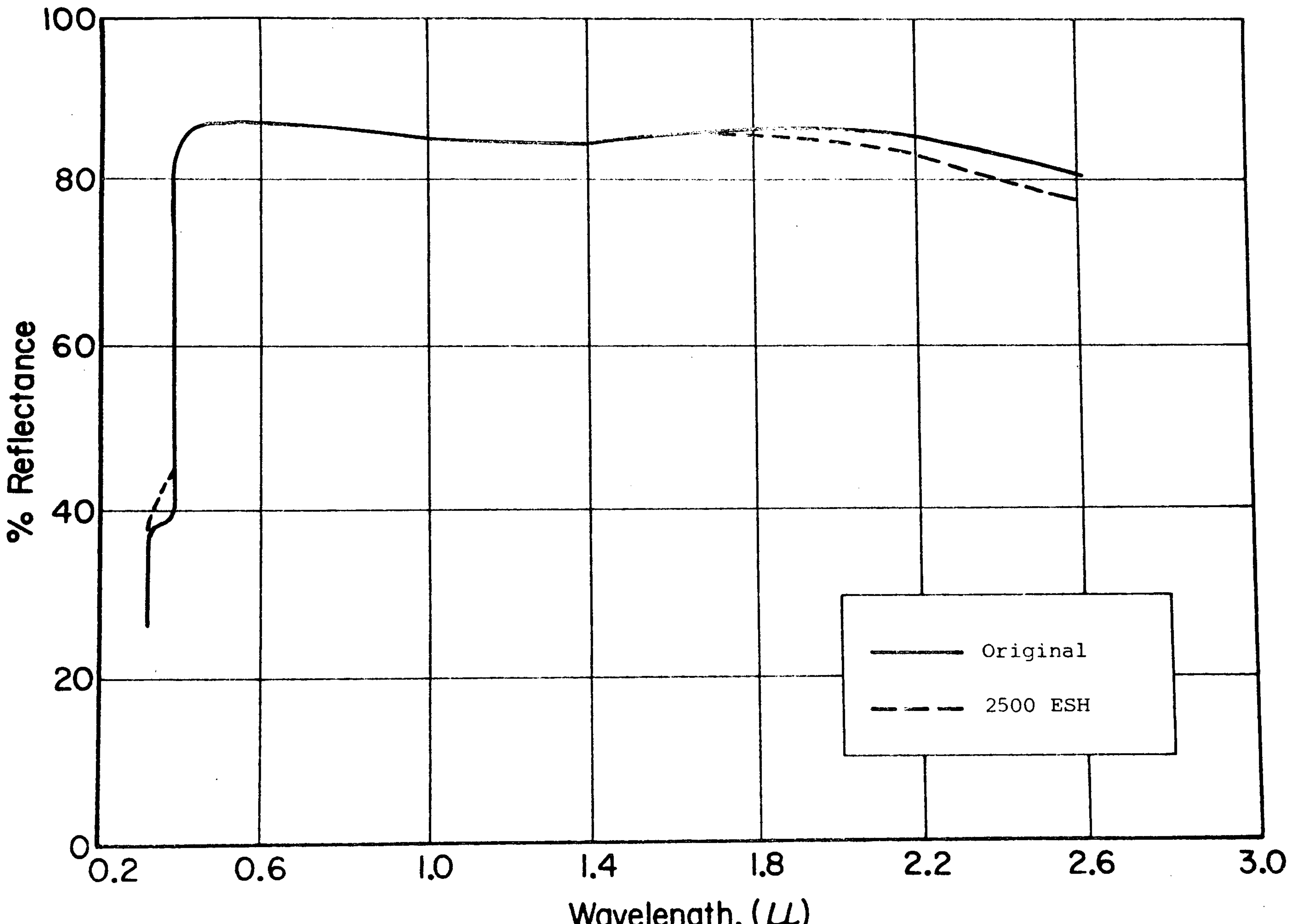

Figure 94 EFFECT OF UV ON 1890°C AT SILICATED Zn_2TiO_4

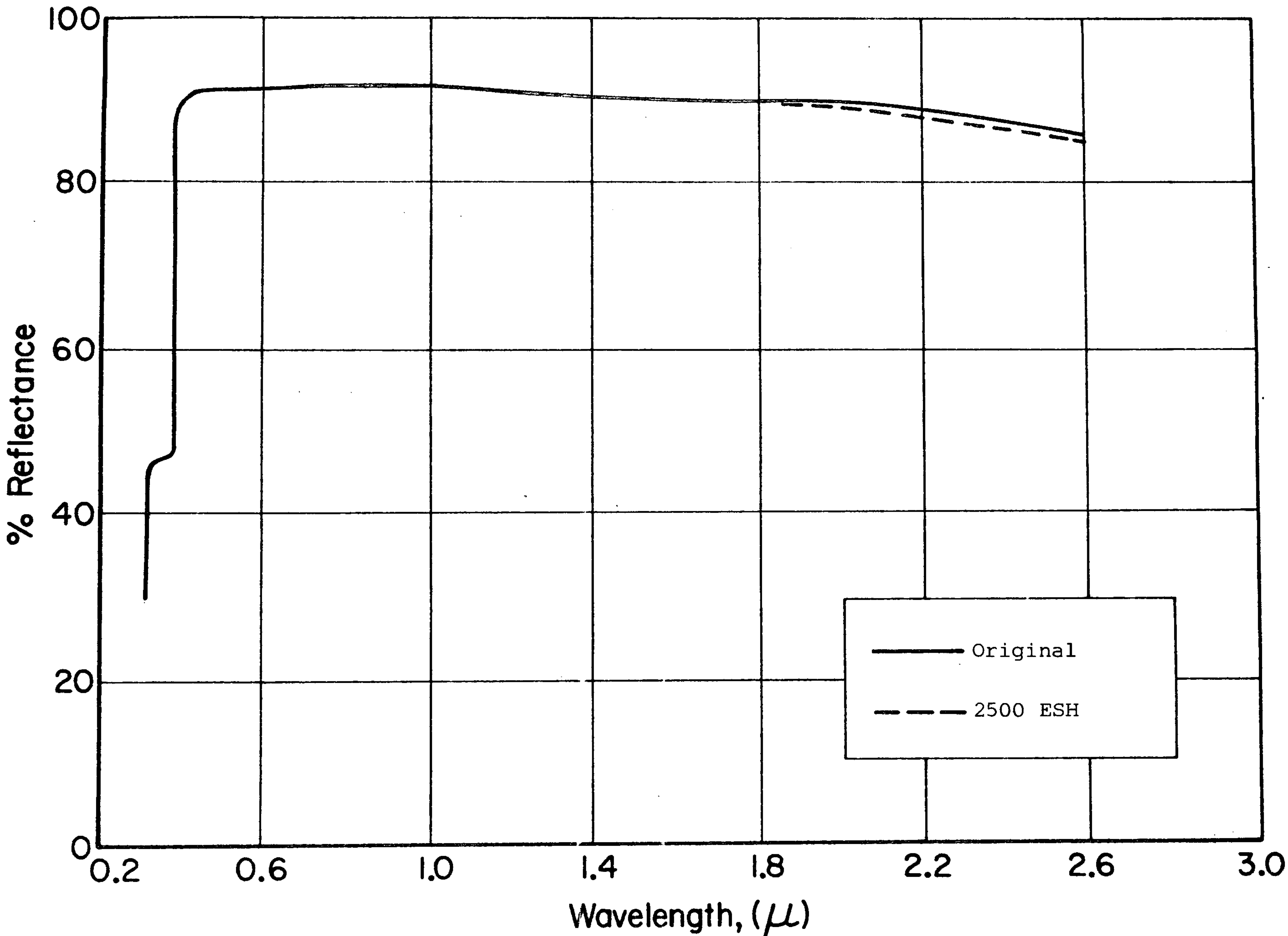

Figure 95 EFFECT OF UV ON 1670°C AT SILICATED Zn_2TiO_4

the greatest ultraviolet stability we have ever observed in a pure pigment powder; this is especially significant when we consider that it was irradiated for 2500 ESH of ultraviolet radiation in vacuum.

8.4.4.3 Silicate Paints

Examination of Table 42 and Figures 96 through 99 confirm the the results obtained previously--namely that potassium silicate paints pigmented with zinc orthotitanate are, even in the absence of reactive encapsulation, quite stable to ultraviolet irradiation in vacuum.

Both specimens B-421 and B-563 possess excellent solar absorptances by virtue of the extraction of the zinc oxide-related shoulder in Zn_2TiO_4 at 368 nm by the acid phosphate and potassium hexafluorosilicate. Although the paint based on ferro/ferricyanide-treated pigment exhibited stability that was superior to the control paint (B-419), its higher solar absorptance of 0.15 is characteristic of iron cyanide-treated pigments.

The excellent stability exhibited by the silicate paint prepared from phosphated pigment should be noted (Batch B-421, Figure 97). In this case, unlike the phosphated-pigment irradiated as a powder, the phosphate treatment preceeded pigmentation in the silicate vehicle and neutralization of any excess acid phosphate was assured by the highly alkaline silicate solution. (A similar formulation has been furnished the British RAE at Farnborough, England for a flight experiment to be flown on the Black Arrow* and to NASA-Goddard Space Flight Center for a flight experiment to be flown on OSO 8**.)

The potassium silicate paint B-563 based on the heat-treated, potassium hexafluorosilicate-treated Zn_2TiO_4, is equally stable to Z93 and possesses the lowest solar absorptance of any of the more stable coatings investigated to date (Figure 99).

---

*Mr. J. Porter (RAE)
**Mr. J. Triolo (NASA-GSFC)

Table 42

EFFECT OF ULTRAVIOLET IRRADIATION ON Zn_2TiO_4-POTASSIUM SILICATE PAINTS

Batch No.	Figure No.	Pigment Treatment: Chemical	Pigment Treatment: Heat Hr	Pigment Treatment: Heat °C	Exposure (ESH)	362	425	700	925	2400	Solar Absorptance α_s	Solar Absorptance $\Delta\alpha_s$
B-419	96	PS7	--	---	2000	4.0	7.0	1.0	1.0	-1.0	0.136	0.020
B-421	97	$HPO_4^{=}$	--	---	2000	7.0	5.5	0.2	-0.4	-2.2	0.122	0.010
B-424	98	Fe-CN	--	---	2000	4.2	5.0	1.8	1.0	-2.2	0.154	0.011
B-563	99	K_2SiF_6	7	500	1200	2.2	2.8	0	0	0.5	0.120	0.002

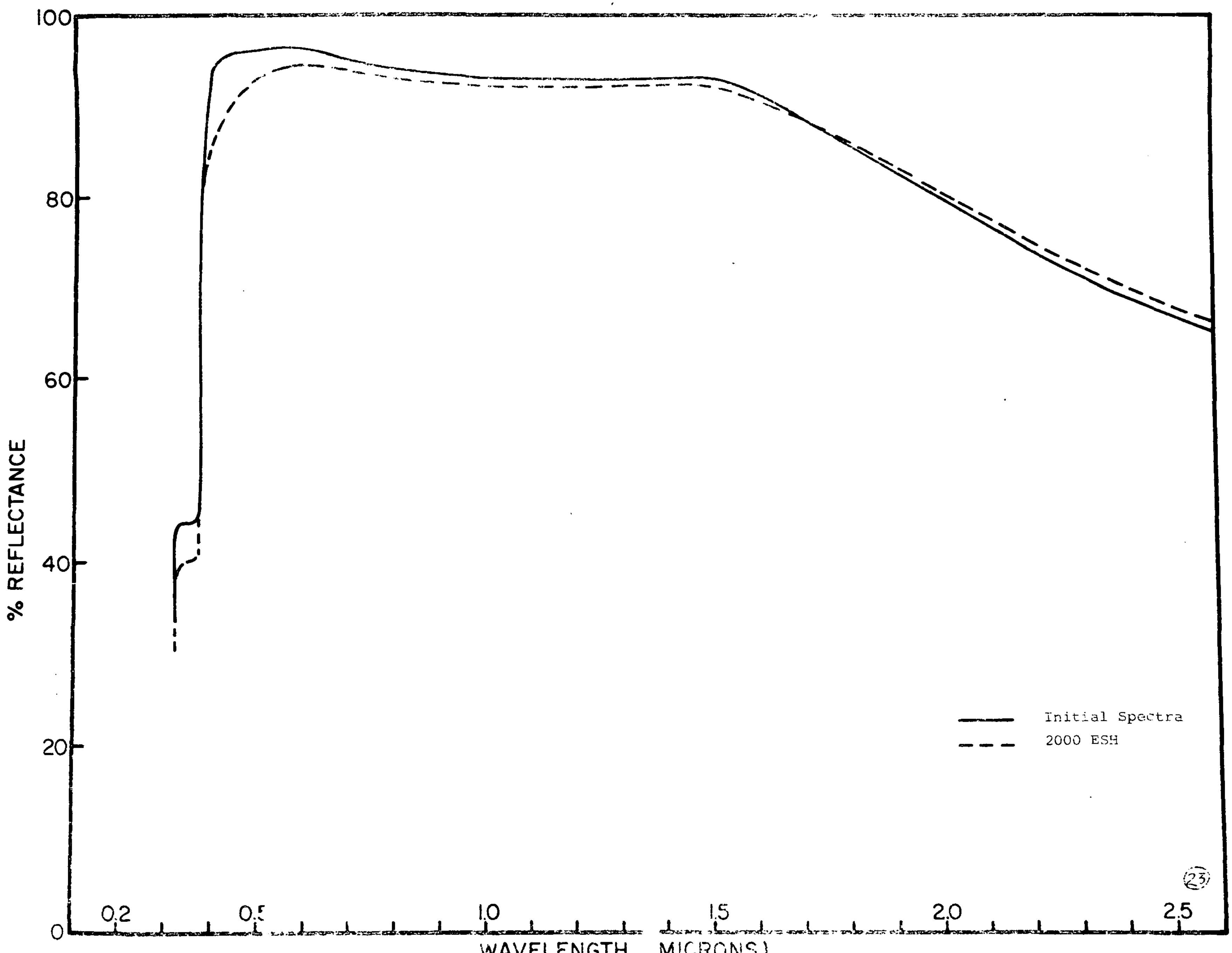

Figure 96 EFFECT OF UV ON B-419 SILICATE PAINT

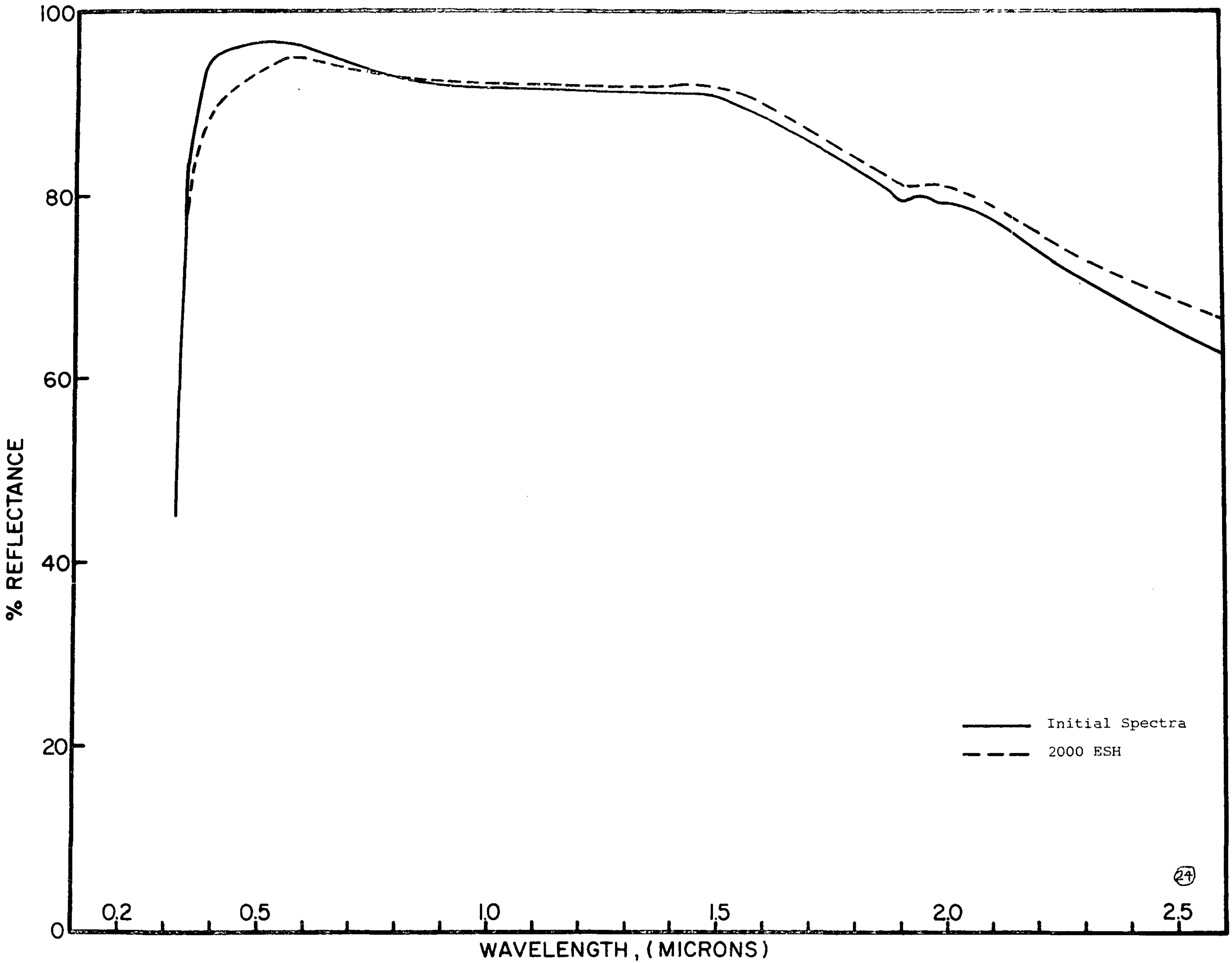

Figure 97 EFFECT OF UV ON B-421 SILICATE PAINT

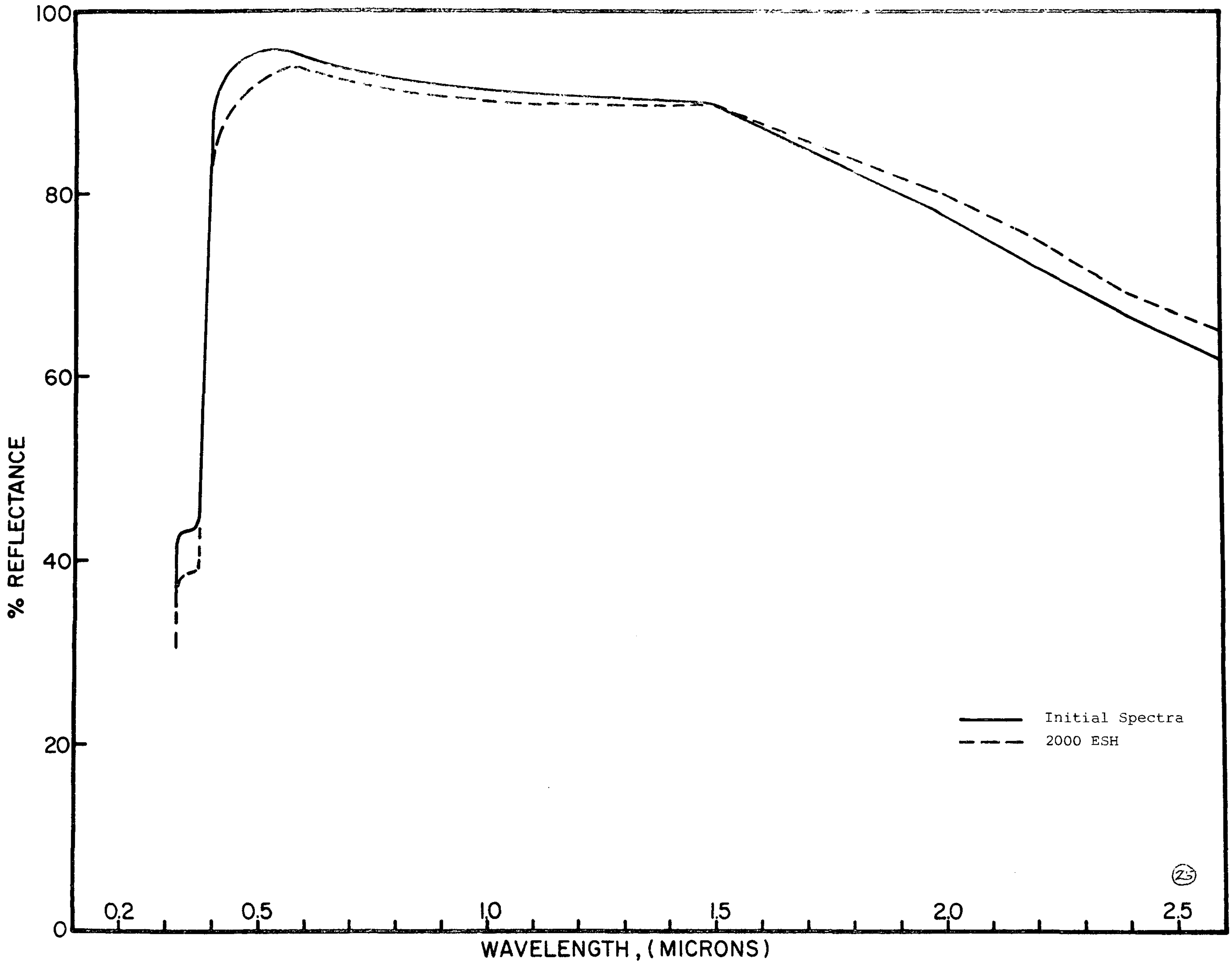

Figure 98 EFFECT OF UV ON B-424 SILICATE PAINT

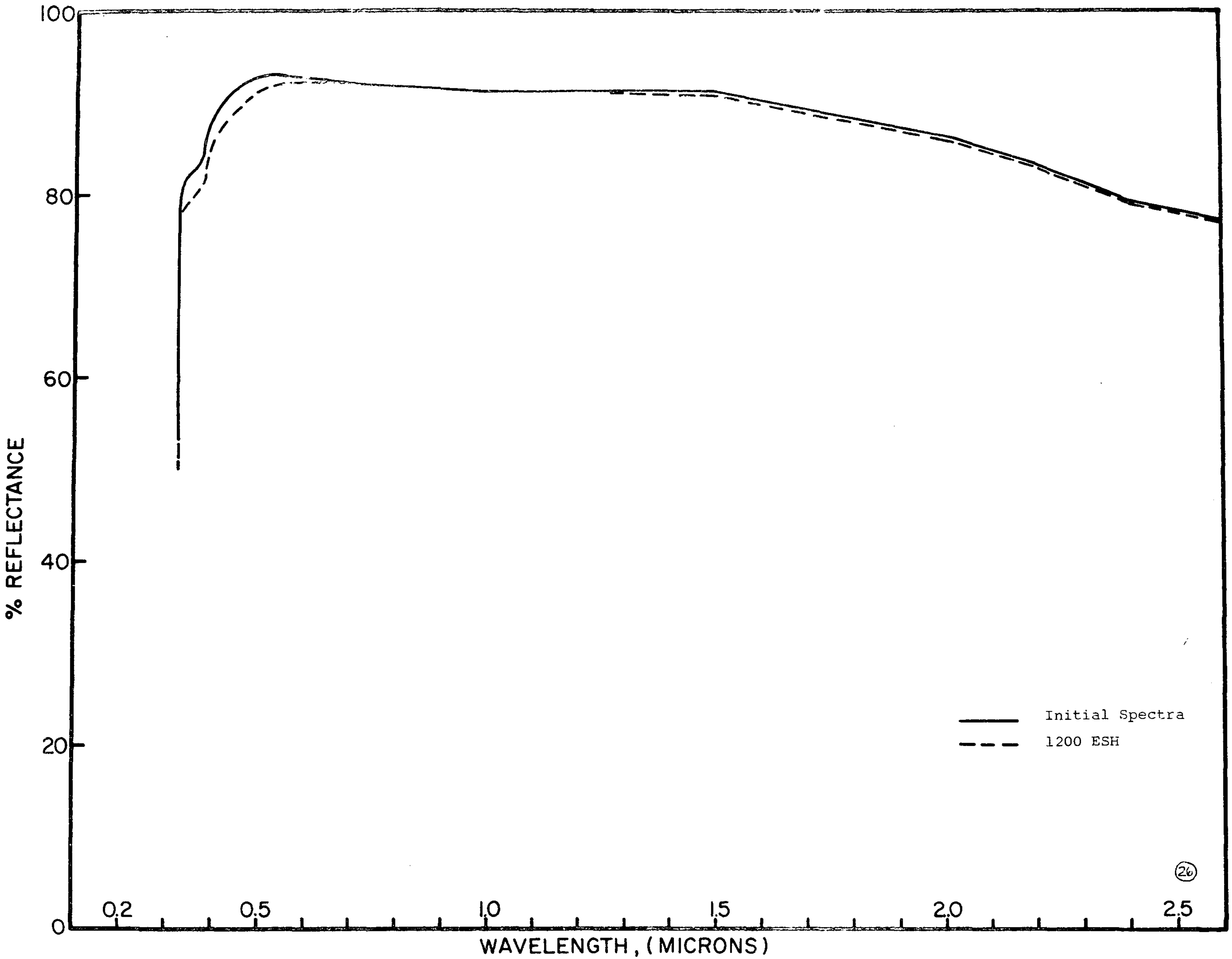

Figure 99 EFFECT OF UV ON B-563 SILICATE PAINT

It should be noted that removal of water during the irradiation of these paints accounts for the increased reflectance in the infrared region with its attendant contribution to the low $\Delta\alpha_s$'s observed (Figures 96 through 98).

8.4.4.4 Silicone Paints

The silicone paint prepared from untreated zinc orthotitanate was less stable in the near infrared (700- to 2600-nm wavelength) than the pigment powder itself (Figures 68 and 100). Indeed Owens-Illinois 650 resin paint prepared from silicated/phosphated pigment (B-427, Table 43) was even less stable than the control paint (Figures 100 and 101). Even the paint prepared from pigment that had been treated with potassium hexafluorosilicate exhibited only slight improvement over the control paint (Figure 102). These disappointing results confirmed earlier studies that an adverse synergistic effect exists between the Owens-Illinois 650 resin and the surface of zinc orthotitanate (see Discussion for an explanation).

The data in Table 43 shows clearly that this adverse synergism between zinc orthotitanate and Owens-Illinois 650 resin can be completely overcome by plasma heat treatment of a silicated/phosphated Zn_2TiO_4. Indeed, irradiation of this paint (Figure 104) resulted in an increase in solar absorptance of essentially zero after 2000 ESH of ultraviolet radiation. The interesting observation is that the character of the spectra in Figures 103 and 104, representing specimen numbers B-704 and B-705, respectively, is identical to the character of the spectra of the pigments alone (Table 41 and Figures 81 and 95, respectively).

The Zn_2TiO_4 paint (Batch B-574 prepared from RTV-602 silicone elastomer and B-229 control pigment) was very badly damaged in the near ultraviolet and visible spectrum in only 1000 ESH (Figure 105). Although this coating did not exhibit a noticeable "belly damage" at 950-nm wavelength, as did the Owens-Illinois 650-resin analog (Figure 100), the O_2-bleaching in the 950-wavelength region is indicative of the $Ti^{+3} \rightleftarrows Ti^{+4}$ transition.

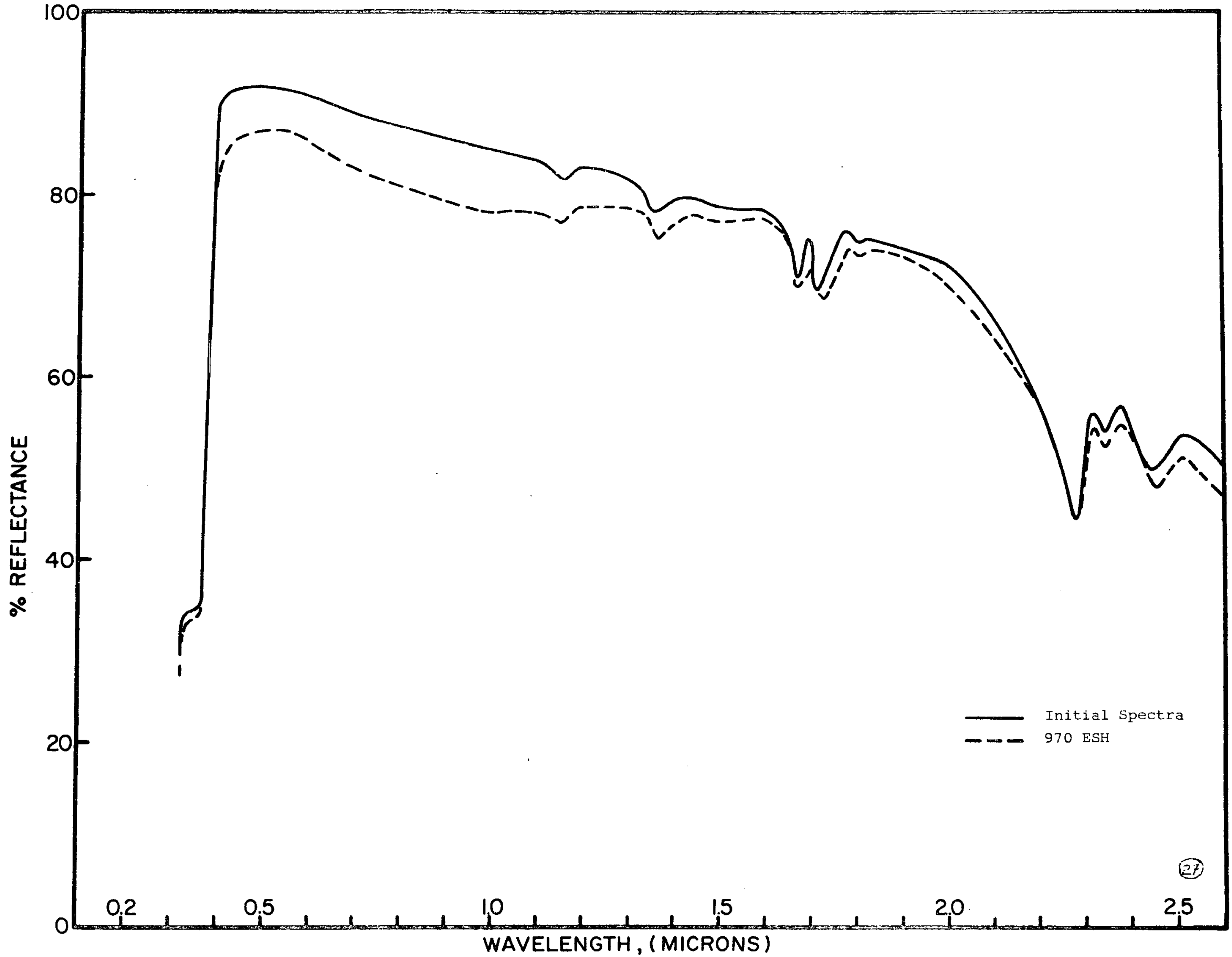

Figure 100 EFFECT OF UV ON B-415 SILICONE PAINT

Table 43

EFFECT OF ULTRAVIOLET IRRADIATION ON Zn_2TiO_4-SILICONE PAINTS

Batch No.	Fig. No.	Binder.	Pigment Batch	Pigment Treatment	Exposure (ESH)	Reflectance Decrease, ΔR_λ (λ = nm), % 362	425	700	950	2400	Solar Absorptance α_s	$\Delta\alpha_s$
B-415	100	OI-650	B-229	---	970	1.0	3.5	6.0	7.8	2.8	---	---
B-427	101	OI-650	B-412	$PS7/HPO_4^=$	970	2.2	5.2	6.0	6.9	3.9	---	---
B-555	102	OI-650	B-458	K_2SiF_6	1200	2.0	4.5	4.5	5.7	3.2	0.212	0.041
B-704*	103	OI-650	B-229	---	2000	-7.5	-0.5	1.2	1.0	3.0	0.250	0.012
B-705*	104	OI-650	B-412	$PS7/HPO_4^=$	2000	-1.0	0	0	0	2.4	0.241	0.002
B-574	105	RTV-602	B-229	---	1000	15.5	40.5	12.0	6.5	0.8	---	---

*Owens-Illinois 650 silicone resin paints prepared from Batch B-412 pigment plasma calcined for 1.1 sec at 1670°C.

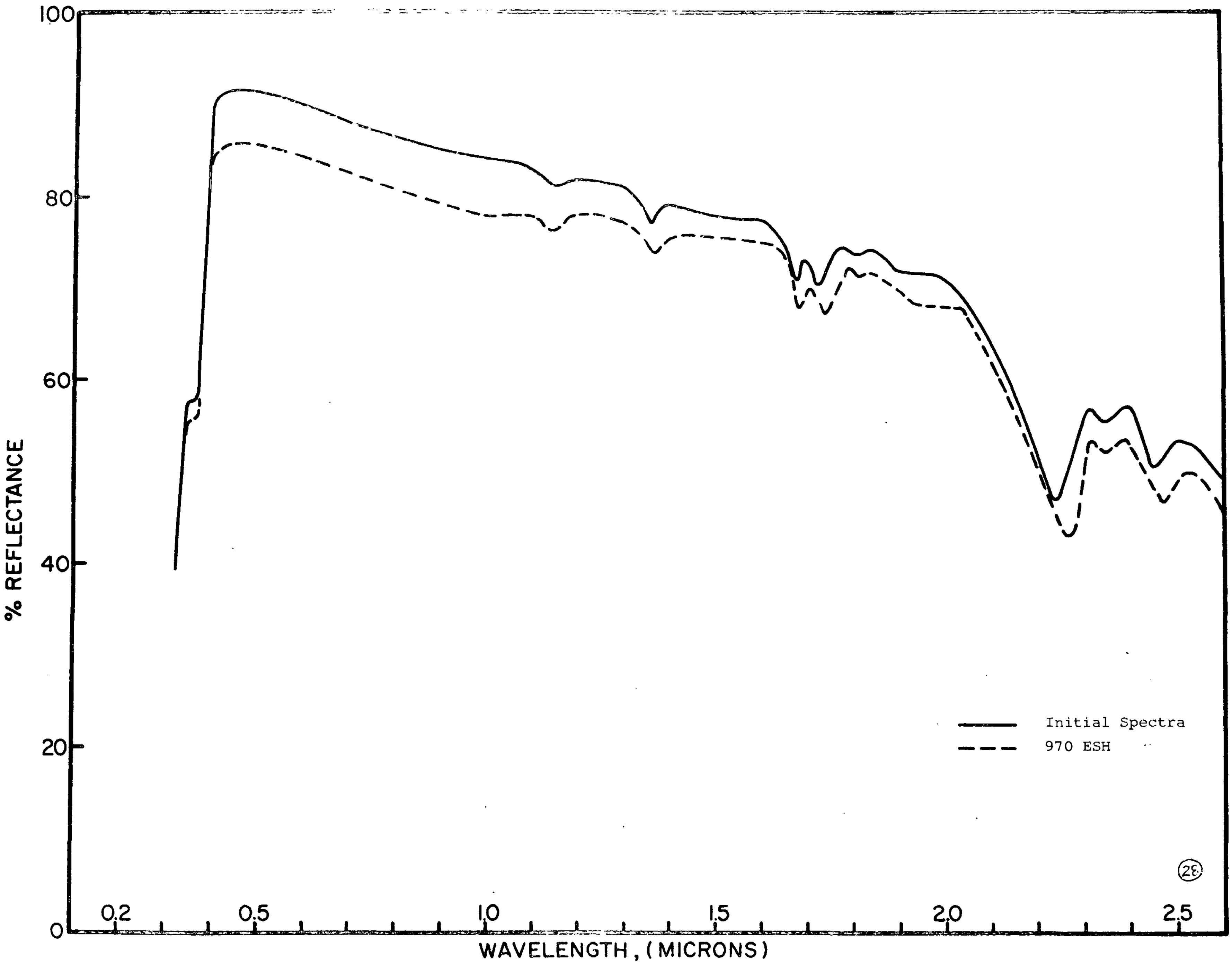

Figure 101 EFFECT OF UV ON B-427 SILICONE PAINT

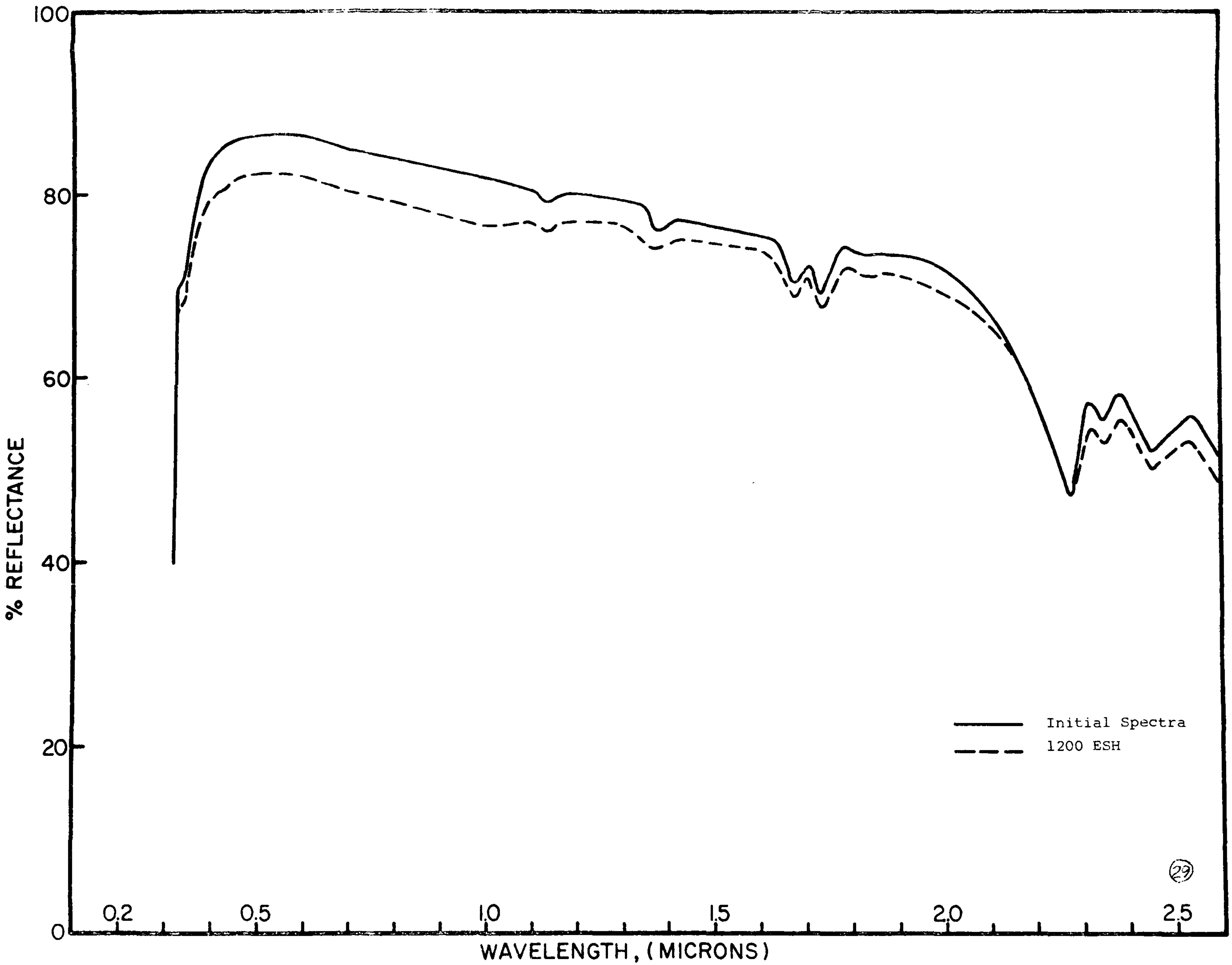

Figure 102 EFFECT OF UV ON B-555 SILICONE PAINT

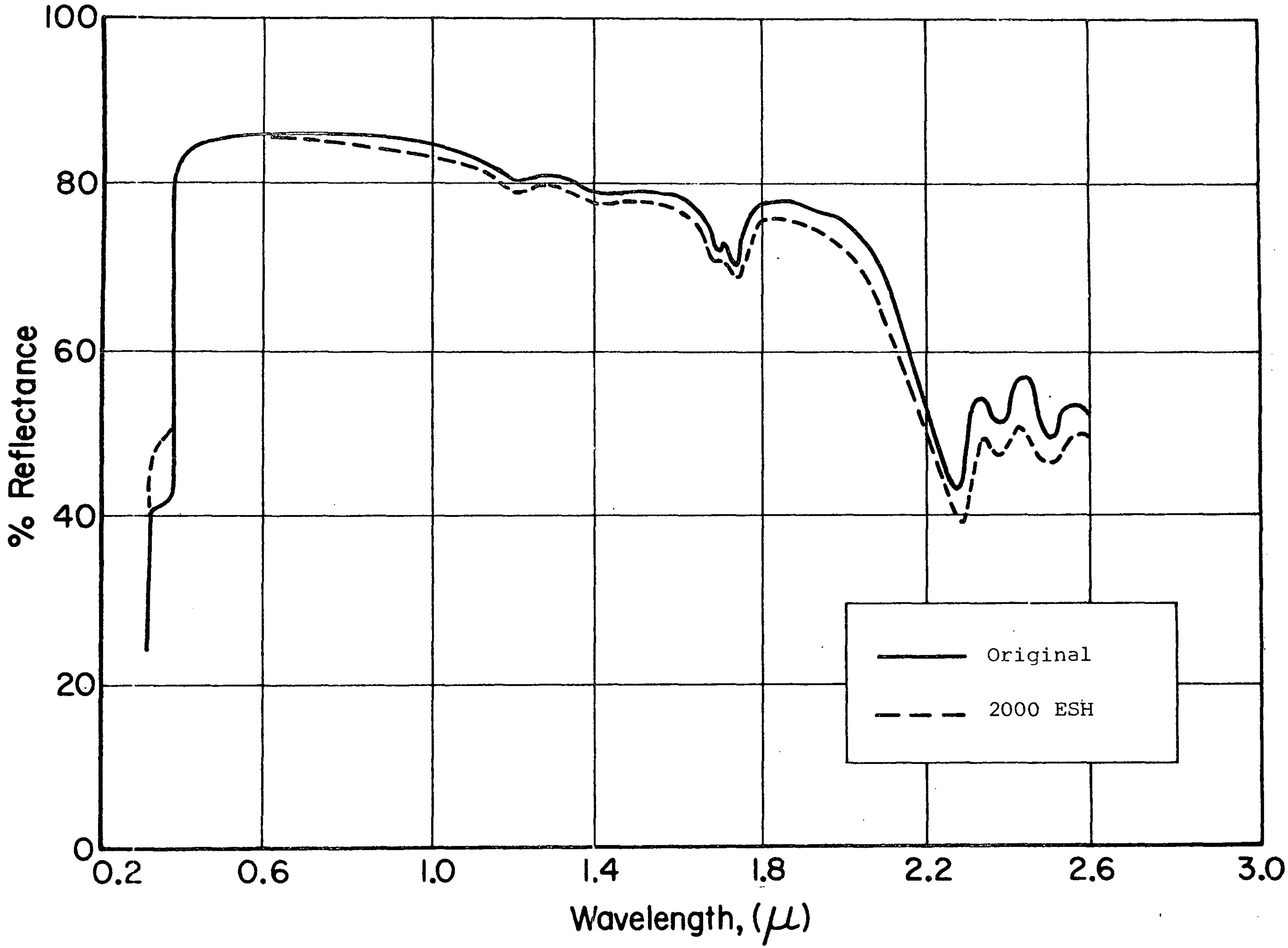

Figure 103 EFFECT OF UV ON B-704 SILICONE PAINT

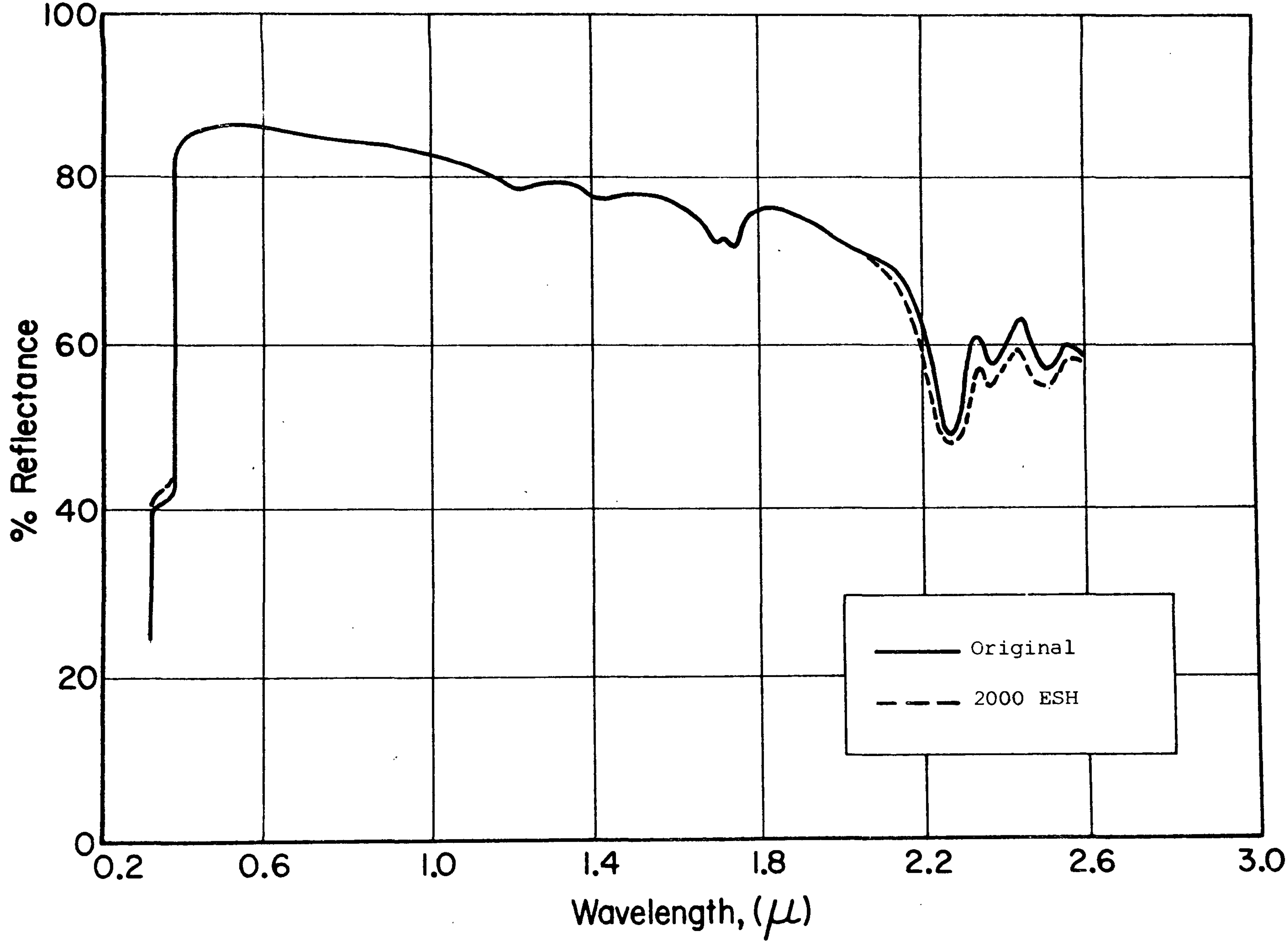

Figure 104 EFFECT OF UV ON B-705 SILICONE PAINT

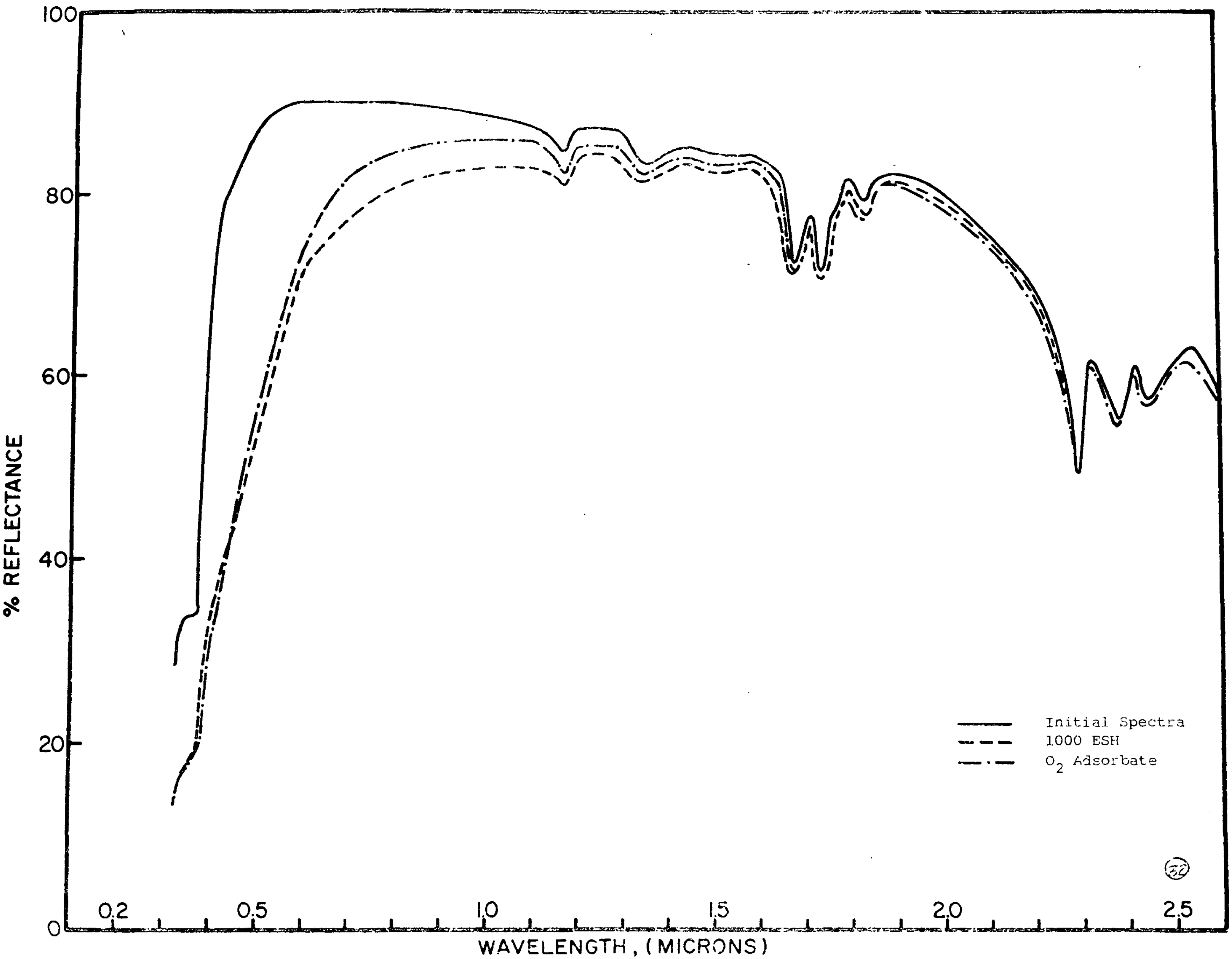

Figure 105 EFFECT OF UV ON B-474 SILICONE PAINT

The severe visible damage is attributed to two synergistic factors: The employment of the near-ultraviolet-scattering Zn_2TiO_4 pigment (compared to the absorber ZnO) in a binder that is less stable than Owens-Illinois 650 resin. (RTV-602 is less stable only by virtue of the requirement for amine curing. Owens-Illinois 650 resin heat cures by residual hydroxyl functionality.)

8.5 Electron Paramagnetic Resonance (EPR) Studies

8.5.1 Summary of Early Results

8.5.1.1 Zn_2TiO_4 Containing Excess TiO_2

In the ground state, zinc orthotitanate material (prepared with a slight excess of TiO_2 and extracted with acetic acid which partially removed the free, residual ZnO) exhibited no paramagnetic centers attributable to ZnO and little or no centers attributable to Ti^{+3} (Ref. 136). Material gamma-irradiated at 77°K exhibited an asymmetric center "x" with g_1 = 1.98 which we attributed to Ti^{+3} and a center "k" with mean g = 2.013 which we attributed to O_2^-. Ultraviolet-irradiation was performed under high vacuum (10^{-7} torr) in the apparatus pictured in Figure 106, at ambient temperatures utilizing uncolumnated light from a mercury AH-6 lamp as described previously (Ref. 141). The effect of ultraviolet irradiation is shown in Figures 107 and 108 indicating the photo-creation of the center "x". If the material was heated to 500°C in vacuum before ultraviolet irradiation, a slightly different resonance was observed (Figure 109). These materials had exhibited their peak near-infrared damage at 800-875 nm.

8.5.1.2 Plasma-Annealed Zn_2TiO_4 (excess TiO_2)

In contrast to the starting material, the nonirradiated higher plasma-annealed orthotitanates (designated ** for $\Delta T \sim 2900°C$; see para. 8.3.3) exhibited both extensive amounts of the center "x" (Ti^{+3}) and a center called "y" with a mean g = 1.960 which we attribute to centers found in ZnO. The g-values of the nonirradiated plasma-annealed materials are listed in Table 44 and the EPR spectra for one sample with low (*) and

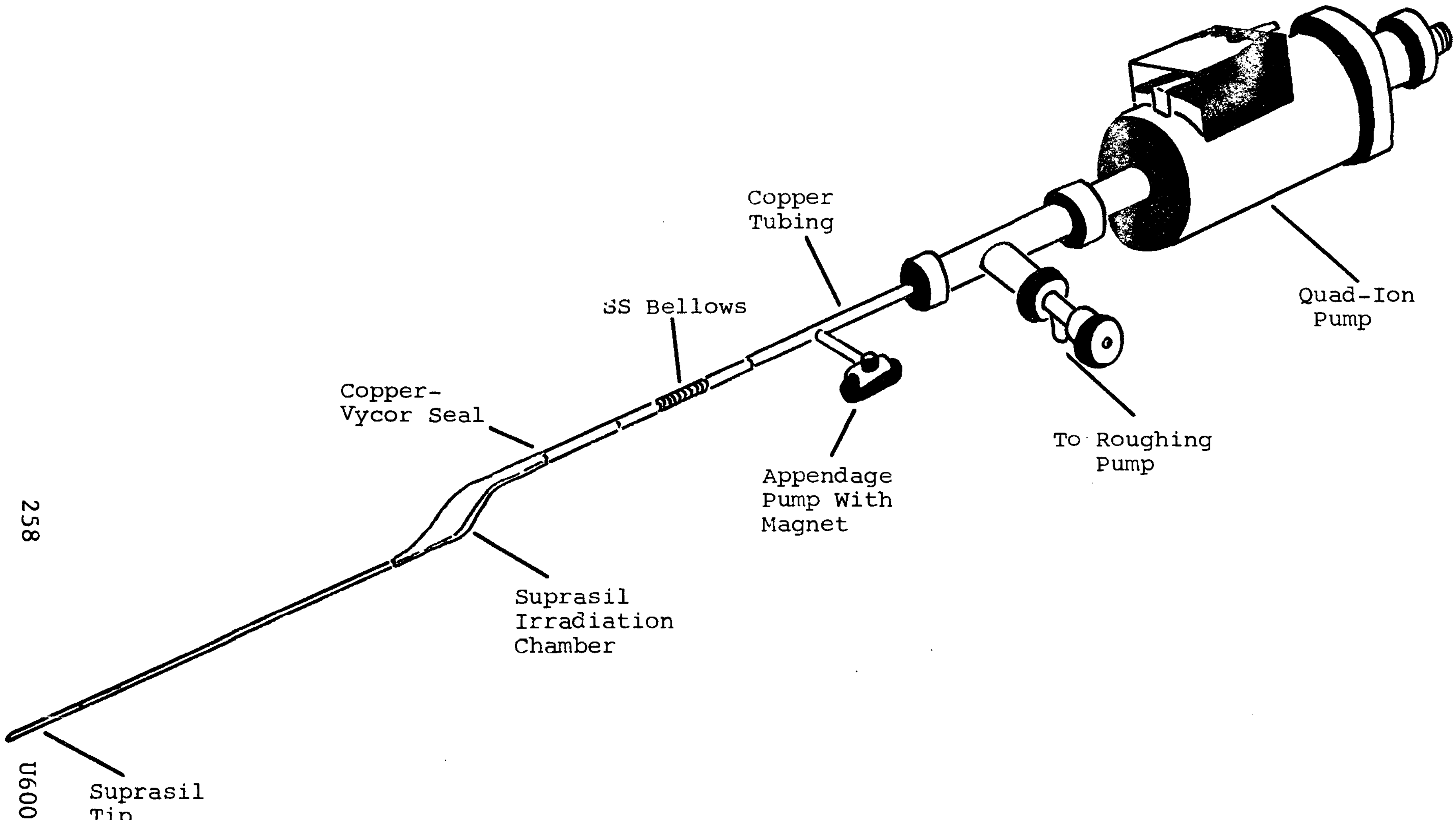

Figure 106 ULTRAVIOLET IRRADIATION APPARATUS (EPR)

U6002-97

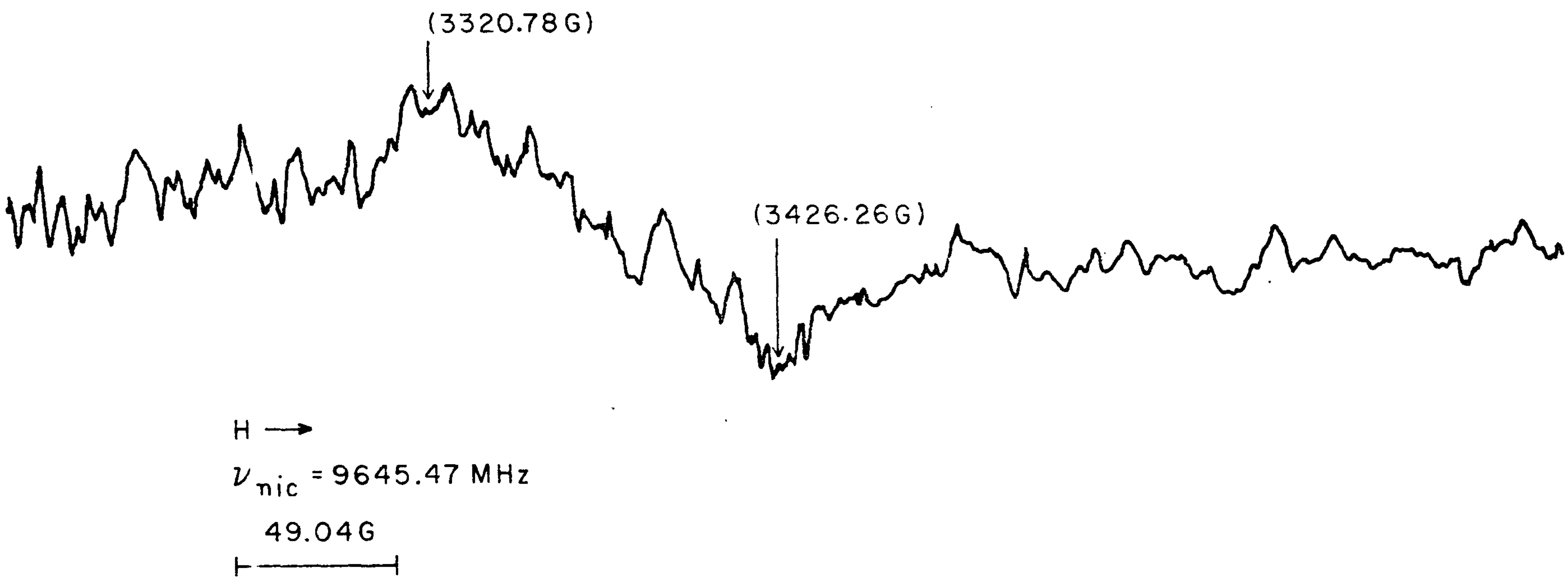

Figure 107 EPR AT ~77°K OF UNIRRADIATED ZINC ORTHOTITANATE, SAMPLE 3, MODULATION - 14.26 G

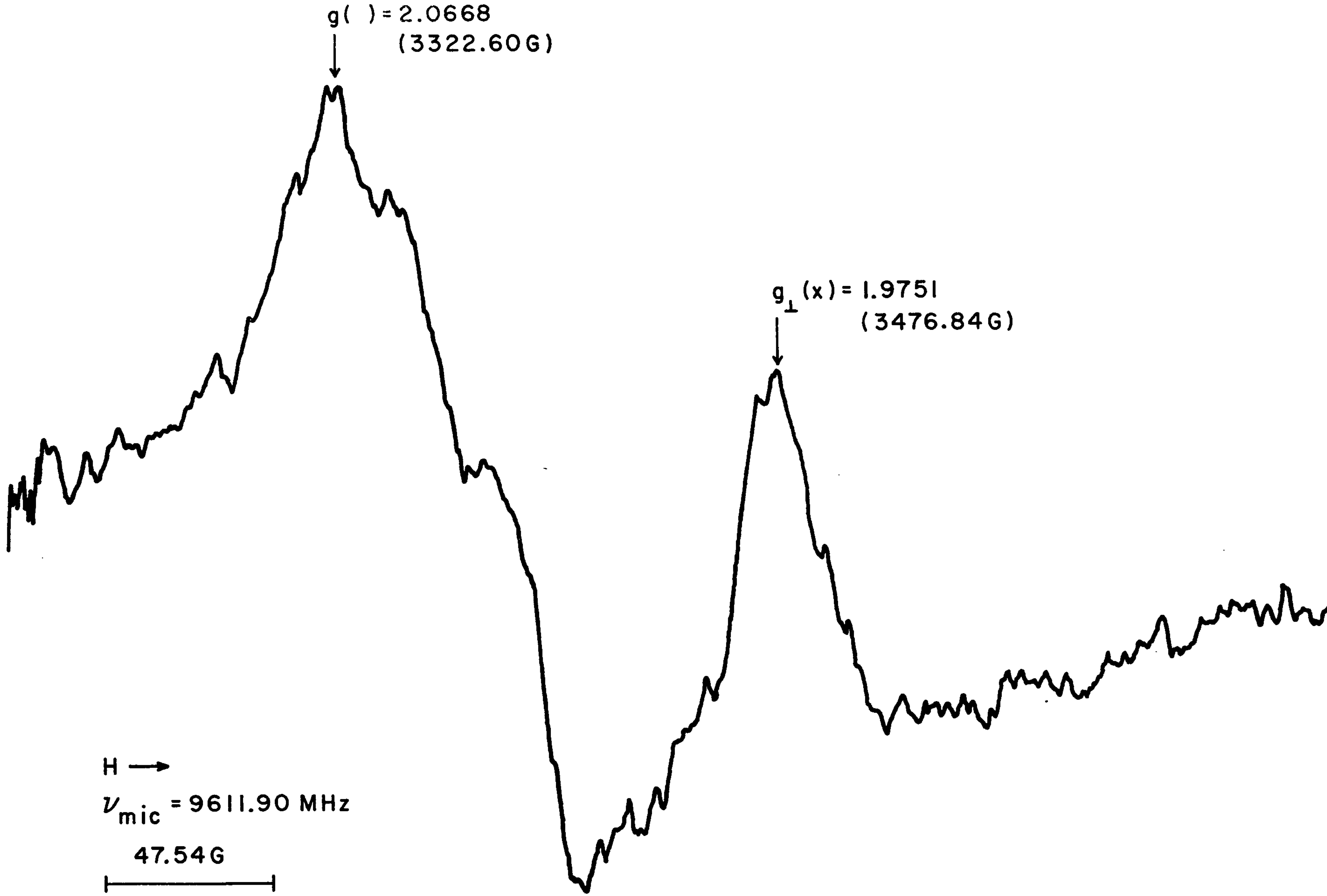

Figure 108 EPR AT ~77°K OF UV-IRRADIATED ZINC ORTHOTITANATE, SAMPLE 3, MODULATION - 14.26 G

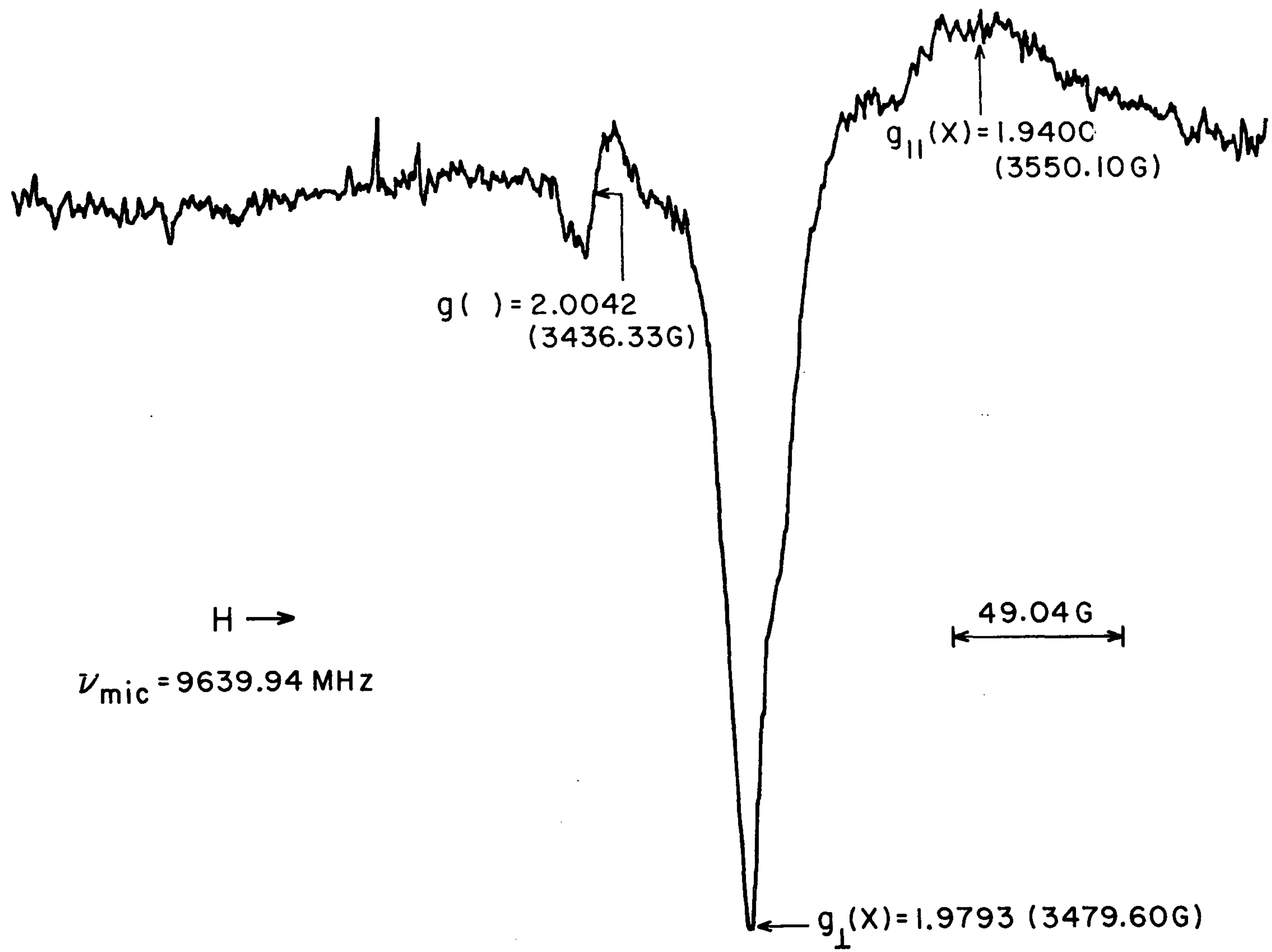

Figure 109 EPR AT ~77°K OF ZINC ORTHOTITANATE, SAMPLE 1, HEATED AT 500°C AT 10^{-7} TORR, ROOM TEMP. OPTICALLY IRRADIATED 23.5 HR. AT 6 SOLAR INTENSITIES, AFTER WARMING TO ROOM TEMPERATURE AND RECOOLING TO ~77°K, MODULATION - 4.78

Table 44

MAGNETIC RESONANCE IN UNIRRADIATED PLASMA ANNEALED ZINC ORTHOTITANATES (g-VALUES)

Resonance	Sample Number					
	3*	3**	4*	4**	6*	6**
g_1 =	--	1.9775	1.9799	1.9789	1.9794	1.9799
g =	--	1.9605	--	1.9601	--	1.9606

high (**) plasma treatment are shown in Figures 110 and 111. Material gamma-irradiated at 77°K also exhibited the centers x and and y and in addition the center k, all with essentially the same g-values as the TiO_2-excess produced, gamma-irradiated orthotitanates. High-vacuum ultraviolet-irradiation of the high temperature plasma-annealed material exhibited a slightly different EPR signal (Figure 112) than non-plasma treated or low-temperature plasma treated materials whose ultraviolet-EPR spectra were the same. There appears to be a systematic shift in the peak position of the near-infrared damage (as well as a broadening) from 800- to 875-nm wavelength for non-plasma treated orthotitanate, ~900-nm wavelength for the lower plasma treatment, to 960- to 1000-nm wavelength for the higher plasma treatment. The reflectance and EPR measurements indicate that two (or even three) kinds of Ti^{+3} may be created in different treatments and may account for the peak shift and broadening of the reflectance spectra.

8.5.1.3 Zn_2TiO_4 Containing Excess ZnO

The unirradiated orthotitanates produced with excess ZnO exhibit the ground-state EPR center y' with $g_1 = 1.9556$ and $g_{11} = 1.9569$, shown in Figure 113 (Ref. 137). The center is identified with ZnO but is not the center "y" observed in the high plasma-treated excess TiO_2-Zn_2TiO_4; no "x" was observed. Various chemical surface treatments of this material yielded the same center and the g-values are listed in Table 45. Material gamma-irradiated at 77°K resulted in the creation of "x" and "k" with essentially the same g-values as in other orthotitanates. Ultraviolet irradiation of these orthotitanates did not result in the creation of x but did produce a change in the low-field side of the center y' indicating that y' is in fact two centers. The spectra are shown in Figure 114.

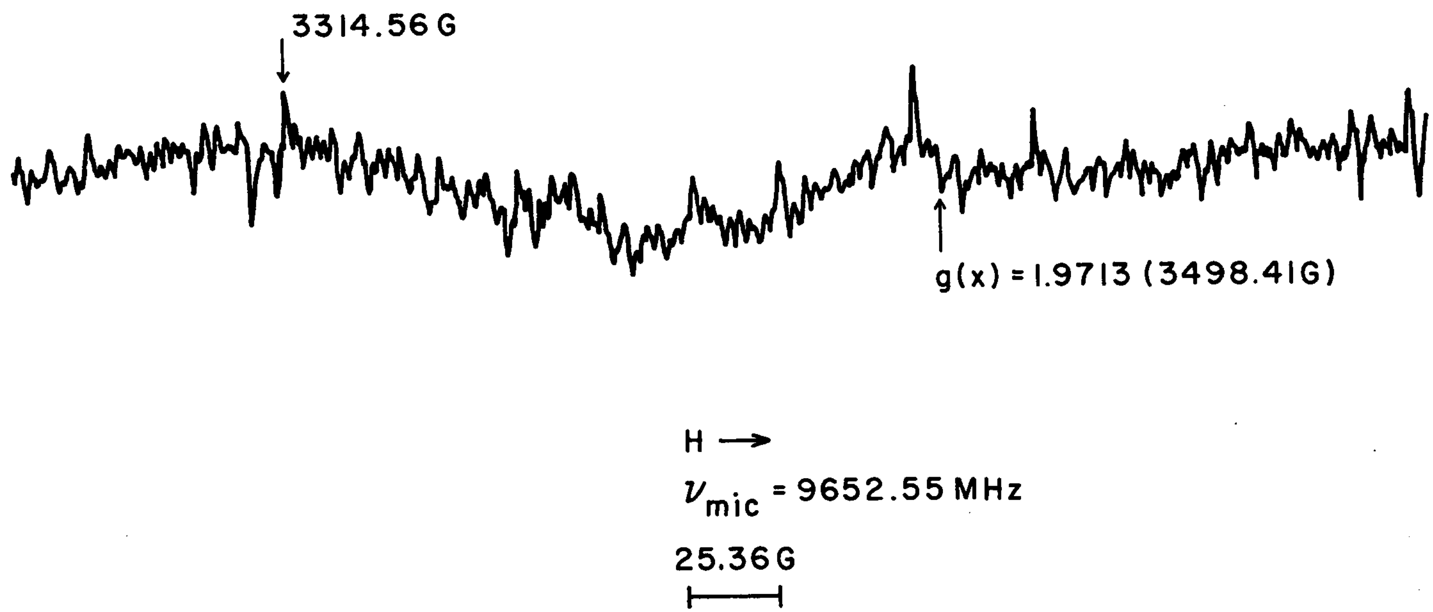

Figure 110 EPR AT ~77°K OF UNIRRADIATED ZINC ORTHOTITANATE, SAMPLE 4* (LOW PLASMA ANNEALED), MODULATION - 4.78 G

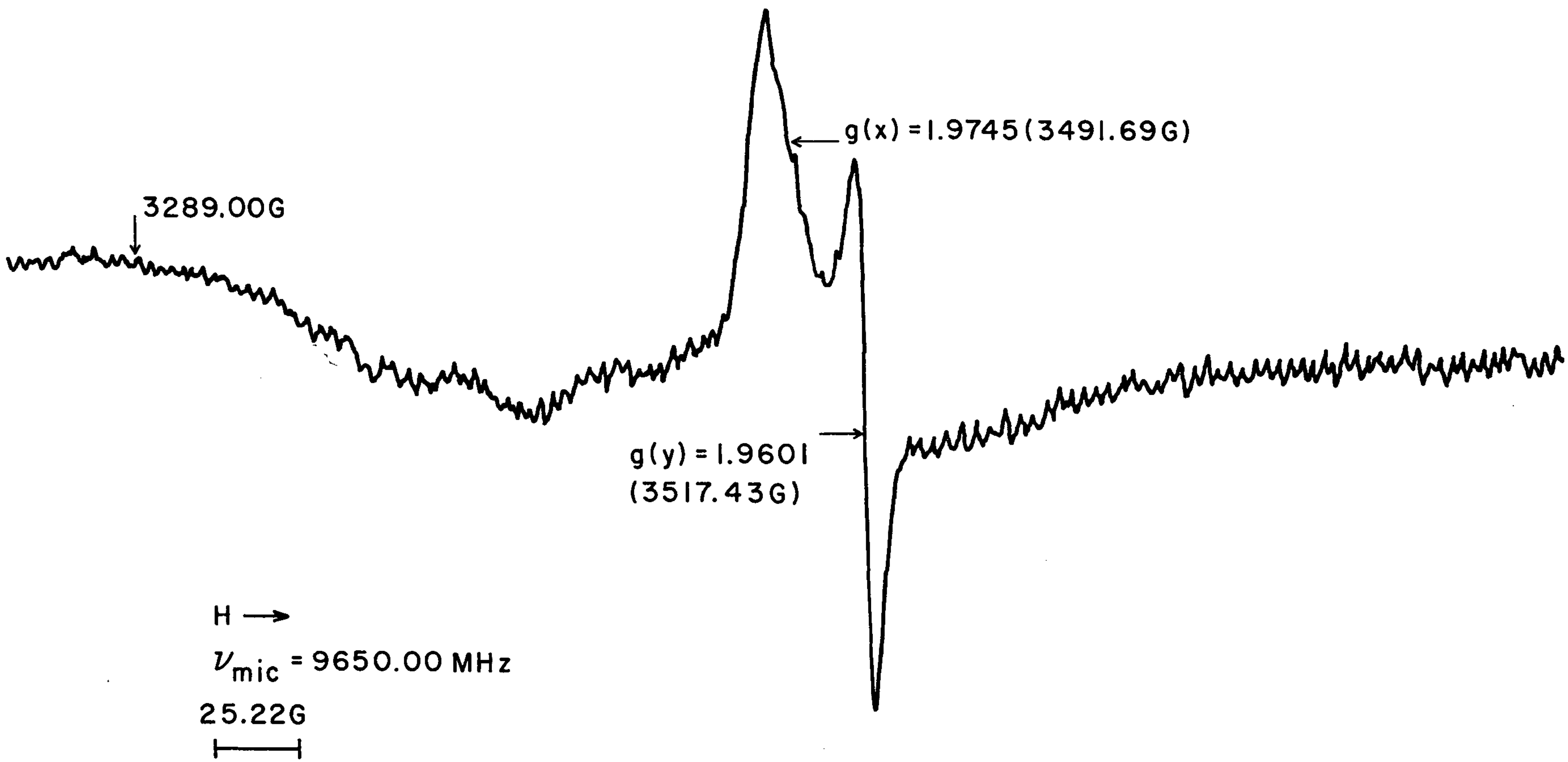

Figure 111 EPR AT ~77°K OF UNIRRADIATED ZINC ORTHOTITANATE, SAMPLE 4**
(HIGH PLASMA ANNEALED), MODULATION - 4.78 G

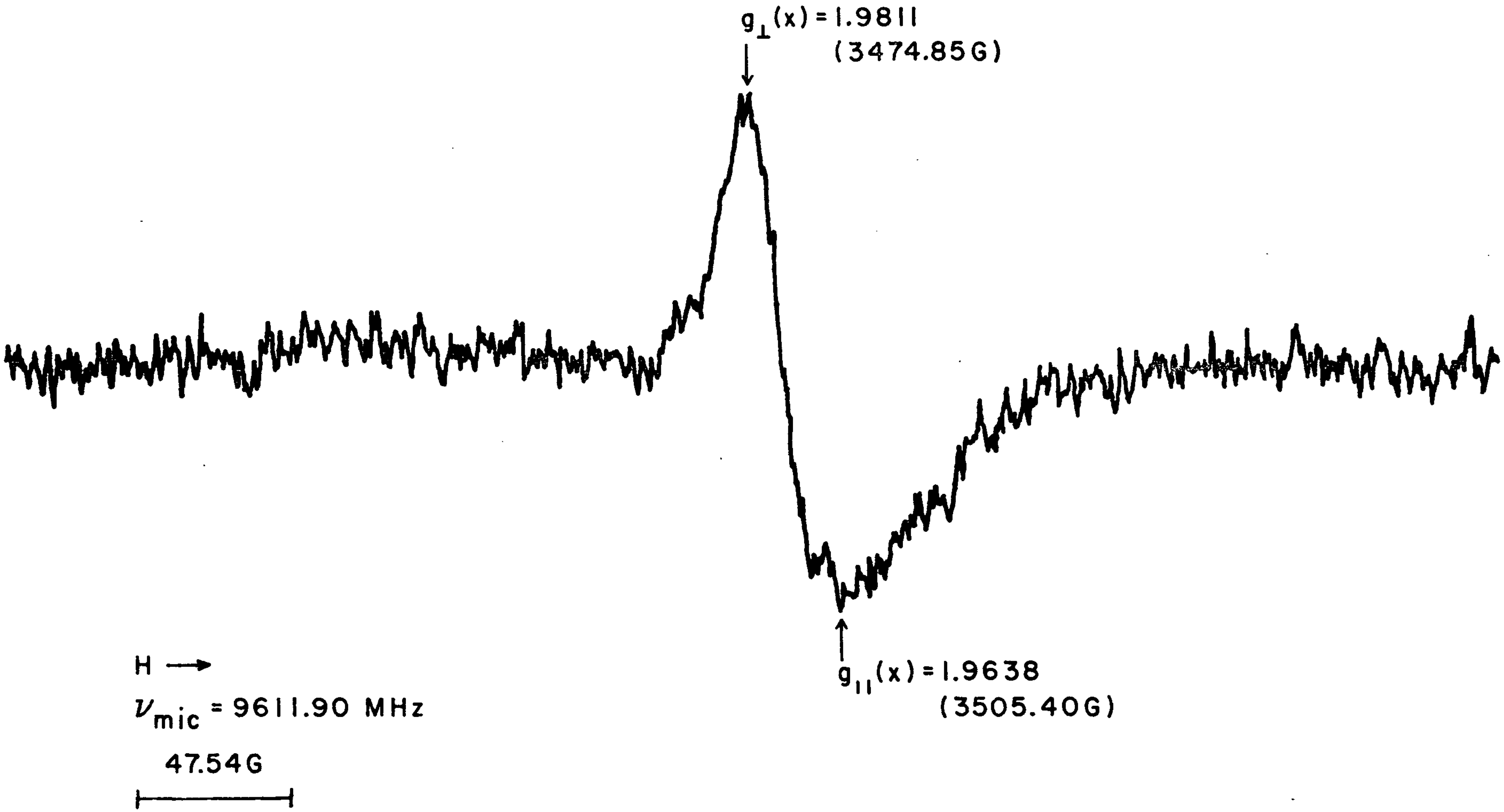

Figure 112 EPR AT ~77°K OF UV-IRRADIATED ZINC ORTHOTITANATE, SAMPLE 3** (HIGH PLASMA ANNEALED), MODULATION - 14.26 G

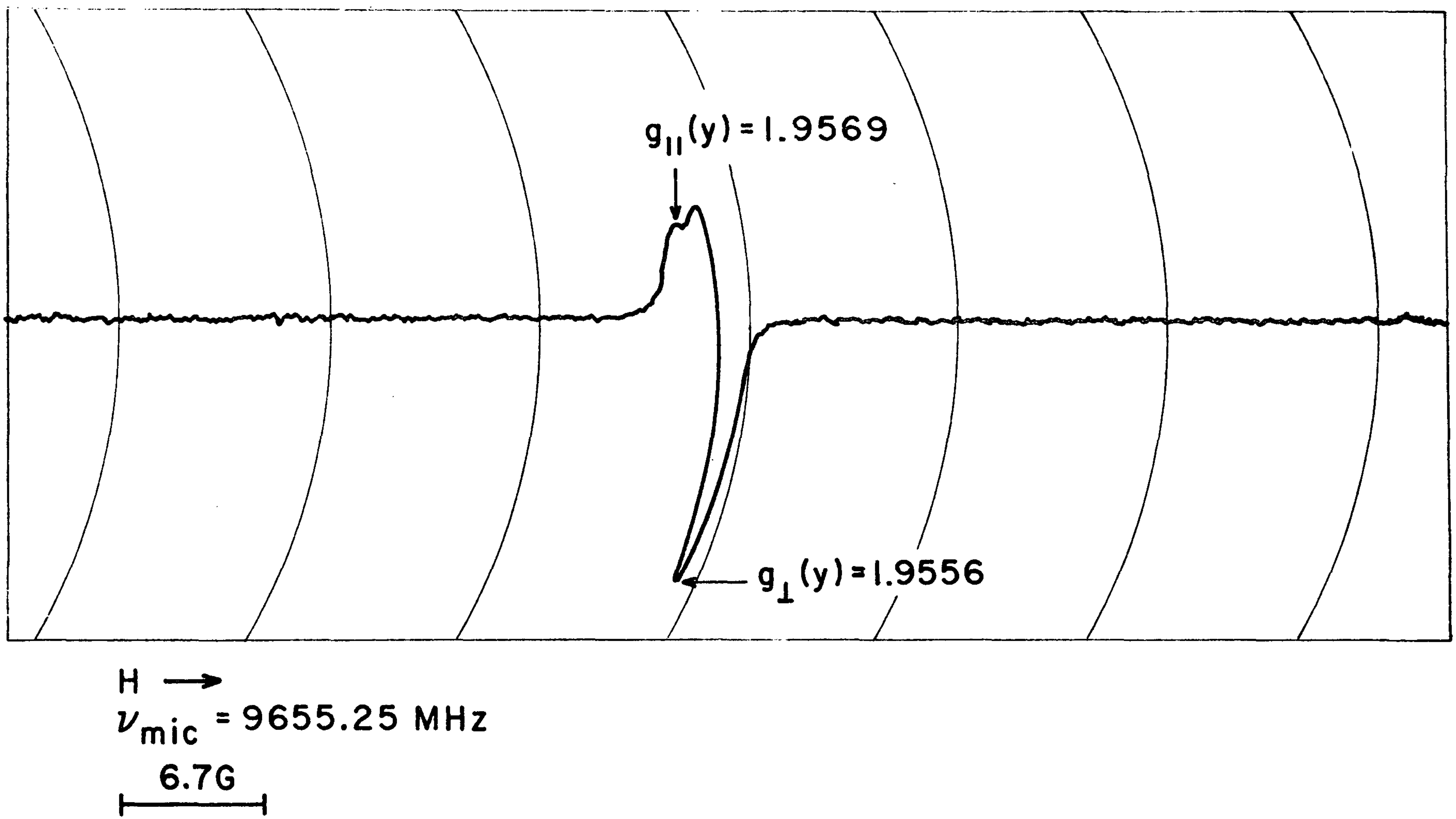

Figure 113 EPR AT ~77°K OF UNIRRADIATED Zn_2TiO_4, SAMPLE B-229, MODULATION - 0.83G

Table 45

MAGNETIC RESONANCE IN UNIRRADIATED SAMPLES (g-VALUES)

Value	Zn_2TiO_4 (B-229)	Zn_2TiO_4 (B-233)	Zn_2TiO_4 (B-234)	Zn_2TiO_4 (B-235)	Zn_2TiO_4 (B-241)	Zn_2TiO_4 (B-226)	Zn_2TiO_4 (B-230)	Lit. Values
g_{11} (y)	1.9570	1.9569	1.9569	1.9569	1.9570	1.9568	1.9569	1.957 (Ref.)
g_1 (y)	1.9556	1.9556	1.9556	1.9555	1.9556	1.9556	1.9556	1.956 (Ref.)

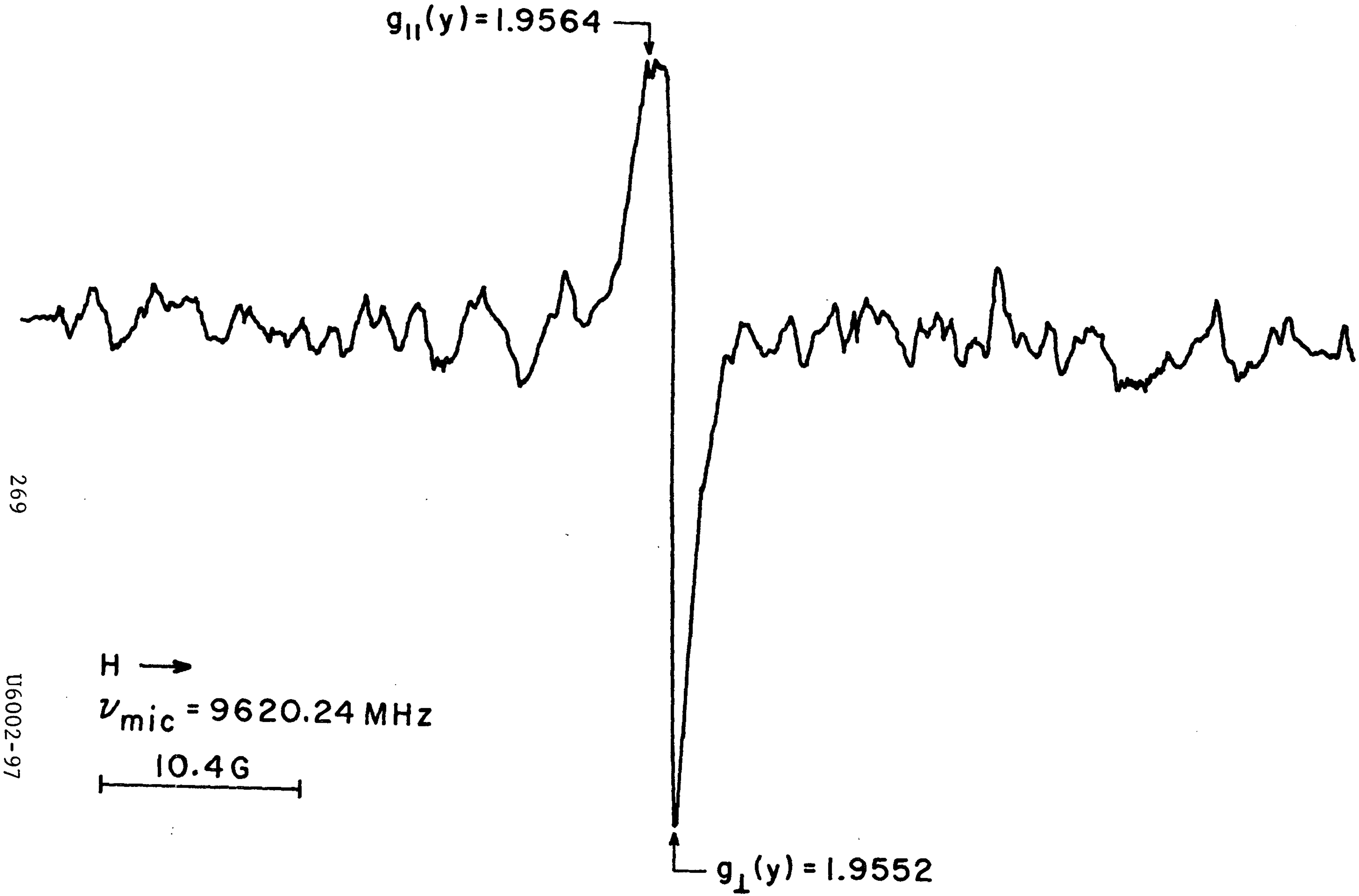

Figure 114 EPR AT ~77°K OF OPTICALLY IRRADIATED Zn_2TiO_4, SAMPLE B-233, MODULATION - 0.34G

8.5.1.4 Summary of Interpretations Based on Previous Work

8.5.1.4.1 The Resonance "y"

Resonance "y" with $g = 1.960$ is identical with the center created by heat treating ZnO at 975°C for 19 hr and attributed to halogen donors (chlorine) by Kasai (Ref. 142). The resonance is only detected in high-temperature plasma-treated Zn_2TiO_4 containing excess TiO_2.

8.5.1.4.2 The Resonance y'

Our g values of $g_1 = 1.9556$ and $g_{11} = 1.9569$ agree well with a second center found after heat treatment by Kasai (Ref. 142) with $g_1 = 1.956$ and $g_{11} = 1.957$ and attributed to (electrons in) oxygen anion vacancies. Kazai reported a slight decrease in this signal intensity on ultraviolet-irradiation. Geisler and Simmond (Ref. 143) further resolved the signal into an ultraviolet-sensitive center at a slightly lower field (~0.6 Gauss) and the heat-created center which is ultraviolet-insensitive. Sancier (Ref. 140), in investigating iron cyanide-treated ZnO finds the ultraviolet-sensitive center (but not the higher field signal) in y' at $g \approx 1.957$ as well as the 1.960 signal. He concludes that both signals are due to conduction electrons and are responsible for the ultraviolet and near-infrared damage in ZnO. His assignment of conduction electrons to the 1.960 signal is not a convincing refutation of Kasai's demonstration that the center is a halogen donor. Furthermore, our observation that y ($g = 1.960$) is present and y' is absent in high-temperature, plasma-annealed orthotitanates with severe infrared damage is at variance with Sancier's conjectures. It may well be that the conduction electrons are not observable at 77°K by EPR methods and that the observation that y ($g = 1.960$) is associated with severe infrared damage is explained by the ionization of an halogen donor: $Cl^- = Cl + e^-$ with the EPR signal y associated with neutral (and paramagnetic) chlorine while the electrons are in the conduction band and are not EPR-observable. The absence of damage at 363-nm wavelength and the failure to detect y' in the high-temperature plasma-treated material, coupled with the observation of 363-nm wavelength damage and the resonance y' in ZnO-excess produced materials, lends support to the thesis that the damage at 363-nm is manifested as the heat-created, ultraviolet-insensitive component of signal y'. Oxygen bleaching experiments planned in the future should help to clarify the problem.

8.5.1.4.3 <u>The Resonance "x"</u>

The resonance "x" too appears to be due to more than one species. The center Ti^{+3} created by high-temperature (500°C) in vacuum with $g_{\perp} = 1.98$ and $g_{11} = 1.94$ is reminiscent of Ti^{+3} found in rutile heated in air at those temperatures. However, since (at least a large part of) the damage at 0.9 microns is oxygen bleachable and since ultraviolet irradiation produces a different (narrower) EPR signal, we recognize that another kind of Ti^{+3} is produced by the photodesorption of oxygen, reducing the Ti^{+4} to Ti^{+3}. Experiments in progress,* to be reported later, indicate that the nature of Ti^{+3} is responsible for damage at 0.9 microns and that Ti^{+3} is associated with orthotitanate material. A complicated solid state chemistry is certainly involved, with the equilibrium dependent on halogen donors, conduction electrons, three centers in ZnO, at least two Ti^{+3} centers and surface and bulk oxygen species.

8.5.2 <u>Summary of Most Recent EPR Studies</u>

8.5.2.1 <u>Introduction</u>

The EPR investigations during the last six months of 1970 were undertaken as initial steps in resolving the following problems:

a. Rationalization of the significant optical damage of otherwise "good" Zn_2TiO_4 pigments when made into O-I 650 paint.

*Contract NAS8-26791, IITRI Project C6233.

b. Elucidation of the mechanisms for alteration of the optical damage in both pigments and paint by surface treatment such as obtained with potassium silicate or Li_2SiF_6.

c. Classification of the nature of the Ti^{+3} species in Zn_2TiO_4 materials and its relation to the optical damage at 0.9μ.

No attempt was made to further investigate the effects of plasma annealing on the defect structure as evidenced by EPR during this period.

8.5.2.2 Experimental

(a) Significant departures from previously used experimental procedures were effected and are described below. In particular, the changes involved (1) in situ ultraviolet-irradiation, rather than transfer of the sample from the irradiation facility (described in Ref. 141) to the EPR cavity and (2) use of a vacuum system which maintained a much poorer vacuum (>10 microns) than that used for previous ultraviolet-irradiation (10^{-5} - 10^{-7} torr). Experiments were performed under these poorer vacuum conditions while a very high-vacuum, in situ epr/irradiation facility was being constructed. These experimental changes are significant and their implications are further amplified in the discussion of results.

(b) Samples and materials examined were as follows:

Sample	Description
3	TiO_2-excess produced Zn_2TiO_4
B-229	ZnO-excess produced Zn_2TiO_4
B-233	Potassium silicate-treated B-229
B-454	Li_2SiF_6-treated B-229
R-900 TiO_2	Rutile TiO_2
FF TiO_2-r	Rutile TiO_2 produced by converting FF anatase
OI-650	Owens-Illinois (non-cured resin)
RTV-602	RTV-602 (uncured liquid)
B-229 OI-650	B-229 in Owens-Illinois "650" paint
R-233 OI-650	B-233 in Owens-Illinois "650" paint.

(c) Ultraviolet-irradiation was carried out in situ in the Varian EPR multi-purpose cavity by irradiation through a grating in the wall of the cavity. The sample in a quartz tube was evacuated to about 10 microns, placed in a Varian quartz dewar situated in the EPR cavity and irradiated at either liquid nitrogen temperatures or at room temperature. The irradiation was accomplished by using an Osram 500-W point-source lamp collimated with a four-inch, fused silica lens and filtered by 5-cm pathlength of an aqueous solution of $NiSO_4 \cdot 6H_2O$ (240 g/l), and $CoSO_4 \cdot 7H_2O$ (45 g/l) which removed most of the visible and infrared-red. For irradiations carried out at room temperatures, liquid nitrogen was added to the dewar just before cessation of illumination. In all irradiations the sample was rotated by $\pi/4$ every fifteen minutes. The total irradiation time was usually 1 to 2 hr, but TiO_2 was irradiated for ~5 hr in some instances. In summary, these irradiations differed from those performed previously in that (1) liquid-nitrogen temperature irradiations were achieved (2) the light was both collimated and filtered and (3) a poorer vacuum was maintained.

All EPR measurements were carried out at liquid nitrogen temperatures.

8.5.2.3 Experimental Results

All EPR measurements were carried out at ~77°K.

B-229

The EPR spectra in the ground-state (non-irradiated) B-229 Zn_2TiO_4 are shown in Figure 115. The resonance y' attributed to electrons in oxygen anion vacancies in ZnO and observed previously is present and another resonance was found at g = 2.000, due to ultraviolet-created centers in the dewar. Ultraviolet-irradiation at 77°K (Figure 116) and at room temperature (Figure 117) produced similar results. The resonance "x" was created in both and a resonance was found which we shall call k', with g-values as indicated on the spectra. It would appear that the resonance "x"

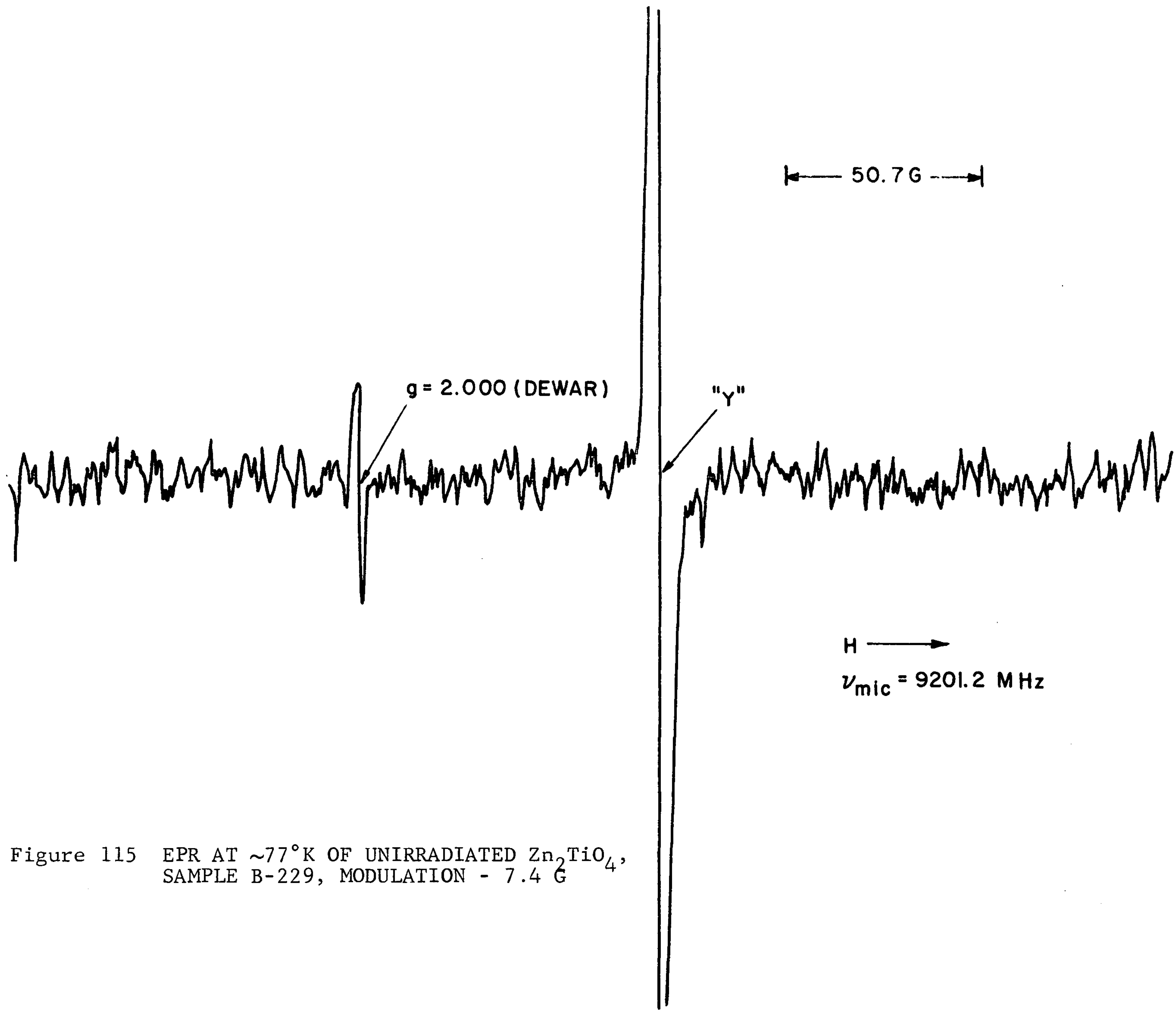

Figure 115 EPR AT ~77°K OF UNIRRADIATED Zn_2TiO_4, SAMPLE B-229, MODULATION - 7.4 G

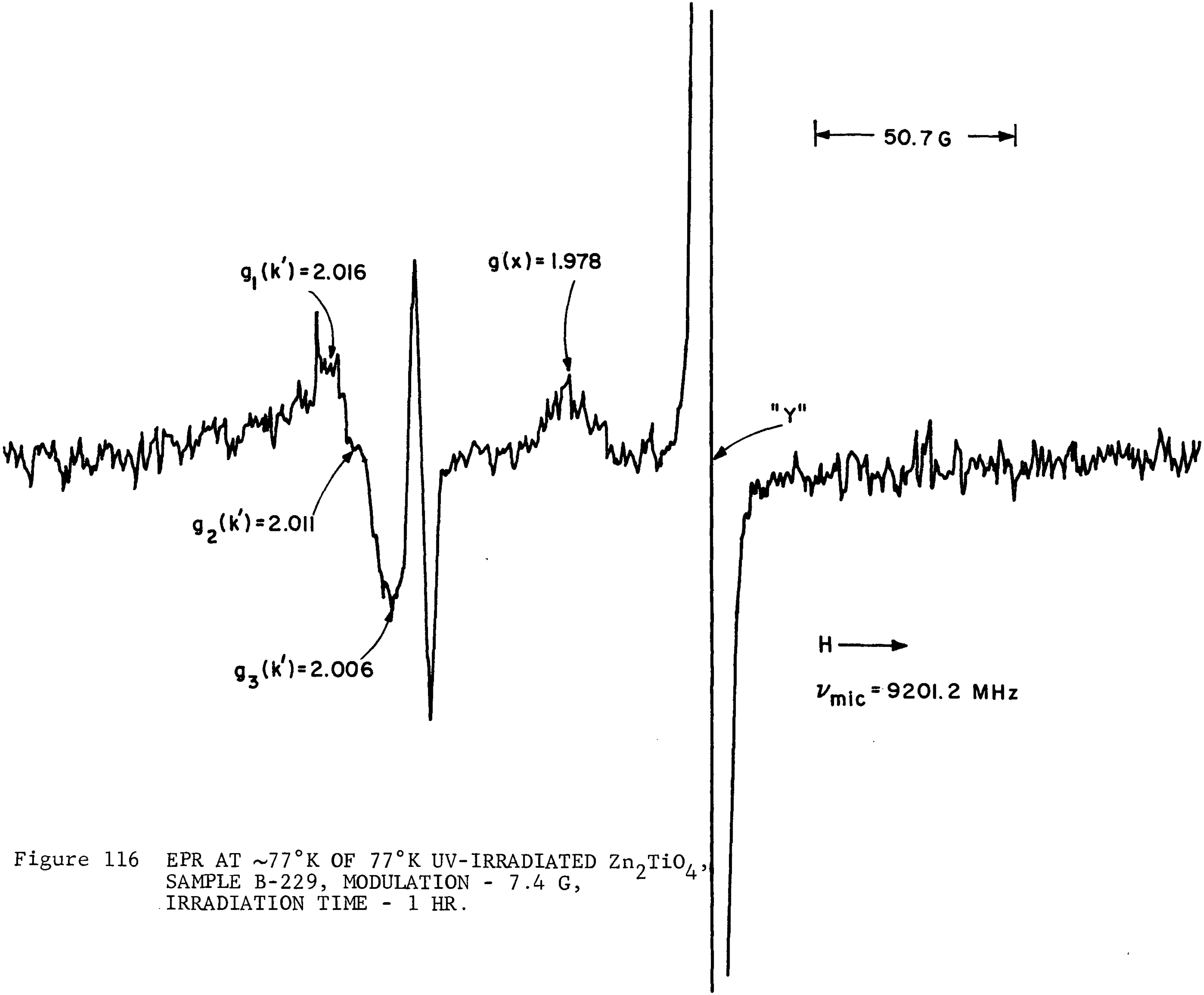

Figure 116 EPR AT ~77°K OF 77°K UV-IRRADIATED Zn_2TiO_4, SAMPLE B-229, MODULATION - 7.4 G, IRRADIATION TIME - 1 HR.

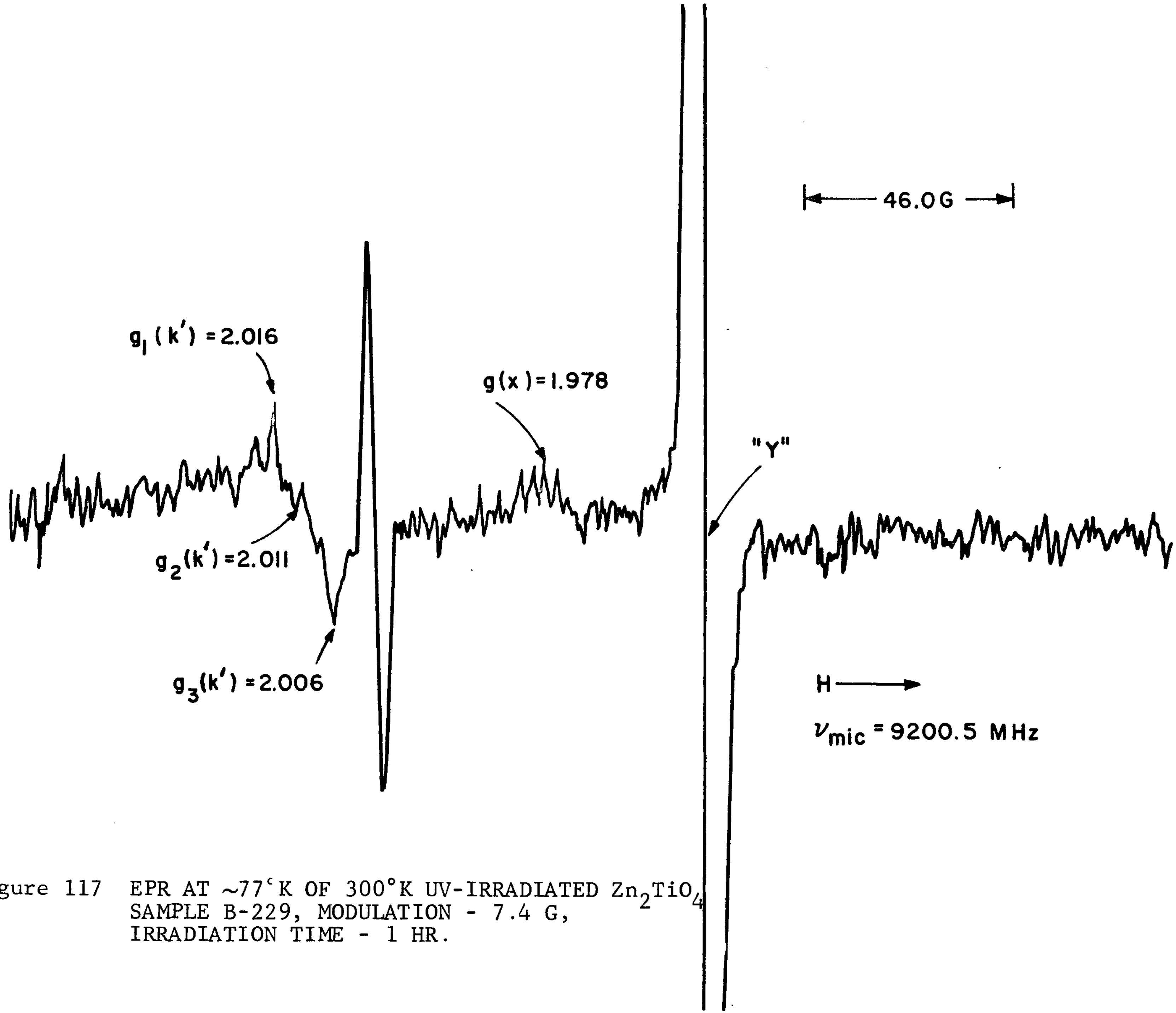

Figure 117 EPR AT ~77°K OF 300°K UV-IRRADIATED Zn_2TiO_4
SAMPLE B-229, MODULATION - 7.4 G,
IRRADIATION TIME - 1 HR.

is more intense in the 77°K irradiated material. Both ultraviolet irradiation doses were the same (1 hr).

B-233 (Silicated B-229)

The EPR spectra of ground-state B-233 are similar to that of B-229 and are shown in Figure 118. Ultraviolet-irradiation at 77°K produced the spectra in Figure 119, showing both "x" and k'. On warming the sample to room temperature both resonances disappeared and were not observable on recooling (Figure 120).

B-454 (Li_2SiF_6-treated B-229)

The EPR spectra of ground-state B-454 showed only the dewar resonance (Figure 121). Ultraviolet-irradiation produced both "x" and k' (Figure 122). No y' was observed.

B-229 OI-650

The EPR spectra of the ground-state paint material is shown in Figure 123. Ultraviolet-irradiation at 77°K (Figure 124) and at room temperature (Figure 125) produced similar results and show both "x" and k'.

B-233 OI-650

The EPR spectra of the ground-state paint material was the same as the pigment alone and is not shown. Ultraviolet-irradiation at 77°K produced a rather strong "x" center (Figure 126) which disappeared upon warming to room temperature and re-cooling (Figure 127).

R900 TiO_2 (Rutile)

Figure 128 shows the EPR spectra of ultraviolet-irradiated rutile at 77°K for 5-1/2 hr. No "x" is observed. Nor is "x" observed by irradiating rutile produced by converting FF anatase to rutile by following the procedure used in making Zn_2TiO_4. The implications of this finding are discussed in the next section. The resonance k' is also not observed in the rutile samples.

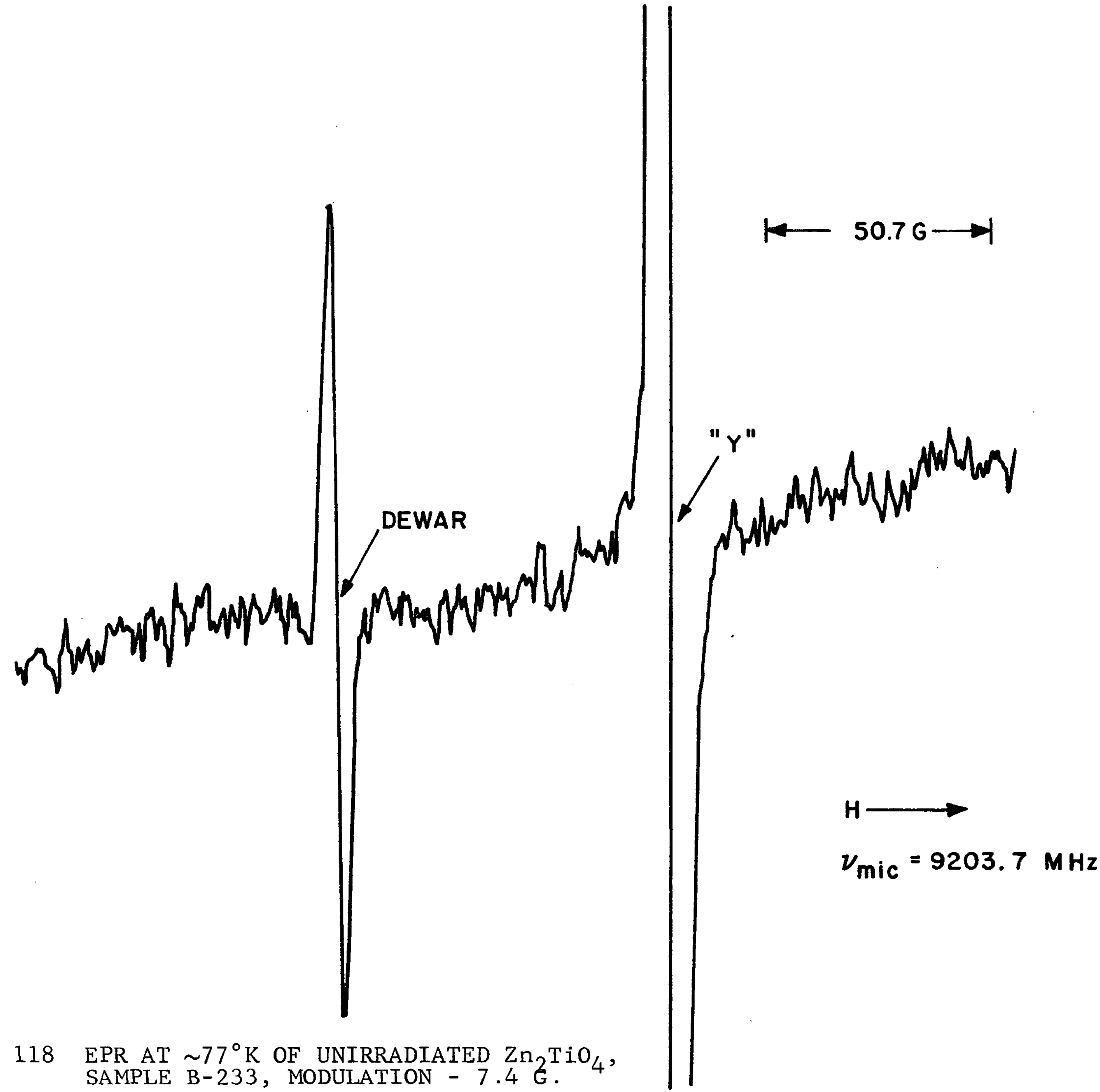

Figure 118 EPR AT ~77°K OF UNIRRADIATED Zn_2TiO_4, SAMPLE B-233, MODULATION - 7.4 G.

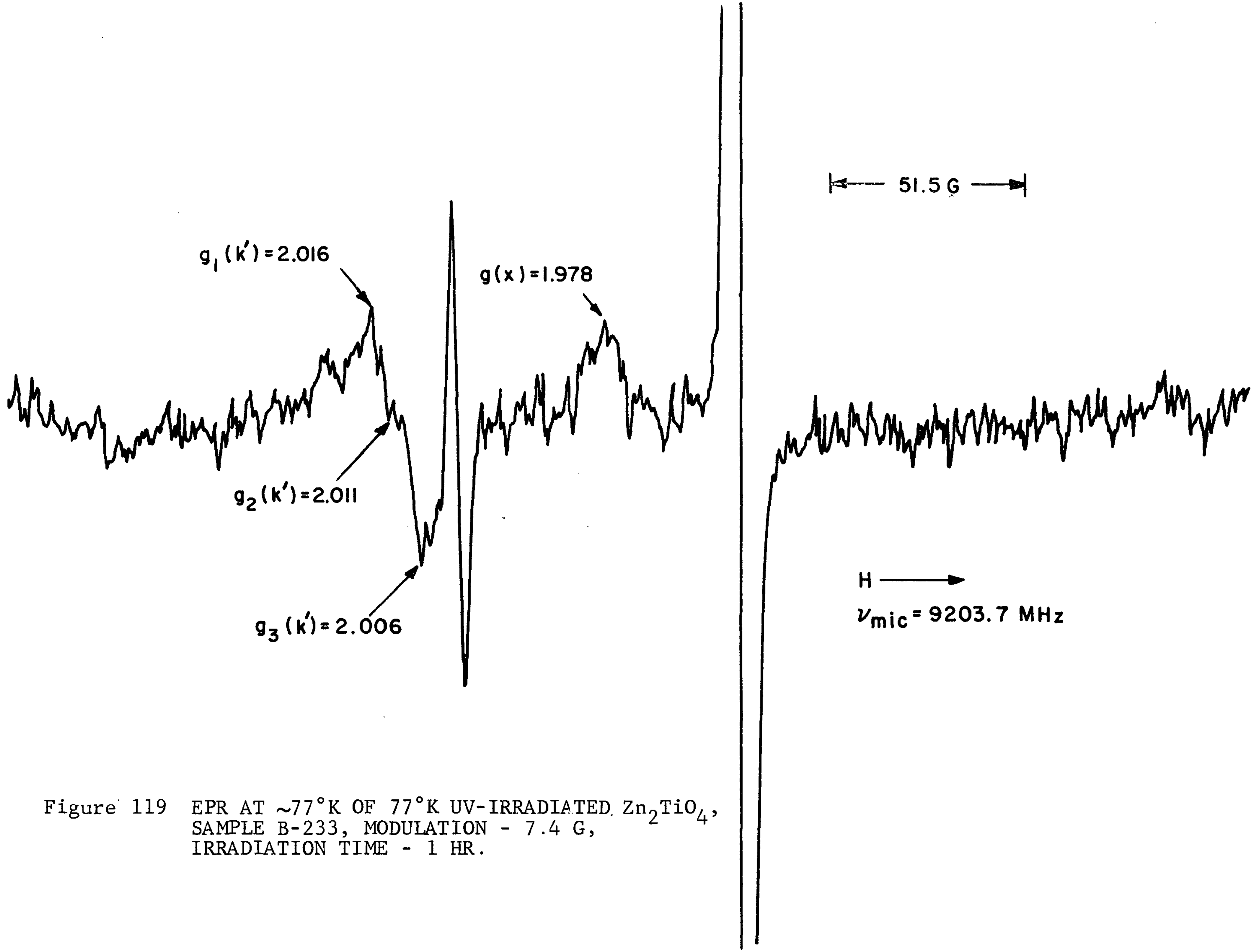

Figure 119 EPR AT ~77°K OF 77°K UV-IRRADIATED Zn_2TiO_4, SAMPLE B-233, MODULATION - 7.4 G, IRRADIATION TIME - 1 HR.

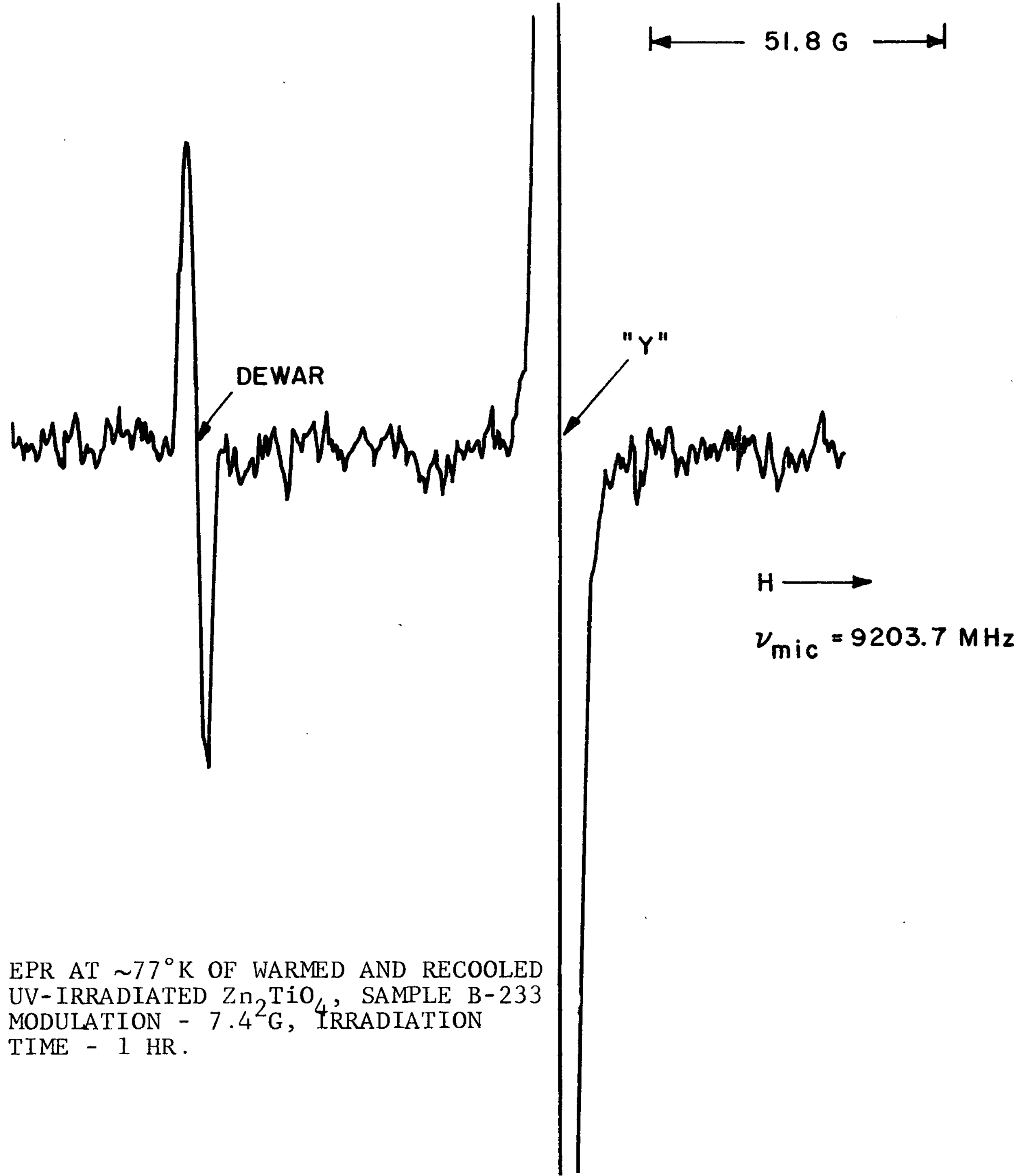

Figure 120 EPR AT ~77°K OF WARMED AND RECOOLED UV-IRRADIATED Zn_2TiO_4, SAMPLE B-233 MODULATION - 7.4 G, IRRADIATION TIME - 1 HR.

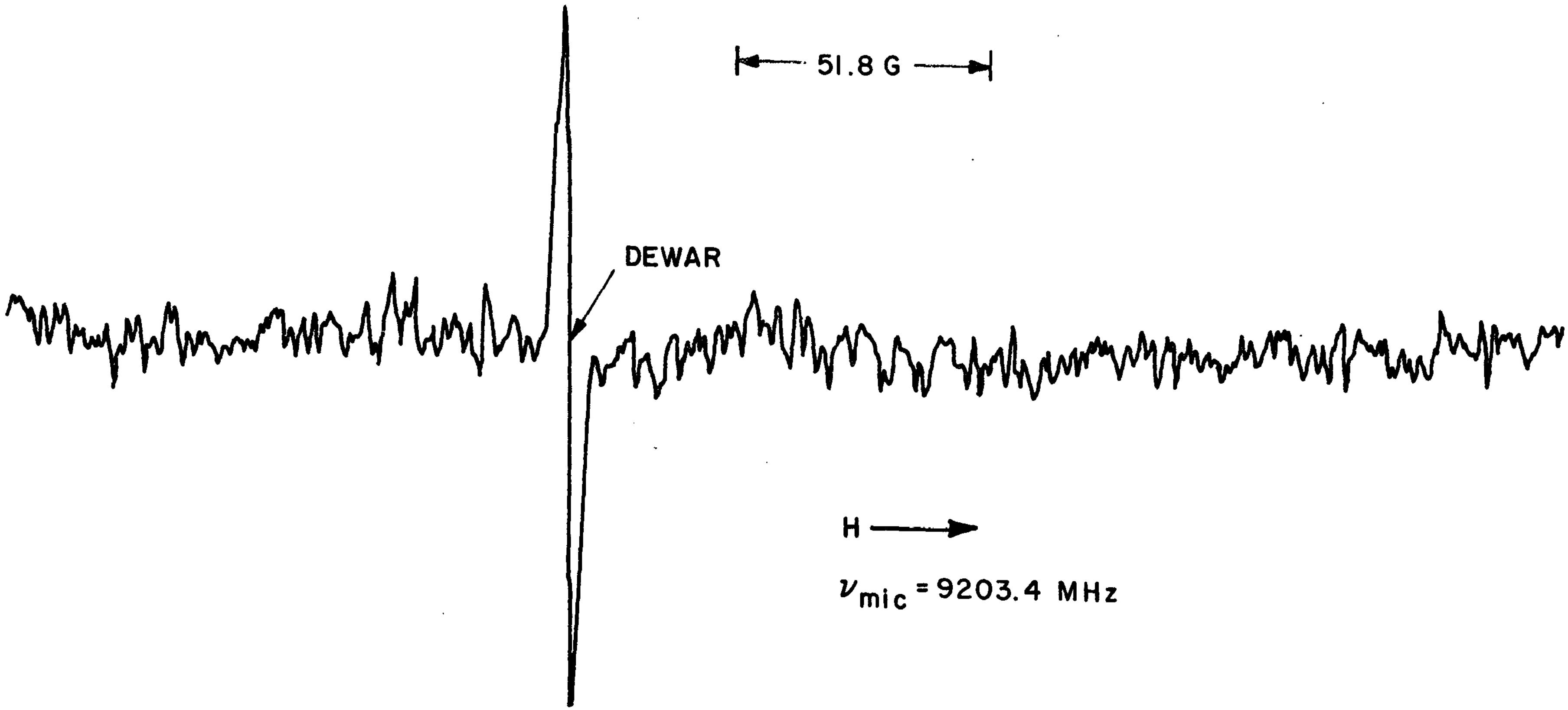

Figure 121 EPR AT ~77°K UNIRRADIATED Zn_2TiO_4, SAMPLE B-454, MODULATION - 7.4 G

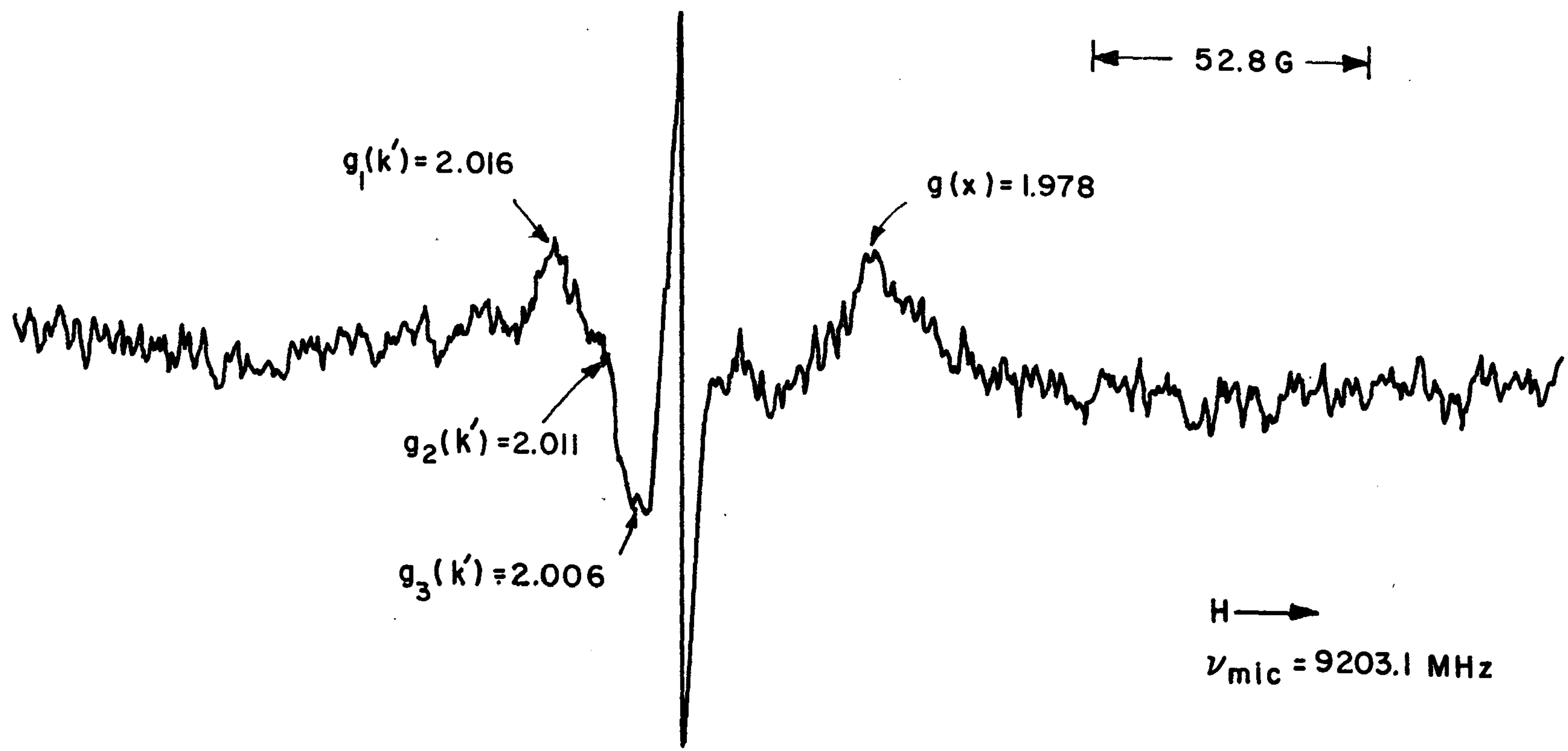

Figure 122 EPR AT ~77°K UV-IRRADIATED Zn_2TiO_4, SAMPLE B-454, MODULATION - 7.4 G, IRRADIATION TIME - 1 HR.

U6002-97

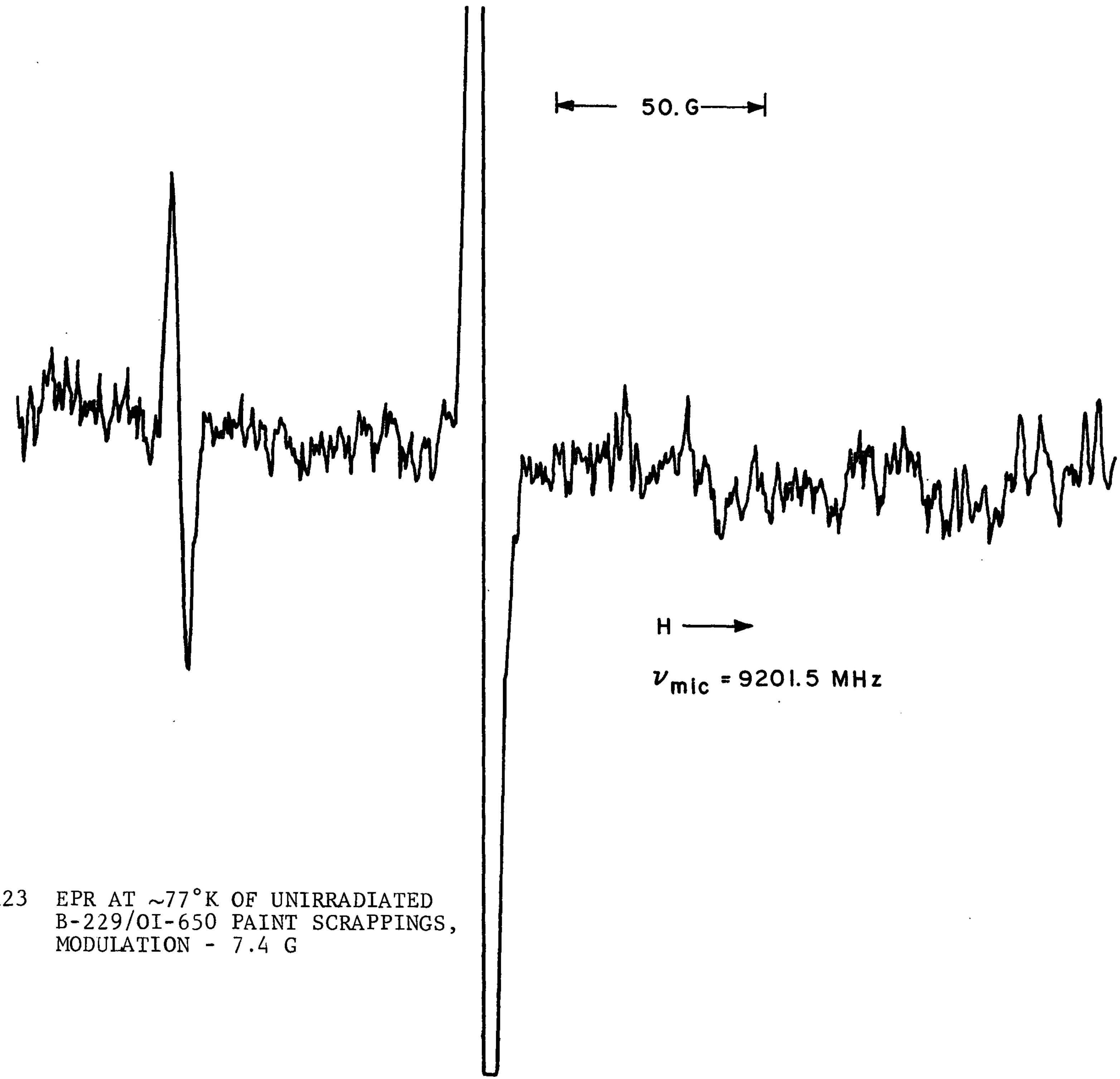

Figure 123 EPR AT ~77°K OF UNIRRADIATED B-229/OI-650 PAINT SCRAPPINGS, MODULATION - 7.4 G

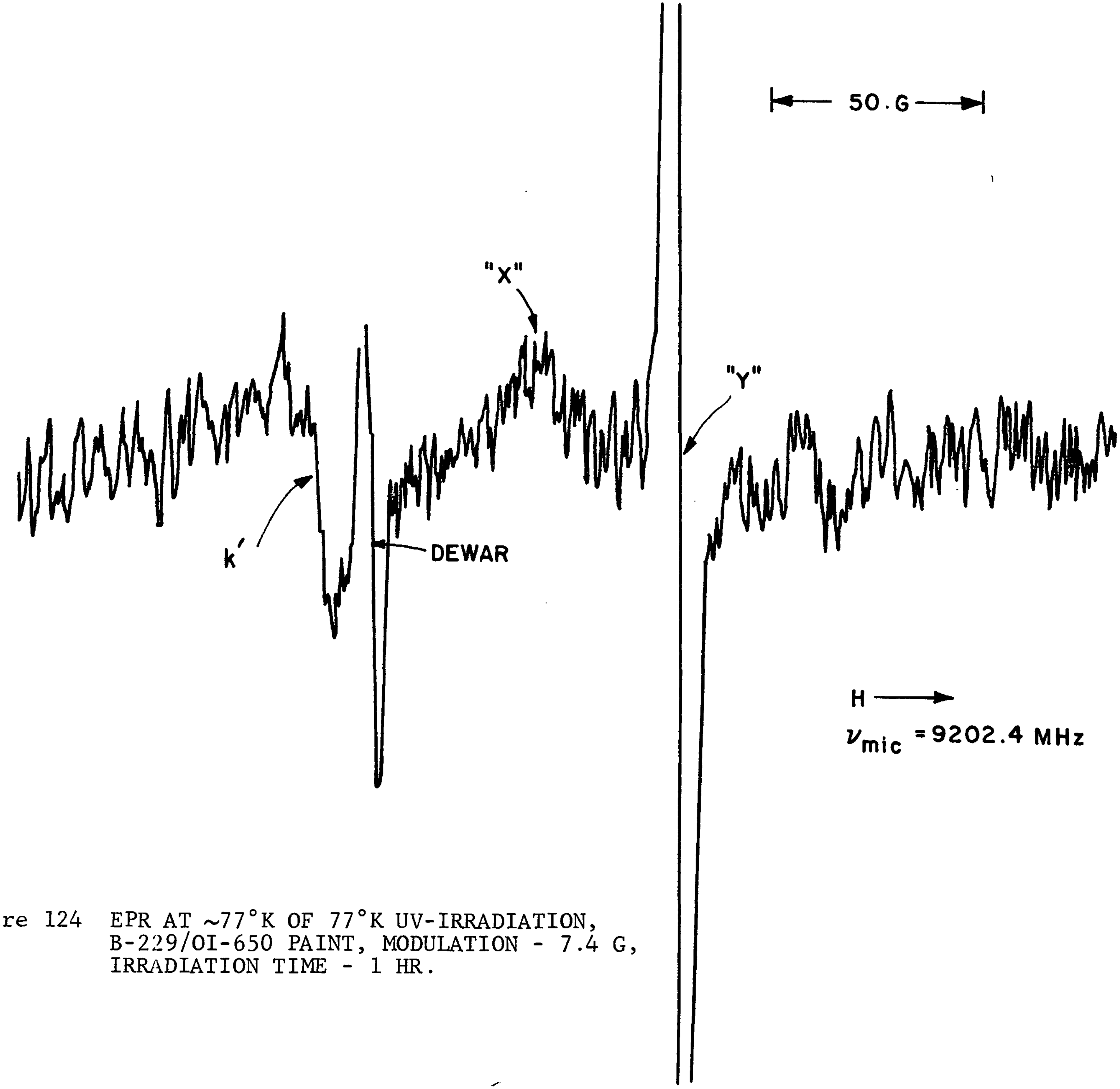

Figure 124 EPR AT ~77°K OF 77°K UV-IRRADIATION, B-229/OI-650 PAINT, MODULATION - 7.4 G, IRRADIATION TIME - 1 HR.

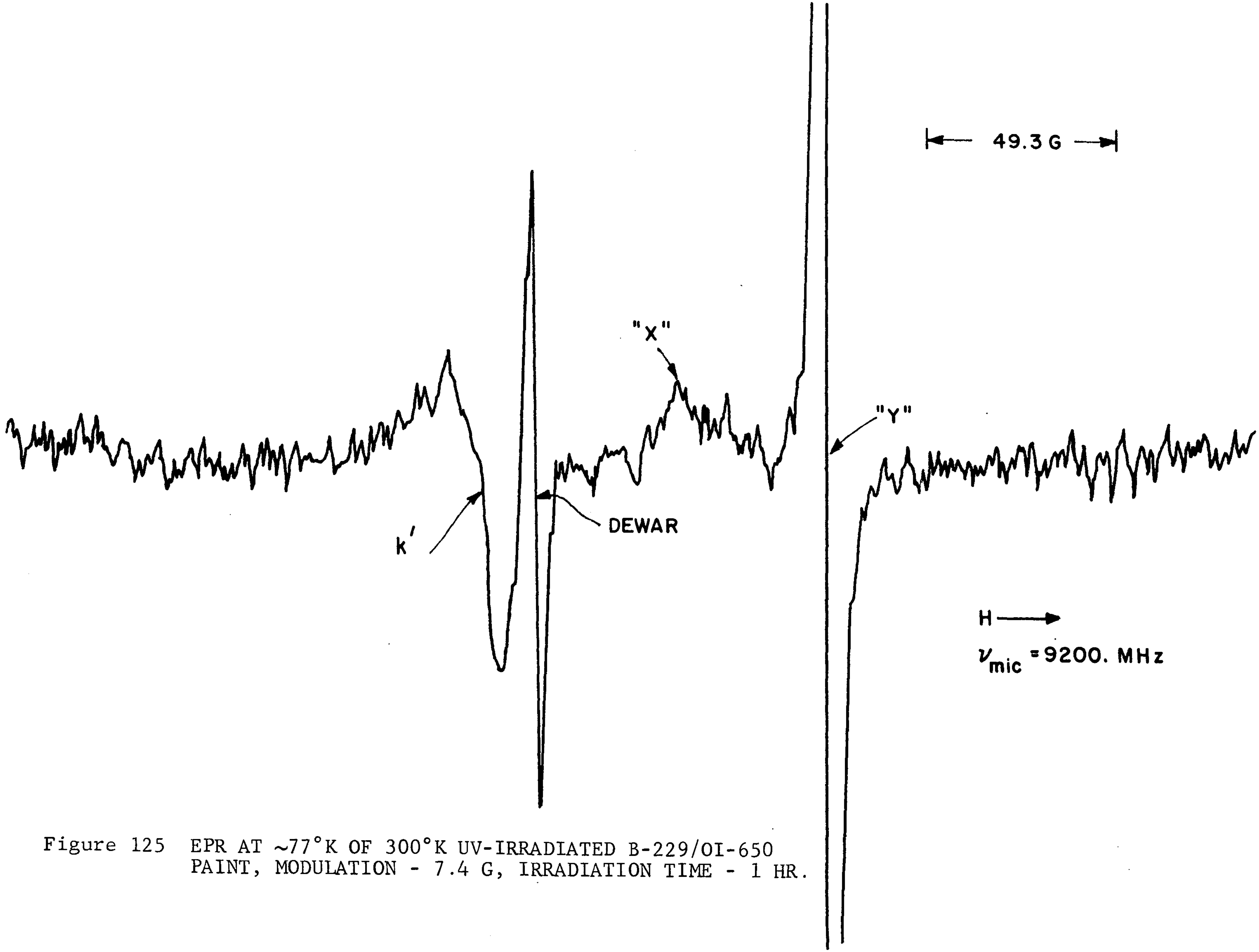

Figure 125 EPR AT ~77°K OF 300°K UV-IRRADIATED B-229/OI-650 PAINT, MODULATION - 7.4 G, IRRADIATION TIME - 1 HR.

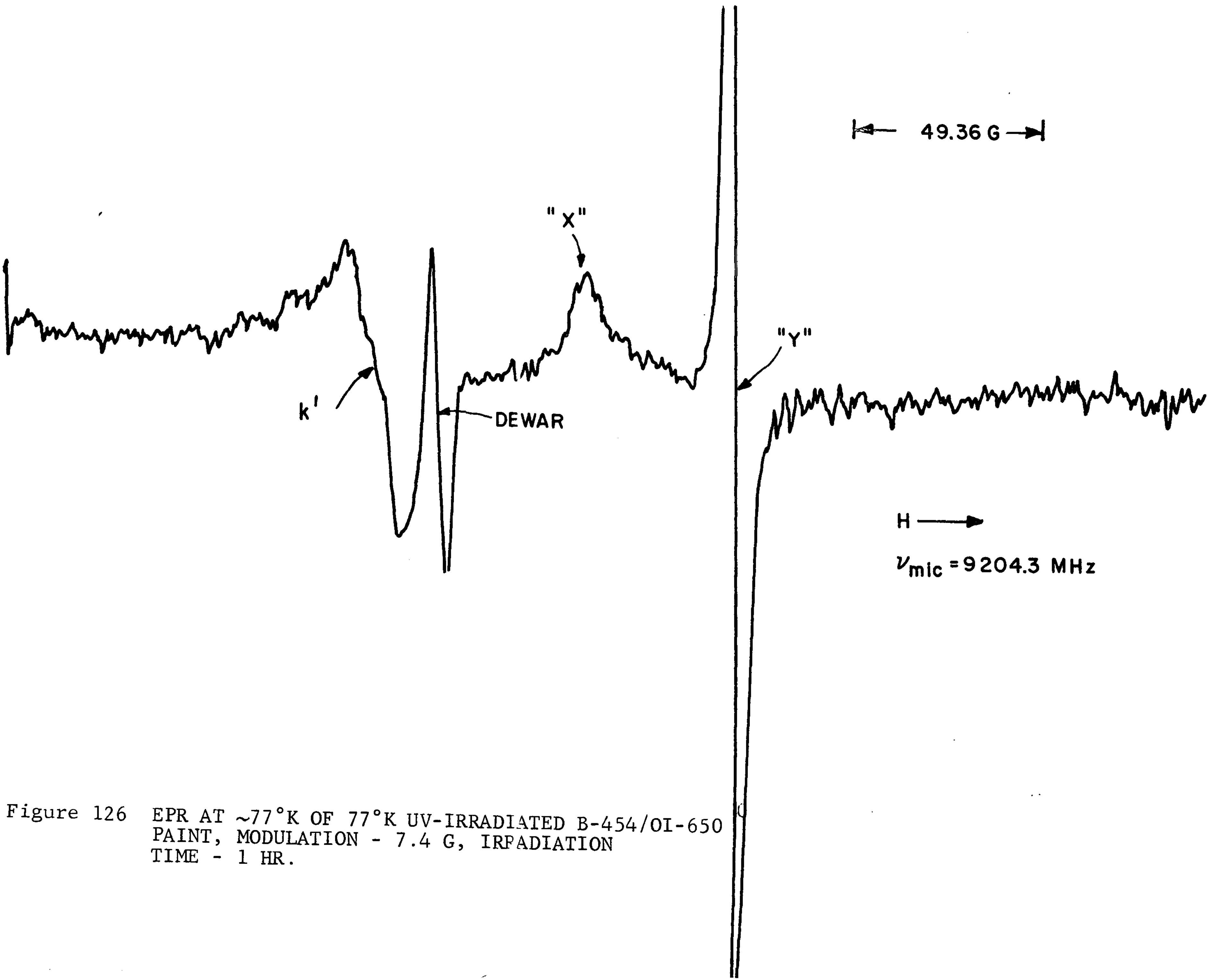

Figure 126 EPR AT ~77°K OF 77°K UV-IRRADIATED B-454/OI-650 PAINT, MODULATION - 7.4 G, IRRADIATION TIME - 1 HR.

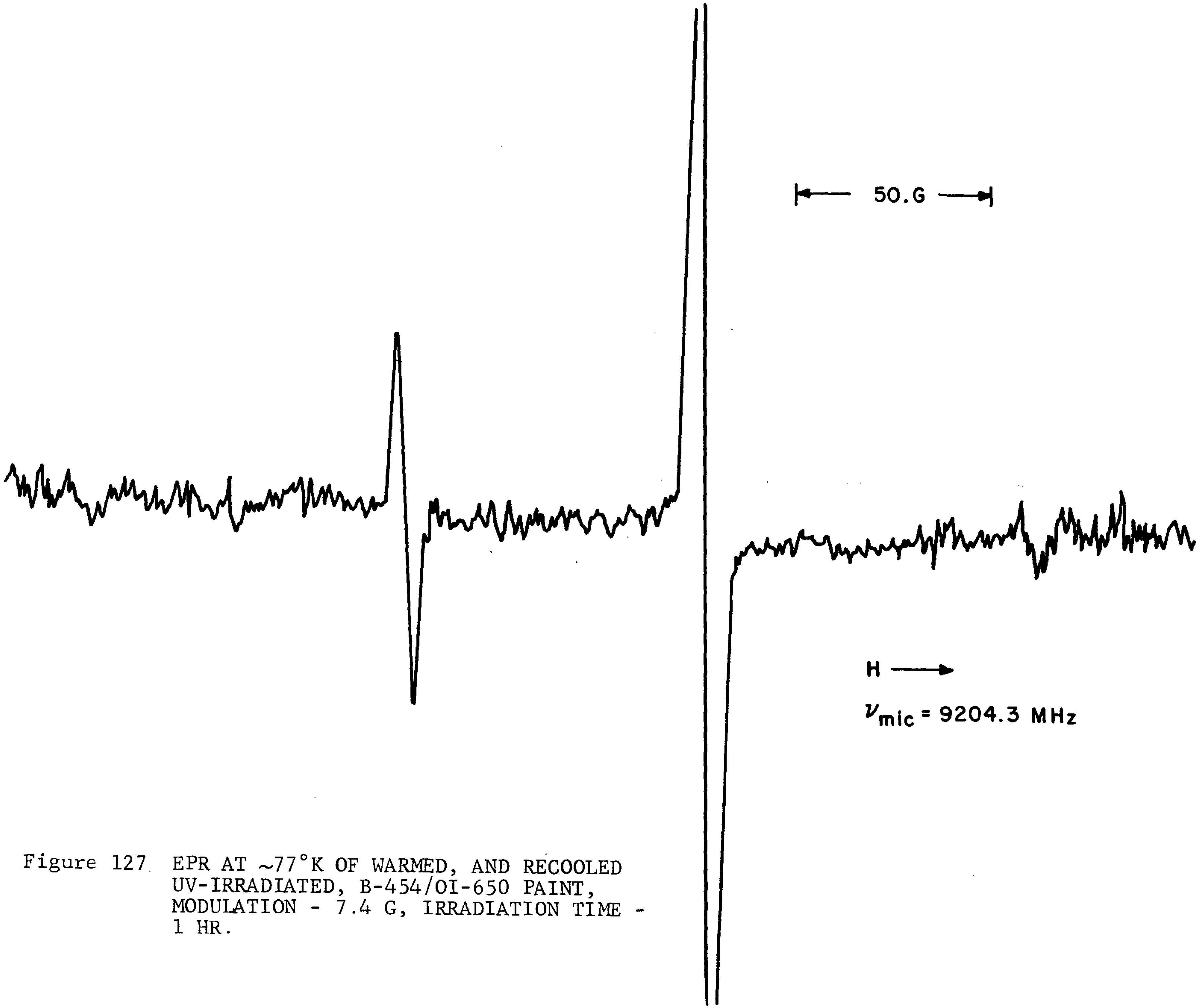

Figure 127 EPR AT ~77°K OF WARMED, AND RECOOLED UV-IRRADIATED, B-454/OI-650 PAINT, MODULATION - 7.4 G, IRRADIATION TIME - 1 HR.

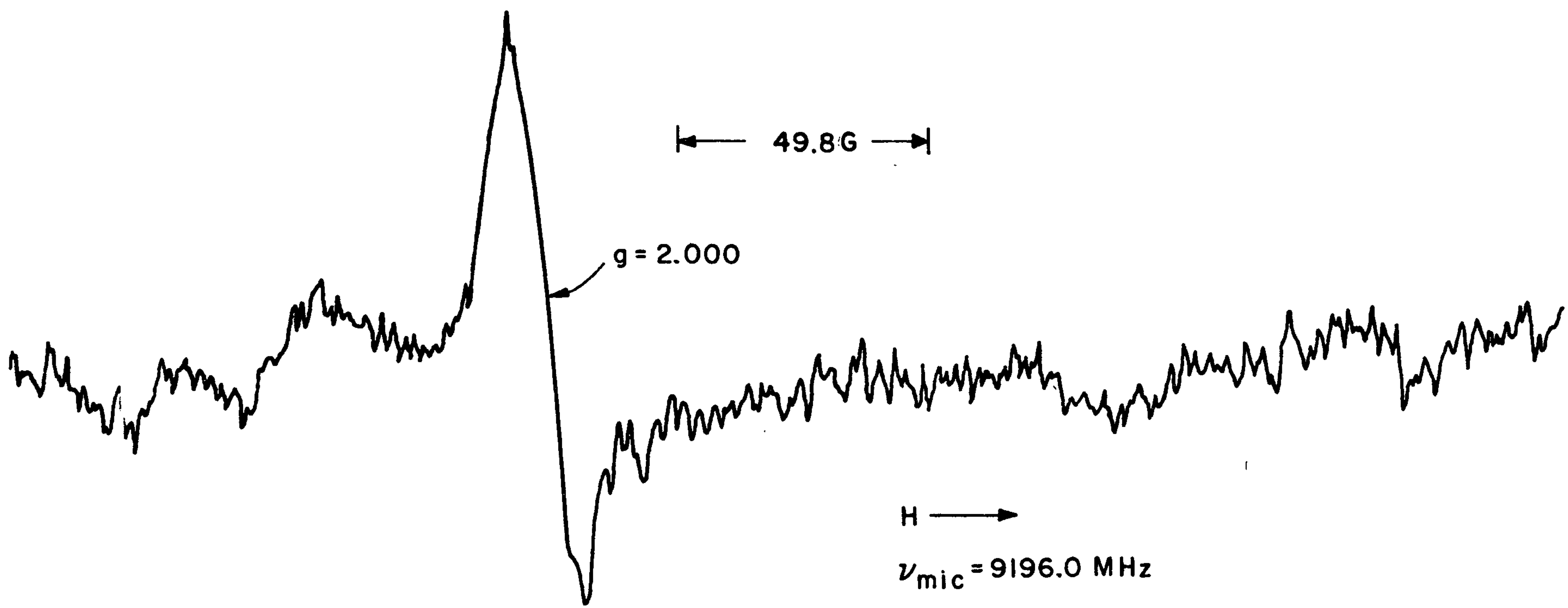

Figure 128 EPR AT ~77°K OF 77°K UV-IRRADIATED RUTILE TiO_2, MODULATION - 7.4 G, IRRADIATION TIME - 5.5 HR.

OI-650 and RTV-602

The EPR spectra of the ultraviolet-irradiated materials at 77°K are essentially identical and are shown in Figures 129 and 130. Free-radicals reported previously (Ref. 12) were observed after a short exposure to ultraviolet (1 hr) and were present in high concentration.

#3

The #3 Zn_2TiO_4 previously investigated, (Figure 31, Ref. 136) was ultraviolet-irradiated again under the new experimental conditions and the EPR spectra are shown in Figure 131. No y' or y is observed, but "x" and k' are.

8.5.2.4 Discussion of Experimental Results

These initial experiments have pointed out some rather significant results. While it may be rationalized that "x" is not observed in rutile TiO_2 on ultraviolet-irradiation--because the vacuum is too low and oxygen, even at >10 microns ($\sim 10^{-2}$ torr), can bleach any Ti^{+3} formed (Ref. 112)--the fact is that "x" is observed in Zn_2TiO_4 material. Obvious possible explanations are that (1) the "x" observed in Zn_2TiO_4 (or TiO_2 present) is bulk rather than surface related (2) the nature of the surface of the Zn_2TiO_4 (or TiO_2 present) is protected from O_2 bleaching or (3) most of the surface "x" is in fact bleached and only residual metastable bulk or surface-protected "x" remains.

Investigation of OI-650 paints made with pigments B-229 and B-233 do not result in significantly different EPR spectra under poor vacuum conditions and lend support for the third explanation since in fact the optical damage in the paints is more severe than for that in the pigments alone. But these explanations need further elucidation. Experiments performed under higher vacuum should settle the anomaly.

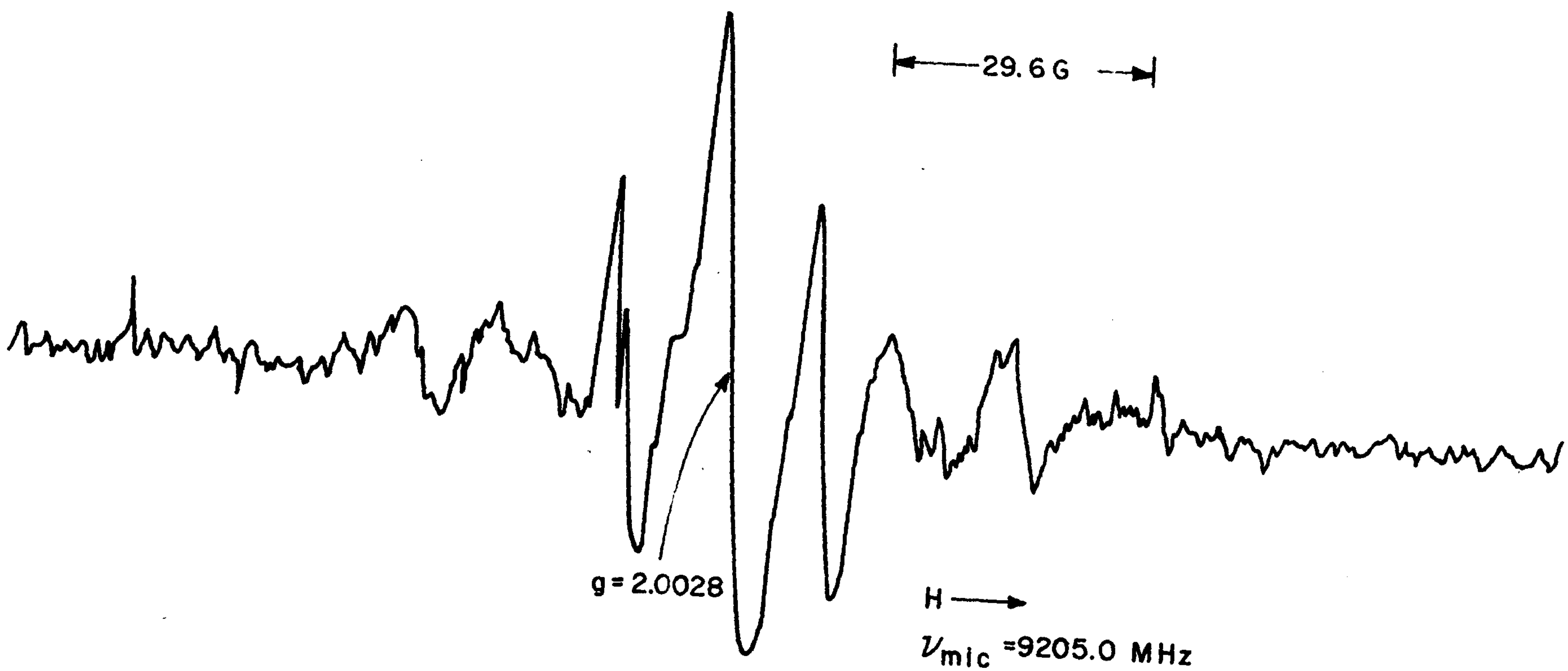

Figure 129 EPR AT ~77°K OF 77°K UV-IRRADIATED OI-650 RESIN, MODULATION - 4.5 G, IRRADIATION TIME - 1 HR.

U6002-97

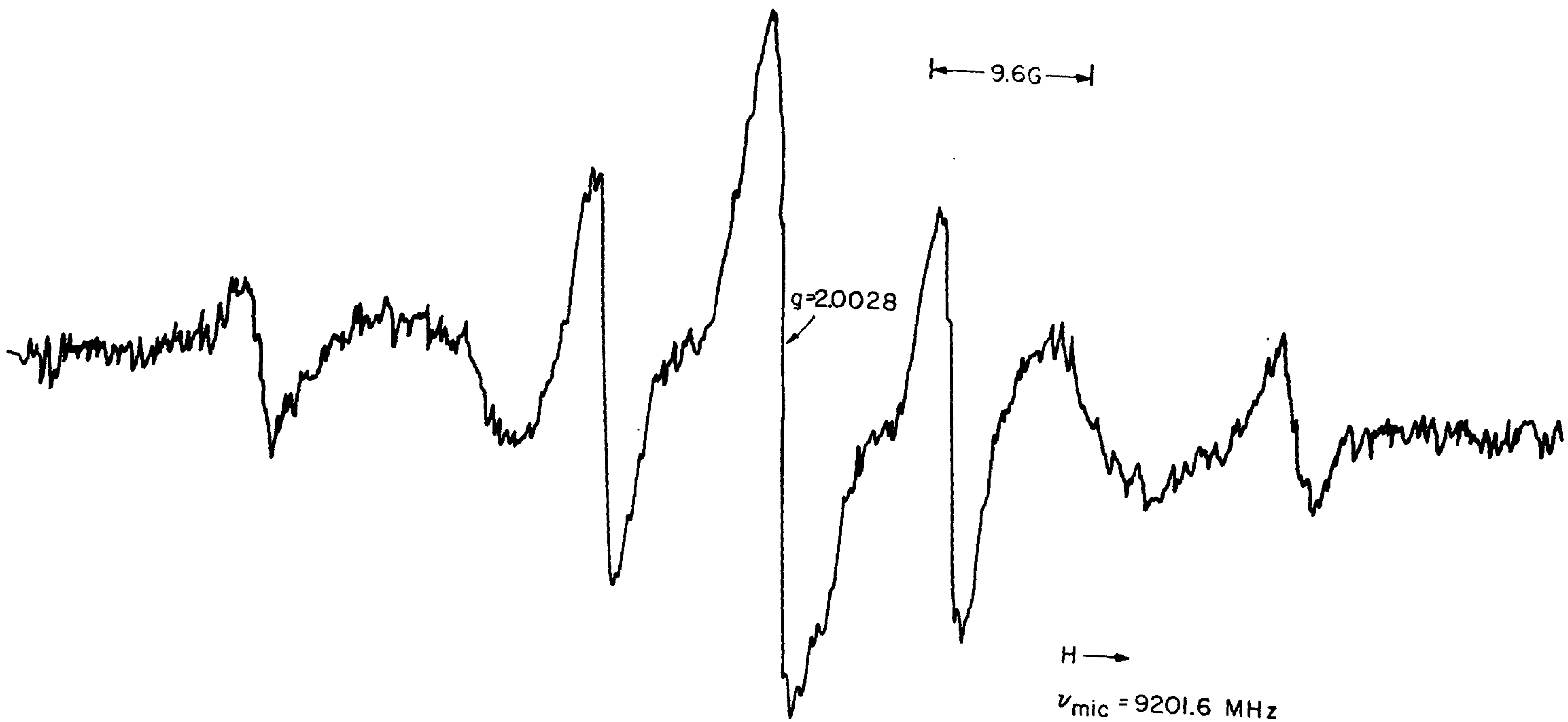

Figure 130 EPR AT ~77°K OF 77°K UV-IRRADIATED RTV-602 RESIN, MODULATION - 7.4 G, IRRADIATION TIME - 2 HR.

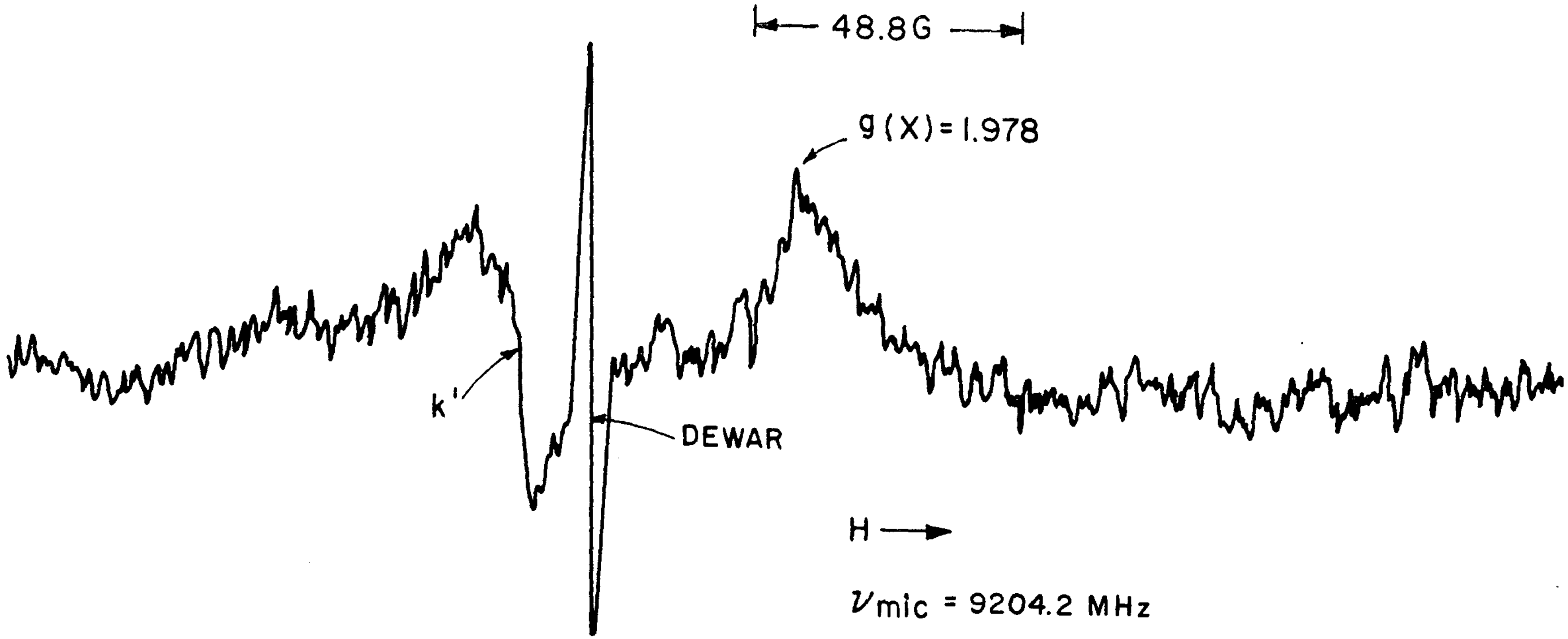

Figure 131 EPR AT ~77°K OF 77°K UV-IRRADIATED Zn_2TiO_4, SAMPLE #3, MODULATION - 7.4 G, IRRADIATION TIME - 1 HR.

The observation that no y' is found in Li_2SiF_6-treated B-229 (B-454), even though excess ZnO is present, is an indication of the alteration of the surface of (the ZnO?) by Li_2SiF_6. The optical spectra show that the pigment is extremely stable to ultraviolet irradiation (Figure 7, Ref. 144).

Perhaps a most suprising observation is that the free-radicals found so easily in OI-650 (and RTV-602) are not observed in Zn_2TiO_4-pigmented Owens-Illinois 650 resin paints. These free-radicals (or their predecessors) may in fact provide damaging electrons for the orthotitanate materials. The fact that Li_2SiF_6 treated Zn_2TiO_4 makes a good (silicate) paint (and a better OI paint than the control)--and yet y' is not observed (in the pigment)--implying an electron scavenging effect and lends support to the thesis that in the absence of electrons capable of reducing Ti^{+4} to Ti^{+3} (x), the pigment and paint will be ultraviolet-stable. The Li_2SiF_6 somehow appears to diminish electron damage.

The resonance k', observed in these ultraviolet-irradiated materials may in fact contain the resonance "k" (attributed to O_2^-) previously observed only in gamma-irradiated material--since (1) it appears to have structure, (2) is broader than "k" and (3) its transition occurs in the area in which "k" would be observed. The center is not observed in the irradiated rutiles and may be associated with Zn_2TiO_4. This is yet to be resolved.

More definitive conclusions from the EPR experiments performed must await the results of in situ high vacuum studies--but it is apparent that the nature of the surface of the pigment can be altered by surface treatment and pigment-binder interactions--and that electrons are the damaging species and can be prevented from producing centers which absorb. These conclusions will appear in Report No. IITRI-C6233-12 on the current contract (NAS8-26791).

8.6 Proton Irradiation

The effects of irradiation of surface-treated pigments with 1.3 keV protons is shown in Table 46 and Figures 132 through 136. The $\Delta\alpha_s$'s of 0.04 for the plasma-treated Zn_2TiO_4 and the phosphated Zn_2TiO_4-pigmented silicate paint are encouraging, since the fluence of 8.4 x 10^{15}p/cm^2 represents greater than one year in the solar wind stream.

The most important observation is the stability exhibited by the Owens-Illinois 650 resin paint that was pigmented with "cyanated" Zn_2TiO_4. The ferro/ferricyanide treatment first utilized by Morrison and Sancier (Ref. 145) in studies of the defect state of ZnO, has been employed at IITRI in treating Zn_2TiO_4 (see para. 8.4.3). We have been generally unsuccessful in using iron cyanide to effectively stabilize either ZnO or Zn_2TiO_4 to ultraviolet irradiation under ambient irradiation conditions. However, the ferro/ferricyanide treatment did indeed militate against the severe damage seen in wet-sprayed powders and silicate paints irradiated at high temperature (Ref. 146).

Although preliminary combined ultraviolet-plus-proton radiation experiments have been performed on untreated Zn_2TiO_4-pigmented potassium silicate and Owens-Illinois 650 paints, these data are the subject of another communication (Ref. 147) and are not included here. The efficacy of reactive encapsulation, of ferro/ferricyanide treatment, or of plasma annealing has yet to be established in terms of either proton irradiation, or combined ultraviolet-plus-proton irradiation.

8.7 Discussion

8.7.1 General

It is necessary that an excess of ZnO (in our studies 0.5%) be present in the preparative stoichiometry to minimize the "surface" Ti^{+4} available in Zn_2TiO_4 for the photodesorption reaction

Table 46

SUMMARY OF 1.2 keV PROTON-IRRADIATION DAMAGE

Figure No.	Material	Binder	Pigment Oxide	Pigment Treatment	Proton Exposure 10^{15} p/cm^2	Proton Exposure 10^9 p/cm^2-sec	Solar Absorptance α_s	Solar Absorptance $\Delta\alpha_s$
132	Z-93	PS7	ZnO		8.4	5.4	0.167	0.027
133	S-13G	RTV-602	ZnO	PS7	2.5	4.9	0.212	0.022
134	Paint	PS7	Zn_2TiO_4	NaH_2PO_4	8.4	5.4	0.149	0.038
135	Paint	OI-650	Zn_2TiO_4	Fe-CN	2.5	4.9	0.269	0.005
136	Powder	H_2O	Zn_2TiO_4	1900°C Plasma	8.4	5.4	0.197	0.041

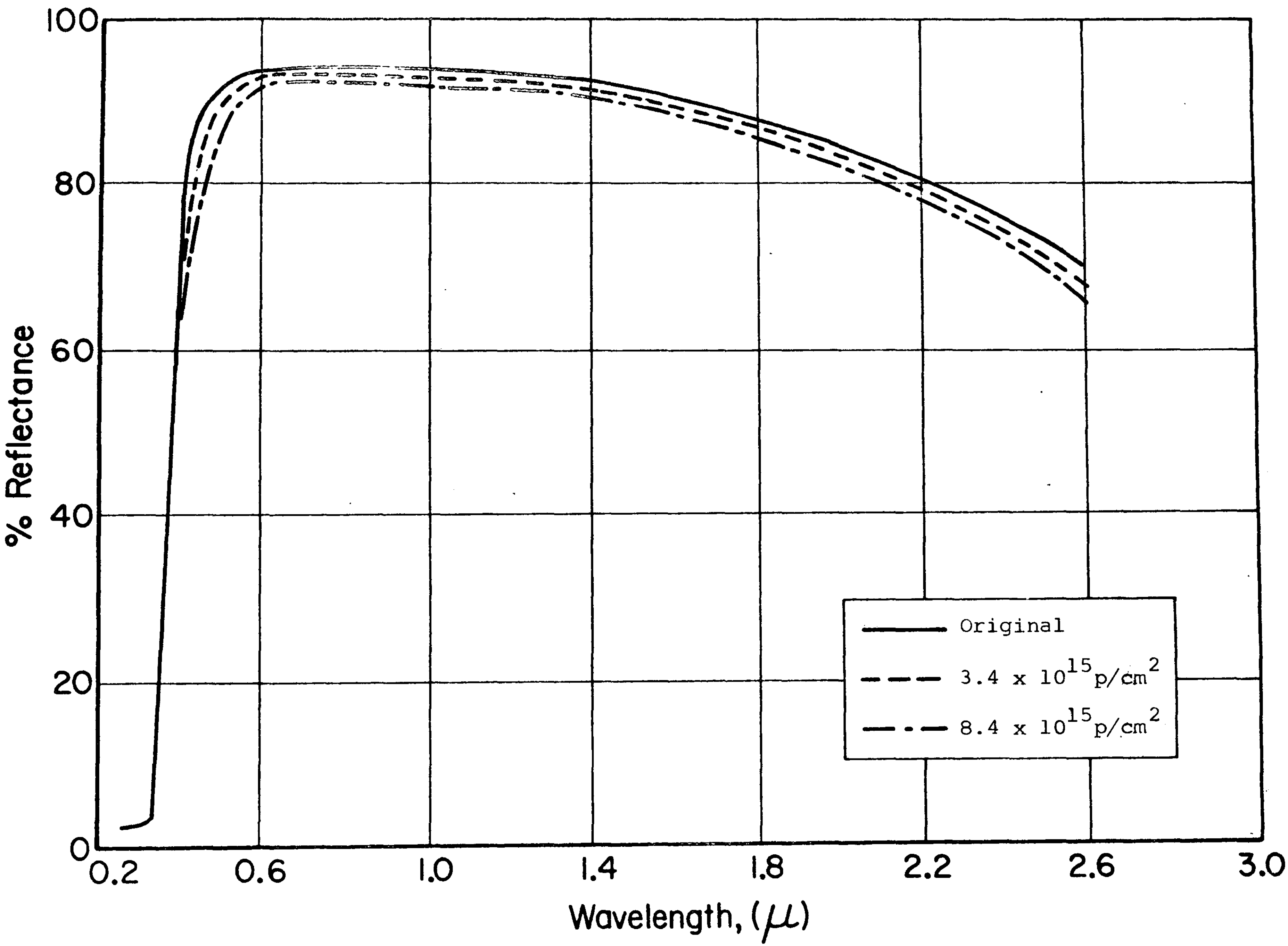

Figure 132 EFFECT OF PROTONS ON Z-93

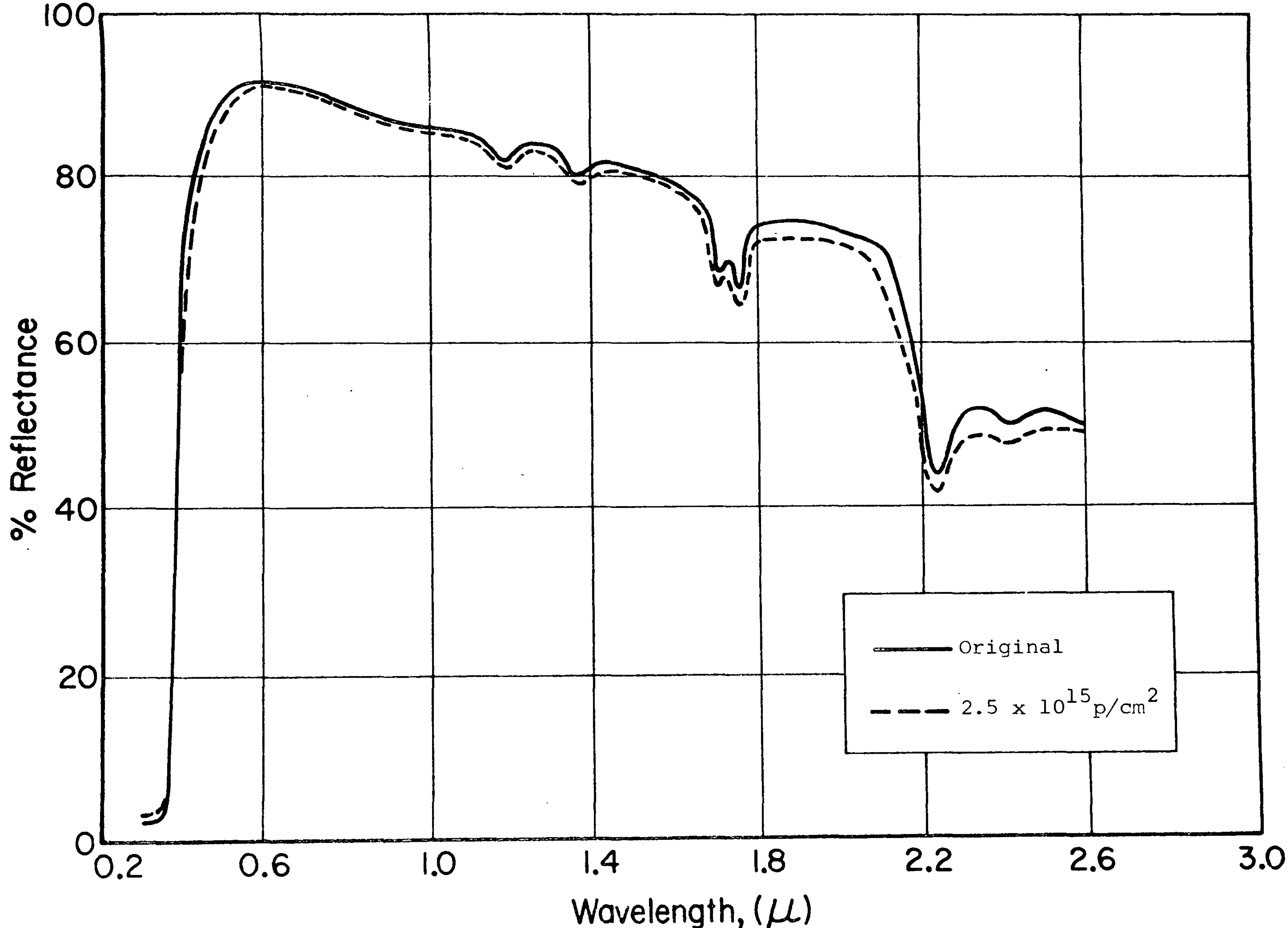

Figure 133 EFFECT OF PROTONS ON S-13G

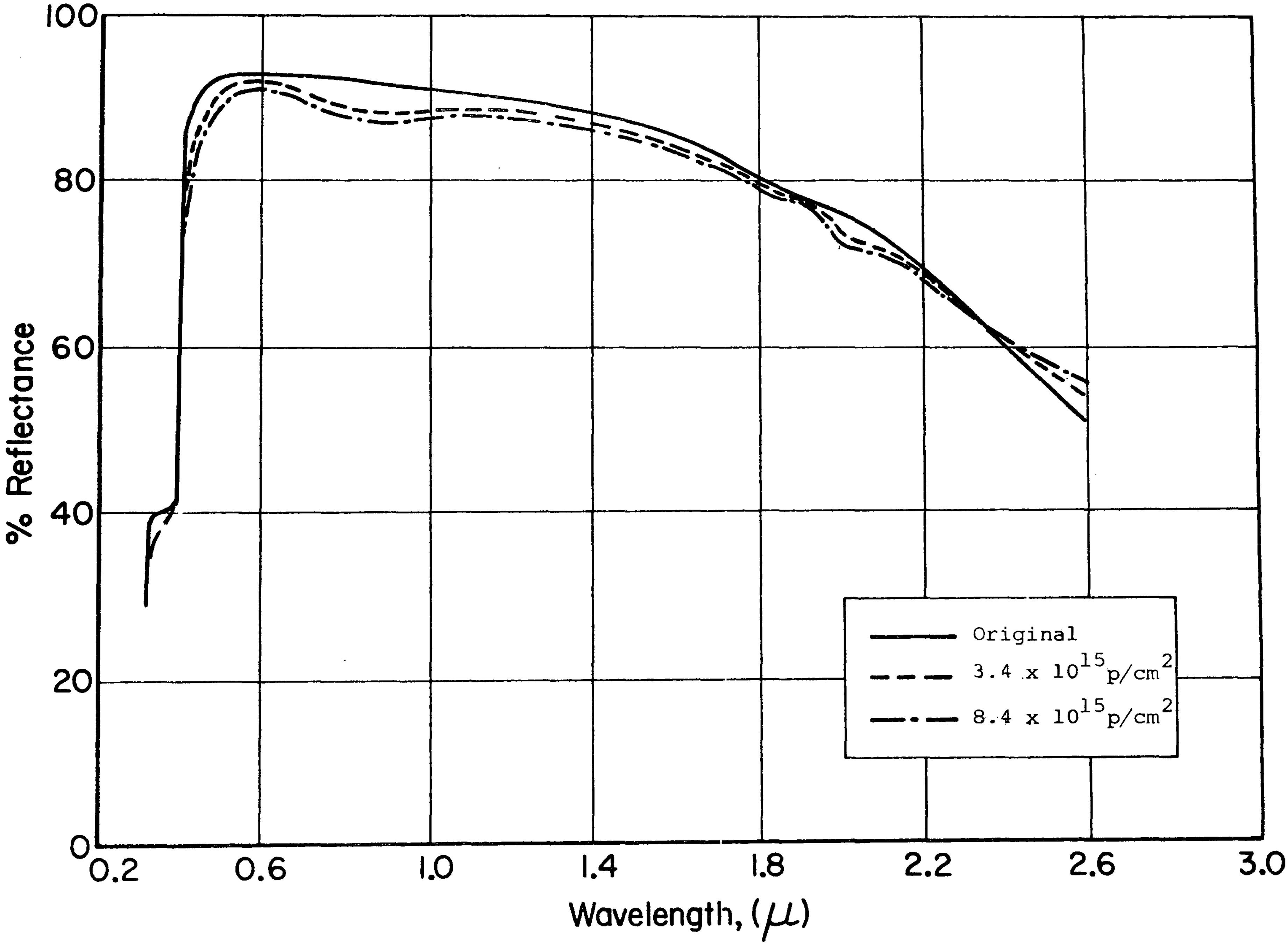

Figure 134 EFFECT OF PROTONS ON B-246 SILICATE PAINT

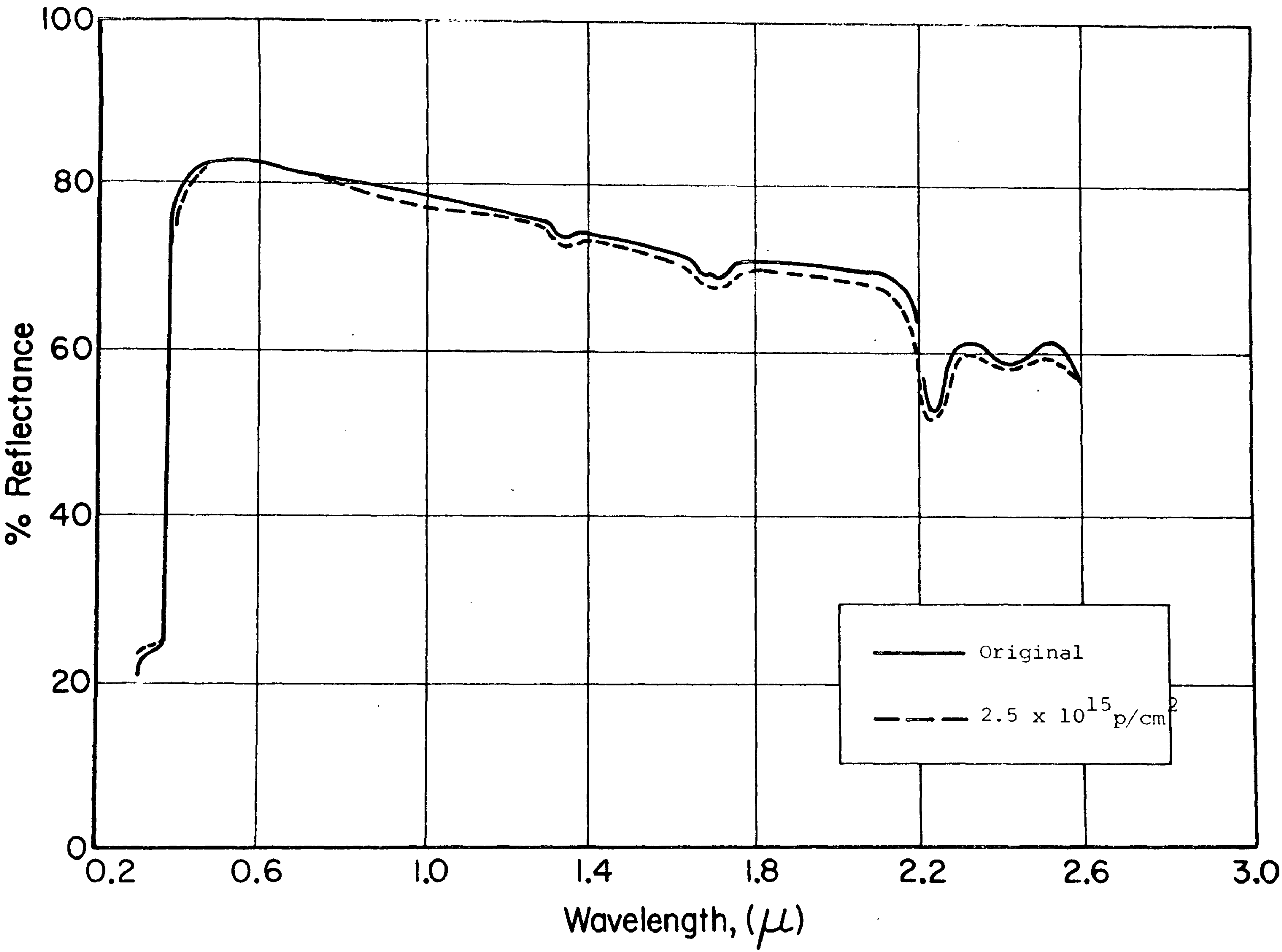

Figure 135 EFFECT OF PROTONS ON B-252 SILICONE PAINT

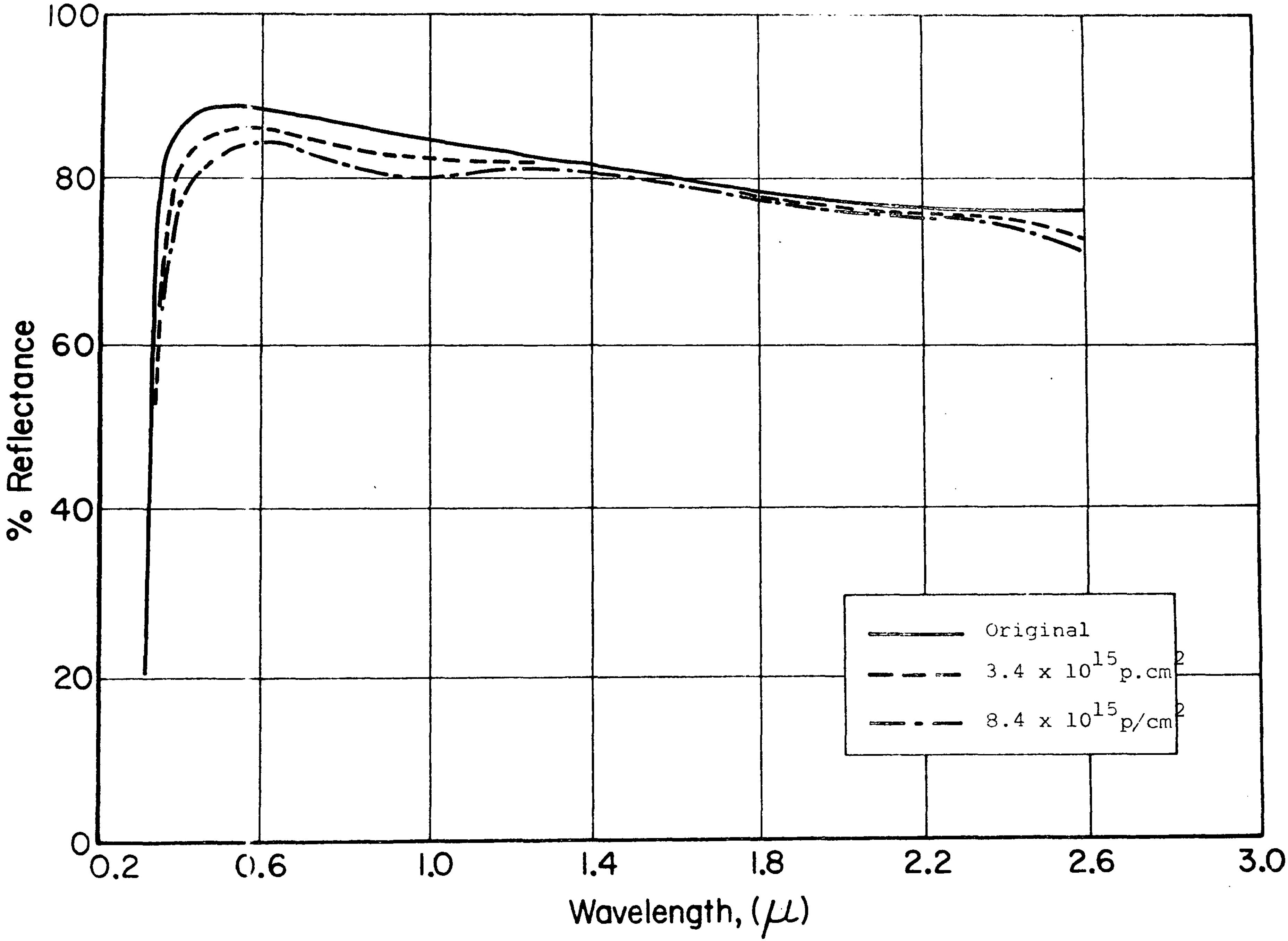

Figure 136 EFFECT OF PROTONS ON B-174 Zn_2TiO_4

$$O_x^{-n} + Ti^{+4} \xrightarrow{h\nu} xO^{-(n-1)} + Ti^{+3} \qquad (13)$$

from occurring, yielding an EPR-observable center and the concomittant broad 950-nm absorption band observable by in situ optical spectroscopy. The 950-nm absorption band is fast oxygen bleachable. On the basis of gas adsorbate kinetic studies reported earlier (Ref. 2), we have shown that the oxygen bleaching process associated with the 950-nm absorption peak depends upon the one-fourth power of oxygen pressure. Since the pressure dependencies of O_2^-, O^- and $O^=$ adsorption are n = 1, 0.5 and 0.25, respectively, we previously concluded that Equation 13 can be rewritten to represent a 2-step bleaching reaction

$$O + 2Ti^{+3} \longrightarrow O^= + 2Ti^{+4} \qquad (14)$$

Similarly, the infrared damage that commences (when present) in the 1500-nm region in Zn_2TiO_4 is associated with ZnO that is thermally produced--either by severe heating in air or by plasma annealing at too high a temperature. The presence of ZnO under both thermal circumstances has been observed by EPR spectroscopy and has been confirmed by x-ray powder diffraction. Furthermore, like conduction-electron absorption in ZnO powder (see the discussion in section 8.4.2) the infrared absorption in Zn_2TiO_4 is broad and still increasing at the limits of the near infrared spectrometer employed,* and, more importantly, is fast bleachable with an oxygen pressure dependence of n = 0.5 (Ref. 2).

Of significance is the fact that residual zinc oxide in Zn_2TiO_4, present in the 925°C product, causes the 350-nm absorption (shoulder) in the reflectance spectra, yet does not result in infrared damage on irradiation, even though the conduction electron center is observable by EPR spectroscopy. However, it is not yet settled whether the EPR center(s) observed at g = 1.96 is in fact due to conduction electrons or is due to electrons

*Beckman DK-2 and DK-2A spectrometers.

in shallow traps (Ref. 140). (We stated earlier, however, that the observable infrared optical damage can only be due to conduction electrons.)

Also, whenever the zinc oxide-related ultraviolet shoulder is present at 350 nm, it can be removed by extraction with acetic acid or reaction with sodium acid phosphate, potassium and lithium hexafluorostannate. Conversely, plasma annealing at too high a temperature always causes the bleachable ZnO-like infrared damage to occur, which is usually accompanied by an increase in absorption at 350 nm. However, we have occasionally observed bulk heat treatments and lower temperature plasma annealing experiments that have resulted in apparently anomalous behavior since conduction electron absorption in the infrared is increased at the same time that the ZnO-related shoulder at 350-nm is reduced, and even eliminated.

Apparently these observations relate to the location of the free ZnO on, in or beneath the Zn_2TiO_4 surface. The ultraviolet and near-infrared spectra, as well as EPR spectra, relate to the concentration of ZnO-related species required to be <u>seen</u> by the three spectroscopic techniques (ultraviolet, infrared and EPR). Residual zinc oxide must reside in the crystal sufficiently below the surface so that it is protected from the electrons remaining after hole/oxygen$_{ads}$ coupling. However, the ZnO is still seen as a 350-nm shoulder since the edge of Zn_2TiO_4 is at 325-nm compared with ZnO's 385-nm wavelength. On the other hand, if created <u>thermally</u> by

$$Zn_2TiO_4 \xrightarrow{\Delta} ZnTiO_3 + ZnO \qquad (15)$$

and

$$ZnTiO_3 \xrightarrow{\Delta} TiO_2 + ZnO, \qquad (16)$$

ZnO may be on the surface in sufficient concentration to permit the necessary quantity of electrons to be associated with the (delocalized) conduction band, such that these conduction electrons are infrared observable, but in insufficient concentration to be seen by ultraviolet spectroscopy.

It should be emphasized that proper plasma annealing results in a pigment without either conduction-electron damage in the infrared or Ti^{+3}-related damage at 950-nm.

8.7.2 Surface Treatments

Reactive encapsulation with potassium silicate, and with potassium and lithium hexafluorosilicate, potassium hexafluorostannate, and potassium silicotungstate, substantially reduces the Ti^{+3}-related damage in Zn_2TiO_4 observed at 950-nm. Heat treatment of the reactively-encapsulated Zn_2TiO_4 powders totally eliminates the possibility of damage at 950-nm for all treatments. Of these, surface treatment with lithium and, especially, potassium hexafluorosilicate stabilizes zinc orthotitanate in the entire solar spectrum. Potassium silicate paints prepared from the reactively encapsulated pigment were all quite stable with the potassium hexafluorosilicate-treated Zn_2TiO_4 producing a paint of exceptional stability ($\Delta\alpha_s$ of 0.002 in 1000 ESH) and solar reflectance ($\alpha_s < 0.12$).

Reactive encapsulation of zinc orthotitanate did not, by itself, result in stable silicone paints based on Owens-Illinois 650 resin. Indeed, these paints exhibit greater damage to ultraviolet irradiation at 950-nm than the pigment powders alone. However, plasma annealing (ΔT = 1670°C) of reactively-encapsulated Zn_2TiO_4 (silicated and phosphated) not only resulted in a pigment that exhibited no damage, but the Owens-Illinois 650 silicone paints produced therefrom exhibit a $\Delta\alpha_s$ of zero in 2500 ESH of ultraviolet radiation in vacuum.

We believe, on the basis of the optical spectroscopy reported here, and EPR studies to be reported later, that the treatments with potassium silicate and hexafluorosilicate provide a barrier to photodesorption of oxygen, as with zinc oxide, wherein the holes are captured by the polynegative anion, thus preventing the photodesorption of O^- and $O^=$ (or O_2^-) by reaction (12).

We attribute the failure of the reactive encapsulants $K_2O \cdot SiO_2$ and K_2SiF_6 to protect the Zn_2TiO_4 (in silicone paints) from 950-nm damage as being due to the interaction with the pigment surface of the free radicals formed in the Owens-Illinois 650 silicone resin (a triethoxymethylsilane condensation product) on ultraviolet irradiation. A <u>possible</u> mechanism might be written as a two step process:

1.

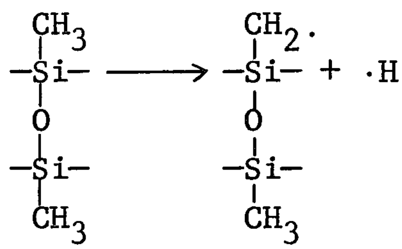

(17)

2. $\cdot H + Ti^{+4} \longrightarrow Ti^{+3} + H^+,$ (18)

--a process that is precluded by plasma annealing of Zn_2TiO_4-- especially if the pigment is first silicated. We believe that, although oxygen species hydrogen-bonded to the surface hydroxyl groups can reduce the surface before plasma annealing, the removal of the hydroxyl groups by plasma annealing and subsequent alteration of the surface, combined with the reactive encapsulant, results in a very different kind of reduction chemistry, certainly involving the free radicals produced in the silicone matrix. Ultimately, the oxygen species, though capable of reducing the surface by itself, most importantly acts as a shuttle for electrons provided by the matrix. Hence, removal or alteration of oxygen species from the surface is the removal of the conduit rather than the predominant source of damaging electrons.

8.8 Summary

In summary, both water and carbon dioxide, among other species, are highly absorbed on the surface of zinc orthotitanate.

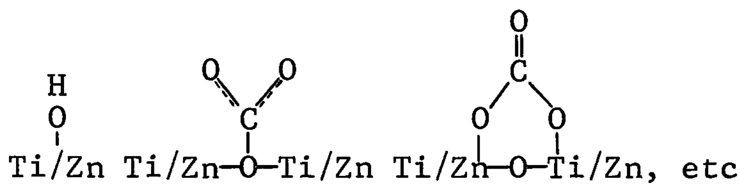

, etc. (19)

We believe that these species promote the association of O^- and $O^=$, as well as O_2^-, on the surface, the photodesorption of which allows an electron to be injected into the surface where, in the case of zinc oxide, it is available for conduction absorption (i.e., broad based, free-carrier absorption) and, in the case of zinc orthotitanate, where it is available for reduction of Ti^{+4} to Ti^{+3}. This concept is wholly consistent with the considerable improvements obtained by plasma annealing and reactive encapsulation of zinc orthotitanate. Plasma annealing dehydroxalates the surface (and oxidizes adsorbed carbonate, as well), thus reducing the sites for absorbed O^- and $O^=$. Similarly, reactive encapsulation is thought to tie up the surface, and again, the availability of sites for absorption of O_x^{-n} is greatly diminished. Thus, photodesorption of oxygen and the injection of an electron into the lattice surface is precluded and ultraviolet-induced damage does not occur.

The role of ferro/ferricyanide in militating against ultraviolet-induced damage in Zn_2TiO_4 powder and Zn_2TiO_4-pigmented <u>silicate</u> (but not in silicone) paints, and in proton-induced damage in Zn_2TiO_4-pigmented <u>silicone</u>, is of interest. This seeming disparity is rationalized in the following manner: The iron cyanide treatment described by Morrison et al (Ref. 145), and later by Sancier (Ref. 140), as providing a high capture cross section for electrons, has not in our studies, as he predicts from his studies of the defect state, provided an effective means of stabilizing ZnO (or, Zn_2TiO_4) to ultraviolet-induced reflectance degradation in vacuum. (It should be pointed out, however, that Sancier* has suggested that we might obtain greater effectiveness at an order of magnitude greater concentration of Fe^{++}/Fe^{+++} in the treatment solution. We point out, however, that this treatment has a deleterious effect on solar reflectance at the concentrations we employ and an increased level of Fe^{++}/Fe^{+++} would seriously impair the reflectance of these coatings.)

The effectiveness of the iron cyanide treatment in stabilizing Zn_2TiO_4 to ultraviolet irradiation at high temperature and proton irradiation as a silicone paint is, however, noteworthy, and is attributed to the electron capture cross section of the Fe^{++}/Fe^{+++} couple. Ultraviolet irradiation of the silicate paint at high temperature (~160°C) changes the kinetics of silicate damage, and, most probably the character, with the result that ionization (as opposed to excitation) of the silicate occurs, injecting electrons into the surface of the Zn_2TiO_4 where the following reaction is enhanced.

$$e + Ti^{+4} \longrightarrow Ti^{+3} \qquad (20)$$

Likewise, proton irradiation, which results in the production of an ionization track in the methyl silicone, along with secondary electrons are produced (a cascade phenomenon), also furnishes electrons for the reduction of Ti^{+4}. In both cases, the presence of the ferro/ferricyanide provides a barrier to Ti^{+4} reduction by the capture of the electrons that are produced in the binder (silicate in the case of high temperature ultraviolet irradiation and silicone in the case of proton irradiation).

Although it is obvious from this discussion that these studies have posed more questions than have been answered, the efficacy of surface treatment by reactive encapsulants and/or plasma annealing, has been firmly established. These techniques offer a very promising and practical approach to the stabilization of the

---

*Private communication.

semiconductor pigment zinc orthotitanate. It is obvious that a total-system (pigment plus binder) approach is required and that this approach has indeed led to the degree of success achieved--namely the development of an ultraviolet-stable Zn_2TiO_4-pigmented potassium silicate paint having a nominal solar absorptance of 0.1, and a cleanable, hard-finish silicone paint of $\alpha_s \sim 0.16$, also of exceptional ultraviolet stability. (Although we would not hesitate to employ the potassium silicate paint on spacecraft at this time, the utilization of the silicone paint must await improved plasma annealing capabilities and the improvement in the physical characteristics of Owens-Illinois 650 resin, which is currently being studied under a current contract.*

Finally, we believe that the potential for stabilizing zinc orthotitanate paints to ionizing charged-particle radiation has at least been suggested and that a different surface treatment, employed in addition to the "hole-capturing" reactive encapsulants, may be required ultimately to do so.

---

*IITRI Project C6233, NASA-MSFC Contract NAS8-26791.

9. RESULTS OF COMBINED RADIATION TESTING EMPLOYING THE CREF

9.1 Proton Irradiation Only

9.1.1 Irradiation Conditions

The results of two solar-wind simulation tests are presented. The figures shown (Figures 137 through 142) represent the form in which the in situ hemispherical reflectance data are displayed. The data, taken with a Beckman DK-1 strip recorder, are typical of those taken with the basic IRIF-II ultraviolet facility.

The irradiations were performed at a pressure of 1×10^{-7} torr and at a specimen temperature of 12°C. Reflectance measurements were performed in-situ, initially at $\sim 6 \times 10^{-8}$ torr pressure. Three specimens were irradiated in each test (Figures 137, 139 and 142 in one test and Figures 138, 140 and 141 in the other). The important conditions and parameters employed in these irradiation tests are listed in Table 47.

9.1.2 Results

The effects of proton irradiation on zinc oxide and the two specification paints based on zinc oxide, Z93 and S-13G, are shown in Figures 137 through 139 respectively. The data are summarized in Table 47. Examinations of the damage spectra show that the SP500 zinc oxide powder underwent damage in both the visible and infrared regions of the spectrum: The Z93 specimen sustained similar, but slightly diminished, damage in these two regions. Surprisingly, the S-13G exhibited only slght damage in the visible spectrum; damage in the infrared was only slightly less than for the Z93 specimen.

The effects of proton irradiation on zinc orthotitanate pigments and paints are presented in Figures 140 through 142. Again, the pigment powder (in this case an early plasma-calcined Zn_2TiO_4), Figure 140, exhibited the greatest damage in the visible spectrum, while the silicone paint (in this case based on Owens-Illinois 650 resin) exhibited no visible-region damage. The acid phosphate-treated pigment prepared as a potassium silicate paint (Figure 141)

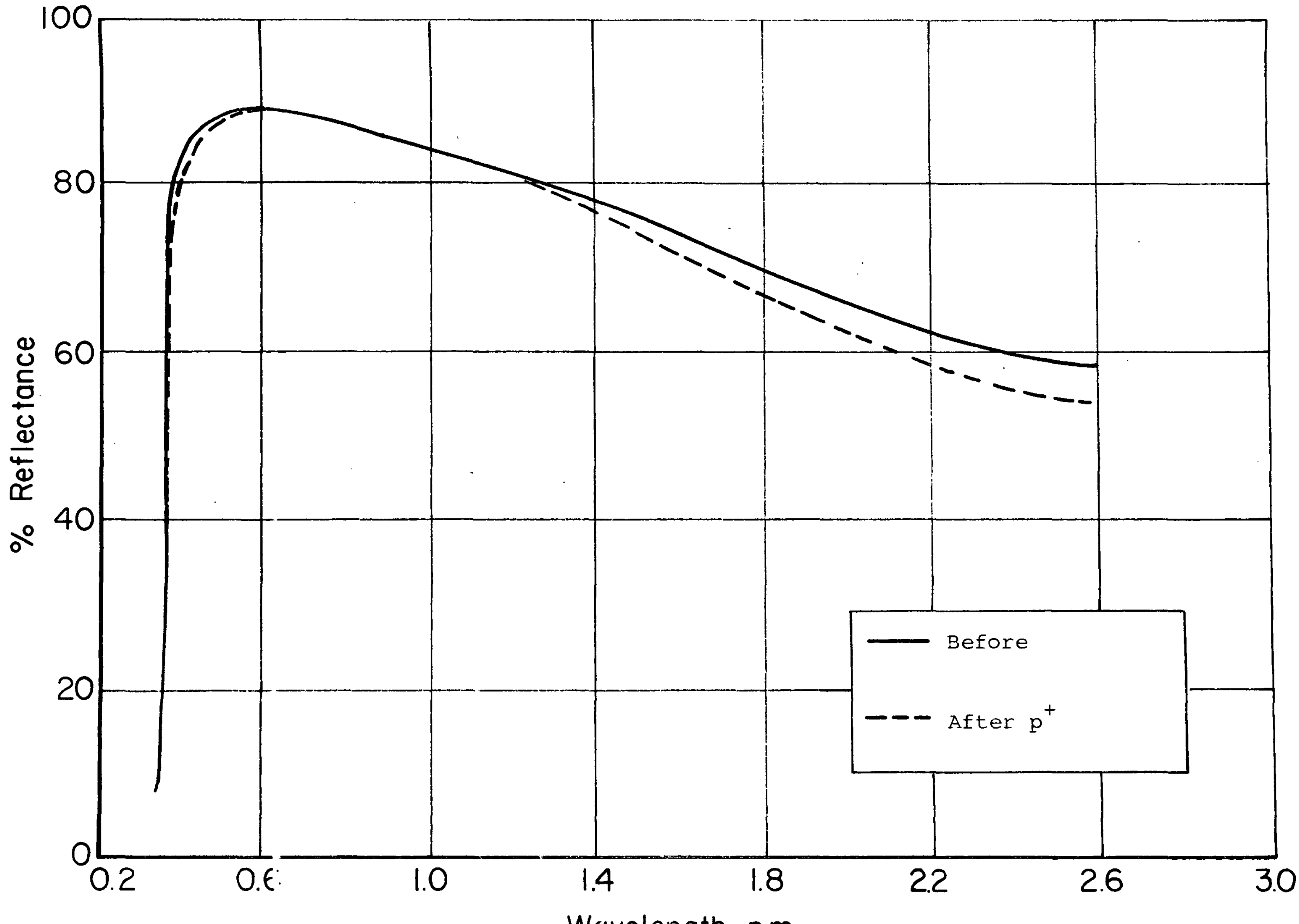

Figure 137 PRE- AND POST-IRRADIATION REFLECTANCE SPECTRA OF ZnO POWDER

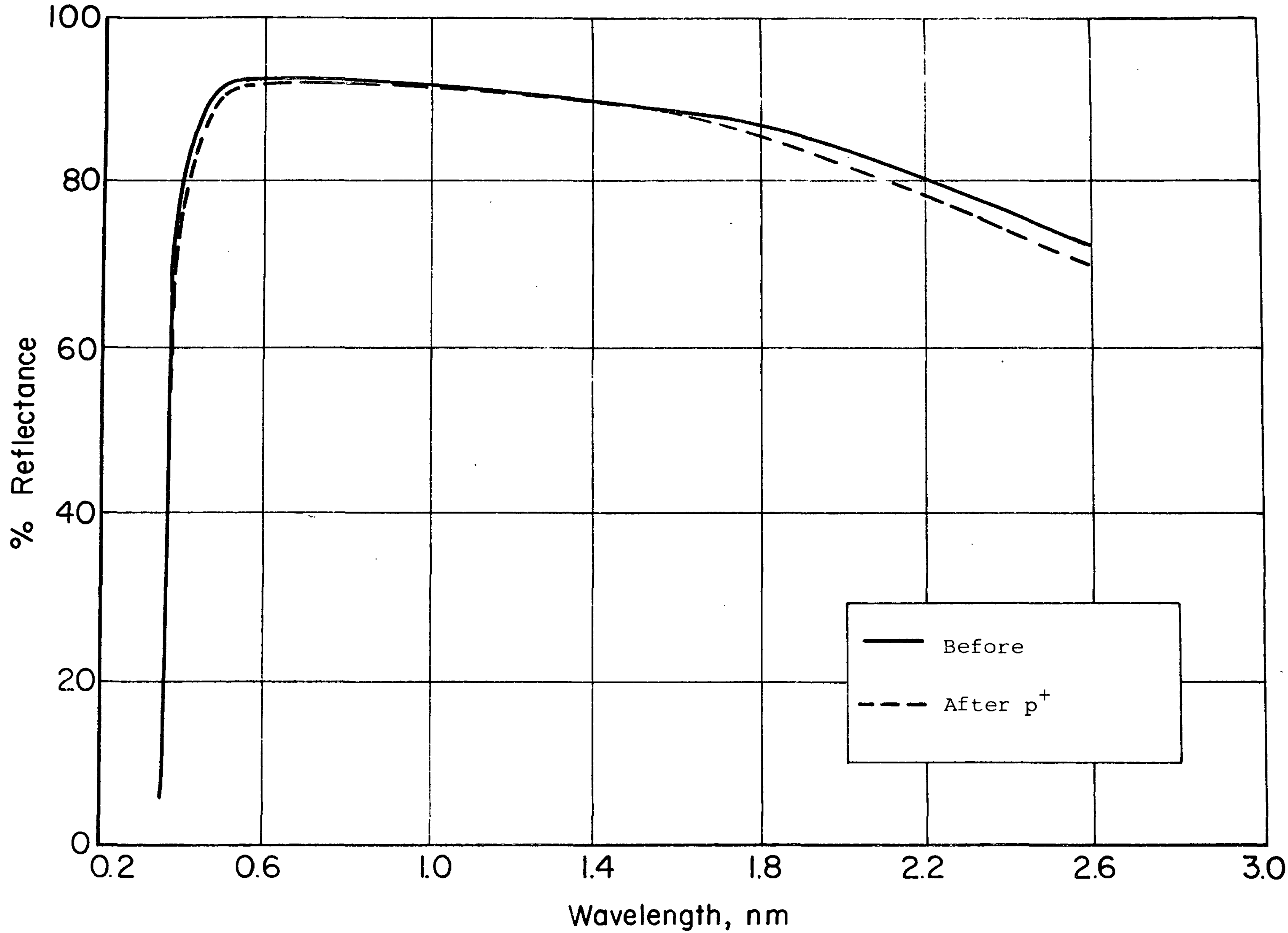

Figure 138 PRE- AND POST-IRRADIATION REFLECTANCE SPECTRA OF Z-93

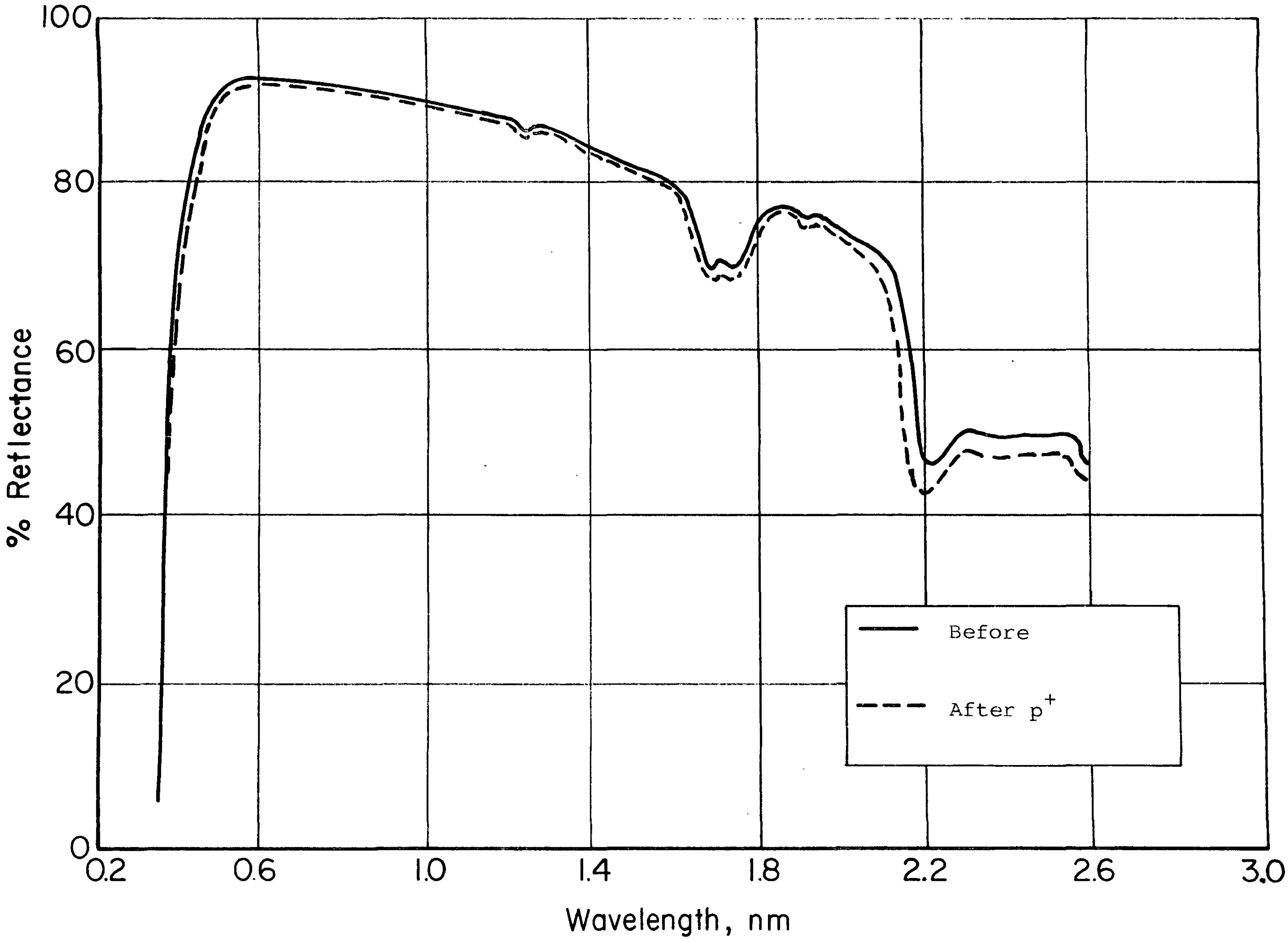

Figure 139 PRE- AND POST-IRRADIATION REFLECTANCE SPECTRA OF S-13G

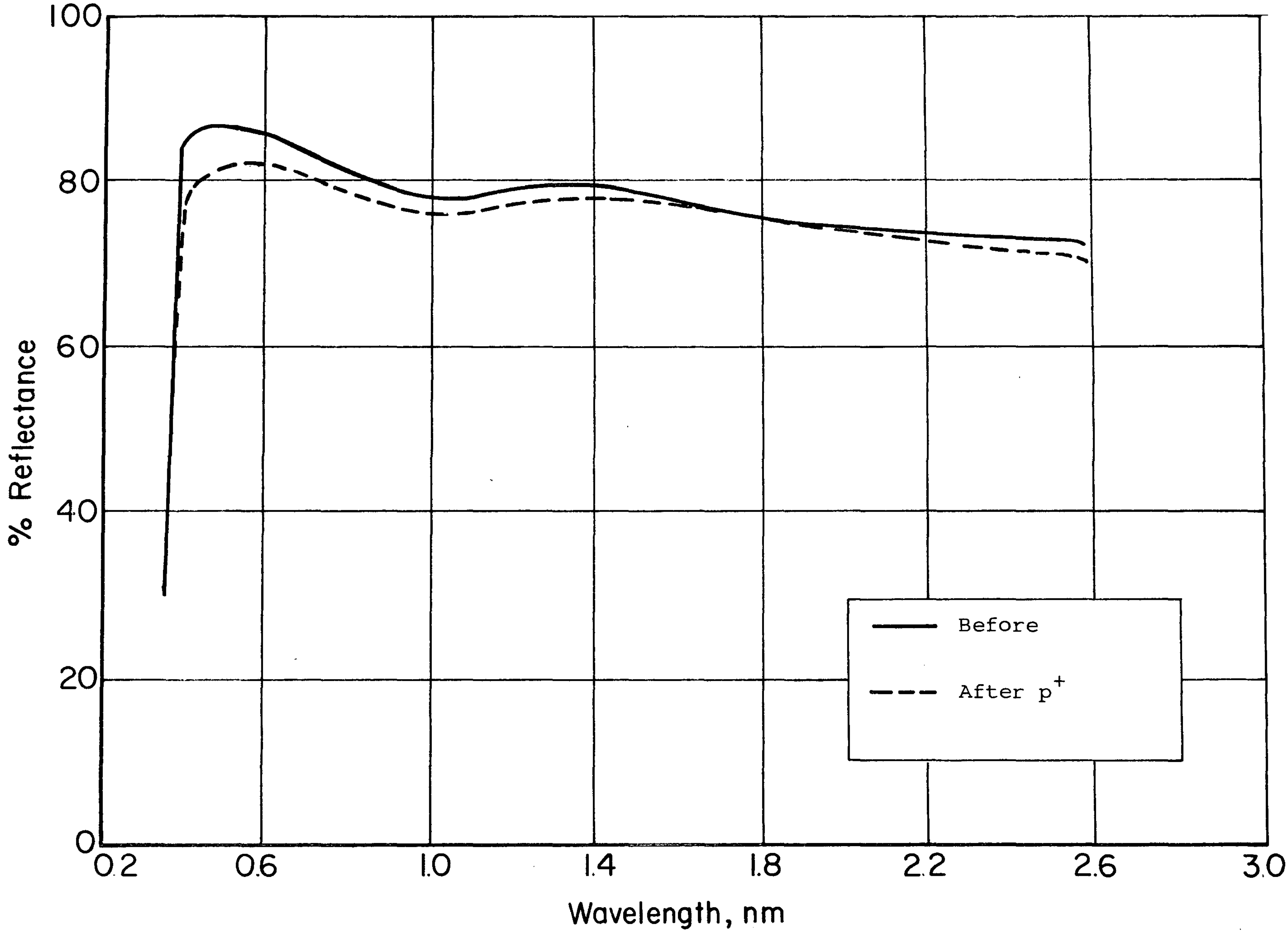

Figure 140 PRE- AND POST-IRRADIATION REFLECTANCE SPECTRA OF Zn_2TiO_4 POWDER

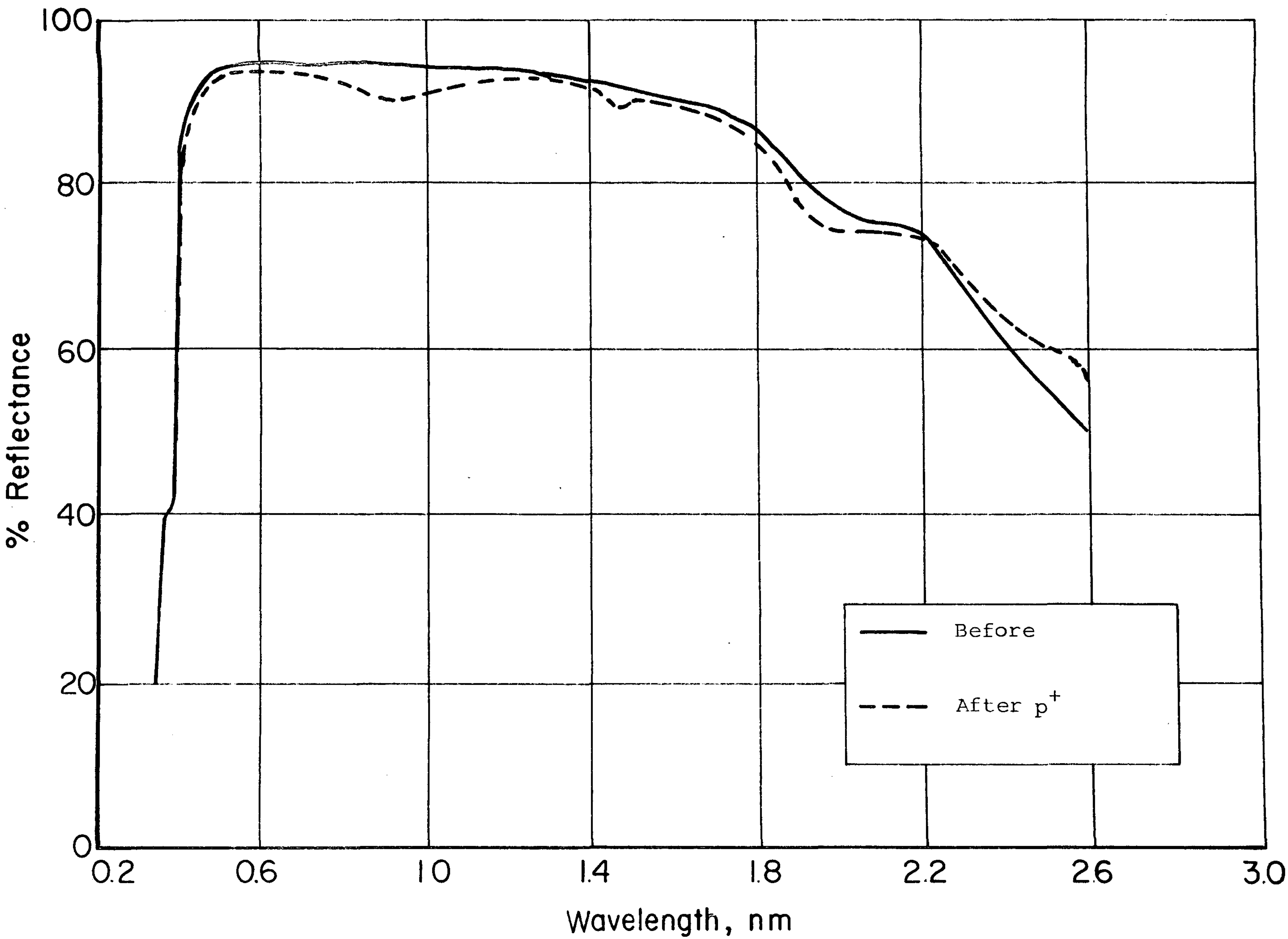

Figure 141 PRE- AND POST-IRRADIATION REFLECTANCE SPECTRA OF Zn_2TiO_4:NaH_2PO_4/PS-7

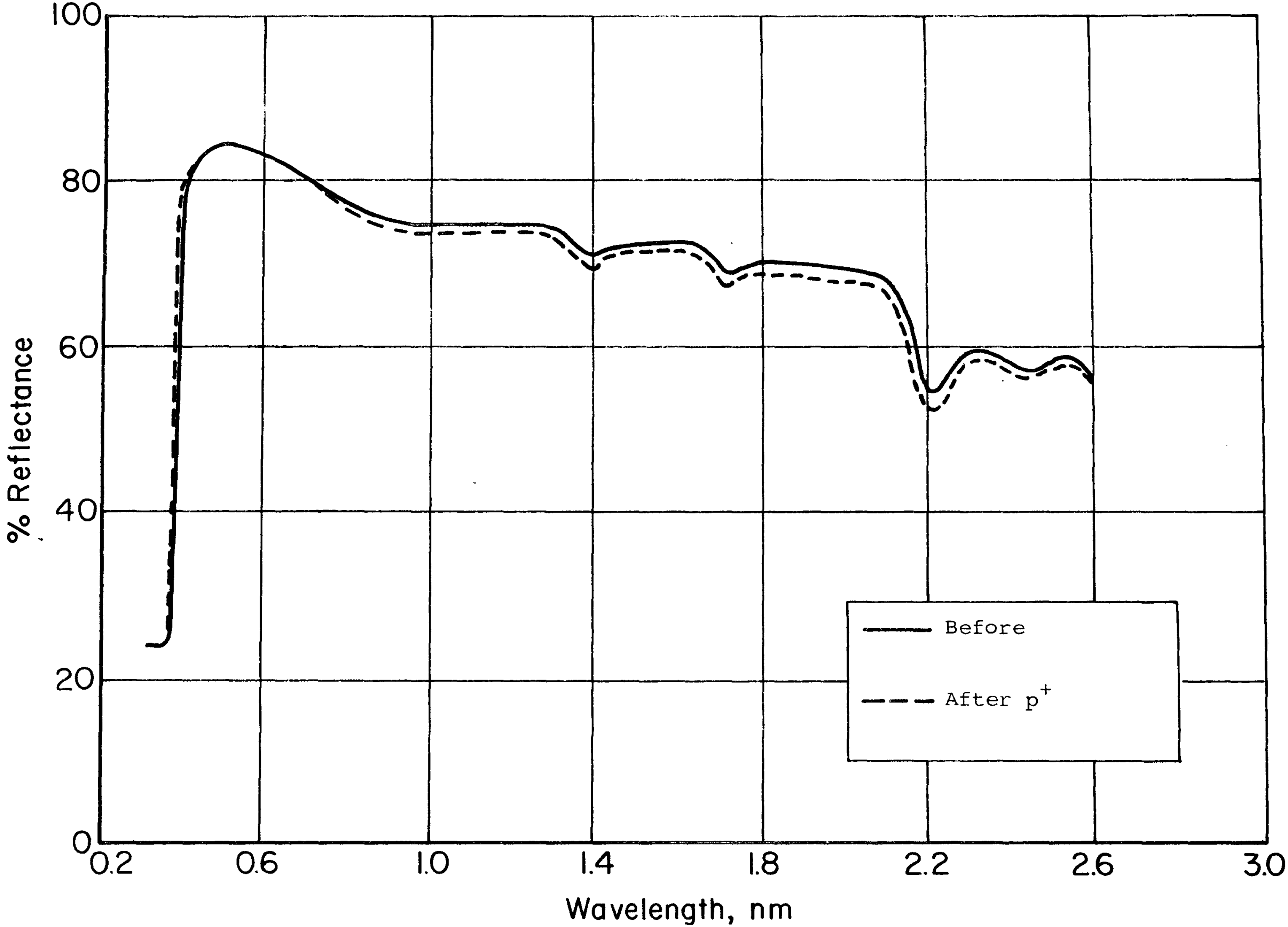

Figure 142 PRE- AND POST-IRRADIATION REFLECTANCE SPECTRA OF $Zn_2TiO_4:Fe^{++}/Fe^{+++}$ CN/OI-650

Table 47

SUMMARY OF PROTON-IRRADIATION DAMAGE

Fig. No.	Material	Proton Exposure (1.2 keV) Fluence 10^{15} p/cm^2	Proton Exposure (1.2 keV) Flux 10^9 p/cm^2-sec	Proton Damage Visible λ_{max} (nm)	Proton Damage Visible ΔR (%)	Proton Damage Infrared λ_{max} (nm)	Proton Damage Infrared ΔR (%)
137	SP500 ZnO	2.5	4.9	425	6.3	2500	6.0
138	Z-93	2.7	5.4	425	5.6	2500	4.0
139	S-13G (B-031)	2.5	4.9	450	1.5	2000	3.2
140	Zn_2TiO_4 (Plasma Annealed)	2.7	5.4	400	5.7	950	2.0
141	Zn_2TiO_4 (NaH_2PO_4-treated) in PS7	2.7	5.4	400	2.0	900	5.0
142	Zn_2TiO_4 (Fe^{++}/Fe^{+++}) in OI-650	2.5	4.9	None		2000	1.5

developed a mildly-intense band at 900-nm wavelength and the powder specimen exhibited a much less-intense band in that wavelength region. The Owens-Illinois 650-resin-based paint prepared from pigment that had been treated with ferric/ferrocyanide exhibited no specific damage at ~900-nm wavelength, and degraded only slightly throughout the infrared region.

9.1.3 Discussion of Results (Protons Only)

Although at this time it is impossible to obtain definitive correlation of preparation and treatment parameters of the zinc orthotitanates with their proton-damage spectra, the behavior of the pure powders versus that of the silicone paints is intriguing. It may be that the binderless pigments are damaged physically by the proton irradiations and develop lattice-strain related damage similar to that attributed to grind of zinc oxide. The explanation might then be that the pigments are physically protected by silicone binders from the "sand-blast" effect of the protons and that the threshhold for damage to the silicone (ionization-wise) is greater than the threshhold for development of a physically induced b-band, as discussed previously by Gilligan (Ref. 74).

The reasons for and results of treatment with potassium ferro/ferricyanide were discussed in Chapter 8. The reader is referred specifically to sections 8.4.3., 8.6 and 8.8.

9.2 Combined Environment Irradiation

9.2.1 Irradiation Conditions

In a second test, the samples were exposed to a series of different irradiation conditions. The irradiations were performed at a pressure of 1 x 10^{-7} torr and at a specimen temperature of 12°C. Reflectance measurements were performed in situ, initially at ~6 x 10^{-8} torr pressure. In the configuration used, all samples were continuously exposed to ultraviolet radiation, but only three at any given time to protons; Table 48 summarizes the sample environment conditions employed in this test. Thus, the ultraviolet exposure sequences were as follows: first,

Table 48

COMBINED TEST EXPOSURE SEQUENCE

Sample No.	Description	Exposure Conditions Part 1* UV + p^+	UV	Part 2* UV + p^+	UV
1	Z-93	X			X
2	S-13G	X			X
3	SP-500 ZnO	X			X
4	Zn_2TiO_4/OI-650		X	X	
5	Zn_2TiO_4/PS-7		X	X	
6	Z-93		X	X	
7	Z-93		X		X
8	S-13G		X		X
9	SP-500 ZnO		X		X
10	Zn_2TiO_4/PS-7		X		X
11	Zn_2TiO_4/OI-650		X		X
12	SP-500 ZnO		X		X

*In Part 1, exposure to ultraviolet and to protons was 600 ESH and 670 EWH (~6 x 10^{14} p^+/cm^2) respectively; in Part 2, the exposure was 700 ESH and 930 EWH (~8.3 x 10^{14} p^+/cm^2).

samples 1, 2 and 3 were exposed, simultaneously to 600 ESH of simulated solar radiation and 670 Equivalent Wind Hours (EWH) of solar wind protons (approximately 6 x $10^{14} p^+/cm^2$). After this irradiation and after measuring the spectral reflectance of all 12 samples again, samples 4, 5 and 6 were then irradiated simultaneously with protons (p^+) and ultraviolet radiations (930 EWH and 700 ESH, respectively). Samples 7 through 12 all received ultraviolet irradiation only, except that some overlap of the proton beam onto samples 7 and 12 apparently occurred. These latter samples, 7 and 12, were adjacent to samples 6 and 1, respectively.

9.2.2 Analysis of Results - Combined Testing

The effect of combined ultraviolet and proton radiation on ZnO can be seen in Figure 143 in which we have shown its reflectance spectra before and after irradiation. These spectra are to be compared with those in Figure 144, which represents ultraviolet-only effects. Only the infrared spectra are comparable. Both protons and ultraviolet cause infrared damage, but only protons induce visible damage. Significantly the proton-induced ultraviolet/visible damage in ZnO is not oxygen-bleachable. These data, as well as for all 12 specimens, are summarized in Table 49.

S-13G and Z93 both exhibit ultraviolet/visible damage when exposed to ultraviolet radiation, but this is because of optical damage in the silicone and silicate vehicles, respectively. This we can deduce from the lack of any such damage in the pigment alone under the same conditions.

In Part 1 of the combined environment test in which samples 1, 2 and 3 were subjected to simultaneous p^+ and ultraviolet radiations, the Z93 displayed very little damage. An additional 700 ESH in Part 2 had scarcely any effect. In S-13G the additional 700 ESH of ultraviolet produced a little more than half again as much damage; and, not surprisingly, the ultraviolet-visible damage is O_2-bleachable. This is because of a silicone/oxygen reaction.

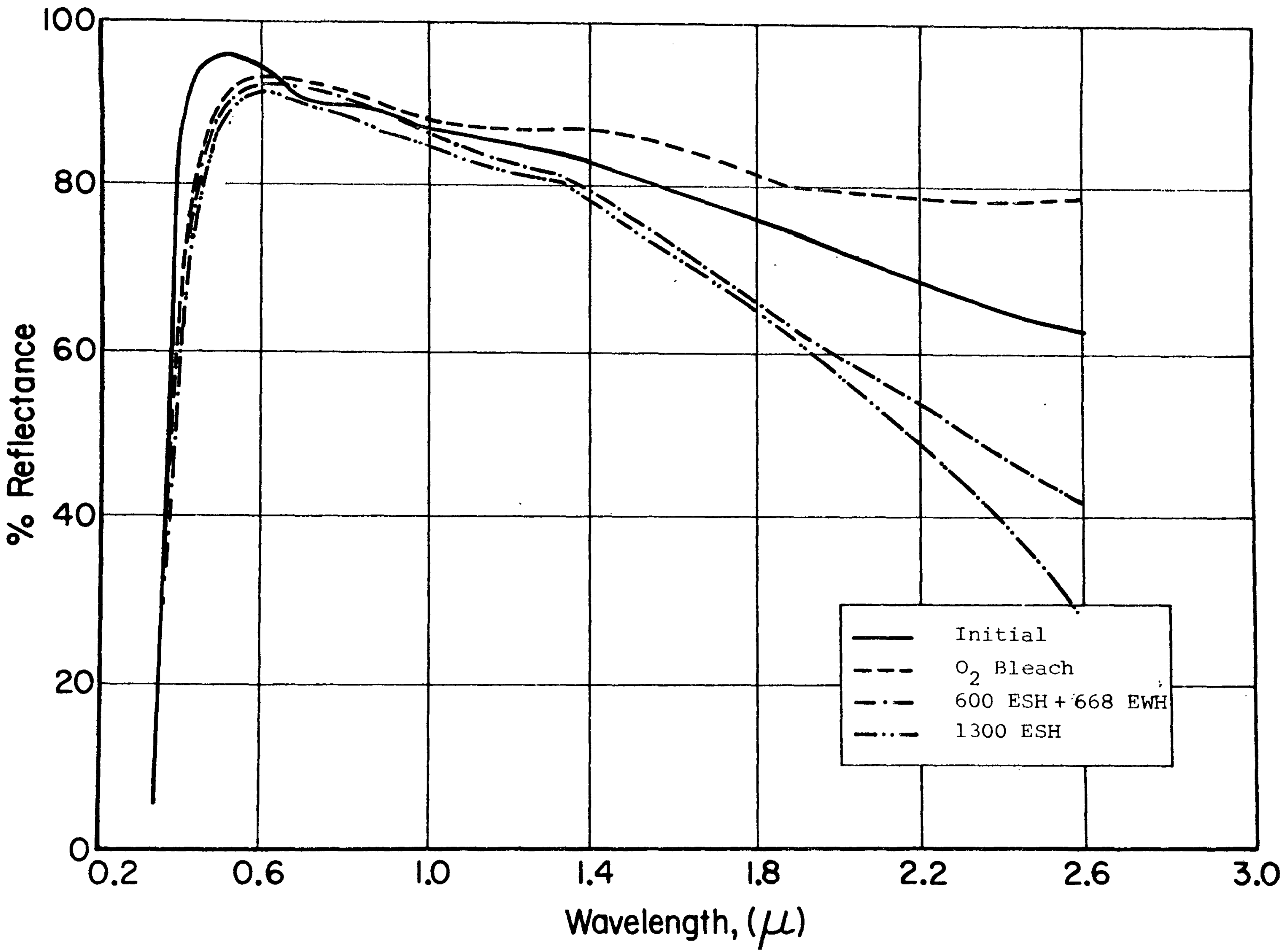

Figure 143 PRE- AND POST-IRRADIATION REFLECTANCE SPECTRA OF SP500 ZnO POWDER

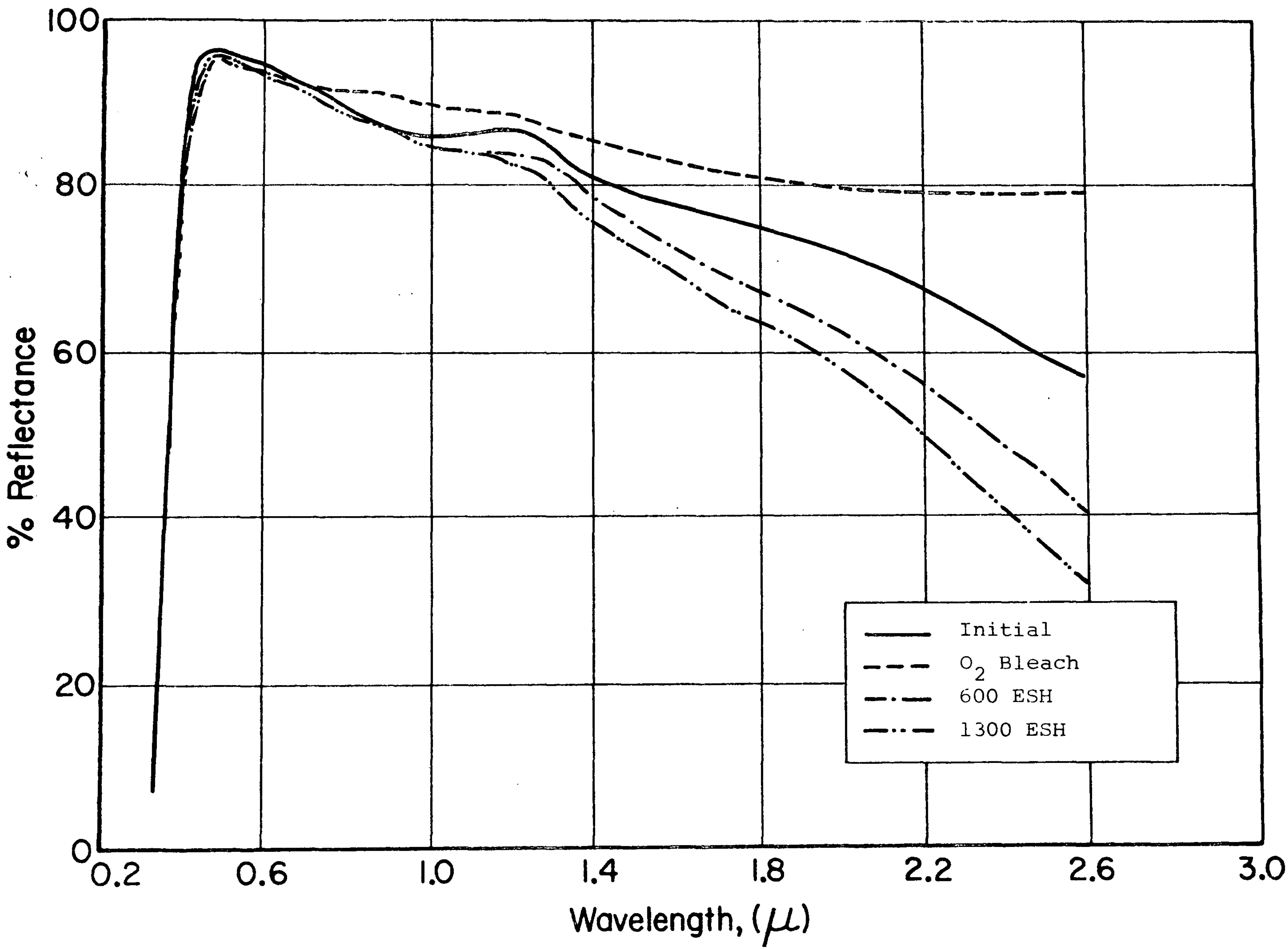

Figure 144 PRE- AND POST-IRRADIATION REFLECTANCE SPECTRA OF SP500 ZnO POWDER

Table 49

SUMMARY OF COMBINED ULTRAVIOLET-PROTON IRRADIATION TEST DATA

Sample No.	Fig. No.	Material	Fluence 10^{15} p/cm^2	Flux 10^9 p/cm^2-sec	Solar Absorptance Changes		
					$UV_1^* + p_1^+$	UV_2^{**}	O_2 Bleach
1	147	Z-93	0.6	1.05	0.012	0.021	0.010
2	150	S-13G	0.6	1.05	0.044	0.065	0.032
3	143	SP500 ZnO	0.6	1.05	0.047	0.064	0.012
					UV_1	$UV_2 + p_2^+$	O_2 Bleach
4	145	Zn_2TiO_4/OI-650	0.83	1.21	0.090	0.113	0.039
5	152	Zn_2TiO_4/PS-7	0.83	1.21	0.033	0.074	0.053
6	148	Z-93	0.83	1.21	0.025	0.057	0.029
					$UV_{1,2}^{***}$		O_2 Bleach
7	149	Z-93	--	--	0.063		0.047
8	151	S-13G	--	--	0.039		0.013
9	144	SP500 ZnO	--	--	0.022		-0.017
10	153	Zn_2TiO_4/PS-7	--	--	0.019		0.010
11	146	Zn_2TiO_4/OI-650	--	--	0.101		0.006
12	154	SP500 ZnO	--	--	0.034		-0.024

*UV_1 p_1^+ - samples 1, 2 and 3 exposed first to 600 ESH and 670 EWH, simultaneously.

**UV_2^{**} - samples 1, 2 and 3 exposed next to additional 700 ESH.

$UV_2 + p_2^+$ - samples 4, 5 and 6 exposed first to 600 ESH, then to 700 ESH + 930 EWH.

***$UV_{1,2}$ - samples 7 through 12, exposed first to 600 ESH then to additional 700 ESH, no protons.

The spectra of zinc orthotitanate in Owens-Illinois 650 resin (Sample #4) shown in Figure 145 indicated that it was exposed to a small "spillage" dose of protons; the sample was in a fringe area during Part 1 of the test. The effect of ultraviolet-only in this material can be seen in Figure 146.

Most significant in these data are the spectral regions in which ultraviolet and protons cause optical damage. In ZnO (Figure 143), protons and ultraviolet cause damage which appears both in the visible and in the infrared regions. Ultraviolet radiation alone, however (Figure 144) produces damage which is predominantly in the infrared, that is, it is essentially free-carrier damage (Ref. 74). The proton induced visible damage, we feel, is due to the "b-band" defect elucidated in Reference 74. The behavior of S-13G and Z93 is consistent with our interpretations of the ZnO damage mechanisms. In these two paint systems, however, the vehicle damage, which occurs primarily in the near ultraviolet and visible regions of the spectrum, adds to the b-band contribution in proton-only and combined ultraviolet-proton irradiations. In ultraviolet-only irradiations, the damage spectra are slightly but yet significantly different from those induced by protons. The slopes of the reflectance spectra in the region of 0.4 - 0.5μ and the O_2-bleaching spectra in this same region clearly indicate these differences. The spectra which result from combined irradiations of component materials often can be predicted on the basis of their behavior in single environments.

Comparing spectra of materials which have been exposed to various sequences of irradiation conditions reveals several important results. Apart from the small differences in total exposure, the only differences in exposure conditions were the sequence of irradiations (see Table 49). Compare the spectra of Z93 in Figures 147, 148 and 149 in which the sequence appears to make a very big difference. Figure 147 shows little visible damage relative to that in Figures 148 and 149. The sample in Figure 147 initially received ultraviolet plus protons, then more

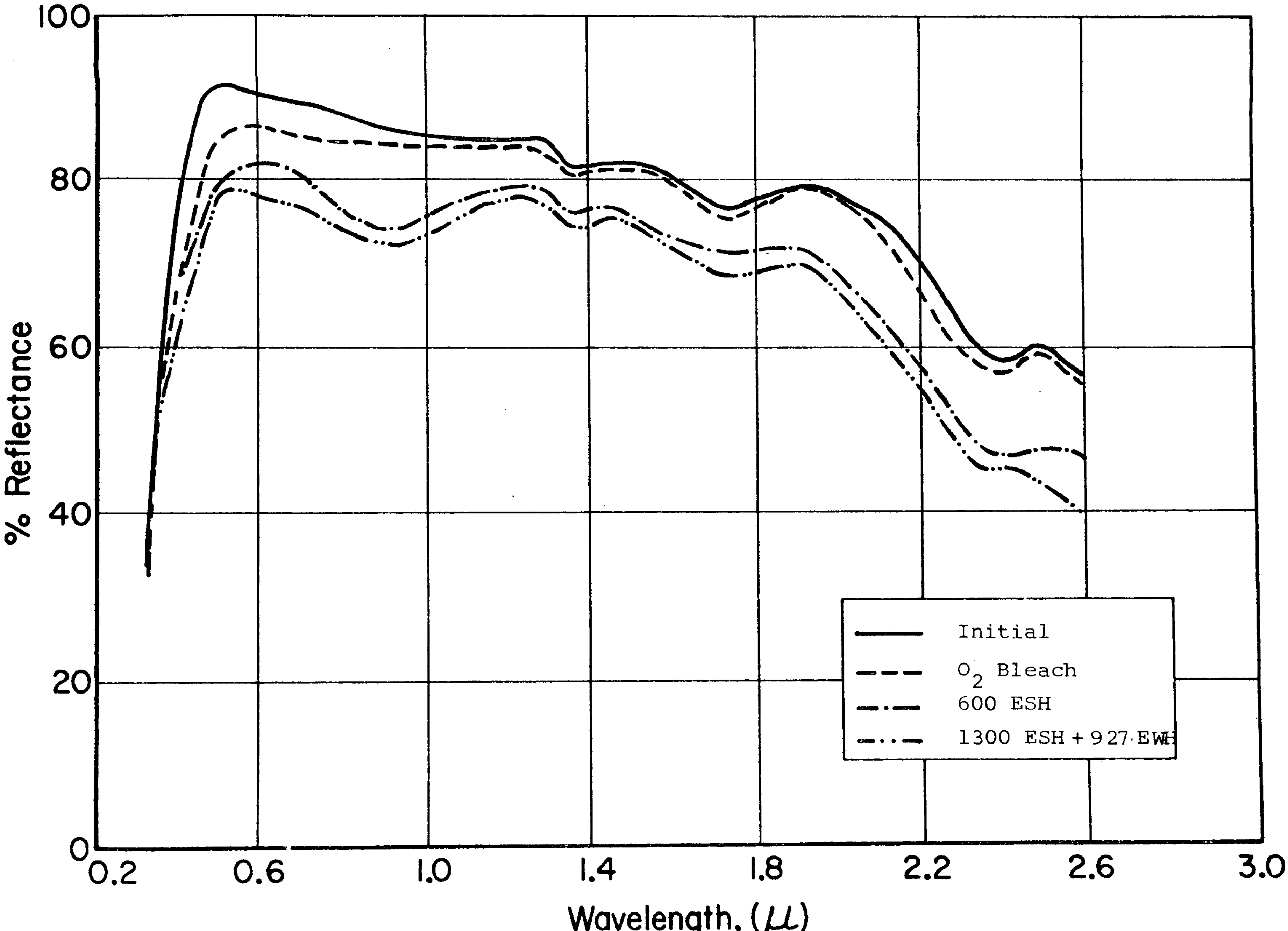

Figure 145 PRE- AND POST-IRRADIATION REFLECTANCE SPECTRA OF Zn_2TiO_4/OI-650

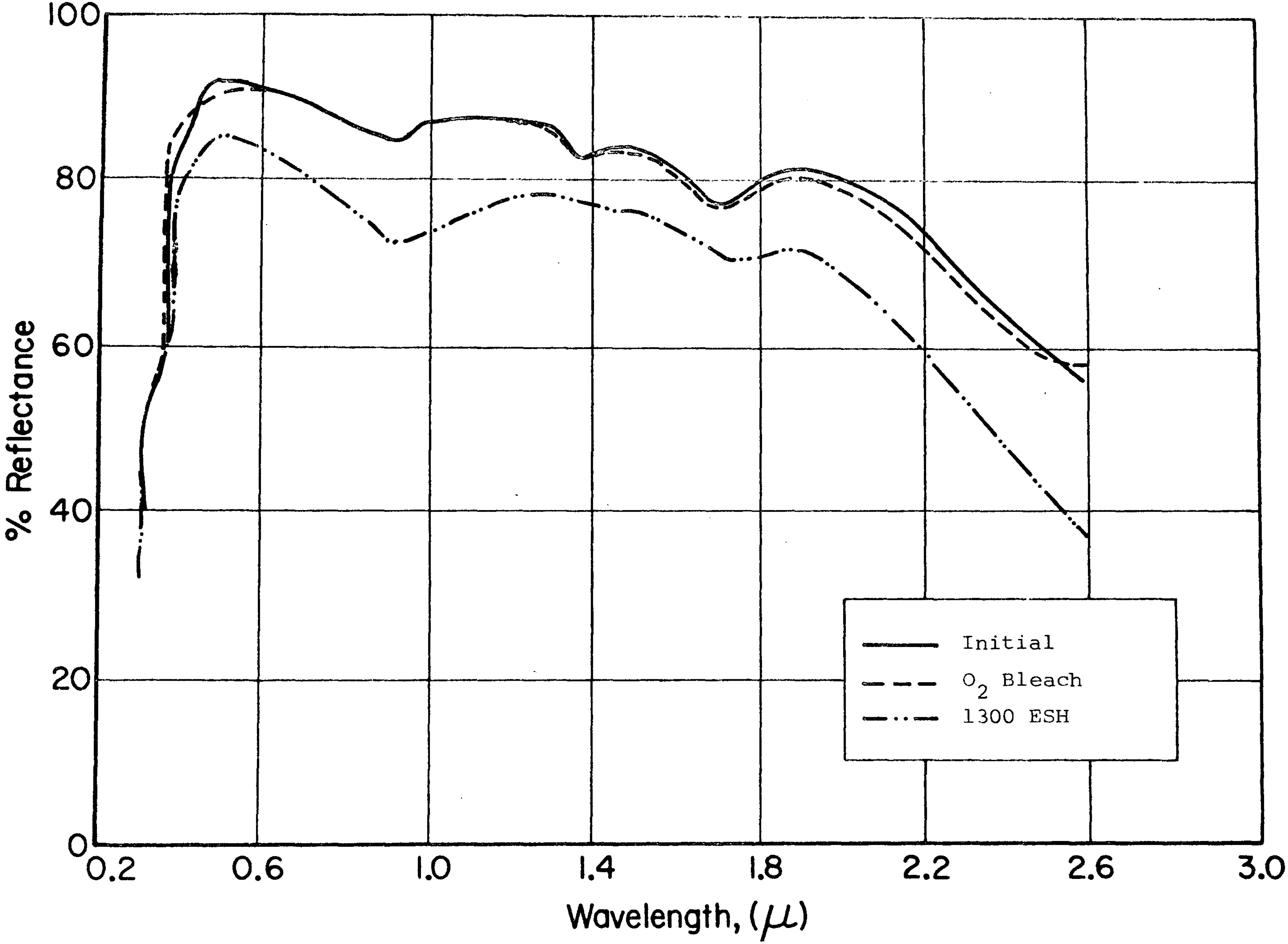

Figure 146 PRE- AND POST-IRRADIATION REFLECTANCE SPECTRA OF Zn_2TiO_4/OI-650

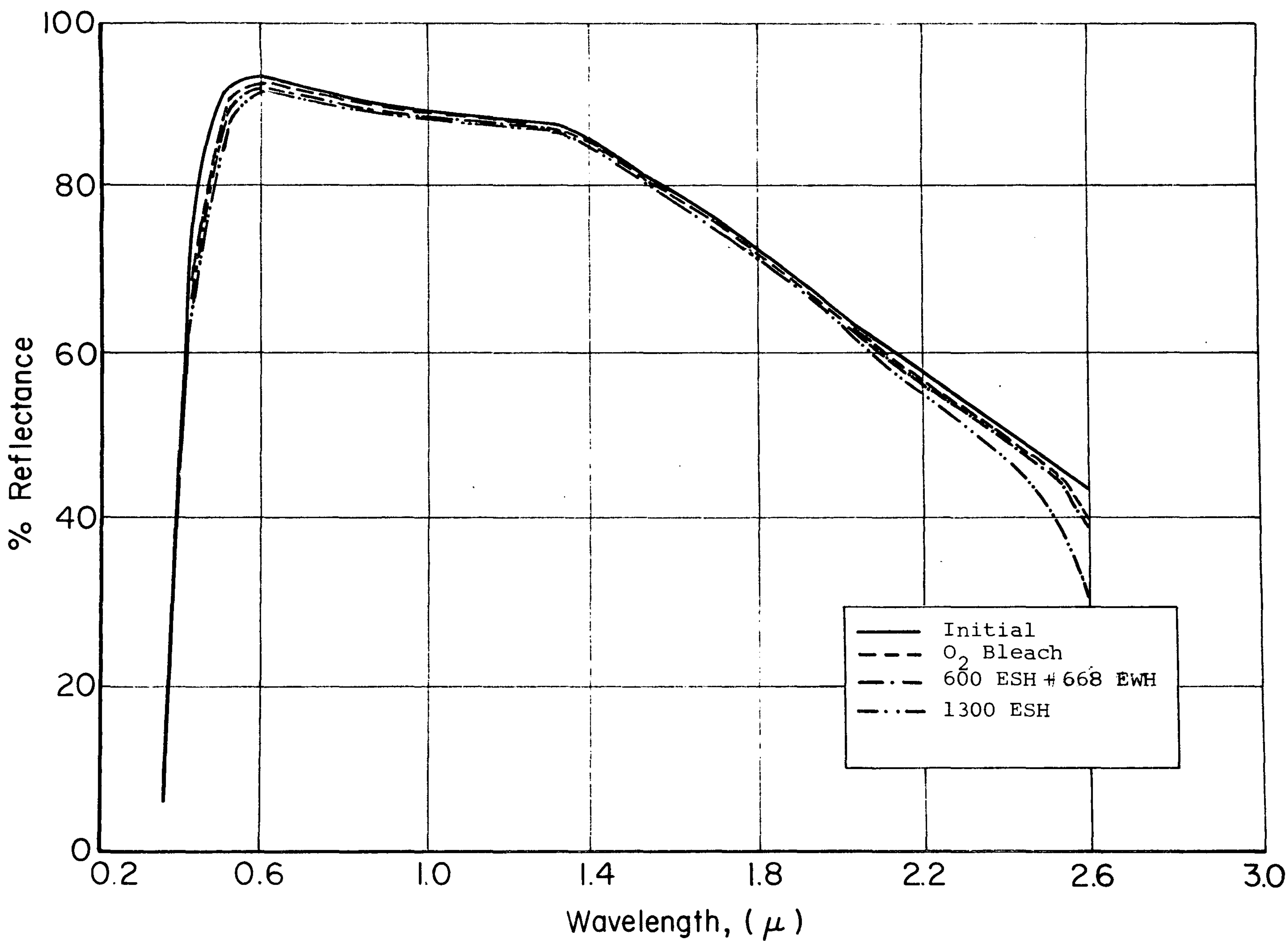

Figure 147 PRE- AND POST-IRRADIATION REFLECTANCE SPECTRA OF Z-93

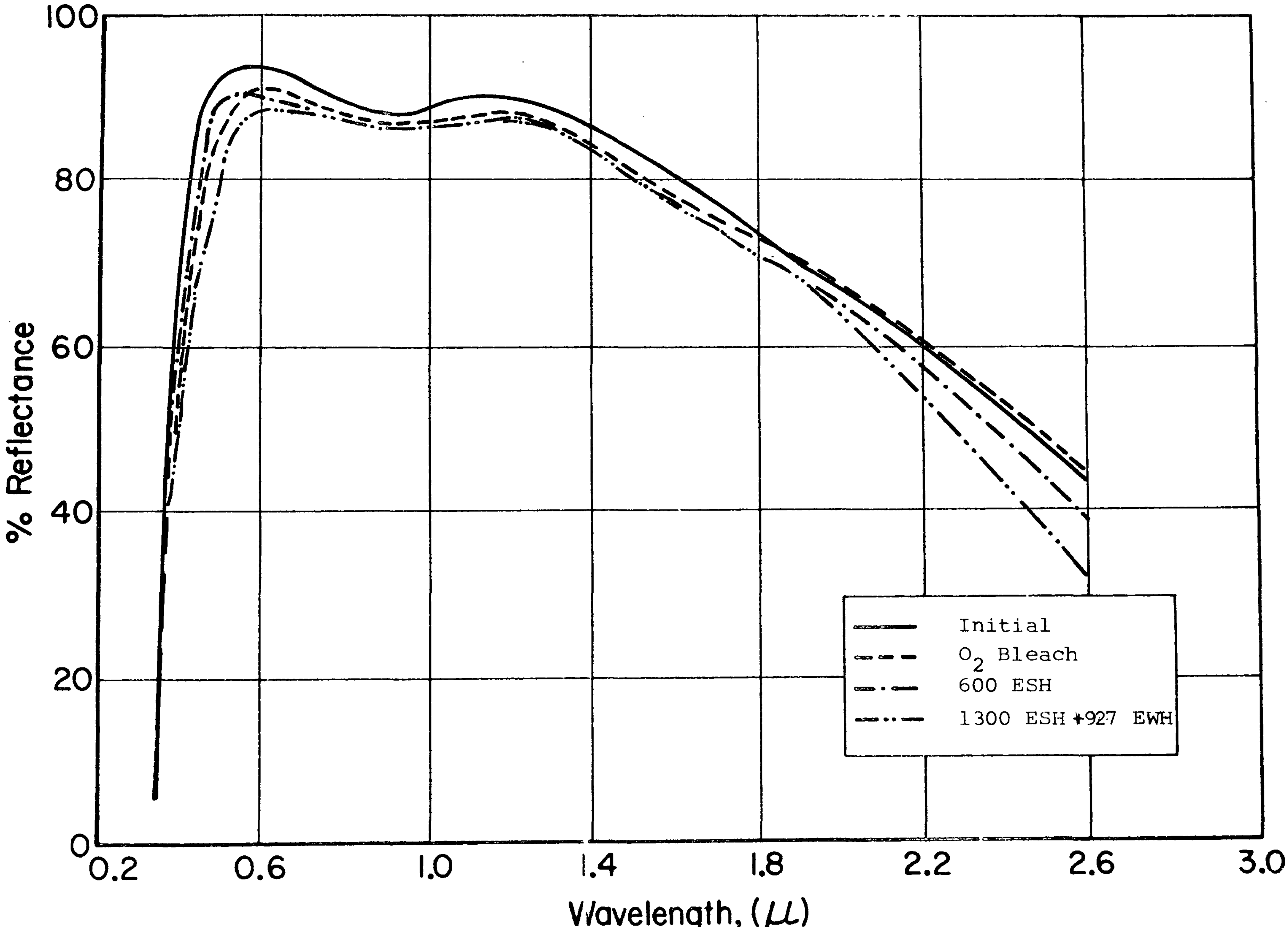

Figure 148 PRE- AND POST-IRRADIATION REFLECTANCE SPECTRA OF Z-93

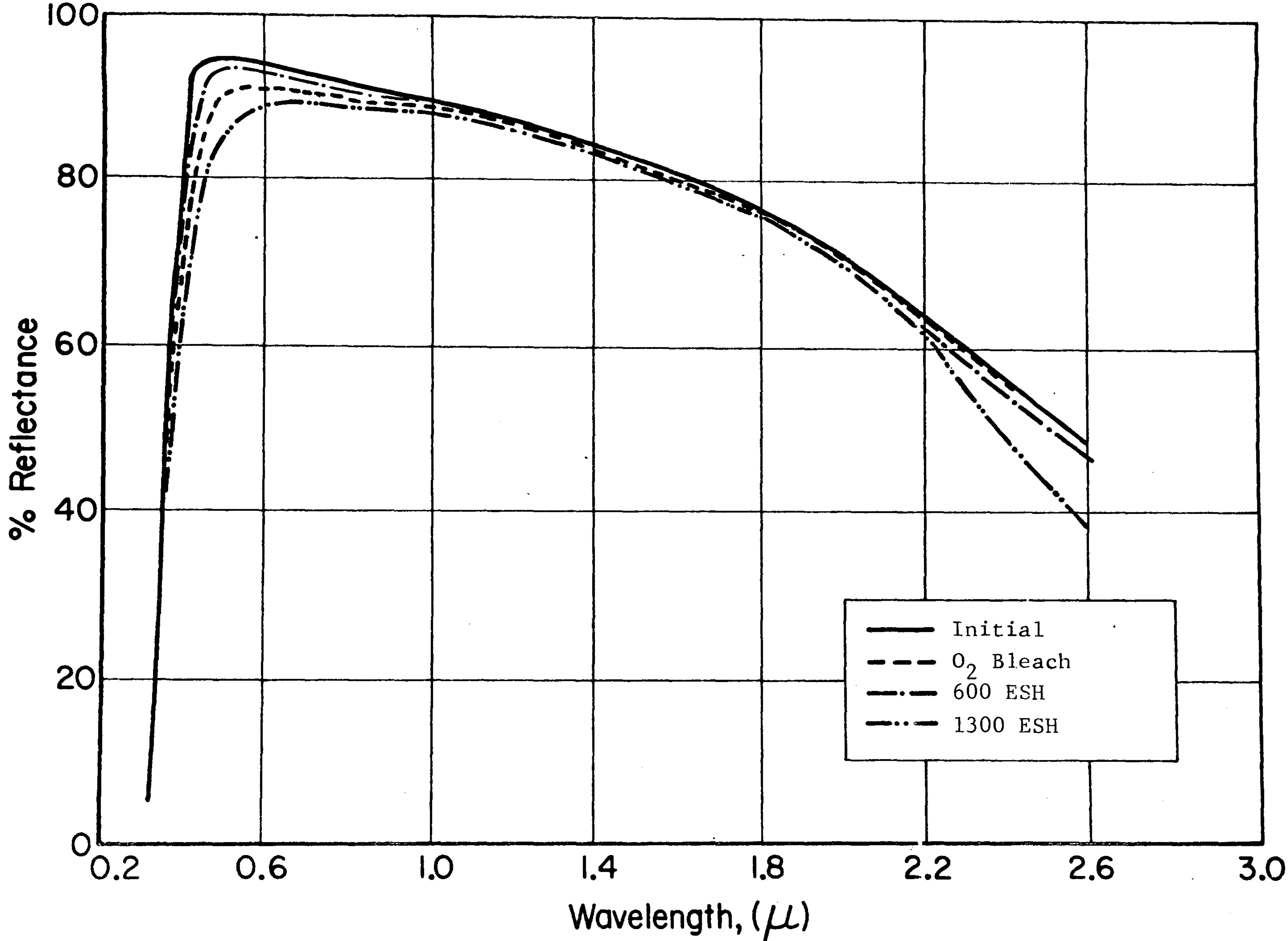

Figure 149 PRE- AND POST-IRRADIATION REFLECTANCE SPECTRA OF Z-93

ultraviolet; the sample in Figure 148 initially received ultraviolet-only, then ultraviolet plus protons; and the sample in Figure 149 received ultraviolet-only, then ultraviolet plus a small spillover of protons. (In the fringe region, the proton flux is roughly 1/10th of the flux in the main beam.)

Analysis of the Z93 spectra indicates that the proton damage due to induced-infrared absorption saturates at about $10^{14} p^{+}/cm^{2}$; that part of the damage caused by the protons in the silicate vehicle is radiatively bleachable, and that some of it is oxygen bleachable. In contrast, analyses of the S-13G spectra (Figures 150 and 151) indicate that the RTV-602 silicone is not as much affected by protons as is the potassium silicate vehicle (in Z93). The damage spectra in the visible region of S-13G show b-band formation in the ZnO and possibly some slight damage in either or both of the silicone vehicle or the silicate encapsulant.

There is some evidence that a slight charge build-up occurred as a result of proton irradiation. The spectra of the ZnO samples (Figures 143 and 144), when compared indicate extensive b-band formation in the proton-irradiation sample and only the typical infrared damage for the ultraviolet-only irradiated sample. Our previous studies of induced b-band formation in ZnO (Ref. 148) indicated that the b-band is not oxygen bleachable. Hence the apparent bleaching in the proton-irradiated sample (Figure 143) is much more likely to be the disappearance of a charge build-up.

Yet unexplained is the response of zinc orthotitanate. In Owens-Illinois 650 "Glass" resin (Figures 145 and 146) the protons clearly have an important effect, but not in the expected spectral region. The oxygen bleaching behavior leads us to suspect that the orthotitanate-silicone interface is unstable. Similarly the behavior of zinc orthotitanate in potassium silicate (Figures 152 and 153) adds further weight to our suspicion of an interfacial stability phenomenon. In later experiments we have indeed shown that zinc orthotitanate can be completely stabilized against

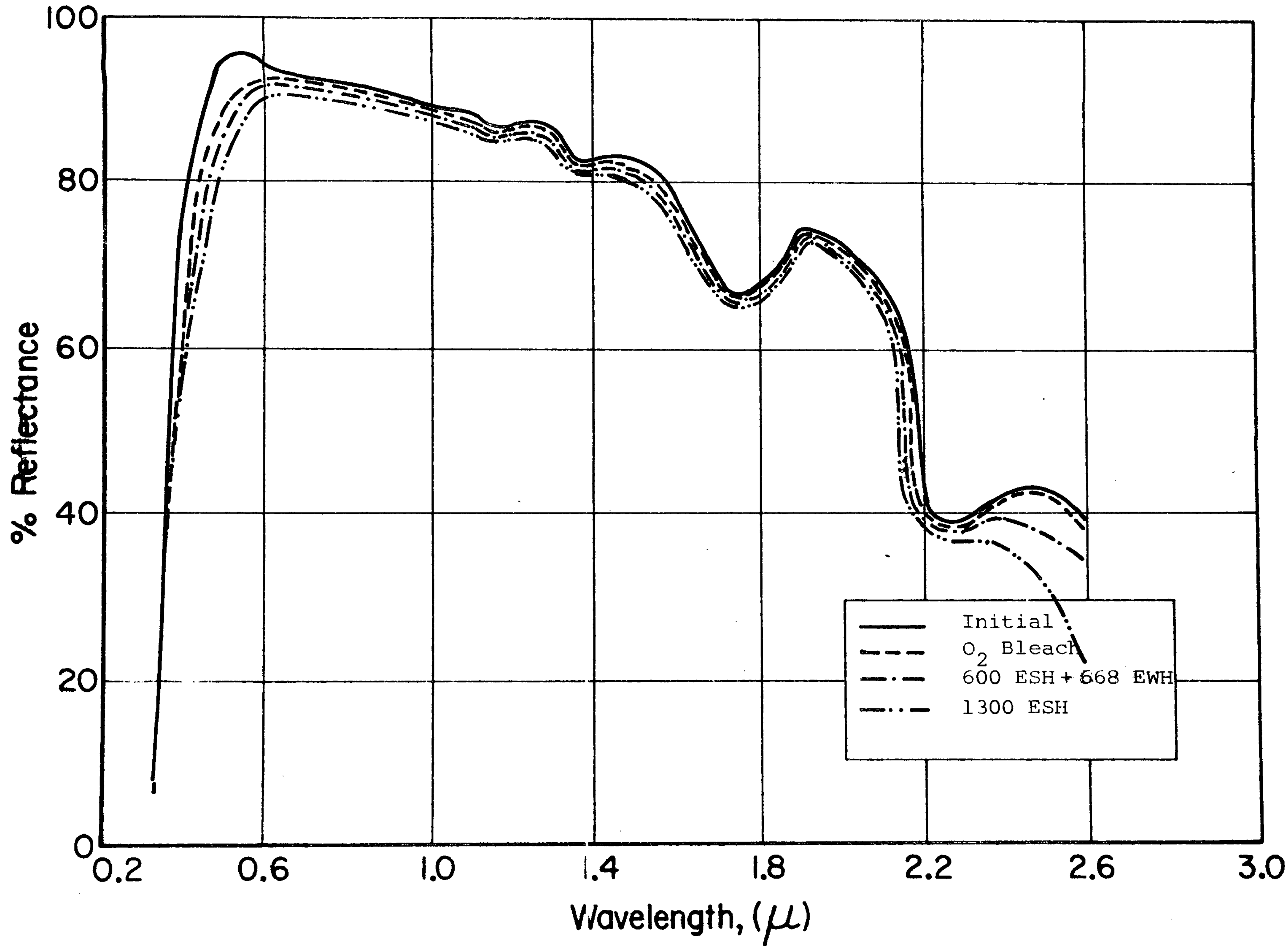

Figure 150 PRE- AND POST-IRRADIATION REFLECTANCE SPECTRA OF S-13G

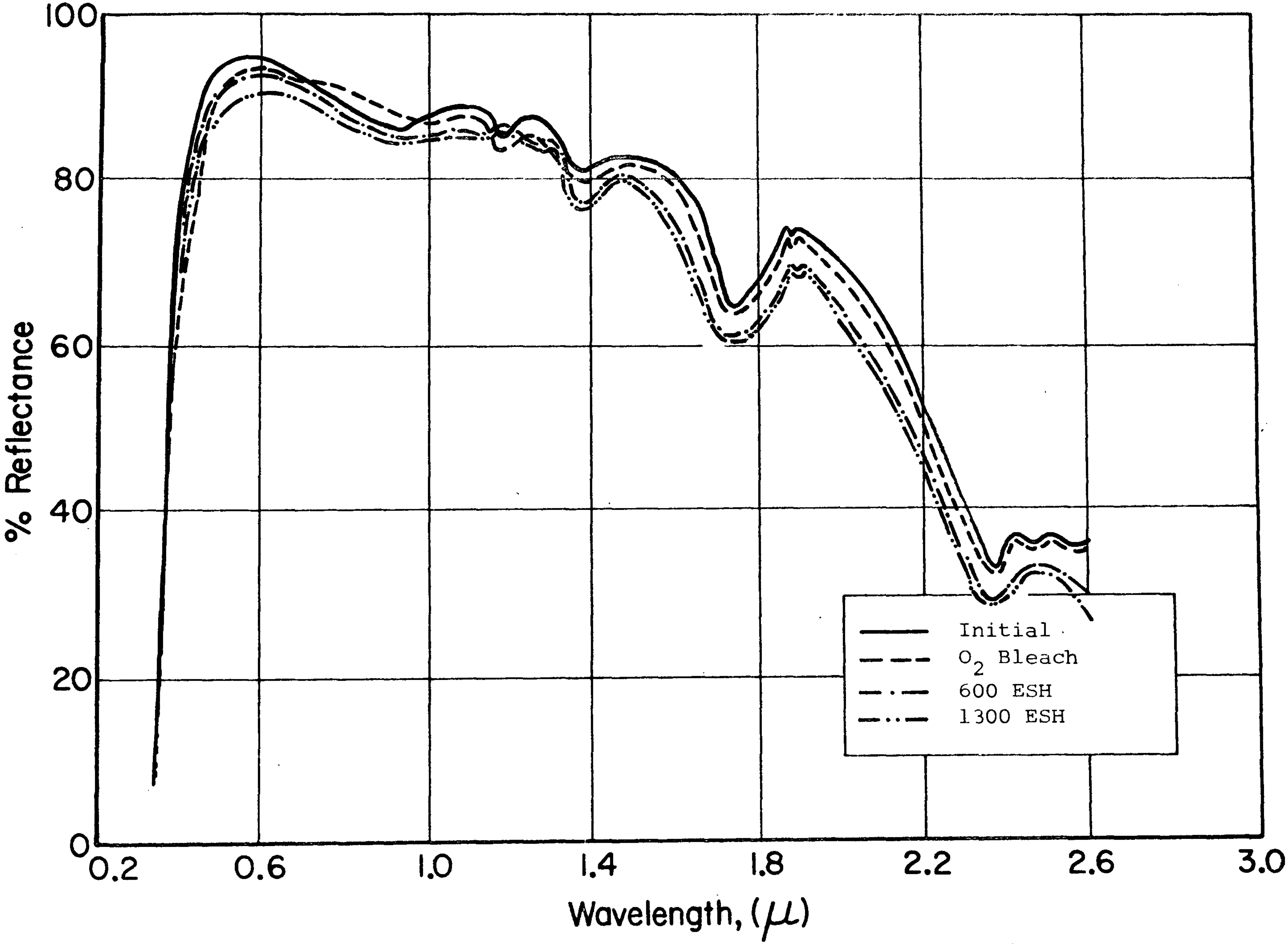

Figure 151 PRE- AND POST-IRRADIATION REFLECTANCE SPECTRA OF S-13G

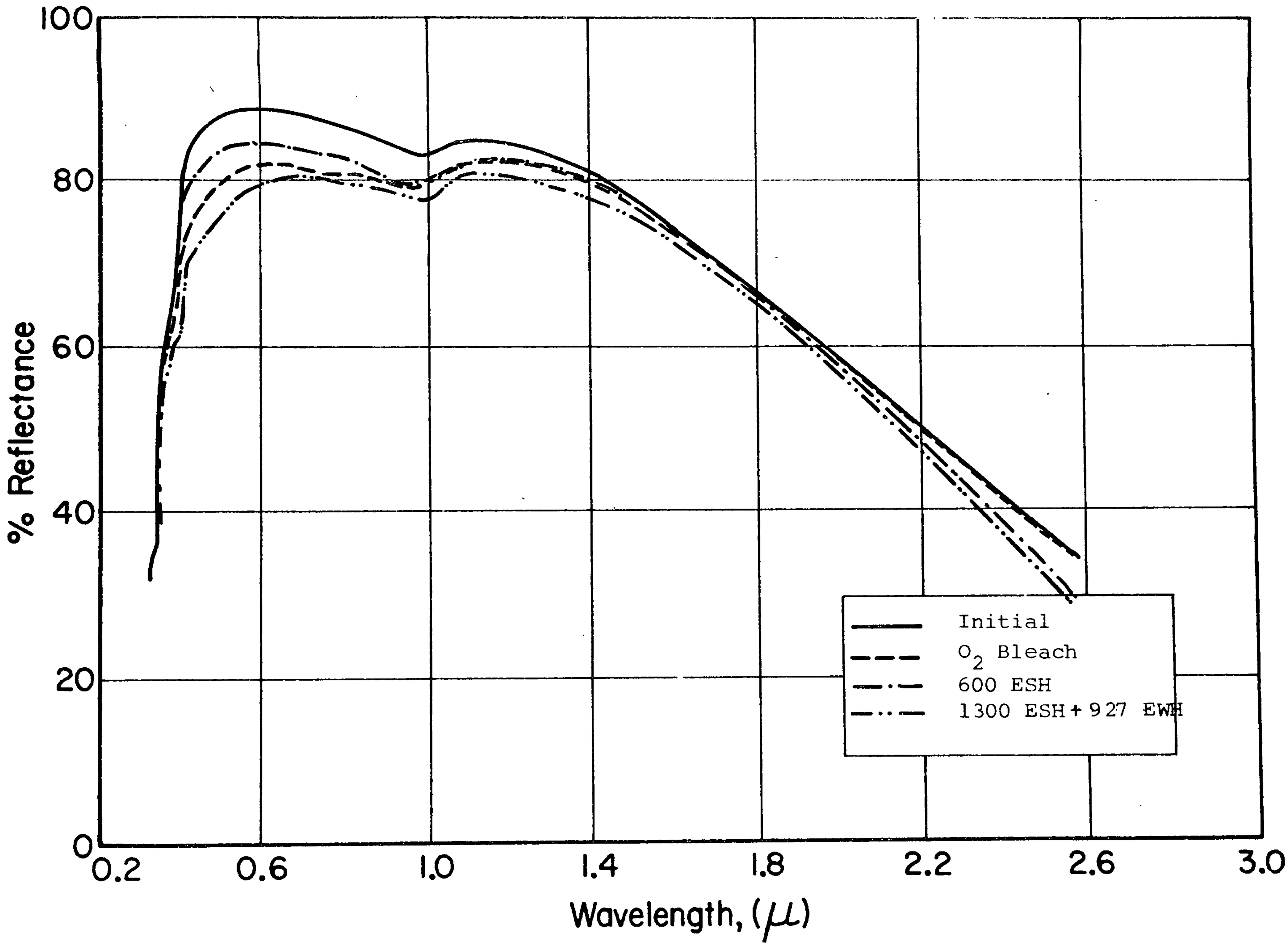

Figure 152 PRE- AND POST-IRRADIATION REFLECTANCE SPECTRA OF Zn_2TiO_4/PS-7

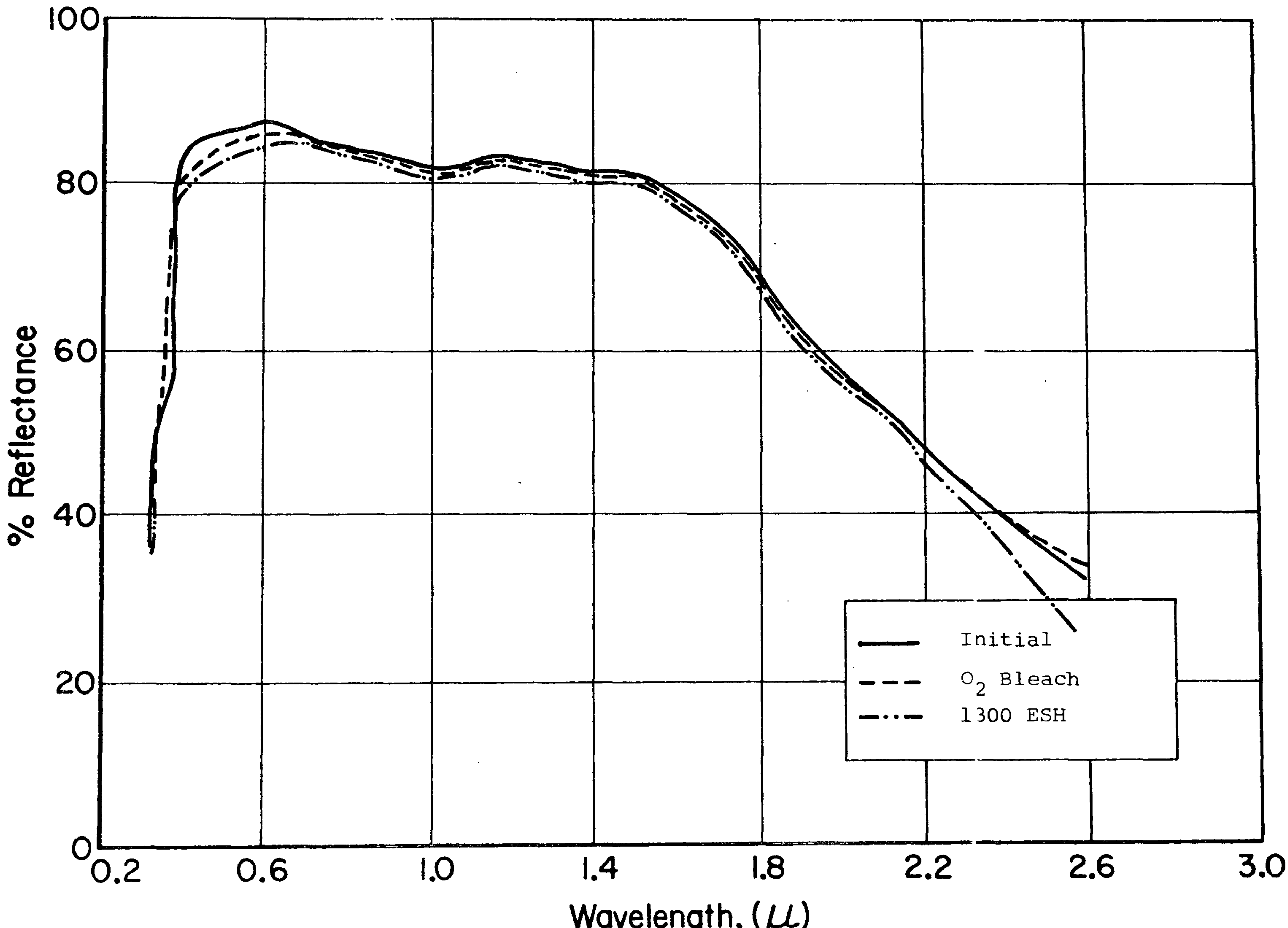

Figure 153 PRE- AND POST-IRRADIATION REFLECTANCE SPECTRA OF Zn_2TiO_4/PS-7

ultraviolet irradiation, if encapsulated in neutral or oxidizing (alkaline) encapsulants. Subsequently, we have shown that these encapsulated pigments, when plasma annealed, can be formulated into very-stable Owens-Illinois 650 resin-based paints.* The zinc oxide sample whose reflectance spectra are displayed in Figure 154 bears out the b-band damage concept in that it was exposed to a very small dose of protons and its damage in the visible is significant (5%) as compared to the sample in Figure 144, which was exposed to ultraviolet-only and sustained about 1% change in this region.

9.3 Conclusions

The simulation of the total space environment becomes an increasingly difficult and complex task as more individual test environments are added. The data presented here obviously show that protons affect the optical performance of IITRI's specification coatings S-13G and Z93. Most importantly, however, analyses of the test results emphasize the fact that experimental test parameters are very critical. It is clear that not only is sequence important, but that the relative rates are very important. All individual radiation fluxes (electromagnetic and particulate) should be the same multiple of actual space rates, and should not exceed rates which will cause temperature effects in the samples.

The use of spectral analyses of the effects of different radiation sources in component materials provides a very important insight into the mechanisms of degradation. Oxygen bleaching following the irradiations also has been a very important diagnostic test. Comparison of oxygen bleaching spectra of materials irradiated in separate and combined environments can greatly aid the interpretation and understanding of test results, and often gives a primary indication of charge buildup. In summary, accurate simulation of the real space environment involves not only the duplication of radiation spectra but the scaling of their rates

---

*IITRI Project C6233, Contract NAS8-26791.

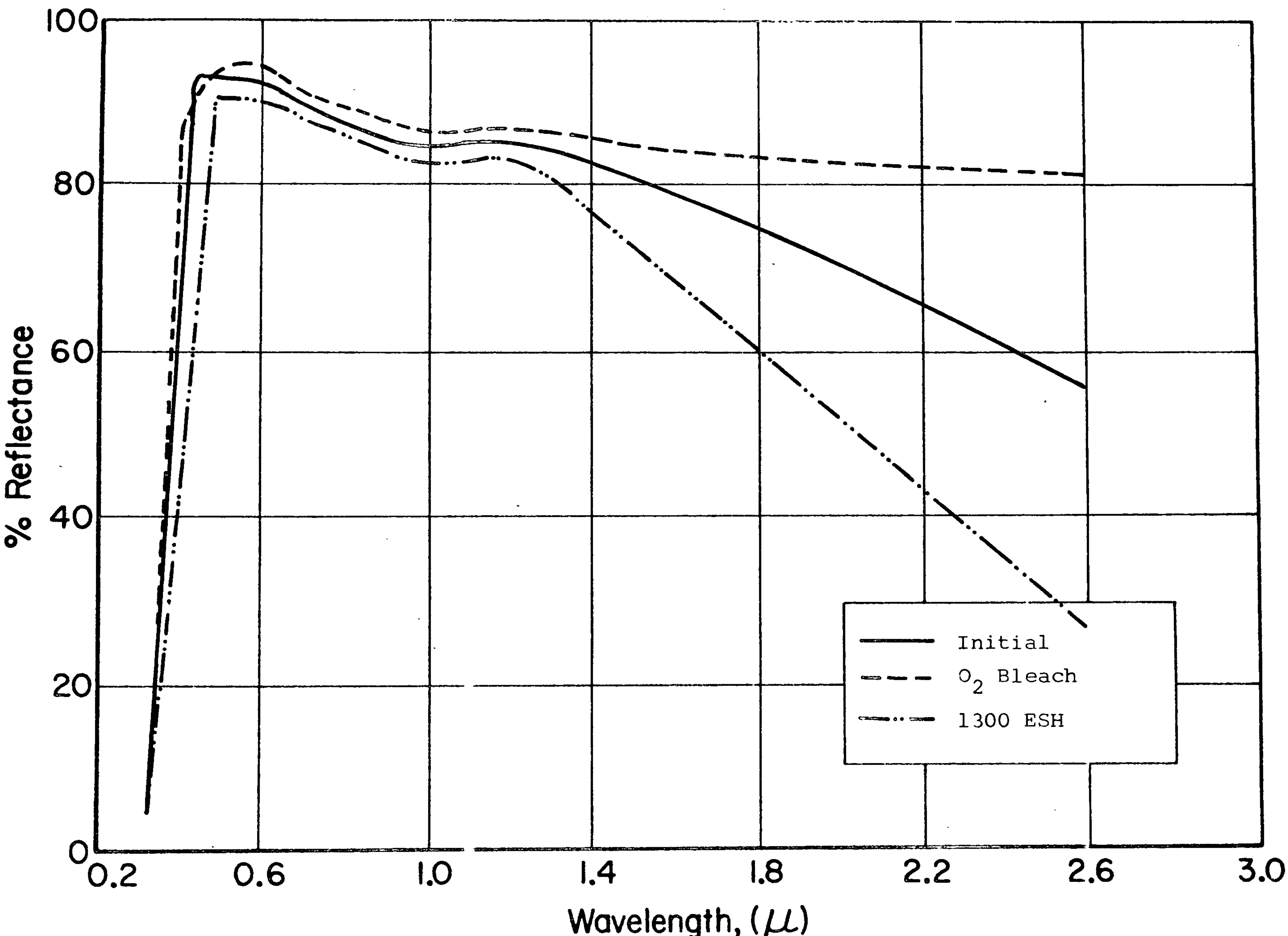

Figure 154 PRE- AND POST-IRRADIATION REFLECTANCE SPECTRA OF SP500 ZnO

to actual environmental rates. When there is an interaction of visible and near-ultraviolet radiation from the solar simulator with charged particle induced defects, the ratio of ultraviolet "suns" to charged particle rates will be especially important. It may well be that the discrepancies between laboratory and flight data can be explained on the basis of unacceptably high and unbalanced environmental flux rates. A final point is that in the real space environment charge buildup would tend to approach a low asymptotic value; whereas, in a laboratory in-situ test facility, such as the CREF, secondary electrons ejected from the test material will usually reach "ground" rather than be attracted back to the sample. The extent to which charge build-up indeed occurs in the real space environment is a question which has a direct bearing on how representative the data from our test devices actually are.

The space environment stability problem in white pigmented coatings will remain obscure until we are certain that our space simulation facilities are indeed accurately simulating the space environment. The stability problem then will become one of knowing the intrinsic responses of materials to specific environments, the optical character and physical interactions of environmentally-induced defects, and the gross reflectance changes these interactions occasion. Because the PVC of white pigmented coatings for spacecraft is so high, the tendency has usually been to emphasize pigment stability. One should be aware, however, of the dilemma wherein the greater the pigment's transparency in the ultraviolet, the lower the solar absorptance, and thus the increased probability of binder photolysis. Accordingly, the further into the ultraviolet the pigment is transparent, the greater will be the demand upon the ultraviolet stability of the binder.

REFERENCES

1. Zerlaut, G.A., Harada, Y. and Tompkins, E.H., "Ultraviolet Irradiation of White Spacecraft Coatings in Vacuum," Symposium on Thermal Radiation of Solids, Katzoff, S. (ed.), NASA SP-55, Washington, D.C., 1965.

2. Gilligan, J.E. and Zerlaut, G.A., "The Role of Gaseous Adsorption in Thermal Coatings Degradation," AIAA Paper 69-1025, AIAA/ASTM/IES Fourth/Space Simulation Conference, Los Angeles, California, September 8-10, 1969.

3. Zerlaut, G.A. and Courtney, W.J., "Space-Simulation Facility for In-Situ Reflectance Measurements," in Thermophysics of Spacecraft and Planetary Bodies," Vol. 20, Progress in Astronautics and Aeronautics, Heller, G. (ed.), Academic Press, New York, pp. 349-368, 1967.

4. Product Data, Hanovia Lamp Division, Englehard-Hanovia, Inc., Newark, New Jersey.

5. Zerlaut, G.A., Tompkins, E.H. and Harada, Y., "Development of Space-Stable Thermal-Control Coatings," NASA-Marshall Space Flight Center Contract No. NAS8-5379, IIT Research Institute Triannual Report No. IITRI-C6014-8, March 5, 1964. (Henceforth all citations pertaining to this contract/project will include only the author(s), report number and date.)

6. Zerlaut, G.A., Harada, Y. and Berman, L.U., Triannual Report No. IITRI-C6014-13, July 20, 1964.

7. Zerlaut, G.A., Gilligan, J.E. and Harada, Y., Triannual Report No. IITRI-C6014-18, December 21, 1964.

8. Zerlaut, G.A., et al, Triannual Report No. IITRI-U6002-31, November 9, 1965.

9. Zerlaut, G.A. and Rubin, G.A., Triannual Report No. IITRI-U6002-36, February 21, 1966.

10. Fajans, K. and Joos, G., Z. Physik, 23, 1, 1924.

11. Moore, L.I., et al, "Evaluation of the Mechanisms Which Affect the Performance of Thermal Radiation Resistant Coatings," WADC TR 57-333, June, 1957.

12. Zerlaut, G.A. and Rogers, F.O., Triannual Report No. IITRI-U6002-47, November 30, 1966.

13. Lundberg, M. and Anderson, S., Acta Chem. Scand., 18, 3, 817, 1964.

14. Reuter, B. and Weber, R., Naturwissenschaften, 53, (10), 251, 1966.

15. Lecerf, A., Compt. Rendus, 254, 2003, 1962.

16. Kutolin, S.A. and Seegeva, A.E., Izv. Akad. Navk SSSR Keorgan. Materialy, 1, (3), 388, 1965.

17. Jonker, G.H., Trabajos reunion intern. reactividad solidos, 3°, 1, 413, Madrid 1956.

18. Yamaguchi, G., J. Japan Ceram. Assoc., 55, 94, 1950.

19. Barblau, F., Schweiz. mineral. petrog. Mitt., 23, 295, 1943.

20. Barblau, F. et al, Helv. Chim. Acta, 27, 1, 88, 1944.

21. Bertant, F. and Durif, A., Comptes Rendus, 236, 212, 1953.

22. Merker, L. and Herrington, K.D., Applied Optics, 3, (11), 1311, 1964.

23. Kestigian, M. and Ward, R., J. Amer. Chem. Soc., 76, 6027, 1954.

24. Johnston, W.D. and Sestrich, D., J. Inorg. and Nuclear Chem., 20, 32, 1961.

25. Collongues, R. et al, Bulletin Soc. Chimique France, (4), 1141, 1965.

26. MacChesney, J.B. and Sauer, H.A., J. Amer. Ceram. Soc., 45, 416, 1962.

27. Kestigian, M. and Ward, R., J. Amer. Chem. Soc., 77, 6199, 1955.

28. Repp, H., Physik Verhandl., 8, (9), 252, 1957.

29. Roth, R.S., J. Res. Nation. Bureau of Standards, 56, 17, 1956.

30. Queyroux, F., Bull. Soc. Franc. Miner. Christ., 86, (3), 295, 1963.

31. Queyroux, F., Comptes Rendus, 259, (8), 1527, 1964.

32. Perez y Jorba, M. et al, Bull. Soc. Franc. Miner. Christ., 84, 401, 1961.

33. Siemens and Halske, A.G., Brit. Patent 720,285, Dec. 15, 1954.

34. Kaczmarek, F., Zeszyty Nauk. Univ. Poznaniu Mat., Fiz. Chem., 5, 3380, 1962.

35. Khodakov, A.L. and Kromakov, O.P., Uchenye Zapiski Fiz. Mat. Fak. Rostov na Donu Univ., 46, (7), 121, 1959.

36. Padurow, N.N., Naturwissenschaften, 43, 396, 1956.

37. Cockayne, B. and Ridley, J.D., Nature, 203, 1054, 1964.

38. Nassau, K. and Broyer, A.N., J. of Applied Physics, 33, 3064, 1962.

39. Chang, L.L.Y., Scroger, M.G. and Phillips, B., J. Am. Cer. Soc., 49 (7), 385, 1966.

40. Kay, M.I., Frazer, B.C., and Almodovar. I., J. of Chem. Physics, 40, 504, 1964.

41. Gillette, R.H., Rev. Sci. Inst., 21, 294, 1950.

42. Shivahare, G.C., Zh. Neorg. Khim., 11, (6), 1478, 1966.

43. Rezukhina, T.N. et al. Izv. Akad. Nauk SSSR, Neorg. Materialy, 2, (2), 325, 1966.

44. Kislyakov, I.P. et al., Tr. Vses Sovesheh, po Fiz. Khim. Rasplaven. Solei, 2nd, Kiev, 116, 1963.

45. Zmud, E.S. and Ostapehenko, E.P., Zhur. Strukt. Khim., 2, 33, 1961.

46. Van Uitert, L.G. and Soden, R.R., J. Appl. Phys., 31, 35, 1960.

47. Shivahare, G.C., J. Sci. Industr. Res., 21 B, 340, 1962.

48. Fesenko, E.G. et al., Izv. Akad. Nauk. SSSR Ser. Fiz, 28, (4), 669, 1964.

49. Belyaev. I.N. et al., Zh. Strukt. Khim., 4, (5), 719, 1963.

50. Dupuis, T., Mikrochimica Acta, II, 737, 1965.

51. Colin, M.L., Bull. Soc. Royal Sciences Liege, 32, (1-2), 110, 1963.

52. Nagay-Szabo, I., Naturwissenschaften, 31, 202, 1943.

53. Megaw, H.D., Proc. Phys. Soc. (London), 58, 133, 1946.

54. Tanaka, Y., Bull. Chem. Soc. Japan, 17, 70, 1942.

55. Smith, A.J. and Welch, A.J.E., Acta Crystallographica, 13, 653, 1960.

56. Couganour, L.W., J. Res. Nat. Bur. Stand., 54, 149, 1955.

57. Rooksby, H.P., Nature, 155, 484, 1945.

58. Troemel, M., Naturwissenschaften, 52, (17), 492, 1965.

59. Wagner, G. and Binder, Z., Anorg. Chem., 297, 1958.

60. Weiss, R. and Faivre, R. Comptes Rendus, 248, 1061, 1959.

61. Natta, G., et Passerini, L., Strukturbericht, 2, 482, 1929.

62. Qureshi, M.H. and Brett, N.H., Trans. Brit. Ceram. Soc., 66 (6) 205, 1968.

63. Berezhnoy, A.S. and Kordyuk, R.A., Refractories, Nos. 1-2, 69, 1962.

64. Belyavskaya, V.V. and Kupriyanova, L.A., Zavodski Lab., 34 (8) 913, 1968; cf. Ceramic Abstracts, 52 (2) 706, 1969.

65. Hossain, D. and Brett, N.H., Trans. Brit. Ceram. Soc., 68 (4), 145, 1969.

66. Chukhlantsev, V.G. and Glakin, Yu. M., Dokl. Akad. Nauk SSSR, 169 (3) 645, 1966; cf. Ceramic Abstracts, 50 (5), 138e, 1967.

67. Smith J.S., Dolloff, R.T. and Mazdiyasni, K.S., "Preparation and Characterization of $SrZrO_3$ and $SrTiO_3$" presented at Am Ceram. Soc. meeting May 4, 1970.

68. Rechter, H.L., IIT Research Institute; unpublished studies.

69. Zerlaut, G.A., Marcour, M. and Noble, G., Triannual Report No. IITRI-U6002-69, October 25, 1968.

70. Zerlaut, G.A. and Gilligan, J.E., "Study of In Situ Degradation of Thermal Control Surfaces," NASA-Marshall Space Flight Center Contract NAS8-21074, IIT Research

Institute Report No. IITRI-U6061-17 (Interim Summary Report), March 7, 1969.

71. Neel, C.B., "Research on the Stability of Thermal Control Coatings for Spacecraft," NASA TMX-51, 196, NASA-Ames Research Center, October, 1963.

72. Zerlaut, G.A., and Harada, Y., "Stable White Coatings," JPL Contract 950111 (Subcontract under NAS7-100), IIT Research Institute Report No. IITRI C207-25 (Summary Report), August 27, 1963.

73. Zerlaut, G.A., Triannual Report No. IITRI-U6002-42, July 11, 1966.

74. Gilligan, J.E., "The Optical Properties Inducible in Zinc Oxide," Progress in Astronautics and Aeronautics: Thermophysics of Spacecraft and Planetary Bodies, Vol. 20, Edited by G.B. Heller, Academic Press, New York, 1967.

75. Pearson, B.D., Jr., "Preliminary Results from the Ames Emissivity Experiment on OSO-II," in Thermophysics and Temperature Control of Spacecraft and Entry Vehicles, Vol. 18, Progress in Astronautics and Aeronautics, Heller, G., (ed.), Academic Press, New York, 1966.

76. Millard, J.P., "Results from the Thermal Control Coatings Experiment on OSO-III," in Thermal Design Principles of Spacecraft and Entry Bodies, Vol. 21, Progress in Astronautics and Aeronautics, Bevans, J. (ed.), Academic Press, New York, 1969.

77. Zerlaut, G.A., Firestone, R.F. and Jameson, W.E., Triannual Report No. IITRI-C6014-26, July 20, 1965.

78. Zerlaut, G.A., "Pigment-Binder Relatingships in Ultraviolet Irradiated Paints in Vacuum," Proceedings, Division of Organic Coatings and Plastics Chemistry (Symposium on Coatings for Space Environment), Vol. 41, No. 2, The American Chemical Society, September, 1961.

79. Zerlaut, G.A. and Kaye, B.H., Triannual Report No. IITRI-C6014-21, February 23, 1965.

80. Charlesby, A., "Radiation Mechanisms in Polymers," in Irradiation of Polymers, N.A.J. Platzer, Ed., Advances in Chemistry Series, No. 66, Am. Chem. Soc., Washington, D.C. 1967.

81. Wall, C.A. and Florin, R.E., J. Appl. Polymer Sci., 5, 251, 1959.

82. Ohnishi, S. et al, ibid. <u>6</u>, 629, 1962.

83. Alexander, A.L. et al., WADD TR 60-703, Part I. Nov. 1960; Part II December, 1960.

84. Miller, A.A., J. Phys. Chemistry, <u>63</u>, 1755, 1959.

85. Chapiro, A., J. Chim. Phys., <u>53</u>, 895, 1956.

86. Loy, B.R., J. Phys. Chem., <u>65</u>, 58, 1961.

87. Yegorova, Z.S. et al., Polymer Sci. (U.S.S.R.), <u>4</u>, 23, 1963.

88. St. Pierre, L.E. and Dewhurst, H.A., J. Chem. Phys., <u>29</u>, 241, 1958.

89. St. Pierre, L.E. and Dewhurst, H.A., J. Phys. Chem., <u>64</u>, 1060, 1960.

90. Zimmerman, J., J. Appl. Polymer Sci., <u>2</u>, 181, 1959.

91. Moore, R.F., Polymer, <u>4</u>, 493, 1963.

92. Zimmerman, J., J. Polymer Sci., <u>46</u>, 151, 1960.

93. Graves, C.T. and Ormerod, M.G., Polymer, <u>4</u>, 81, 1963.

94. Lawton, E.J., et al, J. Poly. Sci., <u>32</u>, 257, 1958.

95. Ormerod, M.G., Polymer, <u>4</u>, 451, 1963.

96. Miller, A.A., J. Am. Chem. Soc., <u>82</u>, 3519, 1960.

97. Miller, A.A., ibid, <u>83</u>, 31, 1961.

98. Ormerod, M.G. and Charlesby, A., Polymer, <u>4</u>, 459, 1963.

99. Charlesby, A. and Garratt, P.G., Proc. Roy. Soc. (London), <u>273A</u>, 117, 1963.

100. Miller, A.A., I. & E.C., Prod. Res. & Dev., <u>3</u>, 252, 1964.

101. Koike, M. and Danno, A., J. Phys. Soc. Japan, <u>15</u>, 1501, 1960.

102. Koike, M., ibid., <u>18</u>, 387, 1963.

103. Patrode, W. and Wilcock, D.F., J. Am. Chem. Soc., <u>63</u>, 358, 1946.

104. Hunter, M.J., et al, J. Am. Chem. Soc., <u>68</u>, 667, 1946.

105. Schwanzkopf Analytical Laboratories, Woodside, N.Y.

106. Hyde, J.F. and Delong, R.C., J. Am. Chem. Soc., 63, 1194, 1941.

107. Tsvetkov, Yu. D., Mulin, Yu. N. and Voeodskii, V.V., Vysokomol. Svedineniya, 1, 1805, 1959.

108. Jen, C.K., Funer, S.N., Cochran, E.L. and Bowers, V.A., Phys. Rev., 112, 1169, 1958.

109. Zerlaut, G.A., Tompkins, E.H. and Harada, Y., Triannual Report No. IITRI-C6014-4, October 25, 1965.

110. Gilligan, J.E. and Ashford, N.A., "Development of Space-Stable, Thermal-Control Coatings for Use on Large Space Vehicles," NASA-Marshall Space Flight Center Contract No. NAS8-26791, IIT Research Institute Triannual Report No. IITRI-C6233-8, October 15, 1971.

111. Akawie, R.I., "Development of Polymeric Materials for the as Binders and Transparent Films," USAF Contract F33615-69-C-1287, Hughes Aircraft Company Quarterly Report No. 4, June 1970.

112. Iyengar, R.D., Kodell, M., Kara, J.S. and Turkevich, J., J. Am. Chem. Soc., 88, 50, 1956.

113. Perny, G. and Lorang, M., J. Chim. Phys., 63, 827, 1966.

114. Zerlaut, G.A., Noble, G. and Rogers, F.O., Triannual Report No. IITRI-U6002-59, January 15, 1968.

115. Rogers, F.O. and Zerlaut, G.A., "Development of S-13G Type Coatings vs Engineering Materials," Jet Propulsion Laboratory Contract No. 951737, IIT Research Institute Report IITRI-U6053-11, March 5, 1969.

116. Zerlaut, G.A., Rogers, F.O. and Noble, G., "The Development of S-13G-Type Thermal-Control Coatings, in Thermal Design Principles of Spacecraft and Entry Bodies, Vol. 21 Progress in Astronautics and Aeronautics, Bevans, J. (ed.), Academic Press, New York, 1969.

117. Streed, E.R. and Beveridge, C.M., "The Study of Low Solar Absorptance Coatings for a Solar Probe," ibid.

118. Zerlaut, G.A., Gilligan, J.E. and Harada, Y., "Stable White Coatings," IITRI Research Institute Report No. IITRI-C6027-16 (Interim Tech. Progress Report), JPL Contract 950746 (Subcontract under NAS7-100), June 30, 1965.

119. Pearson, B. Douglas, Jr., "Preliminary Results from the Ames Emissivity Experiment on OSO-II," Progress in Astronautics and Aeronautics, Heller, G. (ed.), 18, Academic Press, New York, pp. 459-472, 1966.

120. Schafer, C.F. and Bannister, T.C., "Pegasus Thermal Control Coatings Experiment," AIAA 66-419, Los Angeles, California, June 27, 1966.

121. MacMillan, H.F., Sklensky, A.F. and McKeller, L.A., "Apparatus for Spectral Bidirectional Reflectance Measurements During Ultraviolet Irradiation in Vacuum," Progress in Astronautics and Aeronautics, Heller, G. (ed.), 18, Academic Press, New York, pp. 129-149, 1966.

122. Miller, E., NASA-George C. Marshall Space Flight Center, Huntsville, Alabama, Personal Communication, December, 1965.

123. Seitz, F., Disc. Far. Soc., 5, 271, 1949.

124. Johnson, F.S., J. Meteor., 11, 431, 1954.

125. "Solar Electromagnetic Radiation," NASA SP-8005, National Aeronautics and Space Administration, Washington, D.C., June 1965.

126. Parker, E.N., "Interplanetary Dynamical Processes," Interscience Publishers, Inc., New York, N.Y. 1963.

127. Gilligan, J.E. and Zerlaut, G.A., Triannual Report No. IITRI-U6002-90, July 1, 1970.

128. King, H.J. and Zuccaro, D.E., "Solar Wind Simulation Techniques" Hughes Aircraft Coporation, NASA-Ames Research Center Contract NAS2-5585, Final Report, April, 1970.

129. Jaenicke, W., Ieit. fur Elektrochemie, 60, (2), 163, 1956.

130. Dulin, F.H. and Rase, D.E., J. Amer. Cer. Soc., 43, (3), 125, 1960.

131. Bartram, S.F. and Slepetys, R.A., J. Amer. Cer. Soc., 44, (10), 493, 1961.

132. Loshkarev, R.A., Steklo i Keram, 19, (3), 22, 1962.

133. Loshkarev, R.A., Steklo i Keram, 19, (10), 21, 1962.

134. Loshkarev, R.A., Trans. Uralsk Polyt. Inst. Symp., 117, 1962.

135. Kubo, T. and Kato, M. et al, Kogyo Kagsky/Zasshi, 66, (4), 403, 1963.

136. Ashford, N.A. and Zerlaut, G.A., Triannual Report No. IITRI-U6002-77, July 11, 1969.

137. Ashford, N.A., and Zerlaut, G.A., Tirannual Report No. IITRI-U6002-83, November 17, 1969.

138. Bartlett, R.W., "Induction Plasma Calcining of Pigment Particles for Thermal Control Coatings," SRI Report No. 1, PMU-7083, NASA-Marshall Space Flight Center Contract NAS8-21270, August 15, 1968.

139. Farley, E.P. and Bartlett, R.W., "Induction Plasma Calcining of Pigment Particles for Thermal Control Coatings," SRI Report No. 4, PMU-7083, NASA-Marshall Space Flight Center Contract NAS8-21270, February 5, 1971.

140. Sancier, K.W., Surface Science, 21, 1, 1970.

141. Zerlaut, G.A. and Ashford, N.A., Triannual Report No. IITRI-U6002-73, January 31, 1969.

142. Kasai, P.V., Phys. Rev., 130, 989, 1963.

143. Geisler, C.M. and Simmond, G.L. Phys. Letter, 11, 111, 1964.

144. Zerlaut, G.A., Triannual Report No. IITRI-U6002-94, November 30, 1970.

145. Morrison, S.R. and Sancier, K.M., "Effect of Environment of Thermal Control Coatings," SRI Project PAD-6146 Final Report, Jet Propulsion Laboratory Contract 951522, October 15, 1969.

146. Zerlaut, G.A. and Ashford, N.A., Triannual Report No. IITRI-U6002-85, February 20, 1970.

147. Gilligan, J.E. and Zerlaut, G.A., "The Space Environment Stability Problem in White Pigmented Coatings," 17th Annual Meeting, Institute of Environmental Sciences, April 26-30, 1971, Los Angeles.

148. Gilligan, J.E., "Stable White Coatings/ZnO Photolysis," Jet Propulsion Laboratory Contract 950746 (Subcontract under NAS7-100), IIT Research Institute Report No. IITRI-U6004-21 (Summary Technical Report), February 7, 1966.

APPENDIX

MATERIALS PREPARATION

APPENDIX

MATERIALS PREPARATION

A batch of zinc orthotitanate (Zn_2TiO_4) prepared at 925°C, employing 0.5% excess ZnO, was used as the basic pigment for all the studies reported herein. It is designated Batch B-229. The treatments and coatings prepared from them are presented in the following paragraphs. The phylogeny of all specimen preparations are presented schematically in Figures 82 and 83.

B-226

Five hundred (500) g of Batch B-229 Zn_2TiO_4 were slurried with 1250 g of 0.001 M potassium ferrocyanide and 1250 g of 0.001 M potassium ferricyanide for 1 hr at room temperature. With continued agitation, the temperature of the slurry was raised to 80°C and held for 30 min. (Thirty minutes was required to raise the temperature to 80°C.) The slurry was then cooled to room temperature (with agitation) and was then vacuum filtered through a Buchner funnel; the resultant powder was dried for 16 hr at 110°C.

B-233

Five hundred (500) g of Batch B-229 were mixed with 267 g of distilled H_2O and 500 ml of PS-7 potassium silicate. The mixture was refluxed with agitation for 8 hr. After refluxing, 666 ml of distilled H_2O was added to the mixture and the mixture was vacuum filtered through a Buchner funnel. The filter cake was redispersed in 600 ml of distilled H_2O and refiltered. The moist filter cake was broken up and then dried at 110°C for 16 hr.

B-241

Five hundred (500) g of Batch B-229 Zn_2TiO_4 were mixed with 834 g of a 5% solution of NaH_2PO_4. The slurry was refluxed for 4 hr, vacuum filtered through a Buchner funnel, rinsed with 334 ml distilled H_2O and dried for 16 hr at 110°C.

B-412

One hundred (100) g of Batch B-233 (silicate-treated Zn_2TiO_4) were mixed with 167 g of a 5% solution of NaH_2PO_4. The mixture was refluxed for 4 hr, vacuum filtered through a Buchner funnel, rinsed with 67 ml distilled H_2O and dried for 16 hr at 110°C.

B-413

One hundred (100) g of Batch B-233 (silicate-treated Zn_2TiO_4) were mixed with 250 g of 0.001 M potassium ferrocyanide and 250 g of 0.001 M potassium ferricyanide. The mixture was heated to 80°C with agitation and held for 30 min. After cooling, the mixture was filtered through a Buchner funnel and dried for 16 hr at 110°C.

B-414

One hundred (100) g of Batch B-241 (phosphate-treated Zn_2TiO_4) were mixed with 250 g of 0.001 M potassium ferrocyanide and 250 g of 0.001 M potassium ferricyanide. The mixture was heated at 80°C for 30 min with agitation, cooled and filtered through a Buchner funnel. The resultant filter cake was dried for 16 hr at 110°C.

B-415

Twenty (20) g of Batch B-229 were ground with 34 g of a 28% ethanol solution of Owens-Illinois 650 resin (32% PVC). The mixture was ground for 3 hr in a Mini-mill (0000) ball mill. The resultant paint was spray applied on IRIF coupons and baked at 110°C for 16 hr.

B-416

Sixty (60) g of Batch B-229 were ground with 25 ml of PS-7 potassium silicate and 35 ml of distilled H_2O. The mixture was ground for 2 hr in a Mini-mill (000) ball mill. Two sets of IRIF coupons were spray coated with the resultant paint and allowed to air dry for 16 hr. One set was then baked for 16 hr at 110°C and the other set was heat treated for 16 hr at 427°C.

B-417

Fifteen (15) g of Batch B-233 (silicate-treated Zn_2TiO_4) were ground with 35 ml of distilled H_2O for 15 min in a Mini-mill (000) ball mill. The resultant slurry was "wet" sprayed on "hot" IRIF coupons.

B-419

Thirty (30) g of Batch B-233 (silicate-treated Zn_2TiO_4) were ground with 12.5 ml of PS-7 potassium silicate and 12.5 ml of distilled H_2O. The mixture was ground for 1 hr in a Mini-mill (000) ball mill. Two sets of IRIF coupons were spray coated with the resultant paint and allowed to air dry for 16 hr. One set was then baked for 16 hr at 110°C and the other set was heat treated for 16 hr at 427°C.

B-420

Ten (10) g of Batch B-241 (phosphate-treated Zn_2TiO_4) was mixed with 25 ml of distilled H_2O and ground for 15 min in a Mini-mill (000) ball mill. The resultant slurry was "wet" sprayed on "hot" IRIF coupons.

B-421

Twenty-four (24) g of Batch B-241 (phosphate-treated Zn_2TiO_4) was mixed with 10 ml of PS-7 potassium silicate and 10 ml of distilled H_2O. The mixture was ground for 15 min in a Mini-mill (000) ball mill. Two sets of IRIF coupons were spray coated with the resultant paint and allowed to air dry for 16 hr. One set was then baked for 16 hr at 110°C and the other set was heat treated for 16 hr at 427°C.

B-422

Twenty (20) g of Batch B-241 (phosphate-treated Zn_2TiO_4) were mixed with 34 g of a 28% ethanol solution of Owens-Illinois 650 resin. The mixture was ground for 3 hr in a Mini-mill (000) ball mill. The resultant paint was spray coated on IRIF coupons, air dried for 16 hr, and then baked for 16 hr at 110°C.

B-423

Fifteen (15) g of Batch B-226 (Fe^{++}/Fe^{+++}-treated Zn_2TiO_4) were mixed with 35 ml distilled H_2O and ground for 20 min in a Mini-mill (000) ball mill. The resultant slurry was "wet" sprayed on "hot" IRIF coupons.

B-424

Thirty (30) g of Batch B-226 (Fe^{++}/Fe^{+++}-treated Zn_2TiO_4) were ground with 12.5 ml PS-7 potassium silicate and 12.5 ml distilled H_2O. The mixture was ground for 1 hr in a Mini-mill (000) ball mill. The resultant paint was spray coated on two sets of IRIF coupons and allowed to air dry for 16 hr. One set was baked for 16 hr at 110°C and the other set was heat treated for 16 hr at 427°C.

B-425

Twenty (20) g of Batch B-226 (Fe^{++}/Fe^{+++}-treated Zn_2TiO_4) were ground with 34 g of a 28% ethanol solution of Owens-Illinois 650 resin. The mixture was ground for 3 hr in a Mini-mill (000) ball mill. The resultant paint was spray coated on IRIF coupons, air dried for 16 hr, and then baked for 16 hr at 110°C.

B-426

Thirty (30) g of Batch B-412 (phosphate- and silicate-treated Zn_2TiO_4) were mixed with 12.5 ml of PS-7 potassium silicate and 12.5 ml distilled H_2O. The mixture was ground for 1 hr in a Mini-mill (000) ball mill. The resultant paint was spray coated on two sets of IRIF coupons and allowed to air dry for 16 hr. One set was then baked for 16 hr at 110°C and the other was heat treated for 16 hr at 427°C.

B-427

Twenty (20) g of Batch B-412 (phosphate- and silicate-treated Zn_2TiO_4) were mixed with 34 g of a 28% ethanol solution of Owens-Illinois 650 resin. The mixture was ground for 3 hr in a Mini-mill (000) ball mill. The resultant paint was spray coated on IRIF coupons, air dried for 16 hr, then baked for 16 hr at 110°C.

B-428

Thirty (30) g of Batch B-413 (Fe^{++}/Fe^{+++}-silicate treated Zn_2TiO_4) were mixed with 34 g of a 28% ethanol solution of Owens-Illinois 650 resin. The mixture was ground for 1 hr in a Mini-mill (000) ball mill. The resultant paint was spray coated on two sets of IRIF coupons and air dried for 16 hr. One set was then baked for 16 hr at 110°C and the other was heat treated for 16 hr at 427°C.

B-430

Thirty (30) g of Batch B-414 (Fe^{++}/Fe^{+++}-phosphate treated Zn_2TiO_4) were mixed with 12.5 ml PS-7 potassium silicate and 12.5 ml distilled H_2O. The mixture was ground for 1 hr in a Mini-mill (000) ball mill. The resultant paint was spray coated on two sets of IRIF coupons and air dried for 16 hr. One set was then baked for 16 hr at 110°C and the other set was heat treated for 16 hr at 427°C.

B-431

Twenty (20) g of Batch B-414 (Fe^{++}/Fe^{+++}-phosphate treated Zn_2TiO_4) were mixed with 34 g of a 28% ethanol solution of Owens-Illinois 650 resin. The mixture was ground for 3 hr in a Mini-mill (000) ball mill. The resultant paint was spray coated on IRIF coupons, air dried for 16 hr, and then baked for 16 hr at 110°C.

B-453

Five (5) g of lithium silicofluoride ($Li_2SiF_6 \cdot 2H_2O$) were dissolved in 1000 ml distilled H_2O. One hundred (100) g of B-229 (Zn_2TiO_4) were added to the solution and the mixture was refluxed for 6 hr with agitation. On cooling, the mixture was filtered through a Buchner funnel, rinsed 4 times with 600 ml quantities of distilled H_2O, and dried for 16 hr at 110°C. Five (5) g of the dry pigment were dispersed in forty-five (45) ml of distilled H_2O by hand shaking and the resultant slurry was "wet" sprayed on "hot" IRIF Coupons.

B-454

Approximately fifty (50) g of Batch B-453 were placed in a porcelain crucible and heat treated for 7 hr at 500°C. Five (5) g of the pigment were dispersed in forty-five (45) ml of distilled H_2O by hand shaking and the resultant slurry was "wet" sprayed on "hot" IRIF coupons.

B-457

Five (5) g of potassium silicofluoride (K_2SiF_6) were dissolved in 1000 ml distilled H_2O. One hundred (100) g of B-229 (Zn_2TiO_4) were added to the solution and the mixture was refluxed for 6 hr with agitation. On cooling, the mixture was filtered through a Buchner funnel, rinsed 4 times with 600 ml quantities of distilled H_2O, and dried for 16 hr at 110°C. Five (5) g of the dry pigment were dispersed in forty-five (45) ml distilled H_2O by hand shaking and the resultant slurry was "wet" sprayed on "hot" IRIF coupons.

B-458

Approximately 50 g of Batch B-457 were placed in a porcelain crucible and heat treated for 7 hr at 500°C. Five (5) g of the pigment were dispersed in forty-five (45) ml of distilled H_2O by hand shaking. The resultant slurry was "wet" sprayed on "hot" IRIF coupons.

B-459

Five (5) g of silicotungstic acid ($H_4Si_4W_{12}O_{40}$) were dissolved in 1000 ml distilled H_2O. One hundred (100) g of B-229 (Zn_2TiO_4) were added to the solution and the mixture was refluxed for 6 hr with agitation. On cooling, the mixture was filtered through a Buchner funnel, rinsed 4 times with 600 ml quantities of distilled H_2O and dried for 16 hr at 110°C. Five (5) g of the pigment were dispersed in forty-five (45) ml of distilled H_2O by hand shaking. The resultant slurry was "wet" sprayed on "hot" IRIF coupons.

B-460

Approximately fifty (50) g of Batch B-459 were placed in a porcelain crucible and heat treated for 7 hr at 500°C. Five (5) g of the pigment were dispersed in forty-five (45) ml distilled H_2O by hand shaking. The resultant slurry was "wet" sprayed on "hot" IRIF coupons.

B-461

Five (5) g of potassium hexafluorostannate ($K_2SnF_6 \cdot xH_2O$) were dissolved in 1000 ml distilled H_2O. One hundred (100) g of B-229 (Zn_2TiO_4) were added to the solution and the mixture was refluxed for 6 hr with agitation. On cooling, the mixture was filtered through a Buchner funnel, rinsed 4 times with 600 ml quantities of distilled H_2O, and dried for 16 hr at 110°C. Five (5) g of the pigment were dispersed in forty-five (45) ml distilled H_2O by hand shaking. The resultant slurry was "wet" sprayed on "hot" IRIF coupons.

B-462

Approximately 50 g of Batch B-461 were placed in a porcelain crucible and heat treated for 7 hr at 500°C. Five (5) g of the pigment were dispersed in forty-five (45) ml distilled H_2O by hand shaking. The resultant slurry was "wet" sprayed on "hot" IRIF coupons.

B-546

Five (5) g of potassium silicotungstate ($K_4Si_4W_{12}O_{40} \cdot 18H_2O$) were dissolved in 1000 ml distilled H_2O. One hundred (100) g of B-229 (Zn_2TiO_4) were added to the solution and the mixture was refluxed for 6 hr with agitation. On cooling, the mixture was filtered through a Buchner funnel, rinsed 4 times with 600-ml quantities of distilled H_2O, and dried for 16 hr at 110°C. Five

(5) g of the dry pigment were dispersed in forty-five (45) ml of distilled H_2O by hand shaking. The resultant slurry was "wet" sprayed on "hot" IRIF coupons.

B-547

Approximately 50 g of Batch B-546 were placed in a porcelain crucible and heat treated for 7 hr at 500°C. Five (5) g of the pigment were dispersed in forty-five (45) ml distilled H_2O by hand shaking. The resultant slurry was "wet" sprayed on "hot" IRIF coupons.

* * * * *

The following paints were prepared in identical fashion. The procedure used in their preparation was as follows: Five (5) g of the pigment being studied were mixed with 8.5 g of a 28% ethanol solution of Owens-Illinois 650 resin. The mixture was ground by means of a mortar and pestle. The resultant paint was sprayed on IRIF coupons and baked for 17 hr at 110°C. The pigments studied are tabulated below.

Coating No.	Pigment Batch No.	Pigment Description
B-552	B-453	Li_2SiF_6 treated Zn_2TiO_4
B-553	B-454	Heat treated B-453
B-554	B-457	K_2SiF_6 treated Zn_2TiO_4
B-555	B-458	Heat treated B-457
B-556	B-461	K_2SnF_6 treated Zn_2TiO_4
B-557	B-462	Heat treated B-461
B-558	B-546	$K_4SiW_{12}O_{40}$ treated Zn_2TiO_4
B-559	B-547	Heat treated B-546

* * * * *

The following paints were prepared in identical fashion. The procedure used in their preparation was as follows: Seven and one-half (7.5) g of the pigment being studied were mixed with 3.1 ml PS-7 potassium silicate and 3.1 ml distilled H_2O. The mixture was ground by means of a mortar and pestle. The resultant paint was sprayed on IRIF coupons and baked for 16 hr at 110°C. The pigments studied are tabulated below.

Coating No.	Pigment Batch No.	Pigment Description
B-560	B-453	Li_2SiF_6 treated Zn_2TiO_4
B-561	B-454	Heat treated B-453
B-562	B-457	K_2SiF_6 treated Zn_2TiO_4
B-563	B-458	Heat treated B-457
B-564	B-461	K_2SnF_6 treated Zn_2TiO_4
B-565	B-462	Heat treated B-461
B-566	B-546	$K_4SiW_{12}O_{40}$ treated Zn_2TiO_4
B-567	B-547	Heat treated B-546